A TIME DOMAIN APPROACH FOR BRIDGE FATIGUE CONSIDERING THE EFFECT OF MULTIPLE VEHICLES AT RANDOM PASSING RATE

A Thesis Submitted in

Partial Fulfilment of the Requirements

for the Degree of

DOCTOR OF PHILOSOPHY

By

Anjaly J Pillai

DEPARTMENT OF CIVIL ENGINEERING

INDIAN INSTITUTE OF TECHNOLOGY GUWAHATI

GUWAHATI-781039, INDIA

FEBRUARY, 2022

A TIME DOMAIN APPROACH FOR BRIDGE FATIGUE CONSIDERING THE EFFECT OF MULTIPLE VEHICLES AT RANDOM PASSING RATE

A Thesis Submitted in

Partial Fulfilment of the Requirements

for the Degree of

DOCTOR OF PHILOSOPHY

By

Anjaly J Pillai

DEPARTMENT OF CIVIL ENGINEERING

INDIAN INSTITUTE OF TECHNOLOGY GUWAHATI

GUWAHATI-781039, INDIA

FEBRUARY, 2022

DEDICATED

To

My Parents

This work with myself

CERTIFICATE

It is certified that the work contained in the thesis entitled "**A Time Domain Approach for Bridge Fatigue considering the Effect of Multiple Vehicles at Random Passing Rate**", by **Anjaly J Pillai** (Roll No. 166104005) a student of the Department of Civil Engineering, Indian Institute of Technology, Guwahati, submitted for the award of the degree of Doctor of Philosophy, has been carried out under my supervision and that this work has not been submitted elsewhere for a degree.

Dr. S. Talukdar
Professor
Department of Civil Engineering
Indian Institute of Technology
Guwahati, Assam, India

February, 2022

ACKNOWLEDGEMENT

First and foremost, I would like to express my sincere gratitude to my advisor, Prof. S Talukdar for his continuous guidance and support to my PhD research from inception to completion. His patience, motivation, enthusiasm and immense knowledge brought my work to a higher level.

I would also like to thank rest of my Doctoral committee members - Prof. K D Singh, Prof. S K Dwivedy and Dr. Amit Shelke for their encouraging comments and valuable suggestions.

I would like to thank Dr. Atanu Banerjee, Faculty Incharge, Mr Dhruba Jyoti Bordoloi, Scientific Officer and Mr Monuranjan Dowarah, Technical Staff of Vibration and Acoustics Laboratory, Department of Mechanical Engineering, IIT Guwahati for allowing me to conduct damping experiments. I would also like to thank Dr. Ashim Malakar, Junior Technical Superintendent, Central Instruments Facility (CIF), IIT Guwahati for making it possible to carry out fatigue test. The lab works in CIF could not have been completed without the help of my colleagues - Vivekanando Halder, Suman Kr. Mushahary and Mohammed Hashmat Ahmed; and my sincere thanks to all.

I would like to thank Prof. A Dutta, Prof. A Chakraborty, Dr. H Sharma, Dr. Budhaditya Hazra and Prof. K S R Krishna Murthy, IIT Guwahati for their valuable guidance during my course work.

A special thanks to Prof. D C Rai, IIT Kanpur for his inspiration which led me to this path of PhD research. Also, my sincere thanks to Prof. L M Gupta (VNIT, Nagpur), Prof. Sreedeep S, Dr. Sreeja P, Prof. Ganesh Narayanan and Mrs Soudamini A P for their encouragement.

I am grateful to my colleagues - Arnab, Suvendu and Luptesh for their co-operation and support during my research work.

I am thankful to my friends - Manasa, Sagar, Sajitha, Joanne, Akhila, Akhin, Induchoodan and Paromita, who provided stimulating discussions as well as happy distractions to rest my mind outside my research.

My immense gratitude to all my well-wishers and family members – Shri Udit Chaitanyaji, Raji S Nair, Sajimon V, Sathi B Kartha, Late K B Kartha, Aleyamma Rajan, Satish D Jadhav, Sangeeta S Jadhav, Unnikrishnan S, Dr Jimmy Thomas, Pauline Maria, Elsy Thomson and Suresh Kumar for their unconditional loving support and for taking me as one of their own.

Countless people including all my respected teachers supported my efforts on this way – I am always indebted to all of them.

I am extremely grateful to my grandparents also – L Ponnamma, Late P K Sukumara Pillai, Late J Sarojini Amma and Late R V Panicker.

Words cannot express, how much I am grateful to my parents, Padmaja and Jayakumar, for their endless support and sacrifices. They have always stood behind me and this was no exception. Thank you both for the love; and for always reminding me of the end goal. Their prayer is what sustained me so far and in future too.

Anjaly J Pillai

February, 2022

ABSTRACT

Bridges are lifeline structures in transportation network. Smooth flow of traffic through bridges is important consideration for socio-economic development of any regions. The bridges are generally designed with high factor of safety to cater for uncertainty in live load and material properties. With time, the structures may show various forms of degradation. This is mostly common where traffic growth is unexpectedly high and the structures are exposed to aggressive environment, which necessitates a more elaborate approach to estimate fatigue life in design phase itself. Burden of in-situ monitoring of crack growth may thus be reduced.

Most of the bridge design codes evaluate cumulative damage using a uniform fatigue vehicle and applying the Linear Damage Rule (LDR). The shortcomings of LDR are that it neglects the load sequence effect and does not consider the contribution of low amplitude stresses in evaluation of damage index. In the present study, fatigue damage methodology has been developed to overcome the shortcomings of LDR. Loading cycles obtained are segregated into two phases, namely Phase-1 and Phase-2 which represent crack initiation and crack propagation stages respectively. This approach has been further modified to consider opening stress in crack propagation stage. Before applying the fatigue damage analysis to numerical models of bridges, a generic structural model subjected to axially vibrating load has been first taken as pilot study to predict fatigue cycles under variation of operating frequencies, stress range and damping. Thereafter, fatigue testing of axially vibrating specimen was conducted to obtain the actual number of cycles to failure and to compare with the results obtained from presently developed fatigue damage models.

Inspired by the reasonably good agreement between the predicted results and those obtained directly from long duration fatigue testing, further studies have been undertaken to develop the fatigue damage procedure for the analytical and numerical bridge models. The bridge-vehicle dynamic system was developed using continuum bridge models with distributed system parameters. The movement of multiple vehicles has been considered where the vehicle arrival time is assumed to follow a random process. Pavement irregularity is also considered as the realization of non-homogeneous process. The damping matrix, stiffness matrix and force vector contain time dependent random variable. To solve such coupled bridge vehicle equations of motion, a semi analytical time domain approach is developed. The newly developed approach relies on the orthogonal polynomial expansion and its properties. The time domain approach so developed has been used to simulate vehicle induced stress history and to

transfer the same to fatigue damage module to obtain fatigue life of single and continuous span bridges. Different bridge vehicle parameters are taken into account to observe the effect on dynamic amplification factor and fatigue life of bridge.

For real life application, an example of steel concrete composite plate girder bridge has been considered for three dimensional finite element model. Most of the commercial software allows to perform moving load analysis on finite element model of bridge. In such analysis, the dynamic load induced by vehicles due to vibration caused as a result of pavement roughness cannot be incorporated. Thus, an uncoupled iterative scheme is developed to incorporate road roughness in the numerical model. The effect of random arrival time is also considered. Vehicle induced stress history obtained using uncoupled iterative scheme has been utilised to find the fatigue life of plate girder bridge. Study of various influencing parameters on dynamic amplification factor and fatigue life, unveils the significance of vehicle speed, vehicle arrival time, pavement category, eccentricity of load and girder design variables. The detail investigation reveals that early fatigue failure may occur if vehicle arrival rate, eccentricity of vehicle load, variable speed and roughness of bridge deck increase. However, decrease of cross girder spacing and increase of flange-web thickness ratio of plate girders may prolong the fatigue life.

CONTENTS

LIST OF TABLES

LIST OF FIGURES

NOMENCLATURES

A	Area of cross section of bar
A_m	Material constant
A_s	Amplitude of the cosine wave
$A(i)$	i^{th} local peak obtained from stress time history
a	Loading level
a_0	Mass proportional constant
a_1	Stiffness proportional constant
B_m	Material constant
b	Loading level
$\mathbf{C}$	Damping matrix
c	Damping coefficient
c_s	Damping of the sprung mass
c_w	Damping of the unsprung mass
D	Damage index (BLDR)
D'	Damage index (MBLDR)
D_1	Damage index in Phase-1 for BLDR
D_1'	Damage index in Phase-1 for MBLDR
D_2	Damage index in Phase-2 for BLDR
D_2'	Damage index in Phase-2 for MBLDR
E	Modulus of elasticity of the material
$E_f(x,t)$	Standard error of the mean
e	Convergence limit for uncoupled iterative scheme
$F_{dynamic}$	Maximum response due to fluctuating load imposed on bridge
$F_{i,d}$	Vehicle induced dynamic load on the bridge
F_{static}	Maximum static response of the bridge
$\mathbf{F}(t)$	Force vector
f	Stress

f_a	Stress at ath load level
f_e	Stress level at endurance limit
f_{eo}	Original endurance limit of the material
f_f'	Fatigue strength coefficient
f_{max}	Maximum stress
f_{min}	Minimum stress
f_{os}	Opening stress
f_r	Stress range
f_u	Ultimate stress
f_y	Yield stress
$h(x)$	Bridge deck profile
h_0	Amplitude of half sine wave
$h_m(x)$	Deterministic mean surface profile
$h_r(x)$	Road surface unevenness
$\dot{h}(x)$	First derivative of road roughness with respect to time
K	Fatigue detail constant
$\mathbf{K}$	Stiffness matrix
k	Knee-point
k_b	Number of stress range blocks in the histogram
k_s	Stiffness of the sprung mass
k_w	Stiffness of the unsprung mass
L	Span of bridge
L_a	Length of bar
L_f	Expected life
$L_l^j(\lambda t_j)$	Orthogonal function
l_N	Length of Nth span in multi-span continuous bridge
$\mathbf{M}$	Mass matrix
M_n	Generalized mass for nth mode
m	Fatigue exponent

m_b	Mass per unit length of the bridge
m_{i1}	Failure rate at i^{th} Phase obtained using LDR
m_{i2}	Failure rate at i^{th} Phase obtained using BLDR
m_{i3}	Failure rate at i^{th} Phase obtained using MLDR
m_s	Sprung mass
m_w	Unsprung mass
N	Fatigue life
N_1	Number of basic functions with respect to λt_j
N_{actual}	Actual failure cycle obtained from experiment
N_{est}	Estimated failure cycle
N_{est1}	Estimated failure cycle obtained using LDR
N_{est2}	Estimated failure cycle obtained using BLDR
N_{est3}	Estimated failure cycle obtained using MBLDR
N_f	Failure cycles at a given stress level
N_i	Number of cycles to produce failure at i^{th} stress level
N_p	Number of samples considered for evaluating dynamic amplification factor
N_s	Number of terms used to build up the road surface roughness
$N(t)$	Number of vehicles arriving on the bridge during time interval (0,t] following Poisson process
N_1^*	Fatigue life for low cycle of loading (BLDR)
N_1'	Fatigue life for low cycle of loading (MBLDR)
N_2^*	Fatigue life for high cycle of loading (BLDR)
N_2'	Fatigue life for high cycle of loading (MBLDR)
n_d	Number of degrees of freedom
n_i	Number of cycles applied at i^{th} stress level
$P(x,t)$	Exciting force at free end of bar
P_0	Constant mean force
P_j	Amplitude of the j^{th} harmonic excitation
p	Loading level

$p_{t_j}(t)$	Probability density function of the arrival time
$Q_{sl}(t)$	Displacement function varying with respect to time
R	Stress ratio
r_j	Frequency ratio in j^{th} excitation
$S_{g0g0}(\Omega)$	Power spectral density function in the space domain
$S_{GG}(\Omega)$	One sided power spectral density function
$S_{GG}(\Omega_s)$	Power spectral density function of road surface roughness
$S_{g0g0}(\omega)$	Temporal power spectral density function
T	Failure time
T_{max}	Maximum time considered for vehicular movement
t	Time
ti	Interarrival time
t_{pn}	Arrival time of n^{th} vehicle
$u(x,t)$	Axial displacement of the bar
v	Velocity of vehicle
X_a	Amplitude of acceleration
X_k	Knee-point coordinates in x-axis (BLDR)
X_k'	Knee-point coordinates in x-axis (MBLDR)
X_{knew}	New knee-point coordinates in x-axis (BLDR)
X'_{knew}	New knee-point coordinates in x-axis (MBLDR)
$\mathbf{X}(t)$	Response vector
$x_c(t)$	Position of vehicle at time, t
$x_{nc}(t)$	Position of n^{th} vehicle at time, t
Y_k	Knee-point coordinates in y-axis (BLDR)
Y_k'	Knee-point coordinates in y-axis (MBLDR)
Y_{knew}	New knee-point coordinates in y-axis (BLDR)
Y'_{knew}	New knee-point coordinates in x-axis (MBLDR)
$y(x,t)$	Displacement of the bridge
$z_1(t)$	Displacement of the sprung mass

$z_2(t)$	Displacement of the unsprung mass
α	Material constant (BLDR)
α_1	Material constant (MBLDR)
β_{new}	Material constant (MBLDR)
Γ	Gamma function
γ	Applied stress ratio
γ_e	Instantaneous endurance limit ratio
γ_{ec}	Critical endurance limit ratio
ΔD_j	Incremental damage during the cycle j
$\Delta\varepsilon_{eff}$	Effective strain range
$\Delta\varepsilon_i$	Strain corresponding to intrinsic fatigue limit
$\Delta\varepsilon^*$	Net effective strain range
ΔK	Stress intensity factor
Δf_{eff}	Net effective stress range
$\Delta f(t)$	Difference of flexural stress at time instant t from two successive iterations
δ	Dirac delta function
δ'	Logarithmic decrement
δ_{ik}	Kronecker delta function
ε_{max}	Maximum strain
ε_{min}	Minimum strain
ε_{os}	Opening strain
$\eta_i(t)$	Generalized coordinate in i^{th} mode
$\eta_{hi}(t)$	Homogeneous solution of generalized coordinate in time domain in i^{th} mode
$\eta_n(t)$	Generalized time dependent normal coordinate in n^{th} mode for single-span beam
$\eta_{pi}(t)$	Particular solution of generalized coordinate in time domain in i^{th} mode
θ_1	Angle subtended by the damage line due to Phase-1 loading (BLDR)

θ_1'	Angle subtended by the damage line due to Phase-1 loading (MBLDR)
θ_2	Angle subtended by the damage line due to Phase-2 loading (BLDR)
θ_2'	Angle subtended by the damage line due to Phase-2 loading (MBLDR)
θ_s	Random phase angle uniformly distributed from 0 to 2π
λ	Mean arrival rate
$\mu(\lambda t_j)$	Mean of the random variable λt_j
ξ_i	Damping coefficient of the bar in i^{th} mode
ξ_n	Damping ratio of n^{th} mode of single span bridge
ξ_{nr}	Damping ratio of n^{th} mode of r^{th} span of continuous bridge
ρ	Mass density of bar
$\sigma_f(x.t)$	Standard deviation of flexural stress
$\phi_i(x)$	Normalized mode shape function in i^{th} mode for one end fixed and other end free
ϕ_j	Phase angle in j^{th} excitation
$\phi_n(x)$	Normalised mode shape in n^{th} mode for single-span beam
$\phi_{nr}(x)$	Normalised mode shape in n^{th} mode of r^{th} span for multi span continuous beam
Ω	Wave number or spatial frequency
Ω_L	Lower cut-off frequencies of spatial unevenness
Ω_s	Spatial frequency
Ω_U	Upper cut-off frequencies of spatial unevenness
ω	Temporal frequency
ω_{di}	Damped frequency of the bar in i^{th} mode
ω_j	j^{th} excitation frequency
ω_n	Natural frequency in n^{th} mode of single span bridge
ω_{ni}	Natural frequency of the bar in i^{th} mode
ω_{nr}	Natural frequency in n^{th} mode of r^{th} span of continuous bridge

1

INTRODUCTION AND LITERATURE REVIEW

1.1 General

Engineering structures fail due to fatigue, when subjected to repeated applications of loads. Such failures take place at a stress level which is well below the working stress of the material. This phenomenon can be observed in engineering structures of various disciplines. In civil engineering structures, bridges are one of the vivid examples. They are continuously subjected to vehicular loads which varies with space and time. These loads cause stress reversals on the bridge members resulting in stress concentrations in weaker zones that may lead to failure. The study of bridge fatigue due to vehicular movement is very much significant to avoid bridge collapse and to conduct proper maintenance.

1.2 History of Bridge Failure due to Fatigue

Bridges are critical structures of transportation networks necessary for various social and economic activities of modern civilisations that provide smooth flow of goods and people. It is important to evaluate the load effects on bridge accurately while designing the bridge or assessing the performance of bridge in operation so that required levels of safety and serviceability can be assured. The bridge structures are subjected to different types of loads during their lifetimes like vehicular load, wind load and earthquake load. Of interest is the load caused by movement of vehicles since these loads act on the bridge on daily basis unlike strong winds or earthquake. In addition, these vehicular loads also show large uncertainties and considerable variation. This implies that site specific traffic conditions of the bridge should also be considered when estimating the effects due to vehicular loads. Since, these vehicular loads act continuously on the bridge which causes stress variation, it becomes necessary to assess the bridge for fatigue. The bridge failure can take place due to excessive deterioration by corrosion or fatigue cracking (Dexter and Fisher, 2000). The excessive deterioration can be attributed to the inadequate determination of load and lack of proper maintenance which affects the service life. There are several examples of collapse of bridges that has taken place due to various factors such as truck overloading, design deficiencies, fracture in structural joints, failure of the gusset plate, corrosion induced fatigue, wind induced fatigue, fracture in hangers

and so on (Biezma and Schanack, 2007; Deng et al., 2016; Guowen et al., 2021). The collapse of the Silver Bridge in USA in 1967 which spanned the Ohio River between Pt. Pleasant and Kananaga was due to the fracture of one of the eye bars. It was a suspension bridge whose main cables were composed of two cables of eye bars. The rocking pylons were hinged to the pier to balance the movements on the bridge. Thus, the rupture of one chain would lead to immediate overload of the second and rupture of main cable, which implies the loss of anchorage of the pylon and collapse of the structure (Biezma and Schanack, 2007).

Sungsoo Grand steel truss bridge, across Han River in Seoul, Korea collapsed in 1994 (Lee, 1996). Span of the bridge was 1160 m and had a Gerber suspended truss structure with little redundancy. The cantilever truss and 48 m long suspended truss were connected with a hinge and link. It was concluded from the investigations that the fracture of the vertical structural member and the consequential pulling out of the suspended truss was the main reason for bridge collapse (Deng et al., 2016).

Latchford Bridge was built over the Montreal River, Canada which was a steel tied arch bridge with concrete deck. The bridge span was 110 m and consisted of 12 vertical hangers in each plane. A minor defect of one of the hanger's thread combined with seized hanger hinge led to fatigue fracture of the first hanger at the upper connection. Due to this, the adjacent hanger had to carry twice the load which further led to fatigue strains. The third hanger was heavily overloaded as it was the only functional member which also failed due to overload causing the bridge to collapse in 2003. In addition to this, it was also found that the ductility of steel used for construction of the bridge was not appropriate for cold environment, thus favouring brittle fracture (Biezma and Schanack, 2007).

The I-35 W Bridge in Minnesota, USA was 580 m long and it was a steel truss bridge. The bridge collapsed in 2007 due to the failure of the gusset plate and this resulted in brittle collapse of main truss (Deng et al., 2016). A photo of bridge collapse from the reference is shown in Fig. 1.1.

Fig. 1.1 Collapse of the I-35 W bridge in Minnesota in 2007 (Source: Deng et al., 2016)

Nanfang'ao Bridge, Taiwan, China crossing the South Australian sea was a single arch steel bridge of span 140 m. The bridge collapsed in 2019 owing to a steel cable fracture (Guowen et al., 2021), which is shown in Fig. 1.2.

Fig. 1.2 Collapse of the Nanfang'ao bridge in Taiwan in 2019 (Source: Guowen et al., 2021)

From the bridge failures, it can be concluded that the bridges are subjected to usually large number of significant live load cycles and fatigue will occur prior to fracture. Thus, it is important to control fatigue as compared to controlling fracture. The bridge fatigue life can be determined by Cumulative Damage (CD) rule and Linear Elastic Fracture Mechanics Approach (LEFM).

The CD rule is used to compute the bridge fatigue life in design phase and thus it has become part of the bridge design standards in many countries. The LEFM approach is developed on the basis of principles of fracture mechanics, assuming an initial crack length and predicting its propagation till it reaches a critical crack length. Due to this reason, the LEFM approach is applied to existing structures wherein the fatigue cracks have originated under traffic load. This

method also makes it possible to estimate the time for periodic inspections of bridges and the residual life of the bridge.

The works of various authors using CD rule and LEFM in fatigue life evaluation of metals and bridges are discussed in the next section. Heavy and high speed vehicles traverse the bridge. Therefore, the problem of bridge vehicle interaction is important and is studied by various investigators, are discussed in the next section. In addition to the above, the fatigue life of the bridge due to vehicular loads studied by various researchers has also been given.

1.6 Objectives of the Present Work

The following are the objectives of the present study

- To develop a fatigue damage model considering sequence of loading and to verify the model by conducting fatigue testing on several standard specimens in the laboratory.
- To develop bridge-vehicle interaction model using a semi analytical technique incorporating random unevenness of bridge deck and random arrival time of the multiple vehicles, for the purpose of fatigue analysis.
- To obtain response statistics of continuum model of single span and multi-span bridge subjected to multiple vehicle loading at uniform and variable velocity using semi analytical technique in order to predict the fatigue damage of the idealized bridge models from vehicle induced stress history.
- To carry out dynamic analysis of composite plate girder bridge in finite element software using uncoupled iterative scheme subjected to multiple vehicular movement with uniform and variable velocity with the aim of prediction of fatigue damage in the bridge.

1.3 Literature Review

Literature review has been presented in three sections. First section discusses the work done by various authors to predict the fatigue life of metals using CD rule and LEFM approach. Second section provides reviews of fatigue design procedures for bridges, fatigue life evaluation of welded joints in steel bridges, fatigue life of concrete and pre-stressed concrete bridges, bridge vehicle interaction problems and fatigue life evaluation of bridges considering vehicle loads. It also provides a literature survey of the work done on wind induced fatigue in bridges.

1.3.1 Fatigue in Metallic Structures

Metallic structures are widely used in engineering structures and fatigue failure is one of the common failure in this. Fatigue phenomenon takes place when the material is subjected to alternating loads, as this leads to damage accumulation causing failure. The effect of alternating bending stresses on metallic structures was first studied by Ewing and Humphrey (1903). The microscopic observation showed growth of slip bands within the crystals under the action of stresses. Due to the sustained stresses, failure along the slip planes resulted in cracks to spread, leading to failure of specimen. However, no method was developed to estimate the damage due to the bending stresses.

Different methods namely CD rule, energy based and LEFM approach predict fatigue life. This section reviews the techniques for prediction of fatigue life in metallic structures.

1.3.1.1 Cumulative Damage Models

The technique for estimation of fatigue life of a machine part which is subjected to multiple stress levels was developed by Langer (1937). A relationship was developed between the stress cycles and the ratio of crack area at any instant to the crack area necessary to produce failure. However, the nature of the function was not specified and the stresses below the endurance limit were not considered.

Miner (1945) developed the cumulative damage concept for repeated loads. The damage, D was evaluated based on number of cycles applied, n_i divided by the number of cycles to produce failure, N_i, at a given stress level, f_i, expressed as

$$D = \sum_i \frac{n_i}{N_i} \tag{1.1}$$

The concept was experimentally verified on aluminium alloy and found correct. The analysis using cumulative damage concept was found to be simple. This rule is also known as Linear Damage Rule (LDR).

The damage curve concept was developed by Richart and Newmark (1948) to rectify the shortcomings of Miner's rule. The effect of load interaction and load sequence are neglected in Miner's rule. The complex nature of material behaviour during fatigue damage led to the development of damage curve concept. In this, the damage was related to cycle ratio using a term which was dependent on the stress level. An empirical relationship was obtained,

however, the same was not applied due to its complexity in the analysis. The empirical relation developed was further used by Marco and Starkey (1954) to propose a nonlinear damage rule. The damage is related to the cycle ratio using a power function. The power function is dependent on the stress amplitude. The drawback of this rule was that expression for the power function was not readily available in general case.

A factor depending on the load ratio was suggested by Corten and Dolan (1956) to consider the load interaction effect. An empirical relation between the stress dependent ratio, '*R'*, damage exponent, '*a'*, stress ratio and material parameter, '*d'* was developed. This was achieved using two level block loading tests of cold drawn steel wires. The slope of the SN curve was modified to take into account the load interaction effect. The fatigue damage is expressed as

$$D = \sum_{i=1}^{2} \frac{n_i}{N_i} \frac{N_i}{N_1} \left(\frac{f_i}{f_1} \right)^d \tag{1.2}$$

where n_i and N_i are the number of cycles applied and number of failure cycles at i^{th} stress level, f_i respectively. In this, the damage is amplified by a coefficient depending on applied loads, fatigue lives and material parameter, *d*. For high strength steel, *d*, is suggested as 4.8 and 5.8 for other materials.

The amplification of the initial damage by fatigue life with respect to the applied load and life at first loading level may be considered incorrect when more than two load levels were considered for evaluation of fatigue life of the material.

Grover (1960) suggested a two-stage linear damage rule based on crack initiation stage and crack propagation stage. However, a quantitative estimation of fatigue damage in crack initiation and propagation stage was not provided. Manson et al. (1967) and Manson et al. (1981) proposed the Double Linear Damage Rule (DLDR) wherein the crack initiation and crack propagation is considered to signify the two stages of fatigue damage process. On comparing the experimental results obtained from proposed method and Miner's rule, it was observed that Miner's rule overestimated the fatigue life as compared to that of DLDR. In this study, Damage Curve Approach (DCA) was also proposed on the basis of damage curve concept proposed by Marco and Strakey (1954). Using an effective crack growth model which was empirically formulated, the equation for DCA was developed. It was observed from the study that there was a slight difference between fatigue life estimated using DCA and DLDR

for two-level and three-level block loading tests. In case of realistic loading, it was observed that fatigue life estimated using DCA and DLDR will vary significantly. This is because load change effects within a single phase are captured by DCA as compared to DLDR. Further, Double Damage Curve Approach (DDCA) was developed by adding a linear term to the DCA equation for achieving accurate results in lower cycle ratios in the crack initiation stage. However, the effect of load interaction and cycles below the fatigue limit are not considered in all the three models.

The number of cycles at which structures or components fail are random variables when these are subjected to repeated application of random forces. Dowling (1972) proposed a statistical counting method to handle with the complex stress cycles caused by the variable amplitude load.

The fatigue life of materials considering Miner's rule is discussed in Shimokawa and Tanaka (1980). While taking lognormal and Weibull distribution, the conditions required to satisfy the statistical Miners rule are derived. The standard deviation of the log of fatigue life for the lognormal distribution are required to be constant regardless of the stress levels to satisfy the statistical Miner's rule. Wirsching et al. (1982) established a model for predicting metal fatigue in a wide band random process for design purposes.

Bannantine et al. (1990) investigated the theory of fatigue damage in metallic specimens. The fatigue strength of the material was investigated using a constant amplitude test and the results were represented in the form of SN curve.

A stress life relation was given by Basquin's power law equation to examine the influence of low amplitude stresses below the constant amplitude fatigue limit (Basquin, 1910; Kun et al., 2008). This was not considered in Miner's rule, DLDR, DCA, and DDCA. The equation is given as

$$f_a = f_f' \left(2N_f\right)^b \tag{1.3}$$

where f_a represents the stress level, f_f' is the fatigue strength coefficient, b is the fatigue strength exponent and N_f is the failure cycles at a given stress level.

Leipholz et al. (1983) had proposed modified damage parameter life curves to evaluate fatigue life for stochastic or multi-level load history. It was observed that when the structure is subjected to stochastic or multilevel load histories, the different cycles present in the load

history contribute differently to the damage accumulation. The cycles corresponding to equal damaging effect were collected and then used for evaluation of damage. The proposed methodology was experimentally tested on metallic components of Van-80 steel. On comparing the theoretical and experimental results, it was found that they are in good agreement with each other. The identification of cycles contributing to similar damage was found to be cumbersome and the assessment of the scatter of predicted fatigue lives was also required, which was not provided in the study.

Modified Weibull curve has been proposed by Leipholz (1985) for evaluating the fatigue life of metallic specimen considering variable amplitude loading. Effect of interaction of high and low intensity blocks has been considered. Numerical examples with two level loading has been explained. The method becomes difficult to use when multi-level loading is considered.

The steps to reduce the scatter of predicted fatigue lives was suggested by Leipholz (1986) using the modified life law. The life prediction theory proposed by Leipholz et al. (1983) was used here. The theory was also verified using experimental tests on medium carbon steel subjected to three level loading. The scatter for fatigue experiments is found to be within ± 20 % and found to be acceptable. The predicted fatigue life observed was more than Miner's rule. However, the first crack was considered as failure in the experimental results, estimating inaccurate fatigue life since, damage process starts with the crack initiation which is the initial step.

With reference to the works of Corten and Dolan (1956), the material parameter, '*d'* for steel, ranges from 6.2 to 6.9 with a mean of 6.57, which was reported by Rao et al. (2001). A modification of this parameter which depends on the applied stress, instead of being a material constant was suggested by Yang et al. (2003). It was also suggested that Corten-Dolan model can be utilised for evaluating fatigue damage for multi-level loading using the modified parameter. However, the proposed model was not experimentally validated for such type of loadings.

The fatigue strength of friction stir welds in AA6082-T6 under constant and variable amplitude loadings for stress ratio R = -1 was evaluated by Costa et al. (2012) using Linear Damage Rule and Double Linear Damage Rule. The experimental results for stress ratios R = 0 and R = -1 were also compared with the above methods. Comparing the experimental results and fatigue life from the two methods, a good agreement was found for stress ratio R = 0. For stress ratio R = -1, the damage predictions were less conservative.

On the basis of fatigue driving stress, fatigue damage model is proposed by Kwofie and Rahbar (2013). The fatigue driving stress is given as a function of applied cyclic stress and number of loading cycle. The fatigue damage is expressed as a function of life fraction of applied load, life at applied load and life at the initial applied load. The proposed model has been experimentally verified with published data on metallic materials. It is found that predicted lives are in agreement with experimental results. However, it is observed that the fatigue damage can also be a function of lives at various applied loads instead of the life at the initial applied load. The predicted fatigue life taking into account of the lives at various applied load levels may also estimate better than the proposed method.

Gao et al. (2014) suggested a nonlinear fatigue damage model considering load interaction effects. The exponent parameter in Manson-Halford damage model is improved by considering the ratio of stress amplitude. This parameter considers the effect of load interaction. It is observed from experimental results of 16Mn steel subjected to two level loading that suggested model give better predictions in comparison with Manson-Halford model. Although, a comparison has been done with two level loading, it is required to compare the predictions using multi-level or random loading. This helps in better understanding of the proposed method.

Yuan et al. (2015) proposed a modification of DCA taking into account the residual strength degradation, in addition to the load interaction effects. The DCA proposed by Gao et al. (2014) was modified by introducing a residual strength degradation function which is a material property obtained from experimental results and utilising the damage curve.

Fatigue life prediction method considering the effect of overload blocks is developed by Theil (2016). The overload blocks imply the loads around the yield strength and slightly above the yield strength. The nonlinear behaviour of the SN curve is considered. The proposed method has been validated using uniaxial experimental fatigue data carried out on specimens made from isotropic metallic specimens. The predicted fatigue lives using the present method is more accurate than the fatigue lives calculated using Miner's rule. For a better accurate damage prediction, nonlinear damage growth curves can be used. But, this also requires additional material parameters in the calculation.

The material degradation behaviour is introduced using the material memory concept in Peng et al. (2018). The fatigue life of the metallic specimens is evaluated using the material memory concept and residual SN curve approach. The stress life relation of the damaged material

represents the residual SN curve. The slope of the SN curve is assumed to vary with the loading history. The fatigue damage is evaluated using the change in slope. However, the evaluation of residual fatigue life in multi-level loading becomes cumbersome.

A nonlinear fatigue damage model on the basis of damage equivalence concept for multi-level loading is developed by Si-Jian et al. (2018). The load history and load sequence effect is also taken into account. Experimental tests for aluminium alloy under two level block loading is conducted and the results are compared. The results are then compared with the conventional damage methodologies and are found to be conservative.

A fatigue damage model for aluminium alloys correlating the stress ratio, stress amplitude and corrosion fatigue life is developed by Liu et al. (2019). The effect of corrosive medium using sodium chloride in aluminium alloys is also considered in the study. The load interaction effect is also considered in the model using the modified Miner's rule. Notched and unnotched aluminium specimens were tested for random loading. It was concluded from the study that the fatigue life in corrosive environment decreases for notched specimens as compared to unnotched specimens.

The material parameter, '*d*' in Corten-Dolan model depends on experimental results and is difficult to determine. An easier way of finding this parameter using the power form of ratio of applied stress levels is proposed by Liu et al. (2020). This also helps to consider the interaction between different load levels. The results obtained from the suggested model is in agreement with experimental results.

The effect of stress cycles below the fatigue limit in evaluating the cumulative damage is investigated by He et al. (2020). This was achieved by conducting fatigue tests with constant and mixed loading. Mixed loading refers to the combination of high and low stress loading. The stress amplitude below the fatigue limit increases the fatigue damage as compared to the model in which stresses below fatigue limit were neglected.

Using the probability of failure of cumulative damage, a nonlinear damage model is developed by Gao et al. (2021). The nonlinearity of the damage curve and effect of various load level is also considered in this model. The probability distribution function considered is a two parameter Weibull distribution function. It is observed that the shape and scale parameters of the distribution function change according to the stress level. To incorporate this effect, conditional probability distribution function is considered. In case of multi-level loading, this

distribution for a given stress level can be obtained using least square regression analysis. The experimental study is carried out on fiber reinforcement composites. The predicted and experimental results vary within 2% and are found to be satisfactory.

The Corten Dolan model is modified by Xu et al. (2021) using the concept of material residual strength degradation law for variable amplitude load. Using the experimental results of aluminium alloy and titanium alloy specimens, the fatigue life obtained were compared with the Corten Dolan model and the former is found to be conservative. This method can be applied for estimating fatigue life of welded structures.

The model given by Manson and Halford (1981) has been modified for two level loading by Gao et al. (2021). A load interaction factor which is the ratio of load levels are considered. The exponent in the equation given by Manson and Halford (1981) is replaced by ratio of fatigue life and load interaction factor. However, the effect of yield strength and the ultimate tensile strength on the fatigue damage of the material is not considered.

Theories based on stress and strain controlled fatigue damage were presented by Bui-Quoc (1971), Dubuc et al. (1971) and Bui-Quoc et al. (1976). Using the damage models proposed by Shanley (1952), Henry (1955), Gatts (1961) and Valluri (1961), the theory for stress-controlled fatigue was developed. The main assumption in this model is that there is a continuous reduction in fatigue strength of material due to crack growth under cyclic loading. All the parameters in this model were represented by dimensionless ratios with respect to the original endurance limit of the material, f_{eo}. The parameters are the instantaneous endurance limit ratio, $\gamma_e = f_e/f_{eo}$, the applied stress ratio, $\gamma = f/f_{eo}$ and the critical endurance limit ratio, $\gamma_{ec} = f_{ec}/f_{eo}$. The critical endurance limit ratio corresponds to failure. The damage is expressed as

$$D = \frac{r}{r + (1-r)\dfrac{\gamma - (\gamma/\gamma_u)^m}{\gamma - 1}} \tag{1.4}$$

where $\gamma_u = f_u/f_{eo}$, r is the cycle ratio, m is the material constant, f is the stress level, f_e is the stress level at the endurance limit and f_u is the ultimate stress. The stress controlled damage theory was converted to strain controlled by replacing the stress parameters with the corresponding strain parameters. Further improvements in these theories have been made by the same authors to take into account load interaction effect. However, it is observed that endurance limit is a

material property and thus, calculating an instantaneous endurance limit may not be appropriate.

Fatigue life can also be obtained using isodamage lines. The assumption in this method is that SN curve of a material corresponds to a state of failure and combinations of stresses and cycles with identical damage values fall on smooth curves when plotted. A set of straight isodamage lines in S-log(N) diagram was introduced by Subramanyan (1976) and these lines converge near the point where there is no change in fatigue life as the stress levels reduce on the SN curve. The damage is found as the ratio of the slope of the isodamage line to the limiting value of the slope of the S-N curve. According to Hashin and Rotem (1978), the isodamage lines should meet at the point where the S-N curve intersects the stress axis. The approach given by Subramanyan (1976) is more accurate as compared to Hashin and Rotem (1978) as the latter becomes invalid at lower stress amplitudes. However, the stress amplitudes below the constant amplitude fatigue limit are not considered in the study.

The shortcomings of the above mentioned isodamage based models were allievated using the virtual target life curve (VTLC), proposed by El Aghoury and Galal (2013). The VTLC rotates around the S-N curve in clock-wise direction relying on the stress level and the corresponding cycles. The overloading effect and the higher failure cycles are also taken into consideration. Batsoulas (2016) and Xia et al. (2020) established the theory of hyperbolic isodamage lines. In the proposed isodamage lines, the points are apexes of equivalent rectangles. The fatigue damage is obtained by taking the ratio of area of these equivalent rectangles.

1.3.1.2 Linear Elastic Fracture Mechanics (LEFM) Approach

The fatigue damage process consists of three stages namely, crack initiation, crack propagation and sudden fracture of the component. The first stage accounts for major part of the fatigue damage process and has the longest duration. The fatigue crack growth can be modelled using a power law formulated by Paris and Erdogan (1963), given as

$$\frac{da}{dN} = C\,\Delta K^{m} \tag{1.5}$$

The fatigue life N can be obtained as

$$N = \int_{a_i}^{a_f} \frac{da}{C(\Delta K)^{m}} \tag{1.6}$$

where ΔK is the stress intensity factor and C and m are material constants, a_i and a_f represent the initial and final crack lengths respectively. However, in this the assumption is that the material is linearly elastic. For crack growth which do not follow this assumption, elasto-plastic fracture mechanics approach has been introduced where the stress intensity factor in the crack growth equation is replaced by ΔJ which is J integral (Rice, 1968; Wang, 1995).

Using the theory of slip plastic flow, Tanaka and Mura (1981) studied crack initiation in ductile materials. When the surface energy becomes equal to the stored energy, the formation of crack takes place. The fatigue crack initiation was modelled by Tanaka and Mura (1982). In this, the cracks were classified as crack initiation from inclusions named as type A, inclusion cracking by impinging slip bands named as type B and slip band crack emanating from an uncracked inclusion which is type C. Type A mechanism was observed in high strength steels while Type B and C were reported in high strength aluminium alloys. By considering the local plastic flow which was necessary for initiation of crack, a new approach was given by Dang-Van (1993) to measure the crack initiation.

1.3.1.3 Energy Based Models

The methods discussed in the above section can be used for predicting high cycle fatigue only and not low cycle fatigue. Fatigue life in high cycles and low cycles is obtained using a single theory based on the total strain energy density. Such procedure has been adopted by a group of researchers (Lefebvre and Ellyin, 1984; Kujawski and Ellyin, 1984). The fatigue life is dependent on the total energy input, which depends on the damaging plastic strain energy density and elastic strain energy. The fatigue life is described by a power law relation similar to the S-N curve. In the study, the effect of stress amplitudes, strains and the dissipated energy were considered. However, the loading history was not considered. Lagoda et al. (1999) considered the loading history to predict fatigue life under variable amplitude loading.

1.3.1.4 Continuum Damage Mechanics (CDM) Model

The theory for this model is based on mechanical behaviour of a deteriorating medium at a continuum scale. CDM model were developed by various researchers to obtain the fatigue damage of a material considering mechanical deterioration due to fatigue and creep (Rabotnov et al., 1970). The damage was dependent on the load condition and the cycle ratio. A nonlinear damage equation was developed by Chaboche and Lesne (1988) using the effective stress

concept. Further, a constitutive thermo-elasto-plastic-damage model was developed by various researchers to relate the residual material strength and damage threshold evolution (Salomon et al., 2002; Oller et al., 2005). Dattoma et al. (2006) modified the CDM model to take into account the stress level below the constant amplitude fatigue limit. This model can also be used for multi-level loading. The experimental results were then compared with the results obtained from the model and found to have good agreement.

The review of various damage models to predict fatigue life in metals has been given. It has been observed from the review that the even though load interaction effects have been considered by various authors, the applicability to random loading is still not answered. Some of the models are also developed for materials like steel and thus, it limits its use to other materials.

Structures such as bridges are subjected to repeated load cycles. The load cycles generated due to vehicle movement have various uncertainties as a result of vehicle speed, vehicle weight and suspension characteristics as well as unevenness of bridge deck. Thus, assessing the bridge for fatigue is also important. Various studies conducted on bridge fatigue life are discussed in the next section.

1.4 Fatigue Life of Bridges

The first reports of fatigue and fracture failures in metal structures starts form 1800's (Shank, 1954). As the industrial age began, the widespread use of wrought iron and early steels in transportation, manufacturing and industrial industries began. The results of cyclic test on a riveted wrought-iron built-up-I beam, was presented by Fairbairn (1864). The long term effects on the breaking strength during cyclic loading was investigated. The beam was subjected to repeated loading at the mid span and then the level of this load was slightly increased to find the cyclic breaking strength. From the study, it was observed that wrought-iron beams have less strength against fatigue if loaded at a level of one third or more of the static strength. Examples of fatigue failures were reported in railroad bridge members. The earliest welded bridge fracture in welded vierendeel truss bridges in 1920's and 1930's was reported in Germany, Belgium and France (Barsom and Rolfe, 1999). These fractures led to prohibitions against welding to the tension flange of girders. These are also cause of secondary distortion-induced fatigue cracks in structures. Between 1930's and 1960's, cracks were observed in truss hangers and stringer end connection angles which led to further investigation in fatigue and

fracture of bridges. The beginning of modern approach to fatigue and fracture in terms of design and evaluation of bridges began to take form in late 1960's.

The Point Pleasant Bridge collapsed in 1967 and the cause of failure was the brittle fracture of one of the non-redundant I-bars, which was supporting the main span. Development of fracture control plan was initiated by Federal Highway Administration (FHwA) so that higher safety can be provided for non-redundant structures (Frank and Galambos, 1972). The research work by American Iron and Steel Institute to improve the fatigue behaviour of such structures led to the publication of AASHTO Guide Specification for Fracture Critical Non-Redundant Bridge Members and the fatigue critical category for such structures in ASTM A 709 material specification was also included. The test data and theory behind specification development have been given in Barsom (1974). In the AASHTO fracture control plan, two main aspects are there, first being the control of structural flaws and second being specification of material toughness. The first and second aspect are related such that the probability of brittle fracture can be kept low. Keating and Fisher (1986) examined 1500 test data points which was in addition to the fatigue tests data points originally collected in the NCHRP Project 12-7 investigation. The study confirmed the accuracy of the AASHTO fatigue design curves as reasonably predicting the lower bound fatigue life of an expanded population of test data. Minor changes were made to the slopes of the AASHTO design curves and slight adjustment in the infinite life and maximum stress for cover-plated beams were also made. Using the larger data set, a new category 'B' was created to take into account longitudinally loaded group welded attachments. In addition to this category, category 'E' was also created to consider the fatigue strength of thicker web attachments. In revised AASHTO specifications in 2012, the load combinations were modified and a section for constraint induced fracture was also introduced.

Fracture toughness is defined as the ability of a structural member to withstand load and resist fracture in the presence of crack-like flaws. In steel girders, the fracture toughness of steel plates and weld metal determines its ability to withstand load. It depends on the chemistry and processing of steel as well as on the type and strength of steel. It is represented by the impact energy absorbed by a Charpy V-notch specimen, called the CVN energy. It is also called as notch-toughness. In the AASHTO and ASTM specifications in 1974, the requirements for minimum notch-toughness for steel used in bridges were given. Separate CVN values are given for three different temperature zones namely, lower shelf, transition and upper shelf. This is considered to prevent brittle fracture of steel at lower temperatures.

The causes of structural flaws in structural members are welding defects, fabrication imperfection and so on. In order to minimise the weld crack and defects, the Bridge Welding Code (AWS, 1995) has given procedures and standards to minimise the potential for weld cracks and defects during fabrication. In addition to this, the inspection requirements to detect the critical defects and repair of these defects before the bridge is opened to traffic is also set. The defect size is kept sufficiently small so that crack initiation can be prevented and the fatigue crack growth threshold does not exceed under service loads.

Welded details for bridges are designed using nominal stress range. The weld details are segregated in categories having similar fatigue resistance. The fatigue resistance is represented in terms of the nominal stress. Each category of weld details has an associated S-N curve. The S-N curve for steel details in highway and railway bridges is specified in AASHTO (2017), AISC, ANSI/AWS and in AREMA (2000). The categories 'A' to 'E' is given in decreasing order of fatigue strength. The fatigue design criteria discussed above are also used in CEN (2003) and IRC 22 (2015).

Researchers have also pointed out that in case of complicated structural detail or when the loading is complex, then it is difficult to determine the nominal stress of the weld. In addition, the nominal stress method does not consider the actual dimensions of the structural detail (Xiao and Yamada, 2004; Poutiainen et al., 2004). In order to analyse the complicated welded joints for fatigue, an alternative method is used which is called the hot spot stress method. The International Institute of Welding (IIW) has provided detailed procedures in computing the hot spot stress.

Steel bridges are composed of longitudinal and transverse structural members with welded joints at the intersections. The fatigue behaviour of welded joints and the assessment of fatigue strength is investigated by various researchers (Gurney, 1979; van Delft, 1981; Maddox, 1991, Hobbacher, 1996). The hot spot stress can be calculated by multiplying the nominal stress with a factor called as the stress concentration factor (SCF). The fatigue strength and local stress for cope hole details existing in I-section beams by fatigue tests and stress measurements was studied by Miki and Tateishi (1997). Using the results of finite element analysis, an empirical relation was proposed to determine SCF. The results were verified experimentally and found to be in agreement with each other. A numerical and experimental analysis to determine the fatigue strength and to design the welded structures for fatigue using hot spot stress method and also to develop a unified SN curve was done by Han and Shin (2000). The fatigue life of

steel suspension bridge was compared using hot spot stress method and nominal stress method, which was studied by Chan et al. (2003) and Chan et al. (2005). It was observed from the study that the hot spot stress method gives more accurate prediction than nominal stress method.

The effective notch stress method can also be used, in addition to nominal stress method and hot spot stress method. This method focuses on life prediction for crack initiation at root of the notch. The effective notch stress method was proposed by Radaj (1990) and Radaj et al. (2006). Zhang and Ritcher (2000) proposed a new approach relating stress intensity factor and notch stress. This approach can be used for numerical fatigue life prediction of spot welded structures. A comparative study on five selected welded joints, commonly used in steel bridges was reported by Aygul et al. (2013). The accuracy of nominal stress method, hot spot stress method and effective notch stress method was investigated in this study. It was observed from the study that even though modelling and computational efforts required for effective notch stress method are more, it also provides a significant improvement in fatigue strength estimation.

Researchers have pointed out that majority of cracks in bridges are caused due to distortion induced fatigue (Fisher et al., 1979; Fisher, 1984; Fisher et al., 1990). This includes distortion of member cross sections and out-of-plane deformations of webs that induce localised bending stress. The most common occurrence of this type of crack is at connection plates (for cross frames, diaphragms, floor beams) which are not connected to the tension flange of girder i.e., the top flange in the negative moment region of the girder. A proper detailing which eliminates the secondary stresses was recommended to prevent distortion induced fatigue.

The fatigue behaviour of orthotropic steel bridge decks using experimental investigation is presented by Erzurumlu and Toprac (1972). The fatigue test results of steel orthotropic bridge decks with both conventional and biserrated trapezoidal ribs are presented. From the experimental result, it was observed that unflanged rib to deck plate connection and butt joint rib splice exhibit satisfactory fatigue strength. The deck was also subjected to AASHTO wheel loads and the results indicate that fatigue cracks which are developed at lower serration corners do not result in total collapse of the deck. Using the results, an optimum serration radius can be determined.

The effects of repeated loads on slabs of steel concrete composite bridges was investigated by Batchelor et al. (1978). The dimensions of the test specimen were scaled down to $1/8^{th}$ scale of the models. The endurance limit of the slab under repeated concentrated load was determined. Parameters such as stress range and percentage and arrangement of the reinforcement was

varied to observe the effect on endurance limit. It was found that steel concrete composite bridge deck has large fatigue strength. Endurance limit of 50 percent of the ultimate capacity can be expected in such cases. In slabs with 0.2 percent orthogonal reinforcement, endurance limit of 40 percent of the ultimate capacity can be safely adopted for design. Pedikaris et al. (1989) conducted static, fixed pulsating and moving wheel load on a series of scaled down bridge models consisting of concrete bridge decks and steel girders. These models were scaled down to 1/3 and 1/6.6 scale of the original model. The tests were performed to study the deck continuity effect and reinforcing pattern on the ultimate fatigue strength.

The fatigue strength of deformed reinforcing bars was studied by Corley et al. (1978). The experimental program was carried out with each test bar embedded as the main reinforcing element within a concrete beam. Test variables included size of beam, size of bar, grade of bar, bar deformation geometry, minimum stress, and stress range. The test program and the design provisions developed by statistical procedures from the test data were also discussed.

The fatigue strength of plain concrete subjected to flexural loading was investigated by Oh (1986) using experimental results. The SN curve is generated from the test results and equation to predict the fatigue strength is obtained by regression method. The distribution of fatigue life found from the test data for an applied stress level was found to follow Weibull distribution. The fatigue life distributions of concrete for various levels of applied stresses is studied by Oh (1991). The concrete beam specimens are tested in four-point flexural loading condition to obtain the fatigue lives at various stress levels. Three different levels of applied fatigue stresses were considered. It was observed from the study that the probabilistic distributions of fatigue life are dependent on the applied stress levels. The distribution considered in the study was Weibull distribution. It was found that the shape parameter of the Weibull distribution for fatigue life of concrete ranges from 2 to 4 depending on the applied stress levels. Similar values of distribution parameters were obtained using the graphical method, the method of moment and the method of maximum likelihood estimation.

A fatigue crack propagation law for plain concrete is developed by Ray and Kishen (2010) using the theory of population growth model. A closed form expression for specific growth rate parameter is derived using the principle of dimensional analysis. Various parameters are considered in the model such as loading history, fracture toughness, stress ratio, crack length and structural size. The structural size and loading history affect the behaviour of plain concrete in fatigue. The model has been compared with the experimental results of three-point-bend

beams and are found to be in good agreement with each other. In another study, Ray and Kishen (2011) developed an analytical model to predict the fatigue crack growth in concrete using dimensional analysis. A relationship was obtained between the parameters mentioned above using the concept of self similarity. From the study, structural size, loading history and initial crack size were found to affect the fatigue behaviour.

A fatigue crack propagation law was developed by Ray and Kishen (2014) for RC beam using the concept of dimensional analysis wherein the effect of reinforcing bar through a pair of closing force was also considered. The present model was compared with the experimental results and was found to be in good agreement with each other. It was observed from the study that model dimensions affected the fatigue behaviour of concrete. For a critical value of crack length, a method is proposed to obtain the remaining life of RC beam in terms of moment capacity. It was observed that with the increase in relative crack depth, the moment capacity increases in the elastic region and decreases after yielding of steel. The proposed method is further modified to predict the residual strength of member taking the bond-slip at the rebar and concrete interface.

A mathematical model has been derived for prediction of crack growth under fatigue loading in plain concrete members by Bhowmik and Ray (2018). The study considers parameters such as fatigue fracture energy and ratio of maximum aggregate size to structural size along with the other conventional crack growth parameters. The method has been validated with experimental results in the literature to show the applicability. Using the sensitivity analysis, it was observed that structural size and energy release rate affect the fatigue behaviour of concrete.

1.4.1 Bridge Vehicle Interaction

The dynamic interaction between a bridge and moving vehicle is an important problem in structural dynamics. The potential applications of such studies can be found in fatigue design and structural health monitoring of bridges. The bridge and the moving vehicle interact with each other through the contact forces. Several authors have contributed in modelling vehicle, bridge structures, pavement unevenness and the various solution techniques.

1.4.1.1 Vehicle Model

In the middle of the nineteenth century, studies on the dynamic response of bridge due to vehicle movement has been found in the works of Willis (1849) and Stokes (1849). The work

is based on investigation of the collapse of the Chaster Rail Bridge in England in 1847 which was the first case for collapse of a railway bridge in history. This is the first study to consider the effect of vehicle impacts on the design of bridges. In this study, the vehicle is idealized as a concentrated load moving with constant velocity. It has been observed from the study that the dynamic response of the bridge due to vehicular movement is higher than the static response. However, the effect of inertia of the beam was not considered in this study. Further, the dynamic response of simple beam due to concentrated moving loads has been studied by Timoshenko (1922). Similar moving load model was considered by Ayre et al. (1950) and Ayre and Jacobsen (1950) to study the response of a two span beam. The vibration of suspension bridges considering this model was studied by Vellozzi (1967). This model was also used by Chen (1978) to analyze the response of continuous bridges. The moving load model was also adopted by several researchers to examine the dynamic behavior of bridges (Tan and Shore, 1968; Fryba, 1968; Fertis, 1973; Sridharan and Malik, 1979 Wu and Dai, 1987; Weaver et al., 1991; Galdos et al., 1993; Gbadeyan and Oni, 1995; Wang, 1997; Zheng et al., 1998; Rao, 2000; Chen and Li, 2000 and Dugush and Eisenberger, 2002). It is observed from the study that the essential dynamic characteristics of the bridge caused by moving action of the vehicle is captured with sufficient degree of accuracy using the moving load model. However, the interaction between the bridge and moving vehicle is ignored. Thus, the moving load model is appropriate only for the case where the mass of the vehicle is small relative to that of the bridge and when the vehicle response is not of interest.

The inertia effect of the moving vehicle is considered in the moving mass model which was not considered in moving load model. The inertia effect of beam and vehicle was considered by Jeffcott (1929). The vehicle inertia effect has been considered by various researchers to determine the dynamic response of the bridge. Using the Fourier series expansion, the dynamic response of simply supported beam under the action of a number of moving masses is determined by Stanisic and Hardin (1969).

The algorithms for dealing with moving mass problem with the help of Green's function has been considered by Ting et al. (1974) and Sadiku and Leipholz (1987). The closed form solution for a simple beam under the action of a single moving mass using expansion of the eigen functions in series is derived by Stanisic (1985). The same model was considered by Akin and Mofid (1989) to determine the dynamic response of beams with different boundary conditions using an analytical-numerical approach. The drawback of this model is that it does

not consider the bouncing motion of vehicle relative to that of bridge. Thus, bridge deck roughness cannot be incorporated when using the moving mass model.

The vehicle model can still be improved by considering the elastic and damping effects of the suspension systems to consider the bouncing action of the moving vehicle. The simplest model is the sprung mass model in which the moving mass is supported by a spring-dashpot unit. A semi-analytical technique to the problem of a simple beam traversed by a sprung mass is presented by Biggs (1964). The experimental results obtained from the laboratory models and from actual bridge structures in the filed shows good agreement with the theoretical results. It is also observed from the study that the sprung mass model gives realistic results in comparison to the moving load model.

The effect of moving vehicle modeled as sprung mass on a multi-span continuous and suspension bridge was investigated by Chatterjee et al. (1994). Using an iterative procedure, the bridge response was obtained in time domain. The non-linearity of the pavement interactive force at each time step was also taken into account. The response of an elastic continuum to multiple moving oscillators was studied by Pesterev et al. (2001) using the series expansion technique. The asymptotic nature of the solution of the moving oscillator problem has been studied by Pesterev et al. (2003). It was observed that in the limiting case, for a simply supported beam, the moving oscillator problem and the moving mass problem are equivalent in terms of the beam displacements, however it does not follow the same pattern in case of beam stresses. It was also observed that the moving oscillator problem is equivalent to the moving load problem for small value of spring stiffness.

The sprung mass model has been further improved by considering the vehicle as two degrees of freedom system taking into consideration the elastic properties of tyre and mass of the wheel. This type of vehicle model is called the quarter car model. This vehicle model has been considered by various researchers to obtain the bridge dynamic response (Fryba, 1972; Genin et al., 1975; Genin and Chung, 1979; Green and Cebon, 1994). In this vehicle model, the bouncing mode of the vehicle is important as it is often within the range of the first natural frequency of most highway bridges.

The vehicle pitching motion has been incorporated by Wen (1960) in the quarter car model and this model is called as the half car model. A multiple-axle truck or tractor-trailer can be idealised as a number of discrete masses each supported by a set of spring and dashpot using this model (Veletsos and Huang, 1970; Tan et al., 1998). Yang et al., (1999) modeled a rail

road car as a rigid beam supported by two sets of spring-dashpot unit each resting on a wheel mass. The analysis is confined only in the pitching plane and the effect of vehicle roll on the bridge dynamics cannot be considered.

The half car model is further enhanced by considering the vehicle roll and this model is called as 'heave-pitch-roll' model (full car model). Yadav and Upadhyay (1993) have considered full car model for analyzing the response of vehicle moving on a flexible track. Wang et al. (1993) have modeled H20-44 and HS20-44 vehicles as seven and twelve degrees of freedom. These vehicles are the major design vehicles in the AASHTO (2012). Deng and Cai (2009) and Gonzalez et al. (2011) have considered the full car model to obtain the system responses using numerical solution.

1.4.1.2 Modeling of Bridge Deck Unevenness

The surface roughness acts as a source of excitation when the vehicle traverses on the bridge. This causes oscillatory loads on the bridge deck as a result of vehicle vibration. An appropriate model for the deck roughness needs to be chosen by the analyst. The roughness can also be modelled in terms of statistical parameters from profile measurements of a large number of road or bridge surfaces.

The methods to simulate multivariate and multidimensional process with specified cross spectral density is presented in Shinozuka (1971). When the cross-spectral density matrix of an n-variate process was specified its component process can be simulated as the sum of cosine function with random frequencies and random phase angle. It was shown that the homogeneous multidimensional process can also be simulated in terms of sum of cosine functions with random frequencies and random phase angle.

Road surfaces can be considered as a realization of homogeneous and isotropic two dimensional Gaussian random processes, which is shown by Dodds and Robson (1973). The road roughness is described by single auto correlation function, evaluated from longitudinal profile. It is observed that a road surface considered for multi-track vehicle response can be described using a single direct power spectral density function. The classification of road surfaces based on this function is also proposed.

Honda et al. (1982) has shown that Power Spectral Density (PSD) was related to parameters known as roughness and waviness index. These parameters can alter the roughness up and down and thus a guideline for classification of roads in terms of roughness has been outlined.

Henchi et al. (1988) considered the bridge roughness as a periodically modulated random process. The PSD described by Dodds and Robson (1973) was considered in the study. Using the PSD, the deck surface profile is generated using the FFT algorithm with the Monte Carlo simulation.

Coussy et.al. (1989) analyzed the dynamic response of bridge under suspended moving loads considering the effects of random surface irregularities. The vehicle springing system which is a two-axle system is considered by single degree of freedom oscillator for each axle of the vehicle. The surface roughness is represented through stationary normal centered random process. The bridge is idealised as an elastic beam and the surface irregularities are modelled by PSD for frequency domain analysis. The system of equation is solved numerically using Runge-Kutta method of sixth order.

A relationship between PSD of pavement and parameter known as International Roughness Index (IRI) was proposed by Marcondes et al. (1991). The spectral analysis of different measured profiles was evaluated to obtain the relationship. Quarter car simulation model was used to compute IRI.

Shinozuka and Deodatis (1991) proposed a method to generate one dimensional, uni-variate, stationary Gaussian stochastic process using spectral representation method. The stochastic process is simulated using a cosine series and is asymptotically Gaussian as the number of terms tend to infinity. Using Fast Fourier Transform technique, simulation of stochastic process becomes computationally effective. Further, the method is applied to problems wherein material and geometric properties and load are of random in nature.

Deodatis (1996) proposed a simulation algorithm for generation of sample functions of stationary, multivariate stochastic process based on specified cross spectral density matrix and using fast Fourier transform technique. Ergodic sample functions are also generated in this method. The method was applied for simulation of turbulent wind velocity. The longitudinal velocity fluctuations were modelled using a trivariate, stationary stochastic vector process. The power spectral density follows Kaimal spectral model. Apart from this, it can also be used to simulate correlated seismic ground motion time histories at different locations on the ground surface and correlated material properties like mass density, viscous damping and flexural stiffness along the length of beam.

Simulation technique based on spectral representation method to generate sample functions of non-stationary, multivariate stochastic process using non-stationary cross spectral density matrix was proposed by Deodatis (1996). In order to apply it to earthquake ground motion, iterative technique was introduced to generate time histories of seismic ground motion at different locations on the ground surface. The method was also applied to generation of acceleration time histories. For this, trivariate non-stationary stochastic vector process was used. The method can also be extended to generate ground motion time histories for bridges, wherein these are used as input for dynamic seismic analysis.

Sun et al. (2001) compared two PSD functions describing road roughness proposed by Dodds and Robson (1973) and Honda et al. (1982). It has been observed that the PSD proposed by Dodds and Robson (1973) has higher values for frequencies greater than $1/2\pi$ cycle/m. This is because the available PSD functions represent the characteristics of road surface roughness in the longitudinal direction only.

The simulation of road surface profile in transverse direction was proposed by Liu et al. (2002) using the auto-regressive moving average (ARMA). The dynamic behaviour of multi-girder bridges under heavy trucks was investigated using the proposed correlated road surface roughness.

Imine et al. (2005) has carried out studies to evaluate road roughness using longitudinal profile analyser and robotic approach based on sliding mode observer in control theory. The study reveals that road profile can be accurately estimated if vertical displacement of wheels and vehicle body bounce and rotations are obtained correctly. The practical use of the study is to estimate wheel load on the vehicle.

The road surface roughness based on acceleration records of vehicle traversing on the road is obtained by Gonzalez et al. (2011). The time history of the acceleration when the vehicle is traveling on the road with constant velocity is obtained using accelerometers which are fitted to the axles. Using the PSD function of the acceleration response, the PSD of road roughness is obtained from the transfer function of the vehicle. The transfer function can be obtained experimentally by passing the vehicle over a measured profile. The road can be classified as very good, good and poor by identifying the PSD of road.

Road surface roughness has been found to be an important parameter for fatigue damage assessment of heavy vehicle (Bogsjo et al., 2012). It was observed that actual average road

profile contains short segments with above average irregularity and such irregularities cause majority of the fatigue damage. Three new road roughness models have been developed which are homogeneous Laplace moving average (LMA) model, non-homogeneous Laplace process and a hybrid model that combines Gaussian and Laplace process. It was observed from the study that the LMA model works very well for smaller road sections in which homogeneous Gaussian model is an approximation.

1.4.1.3 Bridge Model

Various researchers have studied the dynamic behaviour of bridge due to movement of vehicles on the bridge. Different bridge models have been considered depending on the type and support condition.

Most popularly adopted bridge model is the single span beam to study the vehicle induced bridge response (Willis, 1849; Stokes, 1849; Timoshenko, 1922; Ayre et al., 1950; Biggs, 1964; Fryba, 1972; Sridharan and Mallik, 1979; Green and Cebon, 1994; Tan et al., 1998). The beam model was found to be appropriate as the transverse dimensions are small as compared to that of the length. The beam dynamic stresses have been obtained using the mode superposition method wherein the symmetrical modes are found to contribute to the stresses. The road roughness was not considered in the above mentioned studies.

Different types of bridges have been considered in the study of vehicle induced vibrations. The dynamic response of truss bridge for movement of vehicles was studied by Chu et al. (1979) and Wiriyachai et al. (1982). The truss bridge was modelled as a simple beam model with equivalent properties of the full truss section. Impact factors due to movement of vehicles in the bridge were investigated. The damping of the bridge and vehicle was ignored in the study.

Chatterjee et al. (1993) modelled truss bridge by considering multi-degree of freedom with lumped mass system. The effect bending action on dynamic response of the deck was incorporated by taking sufficient number of in-between nodes or mass points along the deck between two joints of the truss. The stiffness of the truss corresponding to the vertical degrees of freedom at the deck joints is provided by the stiffness of an interconnected springing system. The dynamic analysis of the truss bridge is obtained using the continuum approach. Different types of truss such as Pratt truss, Warren truss with no verticals and Warren truss with inclined upper chord were considered in the study. However, the interaction between vehicle and bridge was ignored in the study.

Parida and Talukdar (2020) analysed Pratt truss bridge subjected to single and multiple vehicles using finite element software. Vehicle induced pavement force is implemented using an uncoupled iterative scheme. Elements of truss bridge such as top chord, bottom chord, lateral bracings, verticals and diagonals, cross beams, floor beams and stringers were modelled using frame elements. Bridge deck is modelled using shell elements. Both the elements have six degrees of freedom at the nodes. Pin and roller supports were modelled using linear type link element. The dynamic load and dynamic amplification factor for various members of truss bridge are obtained for different bridge vehicle parameters. It was observed from the study that dynamic amplification factor is affected by vehicle velocity and road roughness and is not constant in each member of truss.

The dynamic analysis of arch bridge subjected to moving vehicle is studied by Chatterjee and Datta (1995) using a continuum approach. The struts are replaced by a number of interconnected springs located at the deck-strut joints. The mass of the struts and the suitable portion of the mass of the arch are lumped at the beam joints to consider the inertia effect of struts and arch along deck. The lumped masses at the nodes are distributed over small lengths to perform the continuum analysis. It is observed that as the number of spans increases, number of degrees of freedom also increases. Thus, the computation time required also increases.

The response of steel arch bridge under the action of moving load was carried out using finite element analysis (Ju and Li, 2003; Nam et al., 2008; Daniel et al., 2015). A moving wheel element having cubic interpolation function has been used to overcome the difficulty from the use of traditional node to linear algorithms. The criteria to predict bridge vehicle resonance effect was also proposed. The road surface roughness was ignored in the study.

The response of railway bridge, consisting of several box girders was investigated by Chu et al. (1986). The bridge considered is a prestressed concrete having single track. Moment of inertia of individual girder was calculated and multiplied by number of girders to obtain the bridge moment of inertia. Lateral moment of inertia and torsional constant of the bridge were obtained using the similar procedure. The rail irregularities were modelled using PSD function.

Various researchers have investigated the response of multi-span bridges having uniform or non-uniform cross section (Huang et al., 1992; Yang et al., 1995; Kou and DeWolf, 1997; Cheung et al., 1999; Marchesiello et al., 1999). Huang et al. (1992) modelled the continuous multi girder bridge as grillage beam systems. Yang et al. (1995) idealised the continuous bridge as a series of beam elements and the vehicle is idealised as a single degree of freedom system.

Kou and DeWolf (1997) used the finite element method for three dimensional dynamic bridge analysis. The bridge considered in the study is four-span continuous nonprismatic plate girder bridge. The girders and floor beams are modelled as beam elements and the concrete deck is modelled as plate elements. The beam element has six degrees of freedom at each node and the plate element considered is a four-noded quadrilateral isotropic element having six degrees of freedom at each node. The surface roughness considered is based on the Fourier series finite-wavelength profile.

Cheung et al. (1999) used the Lagrangian approach to analyse the response of a multi-span non-uniform bridge subjected to moving vehicle. The modified beam vibration functions are adopted as the assumed modes of a multi span bridge. The assumed vibration modes are the summation of the normal modes of the prismatic beam and the augmenting cubic spline expressions. These are chosen such that the assumed vibration modes satisfy the boundary conditions at the two ends and zero deflection condition at the intermediate supports.

Marchesiello et al. (1999) modelled the multi span continuous bridge as isotropic plate with multi degrees of freedom. Road surface roughness was modelled as a stationary random process.

1.4.1.4 Method of Solution for Bridge Vehicle Interaction Problem

Timoshenko (1922) recognised that imperfect balance of locomotive driving wheels produces impact effect on long span bridges. The induced forced vibration was obtained by considering the bridge as beam of constant cross section with simply supported ends. Differential equation of motion of the beam under the action of a single harmonic force that moves along the span at uniform speed was obtained using energy principles and solved for the boundary conditions wherein the contribution of fundamental mode was considered. In the formulation, damping was ignored.

Jeffcott (1929) developed a method based on successive approximation to address the problems in vibration of railway bridges under the action of moving and fluctuating load. The effect of damping force and inertia effect of moving mass on the beam deflection has also been investigated.

The vibration problems in railway bridge has also been addressed by Inglis (1934) using analytical techniques. The harmonic series method considered showed that the load with shorter wavelength decreases the beam deflection rapidly. It was also observed that the damped

oscillation in railway bridge is due to lack of elasticity in track and ballast and friction at the end bearings. The residual oscillation in case of long span bridges persists for greater duration after the vehicle leaves the bridge.

The three vehicle models are explained by Fryba (1972). The dynamic response of structures under the action of vehicles is also explained. The analytical and numerical solutions pertaining to these models were obtained.

The effect of vehicle braking response on bridge dynamic response was considered by Gupta and Trail-Nash (1980). The bridge was modelled as beam and also as an orthotropic plate. The effect of bridge transverse flexibility is taken into account by including the additional torsional degree of freedom in simple beam representation. The bridge vehicle coupled system of equations were solved using Newmark's algorithm.

Hayashikawa and Watanabe (1981) developed an analytical method to determine the eigenvalues and eigenfunctions of continuous beams with arbitrary boundary conditions. This was obtained using a general solution of differential equation for lateral vibration of beam. The developed method can also be applied to non-uniform cross section beams. Further, the dynamic response of continuous beam traversed by moving load with constant velocity is obtained using modal analysis.

Coussy et al. (1989) studied the effect of time dependent forces on bridges. The effect of road surface roughness on the dynamic response of bridges under suspended moving loads was also considered in the analysis. The beam was idealised as an elastic beam and the surface roughness was modelled by PSD function for frequency domain analysis. The coupled differential equation was solved using the numerical technique. It was observed that dynamic amplification factor is influenced by surface roughness.

Chan and O'Connor (1990) suggested a vehicle model to estimate impact in highway bridges. The axle load consists of a constant load with a sinusoidally varying component. The magnitude of the varying component has been kept as ±10% about the mean. Maximum bending moments in the girder are evaluated varying the span, static axle loads and axle spacing. It was observed that maximum bending moment takes place where the maximum load is leaving the span and simultaneously loads are entering the span.

Hwang and Nowak (1991) analysed dynamic load in bridges. The vehicle has been idealised as a full car vehicle model and the bridge is represented by prismatic beam. The road surface

roughness is described by PSD function. The vehicular load is simulated using Monte Carlo method and the system equations of motion are solved using Newmark- β method. Steel and pre-stressed concrete bridges are considered in the study. The dynamic load factor for different vehicle and bridge parameters is also found and its influence on the above parameters is also investigated.

Wang et al. (1992) investigated the dynamic behaviour of multi girder bridges, modelled as grillage beam system, due to movement of vehicles. Girders and slabs are modelled as longitudinal elements and slabs and diaphragms are modelled as transverse elements. Two nonlinear vehicle models are considered with seven and twelve degrees of freedom. The vehicle models pertain to H20-44 and HS20-44 truck design. The bridge road roughness is generated from PSD function developed by Dodds and Robson (1973). The roughness coefficients for different classes of road are taken according to International Organization for Standardization (ISO) specification (ISO 8608: 1995). The interaction between vehicle and bridge is considered by evaluating interaction forces. The nonlinear vehicle equations of motion are solved using fourth-order Runge-Kutta integration scheme and bridge equation of motion is solved using mode-superposition method based on subspace-iteration method. The bridge deflection and impact factors for different girders of a prestressed concrete multi girder bridge are obtained for different road classes and vehicle parameters. It was observed that road surface roughness greatly influences the impact factor.

The dynamic interaction between the vehicle and guideway of a high speed ground transportation system based on magnetically levitated (maglev) vehicles were studied by Cai et al. (1994). The guideway characteristics are modelled using the Bernoulli-Euler beam equation. Two guideways are considered in the study, one is single-span beam and the second is two-span beam. The vehicle models considered are moving force and quarter car model. In case of the quarter car model, the coupled bridge vehicle equations are solved with the help of numerical method. The maximum guideway deflection for different vehicle and guideway parameter is evaluated and investigated and these parameters are also evaluated for vehicle design in order to take into account better ride quality. However, the irregularities of the guideway are not considered in the study.

The dynamic behaviour of simple-span highway girder bridges due to heavy truck loads is studied by Chang and Lee (1994). The dynamic response of bridges is investigated in time and frequency domain. Form the study it was observed that the main source of bridge vibration due

to movement of heavy vehicles is surface roughness. Impact factor for parameters such as vehicle speed, surface roughness and bridge span were also investigated and empirical formulas for impact factors with the parameters are developed using multiple linear regression analysis. It was also observed from the study that the impact factors used in current bridge design codes were underestimated with rough deck profiles.

Chatterjee et.al. (1994) obtained the flexural-torsional vibration of the suspension bridge under vehicular movement. The non-linear interaction force, vehicle path eccentricity, pavement irregularity, cable-tower connection and end conditions for the stiffening girder are considered for analysis. The pavement irregularity is considered as a stationary random process characterized by a PSD function. The irregular profile of the bridge pavement is generated from the PSD function using Monte Carlo simulation technique. The responses obtained in time domain are compared with three types of vehicles namely, 3-D, 2-D, and single sprung mass system.

Yang and Lin (1995) obtained the response of general vehicle-bridge systems. Vehicle is modelled as lumped mass supported by springs and dashpots and the bridge is modelled as beam. An interaction element is modelled and consists of a bridge element and the suspension units of the vehicle resting on the element. The composition of the interaction element and the parts of vehicle bodies in contact is regarded as a substructure. The degrees of freedom associated with the vehicle existing within each substructure are removed using the dynamic condensation method. This condensation method is done on the element level. The conventional assembly process is used to make it in global level. Newmark's β method with constant average acceleration, that is, with β = 1/4 and γ = 1/2, is used for transforming the finite element equation into finite-difference equation in time domain. This method is suitable for the simulation of bridges under the action of series of vehicles traversing at different velocities.

Michaltsos et al. (1996) investigated linear dynamic response of simply supported beam of uniform cross section under the action of moving load having constant magnitude and travelling at constant velocity wherein the vehicle mass effect is also considered. The individual and coupling effects of the mass of the moving load, velocity and other parameters are also studied. Newmark β scheme was used for the numerical integration of the bridge vehicle coupled system of equations. It was observed from the study that bridge deflection increases at higher velocity with the increase in ratio of vehicle mass to bridge mass.

Yang and Yau (1997) analyzed railway bridges considering high speed trains using vehicle-bridge interaction element. Train is modelled as a series of sprung masses lumped at the bogie positions and the bridge with track irregularities is modelled using beam elements. Newmark's finite difference method is adopted to solve the spring mass equation which is then condensed to the bridge element in contact. It is observed that the vehicle response is affected more as compared to the bridge when higher modes of bridge vibration are considered.

Green and Cebon (1997) studied the interaction between heavy vehicles and highway bridges. Six non-dimensional parameters of the bridge-vehicle system are varied to assess the amount of interaction between the vehicle and the bridge. The equation of motion was evaluated using the convolution integral in frequency domain. The frequency domain method using discrete Fourier transform was considered. The dynamic vehicle response model was calculated using the iterative procedure. It was observed that large mass ratios result in significant interactions in high velocities.

An explicit technique to obtain the solution of coupled dynamic system with the help of mode superposition method for bridge structures and physical components of the vehicles using Lagrange's formulation is proposed by Henchi et al. (1998). Bridge has been idealised as beam and plate model using finite element approach. The dynamic behaviour of bridge subjected to multiple movement of vehicles at different location has been studied using a coupled iterative scheme. However, it was observed from the study that the iterative scheme cannot be used when high frequencies of bridge participate in motion.

Chan et al. (2000) studied the behaviour of prestressed concrete bridge under the action of moving vehicle. Bridge was modelled as beam of uniform cross section having linear viscous proportional damping. The effect of shear deformation and rotary inertia were neglected. Vehicle was modelled as moving load with constant velocity. The dynamic response of beam due to vehicle-induced vibrations were evaluated using Newmark scheme.

The effects of inertia and vehicle moving with constant velocity on the dynamic behaviour of multi span continuous bridge is studied by Ichikawa et al. (2000). The continuous bridge is idealised as Euler-Bernoulli beam. The beam equation of motion is discretised using mode superposition technique. The system response is obtained using numerical integration scheme. It is observed from the study that the inertia of the moving mass greatly affects the second and successive spans as compared to first span.

Dynamic behaviour of bridge considering moving loads using orthotropic plate theory and modal superposition principle is studied by Zhu and Law (2003). The bridge response at different locations are obtained using analytical solution. The numerical example of simply supported beam slab type bridge deck with aspect ratio less than two is considered and the same is used for parametric studies. From the study it is observed that the equivalent beam model of bridge gives better prediction of the impact factor along the centreline of the deck, while the same would underestimate the response at the edge of the structure.

Yang et al. (2004) analysed bridge vehicle interaction using condensation method. In order to consider the bridge vehicle coupled problem, sprung mass equation is first discretised by means of Newmark's finite difference method and further condensed with bridge element in contact. The results have been compared with that obtained using analytical solution and found to be in agreement with each other.

Cai and Chen (2004) presented the framework for dynamic analysis of three dimensional bridge vehicle system. Each vehicle is modelled with several rigid bodies, mass blocks, and spring-damping systems. The vehicle-bridge model is solved using the principle of virtual work. The equation of motion is solved using the second-order Runge-Kutta method. From the study, it was observed that wind speed affects the bridge response in comparison to the vehicle velocity.

The dynamic behaviour of multi-span continuous bridge having non-uniform cross section under the action of traversing vehicle is studied by Law and Zhu (2005). The effect of interaction between bridge and vehicle and the road surface roughness is considered in the study. Braking force was considered by taking a ramp function which was based on the test result on highway vehicle conducted by the Transport and Road Research Laboratory, England. It was found from the study that vehicle barking significantly affects the bridge dynamic response.

Lou (2005) studied vehicle-track-bridge interaction problem based on pitching effect of the vehicle using finite element method. The vehicle is modelled as a two axle mass spring damper system having four degrees of freedom. Rail is idealised as upper beam and deck as lower beam of finite length. The upper beam rests on closely spaced sleepers which are idealised as a series of springs and dampers. System equations are derived using Hamilton principle and are solved using step by step integration method. It is observed from the study that vehicle pitching effect has little influence on vehicle and bridge response when the track irregularity is neglected.

Several researchers have considered the effect of approach span conditions on dynamic response of the bridge due to moving vehicles (Shi et al, 2008 and Cai et. al., 2007). Finite element technique has been adopted to bridge vehicle coupled system model. Generalised coordinates are used for beam and physical coordinates are used for the vehicle to account for computational efficiency. Stochastic road surface which includes approach span are also taken into account in the model. System equations of motion are solved by means of fourth order Runge-Kutta method. Impact factor is evaluated and investigated for several parameters considering the effect of approach span condition. It is observed from the study that the AASHTO specifications undervalue the impact factor for bridge.

Pseudo-excitation method for non-stationary random vibration of vehicle-bridge systems is given by Lu et.al. (2009). 10 degree of freedom vehicle model moving on simply supported and three span continuous bridges were considered for case study. The above method was found to reduce the computational time in comparison to the conventional method. The contribution of vehicle structural mode was ignored although long and slender vehicle of 14m axle spacing was considered in the vehicle model.

A general procedure for stress and acceleration response analysis of coupled vehicle and long span bridge systems using the mode superposition technique is given by Xu et.al. (2010). Number of vibration modes required in the stress analysis was discussed. The results found through the proposed technique were validated with the field test results on long span suspension bridges.

Yin et.al. (2010) studied non-stationary random vibration of bridge considering vehicles with variable speed using the covariance equivalent technique. Simple beam model subject to half car vehicle model was taken for parametric studies. It was observed that road roughness coefficients, initial velocities, accelerations of vehicles and vehicle braking conditions have substantial effect on impact factors considering non-stationary random inputs.

Ouyang (2011) compared analytical formulation for moving load problems such as vehicle-bridge, vehicle-ground, train-track interactions were included in the study. It was concluded that the analytical formulation of the moving load problem has the benefit that its location can be found in the continuous coordinate. But in case of finite element formulation, moving load is located in different element domains at different time which makes it difficult to track its location. Hence, the numerical procedure for a moving load problem using the finite element method is complicated and less accurate than that of analytical method.

Huang (2012) investigated the dynamic behaviour of steel arch bridge considering multiple vehicles moving over a rough deck. The vehicle model considered was a full car vehicle model and Lagrange's formulation was used to construct the equations of motion. The road roughness was considered to be a stationary Gaussian random process. Newmark integration scheme was employed to obtain the bridge response.

Azimi et.al. (2013) investigated the effect of sudden deceleration of vehicle on the dynamic response of the bridge. In vehicle bridge interaction model, effect of deceleration was considered as external load acting on each part of the vehicle masses. Vehicle was modelled as a half car model. In this, the deck roughness was not considered. The response of the bridge was found to increase with higher vehicle speed and an increase in bridge response was found with high rate of deceleration.

The dynamic analysis of highway bridges taking into account the action of vehicles is done in Leitao et.al. (2013). Also it focuses on relating the possible distortions on the bridge when subjected to vehicle dynamic loads and its effect on service life. The FE model was developed in ANSYS adopting the usual mesh refinement techniques. The beam steel sections were modelled using three dimensional beam and shell elements. The top and bottom beam flanges, longitudinal and vertical stiffeners were modelled using three dimensional beam elements accounting for beam and torsional effects. The concrete slab of the bridge was modelled using shell elements. The bridge considered for the study is a simply supported composite bridge. The vehicle model is mass-spring-damper system with three masses and four degrees of freedom i.e., three translational and one rotation. The structural damping of the bridge was considered to be Rayleigh proportional damping. Reference frequencies are generally taken as the two extreme frequencies of the structure spectrum.

The closed form solution to evaluate dynamic behaviour of a multi-span bridge has been determined by Johansson et al. (2013). Boundary conditions of the bridge are assigned to characteristic function of beam to obtain natural frequencies of vibrations and corresponding mode shapes. The governing differential equation was solved for each normal mode in frequency domain using Laplace transformation. Parametric study has been conducted using the data of several existing bridges. In the study, simplest vehicle model was considered. The vehicle is assumed to move at constant velocity. The torsional motion of bridge due to eccentric load was ignored in the formulation.

The response of simply supported beam under the action of arbitrary transient moving load was examined by Zhang and Shepherd (2014). The bridge response was obtained using analytical solution and the results obtained were compared with that obtained from FE approach. It was observed from the study that the analytical method used for the initial configuration study is accurate. It was also observed that FE approach can be used where more complex configurations and alternative support conditions are considered.

The vehicle-bridge coupled vibration was studied by Jin et al. (2015) using random vibration and reliability based approach. System equation of motion was derived using the principle of virtual work utilising a linearized wheel-rail contact equation. In order to avoid iterative solution at each time step of the integration, explicit linearization method was adopted. The results obtained from the proposed method was validated using Monte Carlo simulation. Significant reduction in computational time was found using the proposed method of solution as compared to the traditional methods.

The dynamic behaviour of pre-stressed continuous bridge due to traversing vehicle was studied by Zhong et al. (2015). The bridge was idealised as continuous beam with eccentric pre-stress, while vehicle model considered was half car model. The governing equations of motion for both vehicle and bridge were obtained using virtual work principle and solved by Newmark integration scheme. The FE model was used to validate the results. Parametric studies such as pre-stress amplitude, eccentric load and span length were studied. It was observed that as the pre-stress amplitude increases, bridge dynamic response decreases. However, the effect of road roughness and vehicle body structural modes are not considered in the study.

Train and bridge dynamic interaction response is studied by Duan et al. (2018) using vector form intrinsic finite element method. The train and bridge systems are modelled as mass particles which are linked by a series of massless elements. Central difference method is utilised to solve the equation of motion for each mass particle. Finite set of points are referred to as mass particles in this suggested method. The suggested method was used to find the response of single span beam subjected to a moving train. The response obtained is accurate and efficient in comparison to the numerical methods.

A non-linear multi spring tyre model is suggested by Zhang et al. (2018) to obtain the dynamic response of bridge under the action of moving vehicles. this model is adopted to ensure that vehicle always remains in contact with the bridge. The vehicle model is idealised as quarter car model. The bridge is idealised as single span beam. The road surface roughness is generated

using PSD function. The coupled bridge vehicle equations are solved using combination of Newmark method and Newton method. From the study, it was found that the model is more effective when the vehicle velocity is less.

A three dimensional model for dynamic interaction of train-track-bridge is suggested by Xu and Zhai (2019). Rail is modelled as beam, track slab is modelled as thin plate element and the rail pad is modelled using spring and dashpot, while bridge is modelled as three dimensional beam element. Using continuously distributed spring dashpot elements, bridge and track slabs are connected. For coupling between track and bridge, cubic Hermitian and linear interpolation polynomials are used. The stiffness and damping matrices corresponding to vertical and lateral interactions between bridge and track slab is obtained using energy principle. The train is idealised as a series of vehicle bodies wherein each of them consist of car body, two bogie frames and four wheelsets and all of them are considered as rigid bodies. Only the wheelset has five degrees of freedom, pitch motion is not considered, while the rest have six degrees of freedom. The equations of motions of train-track-bridge system is solved using numerical methods in time domain. It was observed that this method is computationally stable.

A methodology to determine the response of railway bridge under the action of high speed trains using FE software is suggested by Lu et al. (2020). Train was modelled as car body, bogies and wheelsets. These were considered as rigid bodies connected with spring and dashpot. Bridge is modelled using three dimensional solid elements. Using penalty method, interaction between track and wheelset was achieved. Track irregularity was also considered. The method was validated for a simple beam problem subjected to moving mass. The closed form solution and that obtained from FE method are compared and found to be in agreement with each other.

Behaviour of centenary steel arch bridge located in Portugal, subjected to rail loads has been studied by Ribeiro et al. (2021). Using moving load method and vehicle bridge interaction model, bridge response has been obtained. FE models of bridge and vehicle are also developed. Interaction forces are modelled using constraint elements. Bridge vehicle influencing parameters on the bridge response and passenger comfort have also been studied.

In most of the studies discussed, the random nature of vehicular movement on highway bridge is not considered. Since the vehicular loads arrive on the bridge at random times having random magnitude, it is essential to study transverse vibration of bridge by taking into consideration the arrival time of the vehicle as a random variable. The dynamic response of bridge was

evaluated assuming interarrival time of vehicle as a random variable (Śniady et al., 2001; Sniady, 1984). In the above studies, the bridge was idealised as single span beam and the vehicle was idealised as a concentrated moving load. The bridge vehicle equations were solved using stochastic differential equations. It was observed from the study that the mean stresses on the beam decrease with the increase in vehicle speed. The effect of road roughness was not considered in the study.

A stochastic approach for vehicle track bridge system based on probability density evolution method is proposed by Xiao at al. (2019). The vehicle weight is treated as random variable and the track irregularity is also considered as random process. The vehicle bridge coupled equations of motion are solved using principle of virtual work. It is observed from the study that the computational efficiency is significantly better than the Monte Carlo simulation. The track irregularity significantly affects the bridge dynamic response.

1.4.2 Fatigue Life of Bridges due to Vehicle Loads

Bridges are subjected to load histories which consist of cycles with variety of load ranges i.e., variable amplitude loading. The review of fatigue life of bridge considering vehicle load has been separated into three sub sections, fatigue life evaluation using LDR, LEFM approach and spectral method, which are discussed below.

1.4.2.1 Fatigue life evaluation using LDR

Several researchers have studied bridge fatigue considering variable amplitude loading. The sequence effect of blocks in a variable amplitude stress range spectrum which was similar to that recorded on the girders of a Maryland bridge located in Canada was examined by Yamada and Albrecht (1977). Two flange details were tested. First detail was a welded cover plate and second detail was a groove welded connection in the flange-web joint. Control specimens were also tested for constant amplitude fatigue. It was found from the study that the order of blocks did not affect variable amplitude fatigue life.

The effect of minimum stress, load history and type of steel on variable amplitude fatigue strength was investigated by Schilling et al. (1978). 58 specimens of D category cover-plated tensile specimens, 59 specimens of B category welded beams and 153 specimens of E category cover plated beams where welds were laid in different sequences were tested. The specimens were tested under constant amplitude stress range and variable amplitude stress range based on wide-band, medium-band and narrow-band Rayleigh spectra. It was observed from the study

that the band width and minimum stress had a statistically insignificant effect on fatigue strength.

Hahin et.al. (1993) conducted studies on fatigue damage of steel bridges in the state of Illinois from collected field data. The strain gauges were located in the fatigue prone areas. The cumulative damage was calculated by collecting the strain gauge increment by the data acquisition system.

Wang et.al. (1993) calculated the fatigue lives of highway steel bridges using reliability based methodology. The fatigue life of both non-composite and composite steel beam bridges for various vehicle velocities and classes of road surface roughness were calculated from stress time histories.

Dicleli and Bruneau (1995) developed a methodology to evaluate remaining life of steel bridges under the action of heavy permit trucks. It was observed that a large number of special permits can be issued at small reductions in fatigue life.

Mohammadi et.al. (1998) presented the application of filed data for condition assessment and prediction of service life of highway bridges composed of steel girders with reinforced concrete deck slab. The field stress range compiled for each bridge was used along with a probabilistic method to predict fatigue life.

The randomness due to the loading process and the fatigue resistance of the material is considered by Shen et.al. (2000) wherein the randomness of the fatigue resistance of the material is considered by taking a random variable of single cycle fatigue damage. The fatigue life is represented by lognormal distribution. The parameters of the fatigue life are considered as a function of stress amplitude. The cumulative fatigue damage distribution can be calculated using the distribution of single cycle fatigue damage and the distribution of stress amplitude.

Rao and Talukdar (2003) assessed fatigue damage in continuous bridge girder using the stress range frequency histogram. Vehicle induced time history of maximum flexural stresses has been found by Monte Carlo simulation process and used to develop the stress range frequency histogram, considering the annual traffic volume. The fatigue life of the bridge is calculated using LDR. The mass, stiffness and damping properties are assumed uniform along the beam. Vehicle has been modelled as a rigid beam connected by front and rear suspension. The road roughness is described by PSD function. The transverse displacement of the bridge is obtained using mode superposition method. Parametric variations such as effect of the bridge span, road

roughness, vehicle velocity, vehicle weight and vehicle suspension are varied to observe the effect on fatigue life.

Wang et.al. (2005) performed truck loading and fatigue damage analysis using weigh-in-motion data. Fatigue damage analysis according to LDR was carried out.

Alampalli and Lund (2006) evaluated the remaining safe fatigue life of the Patroon Island Bridge using AASHTO (2012) using measured strain data under vehicular traffic. The strain data obtained for the critical structural members were utilised for calculating the remaining fatigue life. In order to transform the strain history, rainflow algorithm and Miner's rule were also used for the analysis.

Mori et.al. (2007) derived the parameters which decide the extent to which the bridge is damaged under the design and maintenance stage. The bridge under consideration is short and medium span I and box girder steel highway bridge. The fatigue load used is the simulated traffic flow and the fatigue life is evaluated based on the stress variations obtained and also based on the Fatigue Design Recommendations of the Japanese Society of Steel Construction. The vehicle weights are expected to follow a log-normal distribution. Vehicle classification was based on Japanese Ministry of Construction. The fatigue life estimating points are chosen such that the points are experiencing higher stress. These points are the center of span in case of a simply supported bridge. In case of three span continuous bridge, the points will be middle span and intermediate supports. The fatigue loads were simulated using the Monte Carlo method. In simulating fatigue load, the vehicle type and weight, and the traffic volume are considered as random variables.

Fatigue damage due to special class of non-Gaussian broadband loadings is considered in Rychlik and Gupta (2007). The loadings considered are transformation of stationary Gaussian random processes. Fatigue damage is obtained using the linear damage accumulation rule.

Chiewanichakorn et.al.(2007) studied dynamic and fatigue response of fiber reinforced polymer decks using FE models. FE models were used for dynamic time history analyses. The loading considered was AASHTO fatigue truck, which however, did reflect the series of vehicles moving at random time as a common case in a busy section of highway in urban areas. Two models were considered for FE modelling. First model was of non-composite reinforced concrete deck while the second one was with FRP decks. The study concludes that fatigue damages are likely to occur in truss joints and intersection of stringer and cross beam.

Fatigue reliability assessment of steel bridges using probability density functions of equivalent stress range, based on field monitoring data is given by Kwon and Frangopol (2010). The fatigue detail coefficient, *A*, and the equivalent stress range, S_{re}, are both treated as random variables in this approach. The fatigue damage is expected to be Lognormal with mean value of 1.0 and coefficient of variation (COV) of 0.3 for metallic materials. The probability density function related to the stress range is assumed as Lognormal, Weibull or Gamma. The equivalent stress range is evaluated from the stress range bin histogram and fatigue exponent value, *m* is considered as 3. It is assumed that small cycles contribute very less to the fatigue damage. It was observed from the study that the field monitoring data can also be used to assess fatigue reliability and predict fatigue life of existing steel bridges.

Fatigue assessment of riveted joints are discussed in Pipinato et.al. (2011). Experiments including physical and physical-chemical tests were conducted on a dismantled short span railway bridge. Fatigue bending laboratory tests were performed on girder and short span diaphragm riveted shear connections. A new design category was suggested for riveted connections based on the experimental results.

The probability of failure under the loading block is evaluated considering the Monte Carlo simulation using Miner's hypothesis, the modified Miner's rule and Haibach's rule in Kang et.al. (2012). An evaluation method was developed which can predict the block number of the failure load and residual fatigue life. The failure loading block is calculated using Monte Carlo simulation. The stress history was measured at the weld joint in the bottom part of the flange and vertical stiffener.

Zhang and Cai (2012) evaluated the fatigue reliability assessment of existing bridges considering the random effects of vehicle speed and road-roughness condition. Equivalent stress range is introduced to include fatigue damage accumulations for one truck passage. The coupled vehicle bridge system is solved considering three dimensional suspension vehicle model and a 3D dynamic bridge model. In current specifications such as AASHTO and LRFD, vehicle speeds and road roughness conditions are not considered. The lateral position of the vehicle, the deterioration of the road surface and traffic increase rate are considered in this paper.

Bilinear S-N curves were developed by Yen et.al. (2013) for fatigue strength categories as per the specifications given in AASHTO (2012). Slope of -4 below the CAFL (Constant Amplitude Fatigue Limit) has been proposed. This slope is based on the analytical derivation by

accounting for the cumulative fatigue damage induced by the stress cycles in the stress range spectra that are sufficient to cause crack. This implies that the stress intensity factor range should be higher than the fatigue crack growth threshold to cause crack. The estimated fatigue life by the bilinear S-N curve is less conservative as compared to AASHTO S-N curve which has a negative slope 3

A statistically consistent damage criterion is established by Sun et.al. (2014). The model is validated using a two-level cyclic loading and experimental verification of fatigue tests for aluminium alloy straight lugs available in the literature, are considered. Fatigue life is assumed to follow a Weibull distribution in this paper. This statistically consistent model is for constant amplitude loading and also variable amplitude loading. The proposed model is in good agreement with the engineering hypotheses and also shows good predictions with the experimental results compared to Miner's model.

The calculation of damage accumulation and probability of failure taking the normalized variable as derived from the probabilistic S-N field is done by Blason et.al. (2016) and is compared with the Miner's rule. The normalized variable is defined as the product of the applied stress or strain range by fatigue life. This normalized variable allows the S-N field to reduce to a simple Weibull or Gumbel cumulative distribution function. The probability of failure is represented by a monotonically increasing function of the normalized variable.

Wang and Deng (2016) suggested a method to determine impact factors for fatigue design of steel I-girder bridges considering the effect of deterioration of the road surface condition, vehicle velocity and bridge span. The coupled vehicle-bridge model developed was three dimensional in nature and simple-span bridge was considered for the study. The impact factors were obtained by considering the maximum of the stress range instead of maximum stress which is used to calculate the conventional impact factor. It was observed that the proposed impact factors were larger than the conventional impact factors for fatigue design of short-span steel bridges. However, for large and medium span steel bridges, the proposed impact factors by AASHTO were found to be suitable.

Wang et.al. (2016) evaluated the number of stress cycles given as per the AASHTO LRFD design specifications for the fatigue design of steel structures. The methodology for evaluating the number of stress cycles for the fatigue design of simply supported steel I-girders is suggested taking into account the dynamic effect of vehicle loading. Three dimensional vehicle-bridge model is considered in which bridge and fatigue load models are adopted from

LRFD code. Parameters such as the road roughness, bridge span, and vehicle velocity are varied to observe the effect on the number of stress cycles.

D'Angelo and Nussbaumer (2017) provides a probabilistic approach for reliable estimation of fatigue characteristic S-N curves of welded joints both for constant and variable amplitude loading conditions. This approach combines Maximum Likelihood method and Monte-Carlo Simulation method.

Analysis of fatigue-loaded vehicle models and theoretical fatigue life of U ribs butt weld of steel box girder is done by Ma et.al. (2018) based on the data collected by Weigh-in-motion system of XiHouMen Bridge in China. The equivalent fatigue load is obtained by the statistical distribution functions of the gross vehicle weight under various loading conditions for each vehicle type.

A practical framework for predicting fatigue life of suspenders under vehicular loads taking three-pylon suspension bridge as an example was studied by Cui et al. (2019). The bridge vehicle interaction is considering by solving the vehicle equations of motion and then utilising interaction forces as input to FE model of the bridge. This is achieved using an iterative scheme. The effect of road roughness is considered. From the study, it was observed that road roughness affects the stresses on the suspenders at the centre and quarter span.

The fatigue performance of a two-way four-lane steel concrete composite continuous bridge deck is studied by Zheng et al. (2021). A spatial finite element model was adopted in the study. Linear elastic constitutive relations were adopted for steel rebars and concrete deck. The parameters such as wheel position, reinforcement ratio and thickness of deck were studied to understand the effect on fatigue life of steel flange in tension and concrete punching shear fatigue. The change in wheel position and reinforcement ratio affect the fatigue life of girder and deck while the change in thickness of deck affects the fatigue behaviour of concrete deck significantly. However, the effect of road roughness was ignored in the study.

1.4.2.2 Fatigue life evaluation using LEFM approach

Fisher and Yuceoglu (1981) compiled qualitative data concerning the cracking of 142 steel bridges in the United States and Canada. Out-of-plane distortion and large initial defects were identified as the two most common specific causes of fatigue crack development.

Zhao et.al. (1994) uses an alternative LEFM method wherein the crack size information can also be considered. The fatigue reliability for full penetration butt welds in the tension flange of a steel box girder is evaluated and the same is compared with the AASHTO method. It is observed that the fatigue life mainly depends on the initial crack size. The initial crack size is modelled using a lognormal distribution. Fatigue growth parameter, *C* is expected to follow a lognormal distribution.

Fatigue evaluation of steel railway bridges was discussed by Fryba (1996). From the field study conducted on steel railway bridges, it was found that main girder endures more number of stress cycles per year. The secondary bridge elements and orthotropic steel deck endure low number of stress cycles per year.

Linear elastic fracture mechanics based reliability model is considered in Zhao and Haldar (1996) which takes into account the uncertainty in the results obtained from non-destructive inspections. The updated model containing the information just after the inspection can be used as a decision making tool to decide on the condition of service life of the bridge. Initial crack size is modelled as lognormal distribution. The stress range parameter is considered to follow Rayleigh Distribution.

Agerskov and Nielsen (1999) studied fatigue damage accumulation in steel highway bridge considering random loading and compared with experimental results and also compared with the results of analysis based on fracture mechanics.

Li et.al. (2001) proposed a methodology and strategy for fatigue damage assessment and life prediction of bridge deck of existing structure (the bridge considered is Tsing Ma Bridge in Hong Kong) with the help of online structural health monitoring. The fatigue damage model is based on Continuum Damage Mechanics model for determining the cumulative damage on the structure. The model consists of structures modelled as elastic members and welded connections are modelled with the accumulated damage. The deformation in the vicinity of the welds follows the constitutive equations of the damaged material. The strain data is collected from online structural health monitoring system. The deformation behaviour of the damaged member is modelled by introducing a scalar variable which corresponds to the damage in the member. The damaged member in this paper implies the member in the vicinity of welds. The results obtained from the damage model were found to be satisfactory.

Dexter et.al. (2004) presented an overview of the state-of-art in design and detailing of steel girders for the fatigue and fracture limit states. The fracture toughness of structural steel plate and weld metal is also discussed.

The development of a probabilistic fracture mechanics methodology for the prediction of fatigue reliability was done by Chryssanthopoulos and Righiniotis (2006). The methodology was developed using an updated crack growth which depends on stress level and fracture assessment criteria.

The fatigue behaviour of welded components under variable amplitude loading is discussed by Baptista et.al. (2017). The experimental crack growth was found using the alternative current potential drop method which showed the detrimental effect of stress ranges below the conventional constant amplitude fatigue limit (CAFL). Two step model with initiation propagation was used to establish the experimental fatigue life.

Wei et.al. (2017) evaluated the fatigue performance of the cope-hole details in welded joints of a steel truss bridge using the structural hot spot stress approach. Fatigue testing of nine specimens were done to evaluate the fatigue strength of cope-hole details in the welded connection between the I-section member and truss joints in steel truss bridges. To study the local stress concentration around the cope-holes, finite element analysis was done. Using the finite element analysis, effect of load type on the local stress distribution was studied. The FE model was prepared considering symmetry of the section and uniform displacement was applied at the end of the section and subjected to pure tensile loading. Based on the fatigue test conducted under axial tensile loading condition, it was observed that the fatigue crack in all specimens first occurred at the welded toe at the flange plates inside the cope-holes. The structural hot spot stress was evaluated using the extrapolation method. The extrapolation can be quadratic based on the three reference points and linear based on two reference points. From the FEM analysis results, it was also observed that the SCF will increase with the increasing ratio of the shear force to the bending moment at the weld toe of cope-hole details in a beam. SCF will also increase with the increasing ratio of the shear force to the axial force at the weld toe of cope-hole details in a tension member.

1.4.2.3 Fatigue Life Evaluation using Spectral Method

Lutes et.al. (1984) presented a stochastic fatigue damage theory to model uncertainty about stress time history. Numerical simulations were performed based on the existence of S-N curves for constant amplitude fatigue.

Lutes and Larsen (1990) conducted study on the variable amplitude fatigue prediction characterizing the stress by PSD function. The accuracy of this method was tested with the rainflow analysis of both unimodal and bimodal power spectral density functions. A new spectral method with one spectral moment was found to be more accurate than the Rayleigh approximation method. Also the single moment method was simpler than other spectral methods which involved three or four moments.

Fu and Cebon (2000) investigated fatigue failure of component subjected to random stress histories with bi-modal spectral densities. The methods for predicting fatigue damage using frequency domain statistics of random stress processes were reviewed.

Holmes (2002) has derived closed-form expressions for estimating the upper and lower limits of fatigue life of structures subjected to wind loading assuming that the mean wind speed follows a Weibull distribution. The results could be used for initial calculations to determine fatigue life of structures subjected to wind loading thereby avoiding extensive calculations.

The need to establish the bounds of fatigue life as a necessary condition in design of structures was emphasized by Repetto (2005). The method was illustrated for the case of wind induced fatigue. The study used cycle counting methods. The cycle counting methods for stationary Gaussian narrow-band and broad-band process is explained. Focusing attention on bi-modal processes, which were used in dynamic response of structures, the cycle histograms obtained by the peak and peak-valley counting methods were expressed in closed form. Benasciutti and Tovo (2006) discussed the fatigue analysis of broad band Gaussian random processes considering the rain flow cycles and the linear fatigue damage rule. Several spectral methods were reviewed.

Nallasivam et.al. (2008) estimated the fatigue damage accumulation rate of horizontally thin walled box-girder bridge from vehicle-induced stress history. Fatigue life is estimated using the rainflow cycle counting method in time domain and is compared with the life estimated using the PSD of response in frequency domain. The frequency domain method used spectral moment characteristics of stress response.

Fatigue life of bridges subjected to wind loading is also studied by various researchers. Gu et. al. (1999) suggested a method in the mixed frequency-time domain to predict the fatigue life of steel girders of the Yangpu cable-stayed bridge due to buffeting taking into consideration the effects of wind direction and the component of the buffeting response on the critical stress. It was observed that the effects of wind direction on the fatigue life of Yangpu Bridge were significant.

Chen et.al. (2011) proposed a framework for fatigue analysis of long span suspension bridges using computer simulation with structural health monitoring system. The bridge considered is Tsing Ma Bridge in Hong Kong. The dynamic stress of the bridge when subjected to trains, vehicle and wind loading is evaluated. The coupled effects of multiple load-induced dynamic stresses and dynamic magnification related to vehicular loads are neglected. Bridge stress caused due to combined effects of three types of loading can be approximately obtained by the superposition of stress for individual loadings. Load due to trains and moving vehicles are modelled as a series of moving loads on the bridge deck. Hence, the bridge stress responses due to train and vehicles are evaluated using the stress influence lines. While obtaining the dynamic stress due to the vehicular loads, it is assumed that the velocity of the vehicle is constant. It was observed that the load due to railway plays an important role in fatigue damage of the bridge. The damage caused due to vehicular loading is greater than the wind loading at some locations and it is reversed in some other locations.

Zhang et al. (2014) studied the fatigue damage assessment of existing bridges with corrosion under vehicle and non-stationary extreme hurricane loads. The non-stationary hurricane load is simulated as a summation of time-varying mean and fluctuating non-stationary components with a time-varying spectrum. The dynamic stress histories are obtained by solving vehicle bridge wind dynamic systems. It is observed from the study that the effect of wind loads in addition to the vehicular load increases the fatigue damage on the bridge.

After literature survey, it appears that there are some key issues on bridge-fatigue analysis that were not adequately addressed by the past researchers. There are various uncertainties involved in vehicle–bridge interaction such as random arrival rate, non-stationary excitation due to variation of vehicle velocities and pavement unevenness in poorly maintained bridge. There are scanty of literatures where combined effects of the above factors were considered in bridge-fatigue analysis. It is the need of the days that during design phase, bridge engineers be able to

know the effect of various unfavourable factors on fatigue life of the structures instead of solely based on empirical relationships of the design codes.

1.5 Scope of the Present Work

Bridge fatigue is primarily caused by the vehicle induced stress that goes on accumulating during life time of the structure. Usually, the fatigue life of a structure is estimated in design phase and in service. Reliable estimate in design phase considering various uncertainties will lead to the construction of safer structure with reduction of maintenance and retrofitting cost. From the literature review, it has been found that the most of the published works on bridge fatigue was based on standard loading, however, in present day's scenario of growing traffic of diverse nature, the dynamic loading on the bridges are of complex characters which influence the behaviour of bridge-vehicle coupled system. This opens the avenue for further research in bridge fatigue taking into consideration of bridge-vehicle coupled system in theoretical model along with multiple vehicle movement having random arrival time. The theoretical simulation of bridge-vehicle coupled system considering the random arrival time of vehicles over the bridge with unevenness of pavement would help the designer to predict the fatigue life in design phase more realistically. The present work aims to develop a fatigue model considering sequence of loading improving the conventional linear damage rule and to apply the same to estimate fatigue damage of bridge structures from vehicle induced stress history.

1.7 Organization of thesis

The thesis has been organized in seven chapters. References and Appendices are also included. The contents of the chapters are briefly given below.

Chapter-1: This gives introduction to the fatigue phenomenon and its significance in design of structures which are subjected to continuous vibratory load. The detail literature review and scope of the present work has been included. Thereafter, objectives of the present works have been listed.

Chapter-2: This chapter has been devoted to the development of the fatigue damage model that will be used to predict the fatigue life of the bridge. Linear damage rule has been modified first by bifurcating the loading history into crack initiation and crack propagation stage to be named as Bilinear Damage Rule (BLDR) in present work, which has been further improved

considering opening stress in the crack propagation stage, which is called as Modified Bilinear Damage Rule (MBLDR). Parametric studies are first conducted on a generic model of axially vibrating bar to examine influence of frequency of loading, stress range, number of modes and damping of the materials on fatigue failure. Experiments are conducted in the laboratory subjecting the ASTM standard specimen to fatigue loading of multiple levels of stress range. The theoretical results of fatigue failure obtained from stress history has been compared with the number of cycles to failures observed in experiments.

Chapter-3: The model of bridge-vehicle interaction has been developed here. Quarter car vehicle model with linear suspension characteristics and damping has been considered. Tyre mass, stiffness and damping has been included. It is assumed that the bridge is subjected to multiple moving vehicles with random arrival time. In the mathematical model, deck profile was considered to be non-homogeneous in presence of variable mean. The orthogonal polynomial expansion method has been employed to devise a semi-analytical technique to find the response statistics.

Chapter-4: In this chapter, numerical results of idealized single span bridge have been presented based on semi-analytical method developed in the present study. Response statistics have been obtained and their time variation for multiple vehicle movement have been presented which are used to obtain dynamic amplification of maximum flexural stresses and fatigue life using present scheme. The effect of random arrival time of vehicle, non-stationary effect for the variable vehicle velocity, random road surface conditions, axle weights, bridge span and amplitude of mean profile on the dynamic amplification of the maximum flexural stresses and fatigue life have been studied.

Chapter-5: In this chapter, response statistics of two span and three span continuous idealized bridge model were obtained. Dynamic amplification factor and fatigue life of two span and three span continuous bridge have been studied to examine the sensitivity of various bridge vehicle parameters. The fatigue life obtained using the present modified rule have been compared with that found in published report (Hahin et al., 1993), which used strain data from an instrumented bridge.

Chapter-6: This chapter is dedicated to the prediction of fatigue life of a steel-concrete composite plate girder bridge adopting a three dimensional finite element model in CSiBridge version 14 considering bridge-vehicle dynamic interaction. To model bridge-vehicle dynamic interaction in presence of uneven pavement, an uncoupled iterative scheme has been used.

Parametric studies including effect of cross girder spacing and eccentricity of vehicle path on the dynamic amplification of the girder's maximum stress and fatigue life have been conducted.

Chapter-7: This chapter summarizes the works done in the thesis and major conclusions that have been arrived from the study. Future scope of the work is also given.

1.8 Closure

In this chapter, the topic of research has been introduced and its practical significance for aiding structural health monitoring has been discussed. The fatigue of bridge that results from vehicle induced stress indicates necessity of survey of the literatures on fatigue damage methods, bridge-vehicle interaction and their utilization in fatigue analysis. The literature review part, therefore, has been split up into required number of sections and subsections. At the end of the literature review, scopes and objectives of the present study have been provided. The organization of the thesis and brief content of each chapter have been given.

2

FATIGUE DAMAGE METHODOLGY

2.1 General

Fatigue failures in metallic structures are a known phenomenon. The fatigue failures were started to be observed in the early 19th century and the early investigation on these failures were done by Wohler (Juvinall, 1967). It was observed that there will be no damage to the structure under a single load application which is far below the static strength of the structure. But, if the same load is repeated many times, it may lead to a complete failure. Such failures occurred without any previous warning. The term fatigue was coined by Poncelet in France before the middle of the 19th century to indicate that the material involved essentially got stressed due to repeated load application, and eventually lead to failure (Juvinall, 1967). Later in the 20th century, it was noted that repeated load applications induce fatigue mechanism in the material leading to nucleation of a microcrack, crack propagation and then leading to complete failure of the structure. The history of engineering structures till now has been observed by numerous fatigue failures of machinery, moving vehicles, welded structures, aircraft, bridges etc (Manson and Halford, 2006). Various factors which lead to fatigue failure are design deficiencies, improper maintenance, fabrication defects and so forth (Reed et al., 1983). It is clearly understood that there are several causes of fatigue failure.

The evaluation of fatigue life of structure is done in design as well as service stage. However, realistic estimation in design phase is more important so that after construction, need of modification or strengthening does not arise. In recent times, many bridges are instrumented from which strain data may be collected and analysed for fatigue life prediction. However, prediction with such structural health monitoring data cannot be validated with real time test results of fatigue failure of the bridge. In view of this, the present study aims to develop fatigue damage methodology considering sequence of loading by bifurcating the damage process into crack initiation and crack propagation and to validate the estimated number of failure cycles with the help of laboratory fatigue testing of axially vibrated bar. The approach, later on, will be applied to estimate fatigue life of different types of bridge models, considering the interaction of the vehicle with the bridge involving randomness in loading and vehicle arrival time.

2.2 Fatigue Damage Process

The process of fatigue damage consists of three stages which are:

(i). Crack nucleation

(ii). Crack initiation

(iii). Crack propagation and fracture

The process of fatigue damage is explained in the sections below.

2.2.1 Crack Nucleation

Crack nucleation can be observed through a variety of crystallographic features. Common nucleation sites in pure metals are tubular holes which are developed in persistent slip bands, slip band extrusion-intrusion pairs at free surfaces and twin boundaries. In polycrystalline metals, grain boundaries are crack nucleation sites. These sites are preferred for the nucleation at high strain rates. The above-mentioned processes also occur in alloys and heterogeneous materials. It is observed from the study that alloying and commercial production practices introduce segregation, inclusions, second-phase particles, and other features that disturb the structure (Boyer, 1985). These phenomena have a significant influence in the process of crack nucleation.

2.2.2 Crack Initiation

The cracks initiate at points of maximum local stress and minimum local strength. The shape of the component and the type and magnitude of loading affects the local stress. Surface and metallurgical imperfections can be areas of stress concentration. Scratches, dents, burrs, cuts and other manufacturing flaws are surface imperfections and are the sites where fatigue cracks initiate.

2.2.3 Crack Propagation and Fracture

Most of the engineering structures contains defects and these become regions of stress concentration which intensifies the strain. The fatigue cracks initiate and grow from these defects. A plastic zone or region of deformation is developed at the defect tip under the action of sustained cyclic loading. This plastic zone which is a zone of high deformation becomes an initiation site for the crack. The crack further propagates under the action of applied stress and ultimately leads to fracture.

2.3 Load Spectra

The fatigue loads on the structure during service are generally referred to as load spectra. The load spectra of the structure give information on the load-time history. The load spectra vary depending on the structure. The wings of the aircraft are subjected to aerodynamic forces during take-off and landing. Runway roughness, touch-down on the ground, and spin-up of the wheels cause high-frequency cycles leading to bending and torsional moments on the wing. Modern street light posts are mostly loaded by wind forces with different intensities coming from different directions. This leads to bending and torsion load cycles with maximum stresses near the base of the pillar. The load spectra for a bridge are considered by the movement of vehicles on the bridge. The major types of loads can be deterministic and stochastic loads. Depending on whether the statistical properties vary as a function of time, stochastic loads are differentiated into stationary and non-stationary load spectra. In the former case, the statistical properties do not vary as a function of time while in the latter, these properties vary during the service usage of the structure (Schijve, 2001). The dynamic effects generate additional small cycles superimposed on the large cycle. Thus, it is necessary to divide a complicated time history into cycles, to count those cycles and to determine an incremental damage for each cycle. Various statistical counting methods for the classification of random stress time histories are available in literatures (Fryba, 1996). In the present study, rainflow counting method has been used and explained in the section below.

2.3.1 Rainflow Counting Method

This method was reported in Japan in 1968 for the first time. The method acquired its name from a notion that water is flowing along a pagoda-shaped roof. The evaluation of random processes with reference to the fatigue of structures is based on the stress-time history shown in Fig 2.1.

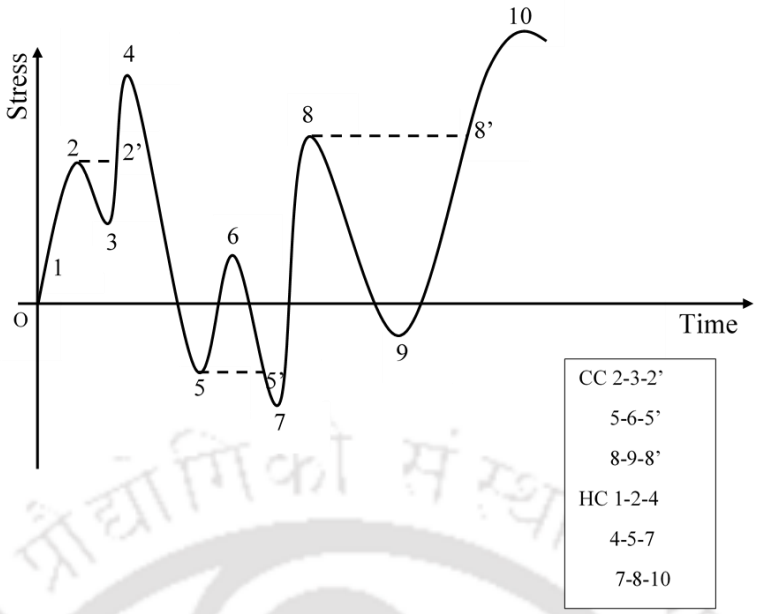

Fig. 2.1 A typical stress time history

Key: CC denotes complete cycles and HC denote half cycles

In Fig. 2.1, *f* and *t* represents stress and time respectively. The basic assumption is that the fatigue damage due to small induced stress cycles may be added to the fatigue damage due to large stress cycles. If the cycle 1- 4 in Fig. 2.1 is interrupted by small cycles 2-3-2', the coordinate of point 2' is very near to the point 2 and the material acts as if no interruption by an inserted cycle has taken place. Moreover, one complete cycle 2-3-2' has remained at disposal.

In rainflow counting method, both the large amplitudes (half cycles) are counted and small inserted stress cycles (complete cycles) are separately counted. The stress time history is then converted into stress cycles and stress ranges after assessment. This method reflects the behaviour of the material and characterizes its hysteresis. For this reason, it is recommended for the evaluation of random stress-time histories with reference to fatigue of materials. Every time interval of stress is counted only once and the same result is obtained, if the evaluation is proceeded in the opposite direction.

The algorithm for rainflow counting (Fryba, 1996) is described below with help of schematic diagram of stress cycle in Fig. 2.2.

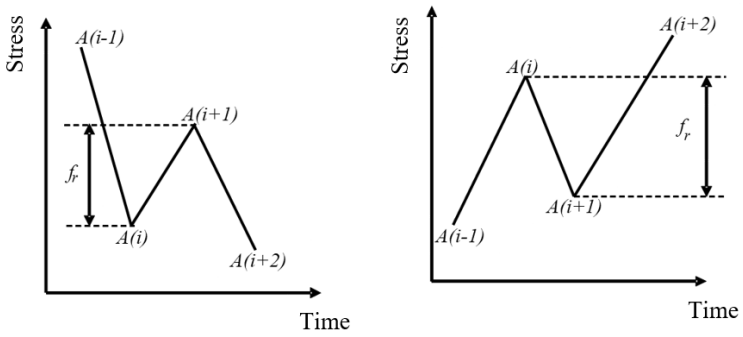

(a) Decaying (b) Rising part of the time history

Fig. 2.2 Two basic cases of complete cycle counting in the Rainflow method

(i). From the stress time history, local peaks $A(0)$, $A(1)$,…, $A(k)$ are read and digitalized.

(ii). The set of local peaks obtained from step 1 is decomposed into half and full cycles.

(iii). The following condition is used for cycle counting (refer Fig. 2.2)

$$A(i-1) \le A(i+1) < A(i) \le A(i+2) \tag{2.1}$$

or

$$A(i-1) \ge A(i+1) > A(i) \ge A(i+2) \tag{2.2}$$

(iv). The computation is proceeded from the lowest $i = 1$ to highest $i = k\text{-}2$. If the above conditions are satisfied, then one cycle will be equal to two half cycles with the stress range,

$$f_r = |A(i) - A(i+1)| \tag{2.3}$$

(v). After computing the stress range in step 4, the peaks $A(i)$ and $A(i+1)$ are eliminated from the sequence of extremes and the sequence is renumbered.

(vi). The steps from 4 and 5 are repeated until at least one cycle is left from the remaining sequence.

(vii). If the stress time history is decomposed into stress ranges and cycles, the stress ranges (absolute values of differences of adjoining extremes) in the remaining sequence are called half cycles.

(viii). The cycles and remaining half cycles of equal magnitude are added after the decomposition. The result obtained is a table of stress range frequencies which is usually represented in the form of frequency histogram and is called the stress range spectrum.

The flow chart depicting the algorithm for rain-flow counting method is shown in Fig. 2.3.

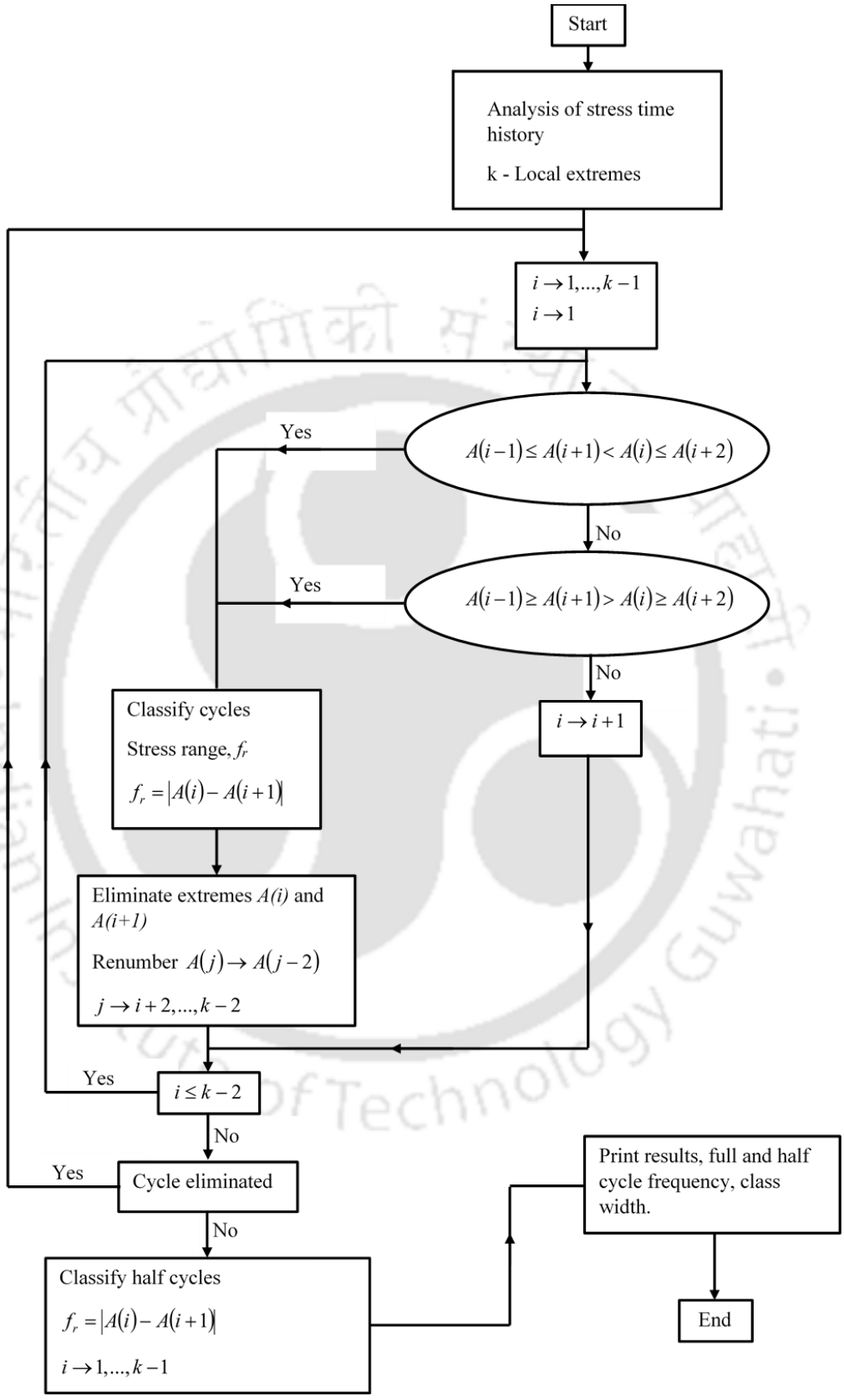

Fig. 2.3 Flow chart of the algorithm for rainflow counting method

2.4 Methods for Determination of Damage Index

The simplest of all deterministic fatigue loads is periodic load, which is defined as constant amplitude load cycle. Empirical data from such constant amplitude tests form the basis for the prediction of fatigue life under complicated time history. In case of complex loading history, the most commonly used damage methodology is Linear Damage Rule (Miner, 1945). Several authors have observed that damage is a non-linear process and it is greatly affected by the sequence of loading (Marco and Starkey, 1954; Manson and Halford, 1981; Benkabouche et al., 2015; Peng et al., 2018). There have been a lot of research on these aspects leading to various damage theories. However, these damage theories are dependent on empirically obtained exponents and have limited evidence in application in real life structure that are exposed to non-deterministic loading. Crack initiation and crack propagation stages play an important role in estimating the total damage index. Present method, however, considers both the stages in estimating damage index, additionally incorporating the effect of crack opening stress with the final aim to apply in bridge models subjected to random vehicular loading.

2.4.1 Damage Accumulation under Deterministic Load

Constant fatigue behaviour is determined experimentally from tests in which a load or deflection is controlled and varied in simple periodic manner until failure. In this, fatigue failure is usually found to depend significantly on only two characteristics of time histories. These two characteristics can be taken as minimum values of stresses f_{min} and maximum values of stresses f_{max} during the cycle shown in Fig. 2.4. An equivalent formulation uses the mean stress value, defined as the average of the minimum and maximum stresses, and stress range value defined as the difference of the maximum and minimum stress.

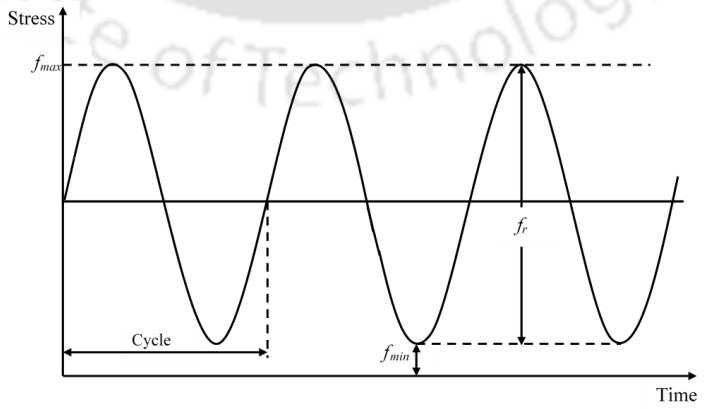

Fig. 2.4 A typical stress history for the constant amplitude loading

Thus, the result of a constant amplitude fatigue test is often described by two bits of information. The stress range, which is denoted by f_r; and number of cycles to failure, denoted by N_f. A typical experimental investigation of constant amplitude fatigue for a specimen of given configuration and material involves a large number of tests. The test results are usually presented in the form of S-N curve with the stress range on the ordinate and the number of cycles on the abscissa.

The typical S-N curve is an ordinary two-dimensional plot shown in Fig. 2.5. Theoretically, though, one can extend the idea of an S-N relationship to more complicated periodic situations, even though the geometry needed to describe the results become more involved. For example, if f_r is a two-dimensional vector representing both stress range and mean stress, then N_f versus f_r is a surface rather than a curve. One could further refine the model by letting f_r include the characteristics of several components of stress, such as a three stress invariants. The basic idea would remain unchanged, though, and the term S-N curve could still be used for the relationship between the observed life N_f and the characteristics of the applied loading which have been included in f_r.

Ignoring any effect of mean stress, we emphasize the dependence of fatigue life on stress range by writing $N_f(f_r)$ for the fatigue life observed for the given stress range value of f_r. In principle, the S-N curve of $N_f(f_r)$ versus f_r could be any non-increasing curve, but experimental data commonly show that a large portion of that curve is well approximated by an equation of the form

$$N_f(f_r) = Kf_r^{-m} \tag{2.4}$$

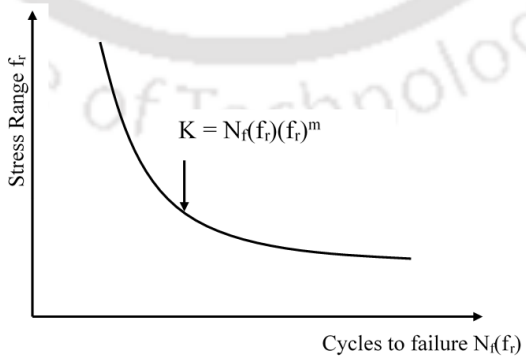

Fig. 2.5 A typical S-N Curve for constant amplitude test results

in which K and m are the positive material constants whose value both depend on both the material and the geometry of the specimen. The S-N plot appears as a straight line on log-log paper shown in Fig. 2.6. For many materials, N_f seems to go to infinity when f_r is smaller than some particular value. This implies that the material can endure infinite number of cycles without failure below this limiting stress and it is known as intrinsic fatigue limit or endurance limit. At the other extreme, a sufficiently large f_r may produce an unstable situation in which failure occurs rapidly.

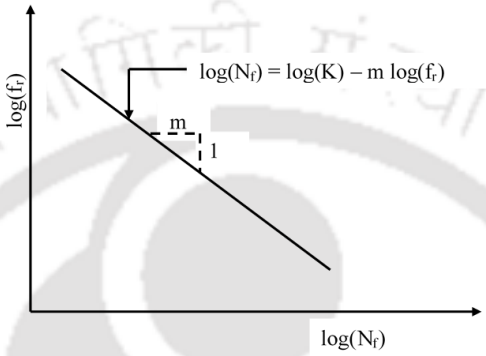

Fig. 2.6 S-N Curve on log-log plot.

The fatigue strength at any particular life is defined as the stress at which the S-N curve cuts the particular value of N_f. A linear equation can be formulated to predict the value of f_r for any particular value of N_f and vice-versa. The following represents the equation of the S-N curve on the log-log plot

$$\log(N_f) = \log(K) - m\log(f_r) \tag{2.5}$$

Once *S-N* curve data is known, a linear damage assumption can be used to evaluate damage index *D*. Let ΔD_j be the incremental damage during the cycle *j* and *N*(*t*) denote the number of applied cycles of load upto time *t*. Thus, one can write

$$D = \sum_{j=1}^{N(t)} \Delta D_j \tag{2.6}$$

Further, let *T* be the failure time, so that $N_f = N(T)$ is the number of cycles to failure. This gives $D = 1$. For periodic constant amplitude loading with stress range f_r, the upper limit of the summation is $N_f(f_r)$. If we assume that the ΔD_j values are all the same throughout the test, the damage per cycle is given by

$$\Delta D_j = \frac{1}{N_f(f_r)} \tag{2.7}$$

2.4.2 Linear Damage Rule (LDR)

Linear Damage Rule (LDR) is one of the easiest methods to predict cumulative damage which was first proposed by Palmgren in 1924 for application to rolling element fatigue of ball bearings made of high-carbon steels (Manson and Halford, 2006). The same hypothesis was proposed in 1945 by Miner and is widely known as Palmgren-Miner rule, LDR or Miner's rule (Miner, 1945). This rule is based on the following assumptions:

(i). The rate of damage accumulation remains constant over each loading cycle.

(ii). Damage occurs and accumulates when the stress level is higher than the intrinsic fatigue limit.

(iii). Failure of the structure or component occurs when cumulative damage reaches unity.

The rule states that failure occurs when the total strain energy due to n cycles of variable amplitude loading is equal to total strain energy from N cycles of constant amplitude loading. The cumulative damage accumulation under variable-amplitude loading is given by

$$D = \sum_{j=1}^{k_b} \Delta D_j = \sum_{j=1}^{k_b} \frac{n_j}{N_j} \tag{2.8}$$

in which ΔD_j is the incremental damage, n_j is the number of stress cycles at stress range level fr_j and N_j is the number of cycles at constant stress range level fr_j from (S-N curve) to cause failure, k_b is the number of stress range blocks in the histogram. The expected life L_f, is then calculated as $L_f = 1/D$.

It has been observed that most metallic materials exhibit complex damage behaviour (Zuo et al., 2015). Metallic materials also exhibit highly non-linear fatigue damage evolution with load dependency (Miller and Zachariah, 1977). Since, the effects of loading sequence and loading history is ignored in the LDR, the cumulative damage accumulation under different loading sequence needs to be further investigated. According to this, research has been conducted to get better and more accurate fatigue life estimates under variable amplitude loading conditions considering the influence of loading sequence and loading history (Aid et al., 2011; Chaboche and Lesne, 1988; Lagoda et al., 2005).

2.4.3 Nonlinear Damage Rule

Richart and Newmark (1948) observed that the damage versus cycle ratio curves should be dependent on the stress level. Taking this into account, a nonlinear damage rule was proposed by Marco and Starkey (1954). The damage is expressed as power function which is load dependent in nonlinear damage rule (Marco and Starkey, 1954). It was observed that a specific functional form for the exponent was not provided by the damage given by Marco and Starkey (1954). Grover (1960) proposed a two stage linearization damage model based on crack initiation and crack propagation. However, the work did not provide a quantitative formulation for separation of life into these two stages. Based on the damage curve concept proposed by Marco and Starkey (1954), Manson and Halford (1981) proposed the Damage Curve Approach (DCA). In this approach, it is assumed that damage accumulation proceeds along a curve associated with the life level at which the cycle ratio is applied. The analytical formulation for the damage curve was based on crack growth model which was empirically formulated. However, the analysis was complex to evaluate the damage index using DCA. The earliest concept proposed for explaining the loading-order effect based on crack initiation and crack propagation was Double Linear Damage Rule (DLDR). The DLDR linearizes the damage curves taking the separation of fatigue process into crack initiation and crack propagation (Manson and Halford, 1981). The assumption in DLDR is that each loading level contributes to crack initiation and crack propagation. But, damage is a cumulative process and only after crack initiation has taken place after a certain loading level, crack propagation will take place.

Taking into consideration various drawbacks of LDR and the non-linearity in damage based on the methods explained above, the following damage evaluation methods known as Bilinear Damage Rule (BLDR) and Modified Bilinear Damage Rule (MBLDR) are proposed in this study. The methods mentioned are explained in detail in section below.

2.5 Proposed Damage Evaluation Methods

In the present study, two damage evaluation methods are proposed. First evaluation method is based on the segregation of crack initiation and crack propagation and second evaluation method is based on the opening stress in the crack propagation phase. The former is BLDR and the latter is MBLDR. Both the methods take into account the load interaction effects.

2.5.1 Bilinear Damage Rule (BLDR)

The stress ranges are segregated into two phases namely Phase-1 and Phase-2 which corresponds to the crack initiation phase and crack propagation phase. Crack initiation phase comprise of low cycles of loading and crack propagation phase comprise of high cycles of loading. The transition point from Phase-1 to Phase-2 is referred to as knee-point in this paper. The equation representing Phase-1 and Phase-2 loading is expressed as (Manson and Halford, 1981)

$$\left(\frac{n_1^*}{N_1^*}\right)^{\left(N_1^*/N_2^*\right)^{\alpha}} + \frac{n_2^*}{N_2^*} = 1 \tag{2.9}$$

where, N_1^* is the fatigue life for low cycle of loading, N_2^* is the fatigue life for high cycle of loading (considering damage of the order of 10^{-3}), n_1^* is the cycles for N_1^* life, n_2^* is the cycles for N_2^* life and α is the material constant (Manson and Halford, 1981). The above equation when plotted results in a continuous curve which is shown in Fig 2.7. On segregating the damage curve into Phase-1 and Phase-2, knee-point, k is formed, which is shown in Fig. 2.8.

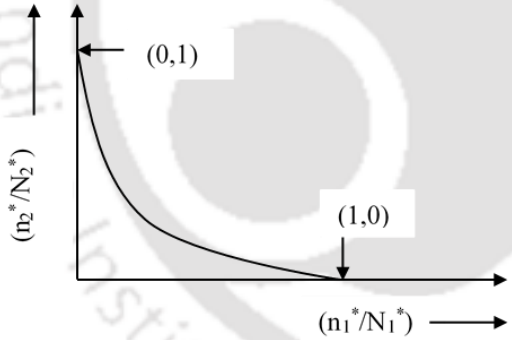

Fig. 2.7 Schematic representation of damage curve

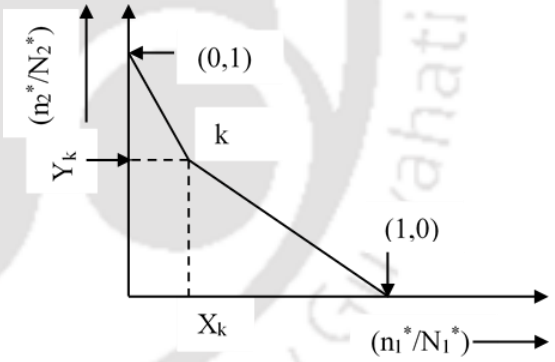

Fig.2.8 Schematic representation of damage curve showing knee-point

In Fig. 2.8, X_k and Y_k denote the knee-point coordinates in X-axis and Y-axis respectively. The knee-point depends on the transition from Phase-1 to Phase-2, which can be observed from Fig. 2.8. Thus, the knee-point coordinates (X_k, Y_k) are dependent on Phase-1 and Phase-2 loading levels (Manson and Halford, 1981). The coordinates of the knee-point (Manson and Halford, 1981) are given in Eq. (2.10).

$$X_k = 1 - A_m \left[\frac{N_1^*}{N_2^*} \right]^{\alpha}$$
$$Y_k = 1 - B_m \left[\frac{N_1^*}{N_2^*} \right]^{\alpha} \tag{2.10}$$

where,

$$\alpha = -0.25, A_m = 0.65, B_m = 0.35 \tag{2.11}$$

The constants α, A_m and B_m correspond to mild steel (Manson and Halford, 1981). The damage line when plotted does not have slope as unity as shown in Fig. 2.9. The slopes for the damage line are tan θ_1 and tan θ_2 as shown in Fig. 2.9. θ_1 and θ_2 are the angles subtended by the damage line due to Phase-1 loading and Phase-2 loading with respect to x-axis respectively. X_{knew} and Y_{knew} are the new knee-point coordinates in x-axis and y- axis respectively which is shown in Fig. 2.9.

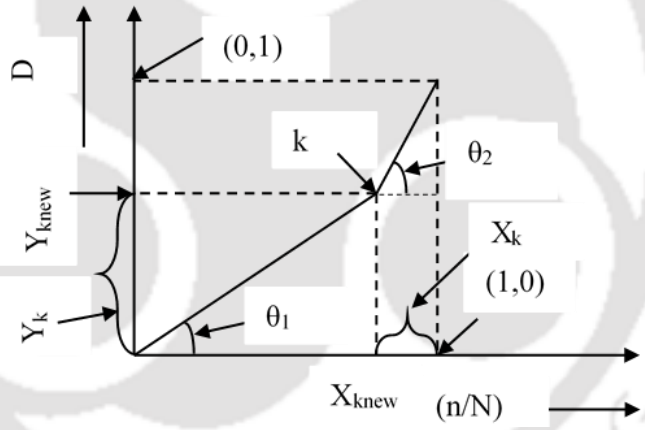

Fig. 2.9 Schematic representation of damage versus cycle ratio

In Fig. 2.9, the new knee-point coordinates are given as,

$$X_{knew} = 1 - X_k$$
$$Y_{knew} = Y_k \tag{2.12}$$

The new knee-point coordinates, (X_{knew}, Y_{knew}) given in Eq. (2.12) are then used to evaluate damage in Phase-1, D_1 and damage in phase-2, D_2.

In Fig. 2.9, the ordinate in Phase-1 represents damage in Phase-1 loading, D_1 which is expressed as,

$$D_1 = \sum_{a=1}^{b} \tan\theta_1 \left(\frac{n_a}{N_a} \right) \tag{2.13}$$

where, b is the loading level and $\tan\theta_1$ is expressed as,

$$\tan\theta_1 = \frac{Y_{knew}}{X_{knew}} \tag{2.14}$$

In order to take into account, the damage caused due to cycles from different stress ranges, a factor β_a is used where, the subscript a denotes the loading level. This factor is introduced in the damage equation which is expressed as,

$$D_1 = \tan\theta_1 \left\{ \left(\frac{n_1}{N_1} \right)^{\beta_1} + \left(\frac{n_2}{N_2} \right)^{\beta_2} + \ldots + \left(\frac{n_{b-1}}{N_{b-1}} \right)^{\beta_{b-1}} + \frac{n_b}{N_b} \right\} \tag{2.15}$$

Although, in the study, the damage is characterized by loading in Phase-1 and Phase-2, there is a need to consider the influence of the previous stress range to the current stress range which is accomplished by the factor, β_a. Since, the number of cycles to failure depend on the stress range, therefore β_a is expressed in terms of the number of cycles to failure,

$$\beta_a = \frac{N_a}{N_{a+1}}; a = 1, 2, \ldots, b \tag{2.16}$$

The ordinate in Phase-2 represents the damage, D_2 which is expressed as,

$$D_2 = \sum_{a=b+1}^{p} \tan\theta_2 \left(\frac{n_a}{N_a} \right) \tag{2.17}$$

where, p is the loading level and $\tan\theta_2$ is expressed as,

$$\tan\theta_2 = \frac{1 - Y_{knew}}{1 - X_{knew}} \tag{2.18}$$

Due to dependence on the stress range, Eq. (2.17) is written as,

$$D_2 = \tan\theta_2 \left\{ \left(\frac{n_{b+1}}{N_{b+1}} \right)^{\beta_{b+1}} + \left(\frac{n_{b+2}}{N_{b+2}} \right)^{\beta_{b+2}} + \ldots + \left(\frac{n_{p-1}}{N_{p-1}} \right)^{\beta_{p-1}} + \frac{n_p}{N_p} \right\} \tag{2.19}$$

The factor β_a is expressed as,

$$\beta_a = \frac{N_a}{N_{a+1}}; a = b+1, ..., p \tag{2.20}$$

The total damage, D is the summation of damage in Phase-1 loading and Phase-2 and is expressed as,

$$D = D_1 + D_2 \tag{2.21}$$

2.5.2 Modified Bilinear Damage Rule (MBLDR)

The effect of opening stress is considered in Phase-2 to compute low life level, N_2'. Damage in Phase-2, D_2' i.e., crack propagation phase is imparted by a crack only if the loading cycle is sufficient to overcome a capacity for resisting fatigue damage intrinsic to the material. An opening stress f_{os}, dependent on cyclic yield stress f_y, maximum stress f_{max} and minimum stress f_{min} corresponding to the largest rainflow cycle, is used to define effective strain range given as (Pereira et. al., 2009),

$$f_{os} = \alpha_1 f_{\max}\left[1 - \left(\frac{f_{\max}}{f_y}\right)^2\right] - \beta_{new} f_{\min} \tag{2.22}$$

where, α_1 and β_{new} are material constants, which are 0.75 and 0 respectively (Pereira et. al., 2009). Assuming that the magnitudes of crack opening stresses occur in a linear elastic region, the opening strain, ε_{os} is determined as,

$$\varepsilon_{os} = \varepsilon_{\min} + \frac{f_{os} - f_{\min}}{E} \tag{2.23}$$

where, ε_{min} is the minimum strain in the particular cycle considered in Phase-2 loading and E is the modulus of elasticity of the material. The opening strain is assumed to be constant throughout. The effective strain range, $\Delta\varepsilon_{eff}$ is defined as,

$$\begin{aligned} \Delta\varepsilon_{eff} &= \varepsilon_{\max} - \varepsilon_{\min}, \varepsilon_{\min} > \varepsilon_{os} \\ \Delta\varepsilon_{eff} &= \varepsilon_{\max} - \varepsilon_{os}, \varepsilon_{\min} < \varepsilon_{os} \end{aligned} \tag{2.24}$$

where, ε_{max} is the maximum strain in the particular cycle considered in Phase-2 loading. The microcracks remain open even below intrinsic fatigue limit, $\Delta\varepsilon_i$ (Pereira et. al., 2009; Yen et al., 2013); the net effective strain range, $\Delta\varepsilon^*$ for each cycle of Phase-2 loading is given as,

$$\Delta\varepsilon^{*} = \Delta\varepsilon_{eff} - \Delta\varepsilon_{i} \tag{2.25}$$

The net effective stress range in Phase-2, Δf_{eff} is then computed using the net effective strain range and is expressed as,

$$\Delta f_{eff} = E\Delta\varepsilon^{*} \tag{2.26}$$

The low life level, N_2' is then computed using the net effective stress range, Δf_{eff}. Using low life level and high life level, N_1' and N_2', knee-point coordinates (X_k', Y_k') is then computed as

$$\begin{aligned} X_k' &= 1 - A_m\left[\frac{N_1'}{N_2'}\right]^{\alpha} \\ Y_k' &= 1 - B_m\left[\frac{N_1'}{N_2'}\right]^{\alpha} \end{aligned} \tag{2.27}$$

where α, A_m and B_m are material constants corresponding to mild steel (Manson and Halford, 1981). The ordinate in Phase-1 and Phase-2, shown in Fig. 2.9, represents the damage, D_1' and D_2' which is expressed as

$$D_1' = \tan\theta_1'\left\{\left(\frac{n_1}{N_1}\right)^{\beta_1} + \left(\frac{n_2}{N_2}\right)^{\beta_2} + \ldots + \left(\frac{n_{b-1}}{N_{b-1}}\right)^{\beta_{b-1}} + \frac{n_b}{N_b}\right\} \tag{2.28}$$

$$D_2' = \tan\theta_2'\left\{\left(\frac{n_{b+1}}{N_{b+1}}\right)^{\beta_{b+1}} + \left(\frac{n_{b+2}}{N_{b+12}}\right)^{\beta_{b+2}} + \ldots + \left(\frac{n_{p-1}}{N_{p-1}}\right)^{\beta_{p-1}} + \frac{n_p}{N_p}\right\} \tag{2.29}$$

where β_b is load interaction factor at bth load level as explained in Eqs. (2.16) and (2.20), $\tan\theta_1'$ and $\tan\theta_2'$ are slopes of two phases of damage line, obtained as

$$\tan\theta_1' = \frac{Y_{knew}'}{X_{knew}'} \tag{2.30}$$

$$\tan\theta_2' = \frac{1 - Y_{knew}'}{1 - X_{knew}'} \tag{2.31}$$

In Eqs. (2.30) and (2.31), new knee point coordinates (X_{knew}', Y_{knew}') is given as

$$\begin{aligned} X_{knew}' &= 1 - X_k' \\ Y_{knew}' &= Y_k' \end{aligned} \tag{2.32}$$

The summation of damage in Phase-1 loading and Phase-2 loading gives the total damage *D'* and is expressed as,

$$D' = D_1' + D_2' \tag{2.33}$$

Failure occurs when the damage is unity.

The damage evaluation methods explained in section 2.5.1 and section 2.5.2 are then implemented on a slender bar subjected to dynamically varying axial loads. A coupon specimen of ASTM E606 standards is then experimentally subjected to axially varying cyclic load using UTM 250 kN and the results obtained are then validated with the fatigue life proposed in the study.

2.6 Implementation of BLDR and MBLDR to Axially Vibrated Bar

In the present study, our aim is to evaluate the fatigue damage of bridge from vehicle induced stress history using the proposed approach. Before applying the approach to a bridge structure with bridge-vehicle interaction, we first illustrate the proposed two approaches with examination of the various influencing parameters considering an axially vibrated bar. The specimen of axially vibrated bar is chosen so that the theories can be verified by conducting fatigue testing with cyclic loading till the failure occurs. The service life of an actual bridge is predicted, in general, from the strain data obtained from an instrumented bridge but the value of such prediction has never been verified or can be verified by conducting in-situ fatigue testing till failure of the bridge. Therefore, the present section illustrates a numerical example of an axially loaded bar and also by validation study of the proposed approaches by conducting fatigue testing till occurrence of failure.

The axial vibration of bar subjected to dynamic load is shown in Fig. 2.10. The length, area of cross-section, modulus of elasticity of the bar and mass density is represented by L_a, A, E and ρ respectively. The exciting force is represented as $P(x,t)$.

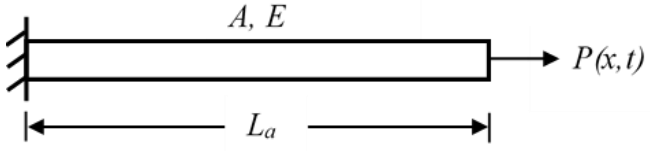

Fig. 2.10. Axially loaded bar with time varying load

The equation of motion is given as

$$AE\frac{\partial^2 u}{\partial x^2} - \rho A\frac{\partial^2 u}{\partial t^2} - c\frac{\partial u}{\partial t} = -P(x,t) \tag{2.34}$$

where, *u(x,t)* is the axial displacement of the bar and *c* is the damping coefficient of the bar. Since, exciting force *P(x,t)* is acting at the free end of the bar, it is expressed in terms of Dirac delta function,

$$P(x,t) = P(t)\delta(x - L_a) \tag{2.35}$$

in which δ is Dirac delta function. The exciting force is considered to be composed of different harmonics. A constant mean force P_0 is considered to be super imposed over the harmonically varying force. The expression for exciting force can now be written as

$$P(t) = P_0 + \sum_{j=1}^{n} P_j \sin \omega_j t \tag{2.36}$$

where, P_0 is the mean force, P_j is the amplitude of the jth harmonic excitation, ω_j is the jth excitation frequency. Using mode superposition method (Meirovitch, 1986), the axial displacement of the bar, *u(x,t)* is given as

$$u(x,t) = \sum_{i=1}^{\infty} \phi_i(x)\eta_i(t) \tag{2.37}$$

where, $\eta_i(t)$ is the generalized coordinate in the i^{th} mode and $\phi_i(x)$ is the normalized mode shape function in the ith mode for one end fixed and other end free and is given as

$$\phi_i(x) = \sqrt{\frac{2}{\rho A L_a}} \sin\frac{(2i-1)\pi}{2L_a} x \tag{2.38}$$

Substituting Eq. (2.37) and Eq. (2.35) in Eq. (2.34),

$$\sum_{i=1}^{\infty}\left\{\frac{d}{dx}\left[AE\frac{d\phi_i}{dx}\right]\eta_i(t) - \rho A\frac{d^2\eta_i}{dt^2}\phi_i(x) - c\frac{d\eta_i}{dt}\phi_i(x)\right\} = -P(t)\delta(x - L_a) \tag{2.39}$$

In Eq. (2.39),

$$-\frac{d}{dx}\left[AE\frac{d\phi_i}{dx}\right] = \omega_{ni}^2 \rho A \phi_i(x) \tag{2.40}$$

In Eq. (2.40), ω_{ni} is the natural frequency of the bar in the i^{th} mode and is given as

$$\omega_{ni} = \frac{(2i-1)}{2}\frac{\pi}{L_a}\sqrt{\frac{E}{\rho}} \tag{2.41}$$

Substituting Eq. (2.40) in Eq. (2.39),

$$\sum_{i=1}^{\infty}\left[\rho A\phi_i(x)\ddot{\eta}_i(t) + c\phi_i(x)\dot{\eta}_i(t) + \omega_{ni}^2\rho A\phi_i(x)\eta_i(t)\right] = P(t)\delta(x-L_a) \tag{2.42}$$

Multiply both sides of Eq. (2.42) by $\phi_k(x)$ and integrate over the domain to use the orthogonality condition of normal modes which is expressed as

$$\int_0^L \rho A\phi_i(x)\phi_k(x) = \delta_{ik} \tag{2.43}$$

where, δ_{ik} is the Kronecker delta function. Substituting the above orthogonality property shown in Eq. (2.43) in Eq. (2.42),

$$\ddot{\eta}_i(t) + 2\xi_i\omega_{ni}\dot{\eta}_i(t) + \omega_{ni}^2\eta_i(t) = Q_i(t) \tag{2.44}$$

where, ξ_i is the damping coefficient of the bar in the i^{th} mode and

$$\begin{aligned} Q_i(t) &= \int_0^{L_a} P(t)\delta(x-L_a)\phi_i(x)dx \\ &= P(t)\phi_i(L_a) \\ &= P(t)\sqrt{\frac{2}{\rho AL_a}}\sin\frac{(2i-1)\pi}{2} \end{aligned} \tag{2.45}$$

The solution of generalized coordinate in time domain is obtained using homogeneous solution, $\eta_{hi}(t)$ and particular solution, $\eta_{pi}(t)$ (Meriovitch, 1986). Homogeneous solution is obtained by taking the forcing function as zero. Let $\eta_{hi}(t)$ be the homogeneous solution expressed as

$$\eta_{hi}(t) = Ae^{st} \tag{2.46}$$

Substitution of Eq. (2.46) in Eq. (2.44) with $Q_i(t) = 0$ yields,

$$s^2 + 2\xi_i\omega_{ni}s + \omega_{ni}^2 = 0 \tag{2.47}$$

The solution of the quadratic equation in Eq. (2.47) is given as

$$s_1, s_2 = \left(-\xi_i \pm \sqrt{\xi_i^2 - 1}\right)\omega_{ni} \tag{2.48}$$

Substituting Eq. (2.48) in Eq. (2.46), one obtains

$$\eta_{hi}(t) = A_1 e^{s_1 t} + A_2 e^{s_2 t} \tag{2.49}$$

Using Eq. (2.48) in Eq. (2.49), the homogeneous solution, $\eta_{hi}(t)$ is obtained as

$$\eta_{hi}(t) = e^{-\xi_i \omega_{ni} t}\left(A_i' \cos \omega_{di} t + B_i' \sin \omega_{di} t\right) \tag{2.50}$$

The particular solution, $\eta_{pi}(t)$ is obtained using Duhamel Integral (Meirovitch, 1986) and is given as

$$\begin{aligned}\eta_{pi}(t) = {} & \frac{P_0}{\omega_{ni}^2}\sqrt{\frac{2}{\rho A L_a}} - \\ & \frac{P_0}{\omega_{di}\omega_{ni}}\sqrt{\frac{2}{\rho A L_a}} e^{-\xi_i \omega_{ni} t}\left\{\xi_i \sin \omega_{di} t + \sqrt{1-\xi_i^2}\cos \omega_{di} t\right\} \\ & + \frac{1}{\omega_{ni}^2}\sqrt{\frac{2}{\rho A L_a}} \sum_{j=1}^{n} \frac{P_j \sin\left(\omega_j t + \phi_j\right)}{\sqrt{\left(1-r_j^2\right)^2 + \left(2\xi r_j\right)^2}}\end{aligned} \tag{2.51}$$

The general solution, $\eta_i(t)$ is obtained by superimposition of homogeneous solution, $\eta_{hi}(t)$ and particular solution, $\eta_{pi}(t)$, as

$$\begin{aligned}\eta_i(t) = {} & e^{-\xi_i \omega_{ni} t}\left\{A_i' \cos \omega_{di} t + B_i' \sin \omega_{di} t\right\} + \frac{P_0}{\omega_{ni}^2}\sqrt{\frac{2}{\rho A L_a}} - \\ & \frac{P_0}{\omega_{di}\omega_{ni}}\sqrt{\frac{2}{\rho A L_a}} e^{-\xi_i \omega_{ni} t}\left\{\xi_i \sin \omega_{di} t + \sqrt{1-\xi_i^2}\cos \omega_{di} t\right\} \\ & + \frac{1}{\omega_{ni}^2}\sqrt{\frac{2}{\rho A L_a}} \sum_{j=1}^{n} \frac{P_j \sin\left(\omega_j t + \phi_j\right)}{\sqrt{\left(1-r_j^2\right)^2 + \left(2\xi r_j\right)^2}}\end{aligned} \tag{2.52}$$

where, ξ_i is the damping ratio, ω_{ni} and ω_{di} is natural frequency and damped frequency of bar in the ith mode, ϕ_j and r_j is the phase angle and frequency ratio in the jth excitation.

Let initial displacement and initial velocity be $\eta_i(0)$ and $\dot{\eta}_i(0)$ respectively. The constants A' and B' are obtained from initial conditions explained below.

At time $t = 0$, the axial displacement and velocity of the bar are given as

$$u(x,0)=\sum_{i=1}^{\infty}\phi_i(x)\eta_i(0) \tag{2.53}$$

$$\dot{u}(x,0)=\sum_{i=1}^{\infty}\phi_i(x)\dot{\eta}_i(0) \tag{2.54}$$

Multiply Eqs. (2.53) and (2.54) by $\phi_k(x)$ and integrate over the domain to use the orthogonality condition of normal modes given in Eq. (2.43). The axial displacement and velocity of the bar at t = 0 is 0. Thus, one obtains $\eta_i(0)$ = 0 and its derivative $\dot{\eta}_i(0)$ = 0 after utilizing the orthogonality condition and the initial conditions. The constant A' and B' are then obtained by solving two simultaneous linear equations. The constants are given below

$$\begin{aligned} A_i^{'} &= -\frac{1}{\omega_i^2}\sqrt{\frac{2}{\rho AL_a}}\sum_{j=1}^{n}\frac{P_j\sin\phi_j}{\sqrt{\left(1-r_j^2\right)^2+\left(2\xi r_j\right)^2}} \\ B_i^{'} &= \frac{1}{\omega_{di}}\left\{\xi_i\omega_i A_i^{'}-\frac{1}{\omega_i^2}\sqrt{\frac{2}{\rho AL_a}}\sum_{j=1}^{n}\frac{P_j\omega_j\cos\phi_j}{\sqrt{\left(1-r_j^2\right)^2+\left(2\xi r_j\right)^2}}\right\} \end{aligned} \tag{2.55}$$

Using mode superposition method (Meirovitch, 1986) the dynamic stresses are given as,

$$f(x,t)=AE\sum_{i=1}^{\infty}\phi_i'(x)\eta_i(t) \tag{2.56}$$

where, $f(x,t)$ is the dynamic stress.

2.6.1 Numerical Example

The present method is illustrated with an example of slender bar of length 100 mm, width 30 mm and thickness 4 mm. The material considered is mild steel. The yield stress is 250 MPa, modulus of elasticity is 2×10^5 MPa, Poisson's ratio is 0.3, fatigue detail constant is 250×10^8 ksi (1.72369×10^{11} MPa) and fatigue exponent is taken as -3 (Fisher, 1977). The dynamic stress obtained from Eq. (2.56), is decomposed using rainflow counting method to obatin stress range versus frequency (cycles) histogram. The effect of frequency of loading, stress range, damping and number of modes are studied to evaluate the fatigue damage on the structural member.

2.6.1.1 Effect of frequency of loading

The mean excitation force and the amplitude of the harmonic force is considered as 10 kN. The damping of the material is considered as 2%. The dynamic stresses obtained by varying the

frequency of loading from 10 Hz to 70 Hz with a difference of 10 Hz is shown in Figs. 2.11 to 2.17. The comparison of histogram of stress range versus number of cycles for different frequncy of excitation is shown in Figs. 2.18 to 2.24. The comparison of frequency of loading and damage index is shown in Fig. 2.25.

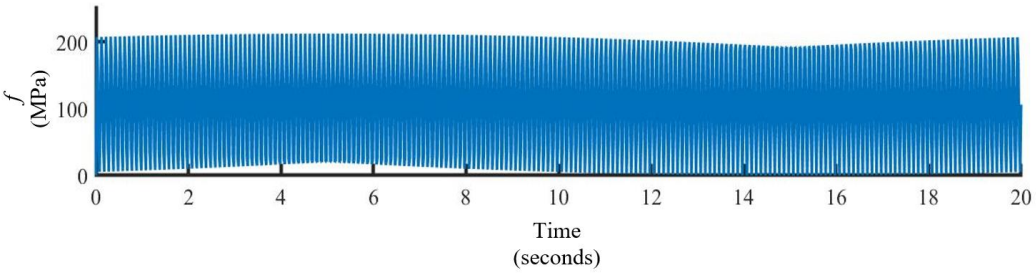

Fig. 2.11 Stress time history for 10 Hz excitation frequency

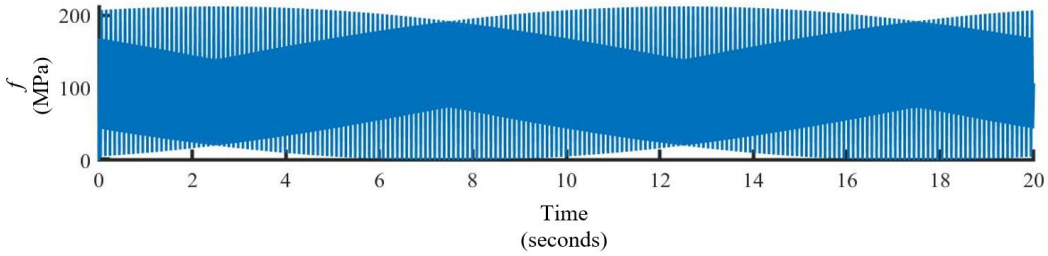

Fig. 2.12 Stress time history for 20 Hz excitation frequency

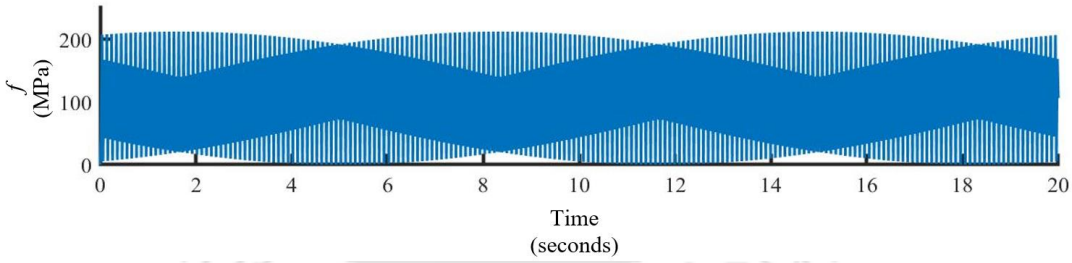

Fig. 2.13 Stress time history for 30 Hz excitation frequency

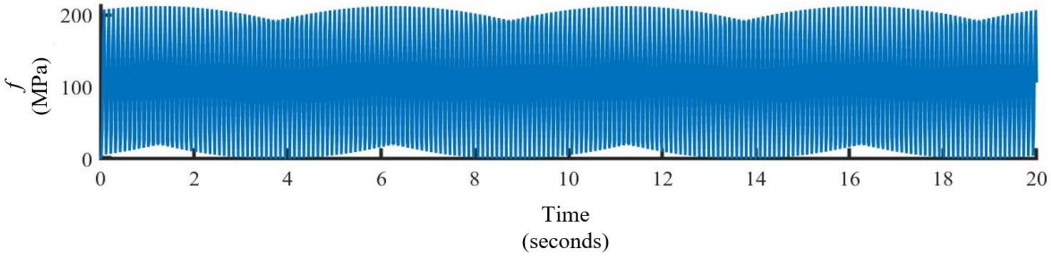

Fig. 2.14 Stress time history for 40 Hz excitation frequency

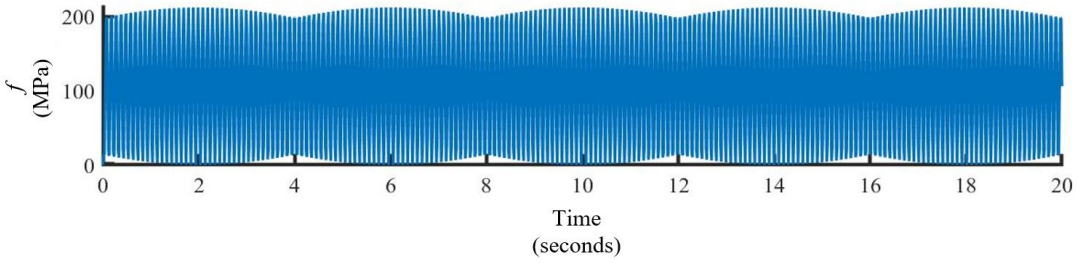

Fig. 2.15 Stress time history for 50 Hz excitation frequency

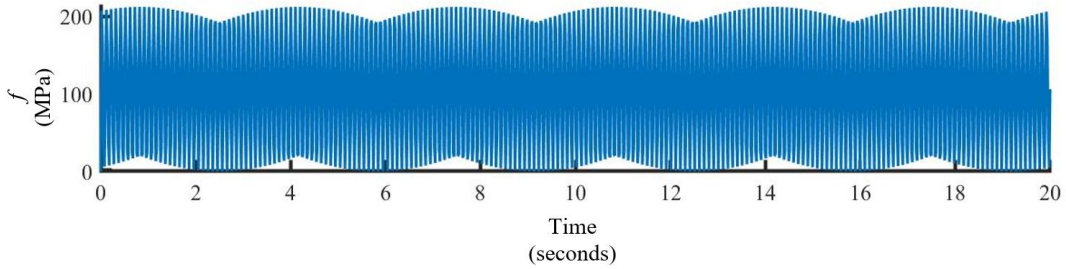

Fig. 2.16 Stress time history for 60 Hz excitation frequency

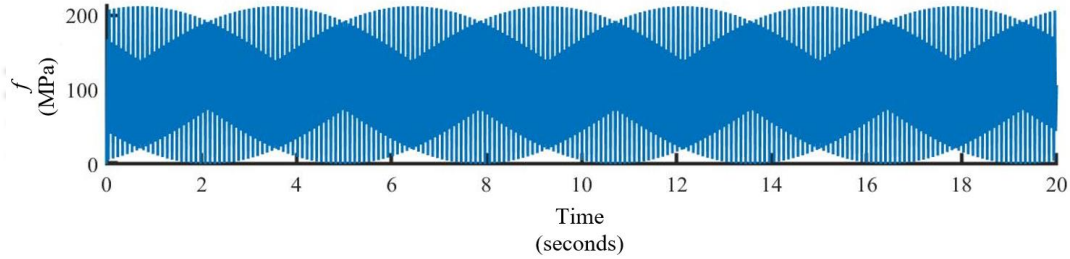

Fig. 2.17 Stress time history for 70 Hz excitation frequency

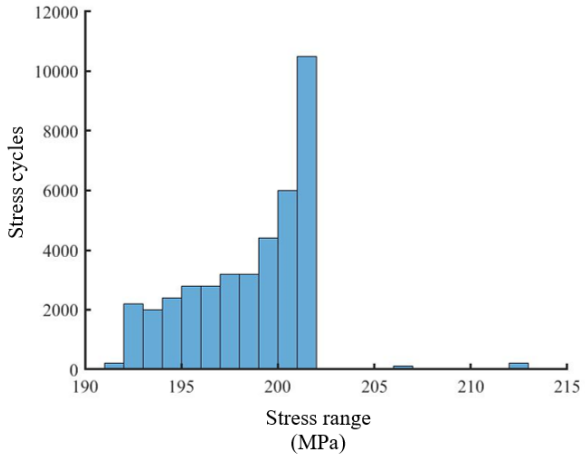

Fig. 2.18 Stress range histogram for 10 Hz excitation frequency

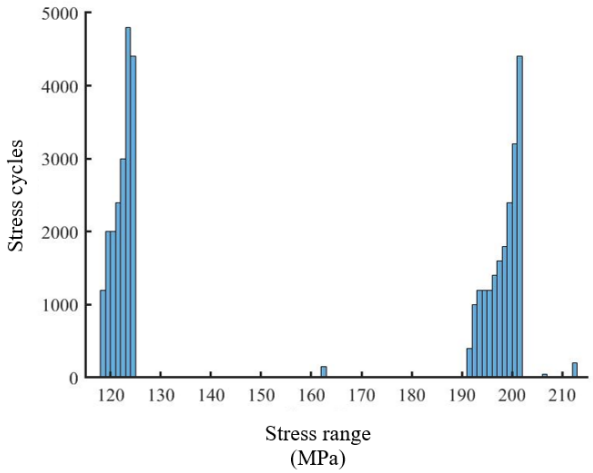

Fig. 2.19 Stress range histogram for 20 Hz excitation frequency

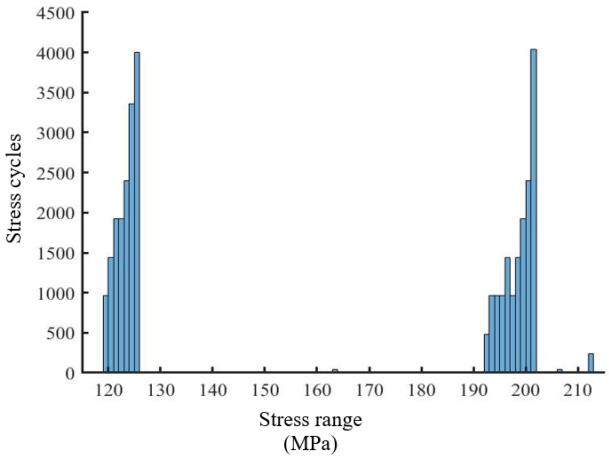

Fig. 2.20 Stress range histogram for 30 Hz excitation frequency

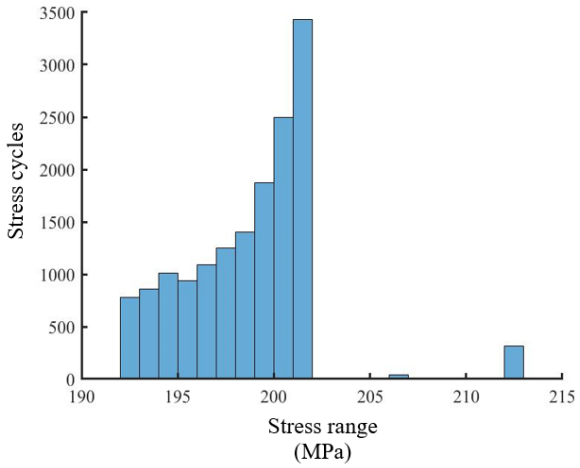

Fig. 2.21 Stress range histogram for 40 Hz excitation frequency

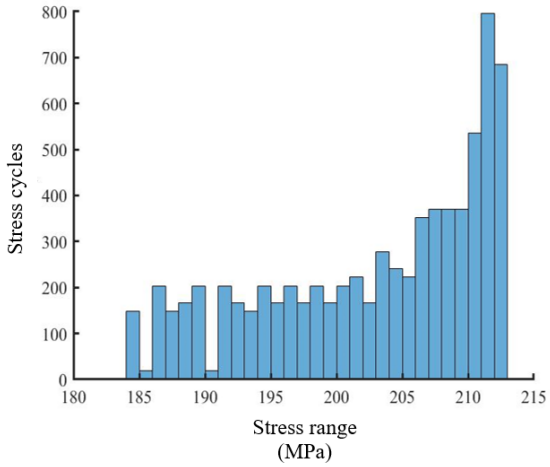

Fig. 2.22 Stress range histogram for 50 Hz excitation frequency

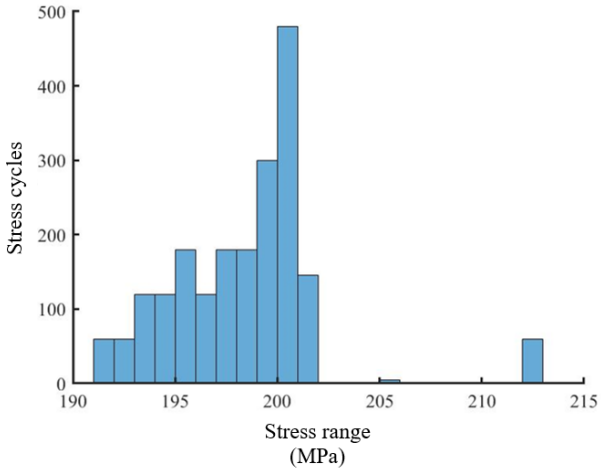

Fig. 2.23 Stress range histogram for 60 Hz excitation frequency

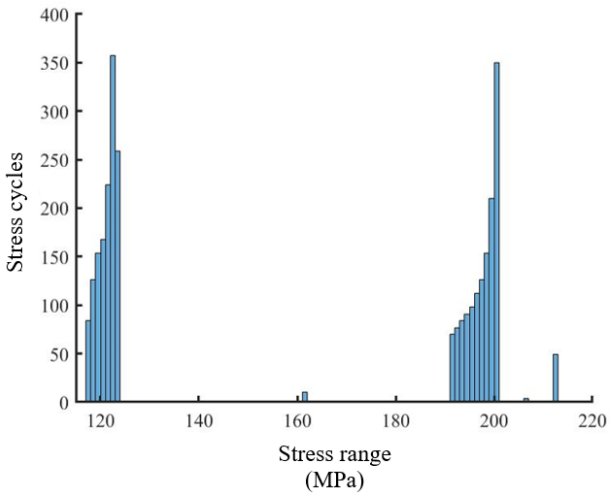

Fig. 2.24 Stress range histogram for 70 Hz excitation frequency

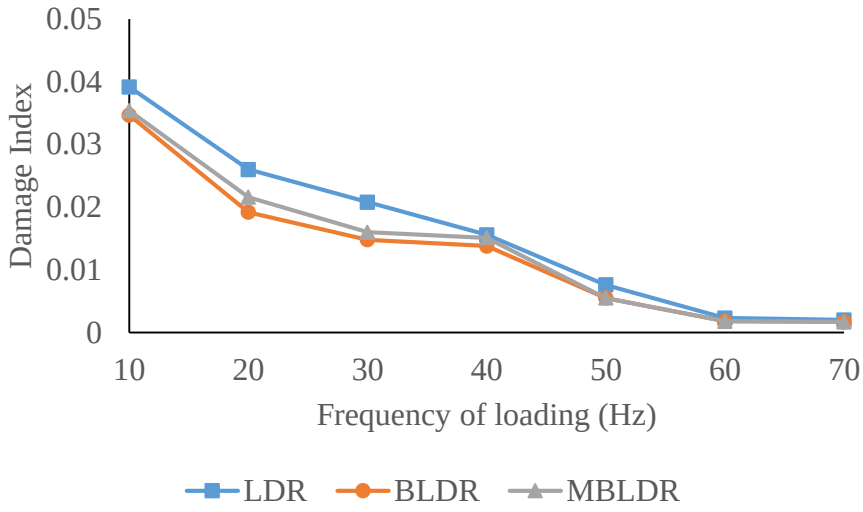

Fig. 2.25. Comparison of damage index with frequency of loading

It is observed from Figs. 2.11 to 2.17 that the dynamic stress time history is oscillatory in nature. The magnitude of maximum dynamic stresses remains the same but the cyclic frequency of stresses increases with the increase in the frequency of loading, as expected in case of linear vibration theory. The stress cycles for stress range is more for lower frequency of excitation thus contributing to higher damage as observed from Figs. 2.18 to 2.24. From Fig. 2.25, it is observed that fatigue strength increases with frequency of loading resulting in lower damage index. Due to increase of loading frequency, the slip systems causing crack propagation tend to be less active. The activation energy required for dislocation of grains possess large value resulting in lower damage index (Papakyriacou et al., 2001).

The damage index evaluated from LDR is more compared to BLDR and MBLDR. The effect of loading order is neglected in LDR resulting in higher damage index. It is also observed that the MBLDR estimates more damage index as compared to BLDR due to the consideration of opening stress in Phase-2. But, as loading frequency increases, the damage index obtained from BLDR and MBLDR are almost the same.

2.6.1.2 Effect of Stress Range

The frequencies of loading are considered as 10 Hz and 20 Hz. The damping of the material is considered as 2%. The amplitude of total excitation force is varied as 3.75 kN, 7.5 kN, 15 kN, 30 kN and 45 kN and the corresponding stress range is varied as 31.25 MPa, 62.5 MPa, 125 MPa, 250 MPa and 375 MPa. The dynamic stresses obtained by varying the stress range is shown in Figs. 2.26 to 2.30. The comparison of histogram of stress range versus number of

cycles for different stress range is shown in Figs. 2.31 to 2.35. The comparison of stress range and damage index is shown in Fig. 2.36.

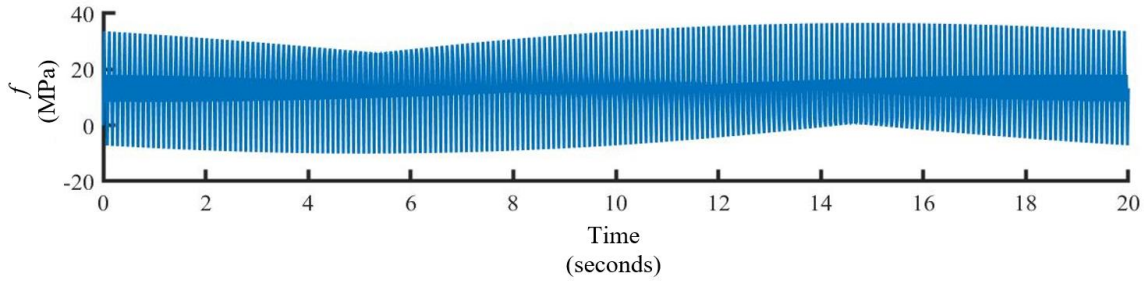

Fig. 2.26 Stress time history for stress range 31.25 MPa

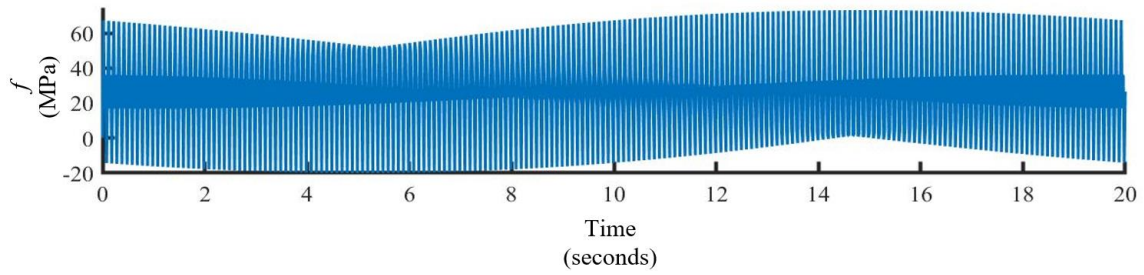

Fig. 2.27 Stress time history for stress range 62.5 MPa

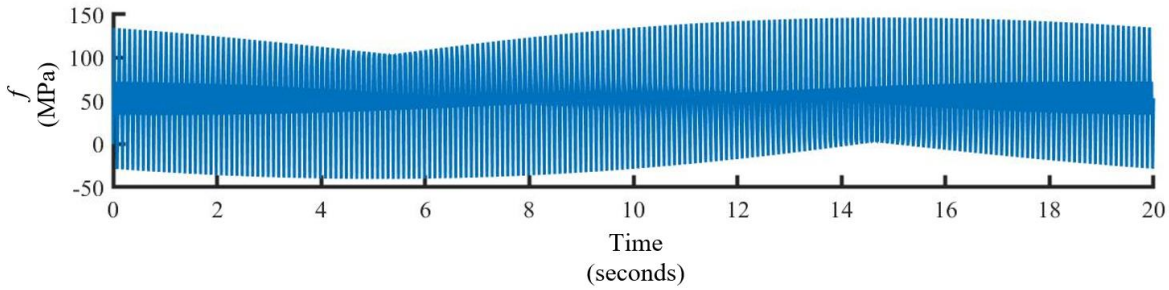

Fig. 2.28 Stress time history for stress range 125 MPa

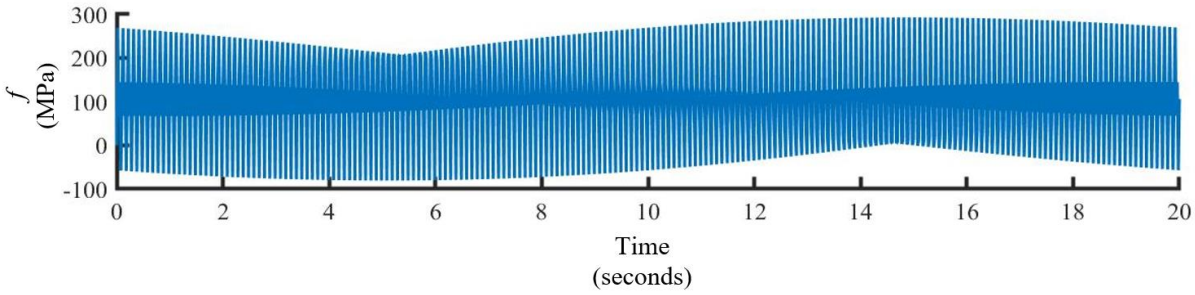

Fig. 2.29 Stress time history for stress range 250 MPa

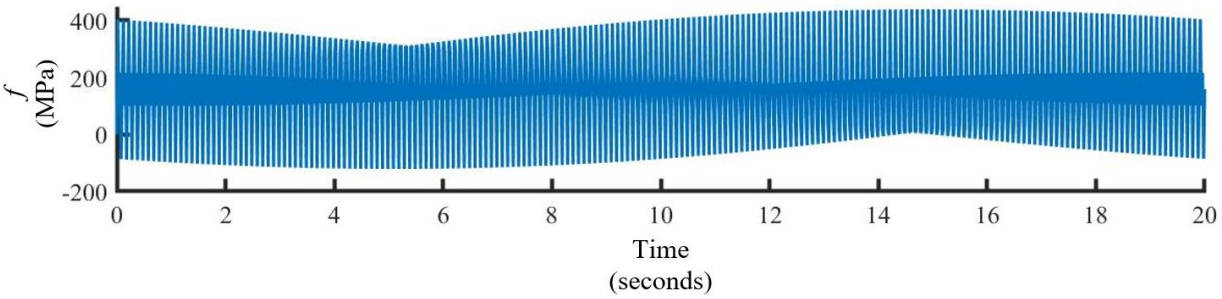

Fig. 2.30 Stress time history for stress range 375 MPa

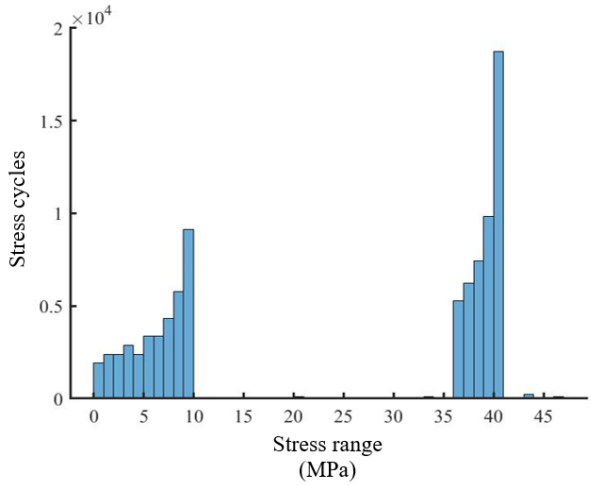

Fig. 2.31 Stress range histogram for stress range 31.25 MPa

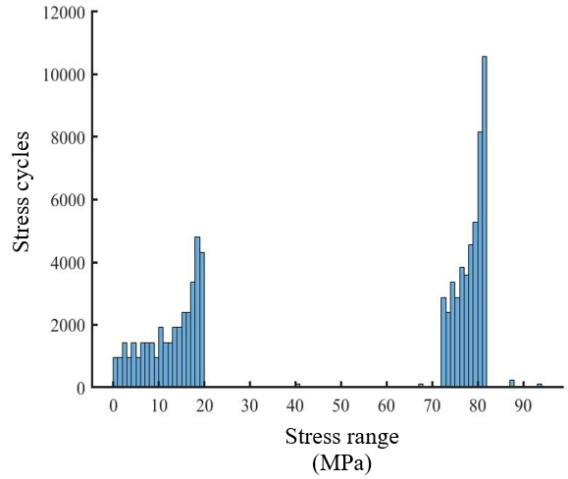

Fig. 2.32 Stress range histogram for stress range 62.5 MPa

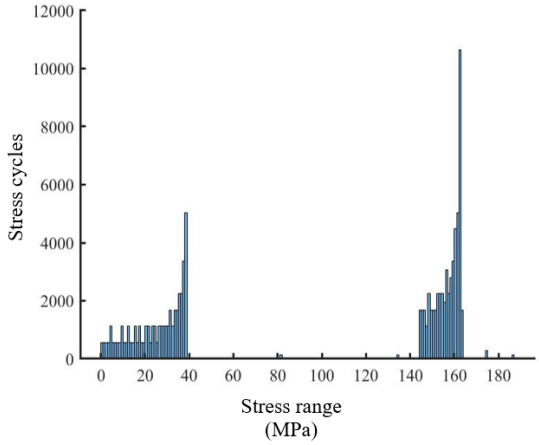

Fig. 2.33 Stress range histogram for stress range 125 MPa

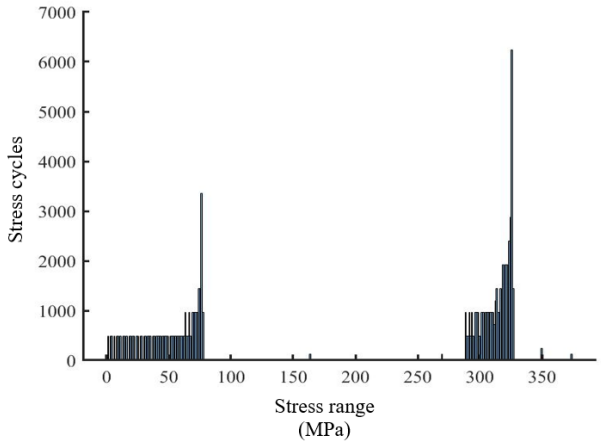

Fig. 2.34 Stress range histogram for stress range 250 MPa

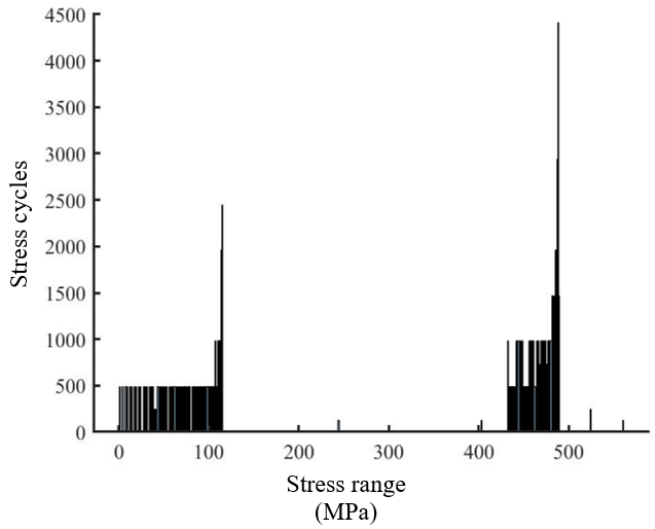

Fig. 2.35 Stress range histogram for stress range 375 MPa

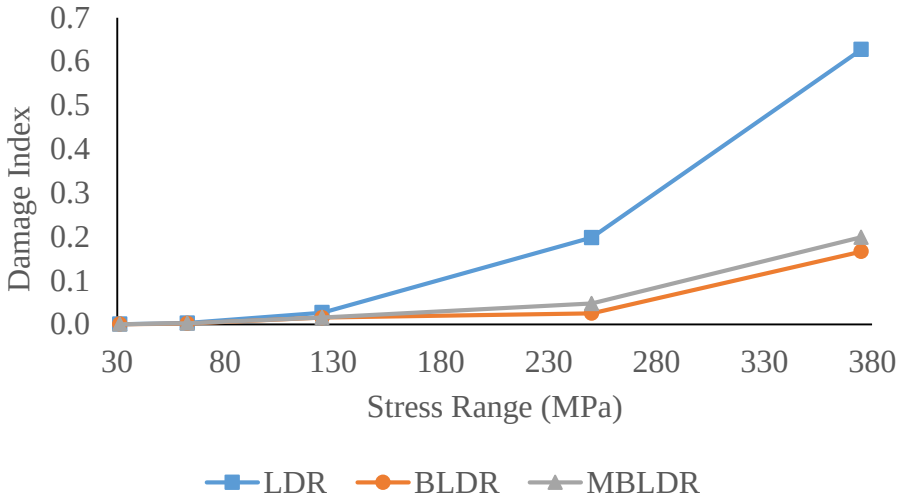

Fig. 2.36 Comparison of damage index with stress range

As the stress range increases, the dynamic stresses increases as shown in Figs. 2.26 to 2.30. This increase leads to higher stress cycles in higher stress ranges as observed in Figs. 2.31 to 2.35 resulting in higher damage index as shown in Fig. 2.36. The damage index evaluated from BLDR and MBLDR is less compared to LDR. The effect of loading order is considered in BLDR and MBLDR due to which the damage index is less. Howevere, this effect of loading order is not considered in LDR leading to more damage index. The effect of opening stress in Phase-2 is considered in MBLDR, thus estimating higher damage index as compared to BLDR which is observed from Fig. 2.36. The damage index evaluated using LDR, BLDR and MBDLR are approximately the same for lower stress range as observed from Fig. 2.36.

2.6.1.3 Effect of Damping

The total excitation force is 15 kN and the frequencies of loading are 10 Hz and 20 Hz. The material damping is varied from 1% to 3% with an interval of 0.5%. There is not much significant change in the dynamic stresses while varying the material damping. Thus, the dynamic stresses obtained for 2% material damping is shown in Fig. 2.28. The same pattern and values are obtained for 1% and 3% material damping. The comparison of histogram of stress range versus number of cycles for 2% material damping is shown in Fig. 2.33. The same pattern and values are obtained for 1% and 3% material damping. The comparison of damping and damage index is shown in Fig. 2.37.

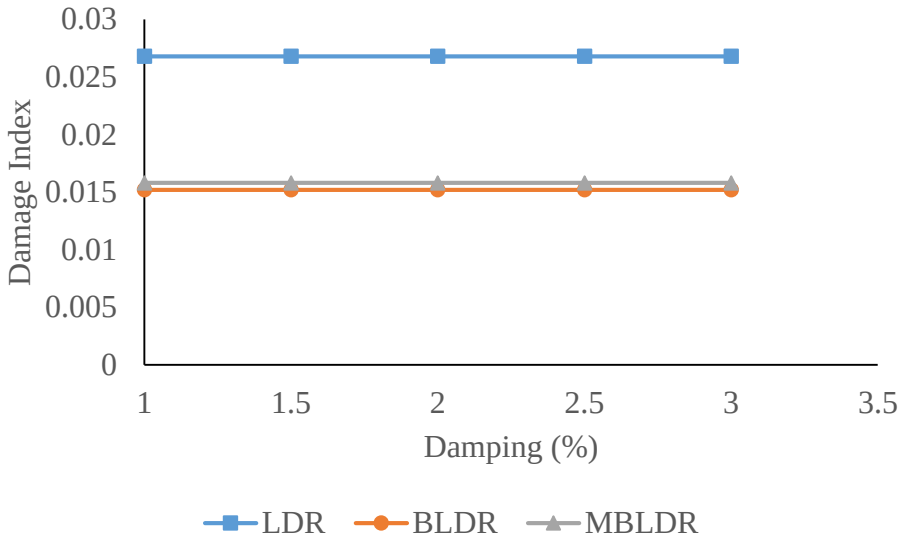

Fig. 2.37 Comparison of damage index with damping

The damage index is constant for all the damping ratios as shown in Fig. 2.37. Although, with increase in damping ratio, there is minute decrement in dynamic stresses which does not significantly affect the damage index.

2.6.1.4 Effect of number of modes

The total excitation force is 7.5 kN and the frequencies of loading are considered as 10 Hz and 20 Hz. The material damping is 2%. The dynamic stresses obtained for first mode, summation of first three, five and seven modes are shown in Figs. 2.38 to 2.41. The stress range histogram for first mode, summation of first three, five and seven modes are shown in Figs. 2.42 to 2.45. The comparison of damage index and summation of mode numbers upto 7 modes is shown in Fig. 2.46.

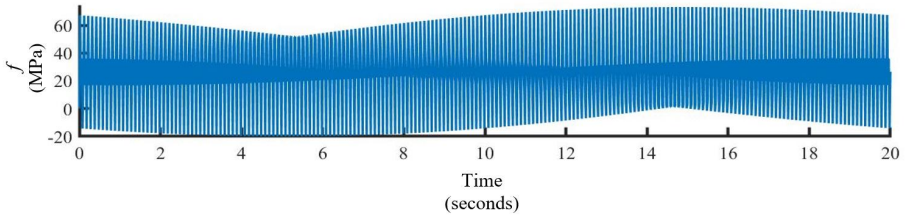

Fig. 2.38 Stress time history considering first mode

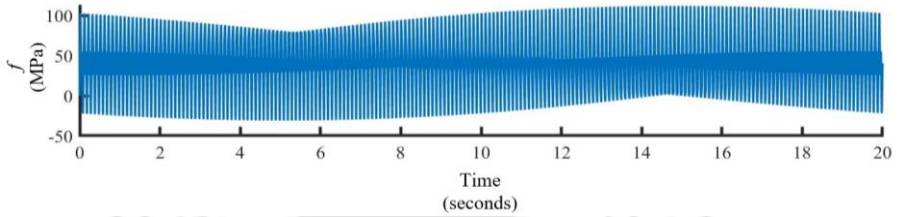

Fig. 2.39 Stress time history considering upto 3 modes

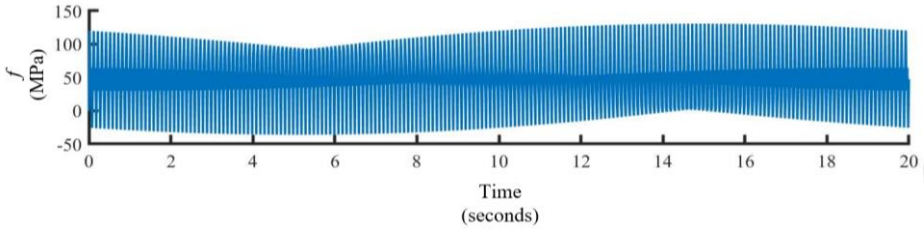

Fig. 2.40 Stress time history considering upto 5 modes

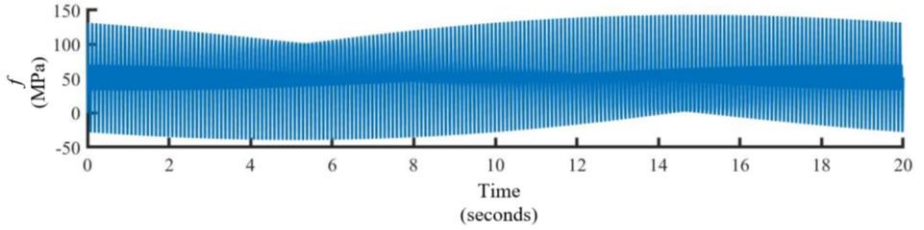

Fig. 2.41 Stress time history considering upto 7 modes

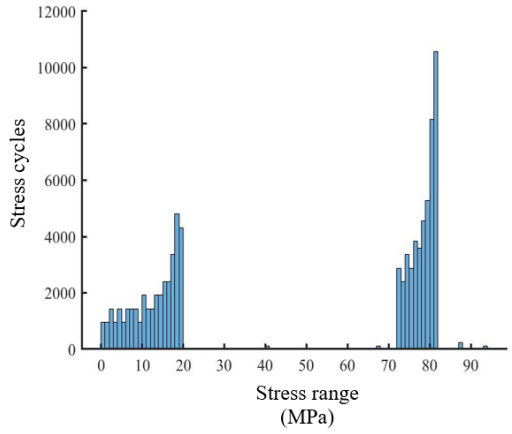

Fig. 2.42 Stress range histogram considering first mode

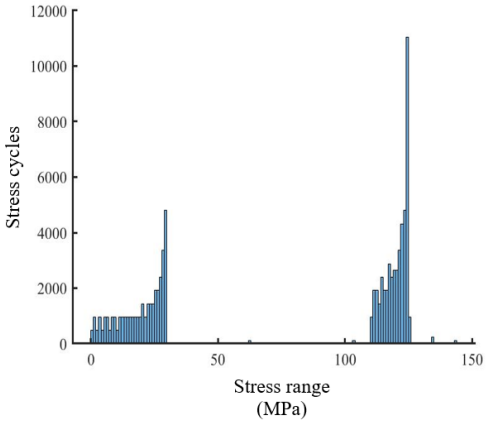

Fig. 2.43 Stress range histogram considering upto 3 modes

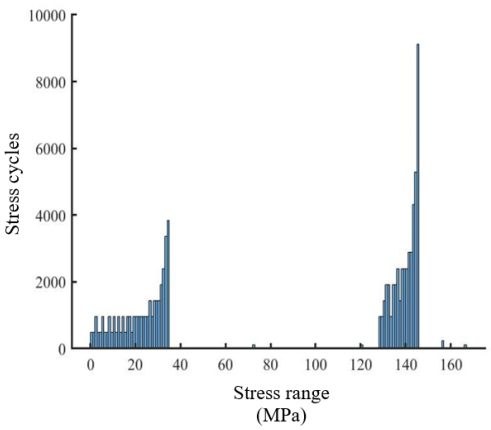

Fig. 2.44 Stress range histogram considering upto 5 modes

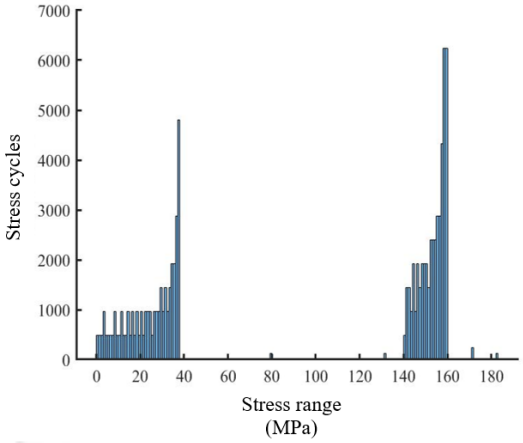

Fig. 2.45 Stress range histogram considering upto 7 modes

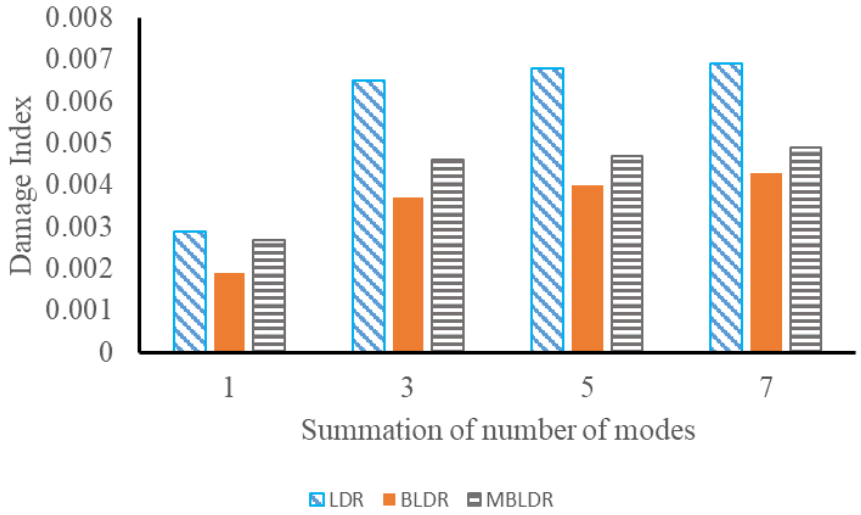

Fig. 2.46 Comparison of damage index with the number of modes

From Figs. 2.38 to 2.41, it is observed that there is little increase in dynamic stresses when the number of modes increases beyond 3. As the number of modes increases, stress cycles in higher stress ranges increases slightly, as observed in Figs 2.42 to 2.45 leading to insignificant change in damage index. The damage index is almost same when number of modes increases from 3 to 7, which is observed from Fig. 2.46. It is also observed that as the number of modes increases, there is no considerable change in the damage index estimated using BLDR and MBLDR.

The experimental validation is done using coupon specimen of ASTM E-606 standard for multi-level loading. The experimental validation is explained in section 2.7.

2.7 Experimental Study

Laboratory tests leading to complete failure under fatigue loading are essential in understanding the fatigue behaviour of specimens and also to gain confidence to adopt a particular model for prediction of fatigue failure in the design stage. The tests can be classified into two categories which are:

(i). In the first category, specimens are subjected to number of stress cycles to initiate a crack and subsequently produce failure by the growth of the initated crack.

(ii). In the second category, a pre-existing crack is made in the specimen and fracture mechanics methods are then used to determine the crack growth rates of pre-existing cracks under cyclic loading.

The crack propagation is affected by various factors such as cyclic stresses in a benign environment, or by the combination of cyclic stresses and an aggressive environment such as corrosion (Boyer, 1985). In the latter case, the process of fatigue damage is called corrosion fatigue.

Common laboratory fatigue testing is done either with alternating axial loading or bending thus generating tensile and compressive stresses. The specimens undergo stresses that usually traverse between a maximum and minimum tensile stress or between a maximum tensile stress and a maximum compressive stress. The maximum compressive stress is considered as negative tensile stress which is represented by negative sign and is taken as minimum stress.

2.7.1Fatigue Testing Machines

The fatigue test specimens are mainly described by the mode of loading which are given as (Boyer, 1985):

(i). Direct (axial) stress
(ii). Plane bending
(iii). Rotating beam
(iv). Alternating torsion
(v). Combined stress

In the present study, axial stresses have been applied on the specimen. Thus, the axial fatigue testing has been used.

2.7.1.1 Axial Fatigue Testing Machine

In the present study, the test has been carried using Universal Testing Machine (UTM) of 250 kN capacity that conforms to ASTM E466 and ISO 1099. The schematic representation of experimental set-up along with the photograph is shown in Fig. 2.47 (a) and (b) respectively. A hydraulic actuator is used to apply load in axial fatigue test. The model number of the instrument is UT-04-0250. The frame stiffness is 2000 MN/m, the column diameter is 125 mm, weight of the test system is 1690 kg and the dimensions of the system are 1250×1500×3600 mm. The working pressure of the system is 210 bar (21 MPa), the load cell is given as per ISO 7500-1; Class 0.5 and the frequency range of the instrument is 0.001-200 Hz. The servo controller is high performance digital 32-bit controller as shown in Fig. 2.48.

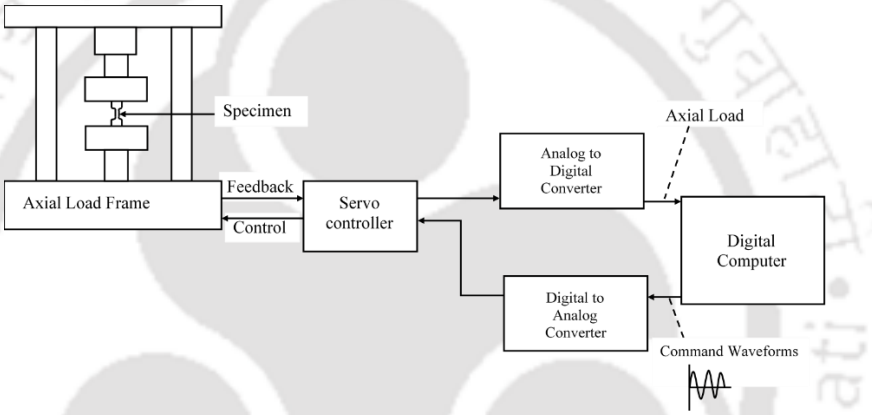

(a)

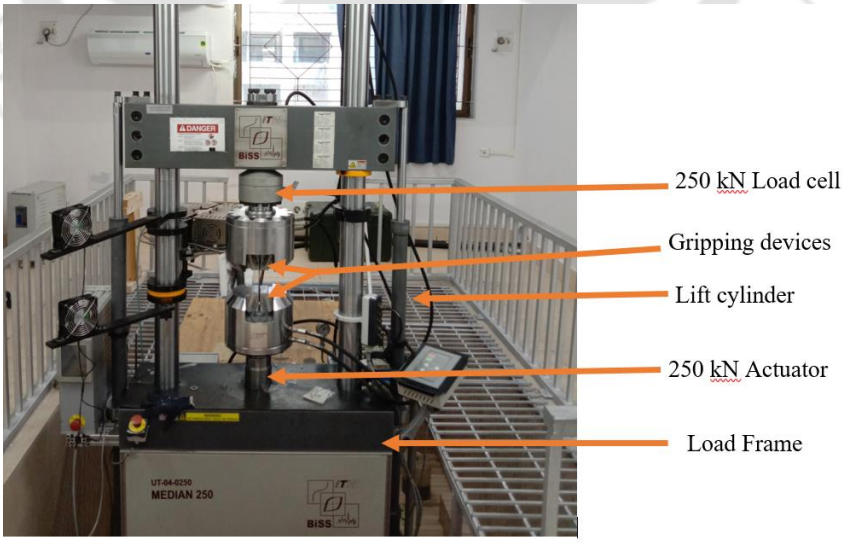

(b)

Fig. 2.47 (a) Schematic representation of experimental set-up (b) Photograph of the experimental set-up

Fig. 2.48 Servo controller of UTM 250 kN

The components of fatigue testing machine are load train, controllers and monitors. The load train consists of load frame, gripping devices, test specimen and drive or loading system which is shown in Fig. 2.47. The load frame is the structure of the machine that reacts to the forces applied to the specimen by the drive system. The most significant feature of the fatigue testing machine is the drive system. This system is electrically powered. The most common systems use electric motors to act on test specimens by means of cams, levers or rotating grips. The motors drive hydraulic pumps to provide service pressure for control of the motion and force of a hydraulic piston actuator in electrohydraulic machines. Electromagnetic excitation is used to excite a mass or inertia system to load the specimen.

The controls or controllers shown in Fig. 2.48 manually or automatically initiate power and test, adjust and maintain the controlled test parameters. Controllers also terminate the test at a predefined status such as failure, load drop and deflection limit. The control of time varying deflection or displacement can be obtained by cam-operated deflection levels, a rotating eccentric mass or hydraulically through a piston limited by stops. Control in most simple machines and drive systems is obtained via the open-loop mode. The magnitude of force and displacement initially set by the control system remains constant throughout the test. In case of uncontrolled parameters, the device provides an output signal to the controller or to a readout device. Common sensors are load cells which are resistance strain gage bridges calibrated to load and are inserted in the load train. Pressure transducers are used in hydraulic or pneumatic actuator devices.

Loading fixtures are used to alter the mode of loading. Fixtures can be designed to convert the axial force provided by a hydraulic actuator to perform four-point bending or torsion test. Fixtures attached to an oscillating pattern of a rotating-eccentric-mass type machine can facilitate axial, bending and torsion fatigue test of specimens. Proper gripping of the specimen is necessary to prevent grip failure prior to specimen failure. The grips shown in Fig. 2.49 are used for axial fatigue tests.

Fig. 2.49 Wedge type flat grips used for flat specimens

2.7.1.2 Fatigue test Specimen

The fatigue test specimen has three areas which are the two grip ends and test section. The grip ends are designed to transfer load from the test machine grips to the test section. The transition from the grip ends to the test section is designed with large, smoothly blended radii to eliminate stress concentrations in the transition. The length of the specimen is 100 mm excluding the grip lengths, the grip lengths are each of 40 mm in length, the radius of curvature in the transition portion is 50 mm, the width at the reduced area is 6 mm and the width at the grip end is 30 mm. The thickness of the specimen is 3 mm. The reduced are of cross section is 18.824 mm^2. The coupon specimen used is conforming to ASTM E606. The dimensional sketch of the coupon specimen is shown in Fig. 2.50 and the fabricated specimen is shown in Fig. 2.51.

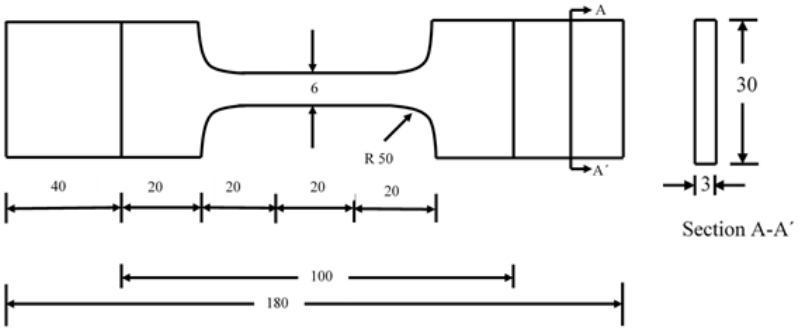

Fig. 2.50 Coupon specimen dimensions (All dimensions are in mm)

Fig. 2.51 Fabricated coupon specimen

2.7.2 Material Properties

Tensile strength

The test is carried out to determine the material properties of the specimen and to obtain the stress-strain curve of the material so that the minimum and maximum load values can be suitably fixed to conduct the fatigue test. Mechanical wedge grips are used for flat specimens. In tensile test, strain is measured using extensometers. The test set-up for tensile test is shown in Fig. 2.52. The gauge length is 25 mm. The stress-strain curve of the material obtained from the tensile test is shown in Fig. 2.53. The results obtained are shown in Table 2.1. The reduced area of cross-section of the specimen is 18.824 mm^2.

Fig. 2.52 Test set-up for tensile test

Fig. 2.53 Stress-strain curve obtained from tensile test

Table 2.1 Mechanical properties of the specimen

Peak Stress	351 MPa
Peak Load	6.62 kN
0.2% Offset Yield Stress	255 MPa
Yield Load	4.80 kN
Modulus of Elasticity	206 MPa

Damping of the specimen

The damping characteristics of the material of the specimen is obtained using vibration experiment. A flat bar of mild steel of uniform size is used. The length, width and thickness of the bar is 400 mm, 30 mm and 3 mm respectively. One end of the beam is fixed and other end is free. The beam is made to vibrate freely with the help of hammer excitation and the response of the beam in the form of acceleration due to the excitation is measured with the help of an accelerometer which is attached to the free end of the beam as shown in Fig. 2.54. This is achieved using Brüel & Kjær Pulse Analyser (0 Hz to 25.6 kHz), DeltaTron Accelerometer 4396 with insulated base (9.8 mV/ms^{-2} to 10.2 mV/ms^{-2}) and five channel dynamic signal acquisition module NI USB-4432. The apparatus consists of a rigid fixture to hold the specimen. The horizontal orientation of the cantilever beam along with test set-up is shown in Fig. 2.54. The acceleration response obtained is shown in Fig. 2.55.

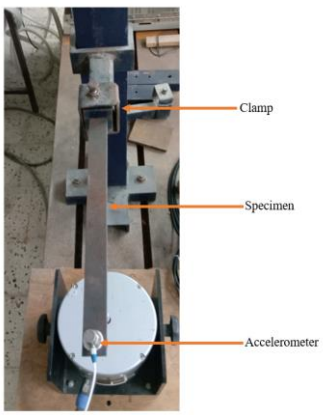

Fig. 2.54 Experimental set-up to obtain the damping characteristics

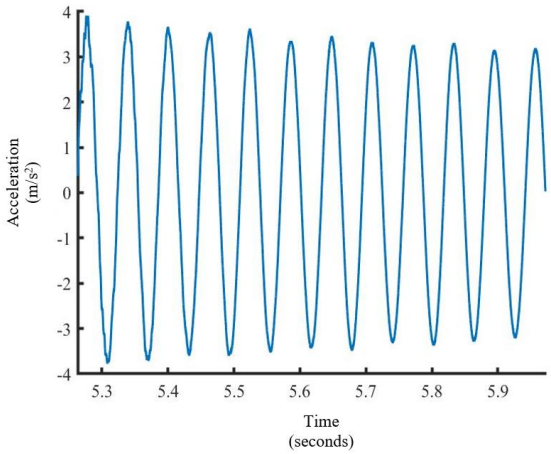

Fig. 2.55 Acceleration at the tip of the cantilever specimen.

The initial amplitude and the amplitude at 3rd cycle of acceleration was recorded. The logarithmic decrement, δ' and damping ratio ξ is calculated using the expression,

$$\delta' = \frac{1}{d}\ln\left(\frac{X_{a0}}{X_{ad}}\right) \tag{2.57}$$

$$\xi = \frac{\delta'}{\sqrt{4\pi^2 + \delta'^2}} \tag{2.58}$$

where, X_{a0} is the initial amplitude of acceleration, d is the number of cycles and X_{ad} is the amplitude of acceleration at the d^{th} cycle. The natural frequency, logarithmic decrement and damping ratio obtained are shown in Table 2.2.

Table 2.2 Results obtained from vibration experiment of cantilever beam

First natural frequency f_{n_1} (Hz)	Initial Amplitude X_{a0} (m/s^2)	Amplitude at the n^{th} cycle X_{ad} (m/s^2)	Number of d^{th} cycle	Logarithmic decrement (δ')	Damping ratio (ξ)
16.03	1.334	1.202	3	0.035	0.005
16.03	1.762	1.574	3	0.038	0.005
16.03	3.907	3.504	3	0.028	0.005

2.7.3 Fatigue Test

The fatigue test has been carried out in Central Instruments Facility, CIF, IIT Guwahati. Total number of specimens tested were three. The specimens were tested for three different loading levels until failure occurs. The specimen was subjected to harmonic excitation. The loading details of the three specimens is shown in Table 2.3. Fig. 2.56 presents test setup with the mounted specimen and the fatigue crack is shown in Fig. 2.57.

Table 2.3 Loading details for each specimen

Specimen No.	Day	Stress Range (MPa)	Frequency of excitation (Hz)	Total time (hrs)
1	1 to 4	150	27	55
	5 to 6	175		
	7	200		
2	1 to 2	160	30	28
	3 to 4	185		
	5	210		
3	1 to 2	170	30	24
	3	195		
	4	220		

Fig. 2.56 Test set up with the specimen

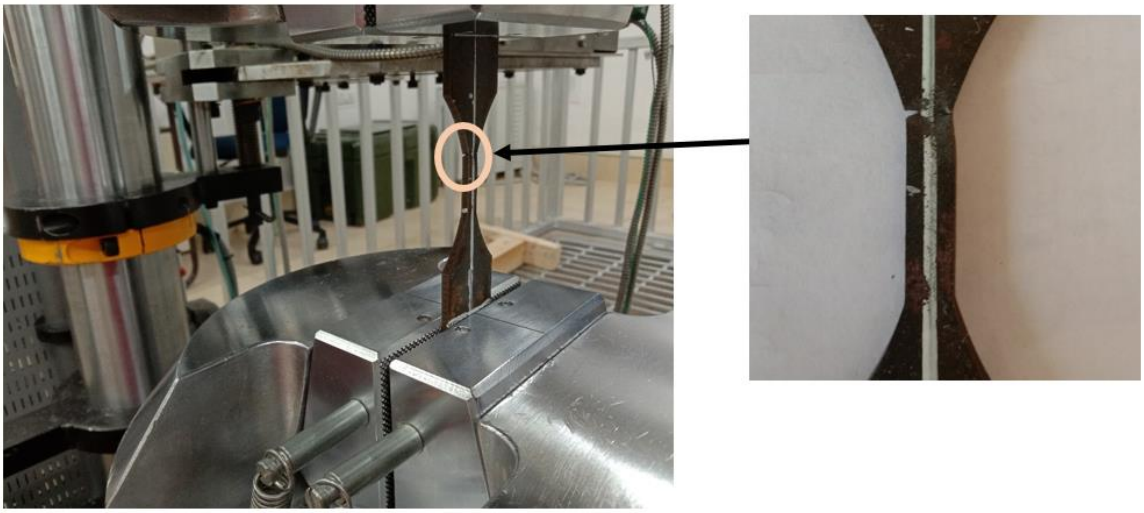

Fig. 2.57 Tested specimen showing fatigue crack

The load time history obtained from the experiment is then given as input to the FE model using the FE software ABAQUS and analysed for dynamic stress. The dynamic stress obtained from the software has been later used to find the fatigue life of the specimen and to compare with experimental results.

2.7.4 Microstructural evolution of the deformed specimens

The fracture surface of the failed specimen was examined under field emission scanning electron microscopy (FESEM) using SIGMA 300, Zeiss Corp. to observe the fracture initiation sites. Fracture features exhibit inclusion induced crack initiation on the reduced area of the specimen, which are caused by stresses during cyclic loading. These inclusions act as potential

sites for stress concentration and are considered to be the region of lowest strength. These lead to crack propagation. Grain boundaries, cleavage steps and slip bands indicate a mixed mode of intergranular and transganular crack propagation. Fatigue striations and fish-eye indicate the occurrence of cyclic deformation in the material and also indicate the intense plastic deformation occurred in the localized region inside the specimen.

The surface induced cracks, fish-eye formation at the subsurface of the specimen, formation of slip bands, grain boundaries and striations indicating fatigue failure are observed in Fig. 2.58.

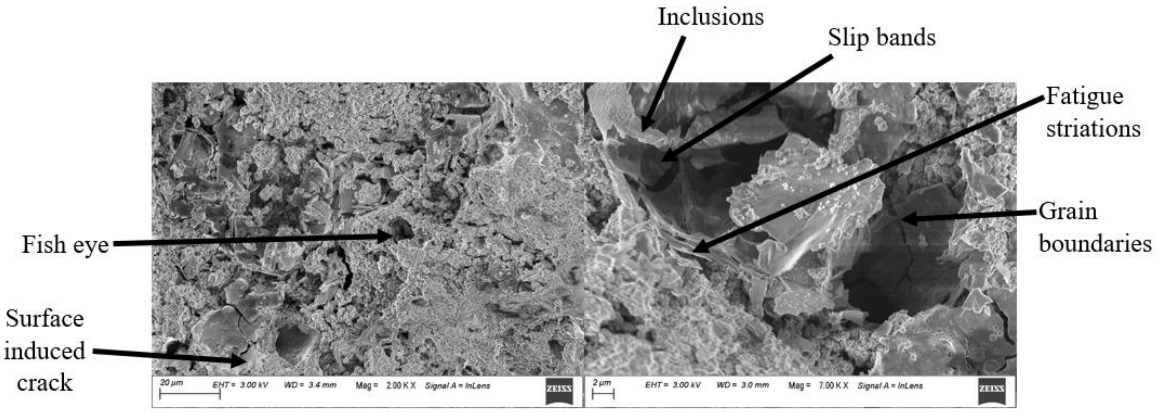

Fig. 2.58 FESEM micrographs of the fracture surface of the specimen

2.8 Finite Element Model

The finite element modelling of a mild steel specimen is used for studying the fatigue damage and to compare this with the experimental results. The specimen is subjected to axial vibration. The coupon specimen is of ASTM standard which is shown in the Fig. 2.50. The specimen is modelled using a 3D solid element. The material properties obtained from the tensile test in section 2.7.2 is used as input. The Rayleigh damping required for dynamic analysis is obtained as

$$\mathbf{C} = a_0\mathbf{M} + a_1\mathbf{K} \tag{2.59}$$

where a_0 and a_1 are mass proportional constants and stiffness proportional constants and have units, sec^{-1} and sec respectively. **M**, **C** and **K** are mass matrix, damping matrix and stiffness matrix respectively. a_0 and a_1 are given as

$$a_0 = \xi\frac{2\omega_{ni}\omega_{nj}}{\omega_{ni}+\omega_{nj}}, \quad a_1 = \xi\frac{2}{\omega_{ni}+\omega_{nj}} \tag{2.60}$$

where ω_{ni} and ω_{nj} are the natural frequencies obtained in i^{th} mode and j^{th} mode respectively. Eigen values have been obtained in ABAQUS using linear perturbation analysis. The results are shown in Table 2.4.

Table 2.4 Natural frequencies in axial mode of the bar model

Mode	Natural Frequency (Hz)
1	1927.7
2	3828.3
3	6318.5
4	7317.9
5	7562.3

The axial forces are applied on the specimen using reference point. This is done using Coupling option under Constraints. The reference point created using the Coupling option is also used for applying the boundary conditions apart from the load. The experiment boundary conditions are being replicated in coupon specimen model where one end is fixed and the other end is allowed to undergo cyclic loading in axial direction. Hence, two reference points are used where one reference point represents the fixed end surfaces and the other reference point represents the surfaces on the free end which is allowed to deform only in the axial direction on which tensile loading is applied. Figs. 2.59 shows the interaction of surfaces of coupon specimen with respect to reference points, RP-1 and RP-2. The axial load is applied on the surface with respect to the reference point, RP-2 as shown in Fig. 2.59.

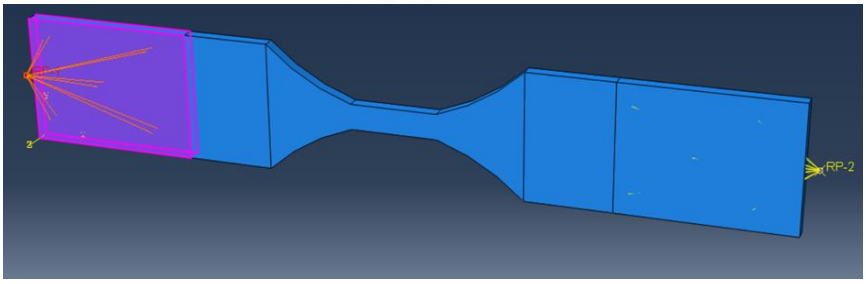

Fig. 2.59 The coupon specimen surface coupled with respect to reference point, RP-1

The surfaces with respect to reference point, RP-2 are allowed to move only in axial direction and the boundary conditions pertaining to the same are assigned. Tensile load is given as input in the experiment. The load time history obtained during experiment is given as excitation to the FE model. A segment of recorded load time history of 40 sec durations has been taken as input to the fatigue damage algorithm. For practical purpose, only a limited duration of stress or strain time history will be used since the duration of fatigue failure is very large and full load time history till failure cannot be used as input in any analytical or numerical scheme. The time history obtained for each stress range is given as input in a tabulated form in ABAQUS. The unit of load is in newton (N). This load is then applied on reference point, RP-2 which represents the surface of the specimen attached in UTM, where the load is acting. The mesh size considered is 1.5 mm. A 3 dimensional 8-noded brick solid element (C3D8R) is used for meshing.

2.9 Validation of Experimental Result

Three specimens of the same material and size have been tested in fatigue till failure. Experimental results have been compared to validate theoretical method developed in the present work. A segment of recorded load time history of 40 secs duration obtained from experiment was taken and given as input in the FE model. The input given to the FE model yields stress time history of the specimen. The fatigue damage has been calculated from the stress time history of each of the specimen. The detailed procedure in evaluating the damage index and fatigue life has been explained for a typical specimen and appended below. The experimental data for specimen-1 has been taken to explain the procedure.

2.9.1 Evaluation of Fatigue Life for a Coupon Specimen

The fatigue testing for specimen-1 is conducted for 55 hrs of constant amplitude cyclic loading to cause failure. The loading details are given in Table 2.2. Since, fatigue damage is caused due to crack initiation and crack propagation, the stress ranges are segregated into two phases of loading. The two phases of loading are Phase-1 which represents crack initiation and Phase-2 which represents crack propagation. An initial surface crack was observed when the stress range was changed from 150 MPa to 175 MPa. This implies that there is a transition from crack initiation to crack propagation on changing the stress range to 175 MPa. Thus, the stress range in days 1 to 4 contribute to Phase-1 loading and stress ranges in days 5 to 7 contribute to Phase-2 loading. The detailed calculation for phase-1 loading is given below.

2.9.1.1 Phase-1 Loading (days 1 to 4)

The 40 secs input stress time history obtained from the experiment is shown in Fig. 2.60. The output stress time history from FE analysis is shown in Fig. 2.61. The stress range histogram obtained using rainflow counting algorithm is shown in Fig. 2.62.

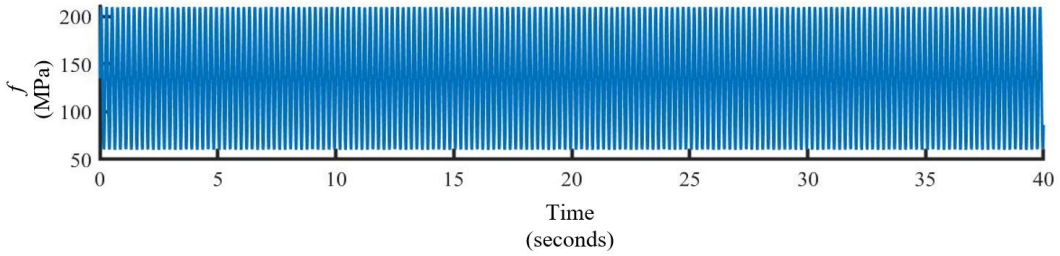

Fig. 2.60 Input of the stress time history given in the FE model

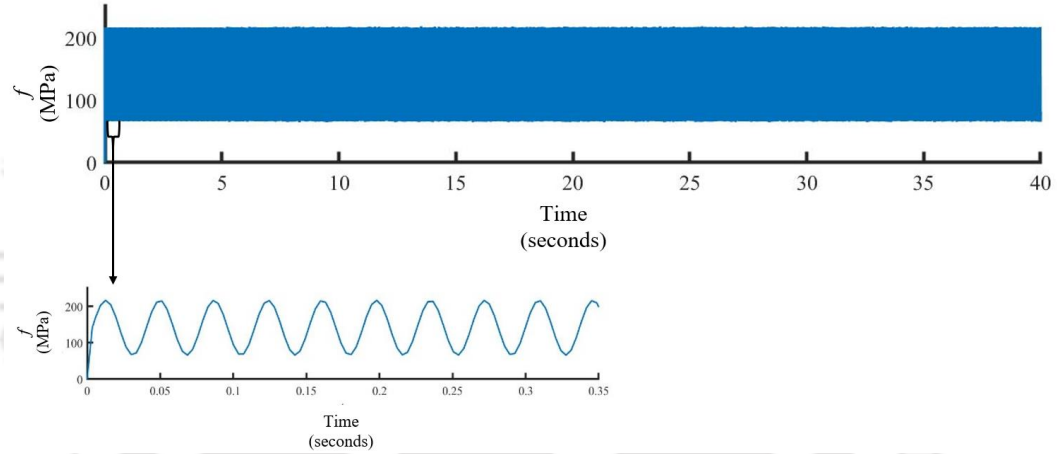

Fig. 2.61 Output stress time history obtained after FE analysis

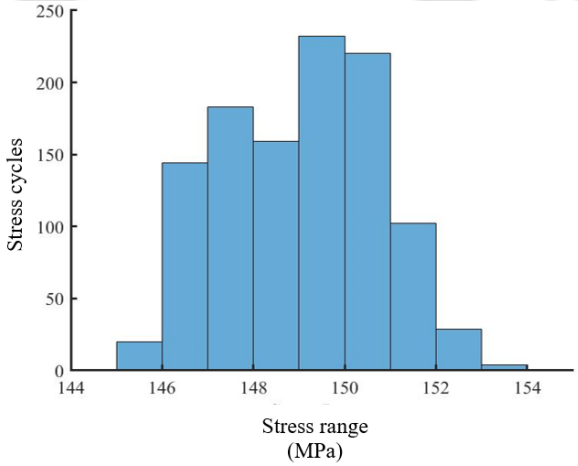

Fig. 2.62 Stress range histogram for 40 secs time history from day 1 to day 4

2.9.1.1.1 Evaluation of damage index using LDR

Damage index obtained using LDR is 4.469×10^{-4}. The estimated cycles to failure, N_{est} is obtained by taking the inverse of damage index and in this case, it is 2238 cycles.

2.9.1.1.2 Evaluation of damage index using BLDR

The stress range in days 1 to 4 contribute to Phase-1 loading i.e., it contributes to the crack initiation. The slope in Phase-1, $\tan\theta_1$ is considered to compute the damage index. The highest life level, N_1^* is considered as 2.4281×10^6 cycles and the lowest life level, N_2^* is considered as 1.53×10^6 cycles as obtained from the histogram in Fig. 2.62. The highest life level considered in the calculation corresponds to stress range 150 MPa. The lowest life level is considered as corresponding to the intrinsic fatigue limit. The intrinsic fatigue limit considered is $0.5 \times f_u$ where f_u is the ultimate tensile strength obtained from the experiment and is 350 MPa. The slope in Phase-1, $\tan\theta_1$ is calculated using Eq. (2.14). The damage index obtained using Eq. (2.15) is 4.355×10^{-4} and the estimated cycles to failure, N_{est} is obtained as 2296 cycles.

2.9.1.1.3 Evaluation of damage index using MBLDR

The maximum stress range obtained from the stress range histogram in Fig. 2.62 is 219 MPa. The stress cycles corresponding to this stress range is 0.5. The contribution to damage by this stress range will be very less due to lower stress cycles although the magnitude of stress range is high. The maximum stress range, f_{max} considered is 153 MPa as observed from Fig. 2.62. The opening stress, f_{os} is evaluated using Eq. (2.22) is 71.771 MPa. The minimum stress range as observed from Fig. 2.62 is 141 MPa and the stress cycles is 1. Since, this contributes to very less damage, the minimum stress range, f_{min} is considered as 146 MPa. The maximum and minimum strain range obtained is 7.427×10^{-4} and 7.087×10^{-4} respectively. The effective strain range obtained using Eq. (2.24) is 3.934×10^{-4} and the strain corresponding to the intrinsic fatigue limit is 8.495×10^{-4}. The new effective strain range evaluated using Eq. (2.25) is 4.522×10^{-4}. The new effective stress range is computed by substituting new effective strain range and modulus of elasticity in Eq. (2.26) and is obtained as 93.771 MPa. The low life level, N_2' is computed using the new effective stress range and is obtained as 9.938×10^6 cycles. The high life level, N_1' is taken as 2×10^7 cycles. The damage index computed using Eq. (2.28) is 4.742×10^{-4} and the estimated failure cycles, N_{est} is 2109 cycles.

2.9.1.1.4 Estimation of failure cycles

The estimated failure cycles obtained from LDR, BLDR and MBLDR is shown in Table 2.4 for 40 secs time history. When computing the estimated failure cycle for 40 secs time history, the failure cycle obtained from the experiment at the start of the 40 secs time history is considered and added with the failure cycle obtained from LDR, BLDR and MBLDR. This is done so that failure cycle at the end of 40 secs can be estimated. The points for estimation of failure rate are taken such that the duration of loading between two points is 40 secs. The points considered are A, B, C, D, E and F and the corresponding time are 448 secs, 488 secs, 930 secs, 970 secs, 850 secs and 890 secs respectively. The duration of loading between points A to B, C to D and E to F is 40 secs and is given in Table 2.5.

Table 2.5 Estimated failure cycles, N_{est} for 40 secs time history using LDR, BLDR and MBLDR

Time instant (sec)	Points at the corresponding time instant	Actual failure cycle obtained from experiment (N_{actual})	Estimated failure cycle obtained using LDR, N_{est1}	Estimated failure cycle obtained using BLDR, N_{est2}	Estimated failure cycle obtained using MBLDR, N_{est2}
448	A	8783			
488	B	9773	11021	11079	10892
930	C	21346			
970	D	22529	23584	23642	23455
850	E	19215			
890	F	20281	21453	21511	21324

It is observed from Table 2.5 that the error between estimated failure cycle N_{est} and actual failure cycle N_{actual} is within 5% for 40 secs time history duration.

The fatigue failure of the specimen takes place by accumulation of damage. The failure rate of the specimen given in Table 2.6 has been obtained by relating the failure cycle and corresponding time for different points. For evaluating the estimated failure cycles, the average failure rate has been considered which is given in Table 2.6.

Table 2.6 Failure rate computed for LDR, BLDR and MBLDR

Reference points (See Table 2.4)	Failure rate for LDR, m_1	Failure rate for BLDR, m_2	Failure rate for MBLDR, m_3
F and A	28.665	28.796	28.373
D and B	26.064	26.064	26.064
E and B	22.635	22.475	22.992
D and A	28.35	28.465	28.107
	Average m_{11}= 26.426	Average m_{12}= 26.45	Average m_{13}= 26.384

The estimated failure cycles for the total duration of time history for days 1 to 4 is obtained by the expression shown

$$Est.N_{1j} = Avg.m_{1j} \times t,\ j = 1,2,3 \tag{2.61}$$

The index j given corresponds to LDR, BLDR and MBLDR which is given as 1, 2 and 3 respectively in Eq. (2.61). *Avg.* denotes average and *t* denotes time in seconds.

2.9.1.2 Phase-2 Loading (Day 5 to7)

The stress range histogram obtained for stress range 175 MPa (day 5 to 6) and 200 MPa (day 7) for 40 secs time history is shown in Fig. 2.63 and Fig. 2.64 respectively.

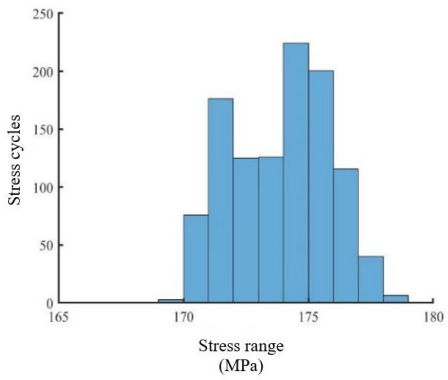

Fig. 2.63 Stress range histogram for 40 secs time history from day 5 to day 6

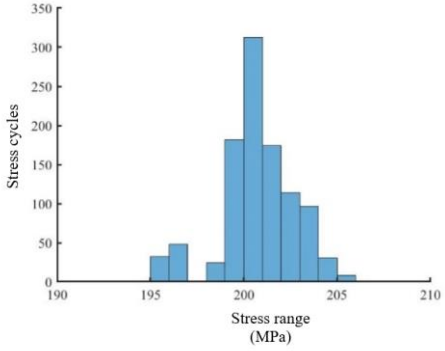

Fig. 2.64 Stress range histogram for 40 secs time history for day 7

2.9.1.2.1 Evaluation of damage index

The damage index and failure cycles obtained using LDR, BLDR and MBLDR for 40 secs time history is given in Table 2.7. The steps for evaluation of damage index and failure cycles explained in sections 2.9.1.1.1, 2.9.1.1.2 and 2.9.1.1.3 are used in this section to evaluate the damage index and failure cycles for Phase-2. Two loading levels are considered i.e., stress range 175 MPa and stress range 200 MPa and are denoted as loading level I and loading level II respectively in Phase-2. In case of BLDR and MBLDR, the slopes in Phase-2, $\tan\theta_2$ and $\tan\theta_2'$ are used and calculated using Eqs. (2.18) and (2.31). Damage index is evaluated using Eq. (2.19) for BLDR and using Eq. (2.29) for MBLDR.

Table 2.7 Damage index and failure cycles obtained using LDR, BLDR and MBLDR for different loading levels in Phase-2

Loading Level	LDR		BLDR		MBLDR	
	D	N_{est} (cycles)	D	N_{est} (cycles)	D	N_{est} (cycles)
I	7.088×10^{-4}	1411	5.520×10^{-4}	1812	5.764×10^{-4}	1735
II	0.001	979	8.145×10^{-4}	1227	8.251×10^{-4}	1212

In Table 2.7, D represents the damage index and N_{est} represents the estimated failure cycles. The estimated failure cycles N_{est} obtained using LDR, BLDR and MBLDR for 40 secs time history for loading level I and II is given in Table 2.8 and 2.9 respectively.

Table 2.8 N_{est} for 40 secs time history using LDR, BLDR and MBLDR for loading level I

Time instant (sec)	Points at the corresponding time instant	Actual failure cycle obtained from experiment (N_{actual})	Estimated failure cycle obtained using LDR, N_{est1}	Estimated failure cycle obtained using BLDR, N_{est2}	Estimated failure cycle obtained using MBLDR, N_{est3}
3978	A	99060			
4018	B	100087	100471	100872	100795
4197	C	104963			
4237	D	107106	106374	106775	106698
5993	E	155377			
6033	F	156500	156788	157189	157112

Table 2.9 N_{est} for 40 secs time history using LDR, BLDR and MBLDR for loading level II

Time Instant (sec)	Points at the corresponding time instant	Actual failure cycle obtained from experiment (N_{actual})	Estimated failure cycle obtained using LDR, N_{est1}	Estimated failure cycle obtained using BLDR, N_{est2}	Estimated failure cycle obtained using MBLDR, N_{est2}
3698	A	1443411			
3738	B	1444453	1444390	1444638	1444623
5248	C	1483787			
5288	D	1484829	1484766	1485014	1484999
5065	E	1479024			
5105	F	1480066	1480003	1480251	1480236

It is observed from Tables 2.8 and 2.9 that the error between estimated failure cycles N_{est} and actual failure cycles N_{actual} is within 2% for 40 secs time history. The prediction is in good agreement with the experimental results. The average failure rates for LDR, BLDR and MBLDR are shown in Tables 2.10 and 2.11 respectively. The failure rate obtained for LDR, BLDR and MBLDR is given in Tables 2.10 and 2.11 for loading level I and II respectively.

Table 2.10 Failure rate for LDR, BLDR and MBLDR for loading level I

Reference points (See Table 2.7)	Failure rate for LDR, m_1	Failure rate for BLDR, m_2	Failure rate for MBLDR, m_3
F and A	28.091	28.286	28.249
D and B	26.954	26.954	26.954
E and B	27.800	27.597	27.636
D and A	28.239	29.787	29.490
	Average m_{21}= 27.711	Average m_{22}= 28.156	Average m_{23}= 28.080

Table 2.11 Failure rate for LDR, BLDR and MBLDR for loading level II

Reference points (See Table 2.8)	Failure rate for LDR, m_1	Failure rate for BLDR, m_2	Failure rate for MBLDR, m_3
F and A	26.007	26.183	26.172
D and B	26.049	26.049	26.049
E and B	26.099	25.912	25.923
D and A	26.009	26.165	26.156
	Average m_{31}= 26.041	Average m_{32}= 26.077	Average m_{33}= 26.075

Since, loading level I and II contributes to phase-2, the estimated failure cycles N_{est} is obtained by taking the average of the average failure rates for LDR, BLDR and MBLDR for the both the loading levels. The estimated failure cycle for the total duration of time history for phase-2 loading is obtained by the expression shown,

$$Est.N_j = \frac{Avg.m_{2j} + Avg.m_{3j}}{2} t,\ j = 1,2,3 \tag{2.62}$$

In Eq. (2.62), the index j corresponds to LDR, BLDR and MBLDR which is given as 1, 2 and 3 respectively.

2.9.2 Comparison of theoretical failure cycle with experimental result

The estimated failure cycles are obtained from the average failure rates for LDR, BLDR and MBLDR. The computation of average failure rate and estimated failure cycles are explained in section 2.9.1.1.4. The same procedure is applied for specimen-2 and specimen-3 and the failure cycles for the total duration of time history till failure is obtained and compared with that of the experimental values. The failure cycles estimated for the three specimens using LDR, BLDR and MBLDR are given in Tables 2.12 to 2.14.

Table 2.12 Comparison of N_{est} with N_{actual} using LDR, BLDR and MBLDR for days 1 to 7 (specimen-1)

Time t (secs)	N_{actual} (cycles)	LDR		BLDR		MBLDR		Day
		N_{est}	Error (%)	N_{est}	Error (%)	N_{est}	Error (%)	
36195.9	912108	972801	6.654	981488	7.607	980077	7.452	1
64868.4	1617523	1743403	7.782	1758971	8.745	1756441	8.588	2
111827	2744661	3005465	9.502	3032303	10.480	3027942	10.321	3
117347	3075462	3153826	2.548	3181989	3.464	3177413	3.315	4
133343	3484044	3583737	2.861	3615740	3.780	3610539	3.631	5
172143	4424915	4626502	4.556	4667816	5.489	4661103	5.338	6
196320	5053156	5276286	4.416	5323403	5.348	5315746	5.197	7

Table 2.13 Comparison of N_{est} with N_{actual} using LDR, BLDR and MBLDR for days 1 to 5 (specimen-2)

Time t (secs)	N_{actual} (cycles)	LDR		BLDR		MBLDR		Day
		N_{est}	Error (%)	N_{est}	Error (%)	N_{est}	Error (%)	
11212.54	323829	320432	-1.049	320858	-0.917	320825	-0.928	1
41560.69	1142077	1187721	3.997	1189301	4.135	1189176	4.124	2
74791.46	1967442	2137390	8.638	2140232	8.782	2140008	8.771	3
88808.33	2390744	2537964	6.158	2541339	6.299	2541073	6.288	4
107213.2	2843492	3063940	7.753	3068014	7.896	3067692	7.885	5

Table 2.14 Comparison of N_{est} with N_{actual} using LDR, BLDR and MBLDR for days 1 to 4 (specimen-3)

Time t (secs)	N_{actual} (cycles)	LDR		BLDR		MBLDR		Day
		N_{est}	Error (%)	N_{est}	Error (%)	N_{est}	Error (%)	
27191.84	745106	787571	5.69	788748	5.85	787530	5.69	1
53419.84	1463490	1547252	5.72	1547573	5.75	1547145	5.71	2
80521.02	2194014	2456213	11.95	2458548	12.05	2458146	12.03	3
86826.45	2364226	2648554	12.02	2651072	12.13	2650638	12.11	4

It is observed from Table 2.12 to 2.14 that the MBLDR estimates lower failure cycles as compared to BLDR. This is because of the consideration of opening stress in Phase-2. It is also observed from the study that the opening stress can occur below the intrinsic fatigue limit. Thus, considering zero slope below the intrinsic fatigue limit can lead to over conservative results. BLDR and MBLDR estimates higher failure cycles as compared to LDR since the load interaction effect is ignored in LDR. The average error falls within 8 % and the prediction is considered to be in agreement with the experimental results.

2.10 Closure

In the present chapter, fatigue damage method considering crack initiation stage and crack propagation stage has been developed. The same has been further extended to include opening stress. The proposed methods have been illustrated with a generic structural model subject to axially vibrating load. The effect of stress range, excitation frequency, damping and number of modes have been considered to examine the damage index. The theoretical method, thereafter, has been compared with the experimental results of fatigue testing of coupon specimen in UTM 250 kN. The comparison of the failure cycles obtained from the proposed methods and that of the experimental results are in good agreement with each other. The average error is approximately 8%. From the study conducted, MBDLR gives more accurate damage predictions as compared to BLDR since opening stresses are considered in the former case in Phase-2. It is also observed from the study that the propagation of crack can take place below the intrinsic fatigue limit and neglecting stresses below the fatigue limit will tend to give over

conservative damage values. Thus, it is observed that zero slope consideration can lead to inaccurate results. Both BLDR and MBLDR give less damage predictions as compared to LDR. This is because in the latter, the load sequence effects are neglected. In the further study for evaluation of damage index, Modified Bilinear Damage Rule (MBLDR) will be used.

3

BRIDGE VEHICLE INTERCATION MODEL

3.1 General

The interaction between the bridge and the movement of the vehicles is a coupled dynamic problem. Conventionally, majority of the research has been focused on obtaining the bridge response by approximating the moving vehicle as a number of moving loads referred to as moving load model. In this model, the effect of interaction between the bridge and the vehicle is ignored. Due to this reason, the moving load model works well for cases where the mass of the vehicle is smaller in relative to that of the bridge (Yang and Lin, 2004). For cases where the mass of the vehicle cannot be ignored, the effect of interaction between bridge and vehicles should be considered. In order to include the interaction between bridge and vehicles, the elastic effects of the tyres and suspension mechanisms are modelled by springs and the damping effects of tyres and suspension systems are modelled by dashpots (Blejwas et al., 1979; Green and Cebon, 1997). The effect of random nature of vehicular movement on the bridge dynamic response which was ignored in earlier research has been considered in the bridge vehicle interaction model. Thus, the present study focuses on solving the dynamic response of the bridge for a stream of vehicles considering interaction between bridge and vehicle and random arrival time of the vehicle following Poisson process. The effect of deck surface irregularity on bridge dynamic response is also considered.

3.2 Idealization of Bridge

The transverse dimension of bridge deck is small compared to its span and therefore, a simplified beam model is a suitable option to establish the connection between bridge response and vehicle parameters (Fryba, 1996). In the present study, a single span bridge and multi-span continuous bridge has been idealized as Euler Bernoulli beam of uniform cross section and damping properties.

3.3 Road Surface Roughness

Irregularities in pavement surface are called roughness. All the pavement surfaces have some irregularities. The National Cooperative Highway Research Program defines roughness as the

deviations of a pavement surface from a true planar surface that affects the vehicle dynamics, ride quality and dynamic pavement loads (Sun, 2013). The vehicles traversing over the bridge are excited by these road conditions at the contact points. These road conditions can be characterized by deterministic mean surface profile superimposed over randomly undulating pavement. Deterministic mean surface profile represents construction defects, pot holes, approach road settlement, expansion joints, development of corrugation, pre-cambering of deck surface, etc. The random unevenness of the pavement profile is assumed to be of Gaussian nature and homogeneous in space (Shinozuka, 1971). In temporal domain, this is a stationary excitation process when the vehicle velocity is constant. However, the process becomes non-homogeneous in space in presence of a variable mean profile (Yadav and Nigam, 1978).

The vertical height of the bridge deck profile along the longitudinal axis measured with respect to flat datum at a point x from the reference station is represented by

$$h(x) = h_m(x) + h_r(x) \tag{3.1}$$

where $h(x)$ is the bridge deck profile, $h_m(x)$ is the deterministic mean surface profile and $h_r(x)$ is the road surface unevenness.

3.3.1 Mean Surface Profile

In the present study, the deterministic mean profile is the pre-cambering of the bridge in the form of half sine wave. The advances in design, construction materials and method of construction has made it possible to construct long span bridges. The problem faced in long span bridges is to control the deflection limit to achieve better serviceability. It is noted that in some cases of bridge design, deck deflection under dead load and live load may cross serviceability limit. The upward pre-cambering of the deck surface is recommended to compensate for the additional vertical deflection. The equation of the pre-camber with reference to origin at the left hand support is given by

$$h_m(x) = h_0 \sin\left(\frac{\pi x}{L}\right) \tag{3.2}$$

where h_0 is the amplitude of half sine wave and L is span of the bridge.

3.3.2 Random Unevenness

The road surface roughness in bridge-vehicle interaction dynamics can be prescribed as a stationary Gaussian random field characterized by its power spectral density (PSD) function (ISO 8608: 1995). The general introduction to random Gaussian processes with their stochastic characteristics, a description of roadway profiles as a random process and an illustration of models for the realizations of roadway profiles is explained in this section.

For a Gaussian stochastic process $g_0(t)$ with an autocorrelation function $R_{g0g0}(\tau)$ and a two-sided power spectral density function $S_{g0g0}(\Omega)$, the following relations hold (Shinozuka and Deodatis, 1991)

$$E[g_0(t)] = 0 \tag{3.3}$$

$$E[g_0(t+\tau)g_0(t)] = R_{g_0g_0}(\tau) \tag{3.4}$$

$$S_{g_0g_0}(\omega) = \frac{1}{2\pi}\int_{-\infty}^{\infty} R_{g_0g_0}(\tau)\exp(-i\omega\tau)d\tau \tag{3.5}$$

$$R_{g_0g_0}(\tau) = \int_{-\infty}^{\infty} S_{g_0g_0}(\omega)\exp(i\omega\tau)d\omega \tag{3.6}$$

where ω denotes the temporal frequency.

Dodds and Robson (1973) suggested a simplified way of describing the road surfaces to avoid a laborious procedure which is often obtained by measuring existing roadways. In the present study, road roughness has been considered as a realization of a stationary Gaussian homogeneous random process described by its power spectral density function in the space domain $S_{g0g0}(\Omega)$ with Ω as the wave number or spatial frequency. The dynamic analysis performed in the study is in time domain, hence a description of the road roughness in time domain is needed. Therefore, the temporal power spectral density function $S_{g0g0}(\omega)$ is to be evaluated. For a constant speed of vehicle, v the relationship between $S_{g0g0}(\omega)$ and $S_{g0g0}(\Omega)$ is derived as follows.

Since, the vehicle is travelling at a constant speed, v, any instant of travel time, τ can be expressed in terms of the distance travelled 'x' as

$$\tau = \frac{x}{v} \tag{3.7}$$

A cycle of wavelength $\lambda = 2\pi/\Omega$ is covered in period T as

$$T = \frac{\lambda}{v} \tag{3.8}$$

Thus, the temporal frequency is written as

$$\omega = \frac{2\pi}{T} = \frac{2\pi v}{\lambda} = v\Omega \tag{3.9}$$

Substituting Eqs. (3.7) and (3.9) in Eq. (3.5),

$$S_{g_0 g_0}(\omega = v\Omega) = \frac{1}{v}\left\{\frac{1}{2\pi}\int_{-\infty}^{\infty} R_{g_0 g_0}(x)\exp(-i\Omega x)dx\right\} \tag{3.10}$$

$$= \frac{1}{v} S_{g_0 g_0}(\Omega) \tag{3.11}$$

Using the relationship in Eq. (3.11), the temporal power spectral density function $S_{g0g0}(\omega)$ can be obtained from the spatial power spectral density function $S_{g0g0}(\Omega)$.

3.3.3 Variable Velocity

Road roughness can be simulated as a stationary random process in space domain when vehicle moves with a constant velocity. This also becomes a stationary process in time domain. Therefore, the response of tire induced by road roughness is a stationary random process in time domain (Honda et al., 1982; Dodds and Robson, 1973; Marcondes et al., 1991). The inclusion of variable mean profile in the road roughness makes it non-homogeneous in space domain which is explained above. However, when a vehicle is traversing the bridge at variable velocity, the response of tire induced by road roughness is a non-stationary random process in time domain (Virchis and Robson, 1971; Nigam and Yadav, 1974; Hwang and Kim, 2000; Zhang et al., 2002). Virchis and Robson (1971) have used the time domain approach to determine the second order statistics of the vehicle response to non-stationary base excitation during variable velocity. The non-stationary response of a vehicle travelling on a homogeneous road roughness is analysed using state-space approach. In this, the vehicle dynamics were modelled by linear ordinary differential equations in time domain and the excitation process of

road roughness was modelled by a differential equation in spatial domain. Another method to solve non-stationary response of a vehicle was presented by Nigam and Yadav (1974) in which differential equations with variable coefficients were first established in space domain and time changing covariance was then computed. Two different improved methods with higher computational efficiency based on the above method were proposed (Hwang and Kim, 2000; Zhang et al., 2002). Sasidhar and Talukdar (2003) used the Monte Carlo simulation technique to simulate deck profile for generating input samples in numerical integration of the system equations.

The variable vehicle velocity can be considered by taking the position of vehicle x_c at any time instant t from a fixed reference point which has been described by a polynomial of degree m and is expressed as

$$x_c(t) = \sum_{k=0}^{m} a_k t^k \tag{3.12}$$

This form can easily be used to represent different conditions of vehicle motions with suitable adjustment of the coefficients of the polynomial. For example, a constant velocity travel requires $a_2 = a_3 = \ldots = a_m = 0$ with a_0 and a_1 having non-zero values. The vehicle with uniform acceleration or deceleration requires $a_3 = a_4 = \ldots = a_m = 0$ with a_0, a_1 and a_2 being non-zero with change of sign to indicate negative acceleration. In a situation where acceleration or retardation is time variable, coefficients a_3, a_4, etc. are to be retained. The velocity of the vehicle, v at any instant time, t over the bridge from a reference station has been obtained by taking the first time derivative of x_c and is given as

$$v(t) = \sum_{k=1}^{m} k a_k t^{k-1} \tag{3.13}$$

In case of variable velocity on the road, the spatial frequency Ω can be mapped to a temporal frequency ω through vehicle forward velocity $v(t)$ as

$$\Omega = \frac{\omega}{v(t)} \tag{3.14}$$

Yadav and Upadhyay (1991) have proposed a generalised power spectral density function for non-stationary ground input. The Fourier transform of road roughness $h_r(x)$ can be written as

$$\tilde{h}_r(\Omega) = \frac{1}{2\pi}\int_{-\infty}^{\infty} h_r(x)\exp(i\Omega x)dx \tag{3.15}$$

Using Riemann-Stieltjes integral, Eq. (3.15) can be written as (Nigam, 1983)

$$\tilde{h}_r(\Omega) = \frac{1}{2\pi}\int_{-\infty}^{\infty}\left\{\int_{-\infty}^{\infty}\exp(-i\Omega_1 x)ds(\Omega_1)\right\}\exp(i\Omega x)dx \tag{3.16}$$

Eq. (3.16) can be written by changing the order of integration as

$$\tilde{h}_r(\Omega) = \frac{1}{2\pi}\int_{-\infty}^{\infty} ds(\Omega_1)\int_{-\infty}^{\infty}\exp\{-i(\Omega_1-\Omega)x\}dx \tag{3.17}$$

Using the definition of Dirac delta function, it is now possible to write road roughness $\tilde{h}_r(\Omega)$ as

$$\tilde{h}_r(\Omega) = \int_{-\infty}^{\infty} ds(\Omega_1)\delta(\Omega_1-\Omega) \tag{3.18}$$

in which δ is the Dirac delta function.

The generalized spatial power spectral density function now can be written as

$$S_{gg}(\Omega_1,\Omega_2) = E\left[\left|\tilde{h}_r(\Omega_1)\tilde{h}_r^*(\Omega_2)\right|\right] \tag{3.19}$$

Substituting Eq. (3.18) in Eq. (3.19)

$$S_{gg}(\Omega_1,\Omega_2) = E\left[\left|\left\{\int_{-\infty}^{\infty} dS(\varepsilon)\delta(\varepsilon-\Omega_1)\right\}\left\{\int_{-\infty}^{\infty} dS^*(\kappa)\delta(\kappa-\Omega_2)\right\}\right|\right] \tag{3.20}$$

Rearranging Eq. (3.20),

$$S_{gg}(\Omega_1,\Omega_2) = \int_{-\infty}^{\infty}\int_{-\infty}^{\infty} E\left[\left|dS(\varepsilon)dS^*(\kappa)\right|\right]\delta(\varepsilon-\omega_1/v_1)\delta(\kappa-\omega_2/v_2) \tag{3.21}$$

Eq. (3.21) is written as

$$S_{gg}(\Omega_1,\Omega_2) = \int_{-\infty}^{\infty}\int_{-\infty}^{\infty} S_{gg}(\varepsilon,\kappa)\delta(\varepsilon-\omega_1/v_1)\delta(\kappa-\omega_2/v_2)d\varepsilon\, d\kappa \tag{3.22}$$

Using the property of Dirac delta function $\int_{-\infty}^{\infty}\delta(u-u_1)f(u)du = f(u_1)$, Eq. (3.22) is written as

$$S_{gg}(\Omega_1,\Omega_2) = S_{gg}(\omega_1/v_1, \omega_2/v_2) \tag{3.23}$$

where v_1 and v_2 are vehicle forward velocities at time instants t_1 and t_2 respectively. In the present study, simulation technique has been used so that at each time instant t, road roughness h_r will vary according to new position of vehicle centre of gravity.

3.3.4 PSD Function of Road Surface Roughness

One-sided power spectral density function is derived for which the following relation holds

$$S_{GG}(\Omega) = 2S_{g_0g_0}(\Omega) \tag{3.24}$$

where $S_{GG}(\Omega)$ is one sided power spectral density function. There are two main models for generating realizations of random processes based on the work of past researchers (Shinozuka and Deodatis, 1991). First one consists of a series of sines and cosines with random amplitudes and second one consists of a series of cosine terms having random phase angles with a specified probability density function. The latter is often adopted for the realization of road profiles for bridge-vehicle interaction dynamics (Olivia et. al., 2013) and is shown below

$$h_r(x) = \sum_{s=1}^{N_s} A_s \cos(2\pi\Omega_s x + \theta_s) \tag{3.25}$$

where $h_r(x)$ is the deck surface random unevenness which is a Gaussian process (Shinozuka, 1971) with an independent random phase angle θ_s uniformly distributed from 0 to 2π, N_s is the number of terms used to build up the road surface roughness, A_s is the amplitude of the cosine wave, Ω_s is the spatial frequency (c/m) within the interval $[\Omega_L, \Omega_U]$ where Ω_L and Ω_U are lower and upper cut-off frequencies of spatial unevenness respectively. The parameters A_s and Ω_s are computed as

$$A_s = \sqrt{S_{GG}(\Omega_s)\Delta\Omega} \tag{3.26}$$

$$\Omega_s = \Omega_L + \left(s - \frac{1}{2}\right)\Delta\Omega \tag{3.27}$$

where $S_{GG}(\Omega_s)$ is the one-sided spatial power spectral density function (m^2/c/m) of road surface roughness as given in Eq. (3.24).

The above equations show that the power spectral density can be discretized into spatial frequency bands of width of $\Delta\Omega$. The entire frequency domain of the power spectral density cannot be used in the realization due to mathematical and physical reasons (Shinozuka, 1971). Therefore, cut-off frequencies are needed for the realizations of road surfaces. The discretizing frequency band is defined as

$$\Delta\Omega = \frac{\left(\Omega_U - \Omega_L\right)}{N_s} \tag{3.28}$$

As mentioned earlier, Ω_L and Ω_U are lower and upper cut-off frequencies respectively and N_s is the number of terms used to build up the road surface roughness.

The long wavelength irregularities correspond to low frequency components and short wavelength irregularities correspond to high frequency components (Newland, 1993). The different wavelengths and their corresponding frequencies excite different vibrational modes of the heavy vehicle. The bouncing mode of the sprung mass is more of low frequency mode with the axle hop and pitching modes are of higher frequencies (Cebon, 1999). The power spectral density function $S_{GG}(\Omega_s)$ (m^2/c/m) of road surface roughness can be expressed as (Huang and Wang, 1992)

$$S_{GG}\left(\Omega_s\right) = S_{GG}\left(\Omega_0\right)\left(\frac{\Omega_s}{\Omega_0}\right)^{-m} \tag{3.29}$$

where Ω_0 is referred as discontinuity frequency and is taken as $1/2\pi$ (c/m). m and $S_{GG}(\Omega_0)$ are the roughness shape coefficient and roughness magnitude coefficient respectively. These factors are indicators of roughness intensity. The ISO suggested that for m = 2, lower cut off frequency Ω_L = 0.1 c/m and upper cut off frequency Ω_U = 2 c/m (Sun and Kennedy, 2002) may be considered to determine dynamic load on the wheel induced by pavement unevenness.

It is observed from Eq. (3.29) that at very low spatial frequency ($\Omega_s \rightarrow 0$), the power spectral density becomes unbounded i.e., $S_{GG}(\Omega_s) \rightarrow \infty$. Yin et al. (2010) suggested an improved equation as follows in view of the former,

$$S_{GG}(\Omega_s) = S_{GG}(\Omega_0)\left(\frac{\Omega_0^2}{\Omega_s^2 + \Omega_L^2}\right) \tag{3.30}$$

The PSD function given by Eq. (3.30) has been adopted in the present study. Using the relation given in Eq. (3.11) for constant velocity and Eq. (3.23) for variable velocity, the temporal power spectral density function $S_{GG}(\omega_s)$ has been obtained from the spatial power spectral density function $S_{GG}(\Omega_s)$ given in Eq. (3.30). ISO classified road into five classes depending on different road surface conditions. Table 3.1 gives ISO specified values for this classification (ISO 8608:1995).

Table 3.1 Road classification based on roughness magnitude coefficient (ISO 8608:1995)

Road Class	Road roughness coefficient $S_{GG}(\Omega_0)$ (10^{-6} m^2/c/m)
Good	$8 < S_{GG}(\Omega_0) \leq 32$
Average	$32 < S_{GG}(\Omega_0) \leq 128$
Poor	$128 < S_{GG}(\Omega_0) \leq 512$
Very Poor	$512 < S_{GG}(\Omega_0) \leq 2028$

3.4 Bridge-Vehicle Model considering Random Arrival Time of Vehicles

In the present study, generic vehicle model known as Quarter Car Model has been adopted. In this model, the vehicle mass is considered to be lumped at the centroid of the vehicle. It is called as sprung mass and is denoted by m_s. The mass of the wheel, tire and part of the suspension is referred to as the unsprung mass m_w. All the motions are in vertical direction, and therefore it is called as heave model. The bridge vehicle model for single-span and multi-span continuous bridge is explained in the section below. The vehicles arrive on the bridge at random times which constitute a Poisson process.

3.4.1 Single Span Bridge Vehicle Model

The schematic representation of single-span bridge with multiple movement of vehicles is shown in Fig. 3.1.

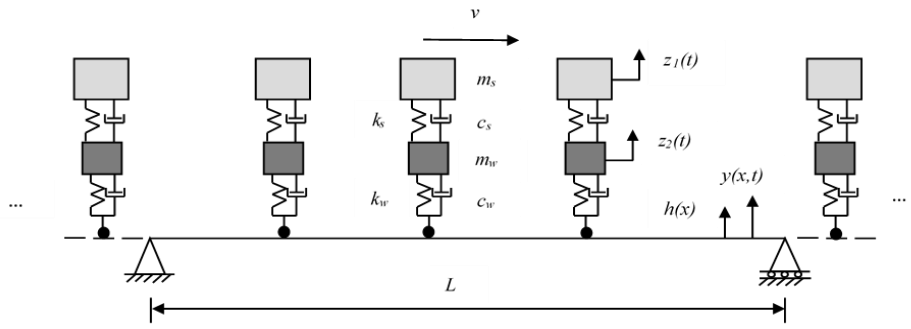

Fig.3.1 Vehicle movement on bridge

In Fig. 3.1, L is the span of the bridge, m_s is the sprung mass, m_w is the unsprung mass, k_s is the stiffness of the sprung mass, k_w is the stiffness of the unsprung mass, c_s is the damping of the sprung mass, c_w is the damping of the unsprung mass, $z_1(t)$ is the displacement of the sprung mass, $z_2(t)$ is the displacement of the unsprung mass, $y(x,t)$ is the displacement of the bridge and $h(x)$ is the bridge deck profile at distance x from the left side of the beam represented in Eq. (3.1).

The equation of motion for sprung mass shown in Fig.3.1 is given by

$$m_s\ddot{z}_1 + c_s\left(\dot{z}_1 - \dot{z}_2\right) + k_s\left(z_1 - z_2\right) = 0 \tag{3.31}$$

The equation of motion for unsprung mass shown in Fig. 3.1 is given by

$$m_w\ddot{z}_2 + c_w\left(\dot{z}_2 - \dot{y} - \dot{h}\right) + k_w\left(z_2 - y - h\right) - c_s\left(\dot{z}_1 - \dot{z}_2\right) - k_s\left(z_1 - z_2\right) = 0 \tag{3.32}$$

The bridge response is assumed as superposition of the normal modes which is given as

$$y(x,t) = \sum_{n=1}^{\infty}\phi_n(x)\eta_n(t) \tag{3.33}$$

where, $\phi_n(x)$ is the normalised mode shape in n^{th} mode for single-span beam given in Appendix I and $\eta_n(t)$ is the generalized time dependent normal coordinate in n^{th} mode. Substituting Eq. (3.33) in Eq. (3.32), we get

$$\begin{aligned} &m_w\ddot{z}_2 + \left(c_s + c_w\right)\dot{z}_2 + \left(k_w + k_s\right)z_2 - c_s\dot{z}_1 - k_s z_1 - \\ &c_w\sum_{n=1}^{\infty}\phi_n(x)\dot{\eta}_n(t) - \sum_{n=1}^{\infty}k_w\phi_n(x)\eta_n(t) = c_w\dot{h} + k_w h \end{aligned} \tag{3.34}$$

in which

$$\dot{h}(t)=\frac{dh}{dt}=\frac{dh}{dx}\frac{dx}{dt}=vh'(x) \tag{3.35}$$

in which v is computed using Eq. (3.13).

The governing differential equation of motion of the bridge in flexure is expressed as

$$EI\frac{\partial^4 y(x,t)}{\partial x^4}+c\frac{\partial y(x,t)}{\partial t}+m_b\frac{\partial^2 y(x,t)}{\partial t^2}=f(x,t) \tag{3.36}$$

in which m_b is the mass per unit length, c is viscous damping per unit length and EI represents the flexural rigidity of the bridge. The imposed vertical force $f(x,t)$ on the bridge due to vehicle interaction is given by

$$\begin{aligned} f(x,t)=&\left\{k_w(z_2-y-h)+c_w(\dot{z}_2-\dot{y}-\dot{h})\right\}\delta\{x-x_c\}\\ &-(m_s+m_w)g\delta\{x-x_c\}\end{aligned} \tag{3.37}$$

in which x_c denotes the location of wheel contact from the same reference station and is given as

$$x_c=\sum_{j=1}^{N(t)}v(t-t_j) \tag{3.38}$$

where, $N(t)$ represents the number of vehicles arriving on the bridge during time interval (0,t] following Poisson process, t_j represents the arrival time of jth vehicle, v is the velocity of the vehicle traversing on the bridge and is given in Eq. (3.13). Substituting Eq. (3.33), Eq. (3.37) and Eq. (3.38) in Eq. (3.36), multiplying both sides of the equation by $\phi_i(x)$ and integrating in the domain of the bridge and using orthogonality conditions (Meirovitch, 1986), Eq. (3.36) is written as

$$\begin{aligned} &\ddot{\eta}_n(t)+2\xi_n\omega_n\dot{\eta}_n(t)+\omega_n{}^2\eta_n(t)=\\ &\frac{1}{M_n}\int_o^L\left\{k_w(z_2-y-h)+c_w(\dot{z}_2-\dot{y}-\dot{h})\right\}\sum_{j=1}^{N(t)}\delta\{x-v(t-t_j)\}\phi_n(x)dx\\ &-\frac{1}{M_n}\int_0^L(m_s+m_w)g\sum_{j=1}^{N(t)}\delta\{x-v(t-t_j)\}\phi_n(x)dx;n=1,2,...\end{aligned} \tag{3.39}$$

where, ω_n is the natural frequency in nth mode, ξ_n is the damping ratio of nth mode, δ is the Dirac delta function and M_n is the generalized mass for nth mode. For practical applications,

the contribution of higher modes is very insignificant and therefore, in the present study, the number of modes are truncated to "n_b".

Using the property of Dirac delta function $\int_{-\infty}^{\infty}\delta(u-u_1)f(u)du = f(u_1)$,

Eq. (3.39) can be further expressed as

$$\begin{aligned}
&\ddot{\eta}_n(t)+2\xi_n\omega_n\dot{\eta}_n(t)+\omega_n^2\eta_n(t)-\frac{c_w}{M_n}\sum_{j=1}^{N(t)}\phi_n\{v(t-t_j)\}\dot{z}_2-\\
&\frac{k_w}{M_n}\sum_{j=1}^{N(t)}\phi_n\{v(t-t_j)\}z_2=\frac{-k_w}{M_n}\sum_{j=1}^{N(t)}\phi_n\{v(t-t_j)\}h-\frac{-c_w}{M_n}\sum_{j=1}^{N(t)}\phi_n\{v(t-t_j)\}\dot{h}\\
&-(m_s+m_w)g\sum_{n=1}^{N(t)}\phi_n\{v(t-t_j)\}-\frac{c_w}{M_n}\sum_{j=1}^{N(t)}\left[\sum_{i=1}^{n_b}\phi_i(x)\dot{\eta}_i(t)\right]\phi_n\{v(t-t_j)\}-\\
&\frac{k_w}{M_n}\sum_{j=1}^{N(t)}\left[\sum_{i=1}^{n_b}\phi_i(x)\eta_i(t)\right]\phi_n\{v(t-t_j)\};n=1,2,\ldots n_b
\end{aligned} \tag{3.40}$$

Rearranging the terms in Eq. (3.40)

$$\begin{aligned}
&\ddot{\eta}_n(t)+\left(2\xi_n\omega_n\dot{\eta}_n(t)+\frac{c_w}{M_n}\sum_{j=1}^{N(t)}\left[\sum_{i=1}^{n_b}\phi_i(x)\dot{\eta}_i(t)\right]\phi_n\{v(t-t_j)\}\right)+\\
&\left(\omega_n^2\eta_n(t)+\frac{k_w}{M_n}\sum_{j=1}^{N(t)}\left[\sum_{i=1}^{n_b}\phi_i(x)\eta_i(t)\right]\phi_n\{v(t-t_j)\}\right)-\\
&\frac{c_w}{M_n}\sum_{j=1}^{N(t)}\phi_n\{v(t-t_j)\}\dot{z}_2-\frac{k_w}{M_n}\sum_{j=1}^{N(t)}\phi_n\{v(t-t_j)\}z_2=-\frac{k_w}{M_n}\sum_{j=1}^{N(t)}\phi_n\{v(t-t_j)\}h-\\
&\frac{c_w}{M_n}\sum_{j=1}^{N(t)}\phi_n\{v(t-t_j)\}\dot{h}-(m_s+m_w)g\sum_{n=1}^{N(t)}\phi_n\{v(t-t_j)\},n=1,2,\ldots n_b
\end{aligned} \tag{3.41}$$

3.4.2 Multi-Span Continuous Bridge Vehicle Model

The multi-span continuous bridge and multiple quarter car vehicle model is shown in Fig. 3.2.

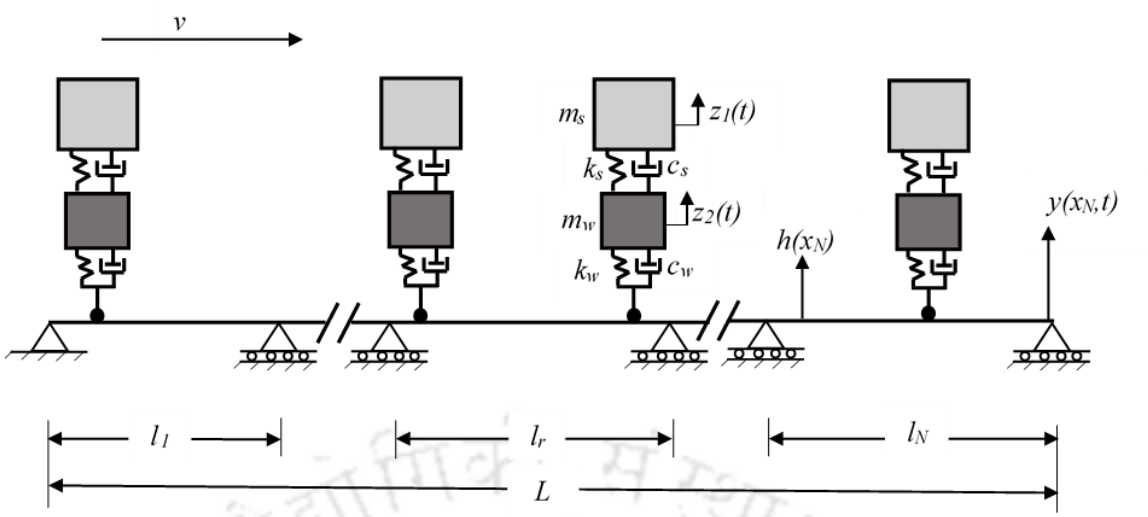

Fig. 3.2 Multi-span continuous bridge subjected to moving vehicle

The variables appearing in bridge-vehicle model in Fig. 3.2 are sprung mass m_s, unsprung mass m_w, suspension stiffness k_s, suspension damping c_s, tyre stiffness k_w, tyre damping c_w, sprung mass displacement z_1 and unsprung mass displacement z_2. For the multi-span continuous bridge, l_N is the length of the bridge in the Nth span, $y(x_N,t)$ is the deflection of the Nth span, $h(x_N)$ is the deck profile of the Nth span and L is the total length of the bridge.

The governing differential equations of the two lumped masses can be written as

$$m_s\ddot{z}_1 + c_s\left(\dot{z}_1 - \dot{z}_2\right) + k_s\left(z_1 - z_2\right) = 0 \tag{3.42}$$

$$m_w\ddot{z}_2 + c_w\left(\dot{z}_2 - \dot{y}_r - \dot{h}\right) + k_w\left(z_2 - y_r - h\right) - c_s\left(\dot{z}_1 - \dot{z}_2\right) - k_s\left(z_1 - z_2\right) = 0 \tag{3.43}$$

Bridge deflection on rth span, $y_r(x_r,t)$ in Eq. (3.43) can be represented as a product of mode shape and normal coordinate which is shown as

$$y_r\left(x_r,t\right) = \sum_{n=1}^{\infty}\phi_{nr}\left(x\right)\eta_n\left(t\right) \tag{3.44}$$

where, $\phi_{nr}(x)$ is the nth bending mode shape function of the rth span (Meirovitch, 1986) and $\eta_n(t)$ is the corresponding generalised time-dependent normal co-ordinate. Since, the contribution of higher modes in the calculation of response is negligible, therefore finite number of first few modes (n_b) is considered in computation. Substituting Eq. (3.44) in Eq. (3.43) and considering the contribution of n_b modes,

$$m_w\ddot{z}_2+\dot{z}_2\left(c_w+c_s\right)+z_2\left(k_w+k_s\right)-c_w\sum_{n=1}^{n_b}\phi_{nr}\left(x\right)\dot{\eta}_n\left(t\right)-k_w\sum_{n=1}^{n_b}\phi_{nr}\left(x\right)\eta_n\left(t\right)-$$
$$c_s\dot{z}_1-k_sz_1=c_w\dot{h}+k_wh \tag{3.45}$$

in which $\dot{h}$ is given in Eq. (3.35).

The equation of transverse vibration for each span is given as

$$EI\frac{\partial^4y_r}{\partial x_r^4}+c\frac{\partial y_r}{\partial t}+m_b\frac{\partial^2y_r}{\partial t^2}=f_r\left(x_r,t\right) \tag{3.46}$$

where, EI, m_b and c denotes the flexural rigidity, mass per unit length and viscous damping per unit length respectively, x_r is the local co-ordinate along the axis of the rth span at time instant t, $f_r(x_r,t)$ is the time-varying external load due to moving loads and is given as

$$\begin{aligned}f_r\left(x,t\right)=&\left\{k_w\left(z_2-y_r-h\right)+c_w\left(\dot{z}_2-\dot{y}_r-\dot{h}\right)\right\}\delta\left\{x_r-x_c\right\}\\&-\left(m_s+m_w\right)g\delta\left\{x_r-x_c\right\}\end{aligned} \tag{3.47}$$

in which x_c is the location of wheel contact in rth span and is given in Eq. (3.12). Using modal expansion technique for linear system and in view of orthogonal nature of normal modes (Meirovitch, 1986) and substituting Eq. (3.44) and Eq. (3.47) in Eq. (3.46), one obtains

$$\begin{aligned}&\ddot{\eta}_n\left(t\right)+2\xi_n\omega_{nr}\dot{\eta}_n\left(t\right)+{\omega_{nr}}^2\eta_n\left(t\right)=\\&\frac{1}{M_n}\int_o^L\left\{k_w\left(z_2-y_r-h\right)+c_w\left(\dot{z}_2-\dot{y}_r-\dot{h}\right)\right\}\sum_{j=1}^{N(t)}\delta\left\{x-v\left(t-t_j\right)\right\}\phi_{nr}\left(x\right)dx\\&-\frac{1}{M_n}\int_0^L\left(m_s+m_w\right)g\sum_{j=1}^{N(t)}\delta\left\{x-v\left(t-t_j\right)\right\}\phi_{nr}\left(x\right)dx;n=1,2,...,n_b\end{aligned} \tag{3.48}$$

In Eq. (3.48), ξ_n, ω_{nr}, $N(t)$, t_j, δ, M_n represents the modal damping ratio of the nth mode, natural frequency in the nth mode of the rth span, number of vehicles arriving on the bridge in the interval (0,t], arrival time of the jth vehicle on the bridge, Dirac delta function and generalized mass in the nth mode respectively. The expression for M_n is given as

$$\begin{aligned}M_n&=\int_0^L m_b\phi_{nr}^2\left(x\right)dx\\&=\sum_{r=1}^N\int_0^{l_r}m_b\phi_{nr}^2\left(x\right)dx\end{aligned} \tag{3.49}$$

Substituting the bridge deflection from Eq. (3.44) and using the property of Dirac delta function $\int_{-\infty}^{\infty}\delta(u-u_1)f(u)du = f(u_1)$ in Eq. (3.48), Eq. (3.48) can be written as

$$\begin{aligned}
&\ddot{\eta}_n(t)+2\xi_n\omega_{nr}\dot{\eta}_n(t)+\omega_{nr}^2\eta_n(t)-\frac{c_w}{M_n}\sum_{j=1}^{N(t)}\phi_{nr}\{v(t-t_j)\}\dot{z}_2-\\
&\frac{k_w}{M_n}\sum_{j=1}^{N(t)}\phi_{nr}\{v(t-t_j)\}z_2=\frac{-k_w}{M_n}\sum_{j=1}^{N(t)}\phi_{nr}\{v(t-t_j)\}h-\frac{-c_w}{M_n}\sum_{j=1}^{N(t)}\phi_{nr}\{v(t-t_j)\}\dot{h}\\
&-(m_s+m_w)g\sum_{j=1}^{N(t)}\phi_{nr}\{v(t-t_j)\}-\frac{c_w}{M_n}\sum_{j=1}^{N(t)}\left[\sum_{i=1}^{n_b}\phi_{ir}(x)\dot{\eta}_i(t)\right]\phi_{nr}\{v(t-t_j)\}-\\
&\frac{k_w}{M_n}\sum_{j=1}^{N(t)}\left[\sum_{i=1}^{n_b}\phi_{ir}(x)\eta_i(t)\right]\phi_{nr}\{v(t-t_j)\};n=1,2,\ldots n_b
\end{aligned} \tag{3.50}$$

Eq. (3.50) can be rearranged as

$$\begin{aligned}
&\ddot{\eta}_n(t)+\left(2\xi_n\omega_{nr}\dot{\eta}_n(t)+\frac{c_w}{M_n}\sum_{j=1}^{N(t)}\left[\sum_{i=1}^{n_b}\phi_{ir}(x)\dot{\eta}_i(t)\right]\phi_{nr}\{v(t-t_j)\}\right)+\\
&\left(\omega_{nr}^2\eta_n(t)+\frac{k_w}{M_n}\sum_{j=1}^{N(t)}\left[\sum_{i=1}^{n_b}\phi_{ir}(x)\eta_i(t)\right]\phi_{nr}\{v(t-t_j)\}\right)-\frac{c_w}{M_n}\sum_{j=1}^{N(t)}\phi_{nr}\{v(t-t_j)\}\dot{z}_2-\\
&\frac{k_w}{M_n}\sum_{j=1}^{N(t)}\phi_{nr}\{v(t-t_j)\}z_2=-\frac{k_w}{M_n}\sum_{j=1}^{N(t)}\phi_{nr}\{v(t-t_j)\}h-\frac{c_w}{M_n}\sum_{j=1}^{N(t)}\phi_{nr}\{v(t-t_j)\}\dot{h}\\
&-(m_s+m_w)g\sum_{j=1}^{N(t)}\phi_{nr}\{v(t-t_j)\};n=1,2,\ldots n_b
\end{aligned} \tag{3.51}$$

3.4.3 General Theoretical Formulation

Eqs. (3.31), (3.34) and (3.41) can be written in matrix form. Similarly, Eqs. (3.42), (3.45) and (3.51) can also be written in matrix form. The general equation in matrix form is shown as

$$\mathbf{M}\ddot{\mathbf{X}}+\mathbf{C}\dot{\mathbf{X}}+\mathbf{K}\mathbf{X}=\mathbf{F}(t) \tag{3.52}$$

The mass matrix **M**, damping matrix **C**, stiffness matrix **K**, force vector **F**(t) and response vector **X**(t) for single span bridge and multi-span continuous bridge along with their respective bending mode shape function and natural frequency is given in Appendix I and II respectively.

It can be noted that in bridge-vehicle dynamics, there are two sub systems. First one is series of moving vehicles and the other is bridge. In studying the response of bridge vehicle systems, two sets of differential equations have been developed. The first set contains vehicle's two

equations of motion for sprung and unsprung mass whereas second set contains discretised equations of bridge continuum. It is the interaction forces existing at the contact points of two sub systems that make the two sub systems coupled. As the contact force changes with respect to time and space and is complicated by their random nature of arrival, the system matrices become time dependents where stiffness and damping matrices as well as force vectors contain random variables as can be observed from Eqs. (3.31), (3.34) and (3.41) in case of single span beam and Eqs. (3.42), (3.45) and (3.51) in case of multi-span continuous beam. To handle such multi-parameter random problem, an orthogonal polynomial expansion method has been outlined in the next subsection.

3.4.4 Orthogonal Polynomial Expansion Method

The damping matrix, stiffness matrix and force vector contain random variable due to arrival time considered as Poisson process. Due to non-linear dependency on the random variable in the form of the sine function (Li and Chen, 2009), the matrices or vectors are expanded using Taylor series as follows

$$\mathbf{C} = \mathbf{C}_m + \mathbf{C}_{\lambda t_j}\left\{\lambda t_j - \mu\left(\lambda t_j\right)\right\} \tag{3.53}$$

$$\mathbf{K} = \mathbf{K}_m + \mathbf{K}_{\lambda t_j}\left\{\lambda t_j - \mu\left(\lambda t_j\right)\right\} \tag{3.54}$$

$$\mathbf{F}(t) = \mathbf{F}(t)_m + \mathbf{F}(t)_{\lambda t_j}\left\{\lambda t_j - \mu\left(\lambda t_j\right)\right\} \tag{3.55}$$

The variable λ corresponds to the mean arrival rate and $\mu(\lambda t_j)$ is the mean of the random variable λt_j. The expression for $\mathbf{C}_m$, $\mathbf{C}_{\lambda tj}$, $\mathbf{K}_m$, $\mathbf{K}_{\lambda tj}$, $\mathbf{F}(t)_m$ and $\mathrm{F}(t)_{\lambda tj}$ are given as

$$\mathbf{C}_m = \mathbf{C}\Big|_{\lambda t_j = \mu(\lambda t_j)},\ \mathbf{C}_{\lambda t_j} = \frac{\partial \mathbf{C}}{\partial \lambda t_j}\Big|_{\lambda t_j = \mu(\lambda t_j)} \tag{3.56}$$

$$\mathbf{K}_m = \mathbf{K}\Big|_{\lambda t_j = \mu(\lambda t_j)},\ \mathbf{K}_{\lambda t_j} = \frac{\partial \mathbf{K}}{\partial \lambda t_j}\Big|_{\lambda t_j = \mu(\lambda t_j)} \tag{3.57}$$

$$\mathbf{F}(t)_m = \mathbf{F}(t)\Big|_{\lambda t_j = \mu(\lambda t_j)},\ \mathbf{F}(t)_{\lambda t_j} = \frac{\partial \mathbf{F}(t)}{\partial \lambda t_j}\Big|_{\lambda t_j = \mu(\lambda t_j)} \tag{3.58}$$

The response $\boldsymbol{X}$ of the generalized coordinates can be sequentially expanded as a set of orthogonal basis functions (Li and Chen, 2009). An element of the response vector is given by,

$$X_s(t) = \sum_{l=0}^{N_1} Q_{sl}(t) L_l^j(\lambda t_j); s = 1, 2, ..., n_d \tag{3.59}$$

where, j is the number of vehicle arrivals which is analogous to the shape parameter of Gamma distribution in the present study, n_d is the number of degrees of freedom considered, N_1 is the number of basic functions with respect to λt_j, $L_l^j(\lambda t_j)$ represents the orthogonal function and $Q_{sl}(t)$ is the displacement function varying with respect to time. The distribution of arrival time considered is Gamma distribution as the arrival time of the vehicle follows Poisson Process which is given by,

$$p_{t_j}(t) = \frac{\lambda^j t^{j-1} \exp(-\lambda t)}{\Gamma(j)} \tag{3.60}$$

where, $p_{t_j}(t)$ is the probability density function of the arrival time, and Γ is the gamma function and is defined as $\Gamma(n) = (n-1)!$, n is an integer and $n > 0$.

The probability density function of λt_j using the property of function of random variable (Nigam, 1983) is given as,

$$p_{\lambda t_j}(\lambda t) = \frac{t^{j-1} \exp(-t)}{\Gamma(j)} \tag{3.61}$$

The orthogonal polynomial function considered as Associated Laguerre Polynomial (Schoutens, 2000) is used which is shown as,

$$L_l^j(\lambda t_j) = \frac{1}{\Gamma(l+1)} \sum_{k=0}^{l} \frac{\Gamma(l+1)}{\Gamma(k+1)}^{j+l} C_{l-k} (-\lambda t_n)^k \tag{3.62}$$

where $\Gamma(n+1) = n\Gamma(n)$. In the expression, n is an integer and $n > 0$.

The response vector is written as,

$$\mathbf{X}(t) = \sum_{l=0}^{N_1} \mathbf{Q}_l(t) L_l^j(\lambda t_j) \tag{3.63}$$

Substituting Eq. (3.63) in Eq. (3.52),

$$\mathbf{M}\sum_{l=0}^{N_1}\ddot{\mathbf{Q}}_l(t)L_l^j(\lambda t_j)+\mathbf{C}\sum_{l=0}^{N_1}\dot{\mathbf{Q}}_l(t)L_l^j(\lambda t_j)+\mathbf{K}\sum_{l=0}^{N_1}\mathbf{Q}_l(t)L_l^j(\lambda t_j)=\mathbf{F}(t) \tag{3.64}$$

Substituting Eq. (3.53), Eq. (3.54) and Eq. (3.55) in Eq. (3.64),

$$\begin{aligned}&\mathbf{M}\sum_{l=0}^{N_1}\ddot{\mathbf{Q}}_l(t)L_l^j(\lambda t_j)+\left(\mathbf{C}_m+\mathbf{C}_{\lambda t_j}\left\{\lambda t_j-\mu(\lambda t_j)\right\}\right)\sum_{l=0}^{N_1}\dot{\mathbf{Q}}_l(t)L_l^j(\lambda t_j)+\\&\left(\mathbf{K}_m+\mathbf{K}_{\lambda t_j}\left\{\lambda t_j-\mu(\lambda t_j)\right\}\right)\sum_{l=0}^{N_1}\mathbf{Q}_l(t)L_l^j(\lambda t_j)=\mathbf{F}(t)_m+\mathbf{F}(t)_{\lambda t_j}\left\{\lambda t_j-\mu(\lambda t_j)\right\}\end{aligned} \tag{3.65}$$

Multiply Eq. (3.65) by $L_k^j(\lambda t_j)$,

$$\begin{aligned}&\mathbf{M}\sum_{l=0}^{N_1}\ddot{\mathbf{Q}}_l(t)L_l^j(\lambda t_j)L_k^j(\lambda t_j)+\\&\left(\mathbf{C}_m+\mathbf{C}_{\lambda t_j}\left\{\lambda t_j-\mu(\lambda t_j)\right\}\right)\sum_{l=0}^{N_1}\dot{\mathbf{Q}}_l(t)L_l^j(\lambda t_j)L_k^j(\lambda t_j)+\\&\left(\mathbf{K}_m+\mathbf{K}_{\lambda t_j}\left\{\lambda t_j-\mu(\lambda t_j)\right\}\right)\sum_{l=0}^{N_1}\mathbf{Q}_l(t)L_l^j(\lambda t_j)L_k^j(\lambda t_j)=\mathbf{F}(t)_m+\\&\mathbf{F}(t)_{\lambda t_j}\left\{\lambda t_j-\mu(\lambda t_j)\right\}L_k^j(\lambda t_j)\end{aligned} \tag{3.66}$$

Eq. (3.66) can be further written as,

$$\begin{aligned}&\mathbf{M}\sum_{l=0}^{N_1}\ddot{\mathbf{Q}}_l(t)L_l^j(\lambda t_j)L_k^j(\lambda t_j)+\left(\mathbf{C}_m\sum_{l=0}^{N_1}\dot{\mathbf{Q}}_l(t)L_l^j(\lambda t_j)L_k^j(\lambda t_j)\right)+\\&\left(\mathbf{C}_{\lambda t_j}\sum_{l=0}^{N_1}\dot{\mathbf{Q}}_l(t)L_l^j(\lambda t_j)L_k^j(\lambda t_j)\lambda t_j\right)-\left(\mathbf{C}_{\lambda t_j}\sum_{l=0}^{N_1}\dot{\mathbf{Q}}_l(t)L_l^j(\lambda t_j)L_k^j(\lambda t_j)\mu(\lambda t_j)\right)+\\&\left(\mathbf{K}_m\sum_{l=0}^{N_1}\mathbf{Q}_l(t)L_l^j(\lambda t_j)L_k^j(\lambda t_j)\right)+\left(\mathbf{K}_{\lambda t_j}\sum_{l=0}^{N_1}\mathbf{Q}_l(t)L_l^j(\lambda t_j)L_k^j(\lambda t_j)\lambda t_j\right)-\\&\left(\mathbf{K}_{\lambda t_j}\sum_{l=0}^{N_1}\mathbf{Q}_l(t)L_l^j(\lambda t_j)L_k^j(\lambda t_j)\mu(\lambda t_j)\right)=\mathbf{F}(t)_m+\mathbf{F}(t)_{\lambda t_j}\left\{\lambda t_j-\mu(\lambda t_j)\right\}L_k^j(\lambda t_j)\end{aligned} \tag{3.67}$$

The recurrence relation shown in Eq. (3.68) is used for terms $\lambda t_j L_l^j(\lambda t_j)$ (Schoutens, 2000),

$$\begin{aligned}&\lambda t_j L_l^j(\lambda t_j)=\alpha_{l-1}L_l^j(\lambda t_j)+\beta_l L_l^j(\lambda t_j)+\gamma_{l+1}L_l^j(\lambda t_j)\\&\alpha_{l-1}=-(l-1+j)\\&\gamma_{l+1}=-(l+1+1)\\&\beta_l=(2l)+j+1\end{aligned} \tag{3.68}$$

Substituting Eq. (3.68) in Eq. (3.67),

$$\begin{aligned}
&\mathbf{M}\sum_{l=0}^{N_1}\ddot{\mathbf{Q}}_l(t)L_l^j(\lambda t_j)L_k^j(\lambda t_j)+\mathbf{C}_m\sum_{l=0}^{N_1}\dot{\mathbf{Q}}_l(t)L_l^j(\lambda t_j)L_k^j(\lambda t_j)+\\
&\mathbf{C}_{\lambda t_j}\sum_{l=0}^{N_1}\dot{\mathbf{Q}}_l(t)L_k^j(\lambda t_j)\left(\alpha_{l-1}L_{l-1}^j(\lambda t_j)+\beta_l L_l^j(\lambda t_j)+\gamma_{l+1}L_{l+1}^j(\lambda t_j)\right)-\\
&\mathbf{C}_{\lambda t_j}\sum_{l=0}^{N_1}\dot{\mathbf{Q}}_l(t)L_l^j(\lambda t_j)L_k^j(\lambda t_j)\mu(\lambda t_j)+\mathbf{K}_m\sum_{l=0}^{N_1}\mathbf{Q}_l(t)L_l^j(\lambda t_j)L_k^j(\lambda t_j)+\\
&\mathbf{K}_{\lambda t_j}\sum_{l=0}^{N_1}\mathbf{Q}_l(t)L_k^j(\lambda t_j)\left(\alpha_{l-1}L_{l-1}^j(\lambda t_j)+\beta_l L_l^j(\lambda t_j)+\gamma_{l+1}L_{l+1}^j(\lambda t_j)\right)-\\
&\mathbf{K}_{\lambda t_j}\sum_{l=0}^{N_1}\mathbf{Q}_l(t)L_l^j(\lambda t_j)L_k^j(\lambda t_j)\mu(\lambda t_j)=\mathbf{F}(t)_m L_k^j(\lambda t_j)+\\
&\mathbf{F}(t)_{\lambda t_j}\left(\alpha_{k-1}L_{k-1}^j(\lambda t_j)+\beta_k L_k^j(\lambda t_j)+\gamma_{k+1}L_{k+1}^j(\lambda t_j)\right)-\mathbf{F}(t)_{\lambda t_j}\mu(\lambda t_j)L_k^j(\lambda t_j)
\end{aligned} \tag{3.69}$$

Multiplying each term of Eq. (3.69) by $p_{\lambda tj}(\lambda t)$ and integrating in the domain of the random variable and using the property of orthogonal polynomials (Schoutens, 2000) shown in Eq. (3.70),

$$\int_0^{\lambda t} p_{\lambda t_j}(\lambda t)L_l^j(\lambda t_j)L_k^j(\lambda t_j)d\lambda t_j = d_l^2\delta_{lk};l,k=0,1,2,...,N_1 \tag{3.70}$$

where, δ_{lk} is Kronecker delta and

$$d_l^2=\frac{\Gamma(l+j+1)}{\Gamma(l+1)\Gamma(j+1)} \tag{3.71}$$

Substituting Eq. (3.70) in Eq. (3.69),

$$\begin{aligned}
&\mathbf{M}\sum_{l=0}^{N_1}\ddot{\mathbf{Q}}_l(t)d_l^2\delta_{lk}+\\
&\sum_{l=0}^{N_1}\dot{\mathbf{Q}}_l(t)\left[\mathbf{C}_m d_l^2\delta_{lk}+\mathbf{C}_{\lambda t_j}\left(\alpha_{l-1}d_{l-1}^2\delta_{l-1k}+\beta_l d_l^2\delta_{lk}+\gamma_{l+1}d_{l+1}^2\delta_{l+1k}\right)-\mathbf{C}_{\lambda t_j}\mu(\lambda t_j)d_l^2\delta_{lk}\right]+\\
&\sum_{l=0}^{N_1}\mathbf{Q}_l(t)\left[\mathbf{K}_m d_l^2\delta_{lk}+\mathbf{K}_{\lambda t_j}\left(\alpha_{l-1}d_{l-1}^2\delta_{l-1k}+\beta_l d_l^2\delta_{lk}+\gamma_{l+1}d_{l+1}^2\delta_{l+1k}\right)-\mathbf{K}_{\lambda t_j}\mu(\lambda t_j)d_l^2\delta_{lk}\right]=\\
&\mathbf{F}(t)_m d_0^2\delta_{0k}+\mathbf{F}(t)_{\lambda t_j}\left(\alpha_{k-1}d_0^2\delta_{0k-1}+\beta_0 d_0^2\delta_{0k}+\gamma_{0+1}d_{0+1}^2\delta_{0+1k}\right)-\mathbf{F}(t)_{\lambda t_j}\mu(\lambda t_j)d_0^2\delta_{0k}
\end{aligned} \tag{3.72}$$

In Eq. (3.72), the value of k varies from 0 to N_1. Eq. (3.72) is solved with the help of Newmark's Method (Chopra, 2011) to obtain $\boldsymbol{Q}$.

3.4.5 Expected Value of Response

The method to evaluate the expectation of the response is shown below. The response ***X*** can be written as

$$\mathbf{X}(t)=\sum_{l=0}^{N_1}\mathbf{Q}_l(t)L_l^j(\lambda t_j) \tag{3.73}$$

Multiplying Eq. (3.73) by $L_0^j(\lambda t_j)$ such that the value of $L_0^j(\lambda t_j)$ is 1

$$\mathbf{X}(t)L_0^j(\lambda t_j)=\sum_{l=0}^{N_1}\mathbf{Q}_l(t)L_l^j(\lambda t_j)L_0^j(\lambda t_j) \tag{3.74}$$

Eq. (3.74) is written in terms of the elements of the response vector as

$$X_i(t)L_0^j(\lambda t_j)=\sum_{l=0}^{N_1}Q_{il}(t)L_l^j(\lambda t_j)L_0^j(\lambda t_j);i=1,2,...,n_d \tag{3.75}$$

Applying expectation operator on both sides of Eq. (3.75)

$$E\left[X_i(t)L_0^j(\lambda t_j)\right]=\sum_{l=0}^{N_1}E\left[Q_{il}(t)L_l^j(\lambda t_j)L_0^j(\lambda t_j)\right] \tag{3.76}$$

Due to the presence of the random variable, Eq. (3.74) can be written as,

$$E\left[X_i(t)L_0^j(\lambda t_j)\right]=\sum_{l=0}^{N_1}Q_{il}(t)E\left[L_l^j(\lambda t_j)L_0^j(\lambda t_j)\right] \tag{3.77}$$

With the help of the property of orthogonal polynomials (Schoutens, 2000) from Eq. (3.70), Eq. (3.77) is reduced to

$$E\left[L_l^j(\lambda t_j)L_0^j(\lambda t_j)\right]=d_l^2\delta_{l0} \tag{3.78}$$

where,

$$d_l^2=\frac{\Gamma(l+j+1)}{\Gamma(l+1)\Gamma(j+1)} \tag{3.79}$$

Substitute Eq. (3.78) in Eq. (3.77),

$$E\left[X_i(t)L_0^j(\lambda t_j)\right]=\sum_{l=0}^{N_1}Q_{il}(t)d_l^2\delta_{l0};i=1,2,...,n_d \tag{3.80}$$

Eq. (3.80) further simplifies due to the presence of Kronecker delta and is given as

$$E\left[X_i(t)\right]=Q_{i0}(t)d_0^2;i=1,2,...,n_d \tag{3.81}$$

3.4.6 Standard Deviation of Response

The covariance of the elements of the response vector is written as

$$Cov\ \left(X_i(t_1),X_i(t_2)\right)=E\left[X_i(t_1)X_i(t_2)\right]-E\left[X_i(t_1)\right]E\left[X_i(t_2)\right];i=1,2,...,n_d \tag{3.82}$$

In Eq. (3.82)

$$E\left[X_i(t_1)X_i(t_2)\right]=E\left[\sum_{l=0}^{N_1}Q_{il}(t_1)L_l^j(\lambda t_j)\sum_{m=0}^{N_1}Q_{im}(t_2)L_m^j(\lambda t_j)\right];i=1,2,...,n_d \tag{3.83}$$

$$\Rightarrow E\left[X_i(t_1)X_i(t_2)\right]=\sum_{l=0}^{N_1}\sum_{m=0}^{N_1}Q_{il}(t_1)Q_{im}(t_2)E\left[L_l^j(\lambda t_j)L_m^j(\lambda t_j)\right];i=1,2,...,n_d \tag{3.84}$$

Using the property of orthogonal polynomials (Schoutens, 2000) from Eq. (3.70), term inside the expectation operator in Eq. (3.84) can be written as

$$E\left[L_l^j(\lambda t_j)L_m^j(\lambda t_j)\right]=d_l^2\delta_{lm} \tag{3.85}$$

where, d_l^2 is given in Eq. (3.79). Substitute Eq. (3.85) in Eq. (3.84),

$$E\left[X_i(t_1)X_i(t_2)\right]=\sum_{l=0}^{N_1}\sum_{m=0}^{N_1}Q_{il}(t_1)Q_{im}(t_2)d_l^2\delta_{lm};i=1,2,...,n_d \tag{3.86}$$

The covariance of the elements of the response vector is obtained by substituting Eq. (3.81) and Eq. (3.86) in Eq. (3.82) which is shown below,

$$Cov\left(X_i(t_1),X_i(t_2)\right)=\sum_{l=0}^{N_1}\sum_{m=0}^{N_1}Q_{il}(t_1)Q_{im}(t_2)d_l^2\delta_{lm}-Q_{i0}(t_1)Q_{i0}(t_2)d_0^4;i=1,2,...,n_d \tag{3.87}$$

In Eq. (3.87), the double summation gets simplified to single summation due to the presence of Kronecker delta. Hence, the above Eq. can be written as,

$$Cov\left(X_i(t_1), X_i(t_2)\right) = \sum_{l=o}^{N_1} Q_{il}(t_1) Q_{il}(t_2) d_l^2 - Q_{i0}(t_1) Q_{i0}(t_2) d_0^4 ; i = 1, 2, ..., n_d \quad (3.88)$$

Substituting $t_1 = t_2 = t$ in Eq. (3.88), the variance of the elements of the response vector is obtained as

$$Var\left[X_i(t)\right] = \sum_{l=0}^{N_1} \left[Q_{il}(t)\right]^2 d_l^2 - \left[Q_{i0}\right]^2 d_0^4 ; i = 1, 2, ..., n_d \quad (3.89)$$

3.5 Dynamic Amplification Factor

In bridge design, complete dynamic analysis for vehicle live load is not usually required as various codes suggested Dynamic Amplification Factor (DAF) to magnify the static effect. As per IRC 6 (2017), DAF is dependent on the span of the bridge. Vehicle parameters such as velocity of the vehicle, road surface roughness, axle weight of the vehicle, arrival time of the vehicle are not considered while evaluating DAF as per IRC 6 (2017). Studies conducted in the past have shown that DAF depends on the above mentioned parameters (Humar and Kashif, 1993; Brady et al., 2006).

The DAF is calculated taking the contribution of mean and standard deviation of the flexural stresses which is shown below. The response variable F is considered as a random process and assuming 95% confidence interval which extends the sample distribution approximately two times the standard error of the mean (SEM) in each direction from the mean, the maximum dynamic response is written as

$$F_{dynamic} = \left| \mu_f(x,t) + E_f(x,t) \right| \quad (3.90)$$

where $F_{dynamic}$ is the maximum response due to fluctuating load imposed on the bridge due to vibratory motion of the vehicle, $\mu_f(x,t)$ is the mean response and $E_f(x,t)$ is the standard error of the mean (SEM) defined as (DeCoursey, 2003)

$$E_f(x,t) = \frac{\sigma_f(x,t)}{\sqrt{N_p/4}} \quad (3.91)$$

in which $\sigma_f(x.t)$ is standard deviation of bridge response and N_p is the number of samples. The Dynamic Amplification Factor (DAF) in this study has been defined as

$$DAF = \frac{F_{static} + F_{dynamic}}{F_{static}} = 1 + \frac{F_{dynamic}}{F_{static}} = 1 + DI \tag{3.92}$$

where, F_{static} is the maximum static response of the bridge and DI represents the dynamic increment.

3.6 Closure

The vehicles entering the bridge are random in nature. In the present study, the arrival time of the vehicles have been considered as a random variable following Poisson process to simulate the actual traffic. The bridge-vehicle coupled system equations have been derived wherein the vehicle arrival rate appears as random variable in damping and stiffness matrices in addition to the force vector casting difficulty in obtaining a direct solution. The solution approach has been devised using Orthogonal Polynomial Expansion method. The non-homogeneous road surface roughness in the presence of variable mean has been incorporated. The variable mean profile can be considered in the study to include the effect of localized defects in the pavement or special provisions in the construction which are not considered while classifying the road conditions by ISO 8608 (1995). In the present work, pre-cambered profile of the bridge has been considered. Pre-cambering is generally adapted to compensate the excessive deflection due to over loading on the bridge. The bridge dynamic response has also been obtained for variable vehicle velocity. The dynamic amplification factor has been obtained by incorporating standard error of the mean in vehicle induced dynamic response, as such response is influenced by several random parameters.

4

FATIGUE LIFE PREDICTION: PART I
SINGLE SPAN BRIDGE USING SEMI ANALYTICAL METHOD

4.1 General

In the present chapter, the dynamic response of single span bridge subjected to multiple vehicle movement has been obtained using the semi analytical method. This approach is based on Orthogonal Polynomial Expansion which yields the expression of mean and standard deviation of response of the bridge. The vehicle arrival time is assumed to be a random process following Gamma distribution. The road surface roughness has been considered non-homogeneous by superimposing variable mean over the random process. The forward vehicle velocity is considered to be uniform and variable. When the vehicle travels at variable velocity, the vibration caused by road surface roughness is considered as a non-stationary random process.

An idealized model of bridge has been represented by partial differential equations of motion coupled with ordinary differential equations of motion of lumped parameter vehicle model. Such coupled system of equations with random parameters embedded in them have been solved by the present Orthogonal Polynomial Expansion method. The method has been described in section 3.4.4 in Chapter 3. The mean and standard deviation of the flexural stresses at the mid span of the bridge has been utilized to obtain the dynamic amplification factor and fatigue life for different bridge vehicle parameters. The results have been discussed to gain understanding of various factors which needs to be considered for design and maintenance of bridge.

4.2 System Parameters

The following system parameters have been adopted to generate numerical results and to conduct parametric study.

4.2.1 Bridge Parameters

The bridge considered is a single span twin cell box girder with span of 30 m. The single lane bridge is composed of reinforced concrete deck and steel girder which is twin cell type. The total width of the twin cell girder is 7.5 m and height is 1.5 m. The cross section of the superstructure of the bridge is shown in Fig. 4.1. The composite section is converted into

equivalent steel section using modular ration E_s/E_c = 8 where E_s is the Youngs modulus of elasticity and E_c is the Youngs modulus of elasticity of concrete. The mass per unit length of the bridge is 1.0288×10^4 kg/m and moment of inertia of equivalent steel section is 0.3391 m^4.

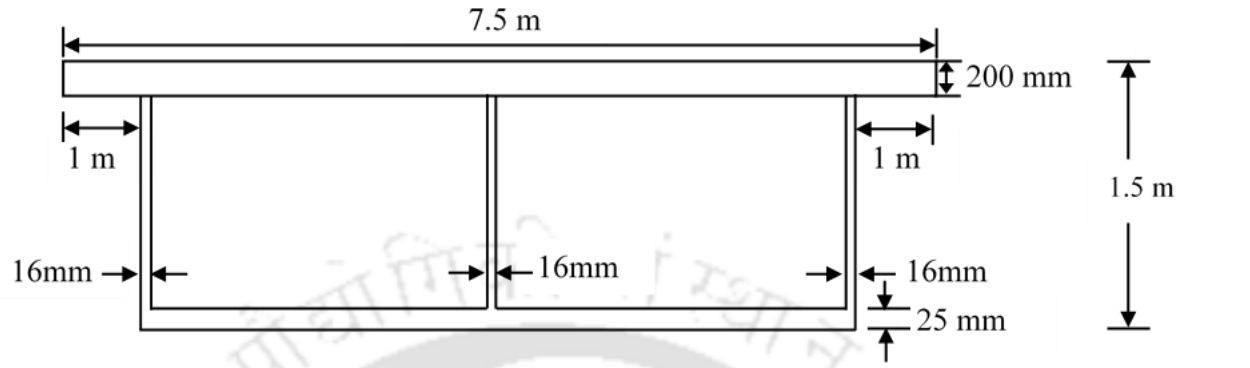

Fig. 4.1 Cross section of the superstructure of the bridge

4.2.2 Vehicle Parameters

The vehicle model considered is Quarter car model having single wheel contact. For this model, sprung mass, m_s is taken as 36000 kg and unsprung mass, m_w is 4000 kg. The vehicle model used is heavy vehicle and total weight $(m_s + m_w)g$ is 40000 N (40 tonnes) where g is 10 m/sec^2. The ratio of vehicle mass to bridge mass is significantly low in case of light vehicles and such vehicles will not be able to excite the bridge transverse mode of vibration (Fryba, 1972). Thus, light vehicles have not been considered in the study. The suspension stiffness k_s, suspension damping c_s, tyre stiffness k_w and tyre damping c_w have been considered as 14.4×10^6 Nm^{-1}, 475.2×10^3 Nsm^{-1}, 3.6×10^6 Nm^{-1} and 24×10^3 Nsm^{-1} respectively.

A video based traffic monitoring and processing has been proposed by Chen et al (2009) to obtain the vehicle arrival rate. According to the survey, it was seen that the average arrival rate is 2 vehicles per second i.e., 120 vehicles per minute. However, the traffic density that is reported is not always applicable in various conditions of road. To test the influence of arrival rate on the fatigue damage of the bridge, it is considered to carry out the parametric study with a deviation of ± 50 %.

4.3 Road Surface Roughness

The details of the procedure for generation of random road roughness from PSD function has been explained in section 3.3.4 in Chapter 3. For modelling deck surface roughness, the values of spectral roughness coefficient, $S_{GG}(\Omega_0)$ have been taken according to International

Organization for Standardization (ISO 8608: 1995) specifications for the class of different road conditions. In the present study, road roughness coefficient considered for good, average, poor and very poor road cases have been considered as 32×10^{-6} m^2/cycle/m, 120×10^{-6} m^2/cycle/m, 512×10^{-6} m^2/cycle/m and 1024×10^{-6} m^2/cycle/m respectively (ISO 8608:1995). As per ISO specifications, roughness shape coefficient m has been taken as 2, lower cut off frequency Ω_L is 0.1 c/m and upper cut off frequency Ω_U is 2 c/m (Sun and Kennedy, 2002). As mentioned in section 4.1, deterministic mean profile has also been considered. The deterministic mean profile in this study is the pre-cambering of the bridge in the form of a half sine wave with amplitude (h_0) as 0.01 m, which is given in section 3.3.1 in Chapter 3.

Using the above data, a typical road roughness, h_r for a very poor road condition is depicted in Fig. 4.2. From simulated road profile, auto-correlation has been computed and then PSD has been obtained using MATLAB function fft, which is shown in Fig. 4.3. The comparison of theoretical and simulated PSD has been presented in Fig. 4.4.

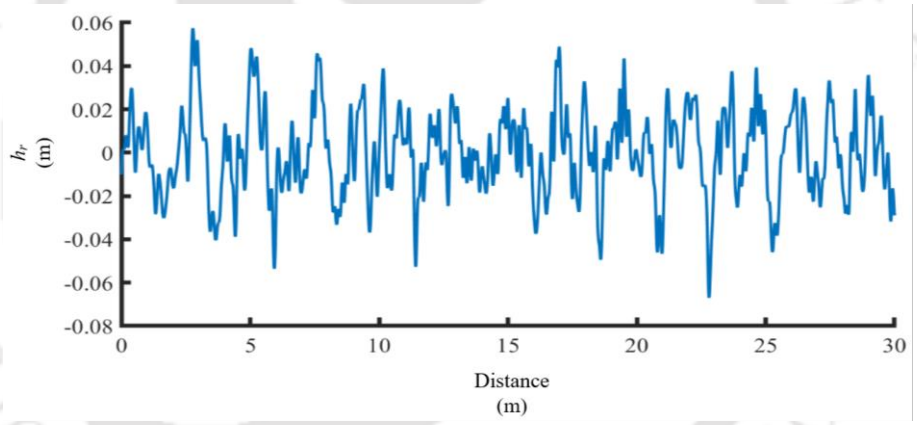

Fig. 4.2 Typical road roughness

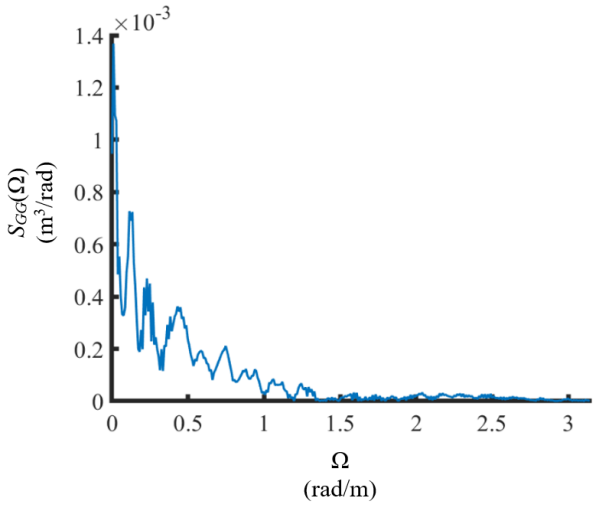

Fig. 4.3 Simulated PSD

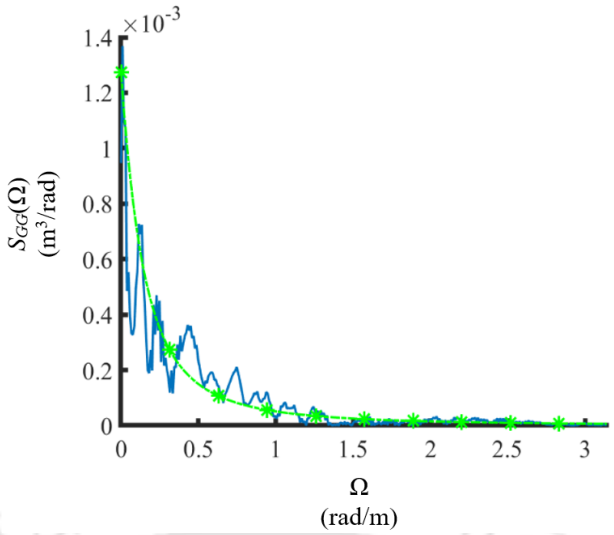

Fig. 4.4 Comparison of theoretical and simulated PSD

Fig. 4.4 reveals close agreement between theoretical and simulated PSD. The agreement is good towards higher cut-off frequencies. In the middle of the frequency range, discrepancy appears mainly because of numerical noise in the simulation process.

4.4 Convergence study

The semi analytical method proposed to evaluate the bridge dynamic response considering vehicle arrival time as random variable following Poisson process depends on the summation of the number of basic functions or the summation of the number of terms of the orthogonal polynomial function, which is explained in section 3.4.4 in Chapter 3.

The Poisson process is simple and widely used stochastic process for modelling the vehicle arrival time on the bridge. It is assumed that the vehicle arrivals on the bridge occurring in an interval of length t is Poisson distributed with mean λt where λ is the arrival rate of the vehicles, the interarrival time of the vehicle follows exponential distribution function with arrival rate λ and the arrival time of the vehicles follow gamma distribution function with arrival rate λ (Solnes, 1997). The orthogonal polynomial function corresponding to Gamma distribution is Associated Laguerre Polynomial (Schoutens, 2000). The size of the mass matrix, damping matrix, stiffness matrix, force vector and response vector depend on the summation of the number of basic functions or the summation of the number of terms considered. The variation of the summation of number of terms with the flexural stresses at mid span of the bridge, when

movement of single vehicle and multiple vehicles are considered is explained in sub section 4.4.1.

Further, the fatigue life of the bridge can be obtained by taking the real time data of the vehicular motion of the bridge. In such cases, the vehicular motion has been recorded for a minimum time span of one month and the stress strain data obtained from the field is used for evaluation of fatigue life. However, acquiring such data is cumbersome for a longer time span. Thus, in order to consider the effect of longer time span and multiple vehicle movement on the bridge, different time windows are kept. The time window fixed for the vehicular movement on the bridge is explained in sub section 4.4.2.

4.4.1 Convergence of Number of Terms of the Associated Laguerre Polynomial

The effect of summation of number of terms of the Associated Laguerre Polynomial on the flexural stresses obtained at mid span of the single span bridge is studied in this section. As explained in section 3.4.4 of Chapter 3, the response $\boldsymbol{X}$ of the generalised coordinates has been sequentially expanded as a set of orthogonal basis functions (Li and Chen, 2009). The response vector is given as

$$\mathbf{X}(t) = \sum_{l=0}^{N_1} \mathbf{Q}_l(t) L_l^j(\lambda t_j) \tag{4.1}$$

where, j is the number of vehicle arrivals which is analogous to the shape parameter of Gamma distribution in the present study, t_j is the arrival time of the jth vehicle on the bridge, λ is the arrival rate of the vehicles, N_1 is the number of basic functions or number of terms with respect to λt_j, $L_l^j(\lambda t_j)$ represents the orthogonal function and $Q_{sl}(t)$ is the displacement function varying with respect to time.

The orthogonal polynomial function considered as Associated Laguerre Polynomial (Schoutens, 2000) which corresponds to Gamma distribution is used, which is shown as,

$$L_l^j(\lambda t_j) = \frac{1}{\Gamma(l+1)} \sum_{k=0}^{l} \frac{\Gamma(l+1)}{\Gamma(k+1)}^{j+l} C_{l-k} (-\lambda t_n)^k \tag{4.2}$$

where Γ is defined as

$$\Gamma(n) = (n-1)! \tag{4.3}$$

$$\Gamma(n+1) = n\Gamma(n) \tag{4.4}$$

where n is an integer and $n > 0$.

The above series given in Eq. (4.2) is convergent as the ratio test given by the limiting value of the ratio of the l^{th} term to $(l\text{-}1)^{th}$ term when number of term approaches infinity is found to be less than 1.

The convergence of the results with the summation of number of terms is checked using the relation shown below

$$\frac{\Delta f\left(\frac{L}{2},t\right)}{f_{N_1}\left(\frac{L}{2},t\right)} \le e, 0 \le t \le T, N_1 = 0,1,2,3,4,5 \tag{4.5}$$

where e is the tolerance limit, T represents the bridge loading time and $\Delta f(L/2, t)$ is given as

$$\Delta f\left(\frac{L}{2},t\right) = f_{N_1+1}\left(\frac{L}{2},t\right) - f_{N_1}\left(\frac{L}{2},t\right) \tag{4.6}$$

In the present study, e is taken as 1×10^{-3} and T is taken as 20 secs.

As per Eq. (4.1), the number of terms, N_1 has been varied from 0 to 5 which corresponds to 1st term, sum of first 2 terms, sum of first 3 terms etc. The flexural stress has been obtained for uniform vehicle velocity 40 km/hr and vehicle arrival rate of 120 vehicles per minute. The road surface condition considered is very poor. The comparison of the flexural stress with the summation of number of terms for single and multiple movement of vehicle is given in Figs. 4.5 and 4.6.

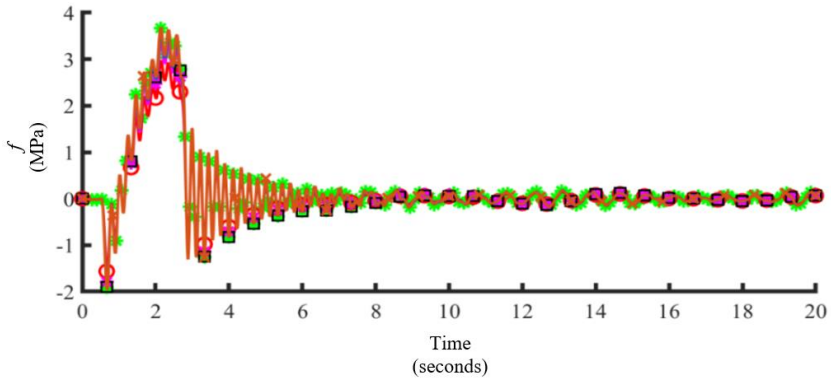

Fig. 4.5 Comparison of flexural stress at mid span of the bridge with the summation of number of terms for single vehicle traversing on the bridge

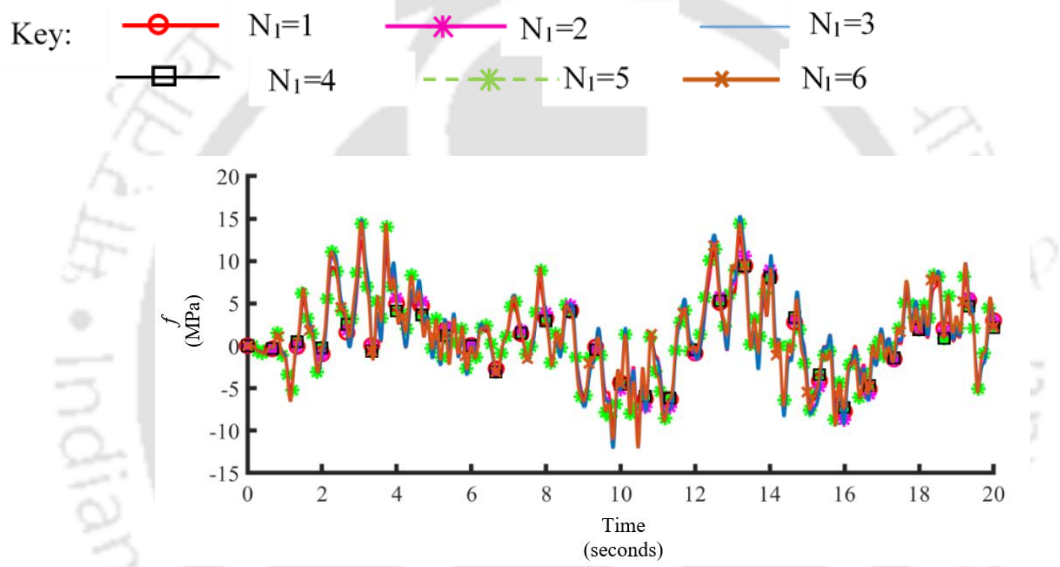

Fig. 4.6 Comparison of flexural stress at mid span of the bridge with the summation of number of terms for multiple vehicles traversing on the bridge

It is observed from Figs. 4.5 and 4.6 that the average tolerance limit obtained is 0.2 for single vehicle and 0.25 for multiple vehicles when the sum of first 2 terms and 1st term (N_1 is 1 and 0) is considered for evaluation of flexural stresses. On considering the sum of first 3 terms and sum of first 2 terms (N_1 is 2 and 1) for obtaining flexural stresses, the average tolerance limit found is 0.022 for single vehicle and 0.035 for multiple vehicles traversing on the bridge. On comparing the flexural stresses obtained from sum of first 4 terms and sum of first 3 terms, the average tolerance limit is 0.016 when single vehicle is traversing on the bridge and 0.021 when

multiple vehicles are traversing on the bridge. However, the average tolerance limit of 0.0016 and 0.0017 is achieved when the summation of number of terms are increased from 4 to 5 i.e., N_1 from 3 to 4 is considered for evaluation of flexural stresses for single vehicle movement and multiple vehicle movement respectively. The flexural stresses for single vehicle and multiple vehicle movement are approximately same when the summation of number of terms are further increased from 5 to 6 (N_1 from 4 to 5). Thus, in the polynomial function, sum of first 4 terms ($N_1 = 0, 1, 2, 3$) are used to evaluate the flexural stresses at mid span of the bridge and the same is used throughout the chapter.

4.4.2 Effect of Time Window

The effect of different time windows on mean and standard deviation of flexural stresses, μ_f and σ_f respectively, obtained at mid span of the bridge has been studied in this section. Time windows are varied from 10 secs to 25 secs with an interval of 5 secs to obtain the optimum time window for multiple vehicular movement. The uniform vehicle velocity is also varied as 20 km/hr, 30 km/hr, 40 km/hr, 50 km/hr and 60 km/hr. The arrival rate of the vehicle is 120 vehicles per minute. The road surface irregularity is varied from good, average, poor and very poor. The comparison of maximum mean and standard deviation of flexural stresses at mid span of the bridge for time windows mentioned above are shown in Figs. 4.7 to 4.10.

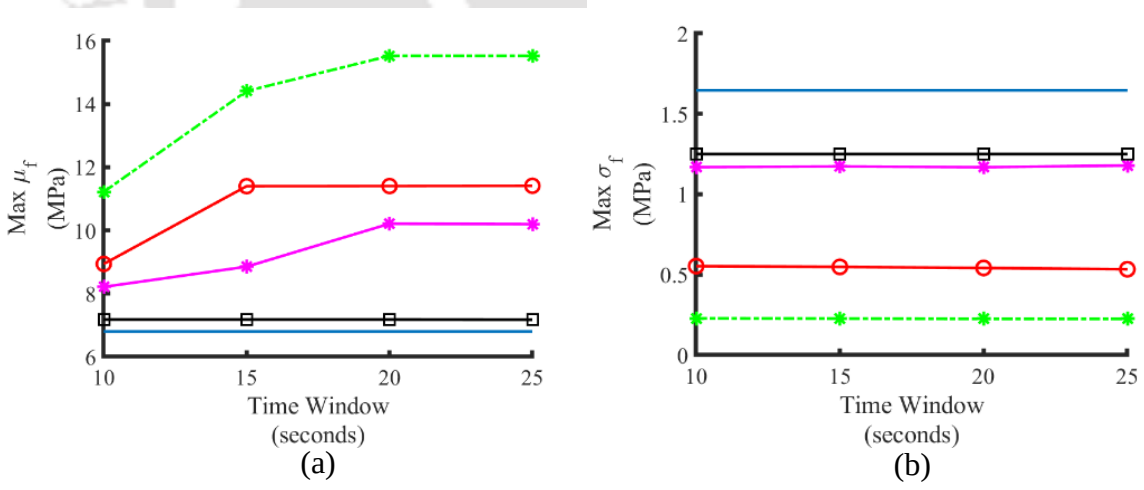

(a) (b)

Fig. 4.7 Comparison of (a): maximum mean and (b): maximum standard deviation of flexural stress at mid span of the bridge with time windows for different uniform vehicle velocities and good road condition ($S_{GG}(\Omega_0) = 32 \times 10^{-6}$ m^2/cycle/m)

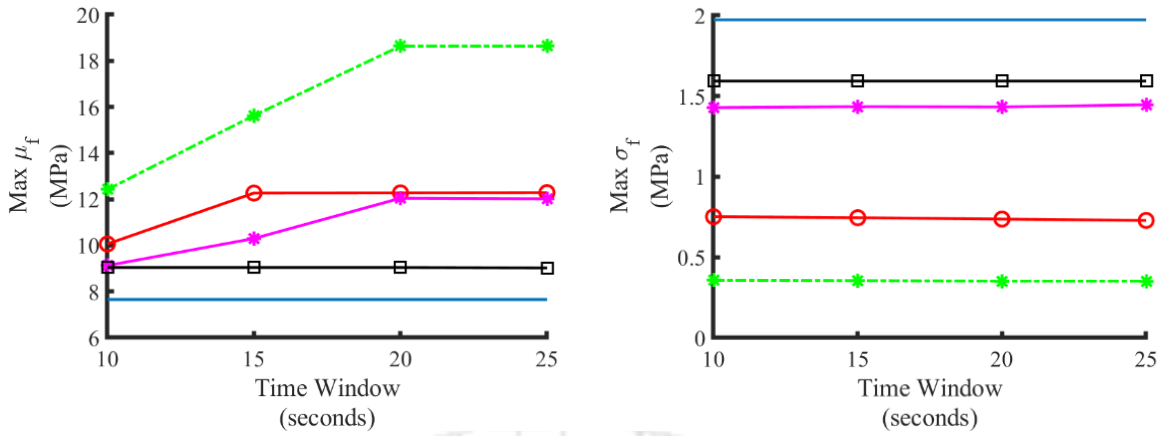

(a) (b)

Fig. 4.8 Comparison of (a): maximum mean and (b): maximum standard deviation of flexural stress at mid span of the bridge with time windows for different uniform vehicle velocities and average road condition ($S_{GG}(\Omega_0)$ = 120 × 10^{-6} m^2/cycle/m)

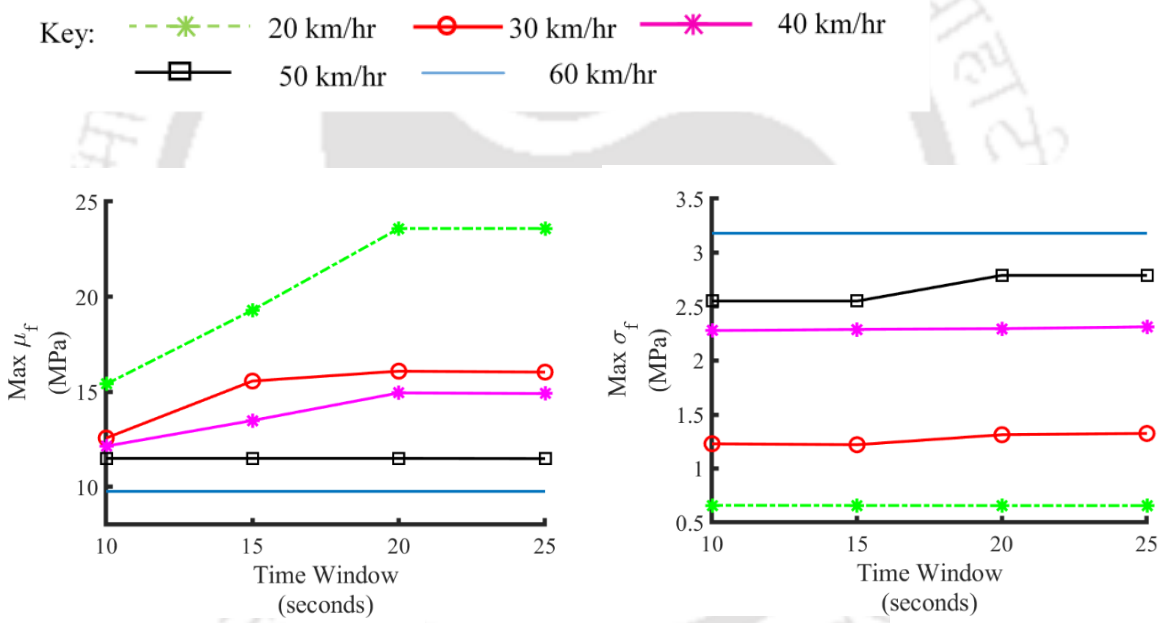

(a) (b)

Fig. 4.9 Comparison of (a): maximum mean and (b): maximum standard deviation of flexural stress at mid span of the bridge with time windows for different uniform vehicle velocities and poor road condition ($S_{GG}(\Omega_0)$ = 512 × 10^{-6} m^2/cycle/m)

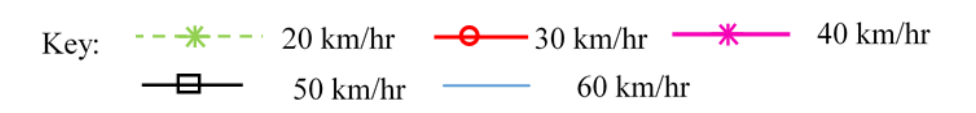

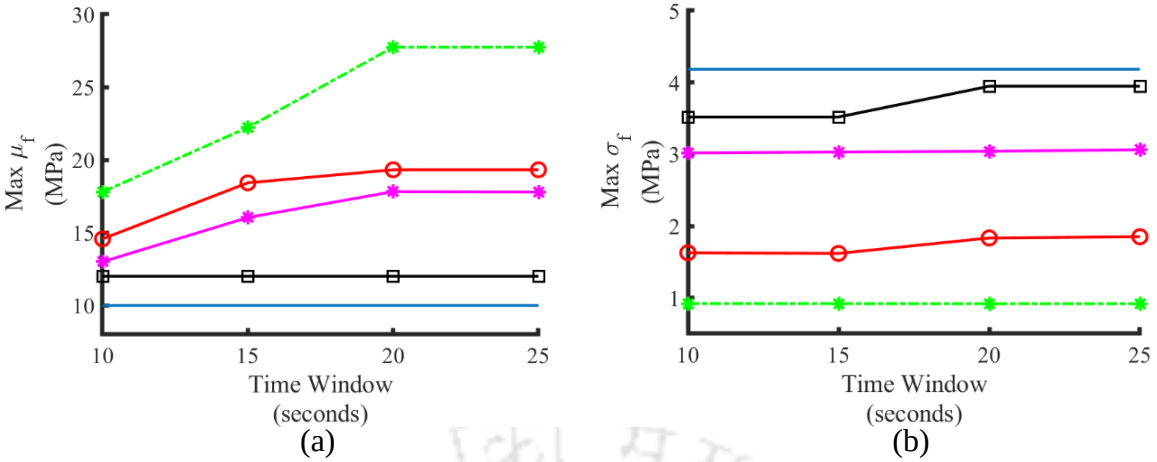

Fig. 4.10 Comparison of (a): maximum mean and (b): maximum standard deviation of flexural stress at mid span of the bridge with time windows for different uniform vehicle velocities and very poor road condition ($S_{GG}(\Omega_0) = 1024 \times 10^{-6}$ m^2/cycle/m)

It is observed form Figs. 4.7 to 4.10 that the maximum mean flexural stresses at mid span of the bridge increase from 10 secs to 20 secs time window and remains approximately same for 25 secs time window. It is also observed from Figs. 4.7 to 4.10 that the maximum standard deviation of flexural stresses at mid span of the bridge does not vary significantly for time windows 10 secs to 25 secs for uniform vehicle velocity 20 km/hr, 40 km/hr and 60 km/hr and for all road conditions. However, there is a significant variation in standard deviation of flexural stresses at mid span of the bridge for uniform vehicle velocity 30 km/hr and 50 km/hr for poor and very poor road condition from time window 10 secs to 20 secs. Thus, considering the above observations, the optimum time window kept for multiple vehicular movement is 20 secs. It is also observed that the fatigue life of the bridge will not be affected drastically after 20 secs time window and the computational time can also be saved. Therefore, 20 secs time window has been considered for all the study in the chapter.

4.5 Validation of Present Semi Analytical Method with State-space solution

The flexural stresses at mid span of the bridge obtained from the present semi analytical method is compared with State-space approach solution (Nigam, 1983). The system matrices are given in section A.1.2 in Appendix-I. The details of the procedure to evaluate the flexural stresses at mid span of the bridge using the semi analytical method are given in section 3.4.4 in Chapter 3. In the semi analytical method, the sum of first 4 terms of the orthogonal polynomial function

is considered in the evaluation of flexural stresses. In state space representation, second order coupled system equations are converted to 2*n* dimensional first order differential equations. In the state space solution, the state transition matrix is first obtained. Using the state transition matrix, the general solution is obtained by the superposition of homogeneous solution and particular solution. The particular solution is obtained using convolution integral. This is done with the help of MATLAB function ss and lsim.

The span of the bridge considered is 30 m, mass per unit length of the bridge is 1.0288×10^4 kg/m and moment of inertia of equivalent steel section is 0.3391 m^4. The sprung mass of the vehicle, m_s is taken as 36000 kg and unsprung mass of the vehicle, m_w is 4000 kg. The suspension stiffness k_s, suspension damping c_s, tyre stiffness k_w and tyre damping c_w are taken as 14.4×10^6 Nm^{-1}, 475.2×10^3 Nsm^{-1}, 3.6×10^6 Nm^{-1} and 24×10^3 Nsm^{-1} respectively. The amplitude of the mean profile is 0.01 m. The comparison of flexural stresses obtained at mid span of the bridge for single vehicle traversing the bridge from the two methods for 20 km/hr uniform vehicle velocity and vehicle arrival rate 120 vehicles per minute in 20 secs time window for good and very poor road surface conditions are shown in Figs. 4.11 and 4.12.

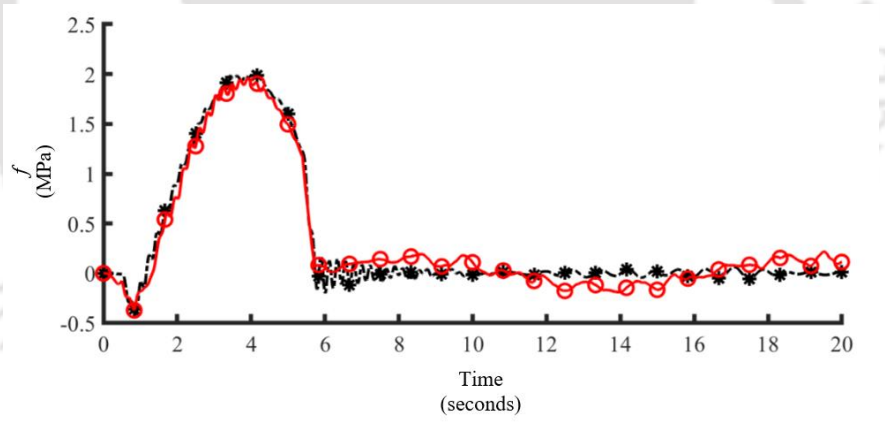

Fig. 4.11 Comparison of flexural stress at mid span obtained from semi analytical method and state space approach for good road condition and 20 km/hr vehicle velocity

Key: – – ✱ – Present Method —○— State space approach

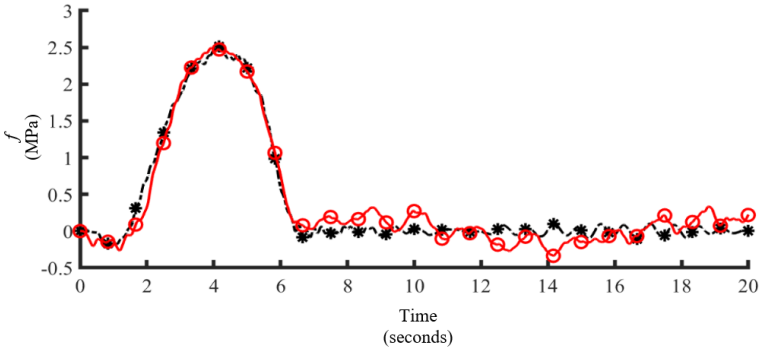

Fig. 4.12 Comparison of flexural stress at mid span obtained from semi analytical method and state space approach for very poor road condition and 20 km/hr vehicle velocity

Key: – – ✱ – Present Method —○— State space approach

It is observed from Figs. 4.11 and 4.12 that flexural stresses at mid span obtained from the present semi analytical method and state space approach are in good agreement with each other.

4.6 Fatigue Life and DAF from Bridge Response Statistics

The fatigue life and dynamic amplification factor (DAF) has been evaluated using the bridge dynamic response of the coupled system which has been obtained using the presently developed semi analytical method, assuming that the vehicle arrival rate follows Poisson process. The effect of road surface roughness and variable mean profile has also been considered in the study. The road roughness becomes a stationary process in time domain when the vehicle moves on the bridge with uniform velocity. The response of wheel induced by road roughness becomes a non-stationary random process in time domain when the vehicle moves with variable velocity (Virchis and Robson, 1971; Nigam and Yadav, 1974). A general polynomial with coefficients that can represent the different vehicle motions have been considered. The position of the n^{th} vehicle on the bridge is modelled using a general polynomial which is given in Eq. (3.12) in Chapter 3. The velocity of the n^{th} vehicle is obtained by taking the first time derivative of Eq. (3.12) and is given in Eq. (3.13) in Chapter 3. The acceleration of the vehicle is considered to be constant, when the vehicle moves with variable velocity. In time domain analysis adopted in the present study, road roughness h_r will vary according to the position of vehicle.

The dynamic amplification factor has been evaluated by incorporating the standard error of the mean in the vehicle induced dynamic response. The design stress history is decomposed using rainflow counting method (Downing and Socie 1982). The number of cycles obtained from

rain flow counting method is converted to annual cycles using a multiplier (annual average daily traffic × 365). The annual average daily traffic depends on the arrival rate of the vehicles considered. The fatigue life has been evaluated adopting Modified Bilinear Damage Rule (MBLDR) as this rule gives accurate damage predictions as compared to Bilinear Damage Rule (BLDR). The error between the predicted fatigue life and the actual fatigue life obtained from experiment is less in case of MBLDR as compared to BLDR, which has been observed in section 2.9.2 in Chapter 2. For a single span box girder bridge corresponding to yield stress f_y = 250MPa, the fatigue detail constant K and material constant m have been taken as 61×10^8 ksi (4.205×10^{10} MPa) and -3 respectively (Fisher, 1977; AASHTO, 2017). The flowchart for the whole procedure to evaluate fatigue life is shown in Fig. 4.13.

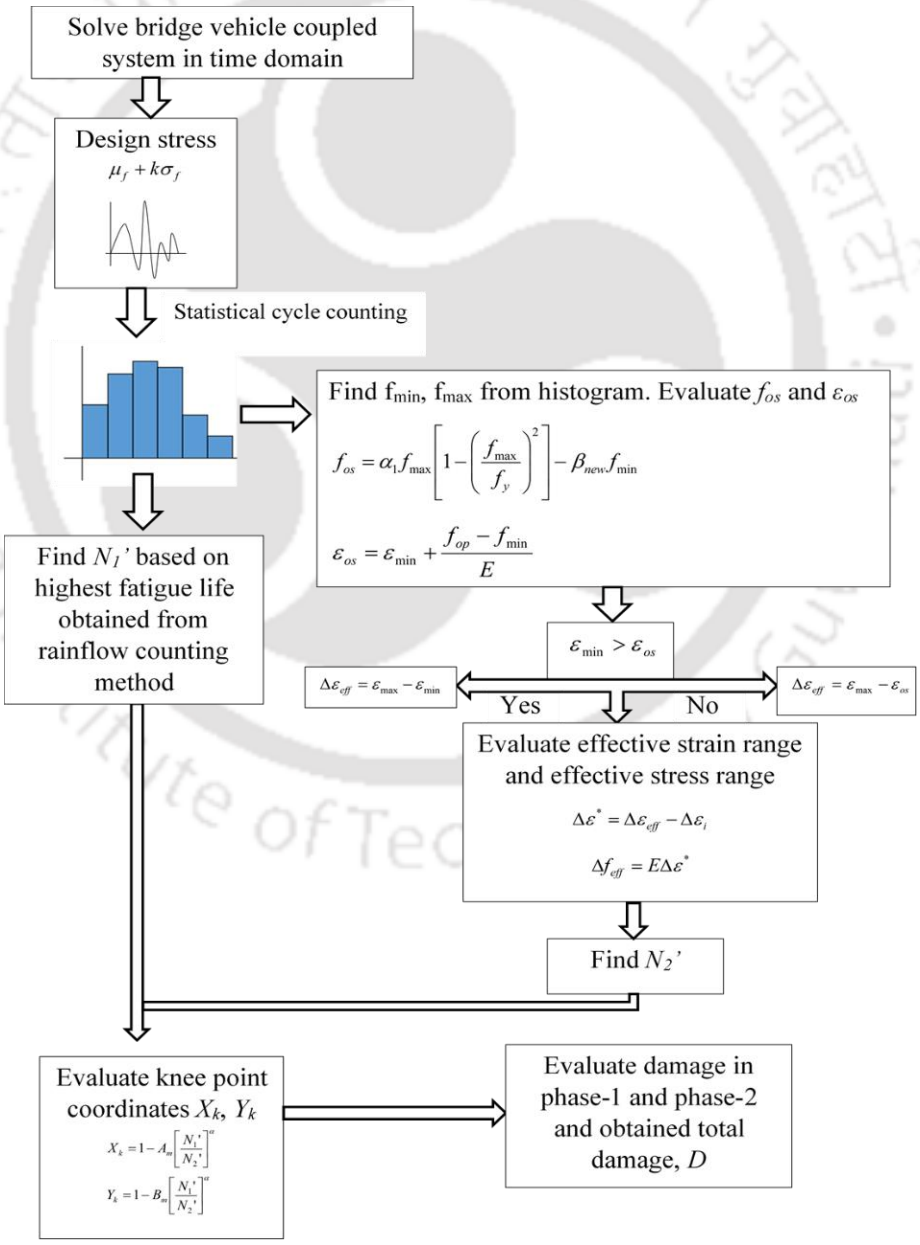

Fig. 4.13 Flowchart for evaluation of fatigue life

4.6.1 Parametric Study

The bridge and vehicle forms a coupled system. The parameters of each of them are significant to result in variation of flexural stress required to cause the cumulative fatigue damage in bridge. In this chapter, the results are obtained using Orthogonal Polynomial Expansion, which takes into account the randomness in vehicle arrival time and road roughness. The purpose of the section is to analyse the sensitivity of variation of vehicle and bridge parameter to dynamic amplification factor and fatigue life of the single span bridge. The different parameters that are considered to study the variation of DAF and fatigue life are given below.

(i). Vehicle forward velocity
(ii). Road surface roughness
(iii). Arrival rate of the vehicle
(iv). Axle weight of the vehicle
(v). Span of the bridge
(vi). Amplitude of mean profile

4.6.1.1 Effect of vehicle forward velocity

The effect of uniform velocity and variable velocity of the moving vehicles on DAF and fatigue life of the bridge has been studied in this section. The mean and standard deviation of the flexural stresses have been generated for very poor category of the road surface. The amplitude of the mean profile is considered as 0.01 m. The response quantities have been obtained at mid span of the bridge for vehicle entry velocities 20 km/hr to 60 km/hr with an interval of 10 km/hr. The vehicle arrival rate is considered to be 120 vehicles per minute. The acceleration of the vehicle is varied from 0.5 m/s^2 to 1.5 m/s^2 with an increment of 0.5 m/s^2 in case of variable velocity. The mean and standard deviation of flexural stresses at mid span of the bridge when the vehicle moves on the bridge with uniform and variable velocity is shown in Figs. 4.14 to 4.17.

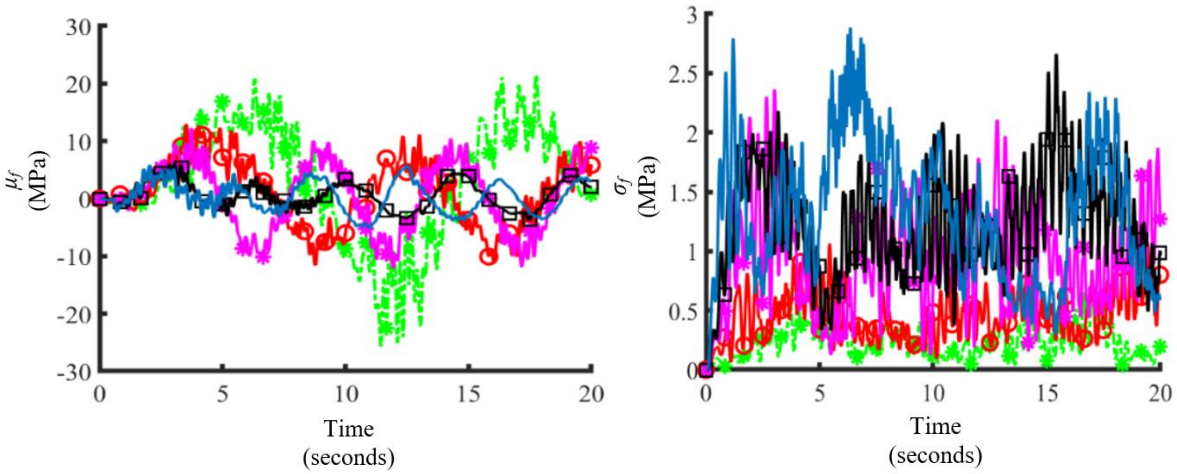

(a) (b)

Fig. 4.14 (a): Mean and (b): standard deviation of flexural stress at mid span of the bridge for different uniform vehicle velocities for very poor road condition ($S_{GG}(\Omega_0)$ = 1024 × 10^{-6} m^2/cycle/m)

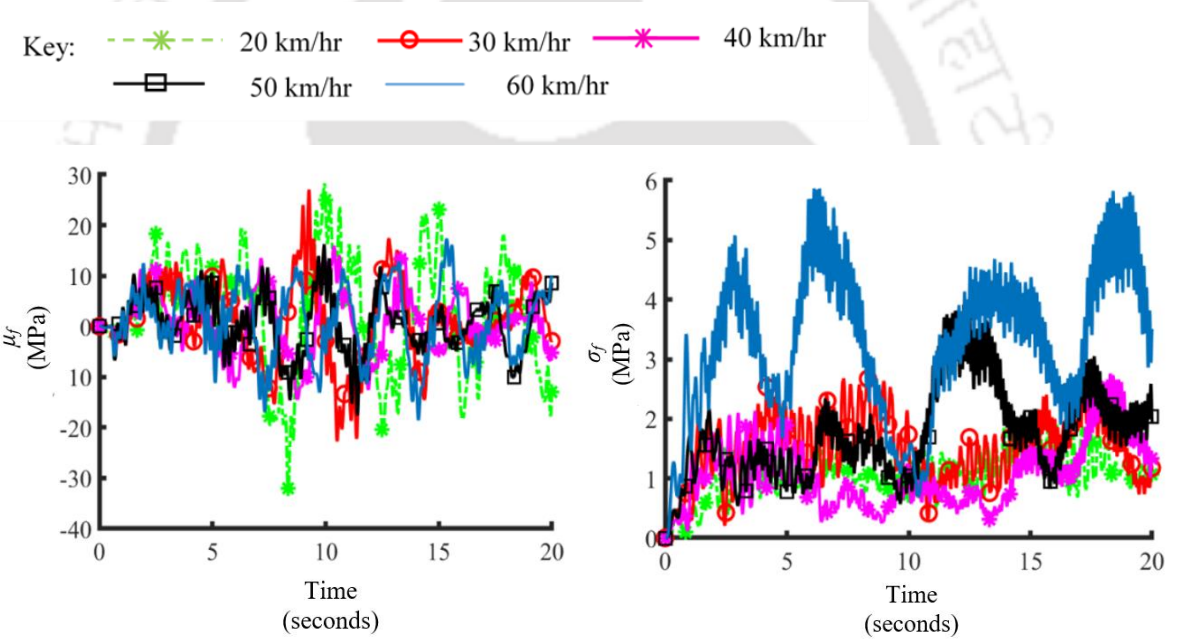

(a) (b)

Fig. 4.15 (a): Mean and (b): standard deviation of flexural stress at mid span of the bridge for different entry vehicle velocities for acceleration 0.5 m/s^2 for very poor road condition ($S_{GG}(\Omega_0)$ = 1024 × 10^{-6} m^2/cycle/m)

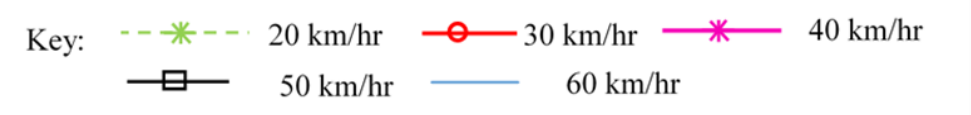

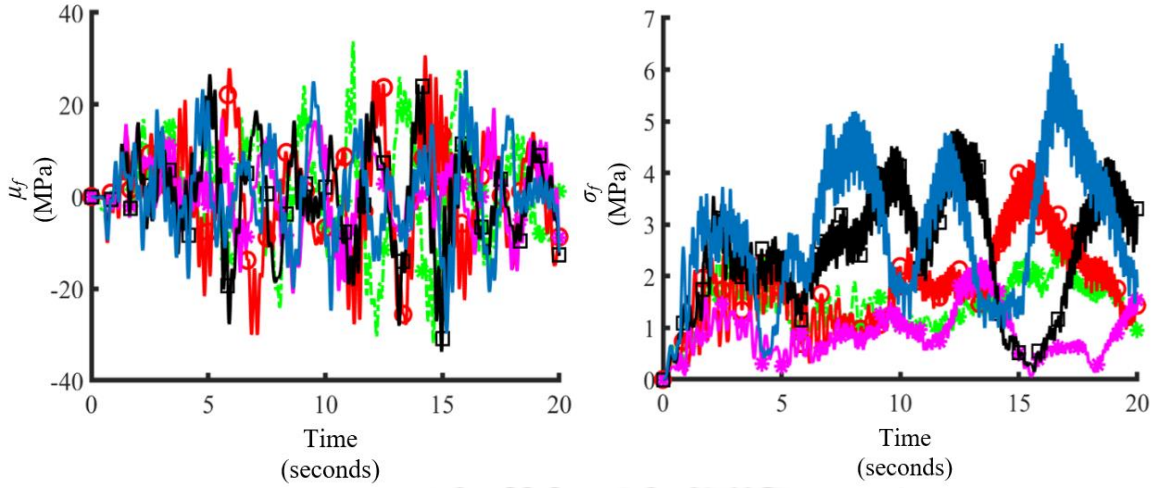

Fig. 4.16 (a): Mean and (b): standard deviation of flexural stress at mid span of the bridge for different entry vehicle velocities for acceleration 1 m/s^2 for very poor road condition ($S_{GG}(\Omega_0)$ = 1024 × 10^{-6} m^2/cycle/m)

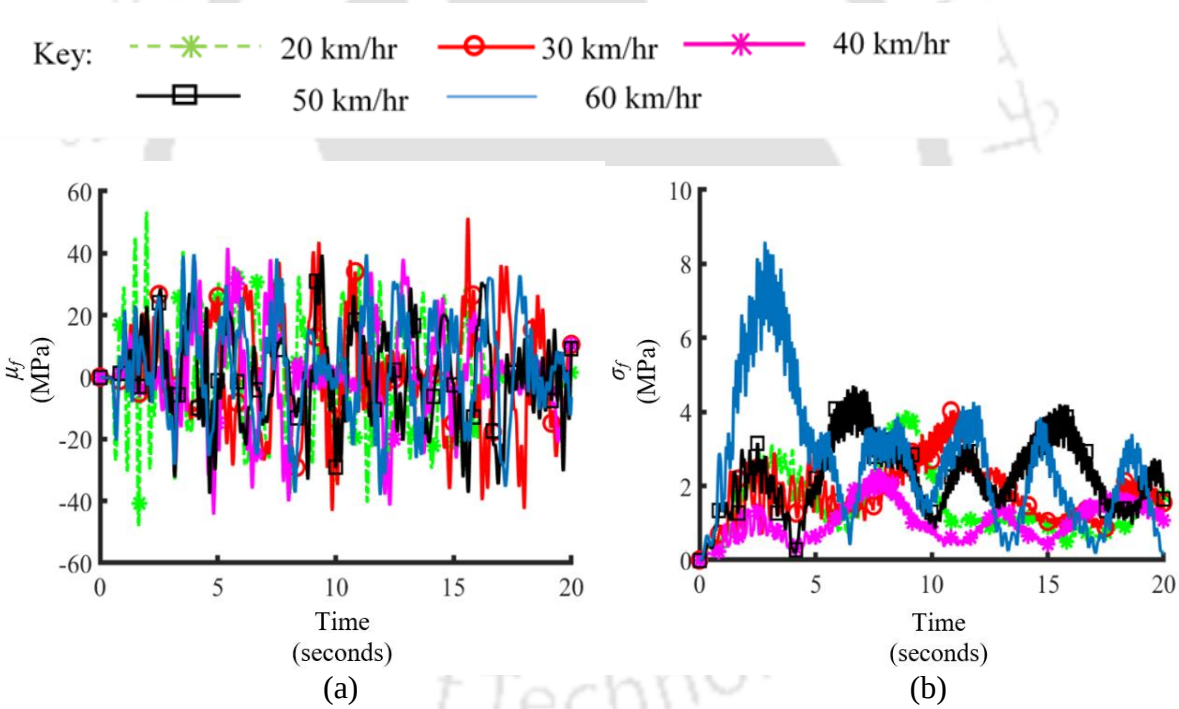

Fig. 4.17 (a): Mean and (b): standard deviation of flexural stress at mid span of the bridge for different entry vehicle velocities for acceleration 1.5 m/s^2 for very poor road condition ($S_{GG}(\Omega_0)$ = 1024 × 10^{-6} m^2/cycle/m)

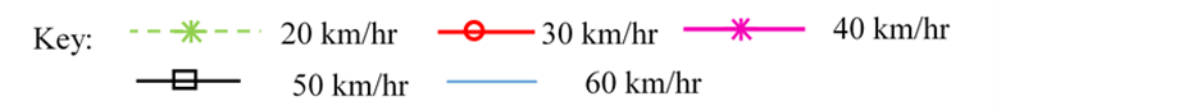

It has been observed from Figs. 4.14 to 4.17, the mean and standard deviation of flexural stresses vary with entry vehicle velocity. The mean flexural stresses are more for lower entry

velocity. The time window considered for multiple vehicular movements on the bridge is 20 secs. The time window of 20 secs is considered same for all entry vehicle velocities, but the action of each vehicular load is restricted to a time span of L/v where L is the span of the bridge and v is the vehicle velocity. This suggests that the number of moving loads acting on the span decreases with increasing entry vehicle velocity. Thus, the mean flexural stresses are more for lower vehicle velocity as observed from Figs. 4.14 to 4.17. The standard deviation of flexural stress of the bridge increases with increase in uniform velocity of the vehicle, which is shown in Figs. 4.14 to 4.17. This can be due to the reason that the mean flexural stresses of the bridge increases with the decrease in velocity of the vehicle. Hence, when calculating the variance, the mean square response is subtracted from the square of the mean response and since, the mean of the response is more for lower velocity of the vehicle, the variance increases as the velocity of the vehicle increases. The same behaviour of flexural stress with vehicle velocity was observed in Savin (2001), Brady et al. (2006) and Sniady (1984). However, a similar variation in standard deviation of flexural stress is not observed when the vehicle is accelerating at 0.5 m/s^2, 1m/s^2 and 1.5 m/s^2.

The mean and standard deviation of flexural stresses increase with increase in acceleration of the moving vehicles as observed from Figs 4.14 to 4.17. This is because the transverse vibration of the bridge increases with the increase in acceleration of the moving vehicles.

Dynamic Amplification Factor (DAF)

The DAF evaluated for uniform and variable vehicle velocities for very poor road condition and arrival rate 120 vehicles per minute is shown in Fig. 4.18.

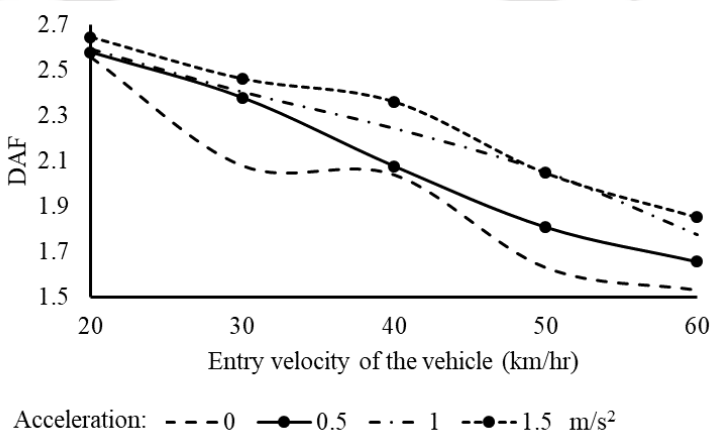

Fig. 4.18 DAF for varying entry velocities of vehicles and acceleration values (m/s^2) for very poor road condition

The DAF increases with the increase in acceleration of vehicles and decreases with the increase in vehicle velocity, which is observed from Fig. 4.18. This is because the mean and standard deviation of the flexural stresses increase with the increase in acceleration of the vehicles. The vehicular load reaches mid-span in less time at higher velocities, resulting in reduced bridge vibration. (Brady et al, 2006; Savin, 2001; and Sniady, 1984; Sieniawksa and Sniady, 1990). As a result, as the vehicle velocity increases, the dynamic stresses decrease, resulting in a reduction in DAF. It is worth mentioning that due to increase in velocity of moving vehicle, temporal frequency of roughness profile increases. This results in vibration of the wheel at higher frequency and therefore, lower value of peak flexural stress is responsible for reduction of DAF. However, in case of vehicles moving with higher acceleration, more number of vehicles pass in a fixed time span and therefore, increased DAF is observed in such cases.

Fatigue Life

The stress range histograms are used to evaluate the fatigue life. The stress range histograms for constant and varying vehicle velocities is illustrated in Figs. 4.19 to 4.22. The fatigue life at various vehicle entry velocities is depicted in Fig. 4.23.

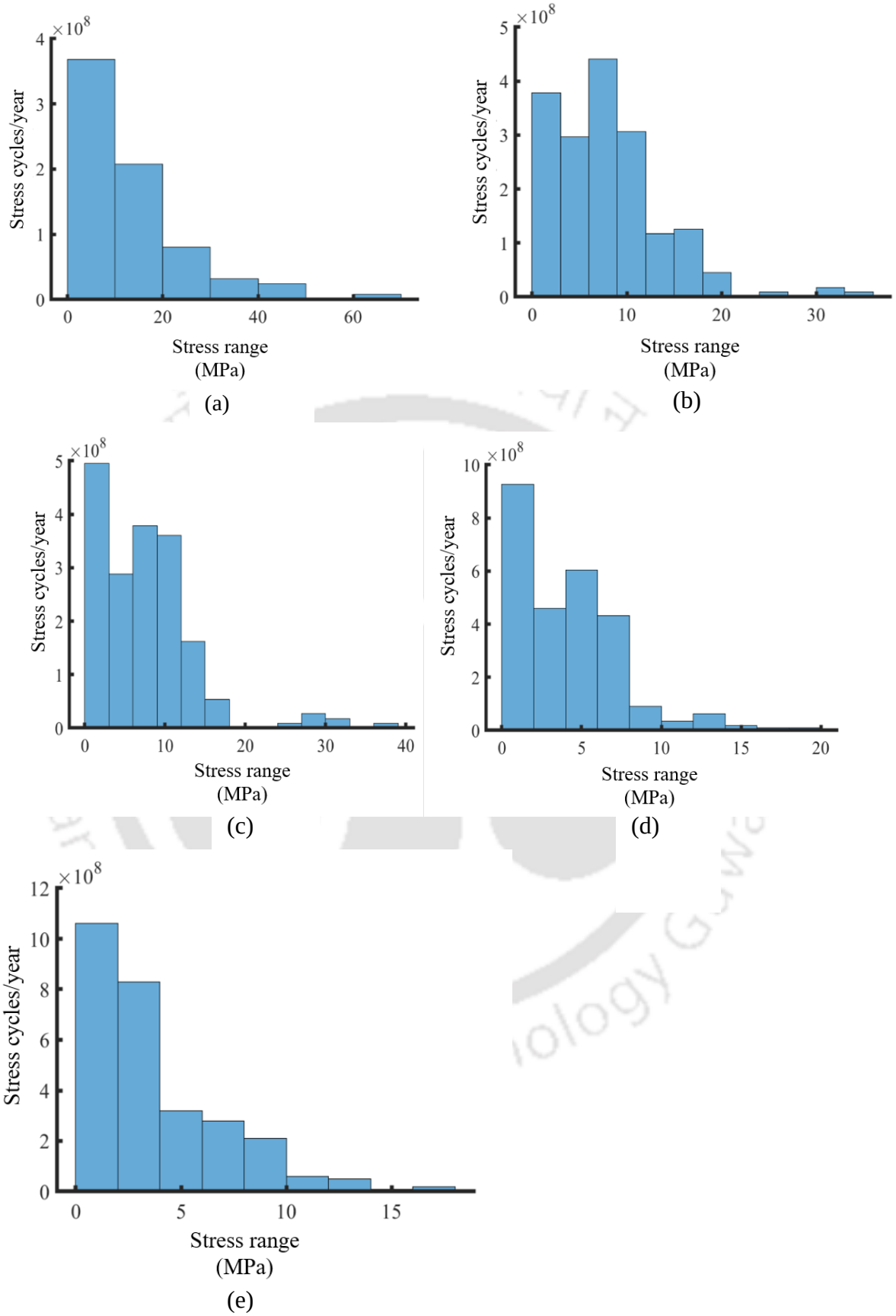

Fig. 4.19 Stress range histogram for uniform vehicle velocity (a): 20 km/hr (b): 30 km/hr (c): 40 km/hr (d): 50 km/hr (e): 60 km/hr for very poor road case

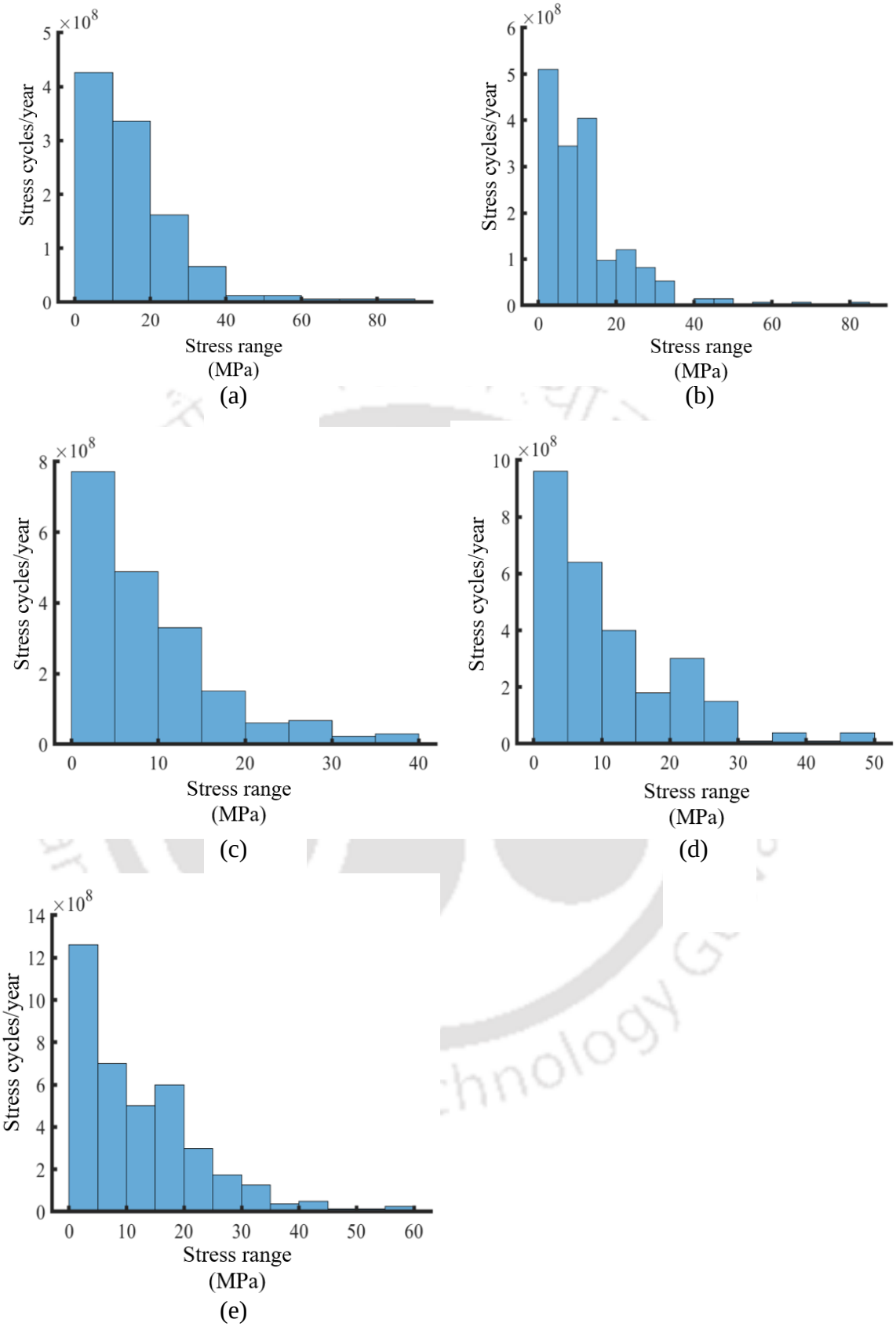

Fig. 4.20 Stress range histogram for vehicle moving with 0.5 m/s^2 acceleration with entry velocity: (a): 20 km/hr (b): 30 km/hr (c): 40 km/hr (d): 50 km/hr (e): 60 km/hr for very poor road case

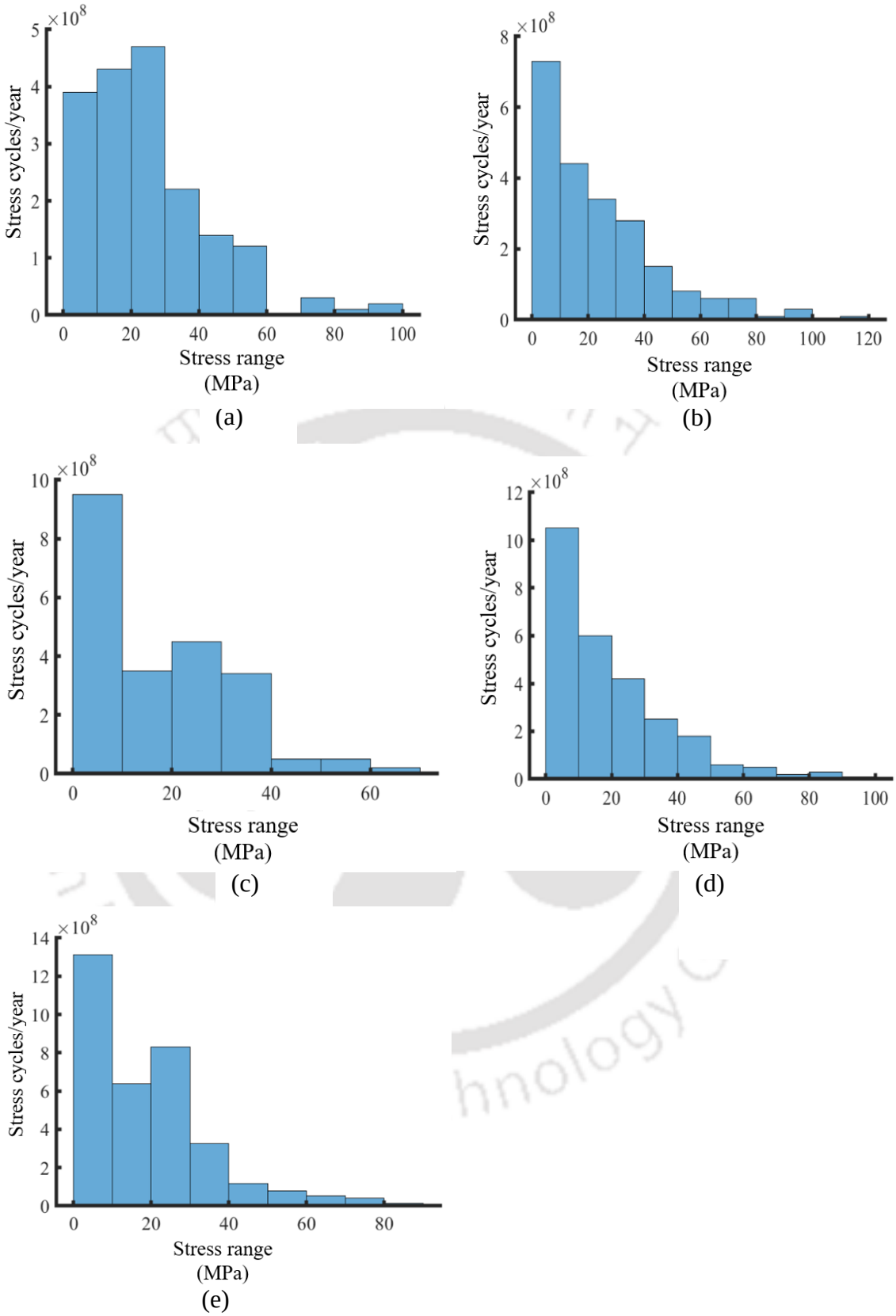

Fig. 4.21 Stress range histogram for vehicle moving with 1 m/s^2 acceleration with entry velocity: (a): 20 km/hr (b): 30 km/hr (c): 40 km/hr (d): 50 km/hr (e): 60 km/hr for very poor road case

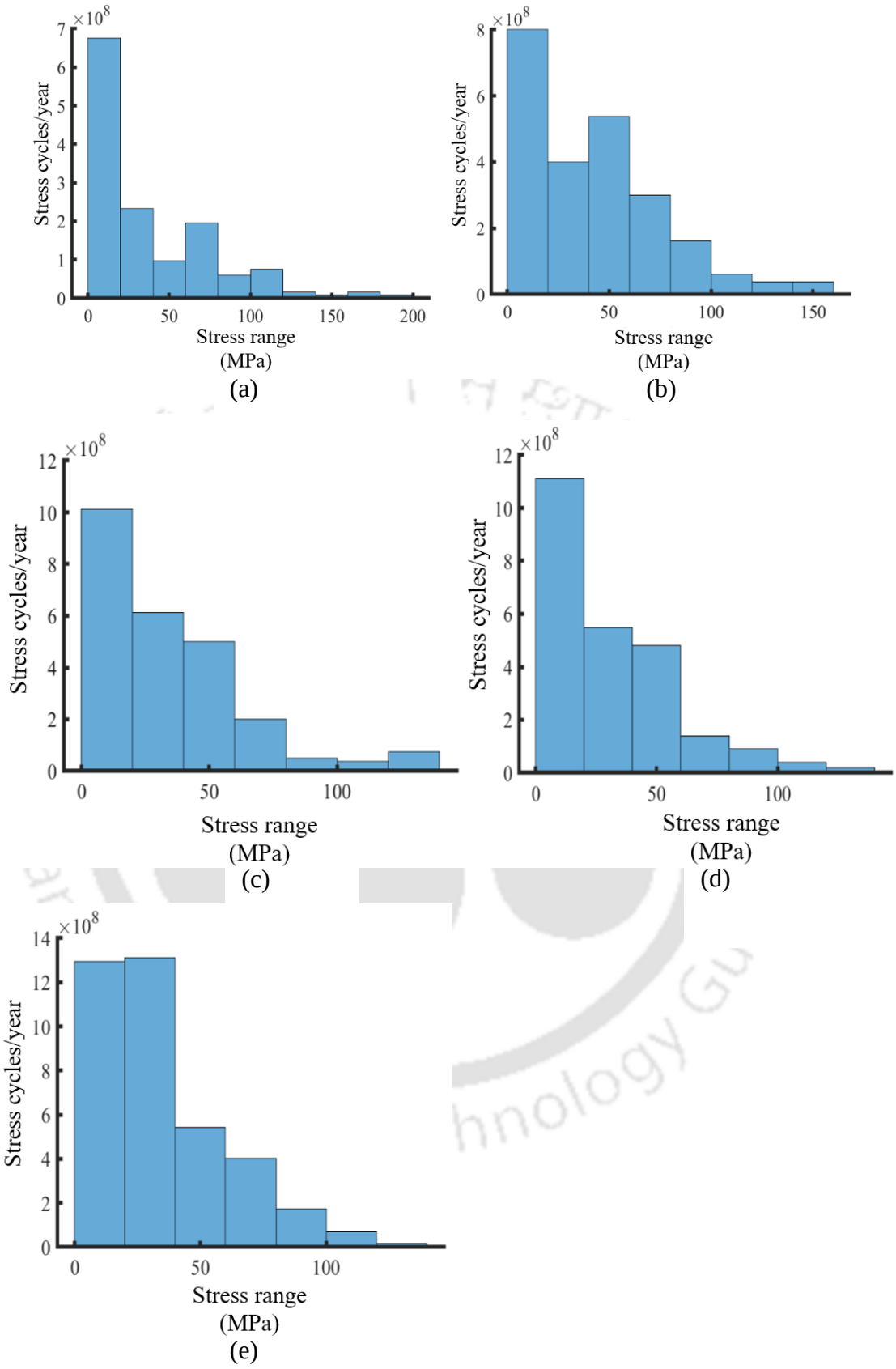

Fig. 4.22 Stress range histogram for vehicle moving with 1.5 m/s^2 acceleration with entry velocity: (a): 20 km/hr (b): 30 km/hr (c): 40 km/hr (d): 50 km/hr (e): 60 km/hr for very poor road case

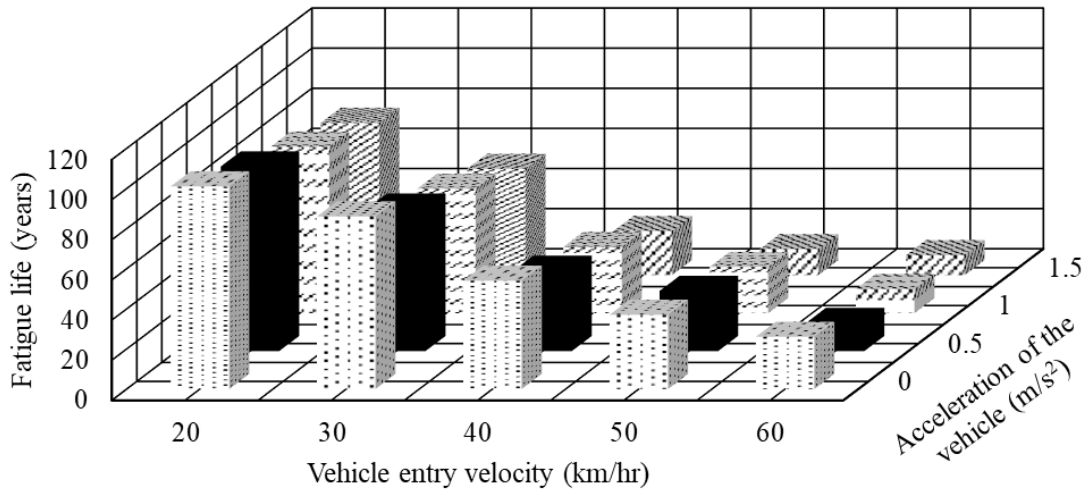

Fig. 4.23 Comparison of fatigue life with different vehicle velocities for very poor road

The low amplitude stress ranges create a reduction in the knee-point coordinates as the vehicle entry velocity increases. The knee-point distinguishes between crack initiation and crack propagation in the fatigue damage process. With increasing vehicle velocity, the rate of crack propagation increases. This contributes to a higher accumulation of fatigue damage in the single span bridge. The static and dynamic stress components owing to vehicle movement over the bridge are included in the stress range histograms illustrated in Figs. 4.19 to 4.22. The number of stress cycles in low amplitude stress ranges are observed to increase in vehicles travelling at higher speed and higher acceleration, which is shown in Figs. 4.19 to 4.22. These characterise the dynamic action of moving vehicles. These stress cycles caused by vehicle bridge interaction contribute to the accumulation of fatigue damage. As a result, the fatigue life of the single span bridge reduces as vehicle velocity increases, which is observed in Fig. 4.23. In Sieniawksa and Sniady (1990), fatigue life varies with vehicle velocity in a similar way. It is also noted that when the vehicle accelerates, the stress cycles for high and low amplitude stress ranges increase, which is observed in Figs. 4.19 to 4.22. The stress ranges increase as the vehicle acceleration increases. This leads to increased fatigue damage and a shorter fatigue life, which is observed in Fig. 4.23.

4.6.1.2 Effect of road surface roughness

This section investigates the impact of road surface roughness on DAF and fatigue life of the single span bridge. The entry vehicle speed is considered as 20 km/hr, and the road surface roughness is categorised as good ($S_{GG}(\Omega_0) = 32 \times 10^{-6}$ m^2/cycle/m), medium ($S_{GG}(\Omega_0) = 120 \times 10^{-6}$ m^2/cycle/m), poor ($S_{GG}(\Omega_0) = 512 \times 10^{-6}$ m^2/cycle/m) and very poor ($S_{GG}(\Omega_0) = 1024 \times 10^{-}$

^{6} m^2/cycle/m). The arrival rate of the vehicles is considered as 120 vehicles per minute. The amplitude of the mean profile is considered as 0.01 m. The mean and standard deviation of flexural stresses at mid span of the bridge for varying road surface roughness while considering uniform and variable vehicle velocity is shown in Figs. 4.24 to 4.27. The vehicle acceleration is varied between 0.5 m/s^2, 1 m/s^2, and 1.5 m/s^2 in case of variable velocity.

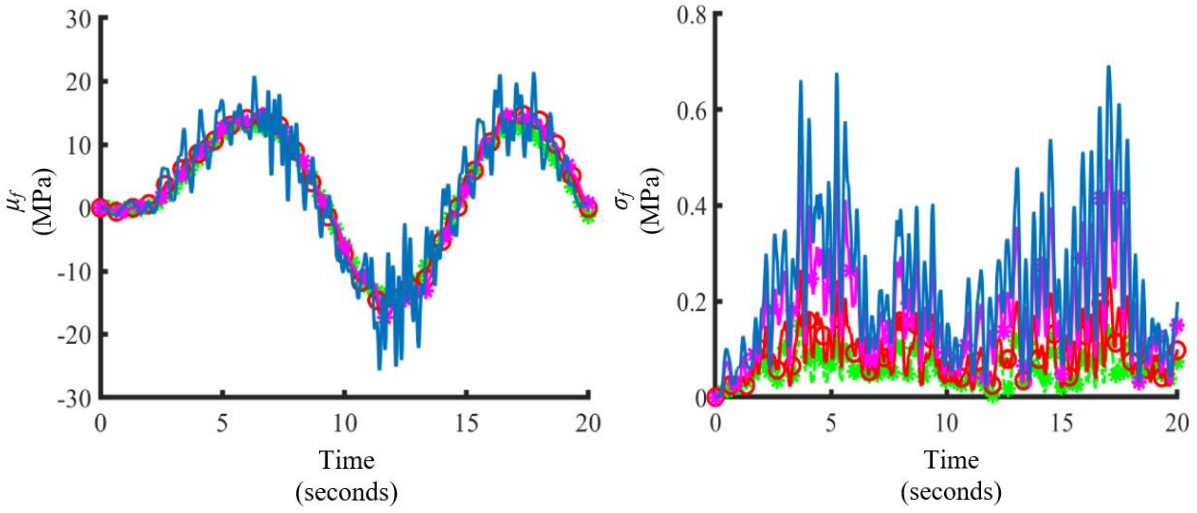

(a) (b)

Fig. 4.24 (a): Mean and (b): standard deviation of flexural stress at mid span of the bridge for uniform vehicle velocity 20 km/hr and arrival rate 120 vehicles per minute

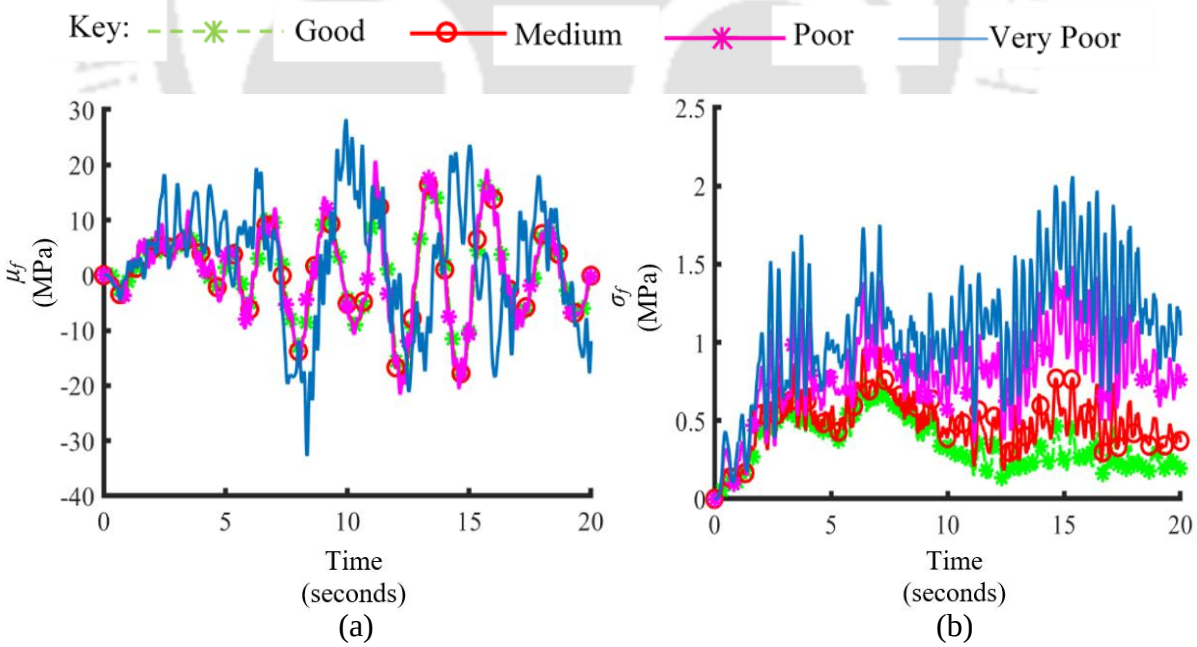

(a) (b)

Fig. 4.25 (a): Mean and (b): standard deviation of flexural stress at mid span of the bridge for vehicle entry velocity 20 km/hr and arrival rate 120 vehicles per minute for vehicles moving with 0.5 m/s^2 acceleration

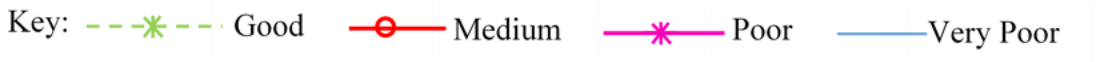

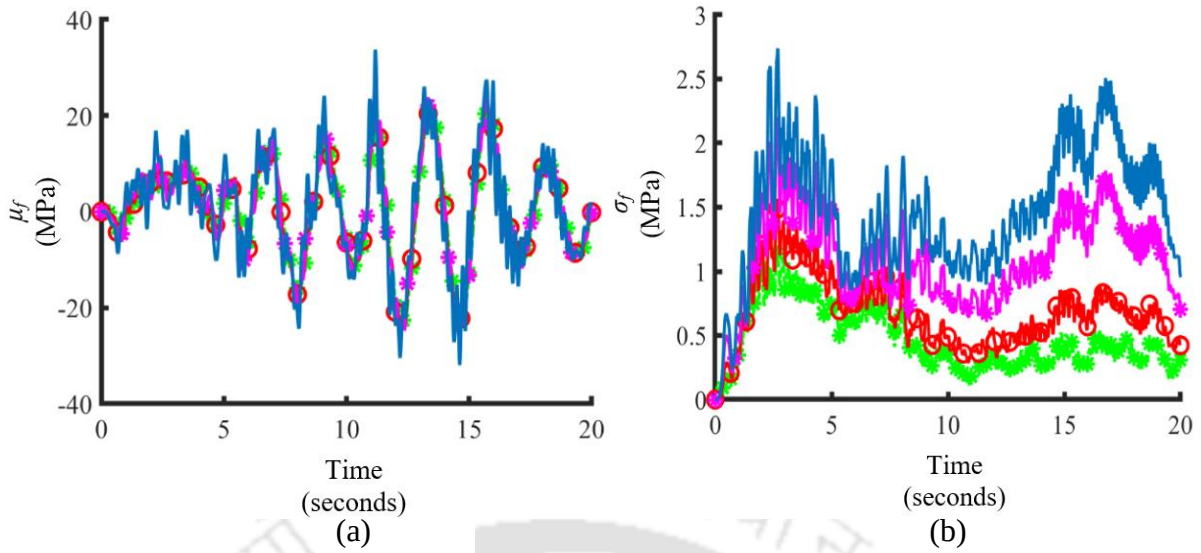

Fig. 4.26 (a): Mean and (b): standard deviation of flexural stress at mid span of the bridge for vehicle entry velocity 20 km/hr and arrival rate 120 vehicles per minute for vehicles moving with 1 m/s^2 acceleration

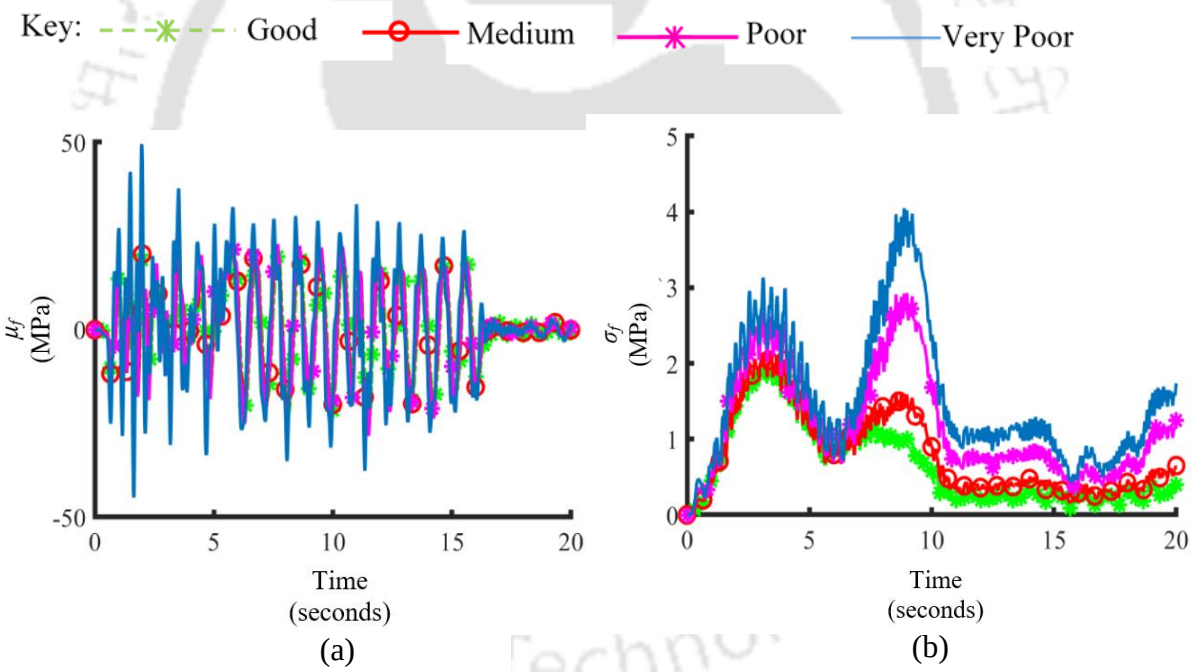

Fig. 4.27 (a): Mean and (b): standard deviation of flexural stress at mid span of the bridge for entry velocity 20 km/hr and arrival rate 120 vehicles per minute for vehicles moving with 1.5 m/s^2 acceleration

When a vehicle travels on a damaged road surface, it generates a large excitation force on the bridge. As a result of the increased dynamic force on the bridge, the mean and standard deviation of flexural stresses increases as the road surface irregularity increases, as shown in

Figs 4.24 to 4.27. A similar trend was observed in Coussy et al., (1988) and Law and Zhu (2005).

Dynamic Amplification Factor (DAF)

The comparison of DAF for vehicles with an entry velocity of 20 km/hr and an arrival rate of 120 vehicles per minute on different road surface irregularities is depicted in Fig. 4.28.

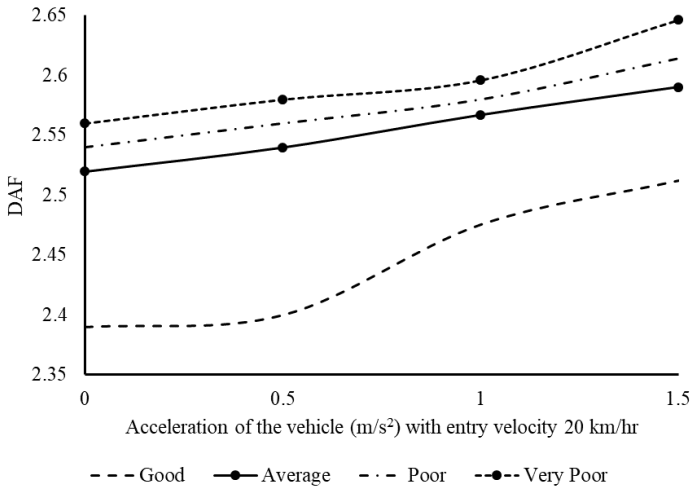

Fig. 4.28 DAF for varying road roughness and acceleration values for vehicles with entry velocity 20 km/hr and arrival rate 120 vehicle per minute

The DAF increases with increasing road surface irregularity, as shown in Fig. 4.28. This is because the dynamic forces caused by vehicular loads increase as road surface irregularity increases, contributing to higher DAF (Inbanthan and Wieland, 1987; Chang and Lee, 1994).

Fatigue Life

The stress range histogram and fatigue life for varying road roughness for vehicles with entry velocity 20 km/hr and arrival rate 120 vehicles per minute is given in Figs. 4.29 to 4.33. The stress range histogram and fatigue life is obtained for uniform and variable vehicle velocity.

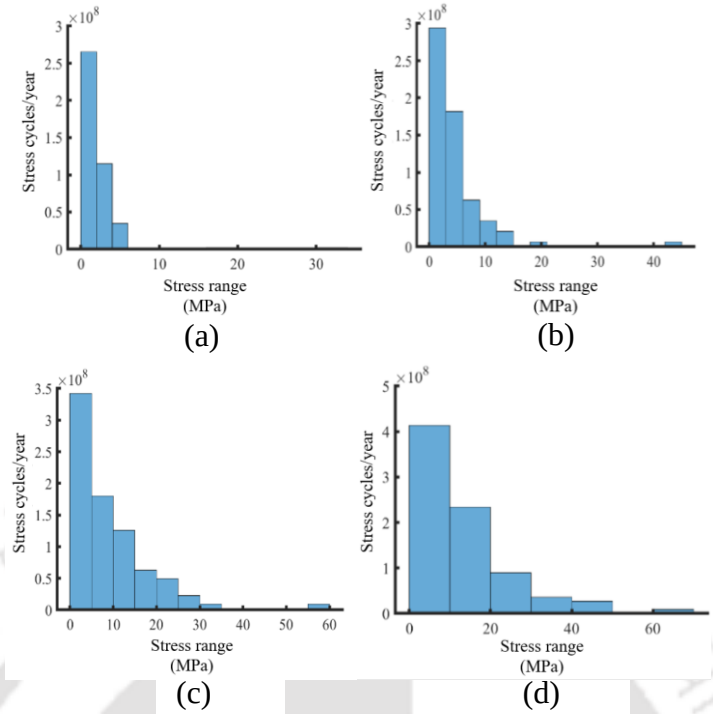

Fig. 4.29 Stress range histogram: (a): good road (b): average road (c): poor road (d): very poor road for uniform vehicle velocity 20 km/hr and arrival rate 120 vehicles per minute

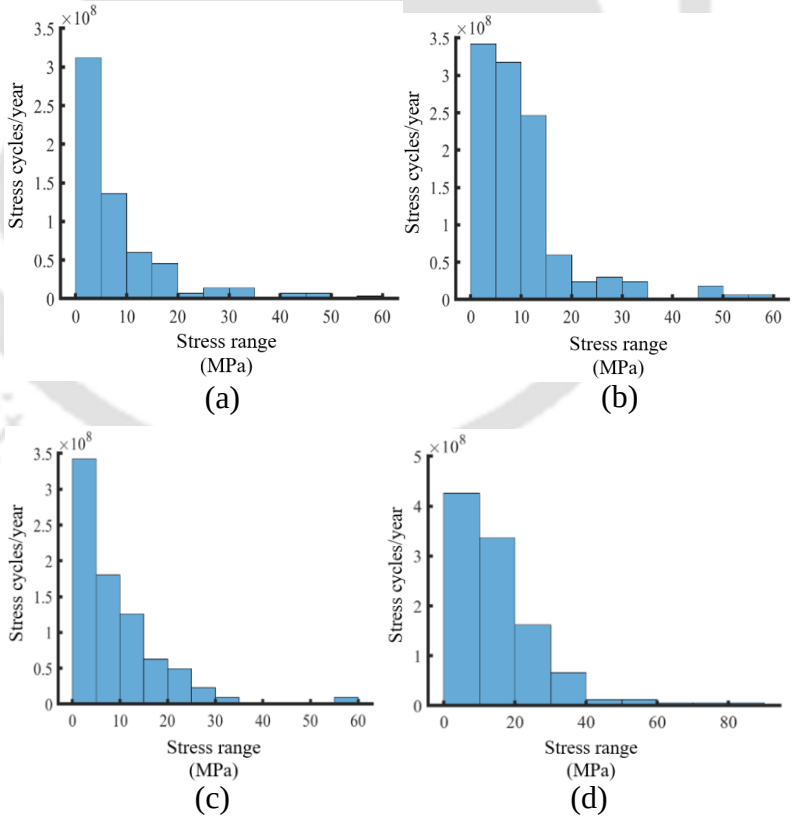

Fig. 4.30 Stress range histogram: (a): good road (b): average road (c): poor road (d): very poor road for vehicle entry velocity 20 km/hr and arrival rate 120 vehicles per minute for vehicle acceleration 0.5 m/s^2

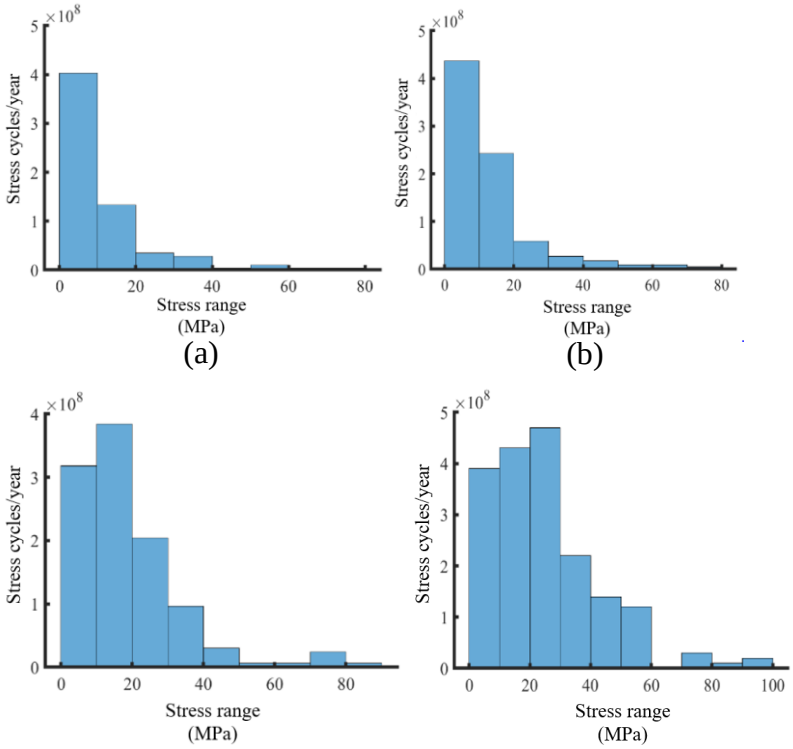

Fig. 4.31 Stress range histogram: (a): good road (b): average road (c): poor road (d): very poor road for vehicle entry velocity 20 km/hr and arrival rate 120 vehicles per minute for vehicle acceleration 1 m/s^2

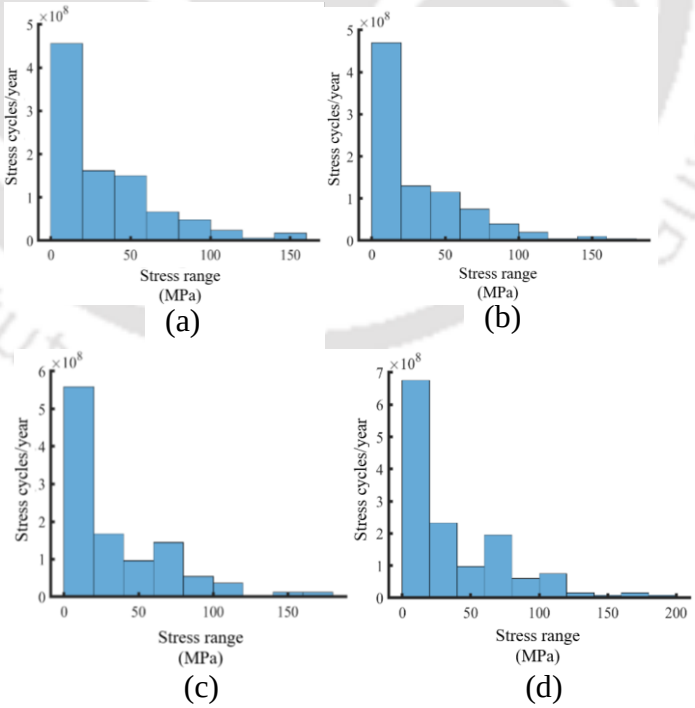

Fig. 4.32 Stress range histogram: (a): good road (b): average road (c): poor road (d): very poor road for vehicle entry velocity 20 km/hr and arrival rate 120 vehicles per minute for vehicle acceleration 1.5 m/s^2

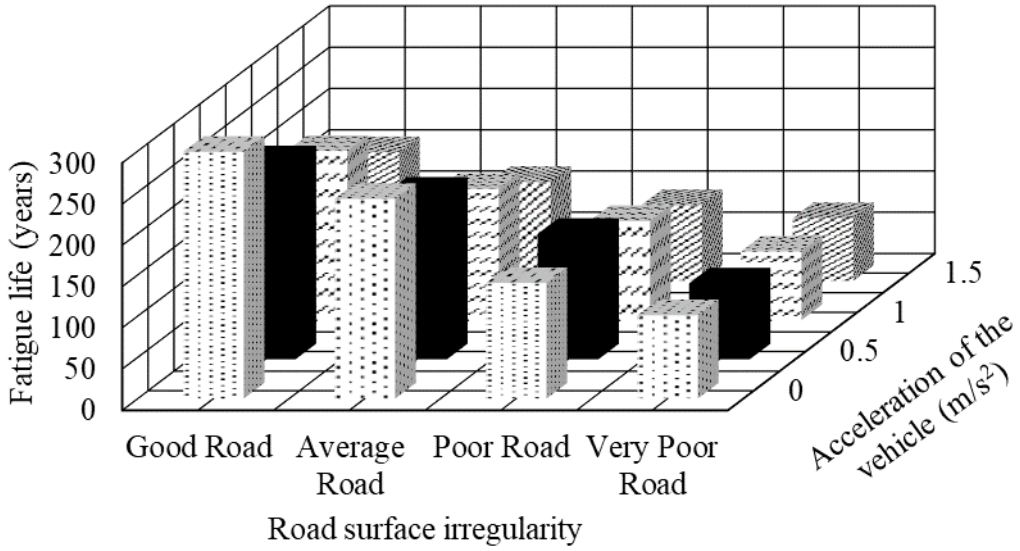

Fig. 4.33 Comparison of fatigue life with different road surface irregularities with entry velocity 20 km/hr

Moving vehicles exert fluctuating forces on the bridge as a result of vibration caused by road surface roughness. As the road surface deteriorates, the fluctuating nature of the dynamic vehicular load increases. This increases the dynamic stresses on the bridge caused by vehicle vibration. Thus, it is observed from Figs. 4.29 to 4.32 that the number of stress cycles in the lower stress range increases as the road surface roughness increases from good to very poor. The stress ranges are subjected to higher stress cycles for very poor road case leading to more damage accumulation as compared to good, average and poor road condition, which is observed from Figs. 4.29 to 4.32. Thus, the fatigue life of the bridge decreases with increasing road surface irregularity as shown in Fig. 4.33.

4.6.1.3 Effect of arrival rate of vehicles

The vehicle arrival rate is varied to examine the effect on DAF and fatigue life. Vehicle arrival rates range from 60 vehicles per minute to 180 vehicles per minute with an interval of 30 vehicles per minute. The uniform vehicle velocity is 20 km/hr. The road roughness considered is very poor. The amplitude of the mean profile is considered as 0.01 m. The mean and standard deviation of the flexural stresses obtained at mid span of the bridge for varying arrival rate is shown in Fig. 4.34.

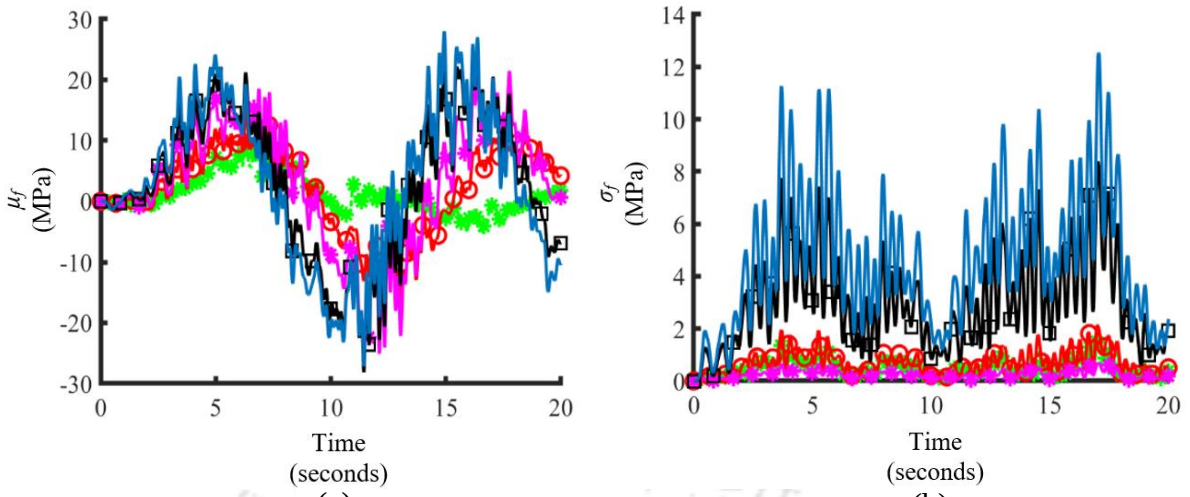

Fig. 4.34 (a): Mean and (b): standard deviation of flexural stress at mid span of the bridge for different arrival rate for uniform vehicle velocity 20 km/hr ($S_{GG}(\Omega_0)$ = 1024 × 10^{-6} m^2/cycle/m)

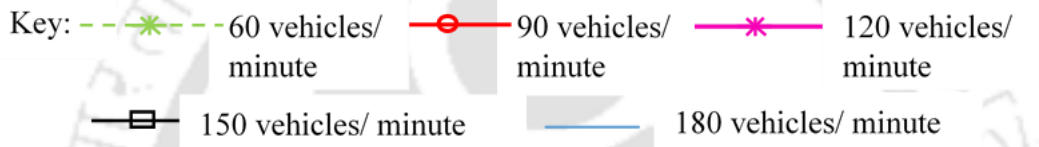

The arrival rate signifies the number of vehicles traversing on the bridge. Increase in arrival rate signifies higher traffic volume thus, leading to higher dynamic stresses, which can be observed from Fig. 4.34.

Dynamic Amplification Factor (DAF)

The DAF for varying arrival rate and acceleration of the vehicle for entry velocity 20 km/hr, 40 km/hr and 60 km/hr is shown in Figs. 4.35 to 4.37. The road case considered is very poor.

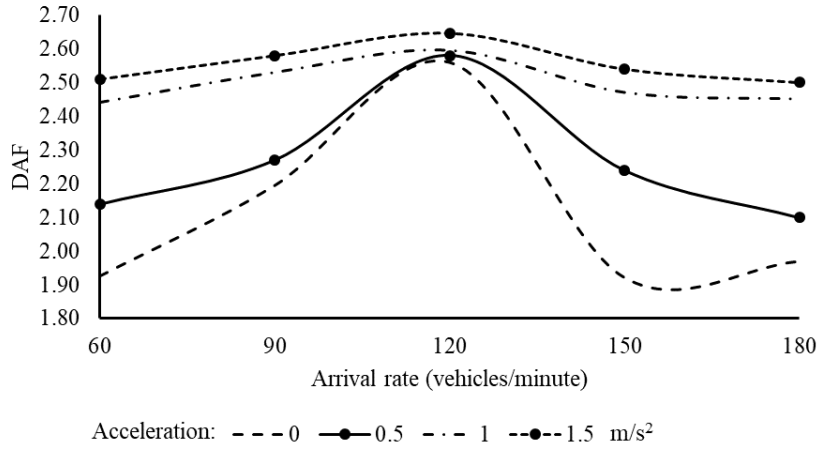

Fig. 4.35 DAF for single span bridge for varying arrival rate and acceleration of the vehicle for entry velocity 20 km/hr for very poor road

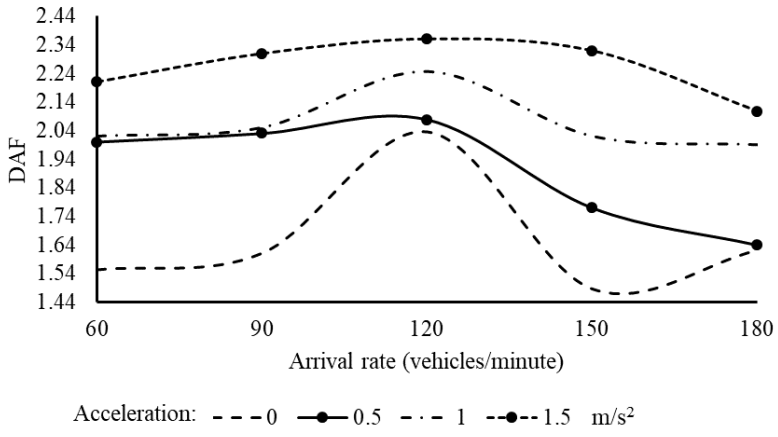

Fig. 4.36 DAF for single span bridge for varying arrival rate and acceleration of the vehicle for entry velocity 40 km/hr for very poor road

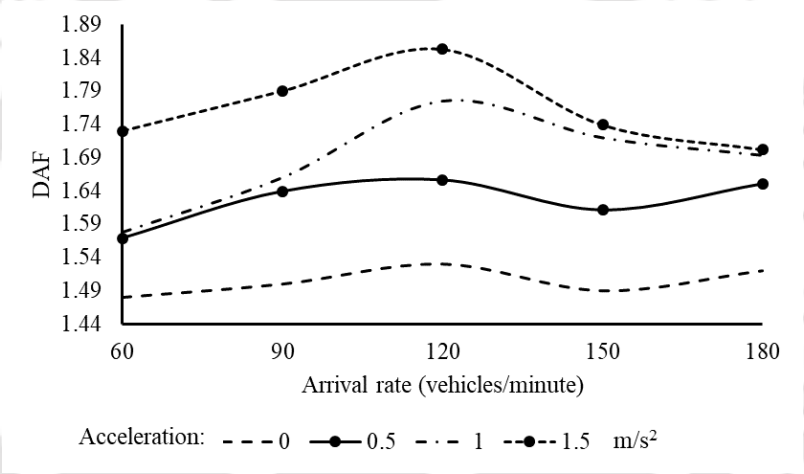

Fig. 4.37 DAF for single span bridge for varying arrival rate and acceleration of the vehicle for entry velocity 60 km/hr for very poor road

The DAF increases for arrival rate up to 120 vehicles per minute and then decreases further, as shown in Figs. 4.35 to 4.37. A higher arrival rate indicates a higher traffic flow on the bridge. However, as the arrival rate increases, the static stresses caused by vehicular movement also increases in addition to the dynamic stresses, which become dominant for arrival rates greater than 120 vehicles per minute. This results in reductions in DAF for arrival rates greater than 120 vehicles per minute.

Fatigue life

The stress range histogram for varying arrival rate for 20 km/hr uniform vehicle velocity and very poor road case is shown in Fig. 4.38. The comparison of fatigue life with arrival rate and

acceleration of the vehicle for entry velocity 20 km/hr, 40 km/hr and 60 km/hr are shown in Figs. 4.39 to 4.41.

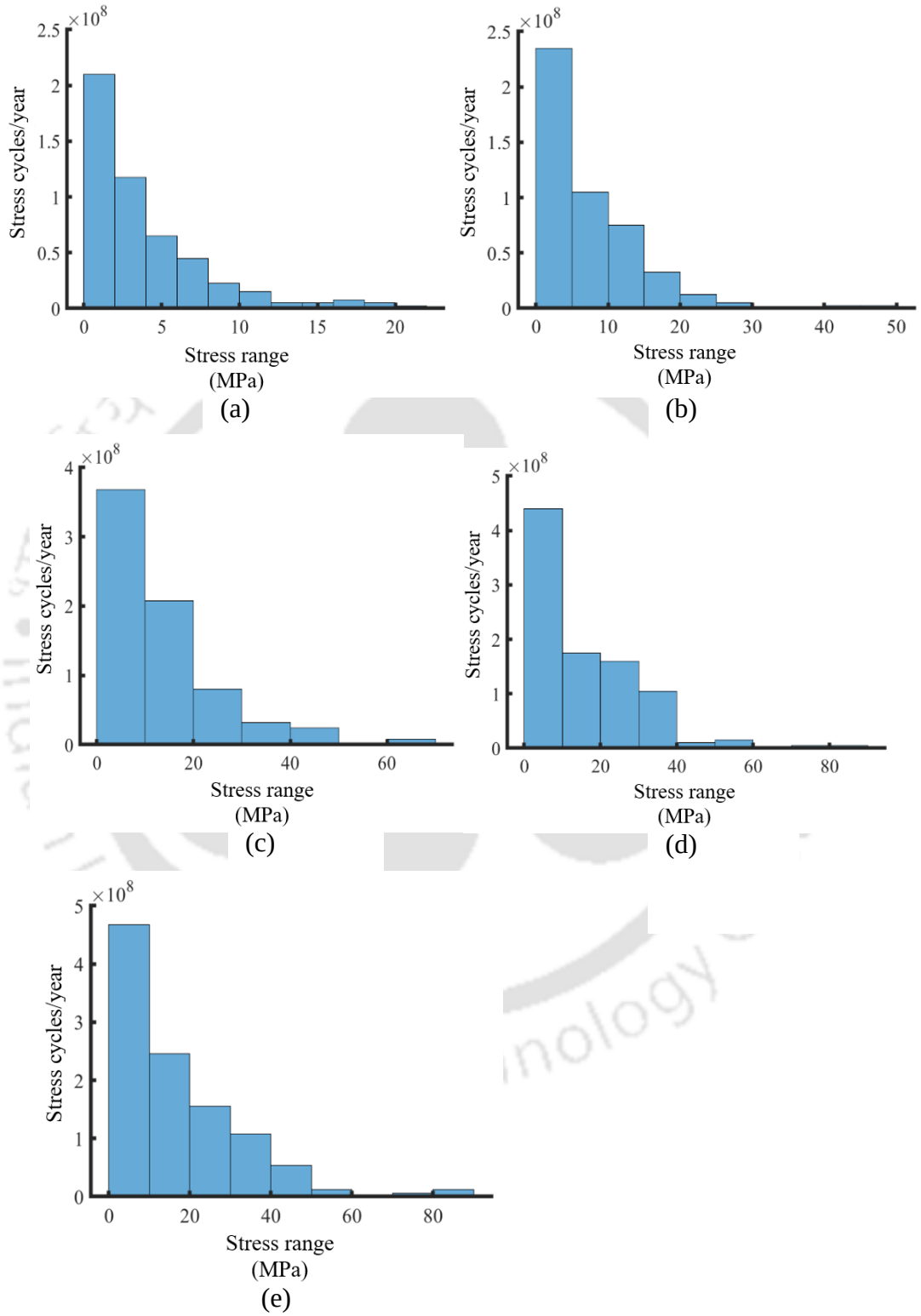

Fig. 4.38 Stress range histogram: (a): 60 vehicles per minute (b): 90 vehicles per minute (c): 120 vehicles per minute (d): 150 vehicles per minute (e): 180 vehicles per minute for uniform vehicle velocity 20 km/hr

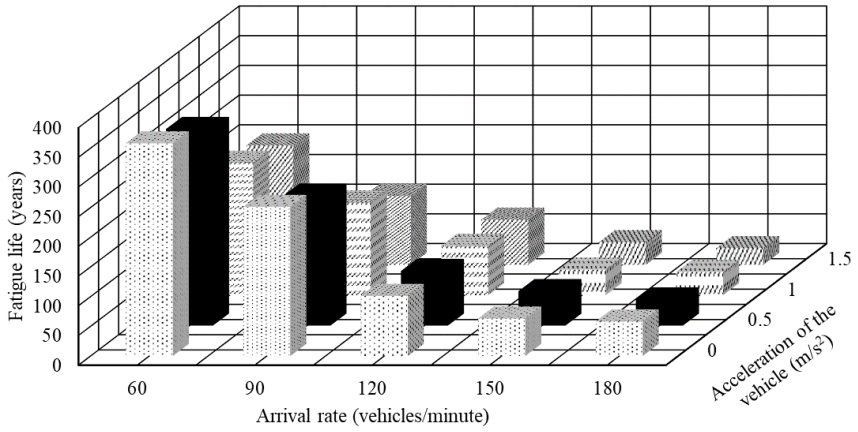

Fig. 4.39 Fatigue life for varying arrival rate and acceleration of the vehicle for entry velocity 20 km/hr for very poor road

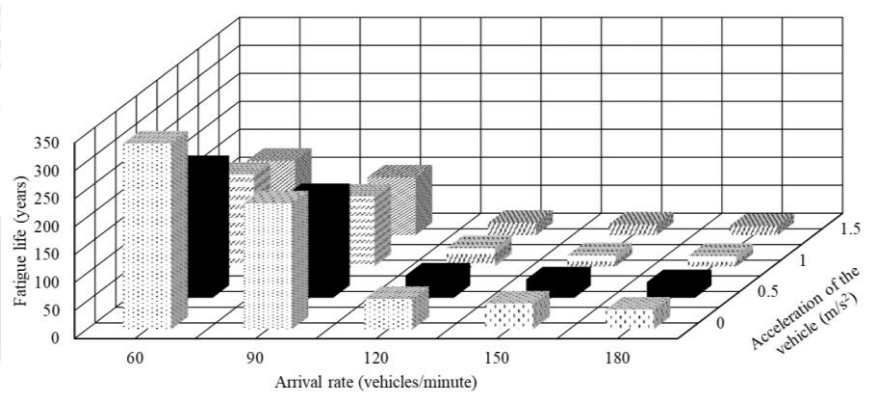

Fig. 4.40 Fatigue life for varying arrival rate and acceleration of the vehicle for entry velocity 40 km/hr for very poor road

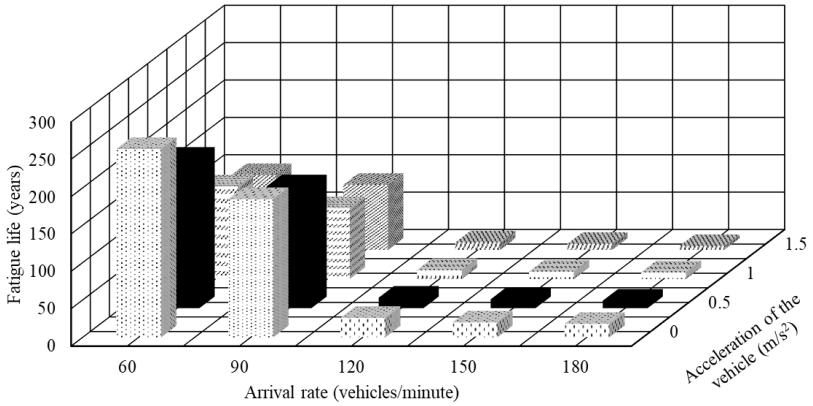

Fig. 4.41 Fatigue life for varying arrival rate and acceleration of the vehicle for entry velocity 60 km/hr for very poor road

As the arrival rate increases, more vehicles traverse the bridge, causing the dynamic force on the bridge to increase. As a result, the presence of multiple vehicles on the bridge amplifies the stress range and increases the number of stress cycles. This causes more fatigue damage than a single vehicle. As shown in Fig. 4.38, the bridge is subjected to higher stress cycles at lower and higher stress ranges as the arrival rate increases. The fatigue life decreases as the vehicle arrival rate increases, as shown in Figs. 4.39 to 4.41. The fatigue life of the vehicle decreases with increasing vehicle velocity and acceleration, as shown in Figs. 4.39 to 4.41.

4.6.1.4 Effect of axle weight of the vehicle

The effect of DAF and fatigue life on the axle weight of the vehicle is studied in this section. The total vehicle weight is varied from 20 tonnes to 100 tonnes with an increment of 20 tonnes. The mean arrival rate is considered as 120 vehicles per minute. The uniform vehicle velocity is 20 km/hr. The road case considered is very poor. The amplitude of the mean profile is considered as 0.01 m. The mean and standard deviation of flexural stresses at mid span of the bridge for varying axle weight of the vehicle is shown in Fig. 4.42.

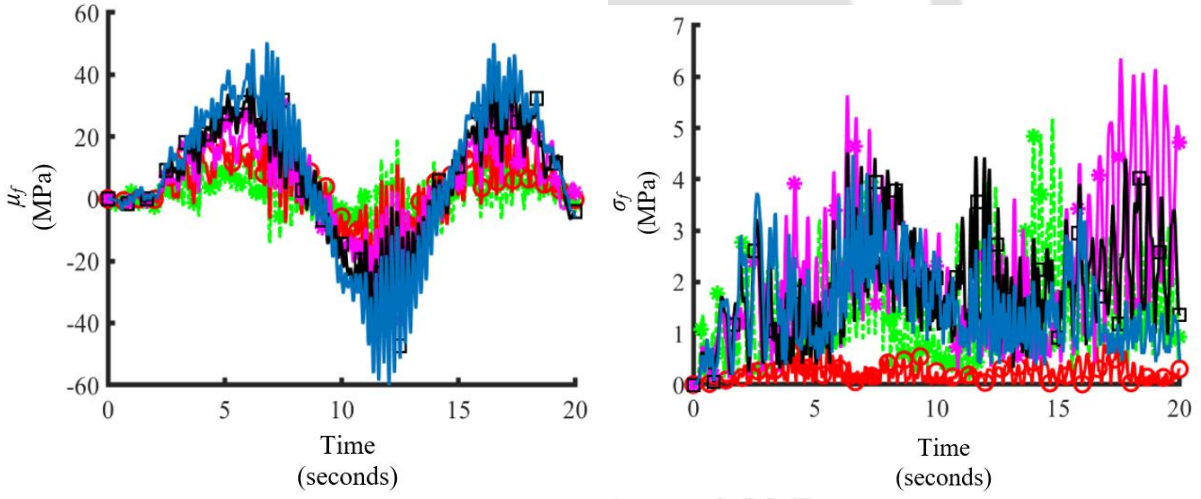

Fig. 4.42 (a): Mean and (b): standard deviation of flexural stresses at mid span of the bridge for different vehicle weight for uniform vehicle velocity 20 km/hr and very poor road condition

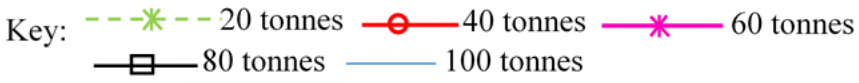

The increase in axle weight of the vehicle increases the dynamic load on the bridge, thus increasing the mean flexural stresses at mid span of the bridge, which is observed from Fig. 4.42. It is observed from Fig. 4.42 that the mean flexural stresses are increased by

approximately 4 times when the axle weight of the vehicle increases from 20 tonnes to 100 tonnes. The standard deviation of flexural stress at mid span do not follow a similar trend. Thus, it can be observed that an overloaded vehicle can cause large dynamic vibrations on the bridge due to vehicular movement when the road roughness is very poor, as compared to that of a light weight vehicle.

Dynamic Amplification Factor (DAF)

The variation of DAF with total vehicle weight and acceleration of the vehicle for very poor road condition for vehicle entry velocities 20 km/hr, 40 km/hr and 60 km/hr are shown in Figs. 4.43 to 4.45.

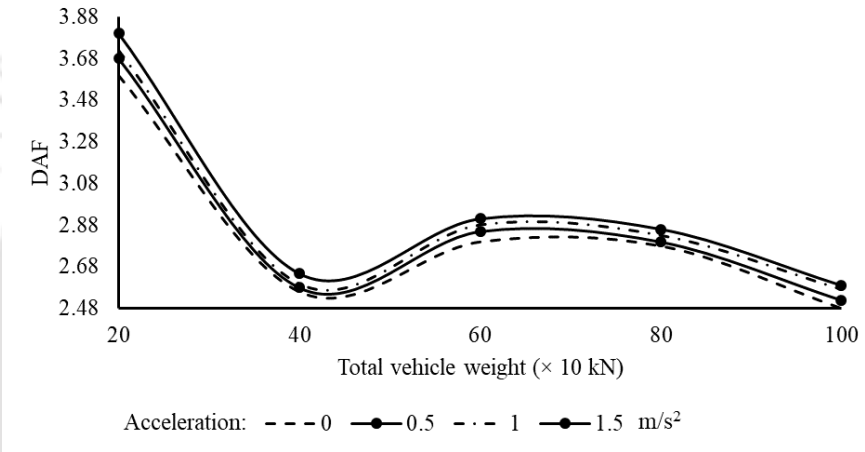

Fig. 4.43 DAF for varying axle weight and acceleration of the vehicle for entry velocity 20 km/hr for very poor road

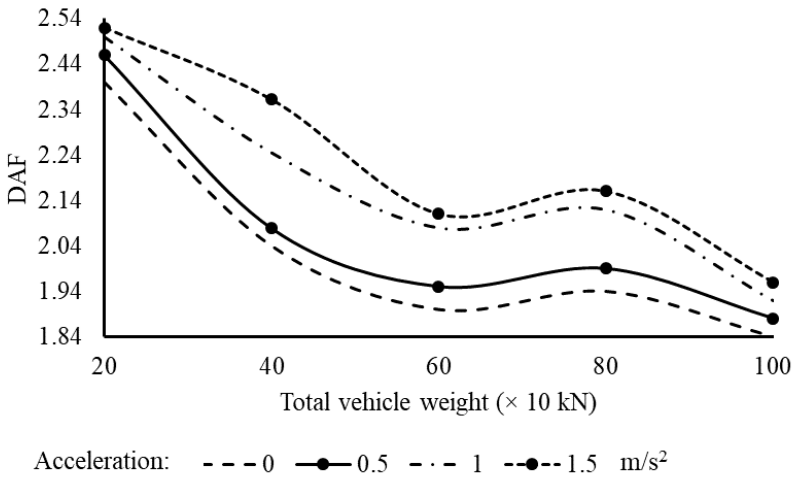

Fig. 4.44 DAF for varying axle weight and acceleration of the vehicle for entry velocity 40 km/hr for very poor road

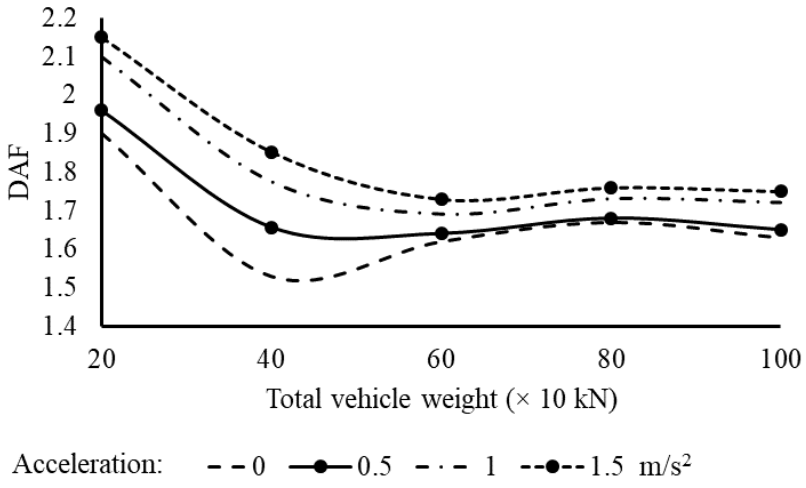

Fig. 4.45 DAF for varying axle weight and acceleration of the vehicle for entry velocity 60 km/hr for very poor road

It is observed from Figs. 4.43 to 4.45 that the DAF decreases as the total vehicle weight increases from 20 tonnes to 40 tonnes and further increase in total vehicle weight does not show a significant change in DAF. The reason for reduced DAF may be attributed mainly due to increase of static stresses that appears superseding the corresponding dynamic part.

Fatigue Life

The stress range histogram for varying axle weight for 20 km/hr uniform vehicle velocity and very poor road case is shown in Fig. 4.46. It is to be noted that the stress range histogram for axle weight 40 tonnes, vehicle arrival rate 120 vehicles per minute, uniform vehicle velocity 20 km/hr and very poor road condition is shown in Fig. 4.19 (a) in sub section 4.6.1.1. The comparison of fatigue life with axle weight and acceleration of the vehicle for entry velocity 20 km/hr, 40 km/hr and 60 km/hr are shown in Figs. 4.47 to 4.49.

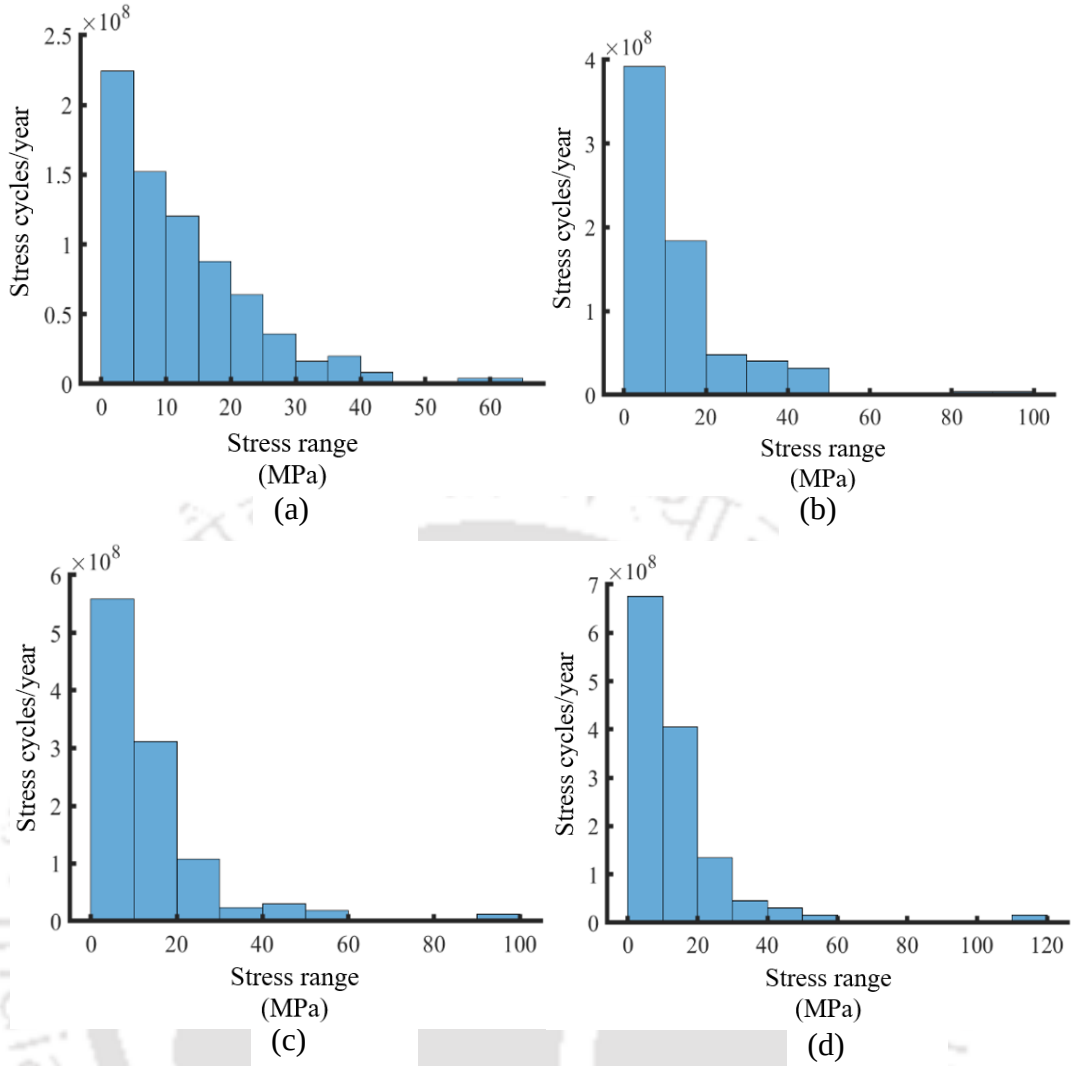

Fig. 4.46 Stress range histogram: (a): 20 tonnes (b): 60 tonnes (c): 80 tonnes (d): 100 tonnes for uniform vehicle velocity 20 km/hr

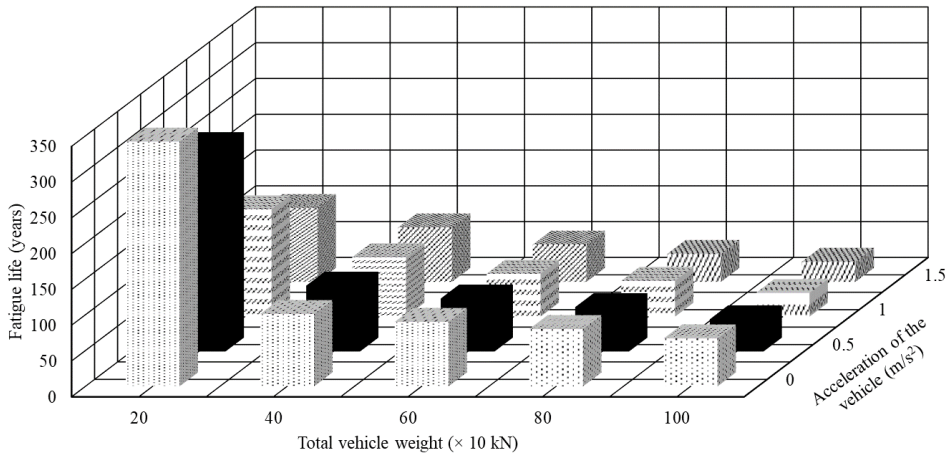

Fig. 4.47 Fatigue life for varying axle weight and acceleration of the vehicle for entry velocity 20 km/hr for very poor road

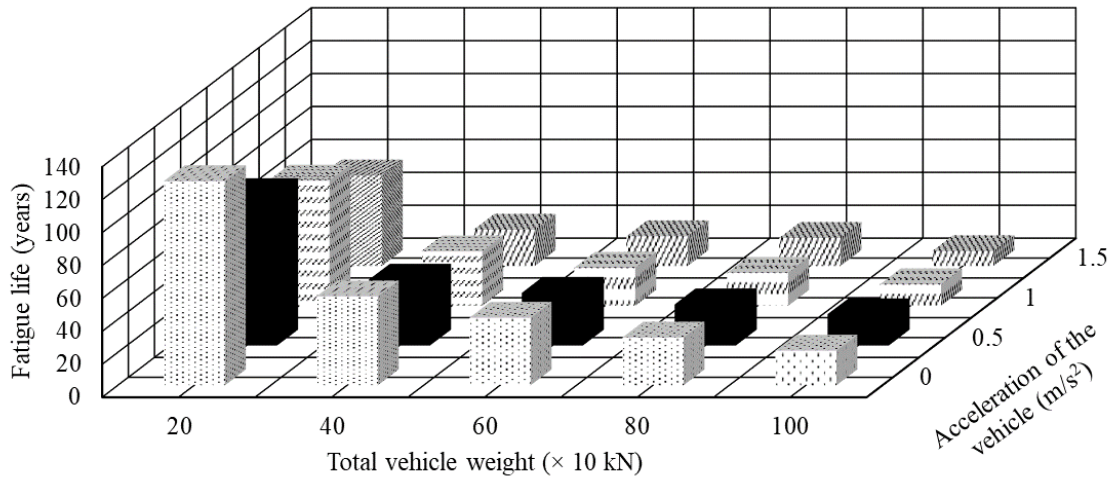

Fig. 4.48 Fatigue life for varying axle weight and acceleration of the vehicle for entry velocity 40 km/hr for very poor road

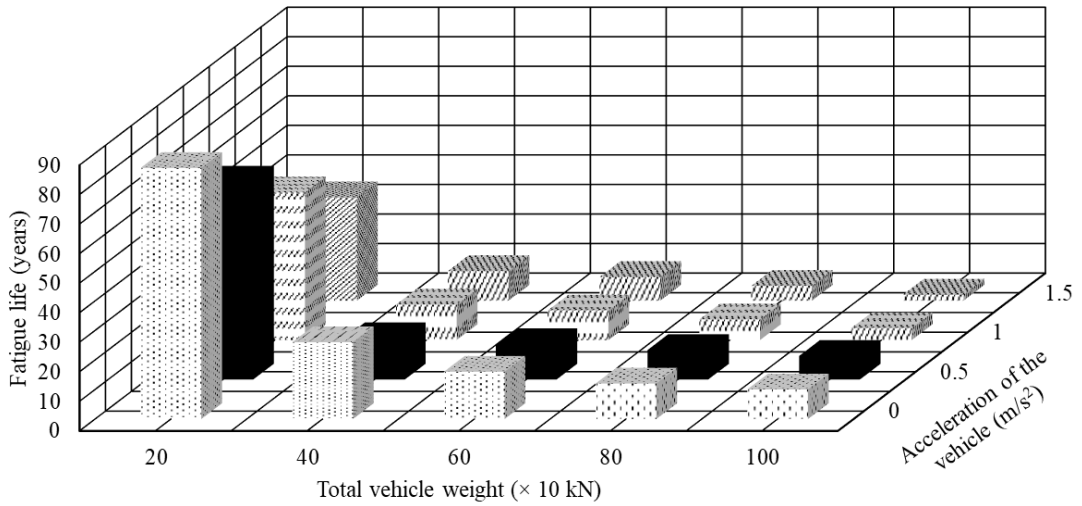

Fig. 4.49 Fatigue life for varying axle weight and acceleration of the vehicle for entry velocity 60 km/hr for very poor road

It is observed form Fig. 4.46 that the stress cycles in lower and higher stress ranges increase as the axle weight increases. The increase is due to the increase in the dynamic flexural stresses of the bridge as the axle weight of the vehicle increases. Due to increase in the stress cycles in lower and higher stress ranges, accumulation of fatigue damage takes place. Thus, the fatigue life of the bridge decreases as the total vehicle weight increases, which is observed from Figs. 4.47 to 4.49. It is also observed that during the service life of the bridge located on a busy highway, there is accumulation of fatigue damage over time with the passage of each heavy

vehicle. The accumulated damage resulting from multiple heavy vehicles leads to more fatigue damage and thereby reducing the fatigue life of the bridge.

4.6.1.5 Effect of span of the bridge

The effect of DAF and fatigue life on the span of the bridge is investigated in this section. The span of the bridge has been varied from 20 m to 40 m with an interval of 10 m considering the mean arrival rate as 120 vehicles per minute. The uniform vehicle velocity considered is 20 km/hr. The amplitude of mean profile is 0.01 m. The mean and standard deviation of flexural stresses obtained at the mid span of the bridge for span 20 m, 30 m and 40 m is shown in Fig. 4.50.

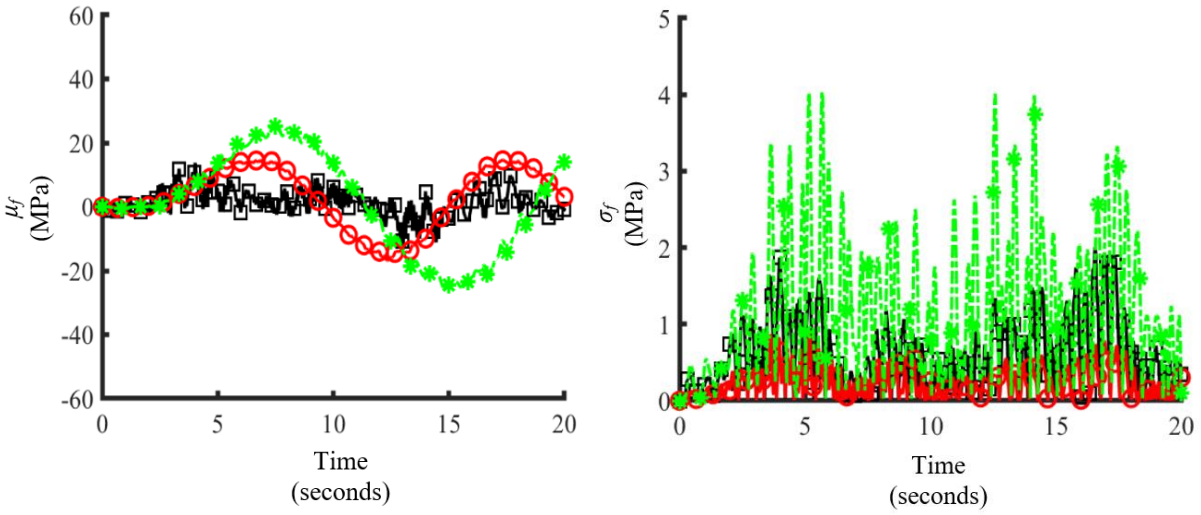

Fig. 4.50 (a): Mean and (b): standard deviation of flexural stresses at mid span of the bridge for different bridge span for uniform vehicle velocity 20 km/hr and very poor road condition

It is observed from Fig. 4.50 that the mean flexural stresses at the mid span of the bridge increases with the increase in span of the bridge. It is observed that the number of vehicles crossing the bridge increases with the increase in span of the bridge, which increases the mean flexural stresses. It is also observed from Fig. 4.50 that the standard deviation of flexural stresses at mid span of the bridge do not follow a similar pattern.

Dynamic Amplification Factor (DAF)

The variation of DAF with span of the bridge and acceleration of the vehicle for vehicle entry velocity 20 km/hr and very poor road condition is shown in Fig. 4.51.

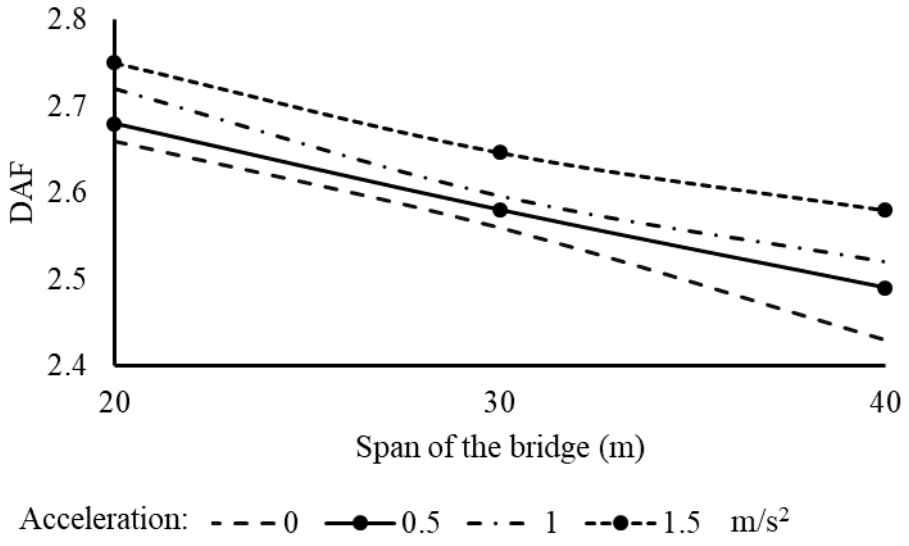

Fig. 4.51 DAF for varying span of the bridge and acceleration of the vehicle for entry velocity 20 km/hr for very poor road

It is observed from Fig. 4.51 that the DAF decreases with the increase in the span of the bridge. The dynamic and static load of the bridge increases as the span increases leading to reduction in DAF. It is also observed the DAF reduces from 7 % to 9 % when the bridge span increases from 20 m to 40 m.

Fatigue life

The stress range histogram for 20 m and 40 m span of the bridge for arrival rate 120 vehicles per minute and uniform vehicle velocity 20 km/hr for very poor road condition is shown in Fig. 4.52. It is to be noted that the stress range histogram for bridge span 30 m with vehicle arrival rate 120 vehicles per minute, uniform vehicle velocity 20 km/hr and very poor road condition is shown in Fig. 4.19 (a) in sub section 4.6.1.1. The fatigue life of the bridge for very poor road condition for varying bridge span and acceleration of the vehicle for vehicle entry velocity 20 km/hr is shown in Fig. 4.53.

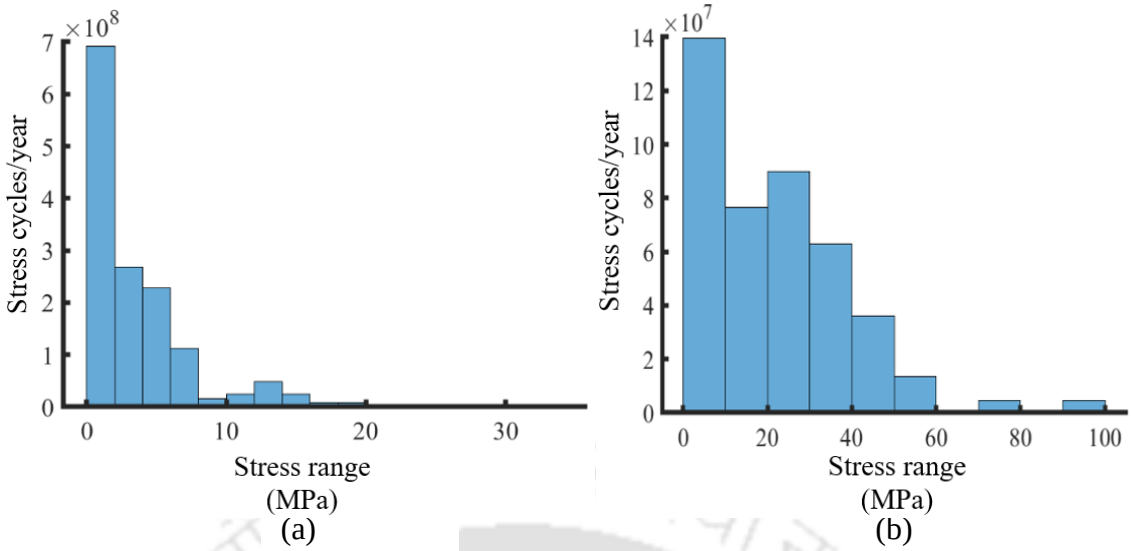

Fig. 4.52 Stress range histogram: (a): 20 m (b): 40 m for uniform vehicle velocity 20 km/hr and very poor road condition

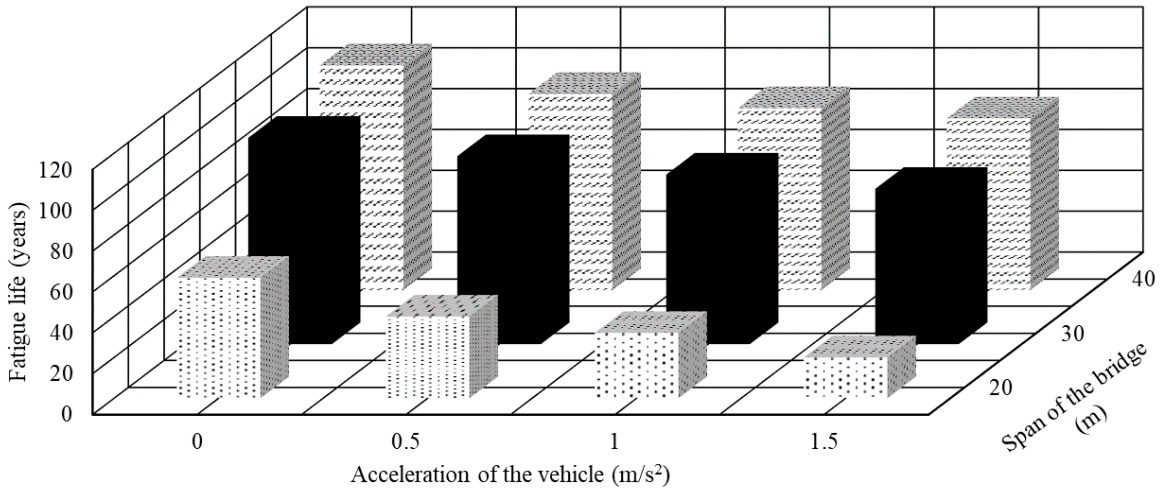

Fig. 4.53 Fatigue life for varying bridge span and acceleration of the vehicle for entry velocity 20 km/hr and very poor road condition

It is observed form Fig. 4.52 and Fig. 4.19 (a) that the fatigue life increases with the increase in the span of the bridge. This is due to decrease in natural frequencies of the bridge in all modes which results in larger amplitude stress cycles. The number of stress cycles in lower stress range increases, which is observed from Fig. 4.52 and Fig. 4.19 (a). This results in lower damage index thereby increasing the fatigue life as observed from Fig. 4.53.

4.6.1.6 Effect of amplitude of mean profile

The effect of DAF and fatigue life on the amplitude of mean profile is studied in this section. The amplitude of the mean profile has been varied from 0, 0.01 m, 0.015 m, 0.02 m. The zero amplitude physically indicates no pre camber is adopted. The vehicle arrival rate is considered as 120 vehicles per minute. The uniform vehicle velocity considered is 20 km/hr. The mean and standard deviation of flexural stresses obtained at the mid span of the bridge for different amplitude of the mean profile is shown in Fig. 4.54.

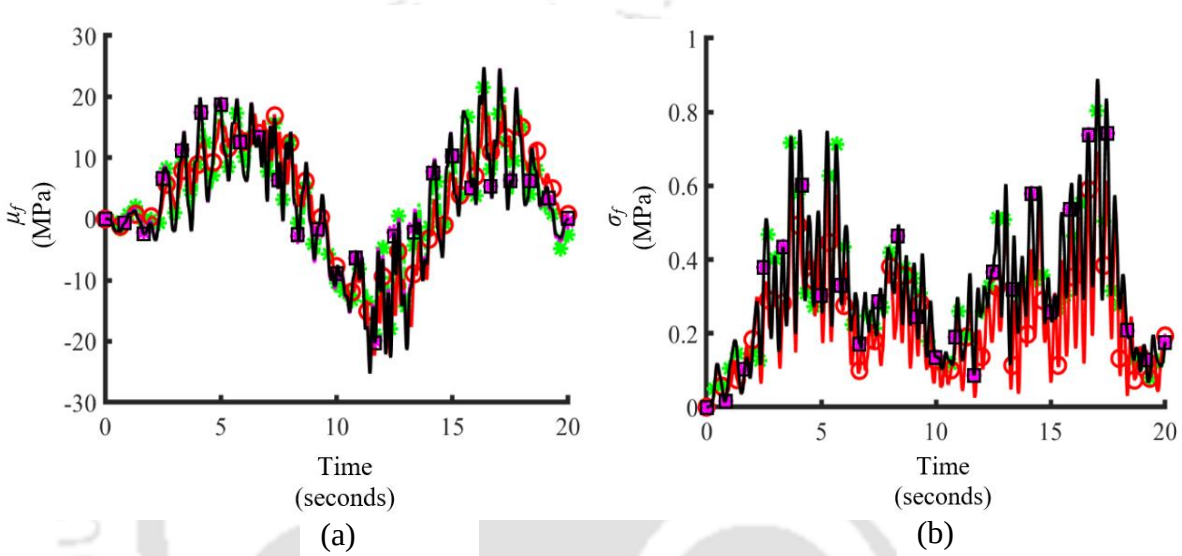

Fig. 4.54 (a): Mean and (b): standard deviation of flexural stresses at mid span of the bridge for different amplitude of mean profile for uniform vehicle velocity 20 km/hr and very poor road

The effect of pre-camber on mean and standard deviation of flexural stress at mid span is observed from Fig. 4.54. The mean and standard deviation of flexural stresses increases with the increase in the amplitude of mean profile. It is also observed from Fig. 4.54 that the flexural stresses are increased by 1.3 times when the amplitude of mean profile is increased from 0 to 0.02 m. It is also observed that there is a significant increase in the flexural stresses when the amplitude of mean profile increases from 0 to 0.01 m. However, gradual increase is observed in the flexural stresses when the amplitude of mean profile is further increased from 0.01 m to 0.015 m.

Dynamic Amplification Factor (DAF)

The effect of DAF with amplitude of mean profile as 0, 0.01m, 0.015 m and 0.02 m and acceleration of the vehicle for vehicle entry velocity 20 km/hr and 60 km/hr with arrival rate 120 vehicles per minute and very poor road condition is shown in Figs. 4.55 to 4.56. It is to be mentioned that in slender bridges, it is customary to provide pre-camber so that excessive deflection due to self-weight and moving vehicular load is compensated and serviceability condition of the structure is maintained.

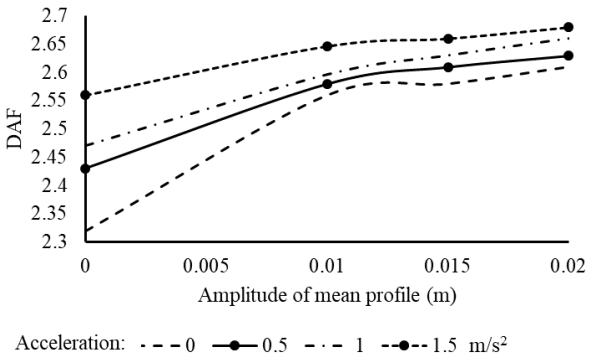

Fig. 4.55 DAF for varying amplitude of mean profile and acceleration of the vehicle for entry velocity 20 km/hr for very poor road

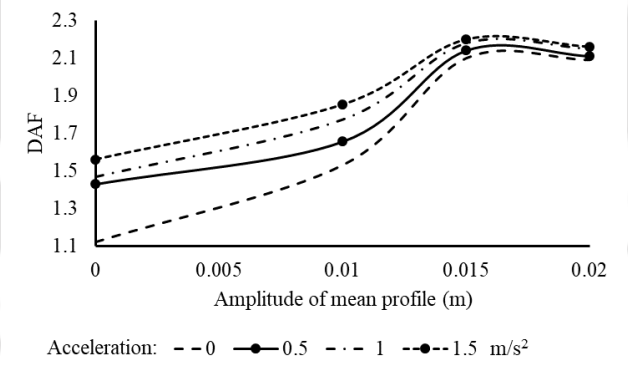

Fig. 4.56 DAF for varying amplitude of mean profile and acceleration of the vehicle for entry velocity 60 km/hr for very poor road condition

It is observed from Figs. 4.55 and 4.56 that the DAF increases with the increase in amplitude of mean profile for vehicle entry velocity 20 km/hr. However, in case of vehicle entry velocity 60 km/hr, DAF increases upto amplitude of mean profile 0.015 m and decreases further. It is also observed that there is a significant increase in the DAF for vehicle entry velocity 20 km/hr and 60 km/hr when the amplitude of mean profile is increased from 0 to 0.01 m. There is

gradual increase in DAF in case of lower entry velocity of the vehicle such as 20 km/hr when the amplitude of mean profile is increased from 0.01 m to 0.02 m. But, the same trend is not followed in case of higher vehicle entry velocity such as 60 km/hr. This may be because the temporal frequency of wheel input due to the pre-cambered profile gets modified by the change of vehicle velocity in time domain analysis, which is adopted in the present method.

Fatigue life

The stress range histogram for amplitude of mean profile as 0, 0.015 m and 0.02 m for arrival rate 120 vehicles per minute and uniform vehicle velocity 20 km/hr for very poor road condition is shown in Fig. 4.57. It is to be noted that the stress range histogram for amplitude of mean profile as 0.01 m with vehicle arrival rate 120 vehicles per minute, uniform vehicle velocity 20 km/hr and very poor road condition is shown in Fig. 4.19 (a) in sub section 4.6.1.1. The fatigue life of the bridge for very poor road condition for varying amplitude of the mean profile and acceleration of the vehicle for vehicle entry velocity 20 km/hr and 60 km/hr is shown in Figs. 4.58 and 4.59.

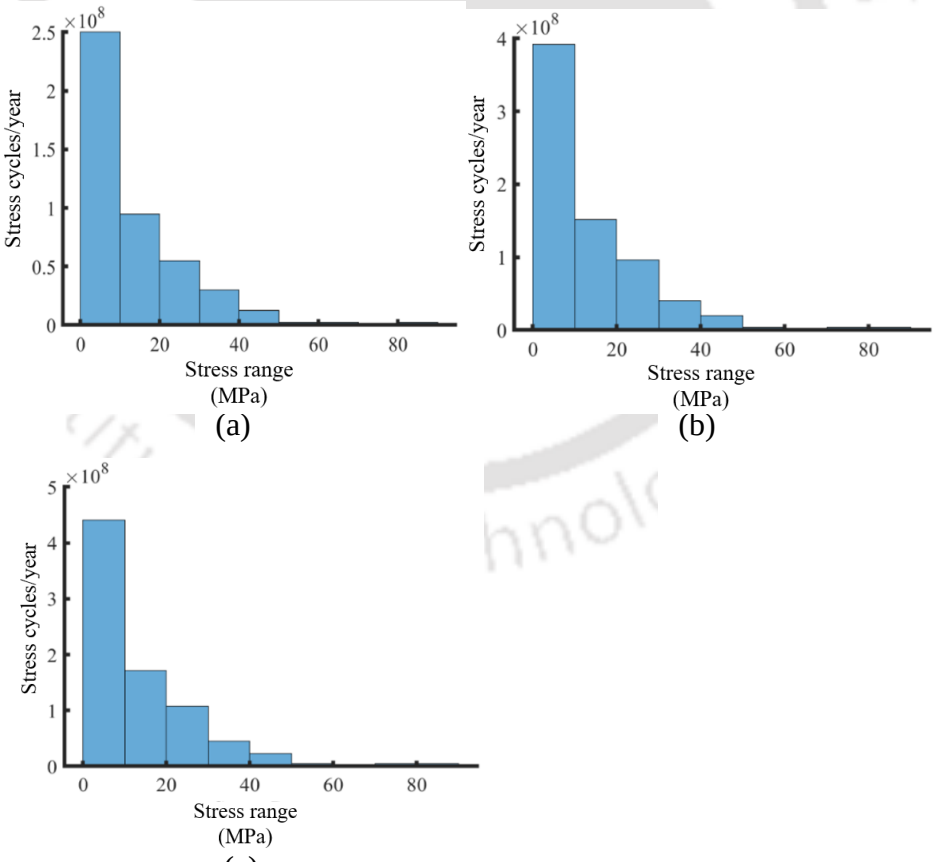

Fig. 4.57 Stress range histogram: (a): h_m = 0 (b): h_m = 0.015 m (c): h_m = 0.02 m for uniform vehicle velocity 20 km/hr and very poor road condition

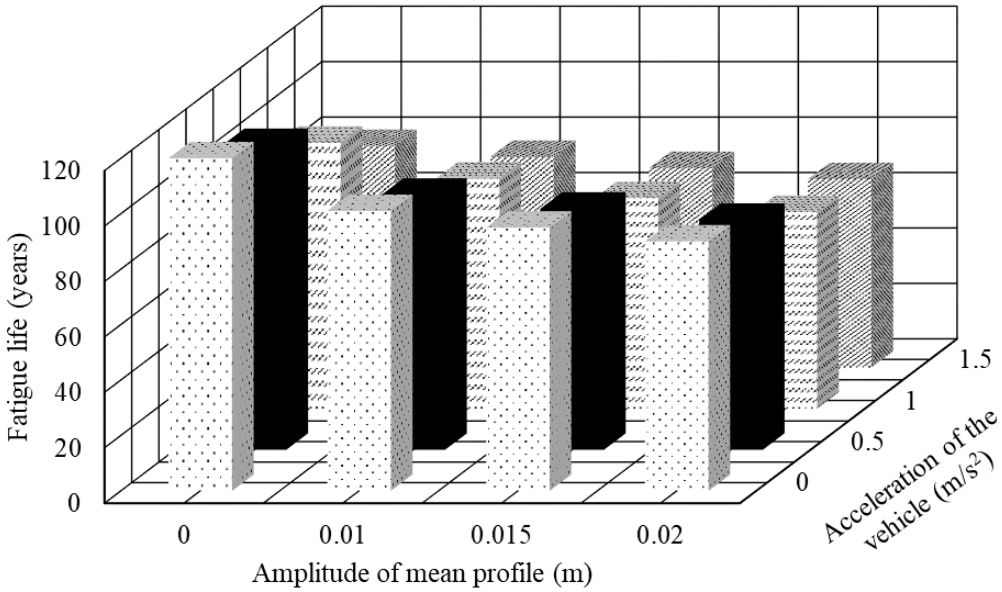

Fig. 4.58 Fatigue life for varying amplitude of mean profile and acceleration of the vehicle for entry velocity 20 km/hr and very poor road

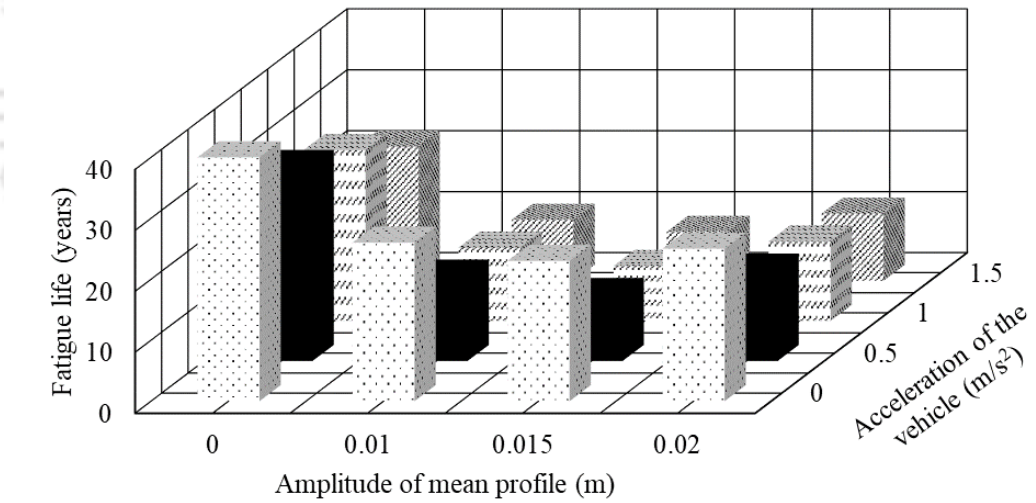

Fig. 4.59 Fatigue life for varying amplitude of mean profile and acceleration of the vehicle for entry velocity 60 km/hr and very poor road

It is observed from Fig. 4.57 that the number of stress cycles in the lower stress range is increased with the increase in amplitude of mean profile. This leads to higher damage accumulation and reduction in fatigue life of the bridge, which is observed from Fig. 4.58 for lower vehicle entry velocity such as 20 km/hr. However, in case of higher vehicle entry velocity such as 60 km/hr, the number of stress ranges in lower and higher stress cycles is reduced leading to lower damage accumulation when the amplitude of mean profile is increased from

0.015 m to 0.02 m. Thus, the fatigue life decreases as the amplitude of mean profile increases from 0 to 0.015 m and increases when the amplitude of mean profile is increased from 0.015 m to 0.02 m, which is observed from Fig. 4.59.

4.7 Closure

In this chapter, the response statistics of the single span bridge due to passage of multiple vehicles has been obtained using the proposed semi analytical method. The convergence study for the number of terms and time window considered have been studied to observe the effect on the mean and standard deviation of flexural stresses at mid span of the bridge. The variable mean profile in the form of pre-camber and variable velocity have been incorporated in the study. Effect of vehicle velocity, acceleration of the vehicle, road surface roughness, arrival rate of the vehicles, axle weight of the vehicle, bridge span and amplitude of mean profile on mean and standard deviation of flexural stresses at mid span of the bridge have been studied. Further, the effect of above mentioned parameters on DAF and fatigue life have also been studied. The study reveals that fatigue damage in bridges would be earlier if road surface condition is not favourable for smooth ride. Moreover, accelerated vehicles will cause increased dynamic stress in the bridge and reduce its fatigue life.

5

FATIGUE LIFE PREDICTION: PART II
MULTI SPAN CONTINUOUS BRIDGE USING SEMI ANALYTICAL METHOD

5.1 General

The dynamic flexural stresses of a multi-span continuous bridge considering multiple vehicle movement where in the vehicle arrival time is assumed to be a random variable following Poisson process has been determined in this chapter using the Orthogonal Polynomial Expansion method. A non-homogeneous road surface roughness has been considered. The mean surface of the bridge deck which resembles the pre-camber is represented by a sine function. The forward vehicle velocity is assumed to be both constant and variable. The mean and standard deviation of flexural stresses at the critical location of two span and three span continuous bridge have been evaluated. For various bridge vehicle parameters, these response statistics have been used in the evaluation of DAF and fatigue life of two and three span continuous bridges.

5.2 Numerical Data

The following subsections detail the system parameters used to determine the response statistics, DAF and fatigue life of two and three span continuous bridge.

5.2.1 Bridge Parameters

The bridge considered for the study is a two and three span continuous twin cell box girder with each span of 30 m. The single lane bridge is composed of reinforced concrete deck and steel girder which is twin cell type. The total width of the twin cell girder is 7.5 m and height is 1.5 m. The cross section of the superstructure of the bridge is shown in Fig. 5.1. The mass per unit length of the bridge is 1.0288×10^4 kg/m and moment of inertia of equivalent steel section is 0.3391 m^4. The natural frequency and mode shapes upto five modes of the two span and three span continuous bridge are shown in Table 5.1, Figs. 5.2 and 5.3 respectively. The natural frequency and mode shape function for a multi-span continuous beam is given in Appendix-II.

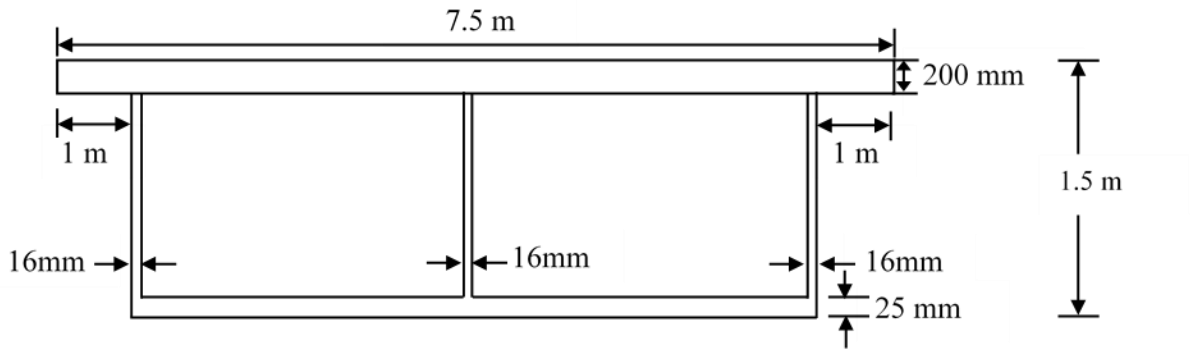

Fig. 5.1 Cross section of the superstructure of the bridge

Table 5.1 Natural frequency of two and three span continuous bridge

Number of span	Natural Frequency (rad/sec)				
	Mode 1	Mode 2	Mode 3	Mode 4	Mode 5
2	28.15	43.99	112.62	142.54	253.41
3	28.15	35.95	52.85	112.64	127.76

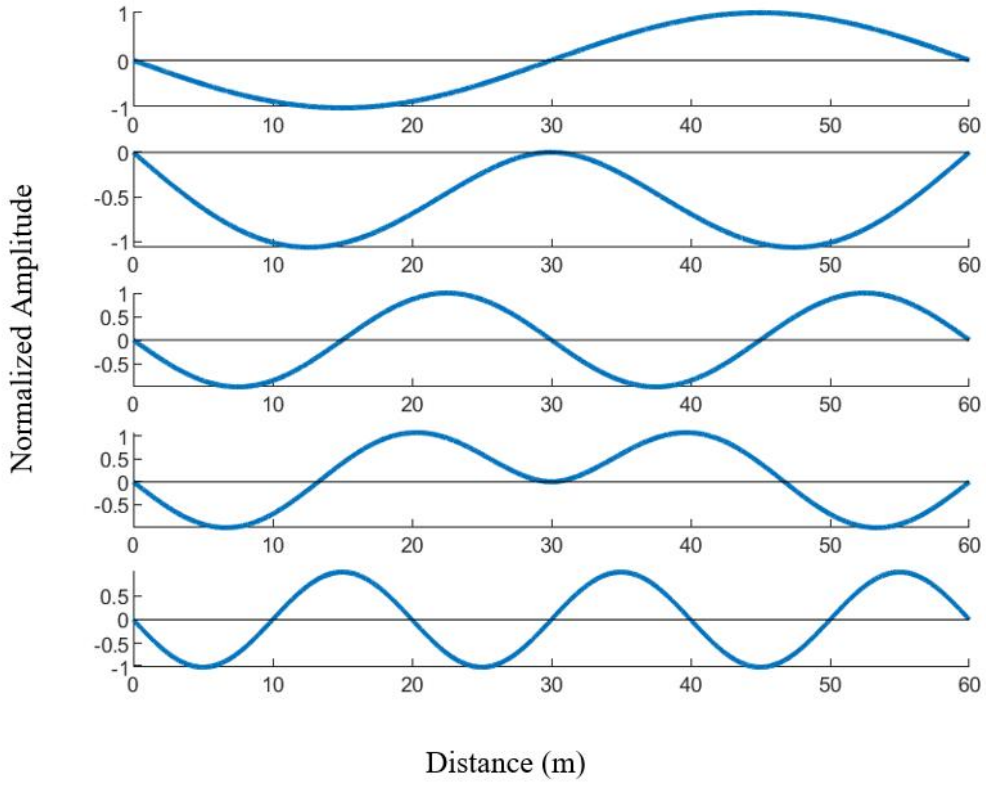

Fig. 5.2 First five mode shapes of two span continuous bridge

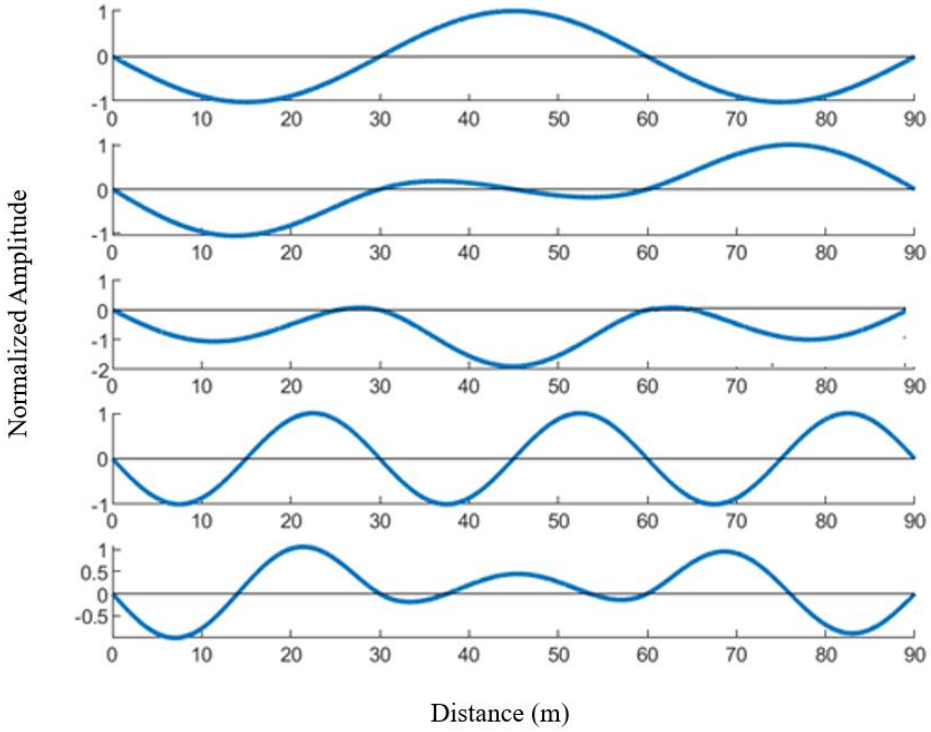

Fig. 5.3 First five mode shapes of three span continuous bridge

5.2.2 Vehicle Parameters

The vehicle model considered is Quarter car model having single wheel contact. For this model, sprung mass, m_s is taken as 36000 kg and unsprung mass, m_w is 4000 kg. The suspension stiffness k_s, suspension damping c_s, tyre stiffness k_w and tyre damping c_w have been considered as 14.4×10^6 Nm^{-1}, 475.2×10^3 Nsm^{-1}, 3.6×10^6 Nm^{-1} and 24×10^3 Nsm^{-1} respectively.

5.3 Convergence Study on Effect of Time Window

The fatigue life of the bridge can be obtained using weigh in motion data. Since fatigue damage of the bridge accumulates over time, the vehicular motion has to be recorded for a time span of one month or more. The stress strain data obtained is used for evaluation of fatigue life. However, acquiring such data is difficult in many situations unless the bridge is instrumented. More important is to examine the fatigue life during design phase such that designer can accordingly choose or modify structural detail considering severe loading. To investigate the effect of multiple vehicle loading, it is necessary to consider a time window for which simulation can be run in a cost effective way. The effect of different time windows on the convergence of the dynamic stresses is discussed in the next section.

5.3.1 Effect of Time Window

This section investigates the impact of various time windows on the mean and standard deviation of flexural stresses measured at the centre of the second span of two and three span continuous bridge. To acquire the optimum time window for multiple vehicular movement, time windows are varied from 15 seconds to 30 seconds with a 5 second interval for two span continuous bridge and time windows are varied from 20 seconds to 35 seconds with a 5 second interval for three span continuous bridge. The uniform vehicle velocity is also varied from 20 km/hr to 60 km/hr with an interval of 10 km/hr. The arrival rate of the vehicle is 120 vehicles per minute. The irregularity of the road surface ranges from good, average, poor and very poor. The maximum mean and standard deviation of flexural stresses at the centre of the second span of two and three span continuous bridge for different time windows is given in Tables 5.2 to 5.5 respectively.

Table 5.2 Comparison of maximum mean flexural stress at centre of second span for two span continuous bridge for different time window

Vehicle Velocity (km/hr)	Road Roughness Coefficient (m^2/cycle/m $\times 10^{-6}$)	Mean Flexural Stress (MPa)			
		15 secs	20 secs	25 secs	30 secs
20	32	2.78	3.01	3.02	3.03
	120	3.14	4	4.12	4.12
	512	4.3	4.54	4.54	4.52
	1024	5.13	5.16	5.16	5.14
30	32	2.55	2.64	2.64	2.68
	120	2.72	2.73	2.73	2.73
	512	2.93	2.93	2.93	2.93
	1024	2.99	2.99	2.99	2.99
40	32	2.4	2.54	2.54	2.54
	120	2.59	2.59	2.59	2.59
	512	2.84	2.84	2.84	2.84
	1024	2.90	2.90	2.90	2.90
50	32	1.91	1.91	1.91	1.91
	120	2.34	2.34	2.34	2.34
	512	2.76	2.76	2.76	2.76
	1024	2.88	2.88	2.88	2.88
60	32	2.05	2.05	2.05	2.05
	120	2.10	2.10	2.10	2.10
	512	2.45	2.45	2.45	2.45
	1024	2.65	2.65	2.65	2.65

Table 5.3 Comparison of maximum standard deviation of flexural stress at centre of second span for two span continuous bridge for different time window

Vehicle Velocity (km/hr)	Road Roughness Coefficient (m^2/cycle/m × 10^{-6})	Standard Deviation of Flexural Stress (MPa)			
		20 secs	25 secs	30 secs	35 secs
20	32	0.36	0.36	0.36	0.36
	120	0.55	0.55	0.55	0.55
	512	1.10	1.10	1.10	1.10
	1024	1.60	1.60	1.60	1.60
30	32	0.37	0.37	0.37	0.37
	120	0.76	0.76	0.76	0.76
	512	1.23	1.23	1.23	1.23
	1024	2	2	2	2
40	32	0.33	0.33	0.33	0.33
	120	0.62	0.62	0.62	0.62
	512	1.15	1.15	1.15	1.15
	1024	1.32	1.32	1.32	1.32
50	32	0.48	0.48	0.48	0.48
	120	0.75	0.75	0.75	0.75
	512	1.20	1.20	1.20	1.20
	1024	1.33	1.33	1.33	1.33
60	32	0.30	0.30	0.30	0.30
	120	0.32	0.32	0.32	0.32
	512	0.44	0.44	0.44	0.44
	1024	0.51	0.51	0.51	0.51

Table 5.4 Comparison of maximum mean flexural stress at centre of second span for three span continuous bridge for different time window

Vehicle Velocity (km/hr)	Road Roughness Coefficient (m^2/cycle/m × 10^{-6})	Mean Flexural Stress (MPa)			
		20 secs	25 secs	30 secs	35 secs
20	32	2.65	2.4	2.4	2.41
	120	2.78	2.76	2.76	2.7
	512	3.08	3.54	3.54	3.52
	1024	3.33	4.16	4.16	4.14
30	32	1.55	1.64	1.64	1.67
	120	1.65	1.89	1.8	1.83
	512	1.89	1.91	1.92	2.21
	1024	2.09	2.23	2.44	2.5
40	32	1.39	1.35	1.34	1.54
	120	1.391	1.52	1.5	1.54
	512	1.4	1.89	1.85	2.1
	1024	1.5	1.79	1.97	1.98
50	32	0.93	0.93	0.93	0.93
	120	1.03	1.03	1.04	1.05
	512	1.36	1.36	1.36	1.37
	1024	1.65	1.65	1.65	1.65
60	32	1.05	1.38	1.7	1.7
	120	1.07	1.43	1.6	1.6
	512	1.37	1.53	1.54	1.64
	1024	1.61	1.61	1.63	1.63

Table 5.5 Comparison of maximum standard deviation of flexural stress at centre of second span for three span continuous bridge for different time window

Vehicle Velocity (km/hr)	Road Roughness Coefficient (m^2/cycle/m × 10^{-6})	Standard Deviation of Flexural Stress (MPa)			
		20 secs	25 secs	30 secs	35 secs
20	32	0.37	0.39	0.39	0.39
	120	0.59	0.68	0.68	0.68
	512	1.18	1.36	1.36	1.36
	1024	1.69	1.91	1.91	1.91
30	32	0.47	0.48	0.48	0.48
	120	0.85	0.85	0.85	0.85
	512	1.66	1.66	1.66	1.66
	1024	2.05	2.15	2.3	2.3
40	32	0.39	0.397	0.397	0.4
	120	0.67	0.67	0.67	0.68
	512	1.3	1.3	1.3	1.3
	1024	1.4	1.7	1.79	1.79
50	32	0.59	0.6	0.6	0.6
	120	0.87	0.87	0.87	0.88
	512	1.27	1.27	1.27	1.27
	1024	1.39	1.55	1.55	1.56
60	32	0.37	0.38	0.38	0.38
	120	0.39	0.39	0.39	0.39
	512	0.46	0.46	0.46	0.46
	1024	0.58	0.58	0.58	0.58

It is observed form Table 5.2 that the maximum mean flexural stresses at centre of the second span of two span continuous bridge increase from 15 secs to 20 secs time window and remains approximately same for 20 secs time window to 30 secs time window. It is also observed from Table 5.3 that the maximum standard deviation of flexural stresses at centre of the second span of two span continuous bridge does not vary significantly for time windows 15 secs to 30 secs for uniform vehicle velocity 20 km/hr to 60 km/hr for all road conditions. Thus, the optimum time window for multiple vehicular movement in two span continuous bridge is 20 secs. Moreover, it is also observed from Tables 5.4 and 5.5 that the on increasing the time window from 20 secs to 35 secs, maximum mean and standard deviation of the flexural stresses at the centre of the second span of three span continuous bridge is not affected significantly. This is because as the time window is increased, some vehicles might have already crossed the bridge while some new vehicles might have entered, thus keeping the number of vehicles per bridge length approximately the same. In view of the insignificant change in the mean and standard deviation of flexural stresses at the centre of second span in two and three span continuous bridge with different time windows, it is apparent that the fatigue life estimate will not significantly change on increasing the time window. Therefore, 20 secs time window has been considered for all the study in the chapter to save the computational time.

5.4 Comparison of Fatigue Damage with Linear Damage Rule

The fatigue life obtained by Modified Bilinear Damage Rule (MBLDR) is compared with that of Linear Damage Rule (LDR), wherein the stress cycles per day and the corresponding stress range are taken from Hahin et al., (1993). These data correspond to a continuous steel plate girder bridge (Bridge 0160335) located at U.S. 12 and 45, Mannheim Road, near O'Hare. The strain data collected at the ends of the welded cover plates of the girder have been reported in the paper and has been taken to compare the estimated life using the present approach. The data were collected for mixed traffic flow which comprised of a large volume of passenger cars, light and heavy trucks and various other commercial vehicles. The stress cycles obtained for a 24-hour period are multiplied by the number of days in 25 years, i.e., 25 × 365 to obtain the stress cycles for that time period which is shown in Table 5.6. The total cycles available, N were calculated taking the Fatigue coefficient, K as 4.218×10^9 and Fatigue exponent, m as 3.256 (Hahin et al., 1993). The fatigue life is evaluated using LDR, BLDR and MBLDR. In case of BLDR, the life level for minimum damage, N_1^* is taken as 4×10^9 and the life level for maximum damage, N_2^* is taken as 7×10^7. However, in case of MBLDR, low life level N_2' is

taken as 1×10^8 and high level N_1' is taken as 4×10^9. These two life levels are used for evaluating fatigue life. The pictorial representation of the comparison of fatigue life is displayed in Fig. 5.4.

Table 5.6. Stress range and stress cycles per day for Bridge (Hahin et al., 1993)

Stress range (ksi)	ɔtal cycles availab *N*	Stress cycles/day	tress cycles after 2 years, *n*	ɔremental fracti ɔf life consumed *n/N*
1	4.22×10^9	3440	3.14×10^7	0.0074
1.5	1.13×10^9	1074	9.80×10^6	0.0087
2	4.42×10^8	477	4.35×10^6	0.0098
2.5	2.14×10^8	203	1.85×10^6	0.0086
3	1.18×10^8	108	9.86×10^5	0.0084
3.5	7.14×10^7	108	9.86×10^5	0.0138
4	4.62×10^7	69	6.30×10^5	0.0136
4.5	3.15×10^7	75	6.84×10^5	0.0217
5	2.23×10^7	17	1.55×10^5	0.0070
5.5	1.64×10^7	8	7.30×10^4	0.0045

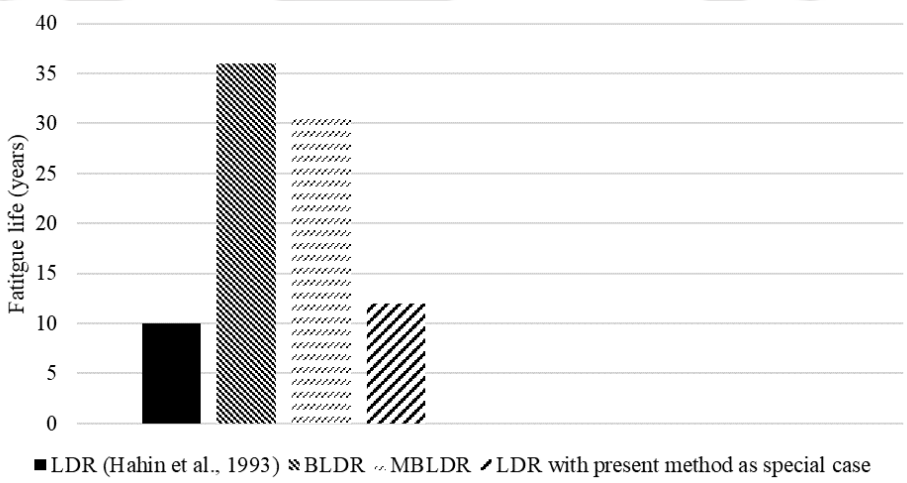

Fig. 5.4 Comparison of fatigue life with LDR (Hahin et al., 1993)

It is observed from Fig. 5.4 that the fatigue life obtained is 10 years as per LDR. However, the MBLDR emphasises the separation of low cycles of loading and high cycles of loading using a knee point and also considers the opening stress in crack propagation stage. The fatigue life obtained is 31 years using MBLDR and 36 years using BLDR. It is observed that the MBLDR estimates more life as compared to LDR, the cycle ratios are interspersed even though the stress cycles are segregated into low cycles and high cycles. The predictions made by the present method seem to predict higher fatigue life on consideration of loading order which was not incorporated earlier by Hahin et al. (1993).

It may be noted that the present formulation to evaluate the fatigue damage can be used for single sloped linear damage curve neglecting sequence of loading as a special case. When one ignores the two phases of loading then a single slope damage curve can be constructed with the average slope of two phases and further if one ignores the sequence of loading taking the factor β = 1, the estimate of damage index becomes 0.0865, yielding fatigue life of 12 years which is very close to the fatigue life given by Hahin et al., (1993), which is observed from Fig. 5.4.

5.5 Fatigue Life and DAF from Bridge Response Statistics

In this section, the fatigue life and dynamic amplification factor (DAF) has been obtained from bridge dynamic response. The bridge dynamic response of two and three span continuous bridge has been obtained using Orthogonal Polynomial Expansion method. In this, the vehicle arrival time follows Poisson process. The effect of road surface roughness and variable mean profile has also been considered in the study. The inclusion of mean profile in road surface roughness renders the road surface roughness to a spatially non-homogeneous random process. The response of the vehicle induced by road surface roughness becomes non-stationary random process in time domain when the vehicle traverses with variable velocity (Nigam and Yadav, 1974). The position of the n^{th} vehicle on the bridge is modelled using a general polynomial which is given in Eq. (3.12) in Chapter 3. The velocity of the n^{th} vehicle is given in Eq. (3.13) in Chapter 3. The vehicle is assumed to move with constant acceleration in case of variable velocity.

The standard error of the mean of the vehicle induced dynamic response is used to calculate the dynamic amplification factor. The fatigue life of the bridge is calculated using the design stress, which is the addition of the mean flexural stress, μ_f and two times the standard variation

of flexural stress, σ_f. The rainflow counting method is used to decompose the design stress history (Downing and Socie 1982). The number of cycles acquired from the rain flow counting method is converted to annual cycles using a multiplier (annual average daily traffic × 365). The annual average daily traffic is determined by the rate at which the vehicles arrive on the bridge. It may be noted that the crack growth in flange plates of the girder, which is the fatigue prone region is seen under direct tensile stress produced due to bending. Different fatigue models described in Chapter 2, shows that MBLDR is close to fatigue cycles observed in fatigue testing under direct axial stress in the laboratory. The fatigue detail constant K and material constant m for two and three span continuous bridge have been taken as 61×10^8 ksi (4.205×10^{10} MPa) and -3 respectively (Fisher, 1977; AASHTO, 2017), which correspond to yield stress f_y = 250MPa.

5.5.1 Parametric Study

The bridge dynamic response is obtained using the semi analytical method which takes into consideration the randomness due to vehicle arrival time and road surface roughness. The bridge vehicle parameters are significant as these cause variations in the dynamic response of the bridge, thereby affecting the fatigue life and DAF. Thus, the study of various parameters on fatigue life and DAF of two and three span continuous bridge is necessary. The fatigue life and dynamic amplification factor (DAF) are obtained considering the following parameters:

(i). Vehicle forward velocity
(ii). Road surface roughness
(iii). Arrival rate of the vehicle
(iv). Axle weight of the vehicle
(v). Amplitude of mean profile

The numerical results for stresses of two and three span continuous girders were obtained for the change of different parameters as mentioned above. It is found that in case of two span continuous bridge, the maximum bending stresses was found to occur at the centre of the span, whereas in case of three span continuous bridge, the maximum bending stresses for the variation of different influencing parameters are observed at the centre of the second span.

5.5.1.1 Effect of vehicle forward velocity

The proposed method studied in this section highlights the influence of uniform velocity and variable velocity of the moving vehicles on DAF and fatigue life of two and three span

continuous bridge. The amplitude of the mean profile is considered as 0.01 m. The entry velocity of the vehicle is varied from 20 km/hr to 60 km/hr with an interval of 10 km/hr. The vehicle arrival rate is considered to be 120 vehicles per minute. The acceleration of the vehicle is varied from 0.5 m/s^2 to 1.5 m/s^2 with an increment of 0.5 m/s^2 in case of variable velocity. The road surface condition is considered as very poor. The mean and standard deviation of flexural stresses at centre of second span of two and three span continuous bridge when the vehicle moves on the bridge with uniform and variable velocity with acceleration 1.5 m/s^2 is shown in Figs. 5.5 to 5.8.

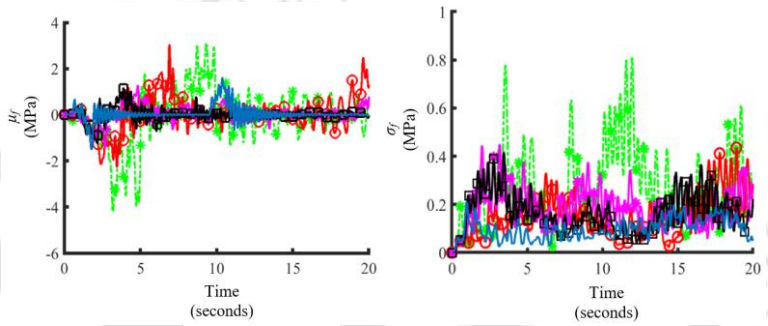

(a) (b)

Fig. 5.5 (a): Mean and (b): standard deviation of flexural stress at centre of second span of two span continuous bridge for different uniform vehicle velocities for very poor road condition ($S_{GG}(\Omega_0)$ = 1024 × 10^{-6} m^2/cycle/m)

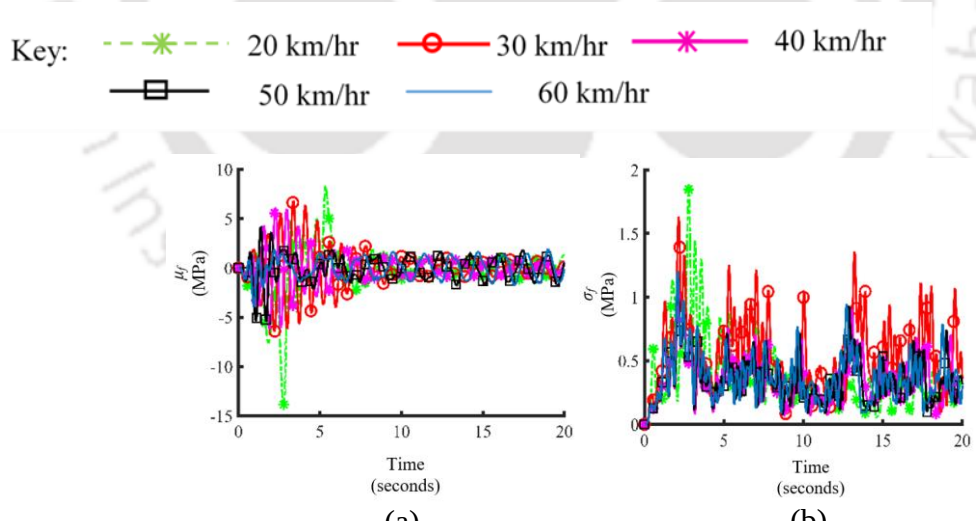

(a) (b)

Fig. 5.6 (a): Mean and (b): standard deviation of flexural stress at centre of second span of two span continuous bridge for different entry vehicle velocities for acceleration 1.5 m/s^2 for very poor road condition ($S_{GG}(\Omega_0)$ = 1024 × 10^{-6} m^2/cycle/m)

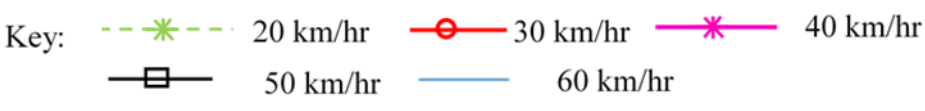

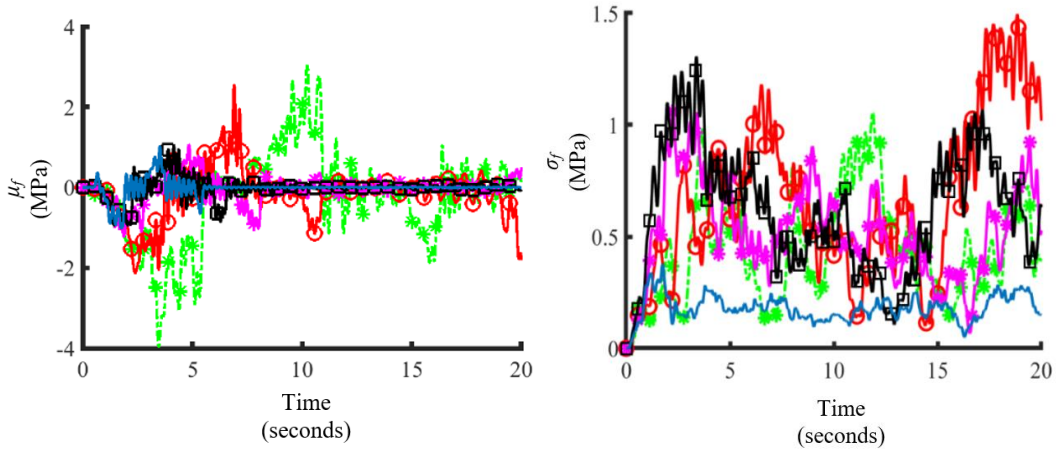

(a) (b)

Fig. 5.7 (a): Mean and (b): standard deviation of flexural stress at centre of second span of three span continuous bridge for different uniform vehicle velocities for very poor road condition ($S_{GG}(\Omega_0)$ = 1024 × 10^{-6} m^2/cycle/m)

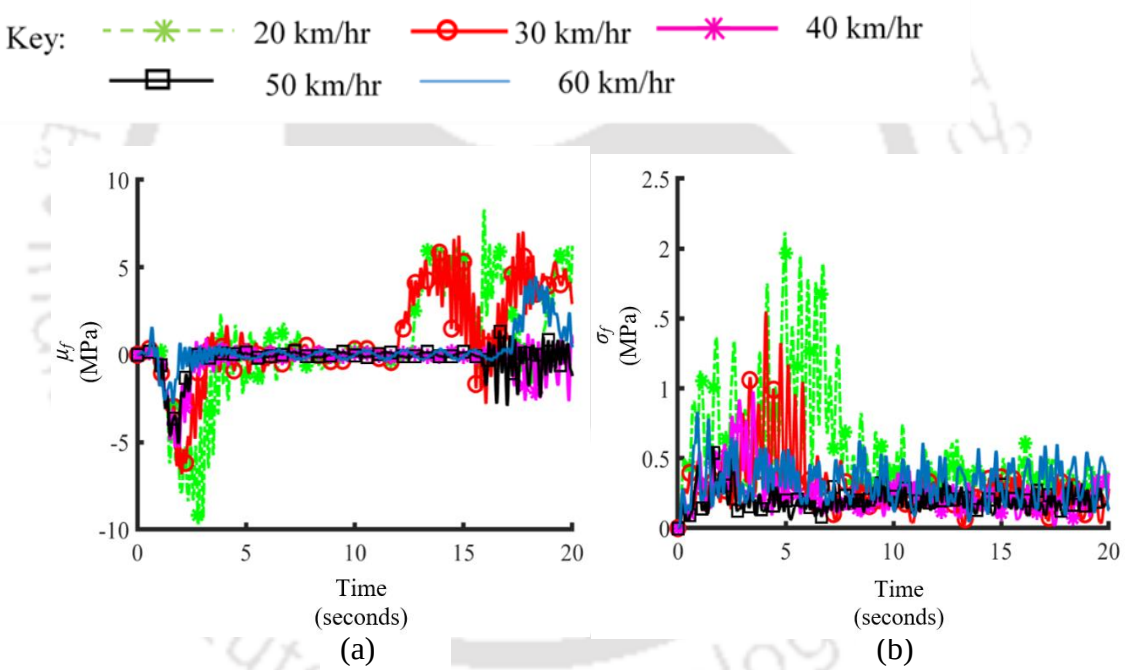

(a) (b)

Fig. 5.8 (a): Mean and (b): standard deviation of flexural stress at centre of second span of three span continuous bridge for different entry vehicle velocities for acceleration 1.5 m/s^2 for very poor road condition ($S_{GG}(\Omega_0)$ = 1024 × 10^{-6} m^2/cycle/m)

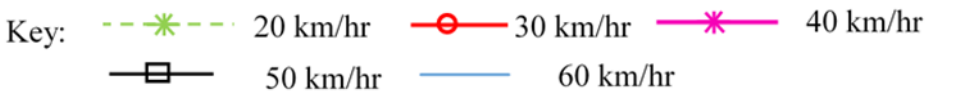

The mean and standard deviation of flexural stresses vary with vehicle velocity and the number of spans considered, which is observed from Figs. 5.5 to 5.8. The vehicles travelling at lower velocities have a longer time span as compared to vehicles travelling with higher velocities.

The effect of each vehicular load is limited to a time span of L/v where L is the span of the bridge and v is the vehicle velocity, even when the same time window of 20 secs is considered for all entry vehicle velocities. The number of vehicular load acting on the span decreases with increasing entry vehicle velocity. Thus, the mean flexural stresses are more for lower vehicle velocity as observed from Figs. 5.5 to 5.8 for both two and three span continuous bridge. The standard deviation of flexural stresses does not follow the same trend as the mean flexural stresses in case of two and three span continuous bridge. It is also observed from Figs. 5.5 to 5.8 that the acceleration of the vehicle influences the mean and standard deviation of flexural stresses. Since the vibration of the vehicle with acceleration is more, the transverse vibration of the bridge also increases as compared to the case when vehicle moves with uniform velocity.

It is also observed from Figs. 5.5 to 5.8 that the mean and standard deviation of flexural stresses are more for two span continuous bridge as compared to that of three span continuous bridge. This is because, three span continuous bridge is structurally redundant as compared to two span continuous bridge. Due to this reason, the dynamic performance is better for bridge with more spans. However, it is also observed that with the increase in the number of spans, the expansion or contraction induced by change of temperature may be larger which has to be taken care in the design (Gao et al., 2015).

Dynamic Amplification Factor (DAF)

The DAF evaluated for two and three span continuous bridge considering uniform and variable vehicle velocities for very poor road condition and arrival rate 120 vehicles per minute is shown in Figs. 5.9 and 5.10.

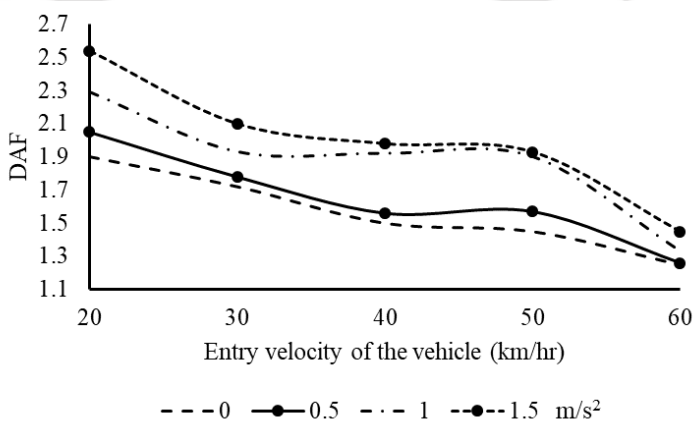

Fig. 5.9 DAF for varying entry velocities of vehicles and acceleration values (m/s^2) for very poor road condition for two span continuous bridge

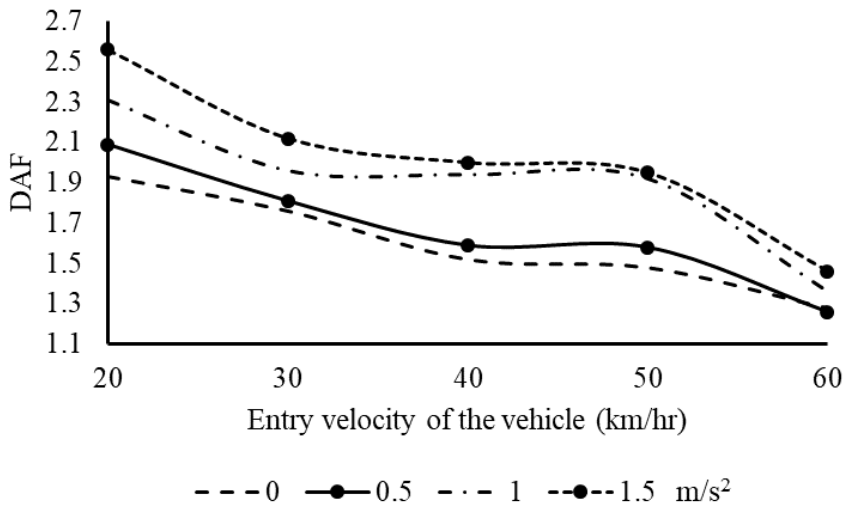

Fig. 5.10 DAF for varying entry velocities of vehicles and acceleration values (m/s^2) for very poor road condition for three span continuous bridge

It is observed from Figs. 5.9 and 5.10 that the DAF is influenced by vehicle velocity and acceleration of the vehicles. The DAF is more for lower entry velocities of the vehicle and vehicles moving with higher acceleration. This is due to the increase in mean and standard deviation of flexural stresses with the decrease in lower entry velocity of the vehicle and increase in the acceleration of the vehicle. The movement of lower vehicle entry velocities causes the excitation frequency to approach the bouncing frequency of the vehicle, thereby increasing the bridge vibration (Law and Zhu, 2005). Also, the vehicles travelling at lower entry velocities take more time to reach the centre of second span of two and three span continuous bridge which also results in increased bridge vibration. The bridge vibration increases with the increase in acceleration of the vehicle, thus increasing the DAF. It is also observed from Figs. 5.9 and 5.10 that the DAF, which is the ratio of dynamic flexural stresses to static flexural stresses, does not change significantly when the number of spans is increased from two to three. This is because both the static and dynamic flexural stresses increase in two span continuous bridge as compared to three span continuous bridge due to reduced structural redundancy in two span continuous bridge.

Fatigue Life

The stress range histograms for constant and varying vehicle velocities for two and three span continuous bridge is depicted in Figs. 5.11 to 5.14. The fatigue life of two and three span continuous bridge at various vehicle entry velocities evaluated using the stress range histograms is shown in Figs. 5.15 and 5.16.

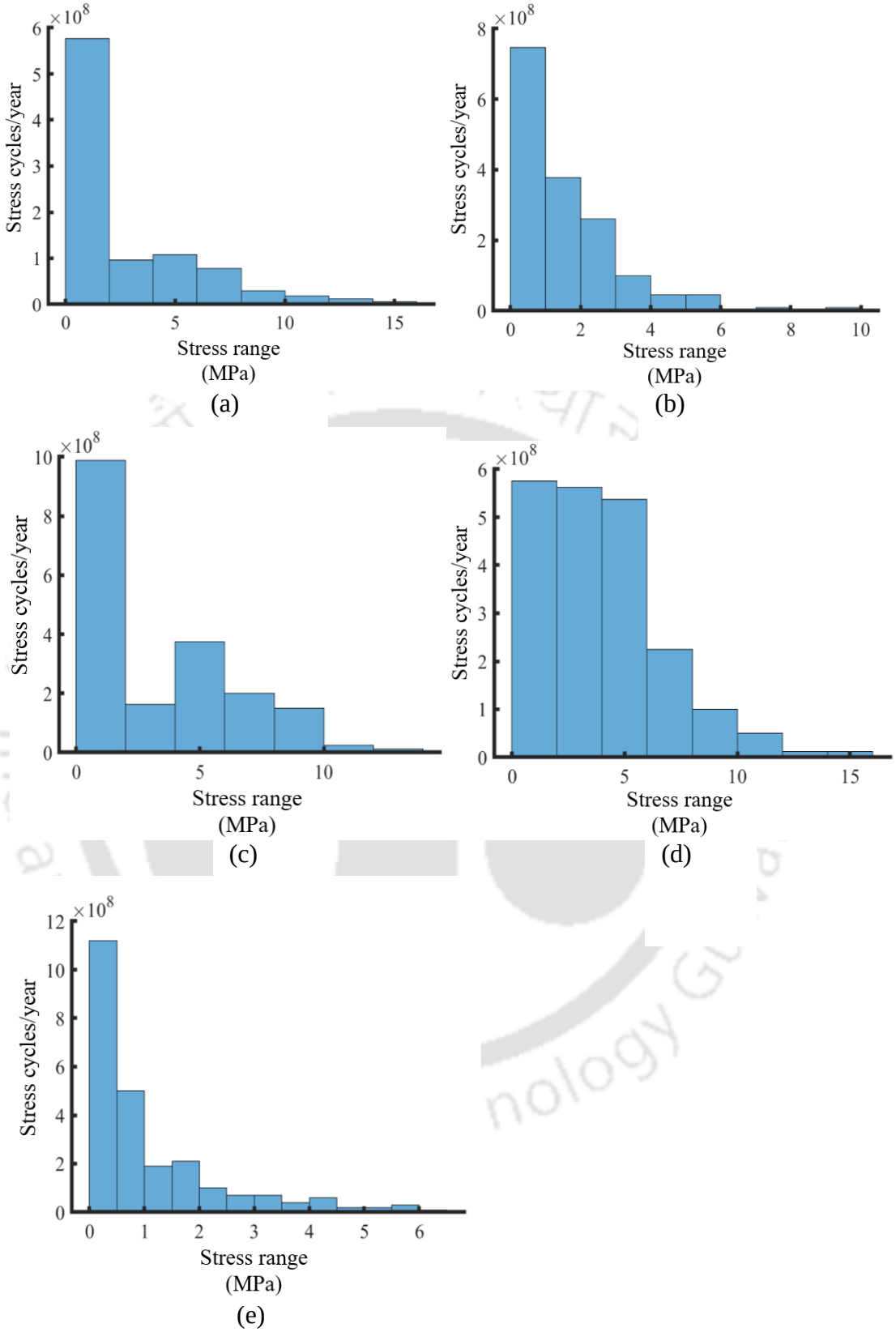

Fig. 5.11 Stress range histogram for two span continuous bridge for uniform vehicle velocity (a): 20 km/hr (b): 30 km/hr (c): 40 km/hr (d): 50 km/hr (e): 60 km/hr for very poor road case

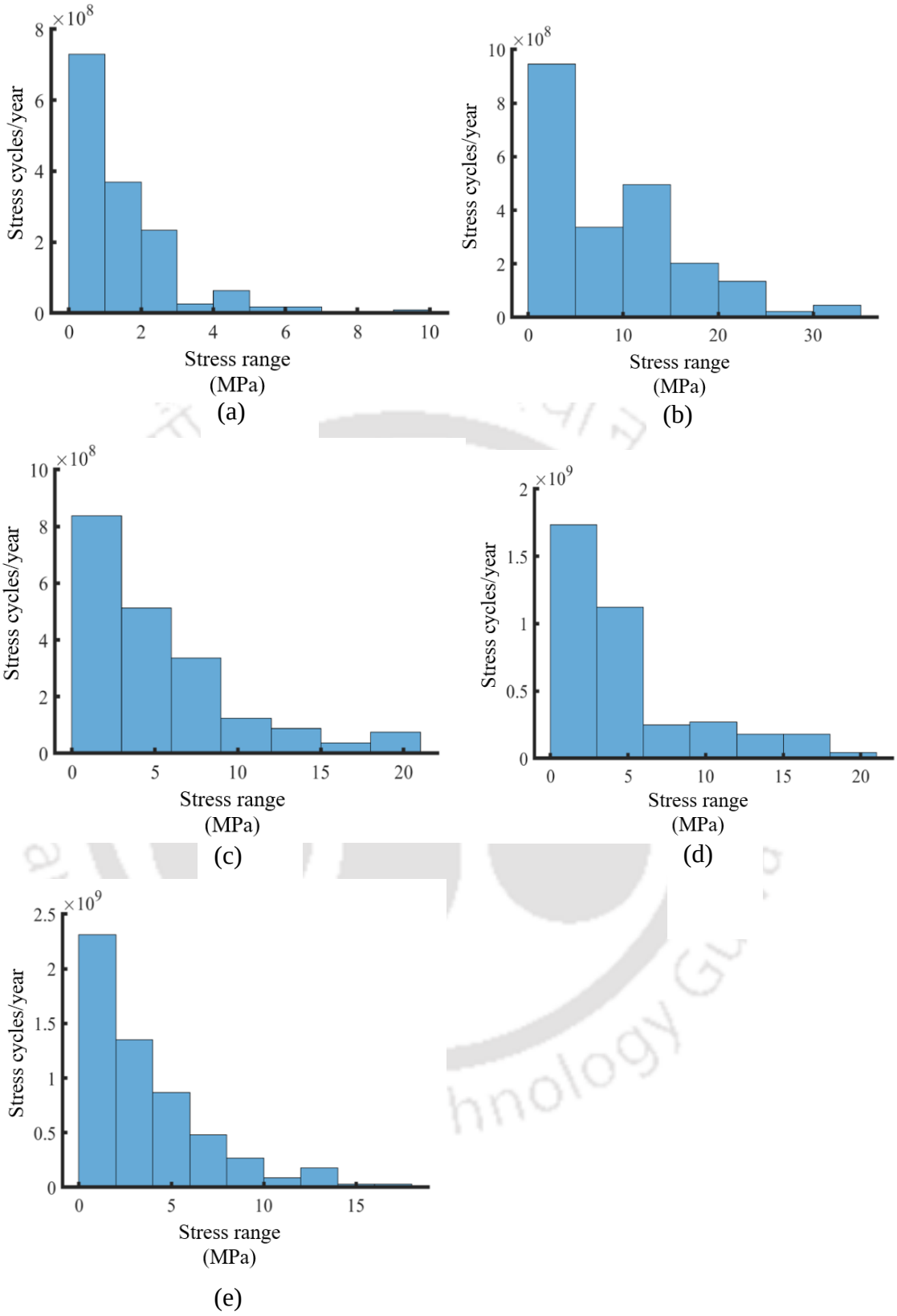

Fig. 5.12 Stress range histogram for two span continuous bridge for vehicle moving with 1.5 m/s^2 acceleration with entry velocity: (a): 20 km/hr (b): 30 km/hr (c): 40 km/hr (d): 50 km/hr (e): 60 km/hr for very poor road case

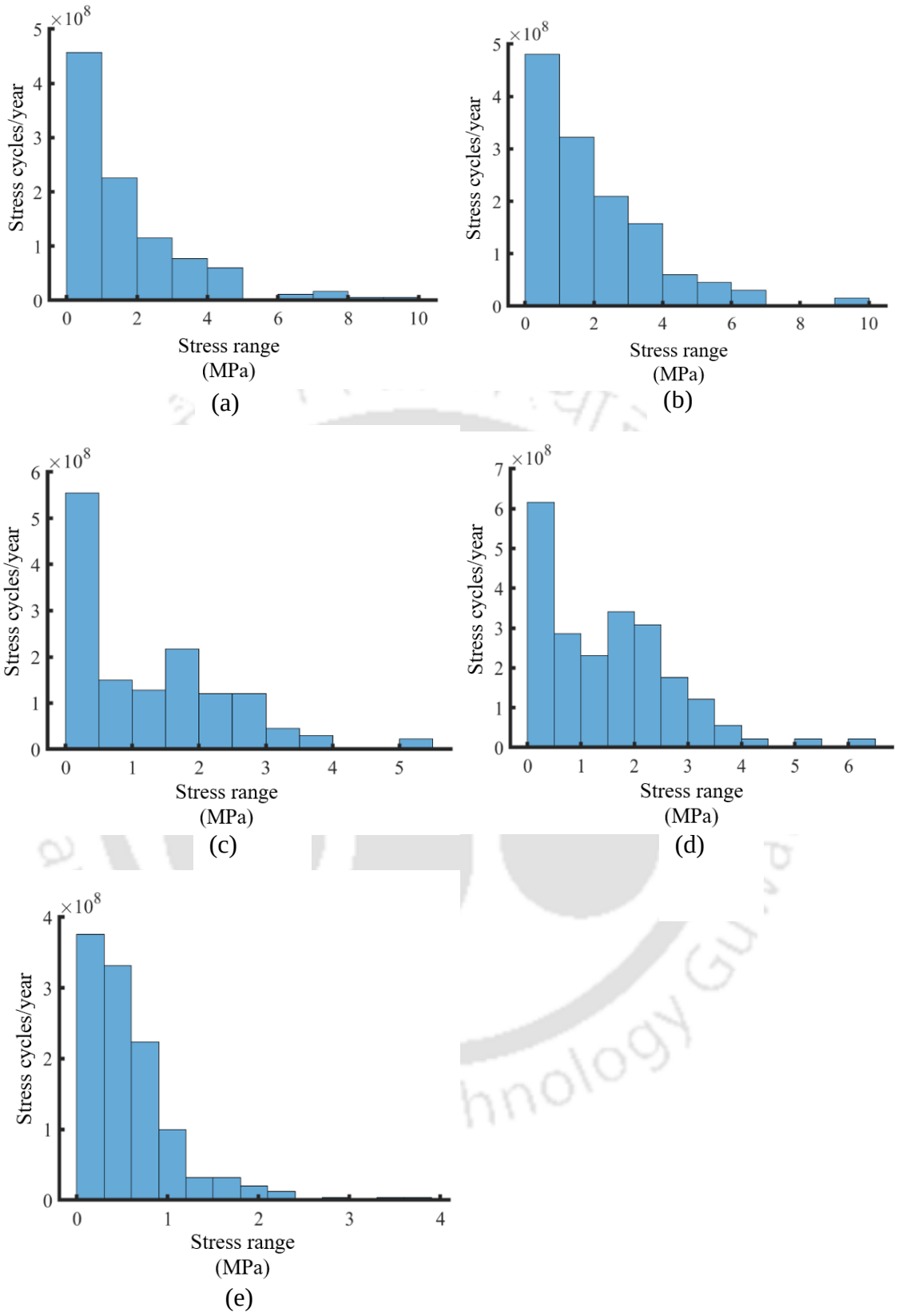

Fig. 5.13 Stress range histogram for three span continuous bridge for vehicle moving with uniform velocity: (a): 20 km/hr (b): 30 km/hr (c): 40 km/hr (d): 50 km/hr (e): 60 km/hr for very poor road case

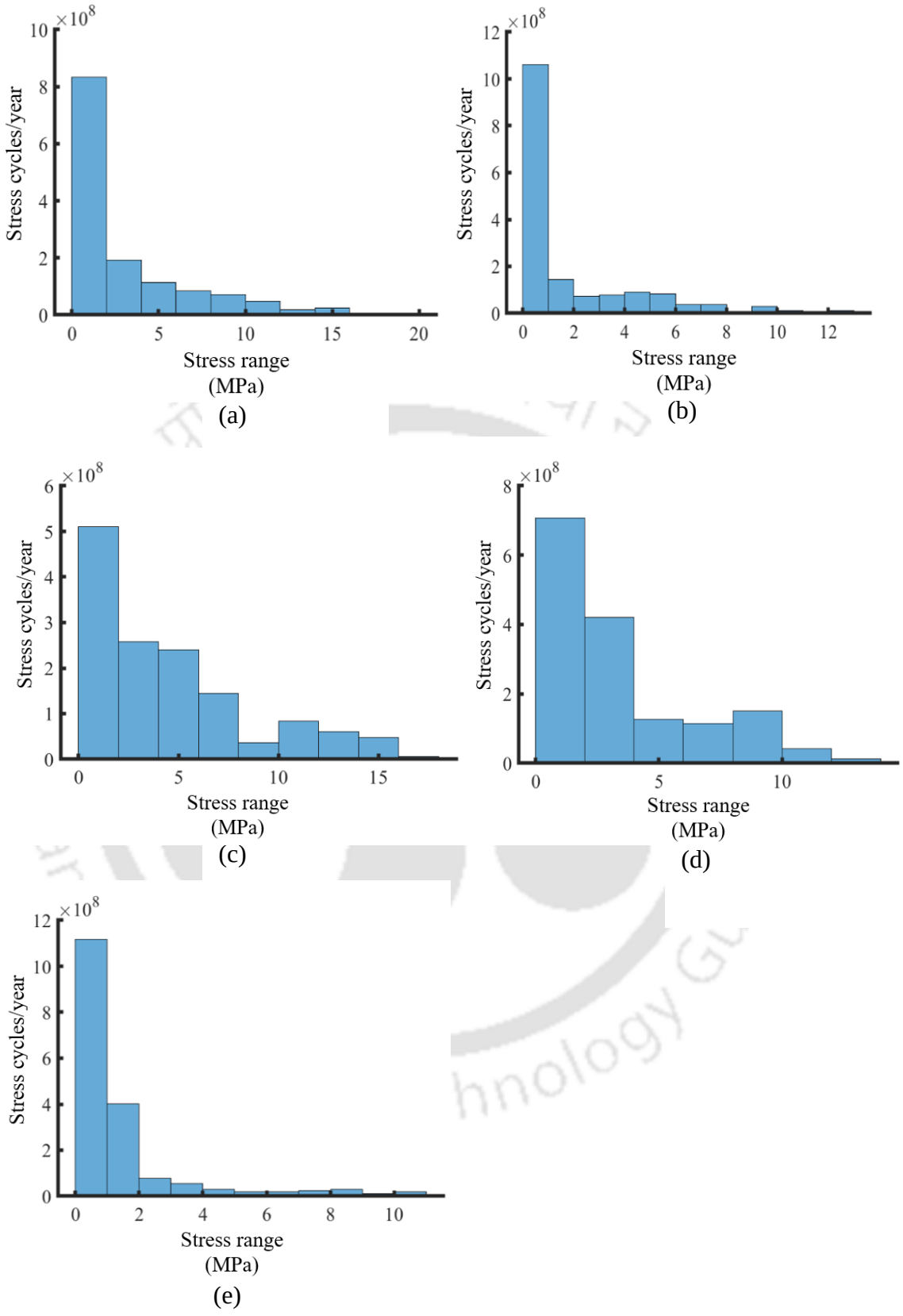

Fig. 5.14 Stress range histogram for three span continuous bridge for vehicle moving with 1.5 m/s^2 acceleration with entry velocity: (a): 20 km/hr (b): 30 km/hr (c): 40 km/hr (d): 50 km/hr (e): 60 km/hr for very poor road case

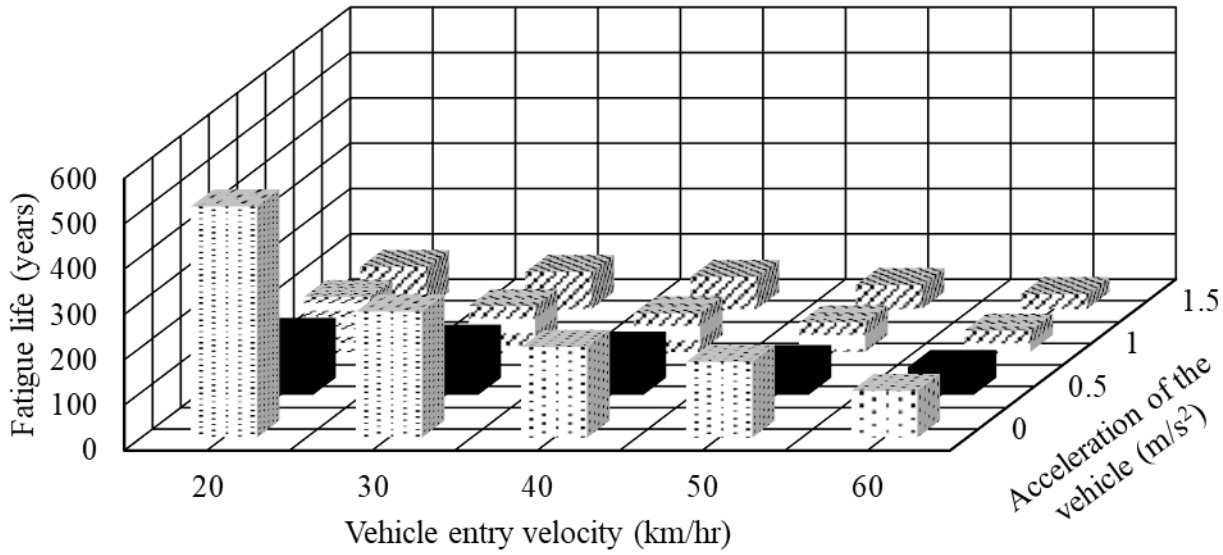

Fig. 5.15 Comparison of fatigue life with different vehicle entry velocities for very poor road for two span continuous bridge

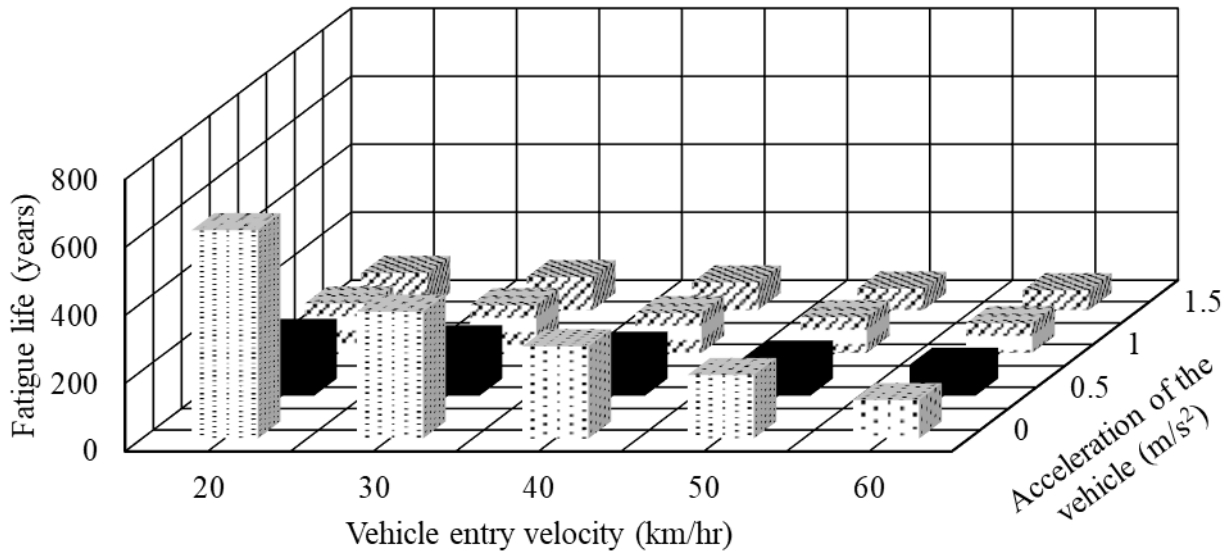

Fig. 5.16 Comparison of fatigue life with different vehicle entry velocities for very poor road for three span continuous bridge

The number of stress cycles in low amplitude stress ranges are observed to increase in vehicles travelling at higher speed and higher acceleration, which is shown in Figs. 5.11 to 5.14. These characterise the dynamic action of moving vehicles. These stress cycles contribute to the accumulation of fatigue damage. Thus, the fatigue life of two and three span continuous bridge reduces as vehicle velocity increases, which is observed in Figs. 5.15 and 5.16. However, the

fatigue life for a two span bridge is less compared to that of three span continuous bridge due to increase in flexural stresses in two span continuous bridge, leading to higher damage accumulation. The two and three span continuous bridge are subjected to higher stress cycles in higher stress range and lower stress range when the acceleration of the vehicle increases. These stress cycles contribute to more fatigue damage and thus reduce the fatigue life.

5.5.1.2 Effect of road surface roughness

The effect of road surface roughness on DAF and fatigue life of two and three span continuous bridge is investigated in this section. The entry vehicle speed is set to 20 km/hr, and the road surface roughness is divided into four categories as, good ($S_{GG}(\Omega_0)$ = 32 × 10^{-6} m^2/cycle/m), medium ($S_{GG}(\Omega_0)$ = 120 × 10^{-6} m^2/cycle/m), poor ($S_{GG}(\Omega_0)$ = 512 × 10^{-6} m^2/cycle/m) and very poor ($S_{GG}(\Omega_0)$ = 1024 × 10^{-6} m^2/cycle/m). The arrival rate of the vehicles is considered as 120 vehicles per minute. The amplitude of the mean profile is considered as 0.01 m. The mean and standard deviation of flexural stresses at centre of second span of two and three span continuous bridge for varying road surface roughness while considering uniform and variable vehicle velocity is shown in Figs. 5.17 to 5.20. The vehicle acceleration is considered as 1.5 m/s^2 in case of variable velocity.

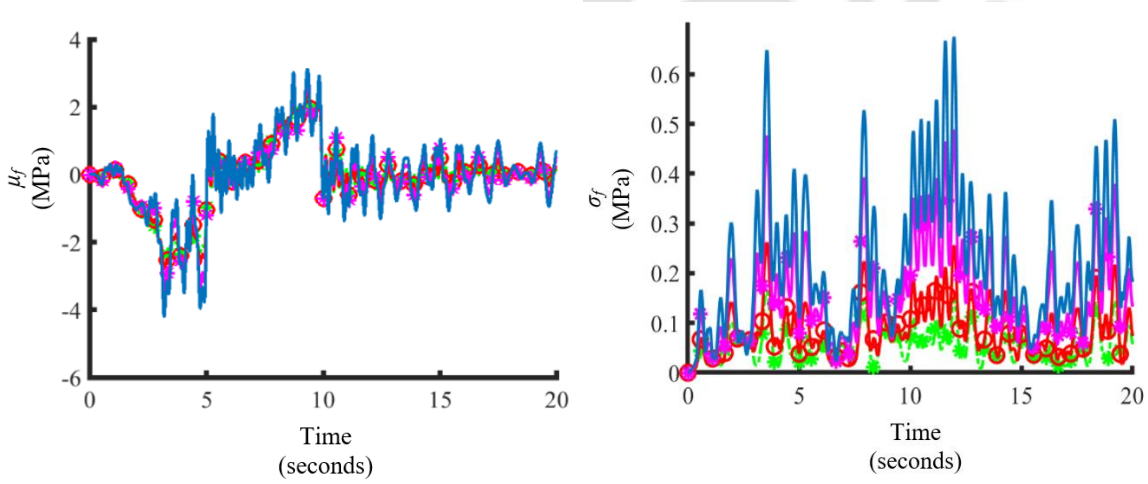

(a) (b)

Fig. 5.17 (a): Mean and (b): standard deviation of flexural stress at centre of second span of two span continuous bridge for uniform vehicle velocity 20 km/hr and arrival rate 120 vehicles per minute

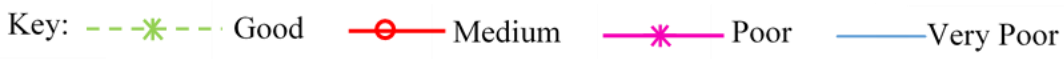

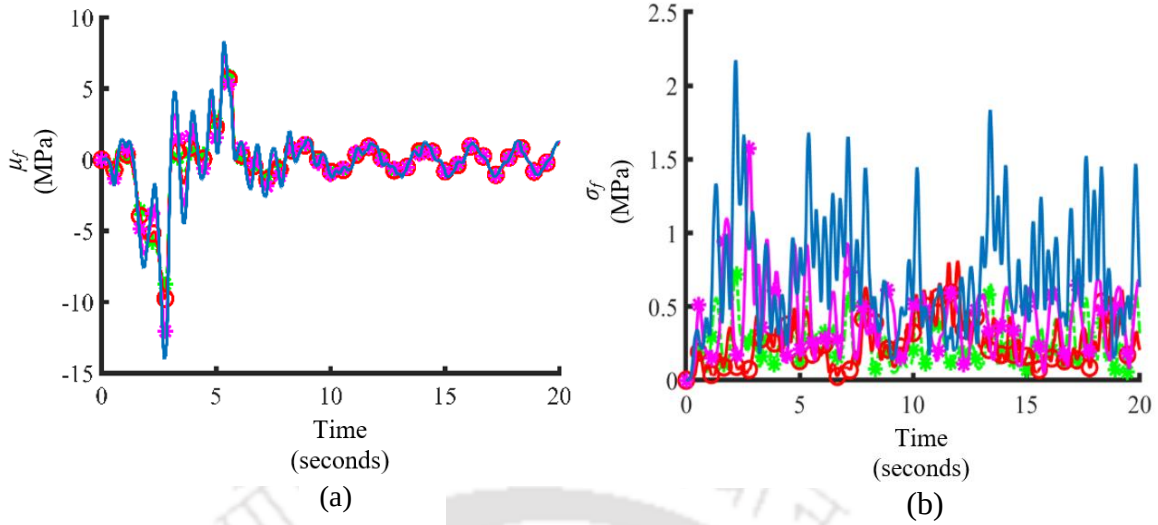

Fig. 5.18 (a): Mean and (b): standard deviation of flexural stress at centre of second span of two span continuous bridge for vehicle entry velocity 20 km/hr and arrival rate 120 vehicles per minute for vehicles moving with 1.5 m/s^2 acceleration

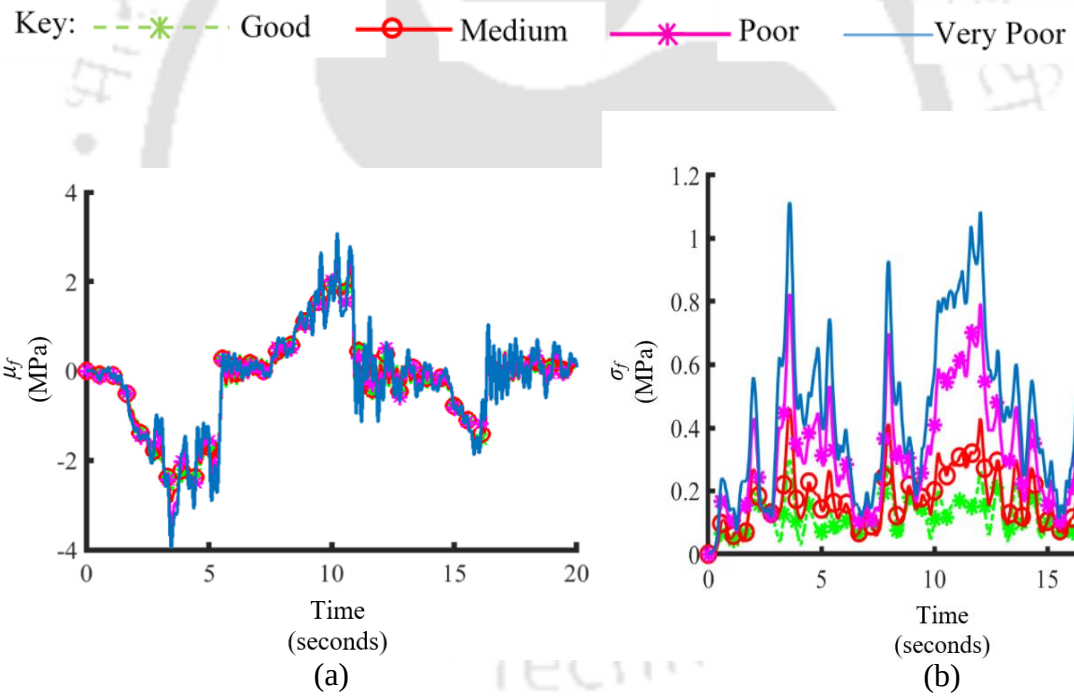

Fig. 5.19 (a): Mean and (b): standard deviation of flexural stress at centre of second span of three span continuous bridge for uniform vehicle velocity 20 km/hr and arrival rate 120 vehicles per minute

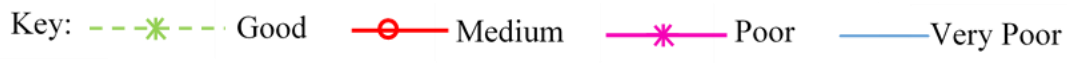

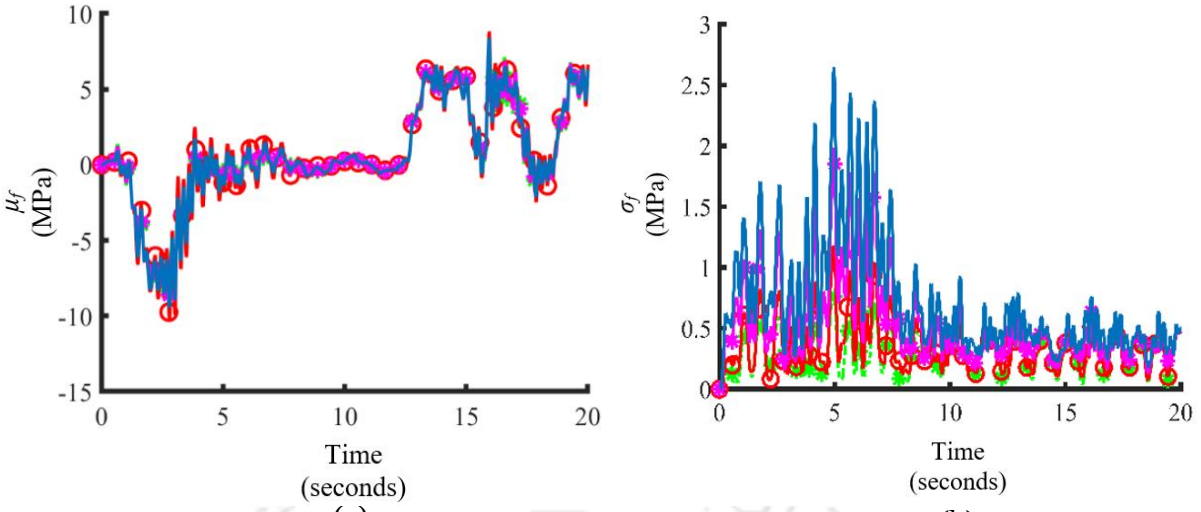

Fig. 5.20 (a): Mean and (b): standard deviation of flexural stress at centre of second span of three span continuous bridge for entry velocity 20 km/hr and arrival rate 120 vehicles per minute for vehicles moving with 1.5 m/s^2 acceleration

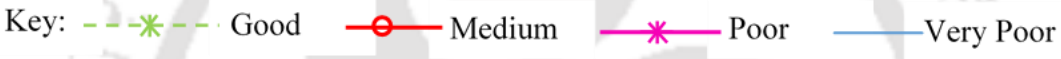

The dynamic response of two and three span continuous bridge results not only from the static weight of moving vehicle but also from the vehicle vibration due to road surface roughness. From Figs. 5.17 to 5.20, it is observed that the deteriorated road may significantly increase the bridge vibration traversed by moving vehicular loads. This causes higher mean and standard deviation of flexural stress at the centre of the second span in two and three span continuous bridge. A similar trend was observed in Law and Zhu (2005). The mean and standard deviation of flexural stresses are more for a two span continuous bridge as compared to three span continuous bridge. Also a larger vehicle vibration induced by deteriorated road will make the passengers uncomfortable to ride.

Dynamic Amplification Factor (DAF)

The comparison of DAF for two and three span continuous bridge for vehicles with an entry velocity of 20 km/hr and an arrival rate of 120 vehicles per minute on different road surface irregularities is depicted in Figs. 5.21 and 5.22.

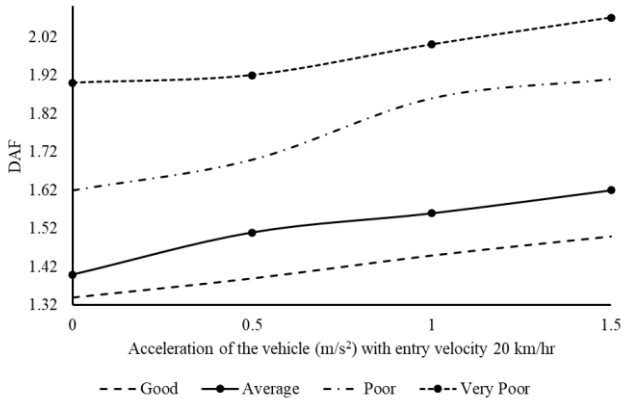

Fig. 5.21 DAF for two span continuous bridge for varying road roughness and acceleration values for vehicles with entry velocity 20 km/hr and arrival rate 120 vehicle per minute

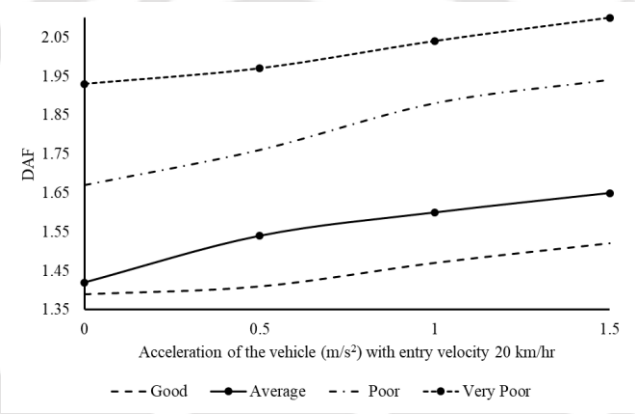

Fig. 5.22 DAF for three span continuous bridge for varying road roughness and acceleration values for vehicles with entry velocity 20 km/hr and arrival rate 120 vehicle per minute

It is observed that the DAF increases by 38 % when the road surface condition is changed from good to very poor in case of two and three span continuous bridge, which is observed from Figs. 5.21 and 5.22. The bridge vibration increases causing higher dynamic flexural stresses when the vehicle traverses on a deteriorated road. The DAF for a two span continuous bridge is found to be approximately same as that of the three span continuous bridge.

Fatigue Life

The stress range histogram and fatigue life for varying road roughness for vehicles with entry velocity 20 km/hr and arrival rate 120 vehicles per minute is shown in Figs. 5.23 to 5.28. The stress range histogram and fatigue life is obtained for uniform and variable vehicle velocity.

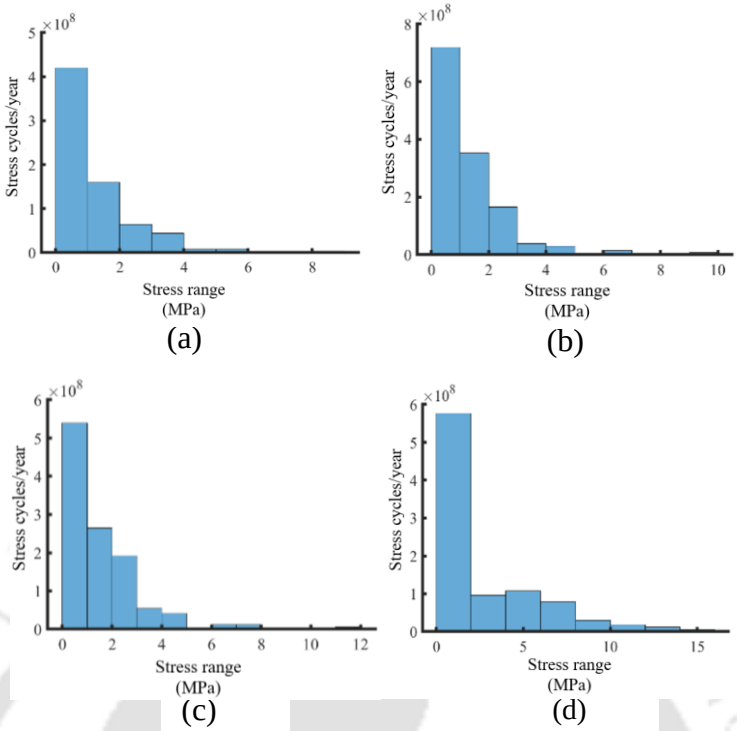

Fig. 5.23 Stress range histogram for two span continuous bridge: (a): good road (b): average road (c): poor road (d): very poor road for uniform vehicle velocity 20 km/hr and arrival rate 120 vehicles per minute

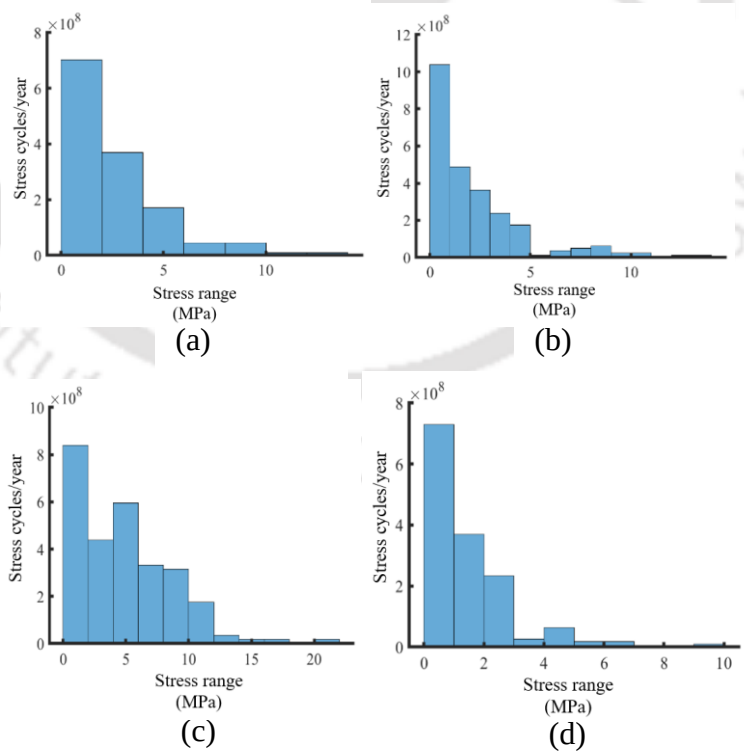

Fig. 5.24 Stress range histogram for two span continuous bridge: (a): good road (b): average road (c): poor road (d): very poor road for vehicle entry velocity 20 km/hr and arrival rate 120 vehicles per minute for vehicle acceleration 1.5 m/s^2

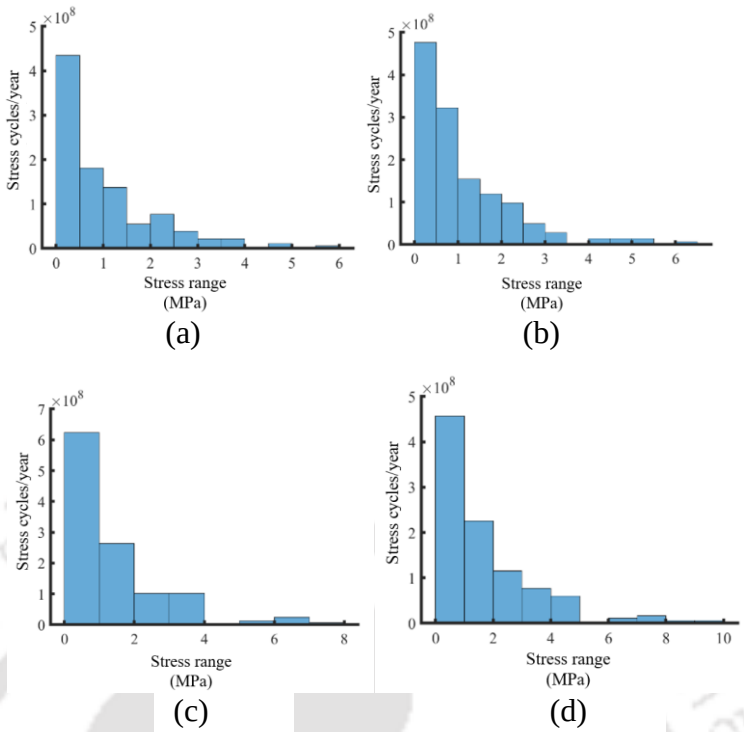

Fig. 5.25 Stress range histogram for three span continuous bridge: (a): good road (b): average road (c): poor road (d): very poor road for uniform vehicle velocity 20 km/hr and arrival rate 120 vehicles per minute

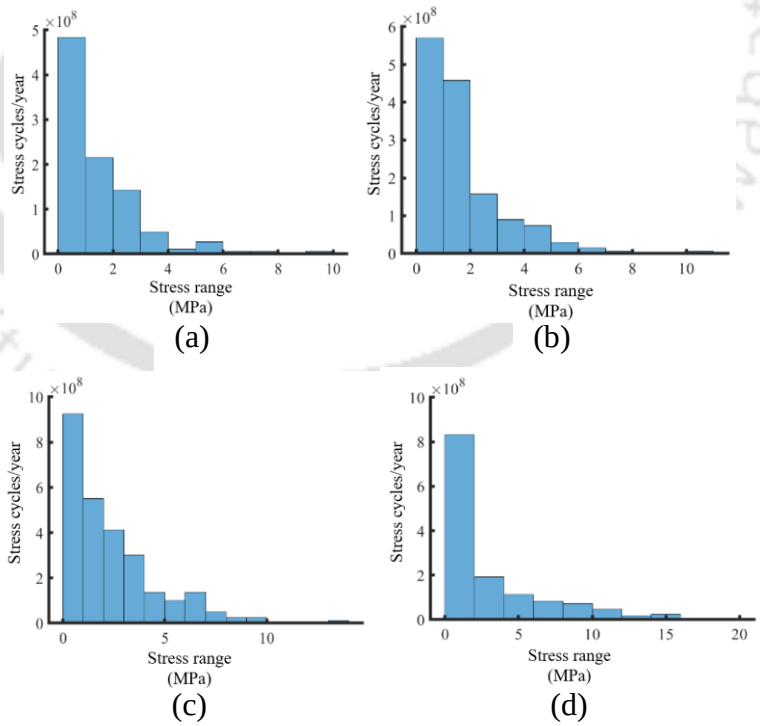

Fig. 5.26 Stress range histogram for three span continuous bridge: (a): good road (b): average road (c): poor road (d): very poor road for vehicle entry velocity 20 km/hr and arrival rate 120 vehicles per minute for vehicle acceleration 1.5 m/s^2

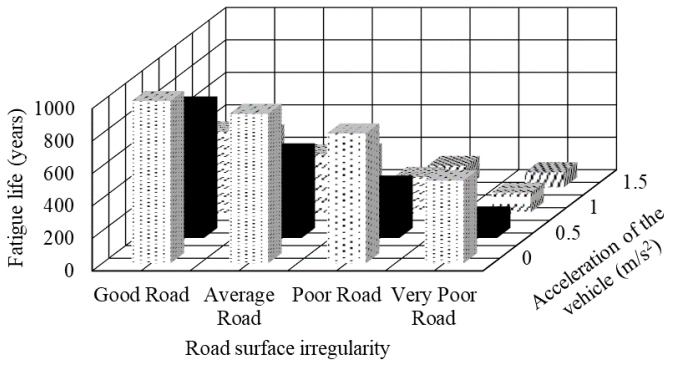

Fig. 5.27 Comparison of fatigue life with different road surface irregularities for two span continuous bridge for vehicle entry velocity 20 km/hr

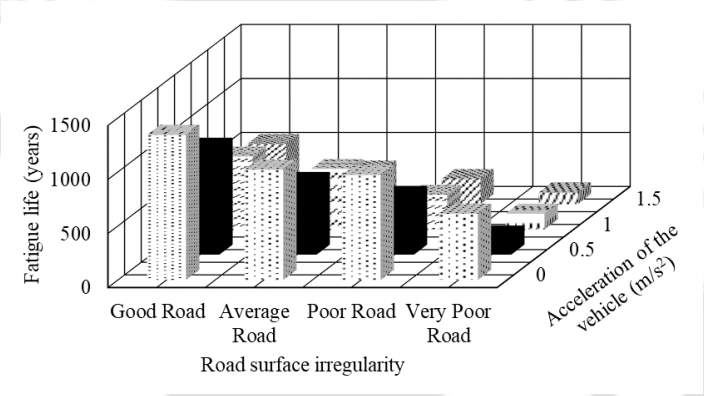

Fig. 5.28 Comparison of fatigue life with different road surface irregularities for three span continuous bridge for vehicle entry velocity 20 km/hr

It is observed from Figs. 5.23 to 5.26 that the number of stress cycles in the lower stress range and higher stress range increases as the road surface roughness increases from good to very poor for two and three span continuous bridge. The stress ranges are subjected to higher stress cycles for very poor road case leading to more damage accumulation as compared to good, average and poor road condition, which is observed from Figs. 5.23 to 5.26. Thus, the fatigue life of two and three span continuous bridge decreases with increasing road surface irregularity as shown in Figs. 5.27 and 5.28. The fatigue life is less for two span continuous bridge as compared to that of three span continuous bridge as the dynamic response of the two span continuous bridge is more, leading to higher fatigue damage accumulation.

5.5.1.3 Effect of Arrival Rate of Vehicles

The effect of arrival rate of the vehicles on fatigue life and DAF for two and three span continuous bridge in investigated in this section. The vehicle arrival rate is varied from 60 vehicles per minute to 180 vehicles per minute with an interval of 30 vehicles per minute. The

vehicle is traversing on the bridge with 20 km/hr uniform velocity. The road roughness considered is very poor. The amplitude of the mean profile is considered as 0.01 m. The mean and standard deviation of the flexural stresses obtained at centre of second span of two and three span continuous bridge for different arrival rate is shown in Figs. 5.29 and 5.30.

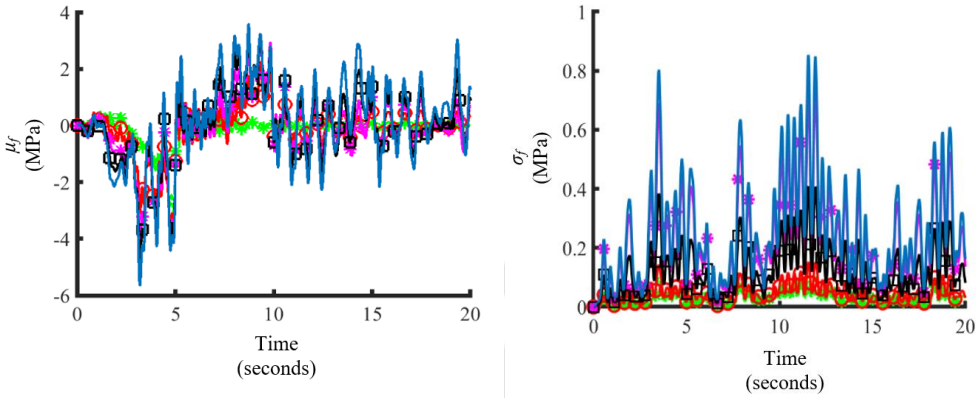

(a) (b)

Fig. 5.29 (a): Mean and (b): standard deviation of flexural stress at centre of second span of two span continuous bridge for different arrival rate for uniform vehicle velocity 20 km/hr ($S_{GG}(\Omega_0)$ = 1024 × 10^{-6} m^2/cycle/m)

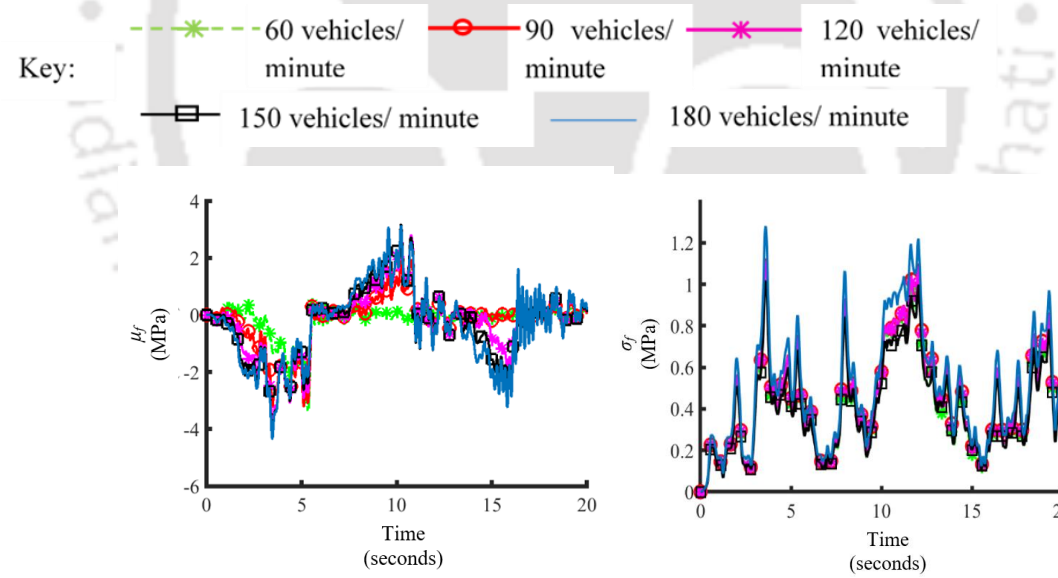

(a) (b)

Fig. 5.30 (a): Mean and (b): standard deviation of flexural stress at centre of second span of three span continuous bridge for different arrival rate for uniform vehicle velocity 20 km/hr ($S_{GG}(\Omega_0)$ = 1024 × 10^{-6} m^2/cycle/m)

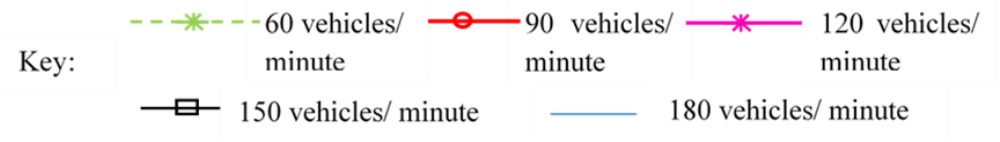

The vehicular load on the bridge is one of the important live loads acting on the bridge which produces a dynamic effect on the bridge because of vibration caused by vehicular movement. The number of vehicles acting on the bridge varies throughout the day. Peak traffic in some durations of the day indicate more number of vehicles are acting on the bridge. The variation in the number of vehicles is taken care by the parameter arrival rate. Higher arrival rate indicates higher traffic volume thus, increasing the mean and standard deviation of flexural stresses at centre of second span of two and three span continuous bridge, which is observed from Figs. 5.29 and 5.30. It is also observed from Figs. 5.29 and 5.30 that the mean and standard deviation of flexural stresses at the centre of the second span of two span continuous bridge is more than that of three span continuous bridge.

Dynamic Amplification Factor (DAF)

The DAF for two and three span continuous bridge for various arrival rate and acceleration of the vehicle for entry velocity 20 km/hr is shown in Figs. 5.31 to 5.32. The road case considered is very poor.

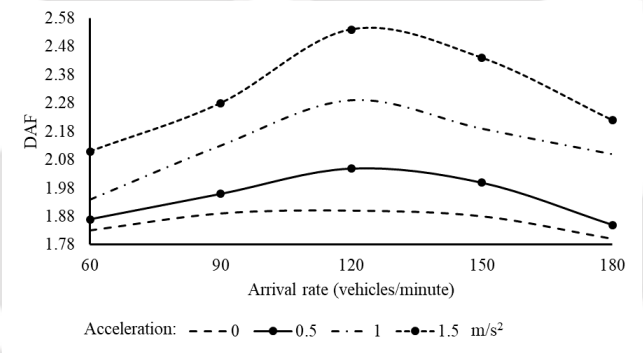

Fig. 5.31 DAF for two span continuous bridge for varying arrival rate and acceleration of the vehicle for entry velocity 20 km/hr for very poor road

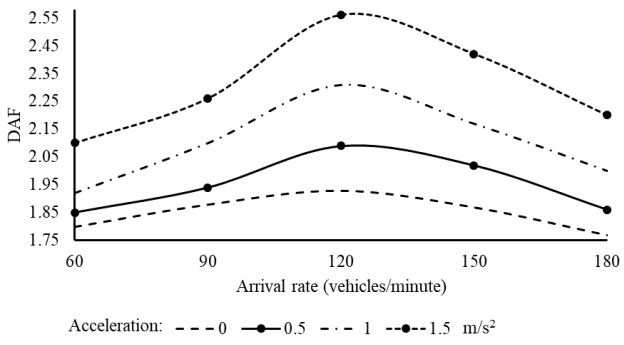

Fig. 5.32 DAF for three span continuous bridge for varying arrival rate and acceleration of the vehicle for entry velocity 20 km/hr for very poor road

It is observed that the static flexural stresses and dynamic flexural stresses increases with the increase in arrival rate of the vehicles. The increase in static stresses caused by vehicular movement is the reason for DAF to reduce, as the arrival rate increases further from 120 vehicles per second. Thus, it is observed from Figs. 5.31 and 5.32 that the DAF for two and three span continuous bridge increases upto arrival rate 120 vehicles per second and decreases further.

Fatigue life

The stress range histogram for two and three span continuous bridge for varying arrival rate for 20 km/hr uniform vehicle velocity and very poor road case is shown in Figs. 5.33 and 5.34. The comparison of fatigue life for two and three span continuous bridge with arrival rate and acceleration of the vehicle for entry velocity 20 km/hr is shown in Figs. 5.35 and 5.36.

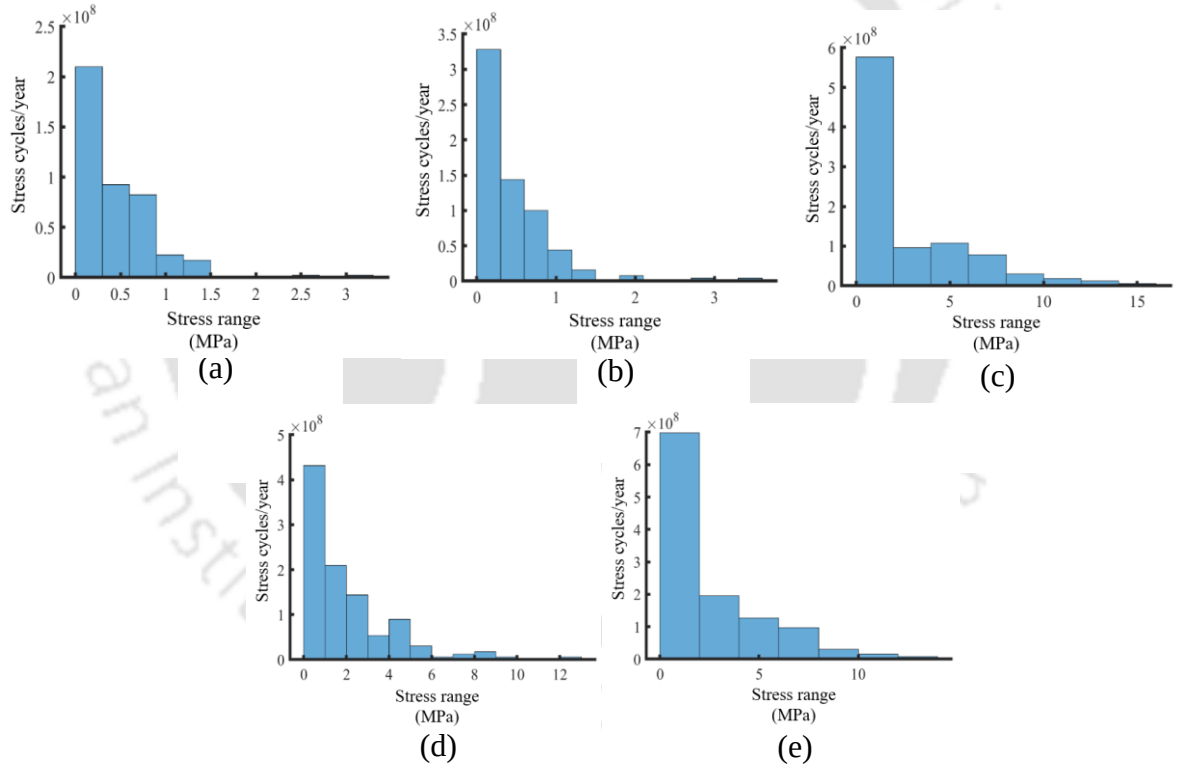

Fig. 5.33 Stress range histogram for two span continuous bridge: (a): 60 vehicles per minute (b): 90 vehicles per minute (c): 120 vehicles per minute (d): 150 vehicles per minute (e): 180 vehicles per minute for uniform vehicle velocity 20 km/hr

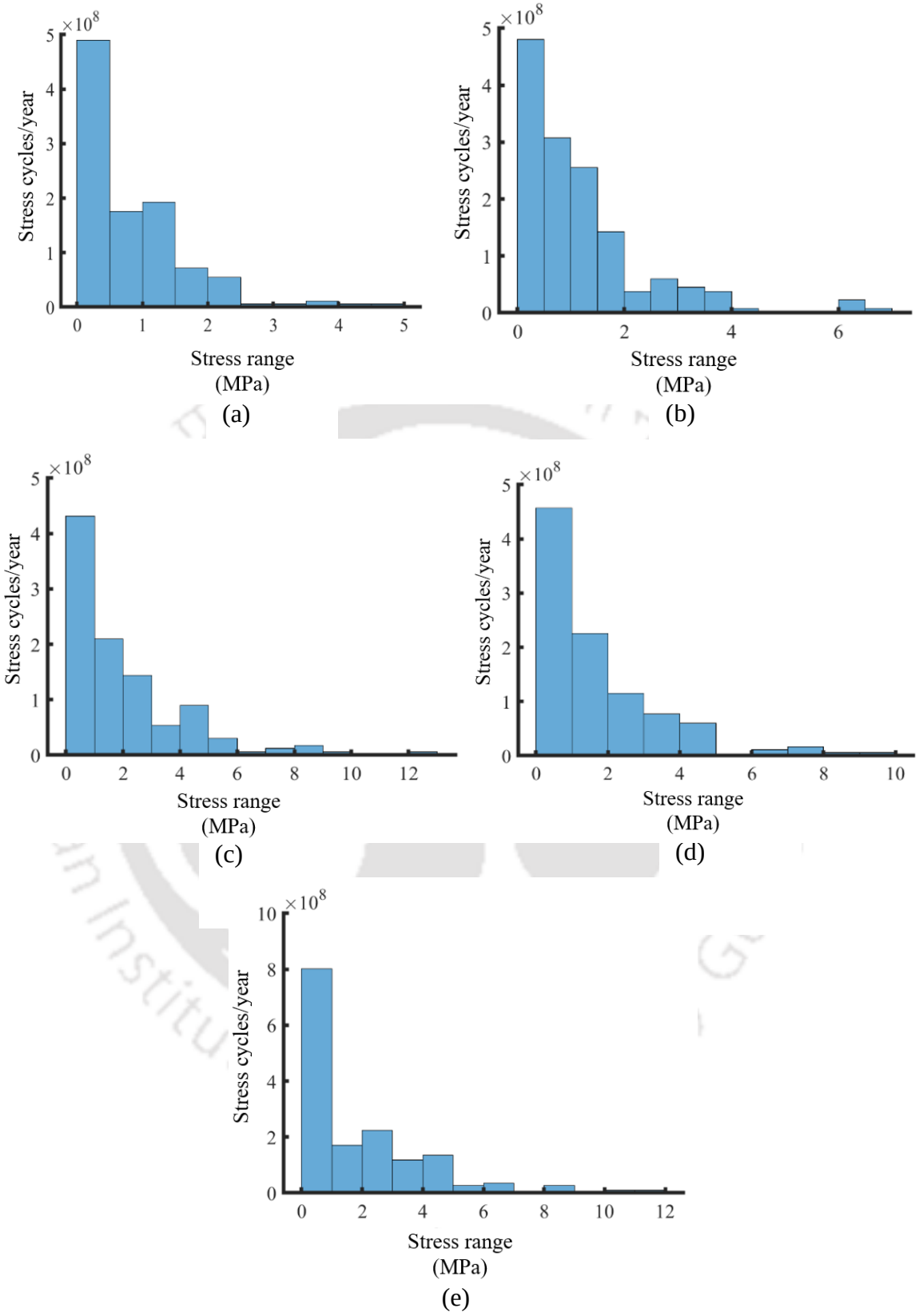

Fig. 5.34 Stress range histogram for three span continuous bridge: (a): 60 vehicles per minute (b): 90 vehicles per minute (c): 120 vehicles per minute (d): 150 vehicles per minute (e): 180 vehicles per minute for uniform vehicle velocity 20 km/hr

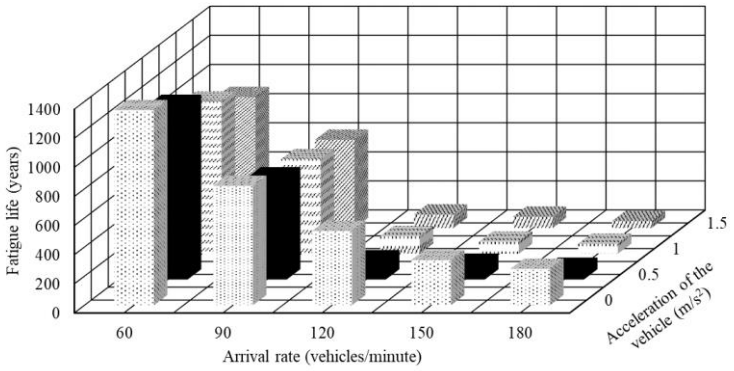

Fig. 5.35 Fatigue life for two span continuous bridge for varying arrival rate and acceleration of the vehicle for entry velocity 20 km/hr for very poor road

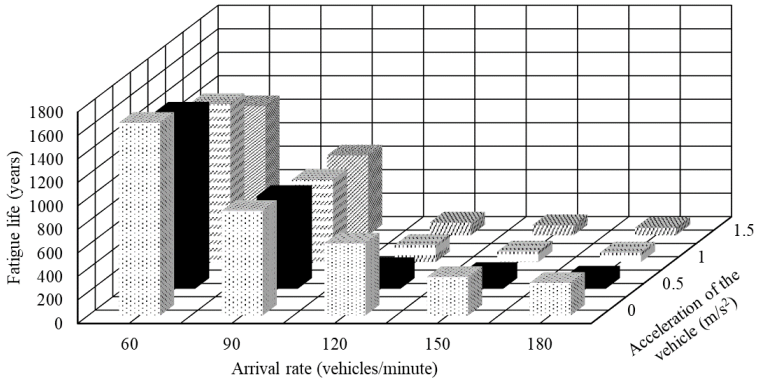

Fig. 5.36 Fatigue life for three span continuous bridge for varying arrival rate and acceleration of the vehicle for entry velocity 20 km/hr for very poor road

The increasing movement of multiple vehicles on the road increases the dynamic flexural stresses on the bridge. The stress ranges and the number of stress cycles increase as the arrival rate increases. Thus, accumulation of fatigue damage is more as compared to the case when a single vehicle is traversing on the bridge. The stress cycles in the lower and higher stress ranges increase in two and three span continuous bridge as the arrival rate increases, which is observed from Figs. 5.33 and 5.34. This causes lower fatigue life with increase in arrival rate in two and three span continuous bridge as observed from Figs. 5.35 and 5.36. However, the fatigue life is less in case of two span continuous bridge as compared to three span continuous bridge.

5.5.1.4 Effect of axle weight of the vehicle

The effect of DAF and fatigue life of two and three span continuous bridge on the axle weight of the vehicle is investigated in this section. The total vehicle weight ranges from 20 tonnes to

100 tonnes with an increment of 20 tonnes. The mean arrival rate is considered as 120 vehicles per minute. The uniform vehicle velocity is 20 km/hr. The road case considered is very poor. The amplitude of the mean profile is considered as 0.01 m. The mean and standard deviation of flexural stresses at centre of the second span of two and three span continuous bridge for varying axle weight of the vehicle is shown in Figs. 5.37 and 5.38.

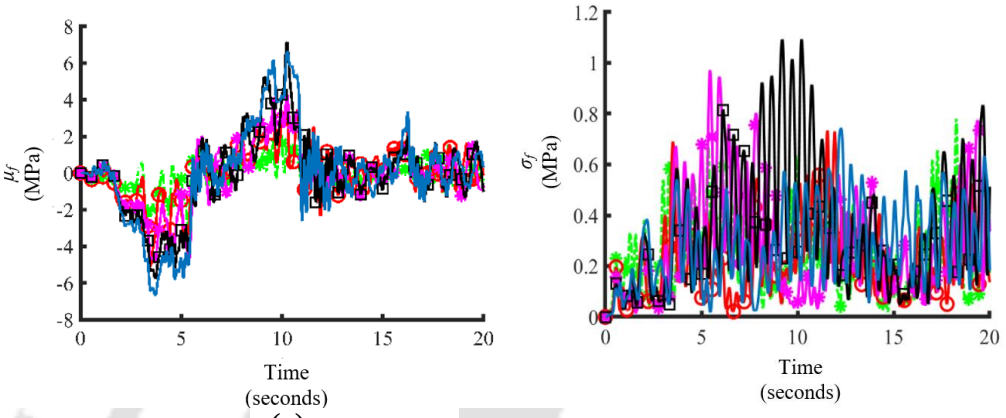

(a) (b)

Fig. 5.37 (a): Mean and (b): standard deviation of flexural stresses at centre of second span of two span continuous bridge for different vehicle weight for uniform vehicle velocity 20 km/hr and very poor road condition

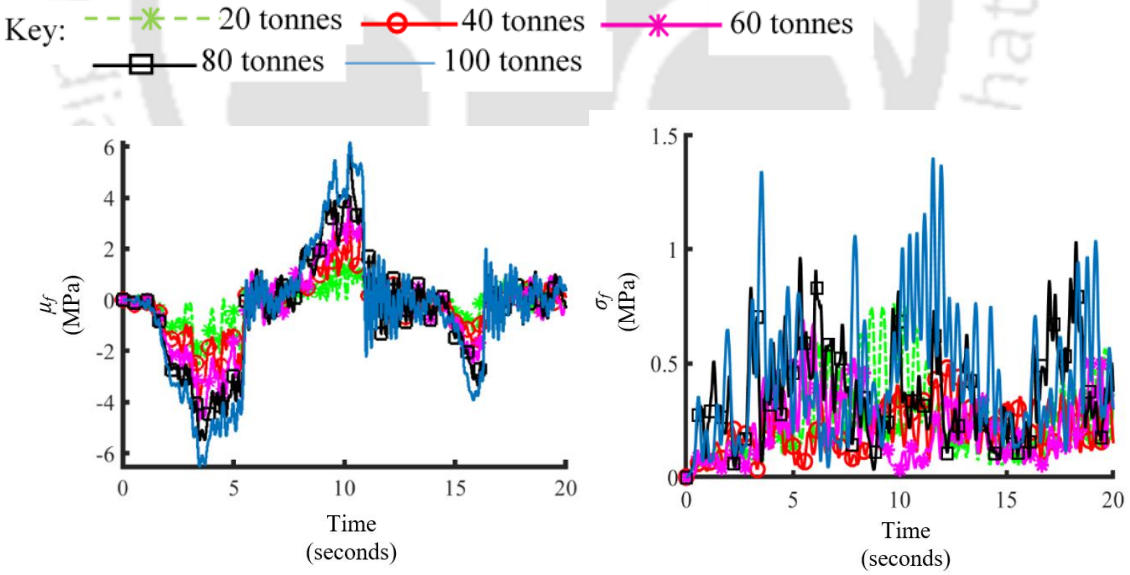

(a) (b)

Fig. 5.38 (a): Mean and (b): standard deviation of flexural stresses at centre of second span of three span continuous bridge for different vehicle weight for uniform vehicle velocity 20 km/hr and very poor road condition

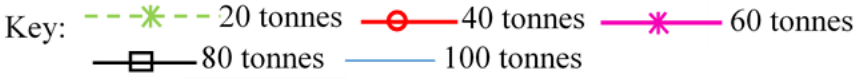

The vehicle weight is found to have a significant effect on the mean and standard deviation of flexural stress at centre of second span of two and three span continuous bridge, which is observed from Figs. 5.37 and 5.38. The increase in axle weight of the vehicle from 20 tonnes to 100 tonnes increases the mean flexural stresses at centre of second span of two and three span continuous bridge by approximately 3 times and 2 times as observed from Fig. 5.37 and 5.38. Thus, it can be observed that vehicle overloading induces large dynamic stresses on the bridge.

Dynamic Amplification Factor (DAF)

The variation of DAF for two and three span continuous bridge with total vehicle weight and acceleration of the vehicle for vehicle entry velocity 20 km/hr and very poor road condition is shown in Figs. 5.39 and 5.40.

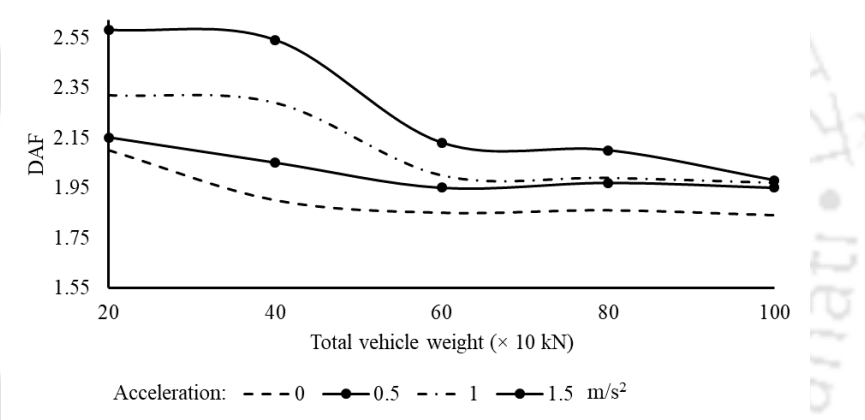

Fig. 5.39 DAF for two span continuous bridge for varying axle weight and acceleration of the vehicle for entry velocity 20 km/hr for very poor road

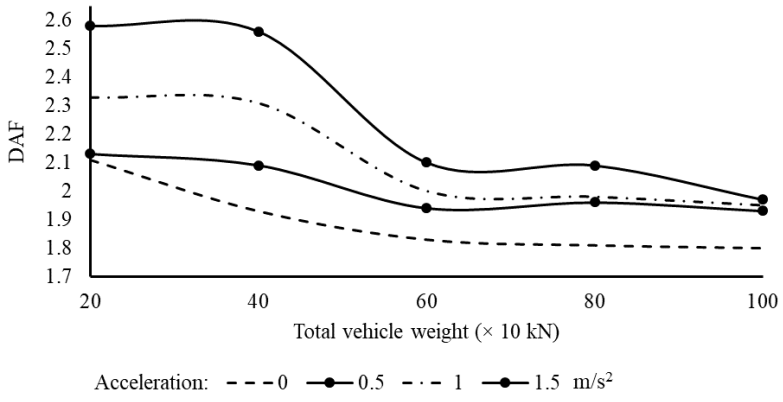

Fig. 5.40 DAF for three span continuous bridge for varying axle weight and acceleration of the vehicle for entry velocity 20 km/hr for very poor road

The DAF reduces when the total vehicle weight increases from 20 to 40 tonnes, as shown in Figs. 5.39 and 5.40, and subsequent increase in total vehicle weight do not result in a substantial change in DAF. As the total vehicle weight increases, the static stresses increase, resulting in lower values of DAF.

Fatigue Life

The stress range histogram for varying axle weight for 20 km/hr uniform vehicle velocity and very poor road case for two and three span continuous bridge is shown in Figs. 5.41 and 5.42. It is to be noted that the stress range histogram for axle weight 40 tonnes, vehicle arrival rate 120 vehicles per minute, uniform vehicle velocity 20 km/hr and very poor road condition for two span continuous bridge is shown in Fig. 5.11 (a) and for three span continuous bridge is shown in Fig. 5.13 (a) in sub section 5.5.1.1. The comparison of fatigue life of two and three span continuous bridge with axle weight and acceleration of the vehicle for entry velocity 20 km/hr is shown in Figs. 5.43 and 5.44.

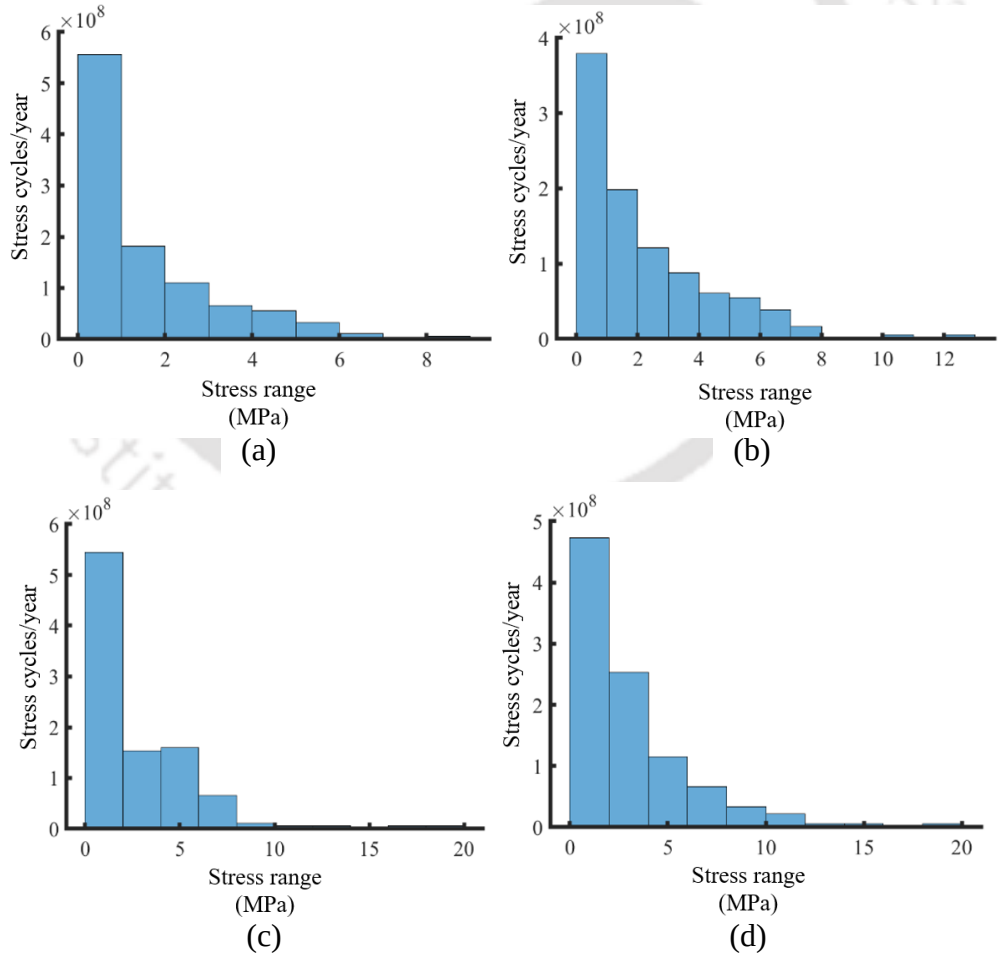

Fig. 5.41 Stress range histogram for two span continuous bridge: (a): 20 tonnes (b): 60 tonnes (c): 80 tonnes (d): 100 tonnes for uniform vehicle velocity 20 km/hr

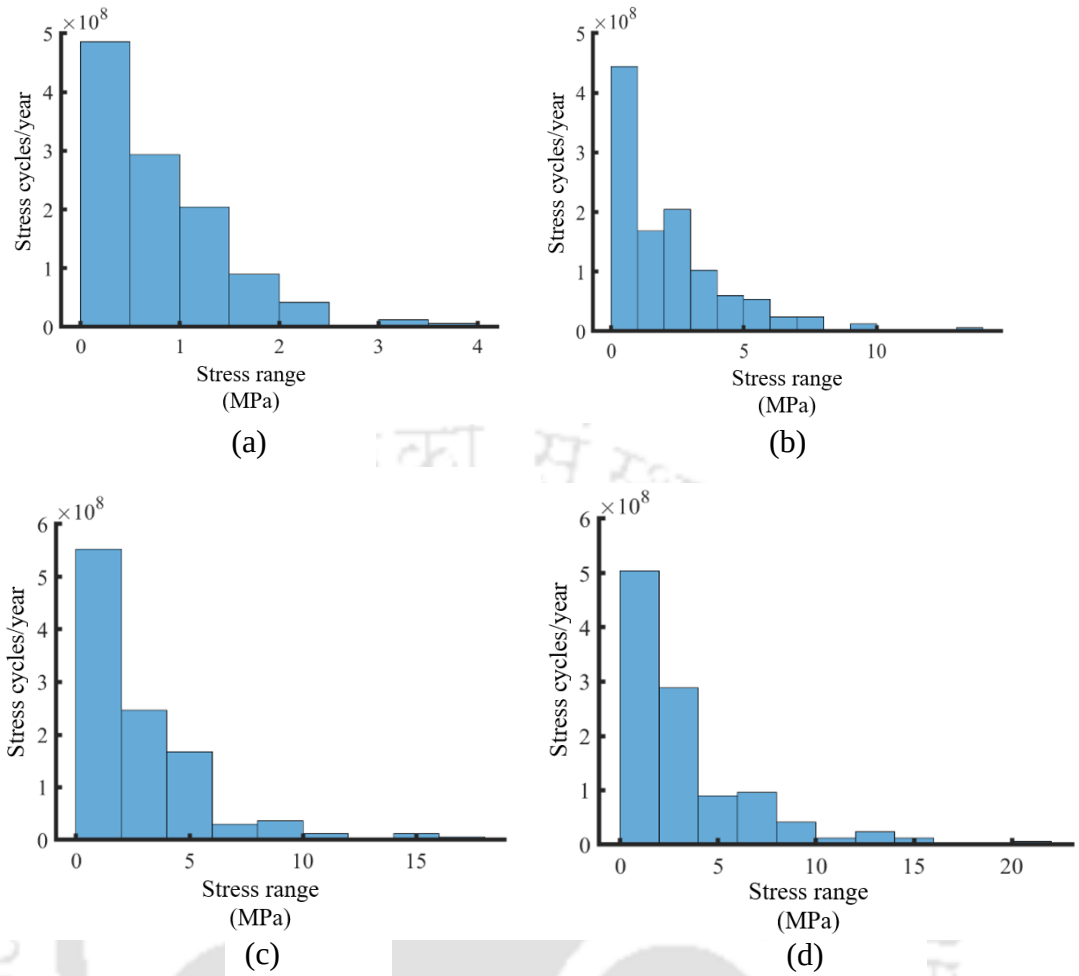

Fig. 5.42 Stress range histogram for three span continuous bridge: (a): 20 tonnes (b): 60 tonnes (c): 80 tonnes (d): 100 tonnes for uniform vehicle velocity 20 km/hr

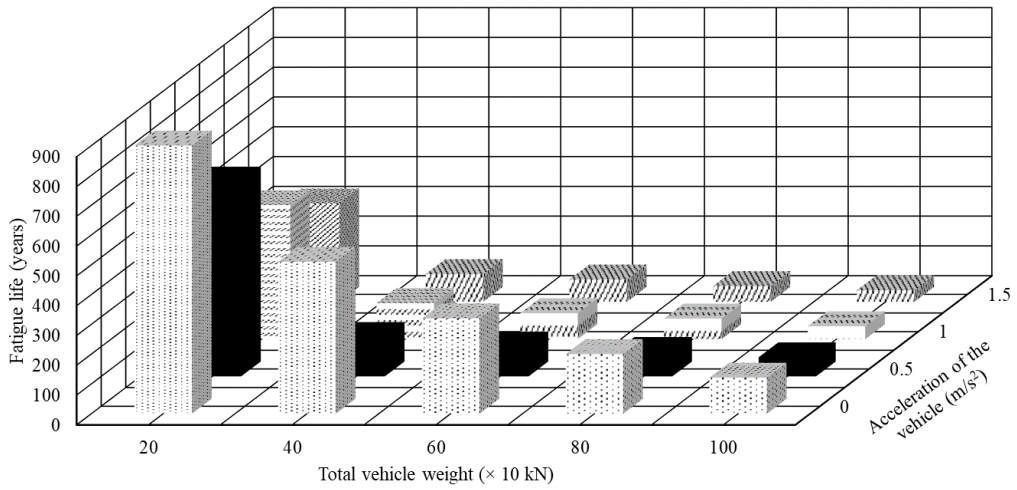

Fig. 5.43 Fatigue life for two span continuous bridge for varying axle weight and acceleration of vehicle for entry velocity 20 km/hr for very poor road

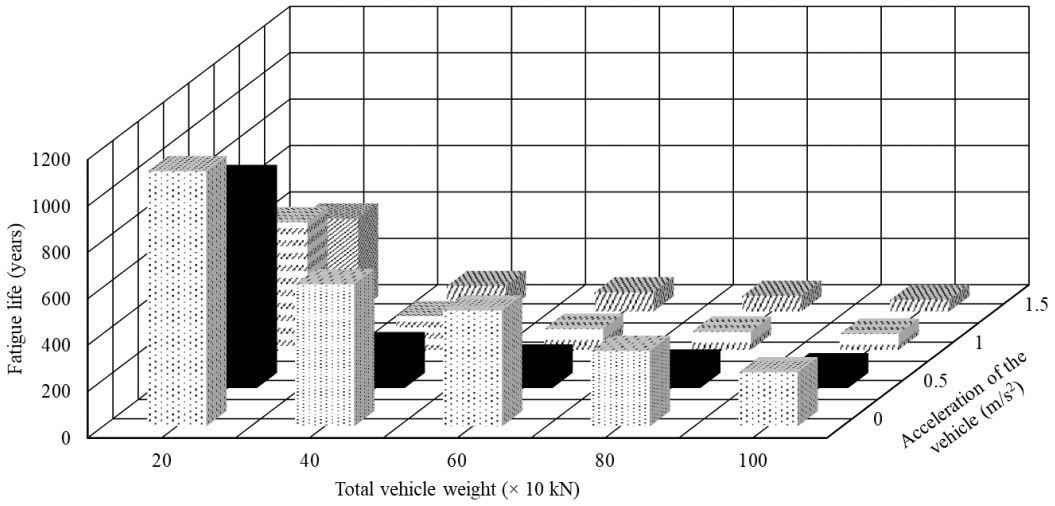

Fig. 5.44 Fatigue life for three span continuous bridge for varying axle weight and acceleration of vehicle for entry velocity 20 km/hr for very poor road

The dynamic flexural stress for two and three span continuous bridge increases with the increase in axle weight of the vehicle. This leads to increase in the stress range. The stress cycles increase in higher stress range, as observed from Figs. 5.41, 5.42, 5.11 (a) and 5.13 (a), leading to more fatigue damage accumulation, thereby reducing the fatigue life with the increase in axle weight. It is also observed that during the service life of the bridge located on a busy highway, there is accumulation of fatigue damage over time with the passage of each heavy vehicle (Unsworth, 2003; Iatsko et al., 2020). The accumulated fatigue damage resulting from multiple heavy vehicles increases and thereby reduces the fatigue life of the bridge, which is observed from Figs. 5.43 and 5.44. The fatigue damage accumulation is more in two span continuous bridge as compared to three span continuous bridge. Thus, the fatigue life for two span continuous bridge is less than that of three span continuous bridge, which is observed from Figs. 5.43 and 5.44.

5.5.1.5 Effect of amplitude of mean profile

The effect of DAF and fatigue life on the amplitude of mean profile is investigated in this section. The amplitude of mean profile has been varied from 0, 0.01 m, 0.015 m, 0.02 m. Physically, a zero amplitude indicates that no pre-camber is used. The vehicle arrival rate is considered as 120 vehicles per minute. The uniform vehicle velocity considered is 20 km/hr. The mean and standard deviation of flexural stresses obtained at the center of second span of

two and three span continuous bridge for different amplitude of mean profile is shown in Figs. 5.45 and 5.46.

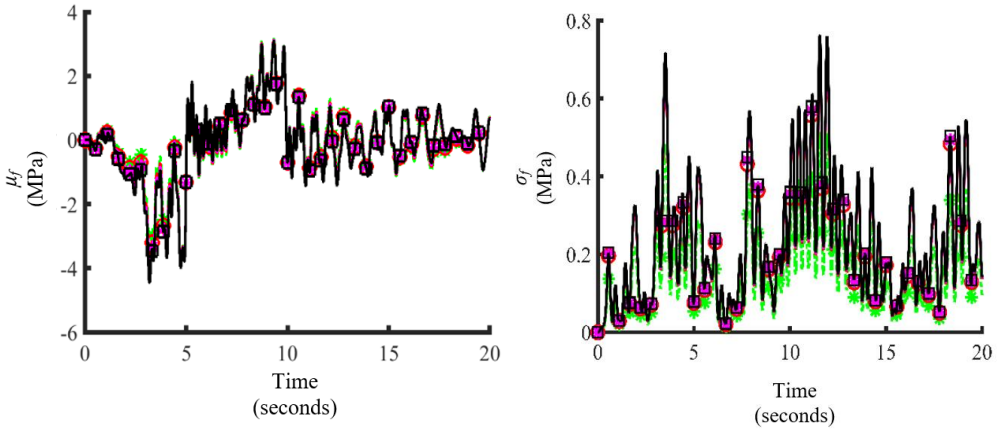

(a) (b)

Fig. 5.45 (a): Mean and (b): standard deviation of flexural stresses at centre of second span of two span continuous bridge for different amplitude of mean profile for uniform vehicle velocity 20 km/hr and very poor road

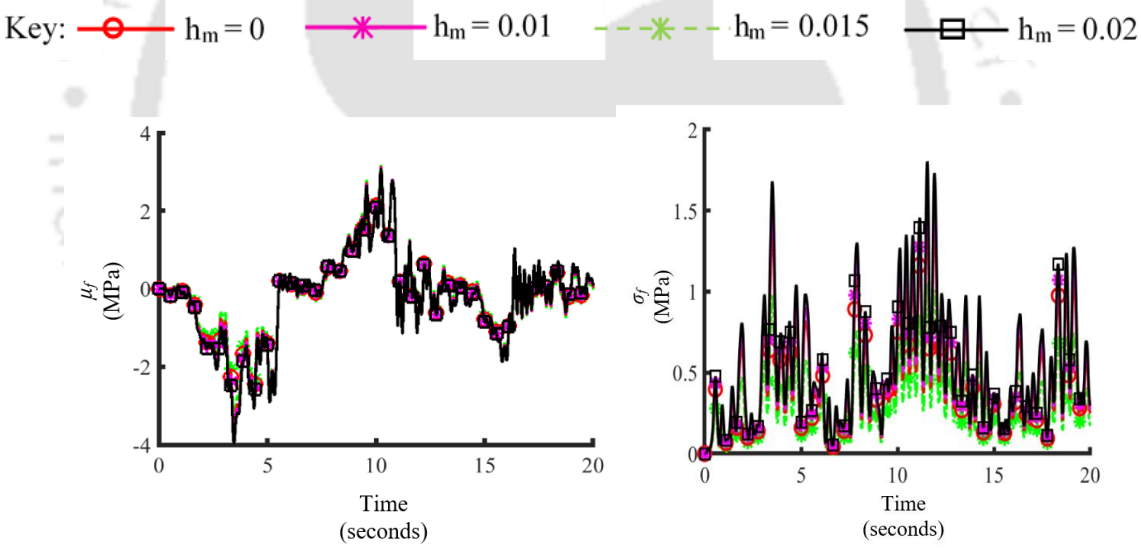

(a) (b)

Fig. 5.46 (a): Mean and (b): standard deviation of flexural stresses at centre of second span of three span continuous bridge for different amplitude of mean profile for uniform vehicle velocity 20 km/hr and very poor road

Key: $h_m = 0$ $h_m = 0.01$ $h_m = 0.015$ $h_m = 0.02$

The effect of pre-camber on mean and standard deviation of flexural stress at centre of second span of two and three span continuous bridge is observed from Figs. 5.45 and 5.46. The mean and standard deviation of flexural stresses increases with the increase in the amplitude of mean

profile. It is also observed from Figs. 5.45 and 5.46 that the flexural stresses are increased by 10% when the amplitude of mean profile is increased from 0 to 0.02 m.

Dynamic Amplification Factor (DAF)

The effect of DAF of two and three span continuous bridge with amplitude of mean profile as 0, 0.01m, 0.015 m and 0.02 m and acceleration of the vehicle for vehicle entry velocity 20 km/hr with arrival rate 120 vehicles per minute and very poor road condition is shown in Figs. 5.47 and 5.48.

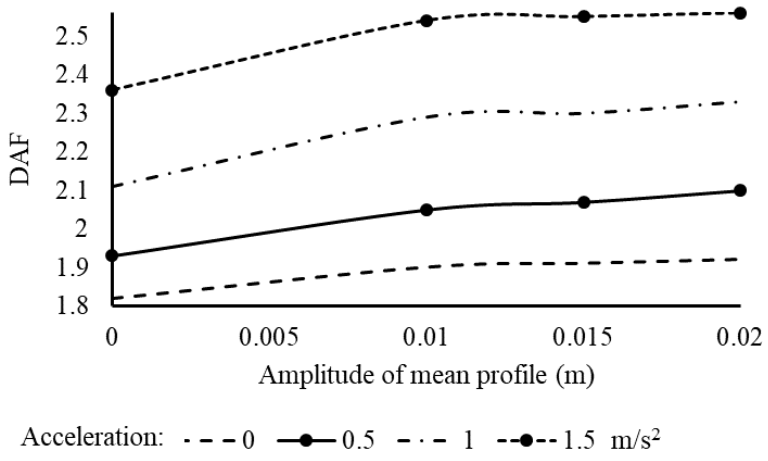

Fig. 5.47 DAF for two span continuous bridge for varying amplitude of mean profile and acceleration of the vehicle for entry velocity 20 km/hr for very poor road condition

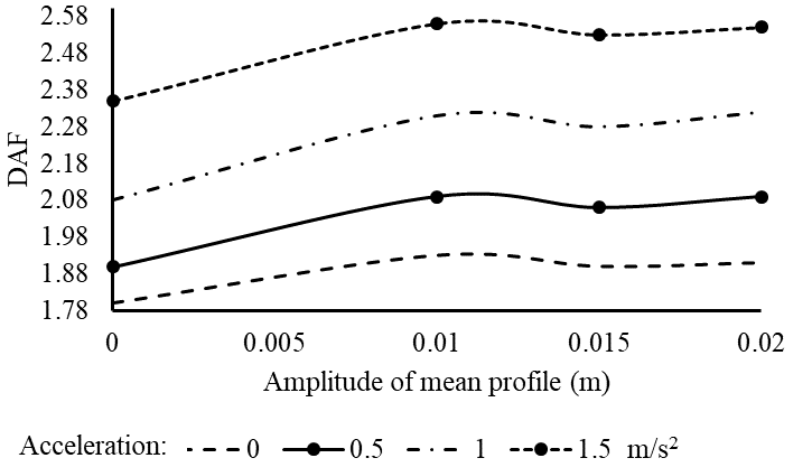

Fig. 5.48 DAF for three span continuous bridge for varying amplitude of mean profile and acceleration of the vehicle for entry velocity 20 km/hr for very poor road condition

The DAF is increased when the amplitude of mean profile is increased from 0 to 0.01 m, which is observed from Figs. 5.47 and 5.48. It is also observed that the further increase in amplitude of mean profile leads to a gradual increase in DAF in case of two and three span continuous bridge.

Fatigue life

The stress range histogram for two and three span continuous bridge for amplitude of mean profile as 0, 0.015 m and 0.02 m for arrival rate 120 vehicles per minute and uniform vehicle velocity 20 km/hr for very poor road condition is shown in Figs. 5.49 and 5.50. It is to be noted that the stress range histogram for amplitude of mean profile as 0.01 m with vehicle arrival rate 120 vehicles per minute, uniform vehicle velocity 20 km/hr and very poor road condition is shown in Fig. 5.11 (a) and Fig. 5.13 (a) for two and three span continuous bridge in sub section 5.5.1.1 respectively. The fatigue life of two and three span continuous bridge for very poor road condition for varying amplitude of mean profile and acceleration of the vehicle for vehicle entry velocity 20 km/hr is shown in Figs. 5.51 and 5.52.

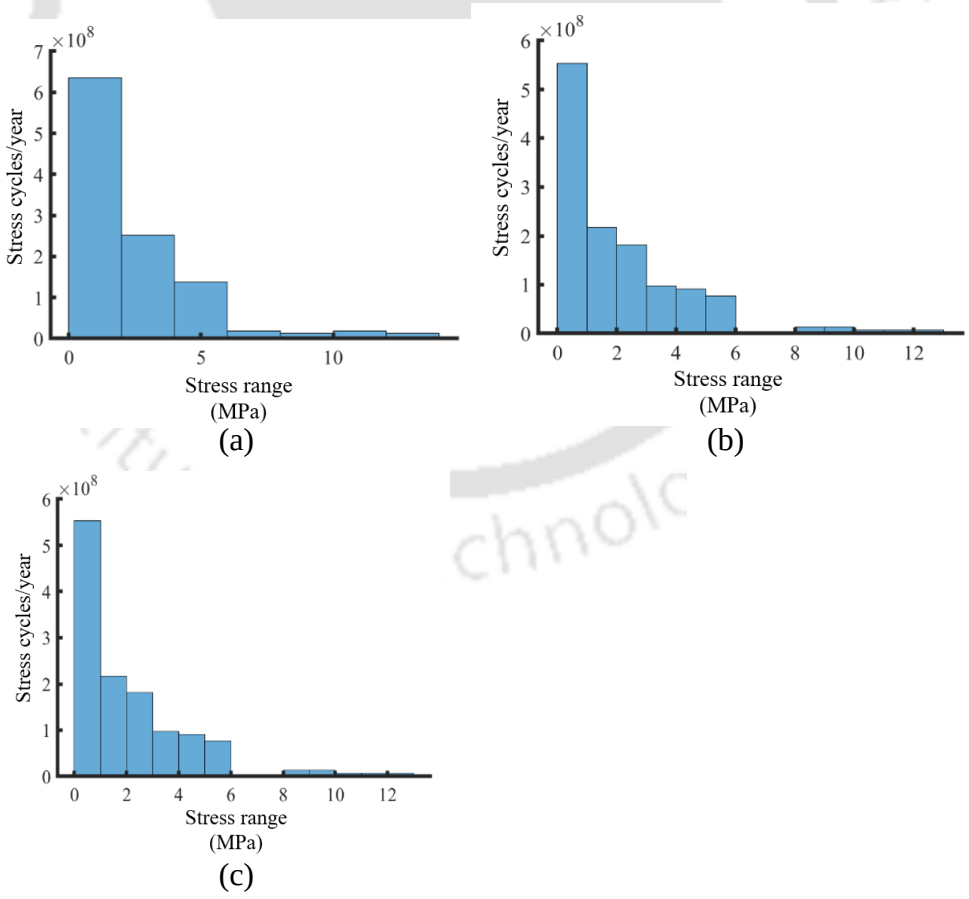

Fig. 5.49 Stress range histogram for two span continuous bridge: (a): h_m = 0 (b): h_m = 0.015 m (c): h_m = 0.02 m for uniform vehicle velocity 20 km/hr and very poor road condition

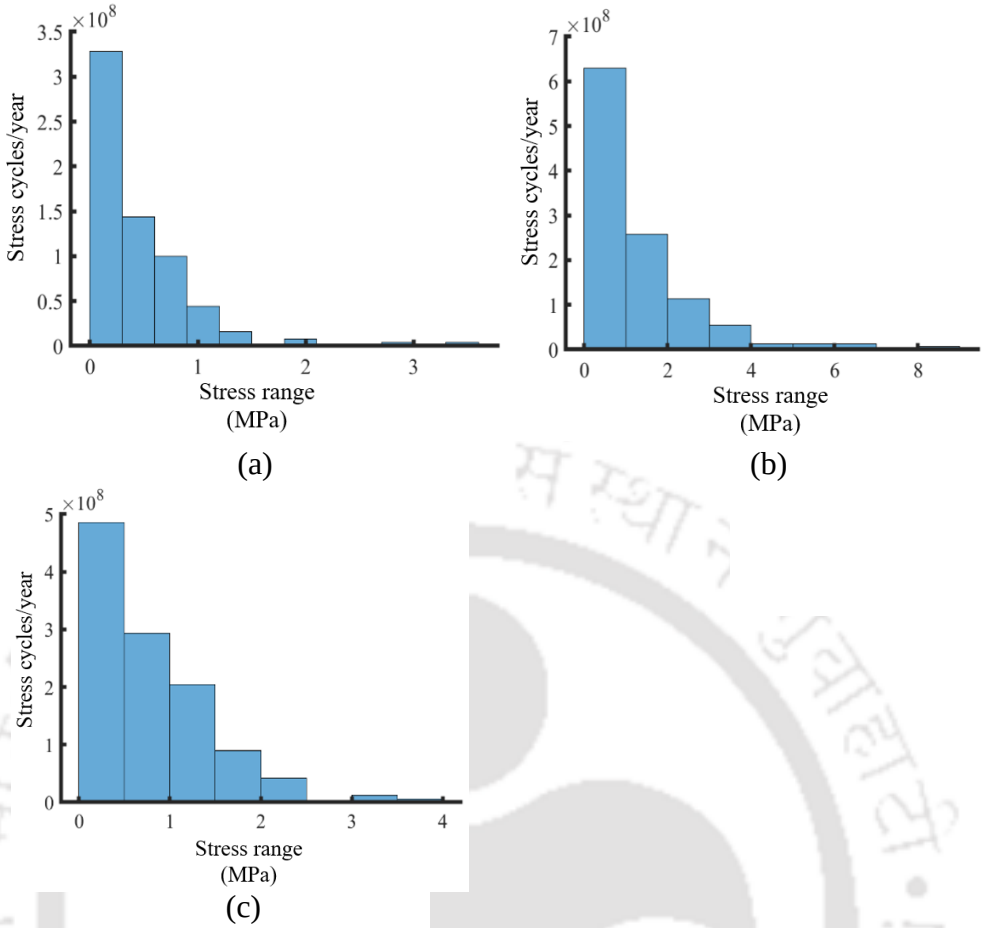

Fig. 5.50 Stress range histogram for three span continuous bridge: (a): $h_m = 0$ (b): $h_m = 0.015$ m (c): $h_m = 0.02$ m for uniform vehicle velocity 20 km/hr and very poor road condition

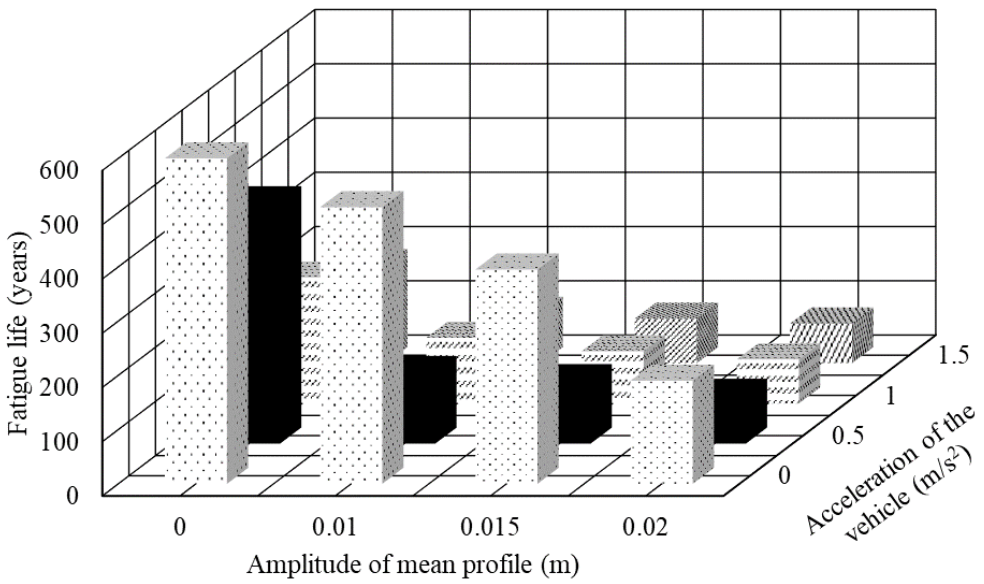

Fig. 5.51 Fatigue life for two span continuous bridge for varying amplitude of mean profile and acceleration of the vehicle for entry velocity 20 km/hr and very poor road

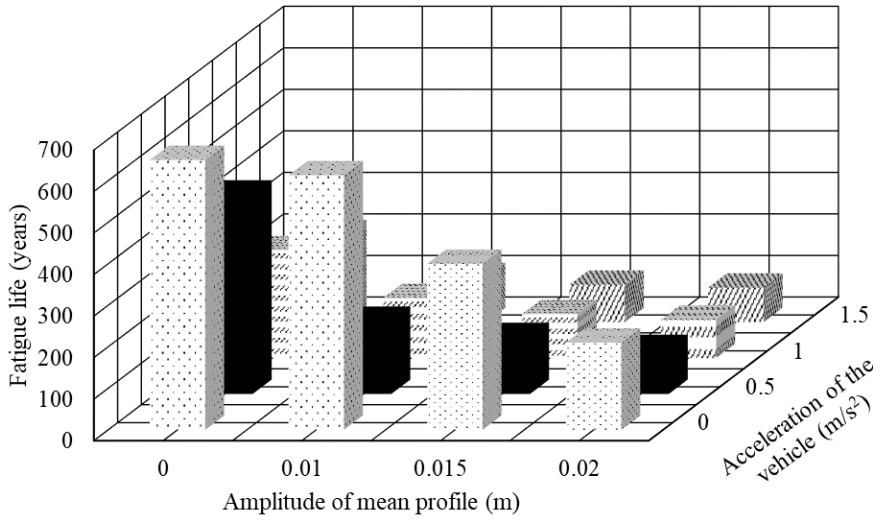

Fig. 5.52 Fatigue life for three span continuous bridge for varying amplitude of mean profile and acceleration of the vehicle for entry velocity 20 km/hr and very poor road

It is observed from Figs. 5.49, 5.50, 5.11 (a) and 5.13 (a) that the number of stress cycles in the lower stress range is increased with the increase in amplitude of mean profile. This leads to higher damage accumulation and reduction in fatigue life of two and three span continuous bridge, which is observed from Figs. 5.51 and 5.52.

5.6 Closure

In this chapter, numerical results of dynamic response of continuous bridge models with two and three span have been presented. The response statistics obtained for continuous bridge at critical location have been used to find out the fatigue life of the bridge. DAF has also been calculated separately and discussed. It may be mentioned that the results are obtained using semi analytical approach for bridge-vehicle interaction problem which forms the most essential and starting step for calculating fatigue life of bridge from the time history of stress at critical location. The effect of vehicle forward velocity, road surface roughness, vehicle arrival rate, vehicle axle weight and amplitude of mean profile on DAF and fatigue damage have been studied. The adverse effect of very poor road condition due to poor maintenance of pavement; and also traffic volume in terms of vehicle arrival rate point out significant fatigue damage. However, due to redundancy present in continuous model and possibility of redistribution of bending moment, the fatigue damage is reduced due to lowering of flexural stress. From fatigue consideration, it is observed that continuous construction may be preferred for long span bridges instead of independent single span resting on separate bearings on pier caps.

6

FATIGUE LIFE PREDICTION: PART-III
PLATE GIRDER BRIDGE USING UNCOUPLED ITERATIVE TECHNIQUE

6.1 General

The mathematical models used to describe the dynamic response of a bridge under the action of moving load is complex in nature. The complexity depends on the type of models considered and the level of accuracy desired. Bridge models can be continuous or can be made of discretized finite elements. The vehicle model is generally lumped parameter multi degree freedom system. The complexity of this model varies depending on the assumptions considered for representing the performance of tyres, suspensions, etc. The equations of motion of bridge and vehicle models are combined together to satisfy the equilibrium of forces and compatibility of displacements at the contact point. The major problem in bridge-vehicle interaction modelling is that the contact points move with time. For each point in time, the displacements of the vehicle are influenced by the displacements of the bridge and this affects the vehicle forces applied on the bridge which in turn again changes the bridge displacement and interaction forces. The above condition makes the two sets of equations of motion coupled and thus the existence of general closed form solutions are rare. Thus, the use of numerical techniques based on Finite Element Method (FEM) is necessary to obtain the solution. In addition to the complexity of bridge-vehicle model, the modelling of road surface roughness is difficult in commercial software. The effect of road surface roughness is an important factor as it increases the bridge dynamic stresses under the action of moving loads (Schenk and Bergman, 2003 and Coussy et al., 1989). Therefore, a need arises to implement the interaction between bridge and vehicle considering the effect of road surface roughness.

The commercial software allows one to carry out moving load analysis on the finite element model of the bridge. However, such analysis cannot incorporate the dynamic load induced by the moving vehicles due to vibration caused by pavement roughness. Keeping this in mind, the present chapter is aimed to develop an uncoupled iterative scheme interfacing the finite element models of bridge in CSiBridge version 14. The vehicle induced stress history will be used to find out the fatigue life of a plate girder bridge along with the study of various influencing parameters on the dynamic amplification factor and fatigue life.

6.2 Finite Element Model (FEM)

The bridge considered for study is a two-lane simply supported composite plate girder bridge with span length 48 m and total width of the bridge 13 m. The width of each lane is 6.5 m. The depth of the bridge deck is 250 mm. The cross section of the plate girder bridge and the detail of plate girder is shown in Figs. 6.1 and 6.2 respectively. Cross bracings are provided at every 6 m interval. As shown in Fig. 6.1, the bridge consists of five girders.

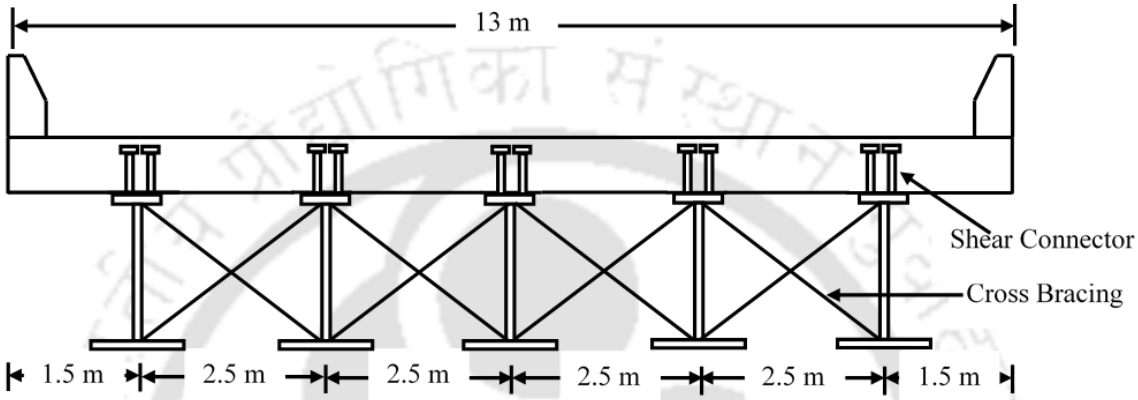

Fig. 6.1 Composite plate girder bridge cross section

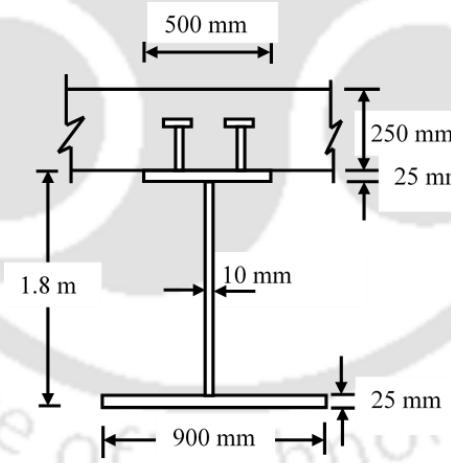

Fig. 6.2 Plate girder cross section

The concrete grade is M 35 and steel grade is E 250. The shear connectors used is stud type as shown in Fig. 6.2. The bracings used are double angle sections of ISA 100 placed back-to-back with gap of 10 mm between them. The FE modelling of the bridge is done using CSiBridge version 14.

Layout lines are defined first in modelling the bridge. The purpose of defining the layout line is that it is used as reference lines for defining the layout of bridge objects such as deck sections and lanes (SAP 2000). The layout line starts from 0 to 48 m where 0 is the start point and 48 m is the end point as the span of the bridge is 48 m. The centreline of the two lanes are then measured with respect to the layout line and given as offset from the layout line. The lane width is also given as input along with the offset.

The deck is modelled as four-noded shell element having six degrees of freedom. The girders and bracings are modelled as frame element having six degrees of freedom. The deck is connected to the girder using shear connectors. Shear connectors are provided to prevent slip which may occur at the interface between steel girder and concrete deck. The composite action between the deck and girder is obtained by using frame insertion point and joint offset (CSiBrdige, 2017). During modelling, the frames and shells are drawn at the elevation of deck centroid sharing the same joints. In order to place the deck above the girder, frame joint offsets and top centre insertion points are used as shown in Fig. 6.3.

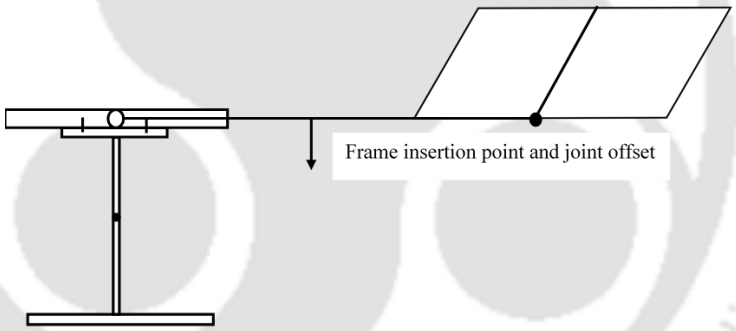

Fig. 6.3 Modelling composite behaviour

The strength of the web plate is increased by providing stiffeners to prevent buckling under heavy concentrated load. The stiffeners are provided under concentrated loads and at the points of supports (Ellobody, 2014; Subramanian, 2008). These stiffeners strengthen the web and transmit heavy concentrated loads or reactions to the flanges of plate girder. In the present study, horizontal stiffeners of size 350 mm × 20 mm and vertical stiffeners of size 360 mm × 20 mm are provided whose total area is 14200 mm^2. The vertical stiffeners are provided at a spacing of 1.5 m. The effect of vertical and horizontal stiffeners is provided using property modifiers option under frame section. Modification factor corresponding to the total web area including the stiffeners and without the stiffeners needs to be evaluated and the ratio between

the two is given as modification factor corresponding to cross section area. The factor considered in the present study is 1.8.

Splices are provided to join the web plates when the length of the plate girder is too long to handle conveniently during transportation and erection. The splices should not be located where maximum bending moment occurs. In the present study, the splices are located at $L/4$ from each end of the span where L is the span of the bridge (IRC 24-2011). The web splices are modelled using rigid links at the locations mentioned.

For the girders at one end of the support, fixed bearing (allows rotation about any axis in horizontal plane) is used in the middle girder. The bearings used for the remaining girders for the same support are Guided POT cum PTFE i.e., it allows movement perpendicular to the direction in which force applied is transmitted and allows rotation about any axis in horizontal plane.

For the girders present at other end of the support, Guided POT cum PTFE bearing is used in the middle girder. Free POT cum PTFE bearings are used for the remaining girders at the same support i.e., it allows movement in any direction in horizontal plane and rotation about any axis in horizontal plane.

The mesh size and the dynamic load applied on the bridge are explained in the sections given below.

6.3 Simulation of Dynamic Load

Multiple vehicles traversing on the bridge are considered in the study. As explained in Chapter 3, the vehicle arrival time on the bridge is considered to be a random variable following Poisson process. The road surface roughness is also considered to be a random process following Gaussian distribution. The modelling of the road roughness is not possible in the commercial FE software. Thus, most of the FE analysis of the bridge has been done taking the movement of single vehicle on the bridge in the absence of road surface roughness (Ding et al., 2016; Zhou et al., 2013). However, in the study, the dynamic analysis of the bridge is considered taking into consideration the movement of multiple vehicles and road surface roughness, causing vibratory load on the bridge deck along the span.

6.3.1 Vehicle Model

As explained in section 3.4.1 in Chapter 3, the generic vehicle model known as Quarter Car Model has been adopted in the study. It is also termed as heave model as all the motions are in vertical direction. The vehicle model can also be extended to account for rotation about the transverse axis (pitch) and rotation about longitudinal axis (roll). However, it is observed that using such degree of sophistication in vehicle model will not affect the stresses on the bridge considered for fatigue assessment (Gonzalez, 2010). Thus, multiple vehicles modelled as quarter car model is considered in the study.

6.3.2 Vehicle Forward Velocity

The vehicle forward motion over the bridge has been considered with variable velocity. A general polynomial with coefficients that can characterize the speed variations have been considered. In the present study, the location of centroid of the n^{th} vehicle is modelled with a general polynomial as

$$x_{nc}(t) = \sum_{k=0}^{m} a_k t^k \tag{6.1}$$

where $x_{nc}(t)$ represents the position of n^{th} vehicle at any time instant, t. The vehicle moves with constant velocity when the constants $a_2=a_3=\ldots=a_m=0$ with a_0 and a_1 having non-zero values. The constants a_3, a_4, etc. are to be retained when considering acceleration or retardation of vehicle motion. The acceleration of the vehicle is considered to be constant for the multiple vehicles traversing on the bridge. The constant or variable velocity is given as input in the FE model while assigning the dynamic load.

6.3.3 Vehicle Arrival Time

The arrival time of the vehicles are random variables following Poisson process. The arrival time of n^{th} vehicle, t_{pn} is represented in terms of interarrival times, ti as

$$t_{pn} = \sum_{i=1}^{n} ti_i \tag{6.2}$$

where n represents the number of vehicles arriving on the bridge, t_{pn} is the arrival time of the n^{th} vehicle on the bridge and ti_i is the interarrival time of i^{th} vehicle.

The arrival time follows Gamma distribution which is given as

$$p_{t_{pn}}(t) = \frac{\lambda^n t^{n-1} \exp(-\lambda t)}{\Gamma(n)} \tag{6.3}$$

where n is the shape parameter of Gamma distribution which represents the number of vehicle arrivals on the bridge and λ represents the arrival rate.

The interarrival time follows an exponential distribution (Lin, 1976) given as

$$p_{ti_i}(t) = \lambda e^{(-\lambda t)} \tag{6.4}$$

where ti_i is the interarrival time of i^{th} vehicle. The interarrival times are generated using random variables following exponential distribution function for a given arrival rate. The first interarrival time will be the arrival time of the first vehicle and the second arrival time will be the sum of first two interarrival time of the vehicles as shown in Eq. (6.2). The vehicles traverse on the bridge from time, $t > 0$ to maximum time, T_{max} depending on the time window considered. The arrival times are generated in the time interval $(0, T_{max}]$.

6.3.4 Road Roughness Simulation

As explained in section 3.3 in Chapter 3, the road roughness is obtained considering the mean profile of the road and road roughness irregularity. The mean profile of the road is considered to be a half sine wave and resembles the pre-camber on the bridge. The power spectral density function of road surface roughness has been given in Eq. (3.30) under section 3.3.4 in Chapter 3.

6.3.5 Vehicle Induced Load on Rigid Pavement

As explained in section 6.3, the movement of multiple vehicles is considered on the bridge and shown in Fig. 6.4.

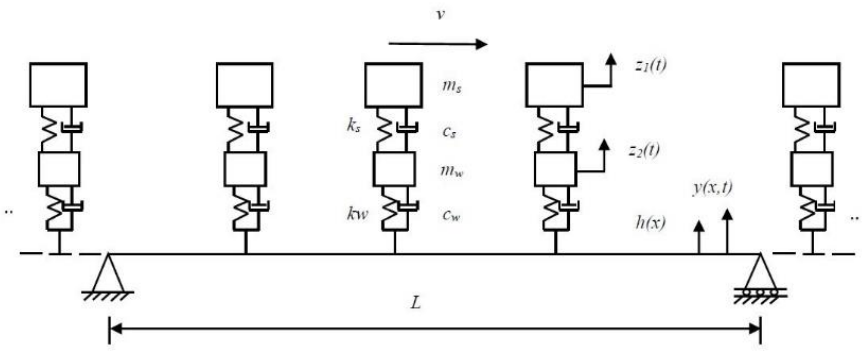

Fig. 6.4 Vehicle movement on the bridge

In Fig. 6.4, m_s represents the sprung mass, m_w represents the unsprung mass, k_s and k_w represents the stiffness of the sprung mass and unsprung mass respectively, c_s and c_w represents the damping of the sprung mass and unsprung mass respectively, $z_1(t)$ and $z_2(t)$ represents the displacement of the sprung mass and unsprung mass respectively, $h(x)$ is the bridge deck profile, $y(x,t)$ is the bridge deflection and L is the span of the bridge.

The vehicle response is obtained by considering bridge as rigid pavement. The vehicle equations of motion are given as

$$m_s\ddot{z}_1 + c_s\left(\dot{z}_1 - \dot{z}_2\right) + k_s\left(z_1 - z_2\right) = 0 \tag{6.5}$$

$$m_w\ddot{z}_2 + \left(c_w + c_s\right)\dot{z}_2 + \left(k_w + k_s\right)z_2 - c_s\dot{z}_1 - k_s z_1 = c_w\dot{h} + k_w h \tag{6.6}$$

In Eq. (6.6), $\dot{h}(x)$ is given as

$$\dot{h} = \frac{dh}{dt} = \frac{dh}{dx}\frac{dx}{dt} = v\frac{dh}{dx} \tag{6.7}$$

In Eq. (6.7), v represents velocity of the vehicle and can be obtained by taking the first time derivative of Eq. (6.1). The vehicle equations of motion as shown in Eq. (6.5) and Eq. (6.6) are solved using Newmark's Method (Chopra, 2011). The vehicle induced dynamic load on the bridge, $F_{i,d}$ is then obtained using the unsprung mass displacement and road roughness and is given as

$$F_{i,d} = k_w\left(z_2 - h\right) + c_w\left(\dot{z}_2 - \dot{h}\right) \tag{6.8}$$

The obtained vehicle induced dynamic load from Eq. (6.8) is then given as input to the FE model to obtain the bridge deflection. The vehicle induced load remains same for vehicles with same mass and suspension characteristics moving with same velocity and same acceleration. Thus, the dynamic load due to vehicular movement is obtained for single vehicle and the same load is applied for 'n' vehicles considering multiple vehicular movement. The method used is called Uncoupled Iterative Scheme and is explained in the section given below.

6.4 Uncoupled Iterative Scheme

The uncoupled iterative scheme employed in the study considers multiple vehicular movement and speed variation. The iterative procedure is explained below.

(i). To start the simulation, deck profile is generated from PSD function of road unevenness and pre-cambered profile is added to it to obtain complete description of the deck elevation.

(ii). The coupled vehicle equation of motions is solved by Newmark β method (Chopra, 2011) to obtain vehicle induced load F_{id}.

(iii). The vehicle weight is added to F_{id} determined in step (ii) which forms the dynamic load for a single vehicle to be passed.

(iv). Since, the present algorithm assumes multiple vehicular motion for fatigue evaluation, dynamic loading for a particular time window is now found for the series of vehicle following Gamma distribution in their arrival rate.

(v). The total load, comprising vehicle's weight and tyre induced load F_{id} for series of vehicles i=1, 2,…n in a time window T is fed to the FE model as input for dynamic analysis to obtain displacement of the bridge $y(t)$ and flexural stress $f(t)$.

(vi). The bridge displacement $y(t)$ is added to the deck profile generated in step (i) and then vehicle induced dynamic load is obtained using the procedure expressed in step (ii) to (v).

(vii). The displacement of the bridge and stress are updated using current loading as in (vi).

(viii). The above steps are repeated till the convergence in bridge displacement is achieved in a particular time window for multiple vehicle motions.

The convergence criteria is set on the maximum flexural stress for the calculation of fatigue damage and in the present study, it is tested by a non-dimensional factor $e \leq 1 \times 10^{-3}$. The factor e is defined as the ratio of the difference of stress at any time instant between the current and previous step to the maximum of the stress between current and previous steps.

6.5 Results and Discussion

The plate girder bridge was subjected to series of vehicular movement using the dynamic interaction force which was given as input to the FE model. The dimensions of the plate girder bridge are given in section 6.2. The sprung mass, m_s of the vehicle is 36000 kg, unsprung mass

of the vehicle, m_w is 4000 kg, the stiffness of the sprung and unsprung mass, k_s and k_w is 14.4 × 10^6 N/m and 3.6 × 10^6 N/m respectively and the damping of the sprung and unsprung mass, c_s and c_w is 475.2 × 10^3 N-sec/m and 24 × 10^3 N-sec/m. The roughness magnitude coefficient $S_{GG}(\Omega_0)$ for different categories of road i.e., good, average, poor and very poor have been considered as 32 × 10^{-6} m^2/cycle/m, 120 × 10^{-6} m^2/cycle/m, 512 × 10^{-6} m^2/cycle/m and 1024 ×10^{-6} m^2/cycle/m respectively (ISO 8608:1995).

The mesh size was fixed depending on the mesh convergence study. The number of iterations required in the study to obtain the flexural stress of the bridge was fixed based on the tolerance limit as given in section 6.4. Both the studies are explained in the section given below. The contribution of mean and standard deviation of flexural stress has been considered in evaluating dynamic amplification factor (DAF), which is discussed in section 3.5 in Chapter 3. The mean and standard deviation of flexural stresses, μ_f and σ_f, obtained were then used to evaluate the design stress. The design stress is obtained after adding the mean with two times the standard deviation of flexural stress, which has been used for evaluating fatigue life. The fatigue life has been evaluated adopting Modified Bilinear Damage Rule (MBLDR) as this rule gives accurate damage predictions as compared to Bilinear Damage Rule (BLDR). The error between the predicted fatigue life and the actual fatigue life obtained from experiment is less in case of MBLDR as compared to BLDR, which has been observed in section 2.9.2 in Chapter 2. For a plate girder corresponding to yield stress f_y = 250MPa, the fatigue detail constant K and material constant m have been taken as 250 × 10^8 ksi (1.723 × 10^{11} MPa) and -3 respectively (Fisher, 1977; AASHTO, 2017).

6.5.1 Mesh Convergence Study

The mesh convergence study is done in an iterative process wherein the mesh size is refined until the FE analysis results are within a reasonable range and further refinement of the mesh size does not affect the analysis results. The girders are modelled as frame elements and the deck is modelled as shell element. The flexural stresses on the girder due to the movement of vehicles is obtained from the FE analysis. To observe the effect of reduced mesh size in the shell elements, the mesh size in the frame elements are kept same and the analysis results i.e., flexural stresses for middle girder for uniform vehicle velocity 20 km/hr and arrival rate 60 vehicle per minute for good road condition ($S_{GG}(\Omega_0)$ = 32 × 10^{-6} m^2/cycle/m) are obtained as shown in Fig. 6.5. For this model, the mesh size in the shell element is varied and is kept as 6m × 2m, 3m × 1m, 2m × 1m and 1m × 1m. The number of shell elements for mesh areas 1 m^2, 2

m^2, 3 m^2 and 12 m^2 are 624, 312, 208 and 52 respectively. The mesh size for frame elements is 240 mm.

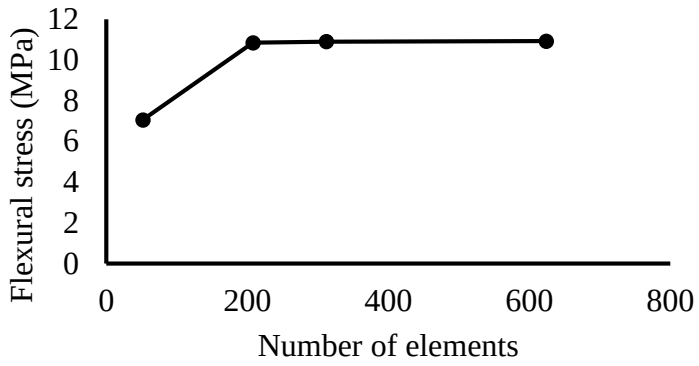

Fig. 6.5 Comparison of flexural stresses with reduced mesh size

As can be seen from Fig. 6.5, the flexural stresses do not change significantly for mesh areas $3m^2$, $2m^2$ and $1m^2$ as compared to $12m^2$ in case of shell elements. Hence, the mesh area is kept as $3m^2$.

Further, the mesh size for the frame elements are varied from 240 mm, 120 mm, 80 mm, 60 mm and 48 mm to observe the effect on flexural stresses. The number of frame elements for mesh size 240 mm, 120 mm, 80 mm, 60 mm and 48 mm are 200, 400, 600, 800 and 1000 respectively. The mesh size for shell elements is kept as 3 m × 1 m. The comparison of flexural stresses for reduced mesh size of frame elements is shown in Fig. 6.6.

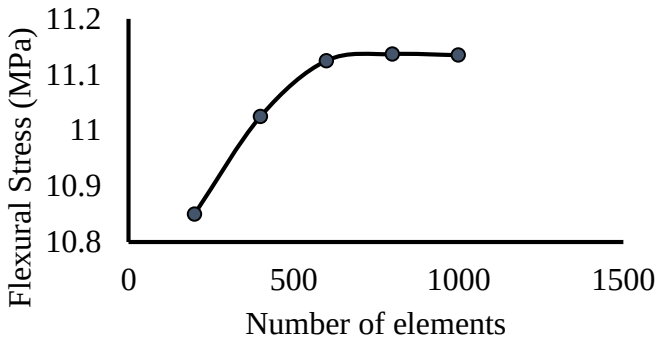

Fig. 6.6 Comparison of flexural stresses with reduced frame size

It is observed from Fig. 6.6 that the flexural stresses do not change significantly for mesh size 80 mm to 48 mm. Thus, optimum mesh size for frame elements is considered as 80 mm. As observed from Figs. 6.5 and 6.6, the final mesh size used for shell elements is 3m × 1m and for

frame elements is 80 mm. The composite plate girder with mesh is shown in Fig. 6.7 and the cross section is shown in Fig. 6.8.

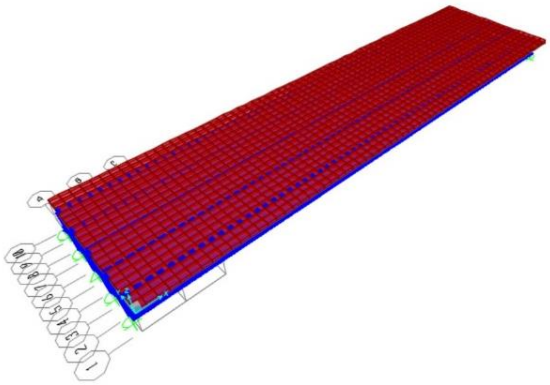

Fig. 6.7 FE model of the composite plate girder bridge with mesh

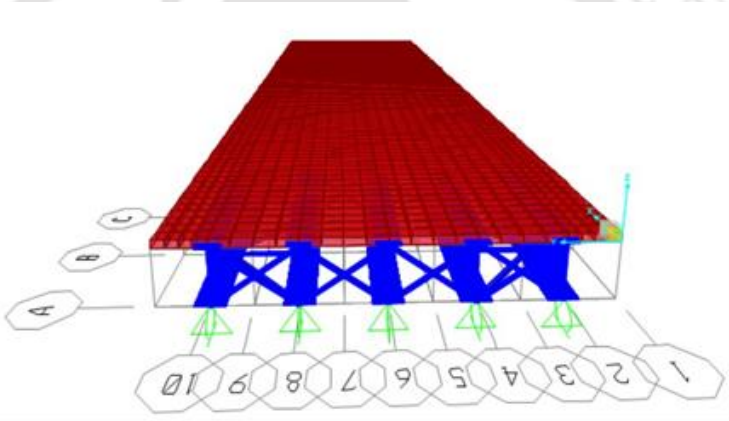

Fig. 6.8 Cross-section of the composite plate girder bridge with mesh

Rayleigh damping is considered in the study which is expressed as

$$\mathbf{C} = a_0\mathbf{M} + a_1\mathbf{K} \tag{6.9}$$

where a_0 and a_1 are mass proportional coefficient and stiffness proportional coefficient respectively, which is obtained by taking the first and second natural frequency. **M**, **C** and **K** are mass matrix, damping matrix and stiffness matrix respectively. The damping ratio is considered as 2 % for all modes. The first natural frequency obtained is 12.59 rad/sec and the second natural frequency obtained is 14.20 rad/sec. The mass proportional coefficient a_0 is 0.267 sec^{-1} and stiffness proportional coefficient a_1 is 1.492×10^{-3} sec.

6.5.2 Simulated Road Roughness

The road roughness was simulated using the equations explained in Chapter 3. A typical road roughness for vehicle velocity 20 km/hr and for very poor road condition is shown in Fig. 6.9.

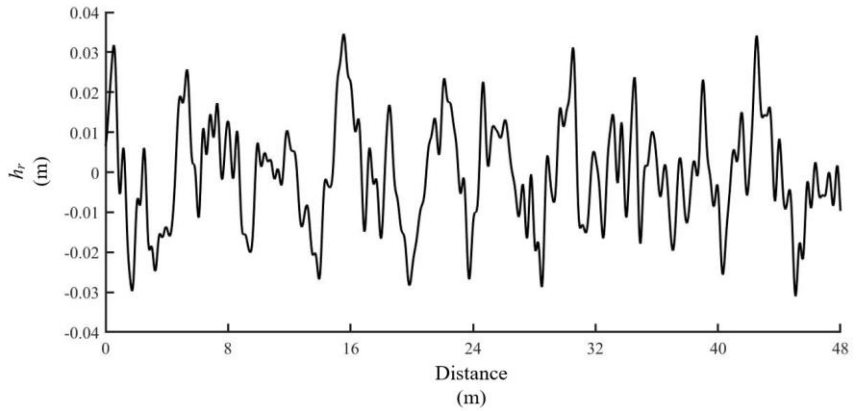

Fig. 6.9 Typical road roughness

In Fig. 6.9, h_r represents the pavement roughness. The pre-camber considered as half sine wave is also added to the road surface roughness and a typical plot is shown in Fig. 6.10. The amplitude of the half sine wave has been considered as 0.01 m.

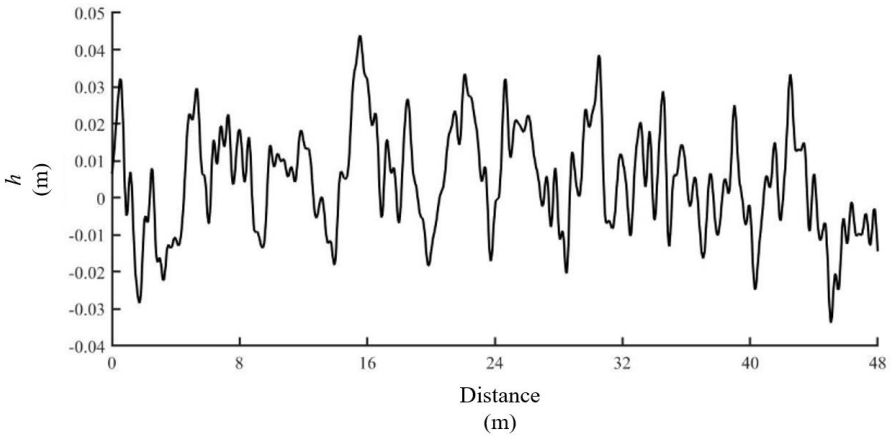

Fig. 6.10 Typical road roughness combined with pre-camber

In Fig. 6.10, h represents the bridge deck profile.

6.5.3 Convergence of Iterative Scheme

The sprung mass m_s of the vehicle is 36000 kg, unsprung mass of the vehicle m_w is 4000 kg, the stiffness of the sprung mass k_s is 14.4×10^6 N/m and unsprung mass k_w is 3.6×10^6 N/m and the damping of the sprung mass c_s is 475.2×10^3 N-sec/m and unsprung mass c_w is 24 ×

10^3 N-sec/m. Using the vehicle data, the vehicle induced dynamic load from Eq. (6.8) is obtained for uniform vehicle velocity 20 km/hr, very poor road condition ($S_{GG}(\Omega_0)$ = 1024 × 10^{-6} m^2/cycle/m) and arrival rate 120 vehicles per minute. The arrival rate is considered for the case when multiple vehicles are traversing on the bridge. The mean profile of the road is also considered and the amplitude is 0.01 m. The vehicle induced dynamic load is given as input to the FE model to obtain flexural stresses. The comparison of flexural stresses, *f* with the number of iterations for single and multiple vehicles traversing on the bridge for the above mentioned vehicle data and road parameter are shown in Figs. 6.11 and 6.12.

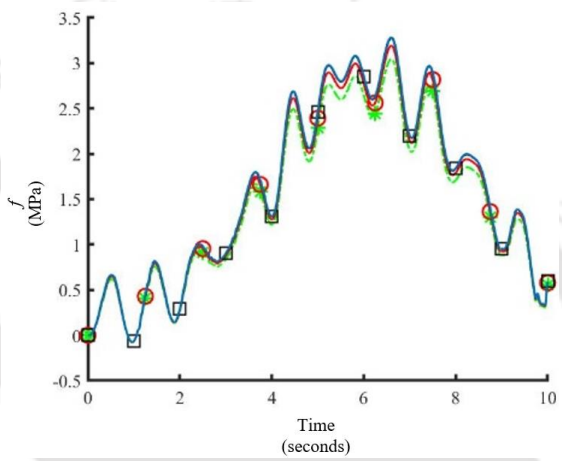

Fig. 6.11 Comparison of flexural stress with the number of iterations for single vehicle traversing on the bridge

Key: 1st iteration 2nd iteration 3rd iteration 4th iteration

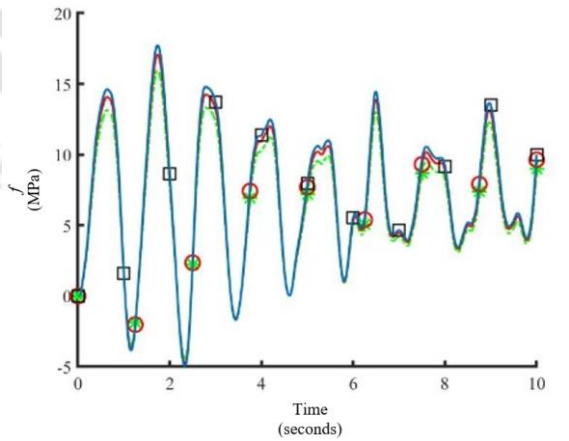

Fig. 6.12 Comparison of flexural stress with the number of iterations for multiple vehicles traversing on the bridge

Key: 1st iteration 2nd iteration 3rd iteration 4th iteration

The maximum flexural stress obtained in the first iteration for single and multiple movement of vehicles is 3.05 MPa and 15.97 MPa respectively which can be observed from Figs. 6.11 and 6.12 respectively. The maximum flexural stress obtained from second iteration is 3.19 MPa and 17.09 MPa for single and multiple vehicular movement respectively. The percentage difference between the value obtained from the second and first iteration is 4.6 % for single vehicle movement on the bridge and 7 % for multiple vehicle movement on the bridge. As observed, the values are not converging and the analysis is carried out to obtain the bridge deflection from second iteration. The bridge deflection is then used to evaluate vehicle induced dynamic load which is given as input in the FE model and the third iteration is carried out. The maximum flexural stress from Figs. 6.11 and 6.12 is 3.28 MPa and 17.73 MPa for single vehicle movement and multiple vehicle movement respectively. On comparing the values obtained from the third and second iteration, the percentage difference is found to be 2.8 % for single vehicle traversing on the bridge and 3.7 % for multiple vehicles traversing on the bridge. Since, the values are not converging till the tolerance limit, the fourth iteration is carried out. It is observed that the maximum flexural stress obtained from the fourth iteration for single vehicle traversing on the bridge is 3.284 MPa and for multiple vehicles traversing on the bridge is 17.75 MPa. The values obtained from the fourth and third iteration for single vehicle traversing on the bridge are differing by 0.12 % and multiples vehicles traversing on the bridge is 0.11 % leading to convergence and thus, the analysis is further stopped. Thus, the total number of iterations carried for FE analysis are four.

The vehicle movement on the bridge have been considered for different time windows. Time windows are considered to account for the multiple vehicle effects in estimating fatigue damage instead of single vehicle movement on the bridge that are traditionally considered for fatigue damage. The optimum time window for vehicular movement is obtained by varying the time windows from 10 secs to 25 secs with an interval of 5 secs. The vehicle velocity is also varied from 20 km/hr to 60 km/hr with an interval of 10 km/hr. The arrival rate of the vehicles is 120 vehicles per minute. The road surface roughness is varied from good, average, poor and very poor. The maximum mean and standard deviation of flexural stresses obtained for different time windows mentioned are given in Table 6.1 and Table 6.2 respectively.

Table 6.1 Comparison of maximum mean flexural stresses for different time windows

Vehicle Velocity (km/hr)	Road Roughness Coefficient ($\times 10^{-6}$ m^2/cycle/m)	Mean Flexural Stress (MPa)			
		10 secs	15 secs	20 secs	25 secs
20	32	12.3	12.45	12.5	12.65
	120	13.17	13.2	13.25	13.3
	512	15.5	15.55	15.6	15.65
	1024	17.75	17.8	17.83	17.83
30	32	12.18	12.25	12.3	12.35
	120	12.73	12.74	12.75	12.75
	512	14.35	14.37	14.37	14.38
	1024	16.67	16.68	16.69	16.7
40	32	12.15	12.155	12.17	12.18
	120	12.69	12.7	12.7	12.7
	512	14.21	14.22	14.24	14.25
	1024	15.77	15.78	15.81	15.82
50	32	12.05	12.06	12.07	12.08
	120	12.52	12.55	12.56	12.57
	512	13.87	13.88	13.89	14
	1024	15.28	15.3	15.31	15.32
60	32	11.8	11.85	11.9	11.9
	120	12.15	12.16	12.17	12.18
	512	13.47	13.48	13.49	13.49
	1024	14.91	14.91	14.91	14.93

Table 6.2 Comparison of maximum standard deviation of flexural stresses for different time windows

Vehicle Velocity (km/hr)	Road Roughness Coefficient ($\times 10^{-6}$ m^2/cycle/m)	Standard Deviation of Flexural Stress (MPa) ($\times 10^{-3}$)			
		10 secs	15 secs	20 secs	25 secs
20	32	1.5	1.52	1.55	1.56
	120	2	2.12	2.15	2.17
	512	2.5	2.55	2.6	2.65
	1024	3.5	3.52	3.55	3.56
30	32	2.3	2.35	2.39	2.40
	120	2.80	2.84	2.85	2.85
	512	3.01	3.07	3.08	3.08
	1024	3.25	16.68	16.69	16.7
40	32	2.23	2.25	2.26	2.26
	120	2.75	2.76	2.76	2.76
	512	2.84	2.85	2.85	2.85
	1024	3.02	3.02	3.02	3.02
50	32	2.10	2.11	2.11	2.12
	120	2.56	2.57	2.58	2.58
	512	2.71	2.72	2.72	2.72
	1024	3.01	3.01	3.01	3.01
60	32	2.05	2.06	2.07	2.07
	120	2.43	2.45	2.46	2.46
	512	2.68	2.69	2.69	2.69
	1024	2.82	2.82	2.82	2.82

It is observed from Table 6.1 and Table 6.2 that the maximum mean and standard deviation of flexural stresses do not vary significantly from time windows 10 secs to 25 secs and will not change fatigue damage. Thus, the time window is considered as 10 secs, keeping in mind that computational time can be saved and overall estimate will not drastically alter the results.

6.5.4 Parametric Study

In order to evaluate the fatigue life and dynamic amplification factor (DAF), the influence of different parameters on the results have been studied. The parameters considered are:

(i). Vehicle Velocity
(ii). Road Surface Roughness
(iii). Arrival Rate of Vehicles
(iv). Eccentricity of Load
(v). Spacing of Cross Bracing
(vi). Ratio of Flange Thickness to Web Thickness of Girder

In the following sub sections, we discuss the effect of each of the above parameters on DAF and fatigue life.

6.5.4.1 Effect of vehicle velocity

In this section, the effect of uniform velocity and variable velocity of the moving vehicles on DAF and fatigue life of the plate girder bridge has been studied. The uniform vehicle velocity is varied from 20 km/hr to 60 km/hr with an interval of 10 km/hr for arrival rate 120 vehicles per minute. The movement of multiple vehicles have been considered. The road roughness considered is very poor ($S_{GG}(\Omega_0) = 1024 \times 10^{-6}$ m^2/cycle/m). The pre-camber of the road along with the road roughness has also been considered. The mean and standard deviation of flexural stresses at mid span of the middle girder and outer girder obtained when the vehicles traverse on the centreline of the lane with uniform velocity is shown in Figs. 6.13 and 6.14.

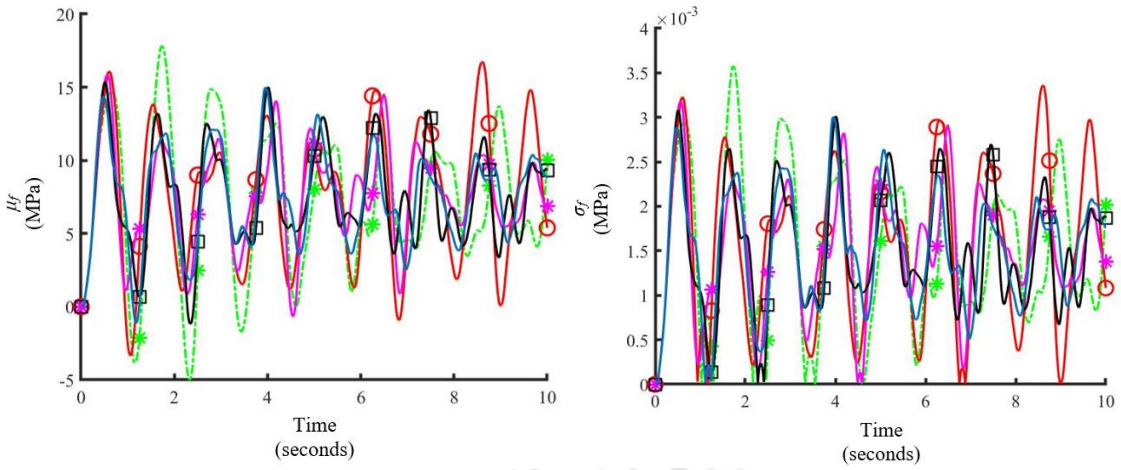

(a) (b)

Fig. 6.13 (a): Mean and (b): standard deviation of flexural stress at mid span of the middle girder for different uniform vehicle velocity for very poor road condition ($S_{GG}(\Omega_0)$ = 1024 × 10^{-6} m^2/cycle/m)

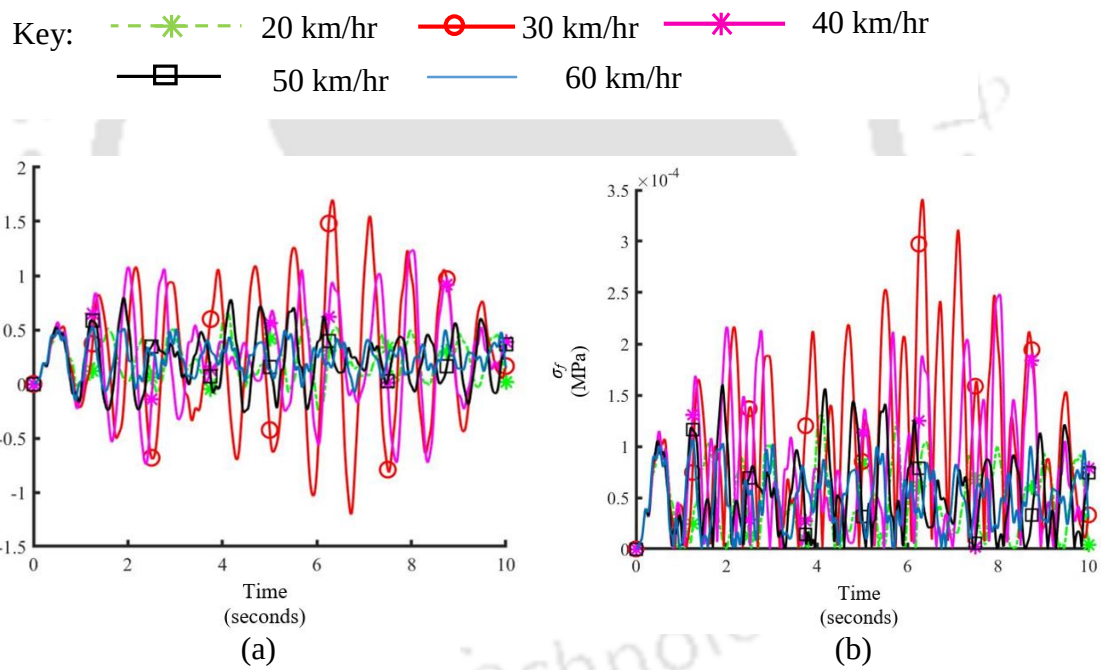

(a) (b)

Fig. 6.14 (a): Mean and (b): standard deviation of flexural stress at mid span of the outer girder for different uniform vehicle velocity for very poor road condition ($S_{GG}(\Omega_0)$ = 1024 × 10^{-6} m^2/cycle/m)

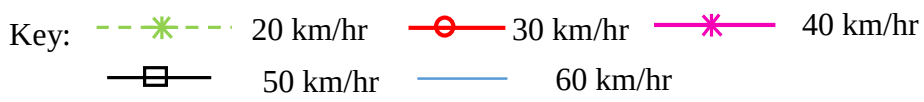

It has been observed from Figs. 6.13 and 6.14 that the mean and standard deviation of flexural stresses vary with vehicle velocity. The mean flexural stresses are more for lower velocity.

However, for the outer girder, the variation with vehicle velocity does not follow a similar trend as shown in Fig. 6.14. Since the load is made to pass through the centreline of the bridge, the middle girder is subjected to more flexural stress as compared to the outer girder.

The movement of multiple loads in 10 secs time window is considered. Although a uniform time window is considered for all vehicle velocities, the action of each load is limited to time intervals of length L/v where L is the span of the bridge and v is the vehicle velocity. This implies that the average number of moving loads acting on the span decreases with increasing vehicle velocity. Thus, the mean and standard deviation of flexural stresses are more for lower vehicle velocity as observed from Fig. 6.13. The same behaviour of flexural stress with vehicle velocity was observed in Savin (2001), Brady et al. (2006) and Sniady (1984).

The effect of variable velocity is considered by varying the entry velocity of the vehicle as 20 km/hr, 30 km/hr, 40 km/hr, 50 km/hr and 60 km/hr and letting the vehicles accelerate at the rate 0.5 m/s^2, 1 m/s^2 and 1.5 m/s^2. The mean and standard deviation of flexural stresses at the mid span of the middle girder for the following entry velocities and acceleration values for very poor road ($S_{GG}(\Omega_0)$ = 1024 × 10^{-6} m^2/cycle/m) and arrival rate 120 vehicles per minute are shown in Figs. 6.15 to 6.17.

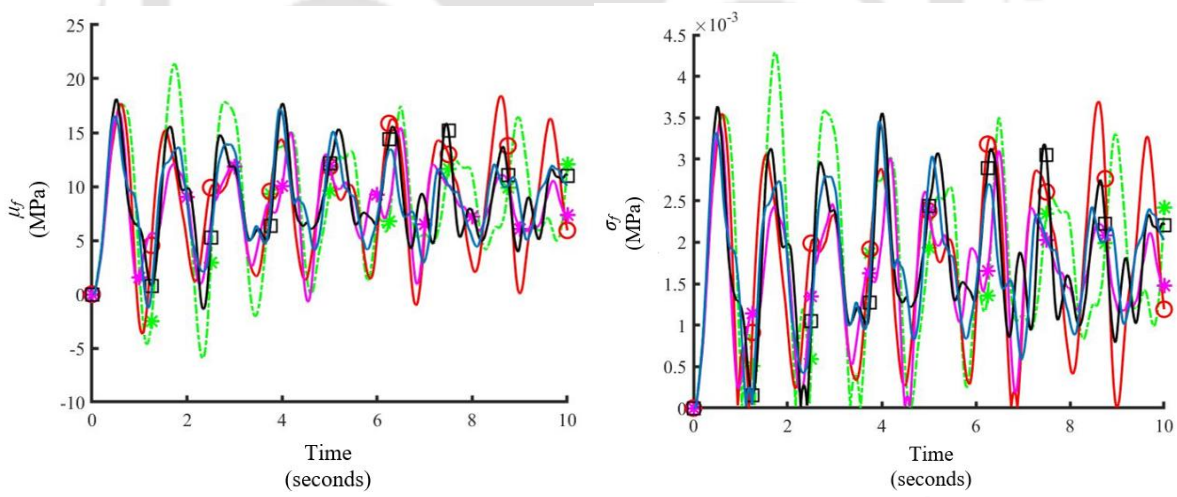

(a) (b)

Fig. 6.15 (a): Mean and (b): standard deviation of flexural stress at mid span of the middle girder for different entry velocities for acceleration 0.5 m/s^2 for very poor road condition ($S_{GG}(\Omega_0)$ = 1024 × 10^{-6} m^2/cycle/m)

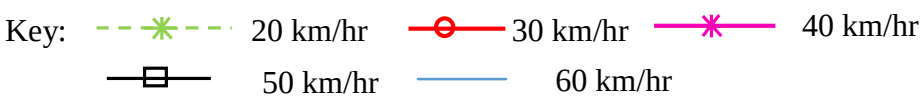

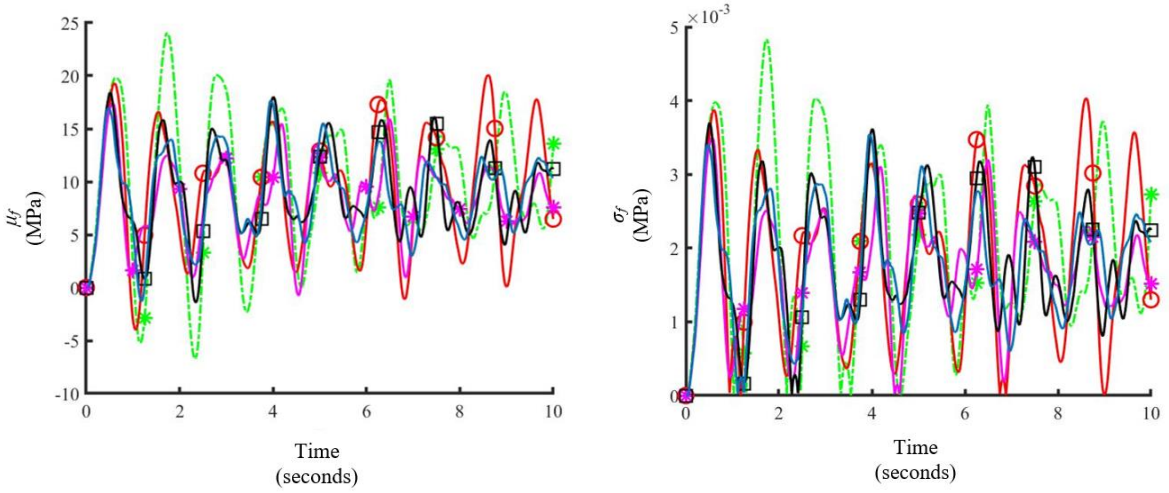

(a) (b)

Fig. 6.16 (a): Mean and (b): standard deviation of flexural stress at mid span of the middle girder for different entry velocities for acceleration 1 m/s^2 for very poor road condition ($S_{GG}(\Omega_0)$ = 1024 × 10^{-6} m^2/cycle/m)

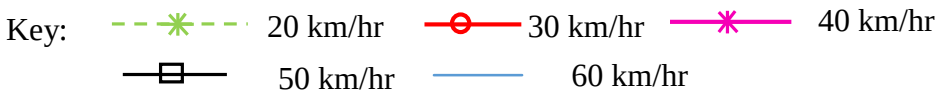

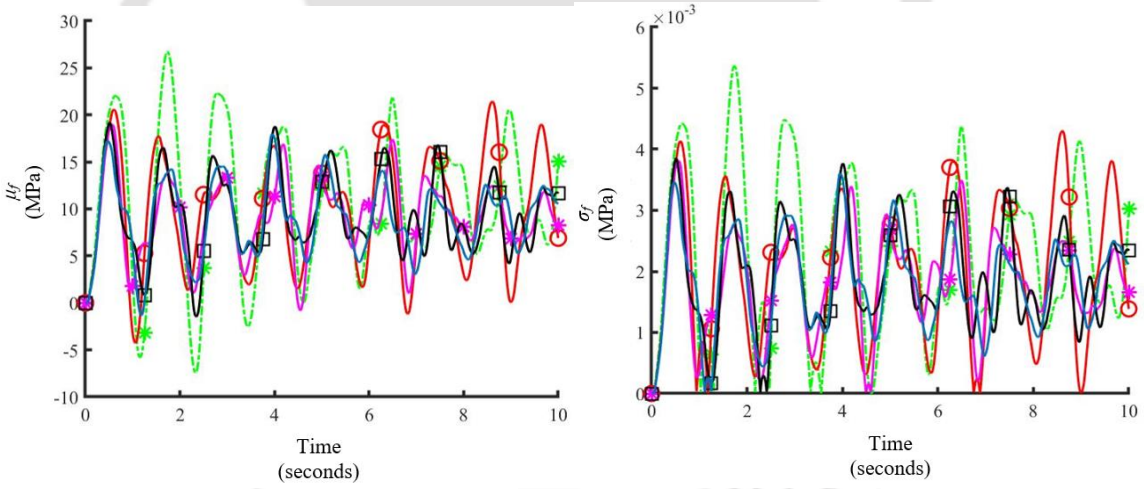

(a) (b)

Fig. 6.17 (a): Mean and (b): standard deviation of flexural stress at mid span of the middle girder for different entry velocities for acceleration 1.5 m/s^2 for very poor road condition ($S_{GG}(\Omega_0)$ = 1024 × 10^{-6} m^2/cycle/m)

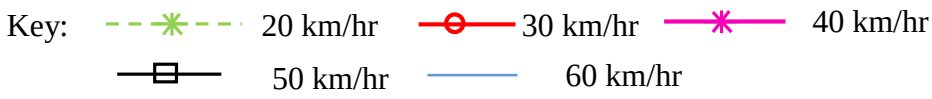

The mean and standard deviation of flexural stresses increase with increase in the acceleration values of the moving vehicles as observed from Figs 6.15 to 6.17. This is because the transverse vibration of the bridge increases with the increase in acceleration of the moving vehicles.

Dynamic Amplification Factor (DAF)

The DAF for the middle girder is evaluated for uniform and variable vehicle velocities for very poor road condition ($S_{GG}(\Omega_0)$ = 1024 × 10^{-6} m^2/cycle/m) and arrival rate 120 vehicles per minute and is shown in Fig. 6.18.

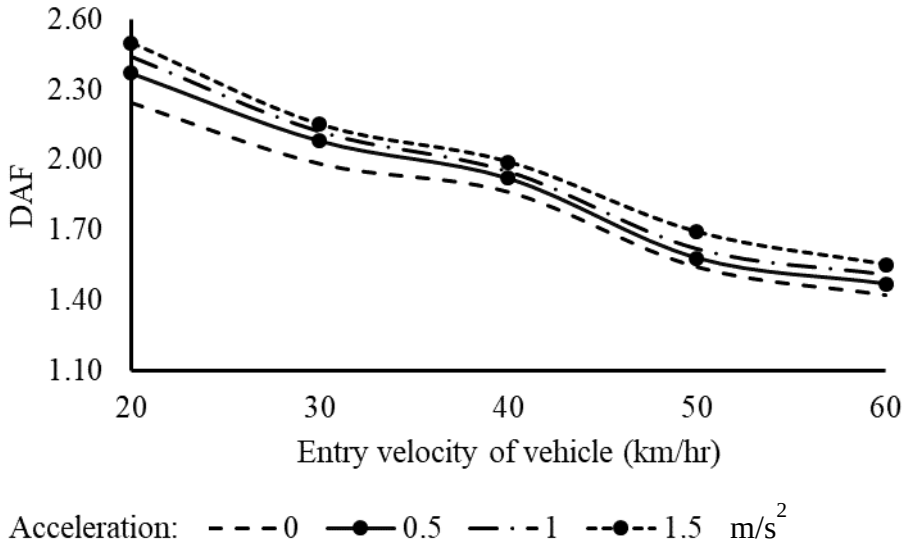

Fig. 6.18 DAF for varying entry velocities of vehicles and acceleration values (m/s^2) for very poor road surface condition

The DAF increases with the increase in acceleration of vehicles and decreases with the increase in vehicle velocity, which is observed from Fig. 6.18. The mean and standard deviation of the flexural stresses increase with the increase in acceleration of the vehicles. This leads to higher DAF as vehicle acceleration increases. However, at higher velocities, the vehicular load reaches mid-span in less time due to which the bridge vibration is less (Brady et al, 2006; Savin, 2001; and Sniady, 1984; Sieniawksa and Sniady, 1990). Thus, the dynamic stresses decrease with higher velocities leading to decrease in DAF with increase in vehicular velocity.

Fatigue Life

The fatigue life is evaluated using the stress range histograms. The stress range histograms for constant and variable velocities are shown in Figs. 6.19 to 6.22. The fatigue life for different vehicle velocity considering constant and variable velocity is shown in Fig. 6.23.

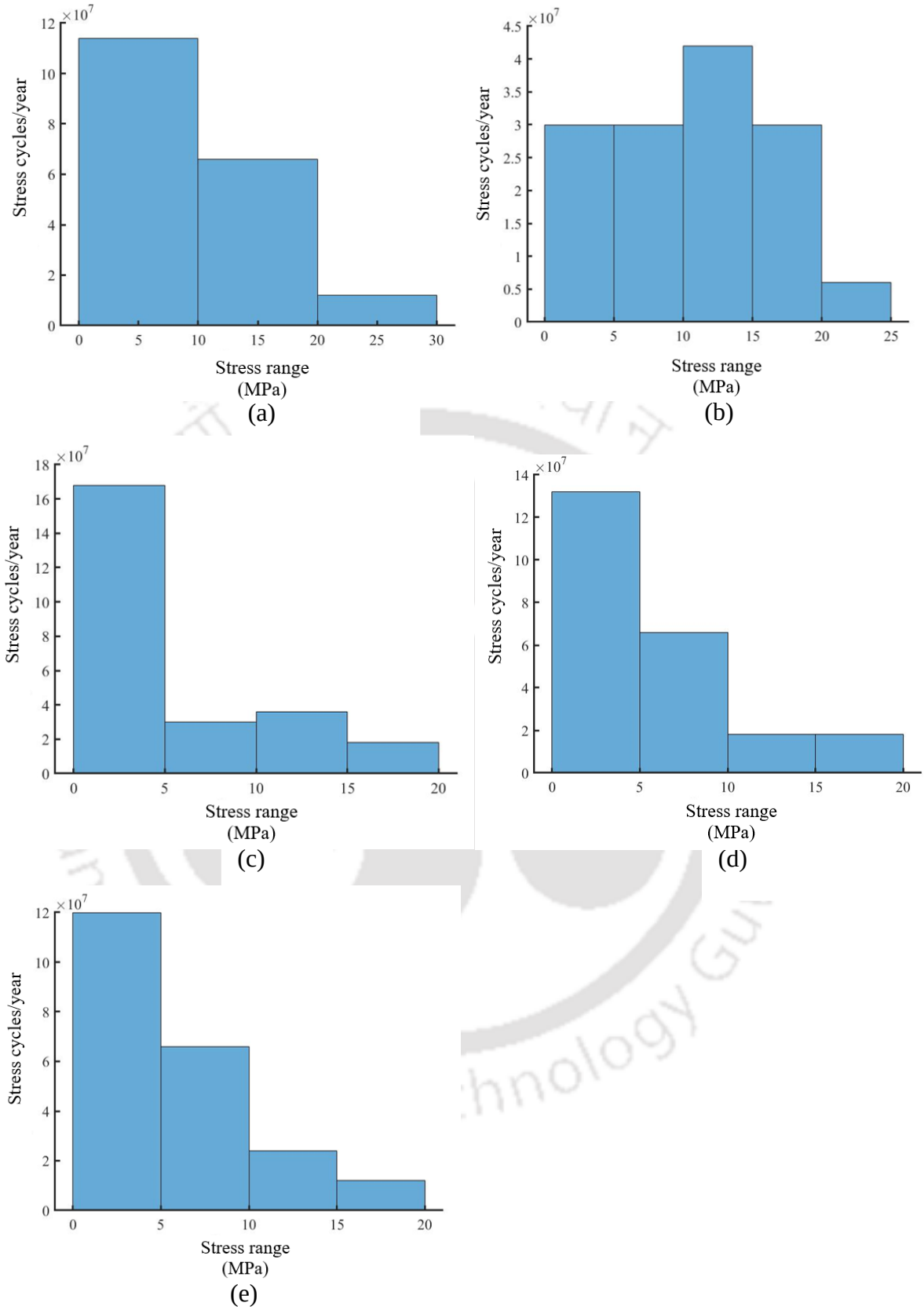

Fig. 6.19 Stress range histogram for uniform vehicle velocity (a): 20 km/hr (b): 30 km/hr (c): 40 km/hr (d): 50 km/hr (e): 60 km/hr for very poor road case

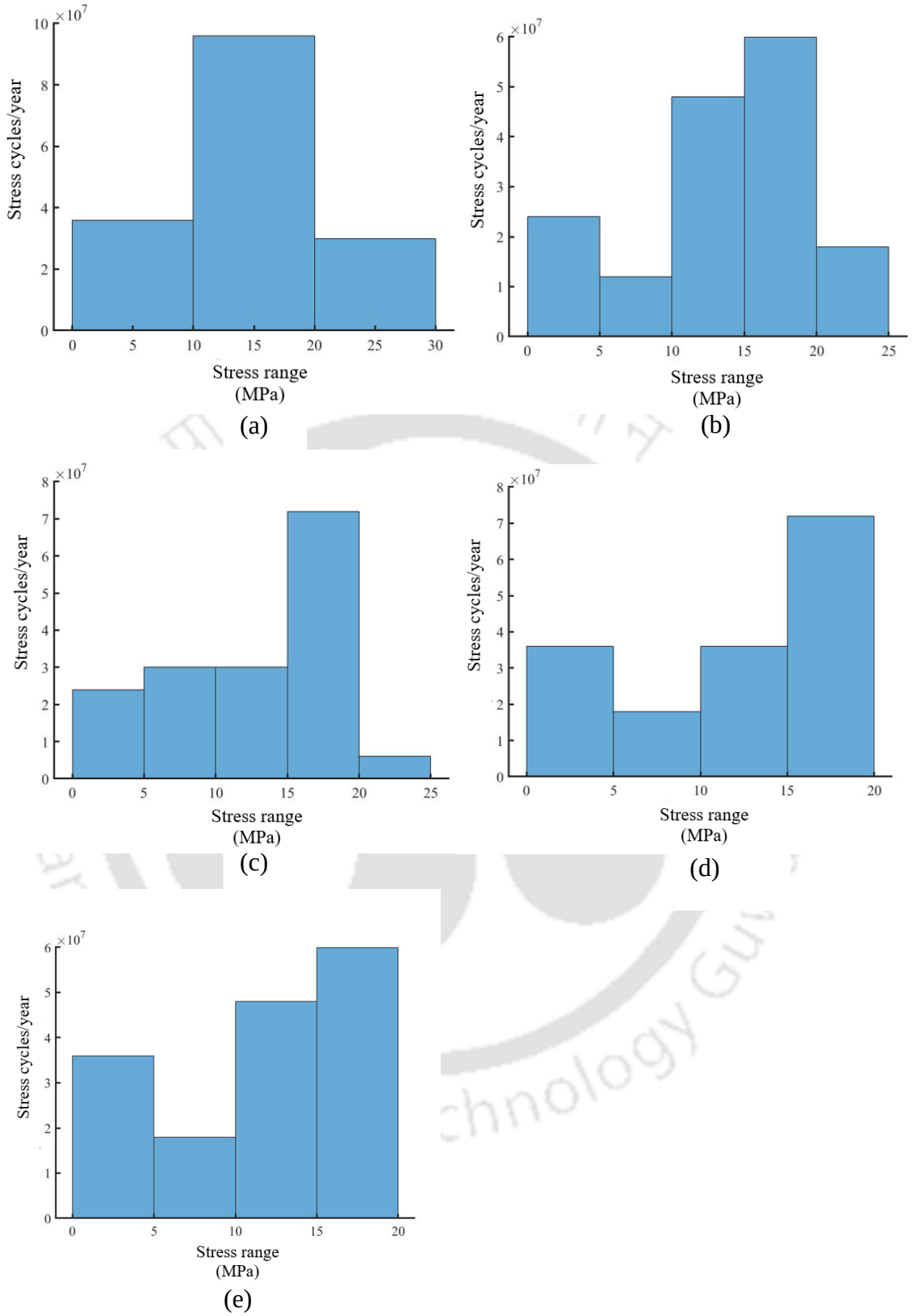

Fig. 6.20 Stress range histogram for vehicle moving with 0.5 m/s^2 acceleration with entry velocity: (a): 20 km/hr (b): 30 km/hr (c): 40 km/hr (d): 50 km/hr (e): 60 km/hr for very poor road case

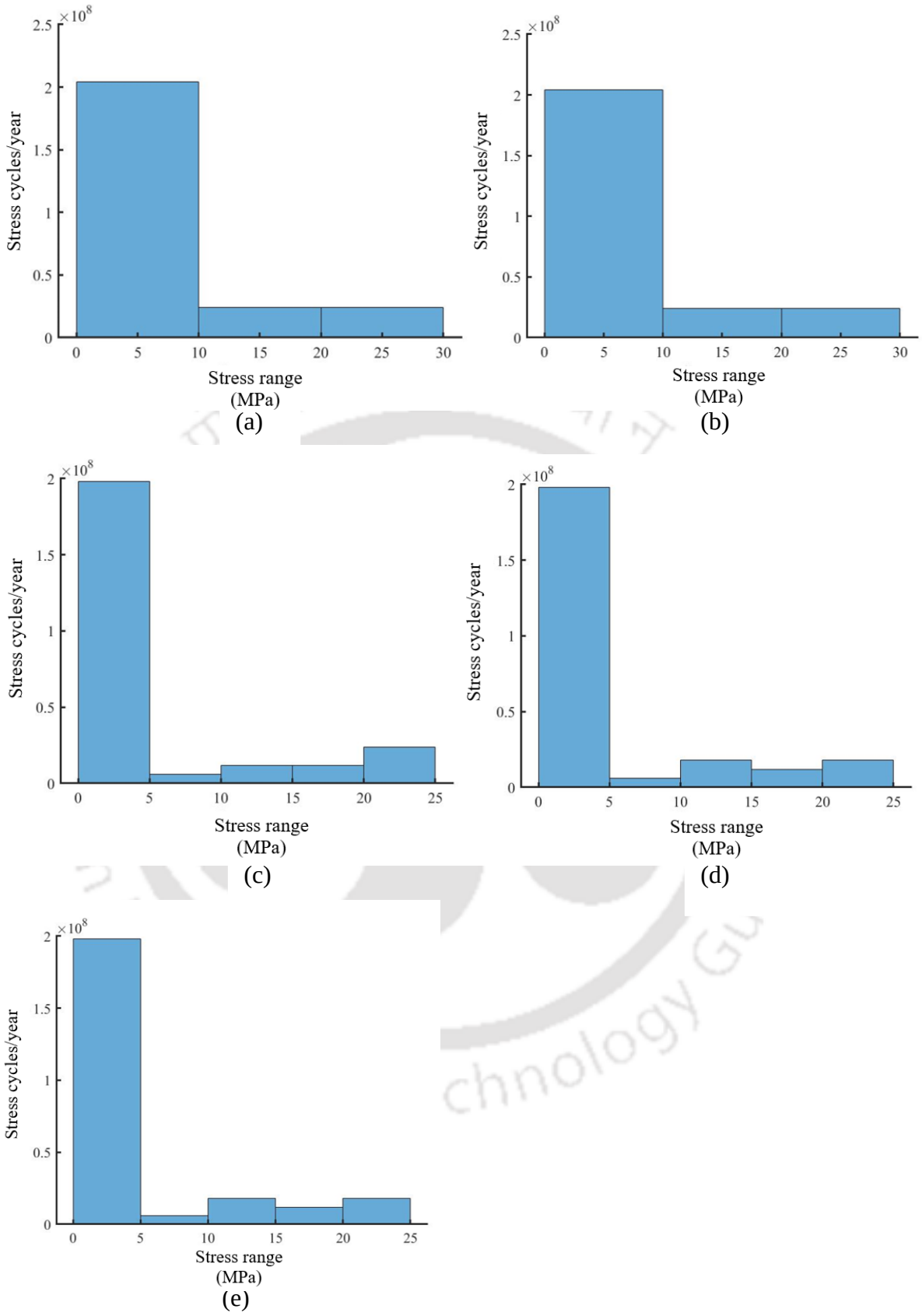

Fig. 6.21 Stress range histogram for vehicle moving with 1 m/s^2 acceleration with entry velocity: (a): 20 km/hr (b): 30 km/hr (c): 40 km/hr (d): 50 km/hr (e): 60 km/hr for very poor road case

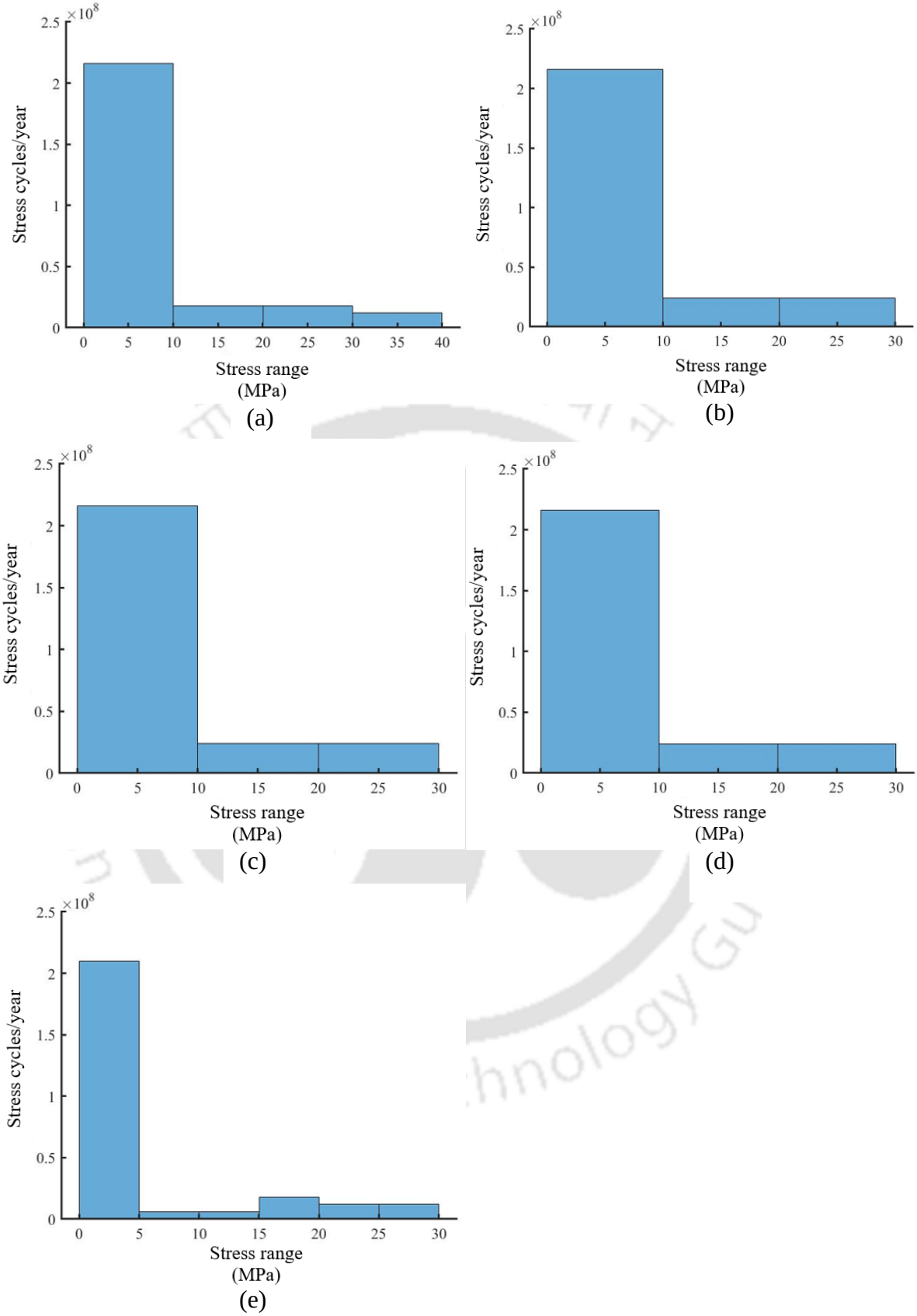

Fig. 6.22 Stress range histogram for vehicle moving with 1.5 m/s^2 acceleration with entry velocity: (a): 20 km/hr (b): 30 km/hr (c): 40 km/hr (d): 50 km/hr (e): 60 km/hr for very poor road case

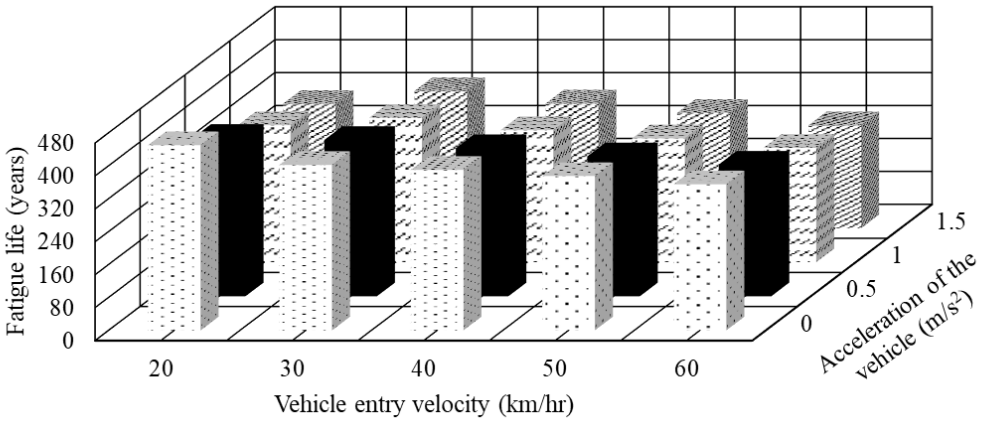

Fig. 6.23 Comparison of fatigue life with different vehicle velocities

It is observed that as the vehicle velocity increases, the low amplitude stress ranges cause reduction in the knee-point coordinates. The knee-point demarcates the fatigue damage process into crack initiation and crack propagation. The reduction in knee-point coordinates lead to reduction in crack initiation phase and increase in crack propagation phase. The rate of crack propagation increases with increase in vehicle velocity. This contributes to higher fatigue damage accumulation in the plate girder bridge with increase in vehicle velocity. The stress range histogram shown in Figs. 6.19 to 6.22 include both the static and dynamic stress components due to the movement of vehicles over the bridge. It is observed from Figs. 6.19 to 6.22 that the number of stress cycles with large amplitude stress range is low and these correspond to the static component of vehicles traversing on the bridge. It is also observed from Figs. 6.19 to 6.22 that the number of stress cycles with small amplitude stress range is high and these characterise the dynamic action of moving vehicles and their effects on vibration of bridges. Vehicles moving with higher velocity exhibit higher stress cycles in low amplitude stress range. These stress cycles due to vehicle bridge interaction contribute to fatigue damage accumulation. Thus, the fatigue life of the bridge decreases as the vehicle velocity increases, which is observed from Fig. 6.23. Similar variation of fatigue life with vehicle velocity is observed in Sieniawksa and Sniady (1990).

It is also observed that as the acceleration of the vehicle increases, the stress cycles increases for high and low amplitude stress ranges. Moreover, it is also observed that at vehicle acceleration 0.5 m/s^2, the number of stress cycles at low and high amplitude stress range is high as compared to the case when the vehicle moves with uniform velocity. This contributes to more fatigue damage and lower fatigue life. While in the case, when the vehicle accelerates at

1.5 m/s^2, the number of stress cycles at low amplitude stress ranges are more as compared to the case when vehicle accelerates at 1 m/s^2, thus decreasing the fatigue life as vehicle acceleration increases, which is observed form Fig. 6.23.

6.5.4.2 Effect of road surface roughness

The effect of road surface roughness on DAF and fatigue life of the plate girder bridge has been studied in this section. The entry vehicle velocity is kept as 20 km/hr and the road surface roughness is varied as good ($S_{GG}(\Omega_0)$ = 32 × 10^{-6} m^2/cycle/m), medium ($S_{GG}(\Omega_0)$ = 120 × 10^{-6} m^2/cycle/m), poor ($S_{GG}(\Omega_0)$ = 512 × 10^{-6} m^2/cycle/m) and very poor ($S_{GG}(\Omega_0)$ = 1024 × 10^{-6} m^2/cycle/m). The arrival rate of the vehicles is 120 vehicles per minute. The mean and standard deviation of flexural stresses at mid span of the middle girder considering uniform and variable vehicle velocity obtained for different road surface roughness is shown in Figs. 6.24 to 6.27. In case of variable velocity, the acceleration of the vehicles is varied as 0.5 m/s^2, 1m/s^2 and 1.5 m/s^2.

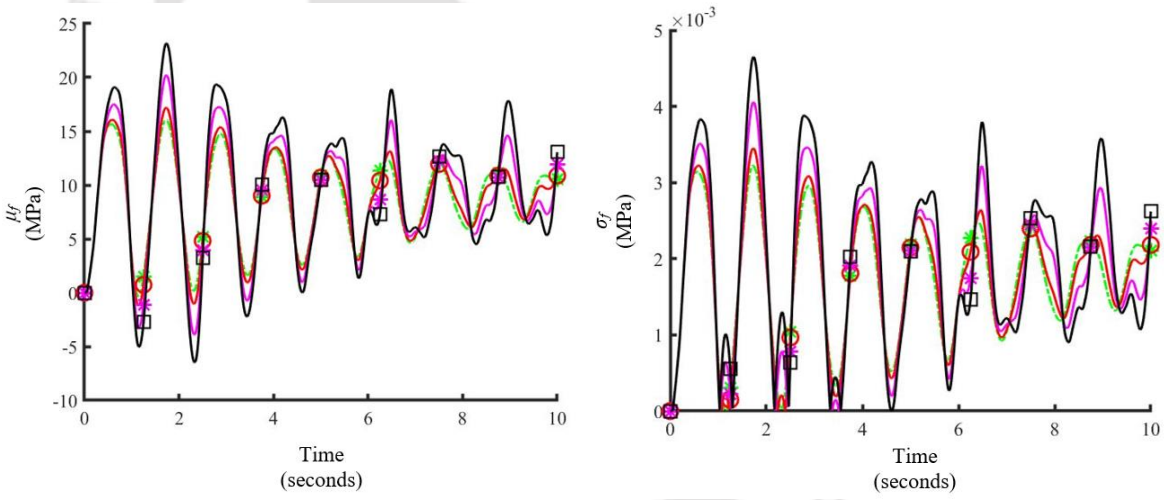

(a) (b)

Fig. 6.24 (a): Mean and (b): standard deviation of flexural stress at mid span of middle girder for uniform vehicle velocity 20 km/hr and arrival rate 120 vehicles per minute

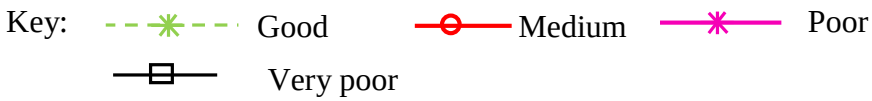

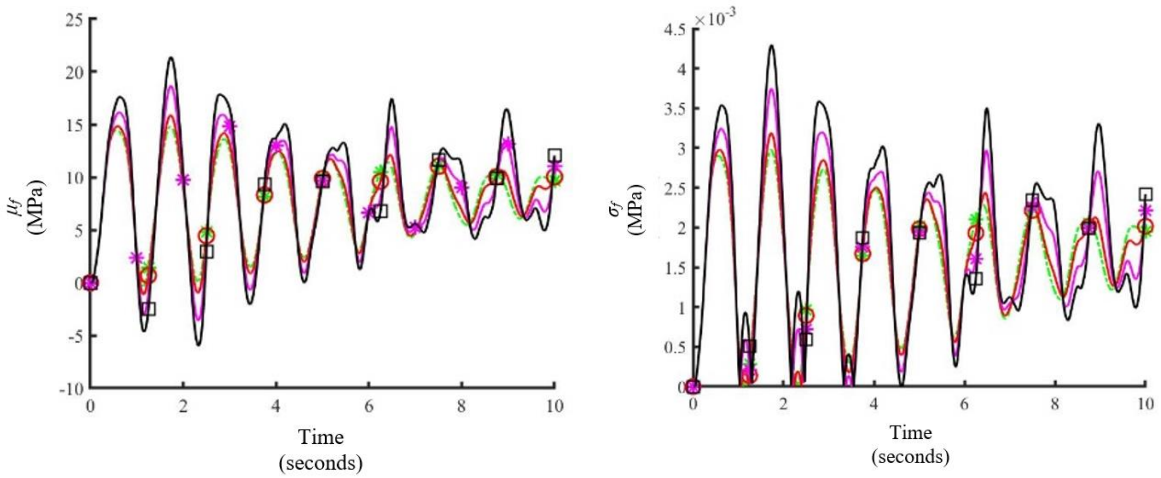

(a) (b)

Fig. 6.25 (a): Mean and (b): standard deviation of flexural stress at mid span of middle girder for entry velocity 20 km/hr and arrival rate 120 vehicles per minute for vehicles moving with 0.5 m/s^2 acceleration

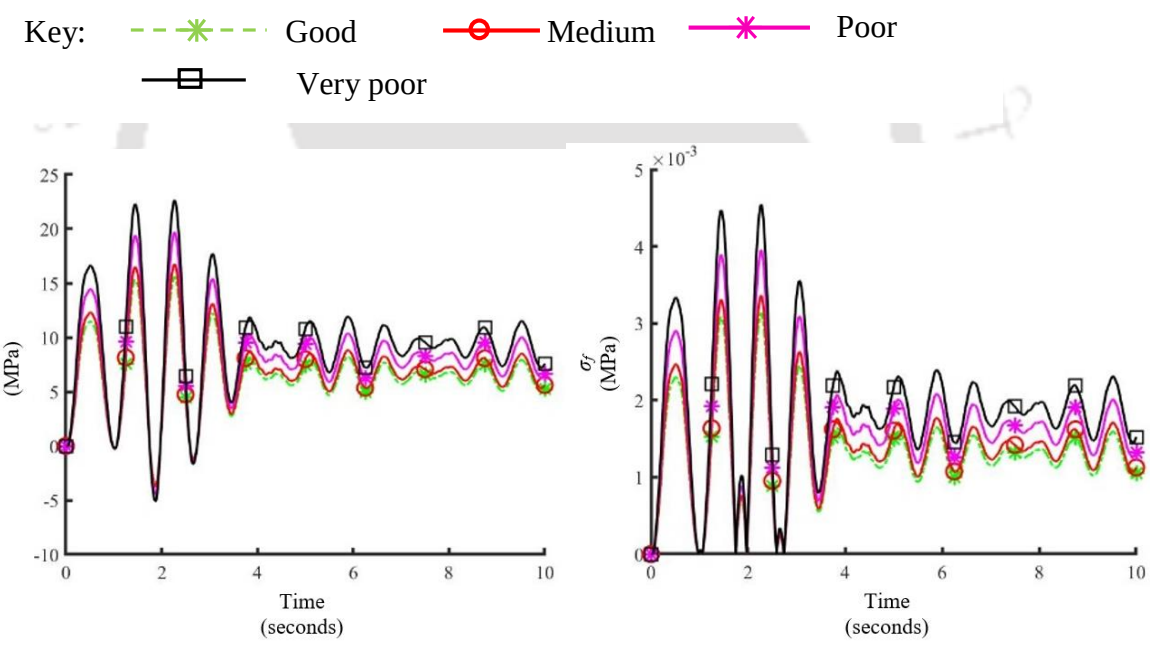

(a) (b)

Fig. 6.26 (a): Mean and (b): standard deviation of flexural stress at mid span of middle girder for entry velocity 20 km/hr and arrival rate 120 vehicles per minute for vehicles moving with 1 m/s^2 acceleration

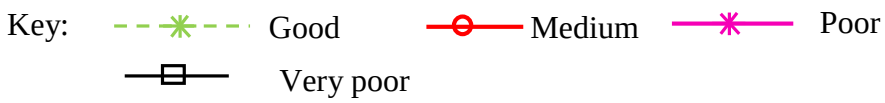

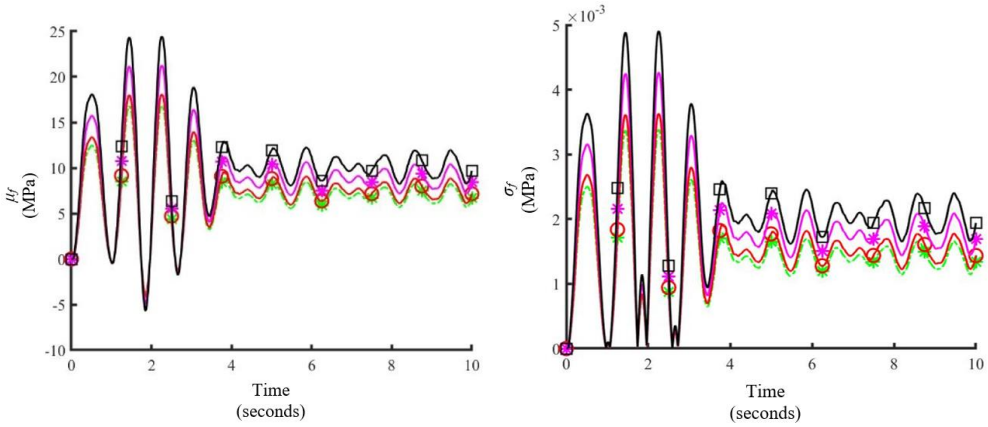

(a) (b)

Fig. 6.27 (a): Mean and (b): standard deviation of flexural stress at mid span of middle girder for entry velocity 20 km/hr and arrival rate 120 vehicles per minute for vehicles moving with 1.5 m/s^2 acceleration

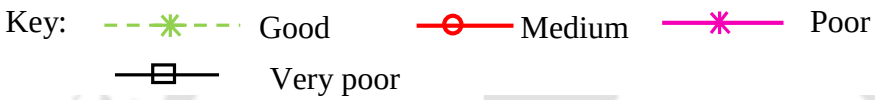

The road surface roughness serves as a source of excitation when the vehicle travels along the bridge (Sun, 2013). The vehicle traversing on a deteriorated road surface generate large excitation force on the bridge leading to large dynamic response (Law and Zhu, 2005). Thus, the mean and standard deviation of the flexural stresses increase with increase in road surface irregularity due to increase in dynamic forces on the bridge as observed in Figs 6.24 to 6.27. The same trend was observed in Coussy et al., (1988), Law and Zhu (2005), Ding et al., (2009) and Wang et al., (2016).

Dynamic Amplification Factor (DAF)

The comparison of DAF for vehicles with entry velocity 20 km/hr and arrival rate 120 vehicles per minute with different road surface irregularities is shown in Fig. 6.28.

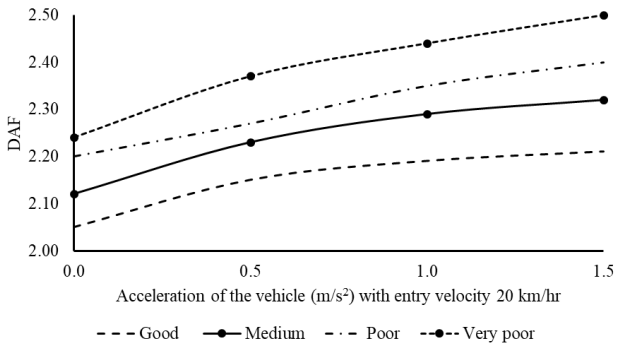

Fig. 6.28 DAF for varying road roughness and acceleration values for vehicles with entry velocity 20 km/hr and arrival rate 120 vehicle per minute

As observed from Fig. 6.28, the DAF increases with increasing road surface irregularity. This is because the dynamic forces due to the vehicular loads increase with increasing road surface irregularity contributing to higher DAF (Inbanthan and Wieland, 1987; Chang and Lee, 1994; Ding et al., 2009; Ho and Nishio, 2020).

Fatigue Life

The stress range histogram and fatigue life for varying road roughness for vehicles with entry velocity 20 km/hr and arrival rate 120 vehicles per minute is shown in Figs. 6.29 to 6.33. The stress range histogram and fatigue life is obtained for uniform and variable vehicle velocity.

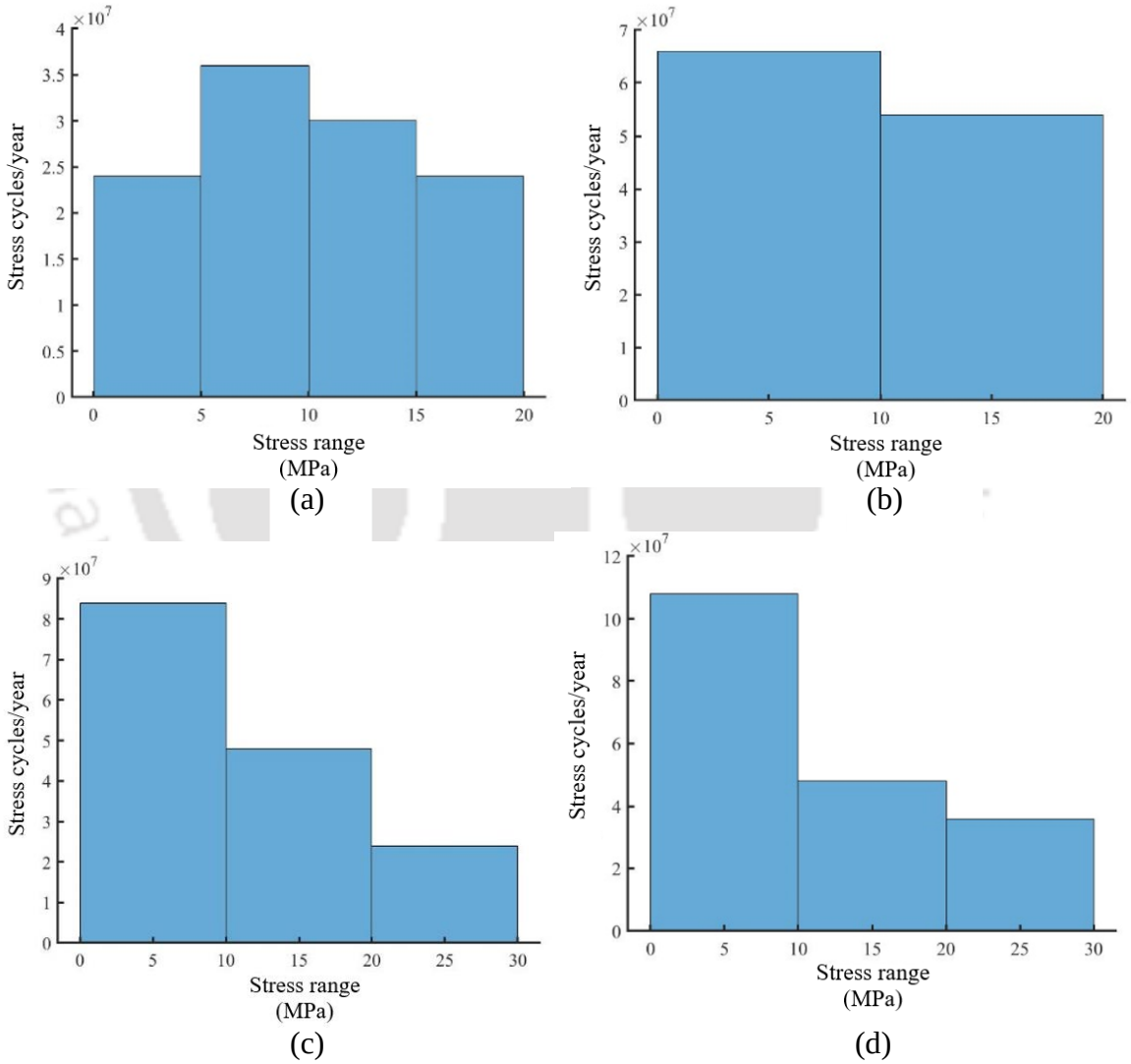

Fig. 6.29 Stress range histogram: (a): good road (b): medium road (c): poor road (d): very poor road for uniform vehicle velocity 20 km/hr and arrival rate 120 vehicles per minute

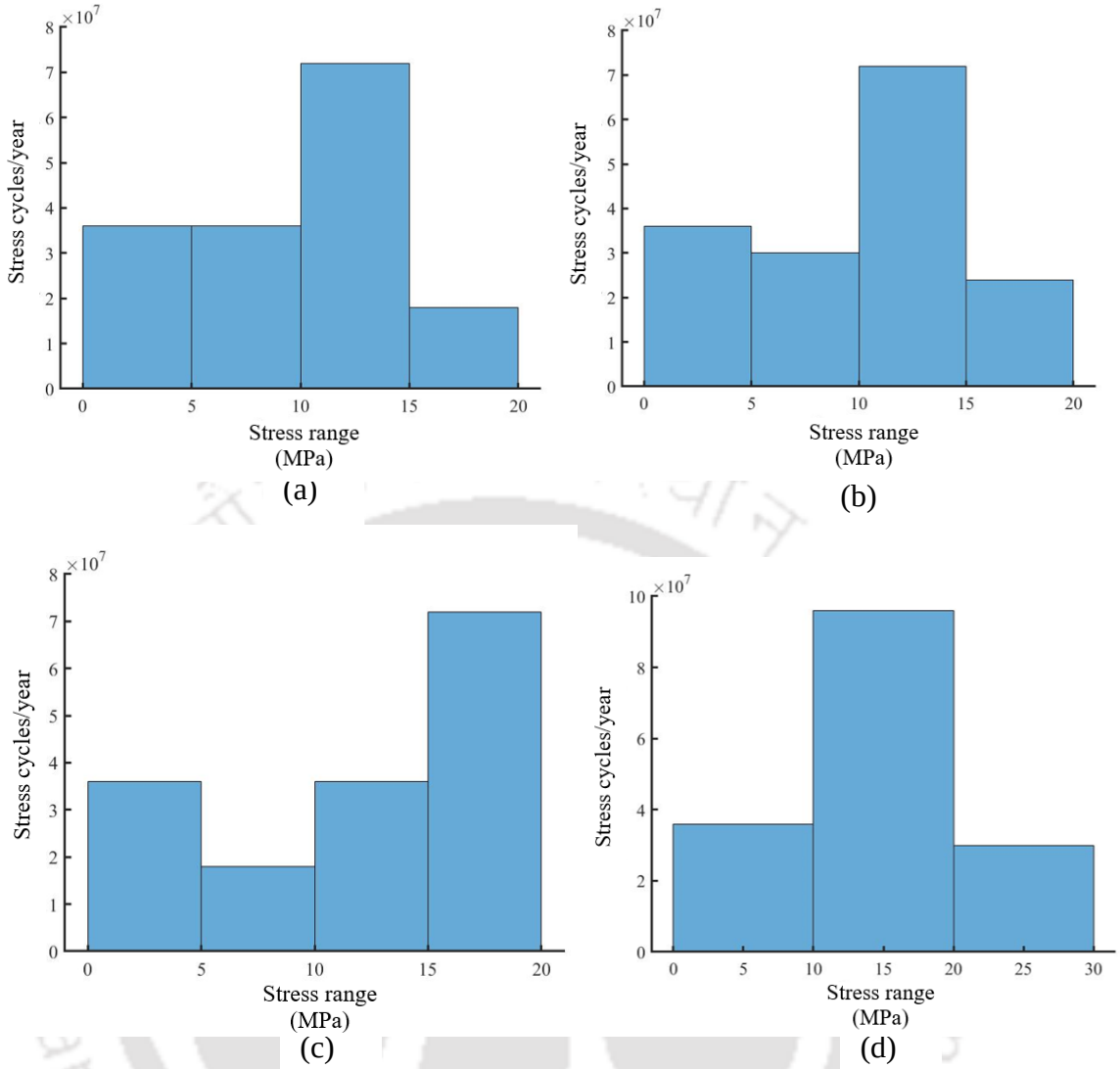

Fig. 6.30 Stress range histogram: (a): good road (b): medium road (c): poor road (d): very poor road for vehicle entry velocity 20 km/hr and arrival rate 120 vehicles per minute for vehicle acceleration 0.5 m/s^2

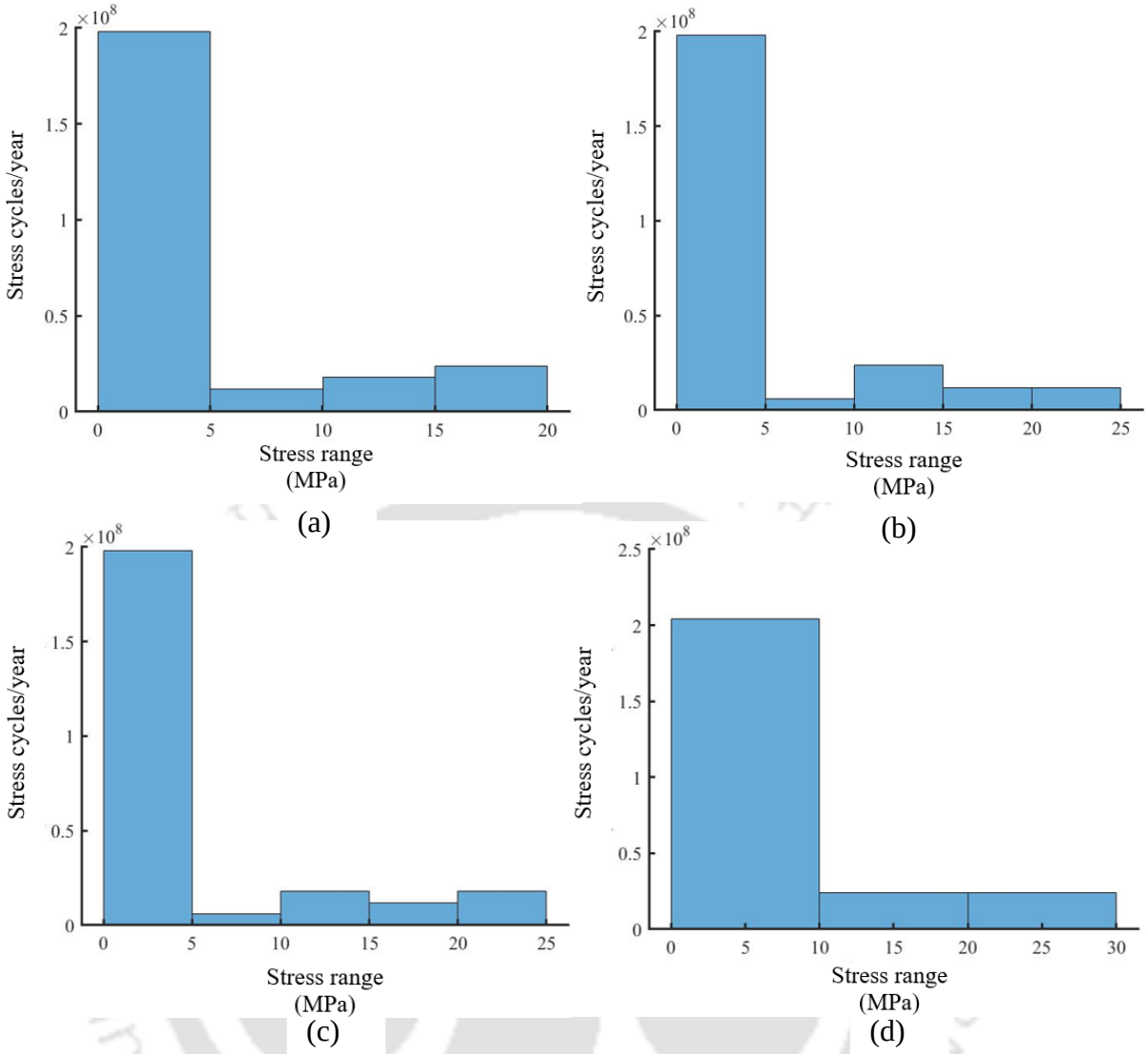

Fig. 6.31 Stress range histogram: (a): good road (b): medium road (c): poor road (d): very poor road for vehicle entry velocity 20 km/hr and arrival rate 120 vehicles per minute for vehicle acceleration 1 m/s^2

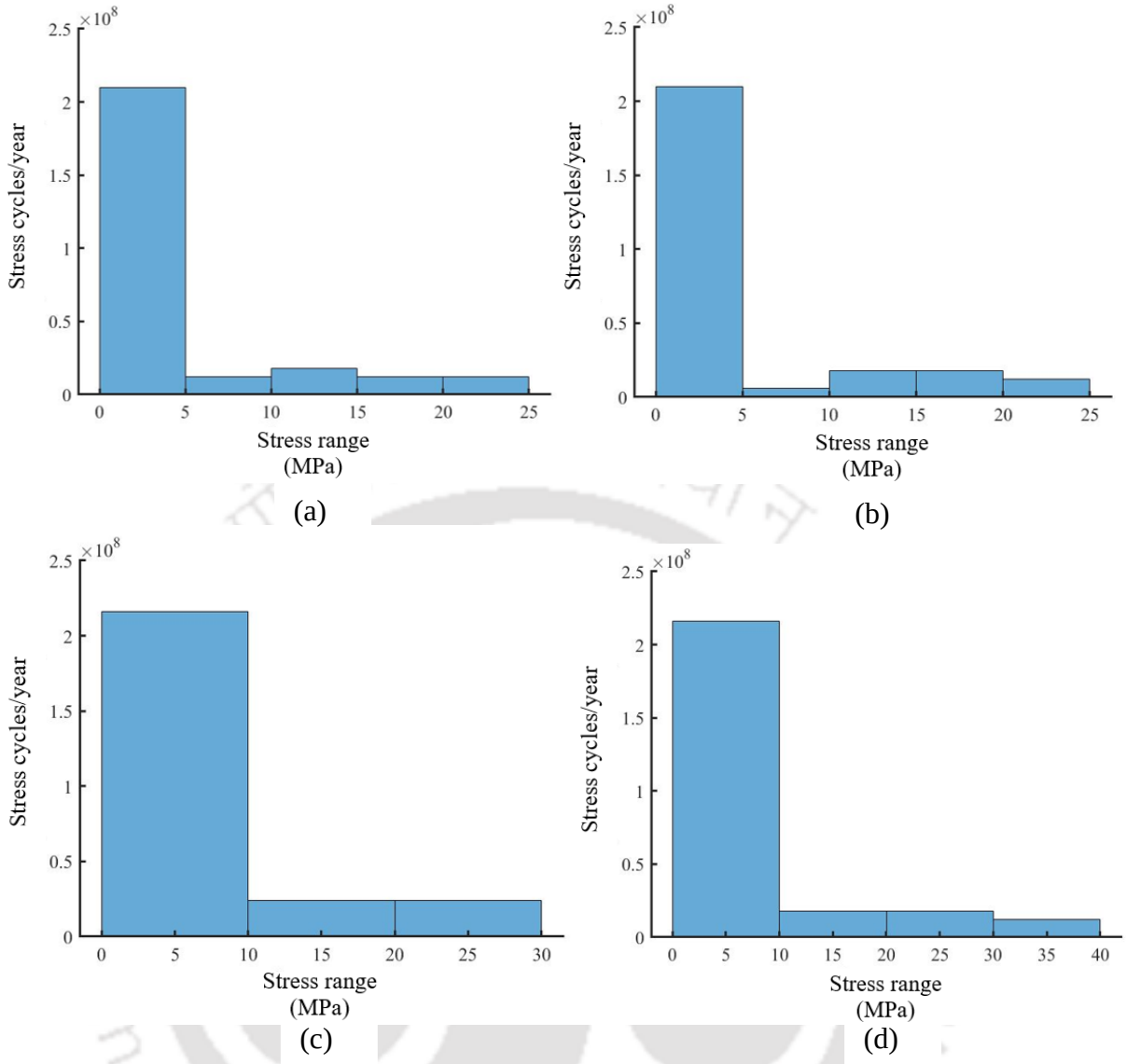

Fig. 6.32 Stress range histogram: (a): good road (b): medium road (c): poor road (d): very poor road for vehicle entry velocity 20 km/hr and arrival rate 120 vehicles per minute for vehicle acceleration 1.5 m/s^2

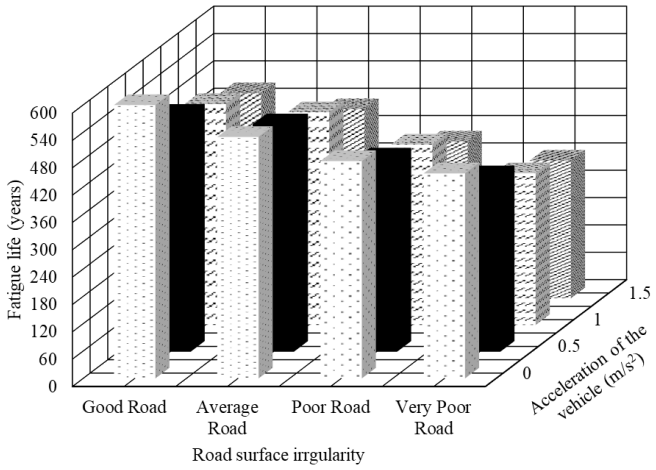

Fig. 6.33 Comparison of fatigue life with different road surface irregularities

The road surface roughness varies from good to very poor due to increase in the magnitude of road roughness coefficient. The moving vehicles exert fluctuating forces on the bridge caused due to vibration resulting from road surface roughness. These fluctuating nature of the dynamic vehicular load increase with the increase in number of load repetitions as the road surface deteriorates. This increases the dynamic stresses caused due to vehicle vibration on the bridge. The road surfaces that have been in-service for some time often develop localized distresses due to application of heavy vehicle load and environmental changes and lead to deterioration of road surfaces and fatigue damage accumulation. This fact can be attributed to the random numbers used to simulate road roughness, which is associated with high and low values reflecting discrete source of excitation, leading to produce stress concentration at weaker location. Thus, it is observed from Figs. 6.29 to 6.32 that the number of stress cycles in the lower stress range increases as the road surface roughness increases from good to very poor. The stress ranges are subjected to higher stress cycles for very poor road case leading to more damage accumulation as compared to good, medium and poor road case, which is observed from Figs. 6.29 to 6.32. Thus, the fatigue life of the bridge decreases with increasing road surface irregularity as shown in Fig. 6.33. It is observed that the increase in road roughness can damage the bridge by fatigue since the fatigue phenomenon of the bridge is closely related to the transverse movement. It is also observed that with the increase in entry velocity of the vehicle, road surface roughness and arrival rate of the vehicles, the crack initiation phase is reduced and the crack propagation phase is increased. The increase in the rate of crack propagation leads to higher fatigue damage leading to lower fatigue life of the bridge.

6.5.4.3 Effect of arrival rate of vehicles

The arrival rate of the vehicles is varied to observe the effect on DAF and fatigue life. The arrival rate of the vehicles is varied as 60 vehicles per minute, 90 vehicles per minute, 120 vehicles per minute, 150 vehicles per minute and 180 vehicles per minute. The vehicle velocity is 20 km/hr and the vehicles are assumed to travel with uniform and variable velocity. The acceleration of the vehicles is varied as 0.5 m/s^2, 1 m/s^2 and 1.5 m/s^2, in case of variable velocity. The road case considered is very poor ($S_{GG}(\Omega_0) = 1024 \times 10^{-6}$ m^2/cycle/m). The mean and standard deviation of the flexural stresses for varying arrival rate is shown in Figs 6.34 to 6.37.

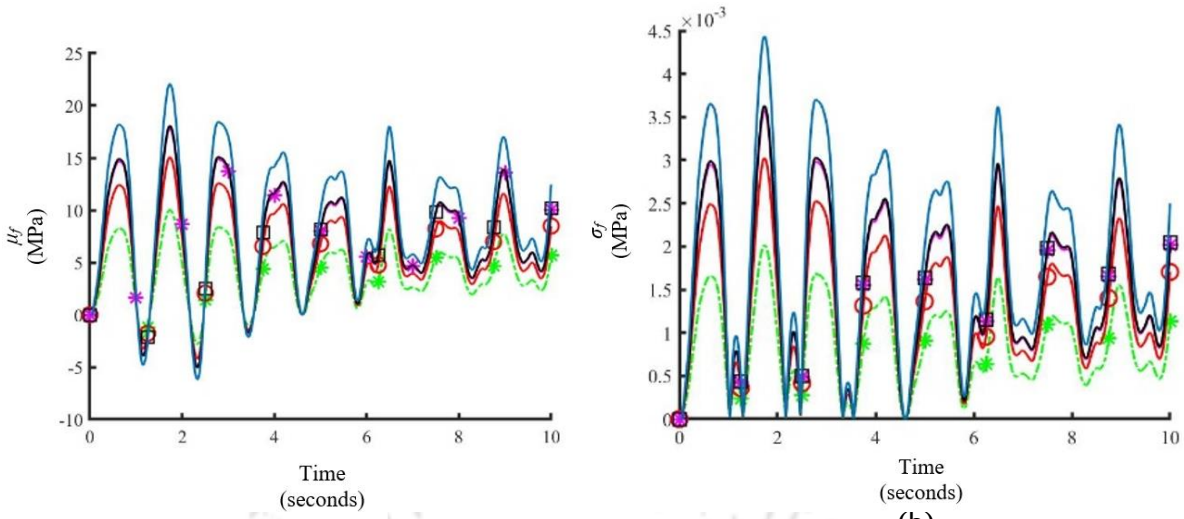

(a) (b)

Fig. 6.34 (a): Mean and (b): standard deviation of flexural stress at mid span of the middle girder for different arrival rate for uniform vehicle velocity 20 km/hr ($S_{GG}(\Omega_0) = 1024 \times 10^{-6}$ m^2/cycle/m)

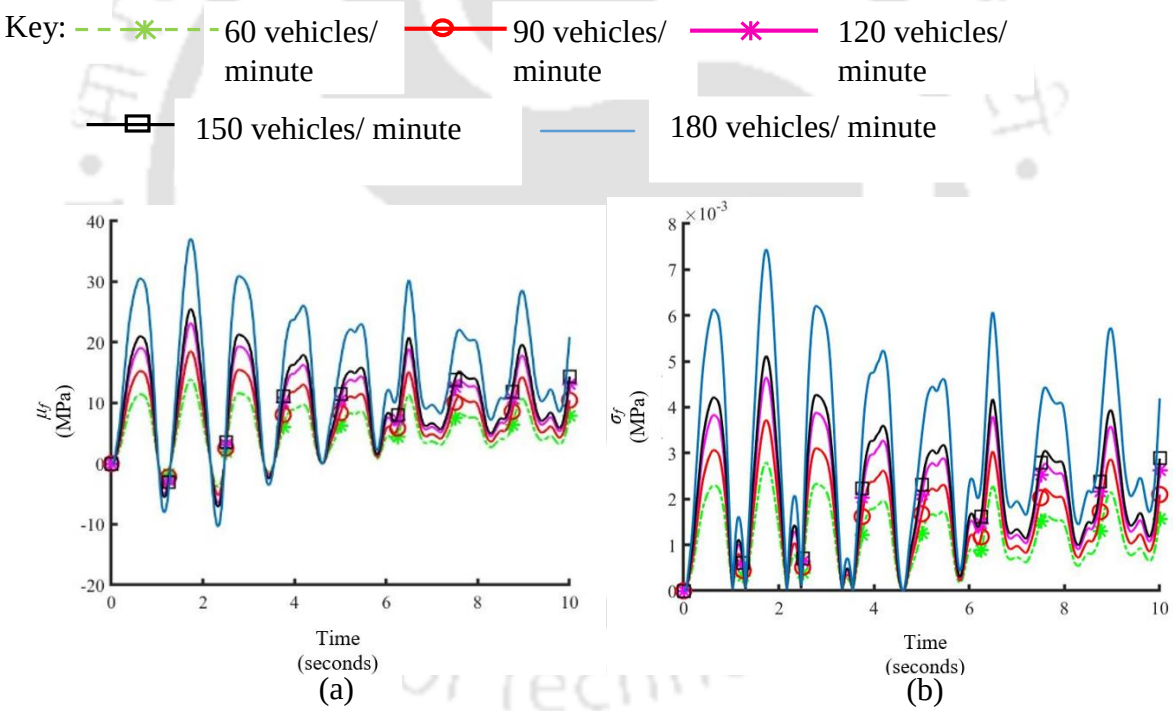

(a) (b)

Fig. 6.35 (a): Mean and (b): standard deviation of flexural stress at mid span of the middle girder for different arrival rate for vehicle entry velocity 20 km/hr and vehicle acceleration 0.5 m/s^2 ($S_{GG}(\Omega_0) = 1024 \times 10^{-6}$ m^2/cycle/m)

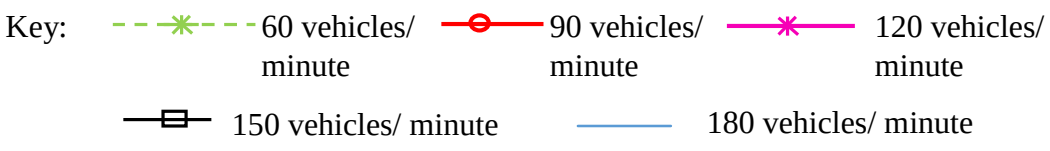

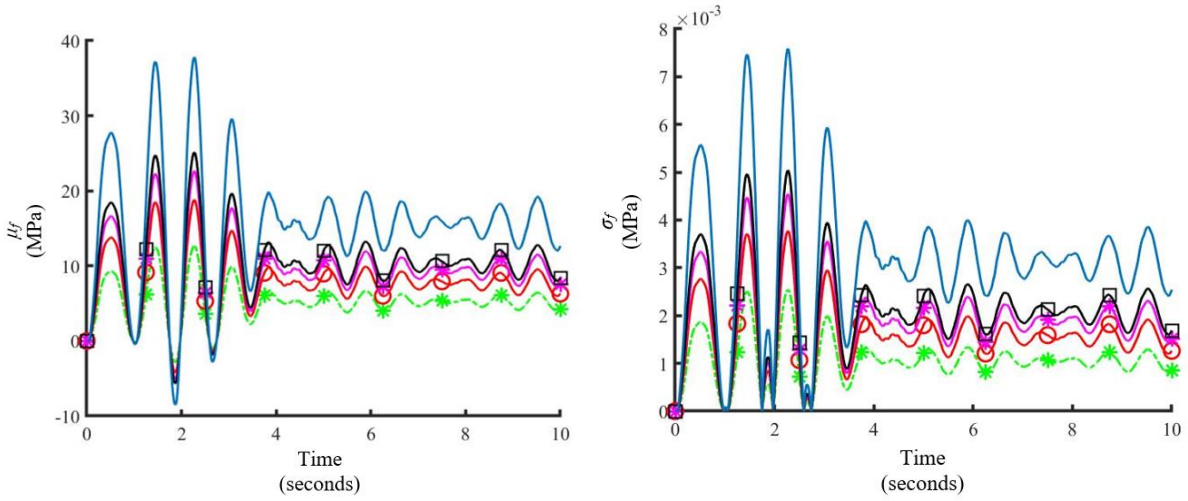

(a) (b)

Fig. 6.36 (a): Mean and (b): standard deviation of flexural stress at mid span of the middle girder for different arrival rate for vehicle entry velocity 20 km/hr and vehicle acceleration 1 m/s^2 ($S_{GG}(\Omega_0)$ = 1024 × 10^{-6} m^2/cycle/m)

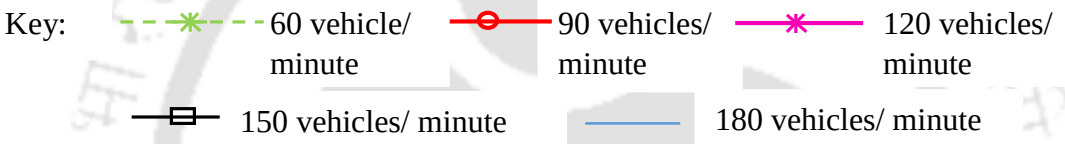

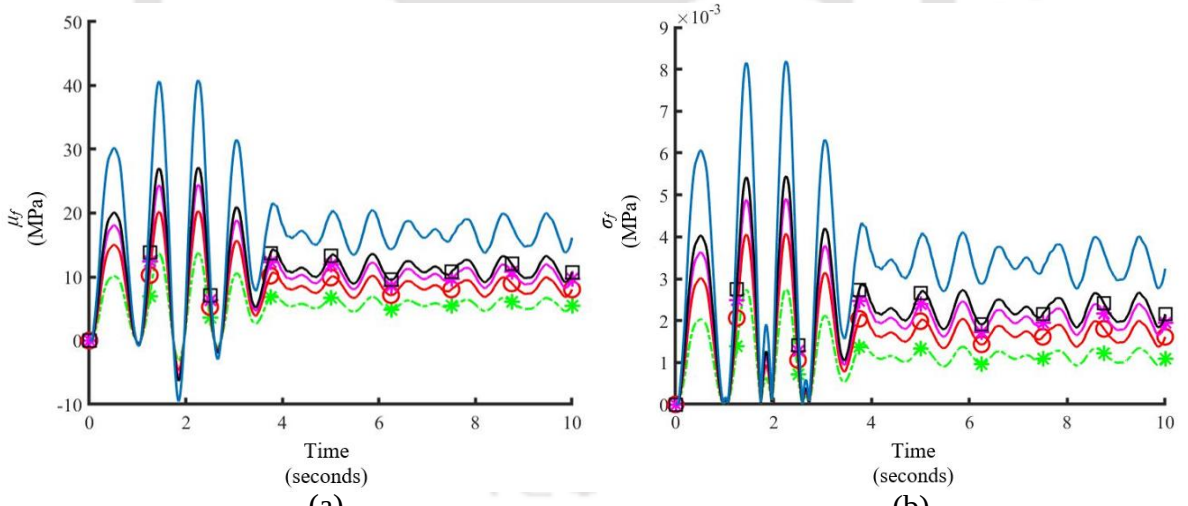

(a) (b)

Fig. 6.37 (a): Mean and (b): standard deviation of flexural stress at mid span of the middle girder bridge for different arrival rate for vehicle entry velocity 20 km/hr and vehicle acceleration 1.5 m/s^2 ($S_{GG}(\Omega_0)$ = 1024 × 10^{-6} m^2/cycle/m)

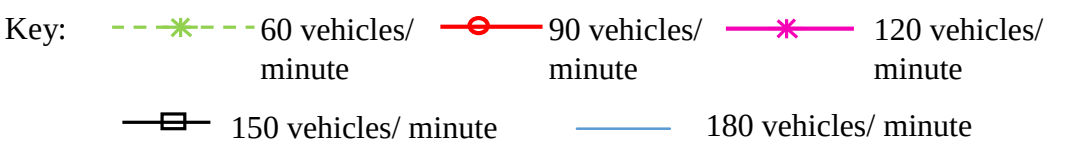

The randomness of traffic flow i.e., traffic volume per unit time is represented by the arrival rate of the vehicles. The arrival rate signifies the number of vehicles traversing on the bridge. Numerous transient responses occur due to each vehicle traversing the bridge as per the arrival rate of the vehicles (Ho and Nishio, 2020). Increase in arrival rate signifies higher traffic volume which implies increased vehicular movement on the bridge leading to higher dynamic stresses, which can be observed from Figs. 6.34 to 6.37.

Dynamic Amplification Factor (DAF)

The DAF for different arrival rate and acceleration of the vehicle for entry velocity 20 km/hr, 40 km/hr and 60 km/hr is shown in Figs. 6.38 to 6.40. The road case considered is very poor ($S_{GG}(\Omega_0) = 1024 \times 10^{-6}$ m^2/cycle/m).

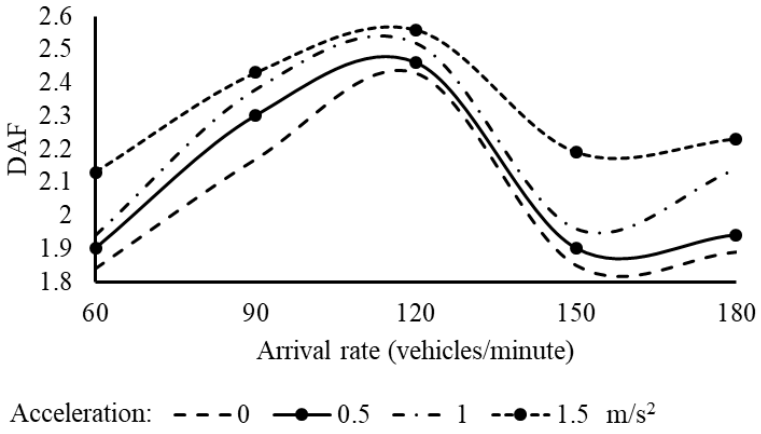

Fig. 6.38 DAF for varying arrival rate and acceleration of the vehicle for entry velocity 20 km/hr for very poor road

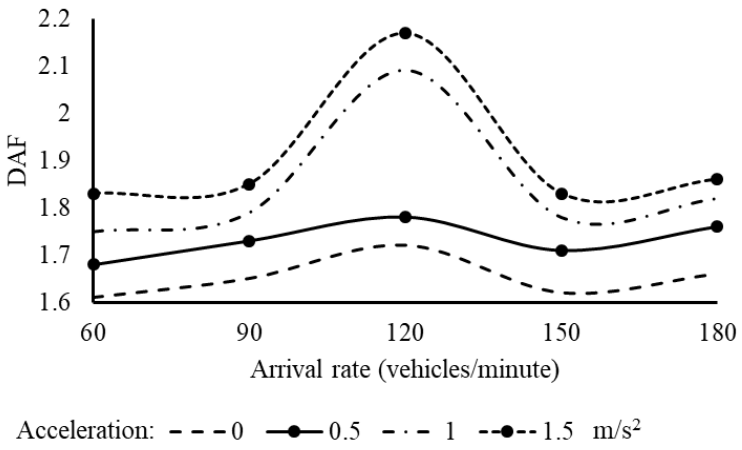

Fig. 6.39 DAF for varying arrival rate and acceleration of the vehicle for entry velocity 40 km/hr for very poor road

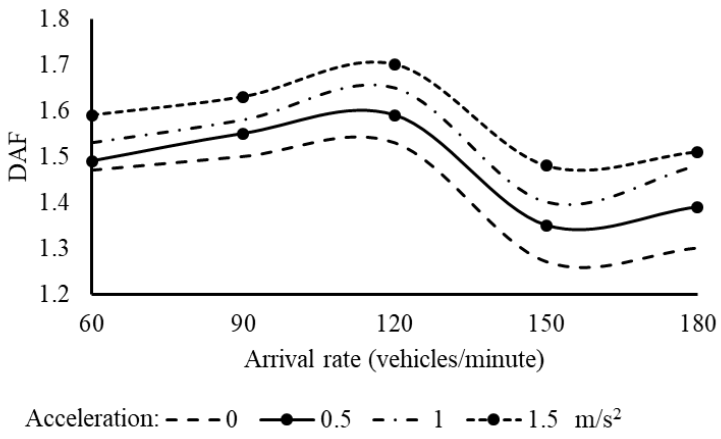

Fig. 6.40 DAF for varying arrival rate and acceleration of the vehicle for entry velocity 60 km/hr for very poor road

It is observed from Figs. 6.38 to 6.40 that the DAF increases for arrival rate upto 120 vehicles per minute and then decreases further. Increased arrival rate indicates increased traffic flow on the bridge. However, with the increase in arrival rate, the static stresses due to vehicular movement also increases in addition to the dynamic stresses, which becomes dominant for arrival rates greater than 120 vehicles per minute. This leads to reduction in DAF for arrival rates greater than 120 vehicles per minute. It is also observed from Figs. 6.38 to 6.40, the traffic flow decreases with the increased vehicle velocity since, the acting time of the vehicular loads on the bridge decreases with the increase in arrival rate. This leads to reduction in DAF with increase in vehicle velocity.

Fatigue life

The stress range histograms for varying arrival rate for 20 km/hr vehicle entry velocity and very poor road case are shown in Figs. 6.41 to 6.44. The stress range histograms for constant and variable velocity is also obtained. The comparison of fatigue life with varying arrival rate and acceleration of the vehicle for entry velocity 20 km/hr, 40 km/hr and 60 km/hr are shown in Figs. 6.45 to 6.47.

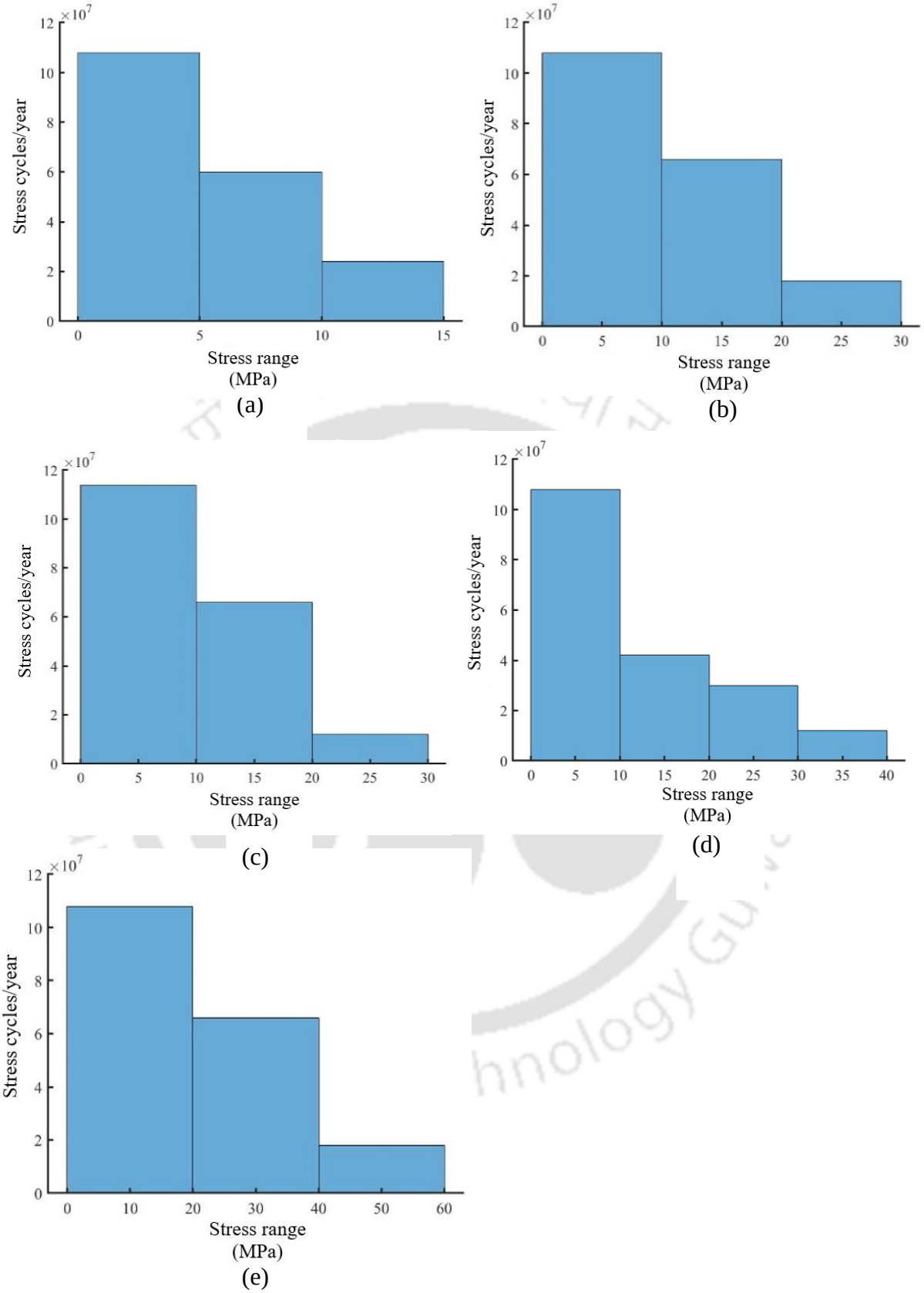

Fig. 6.41 Stress range histogram: (a): 60 vehicles per minute (b): 90 vehicles per minute (c): 120 vehicles per minute (d): 150 vehicles per minute (e): 180 vehicles per minute for uniform vehicle velocity 20 km/hr

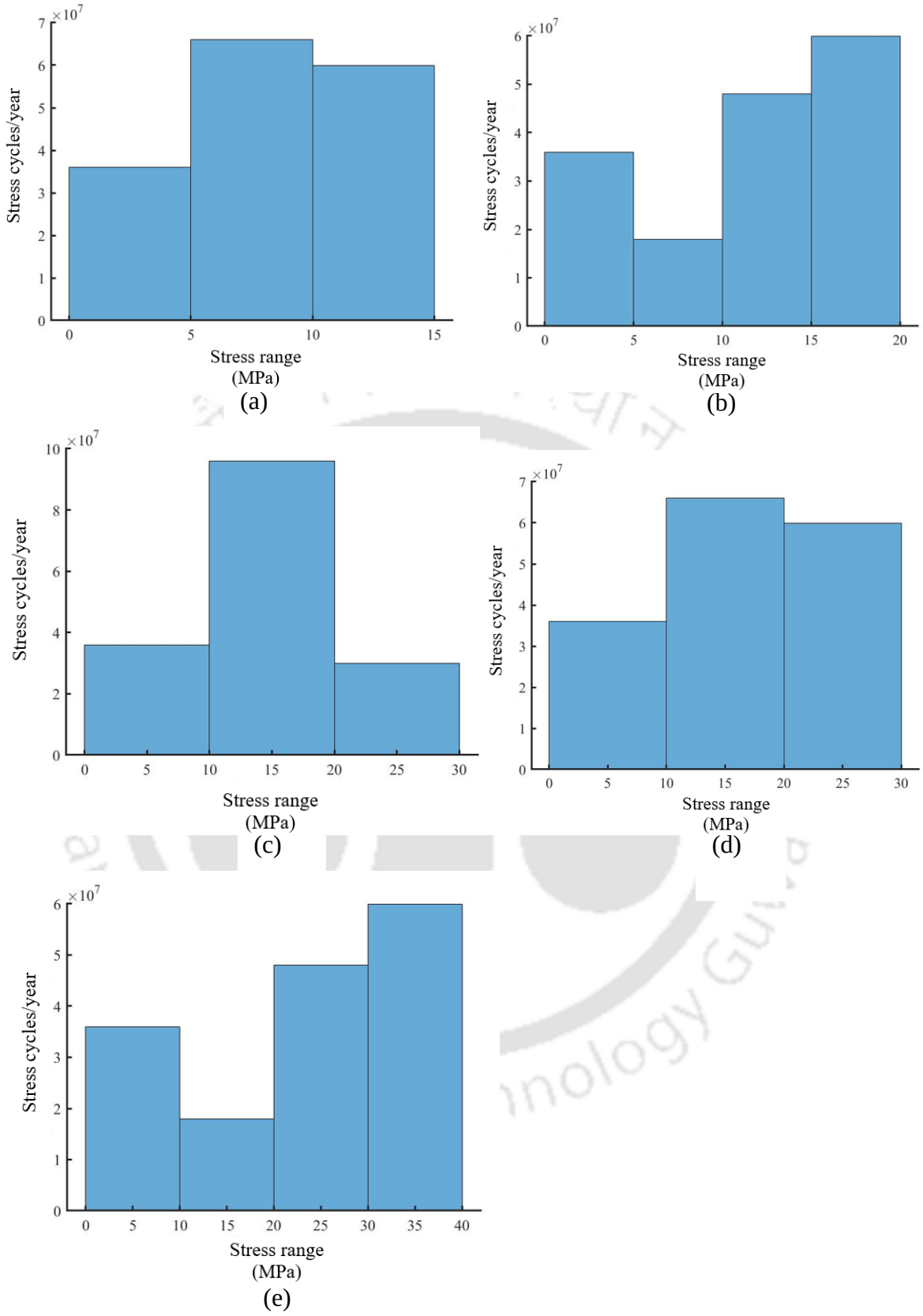

Fig. 6.42 Stress range histogram: (a): 60 vehicles per minute (b): 90 vehicles per minute (c): 120 vehicles per minute (d): 150 vehicles per minute (e): 180 vehicles per minute for entry velocity 20 km/hr and vehicle acceleration 0.5m/s^2

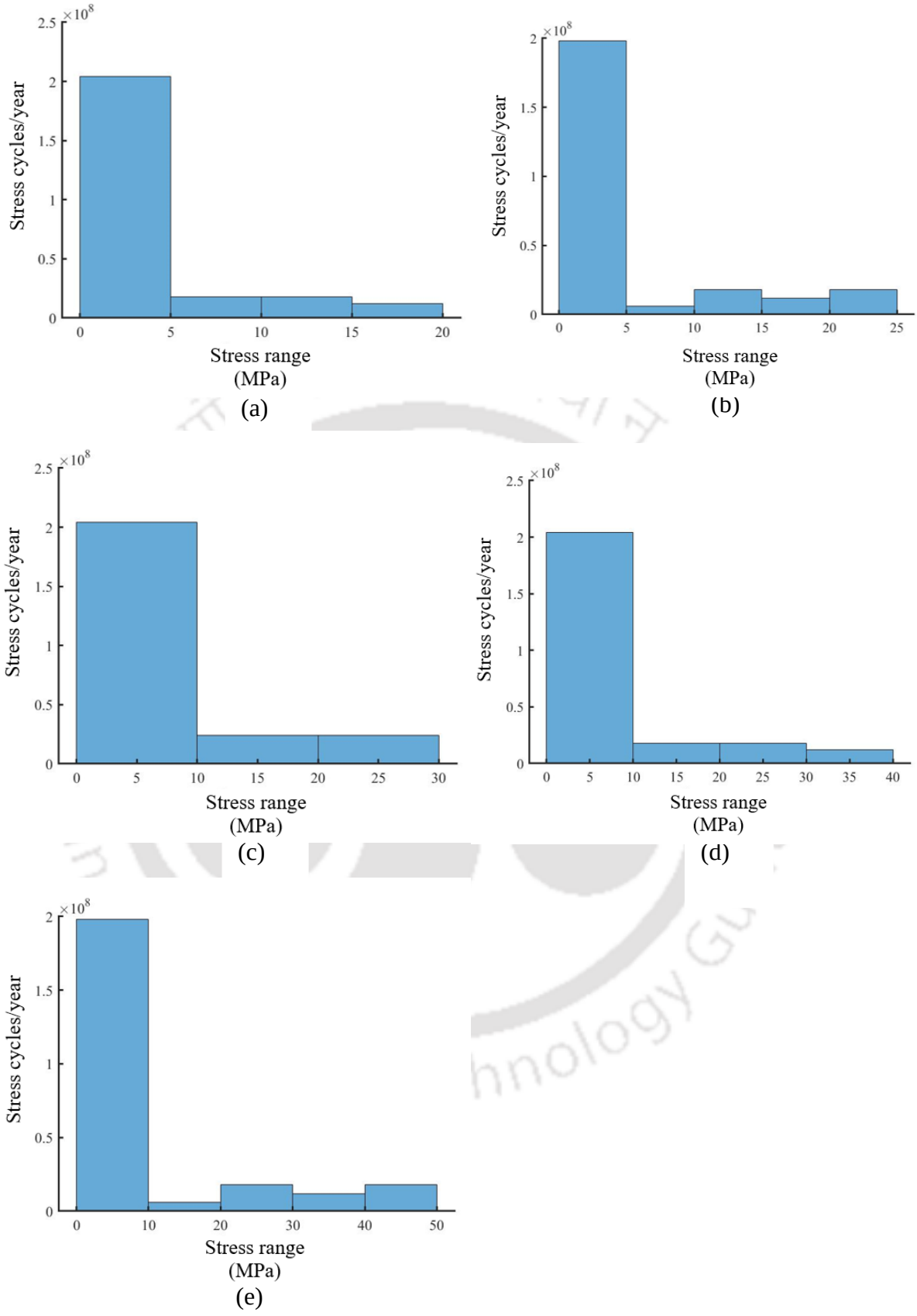

Fig. 6.43 Stress range histogram: (a): 60 vehicles per minute (b): 90 vehicles per minute (c): 120 vehicles per minute (d): 150 vehicles per minute (e): 180 vehicles per minute for entry velocity 20 km/hr and vehicle acceleration 1 m/s^2

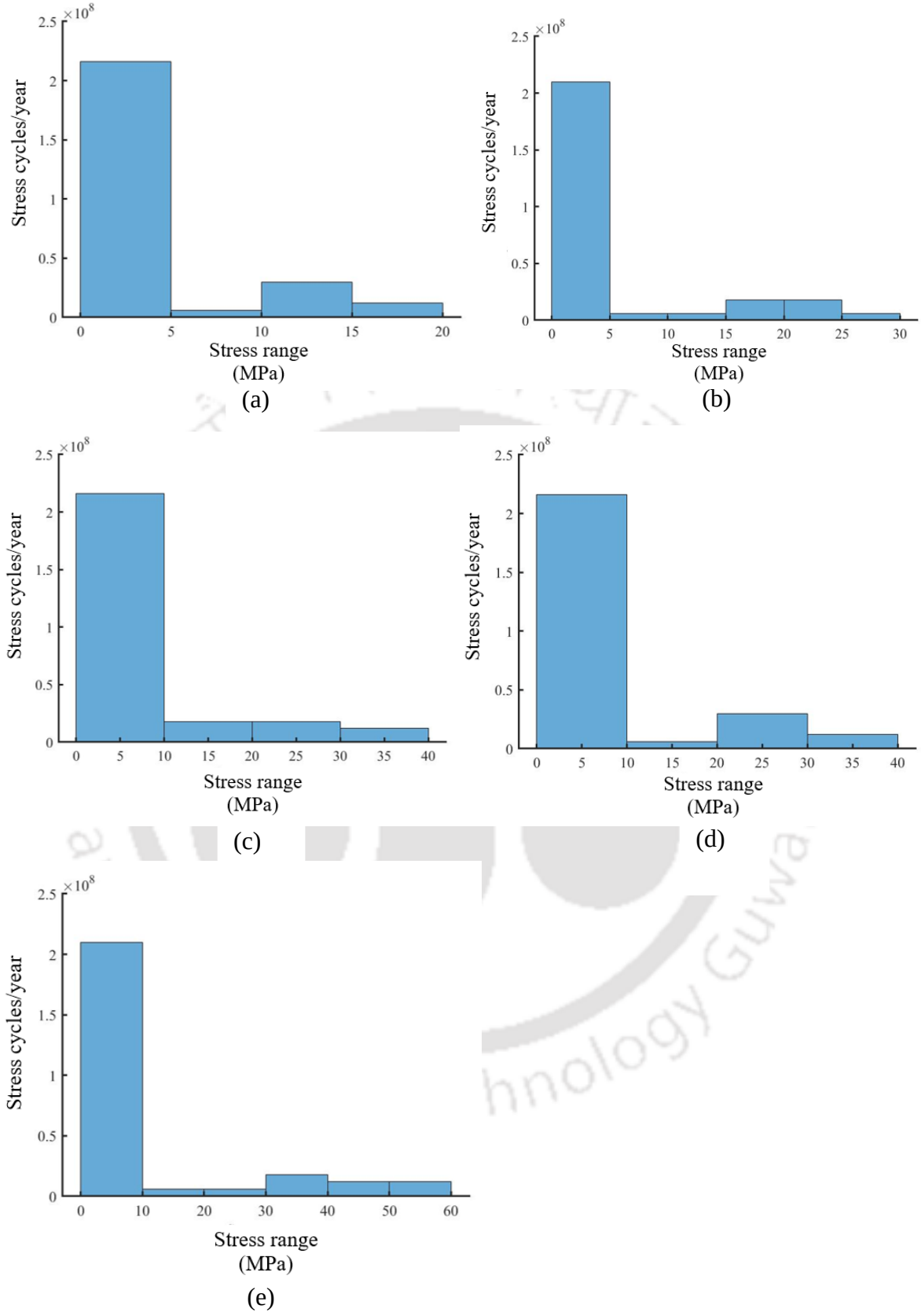

Fig. 6.44 Stress range histogram: (a): 60 vehicles per minute (b): 90 vehicles per minute (c): 120 vehicles per minute (d): 150 vehicles per minute (e): 180 vehicles per minute for entry velocity 20 km/hr and vehicle acceleration 1.5 m/s^2

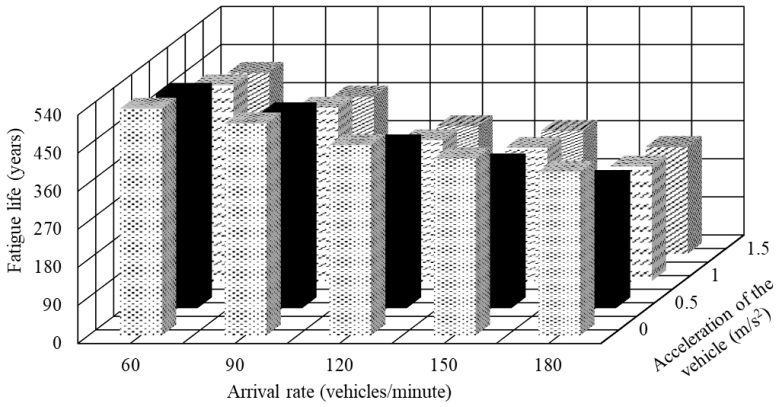

Fig. 6.45 Fatigue life for varying arrival rate and acceleration of the vehicle for entry velocity 20 km/hr for very poor road

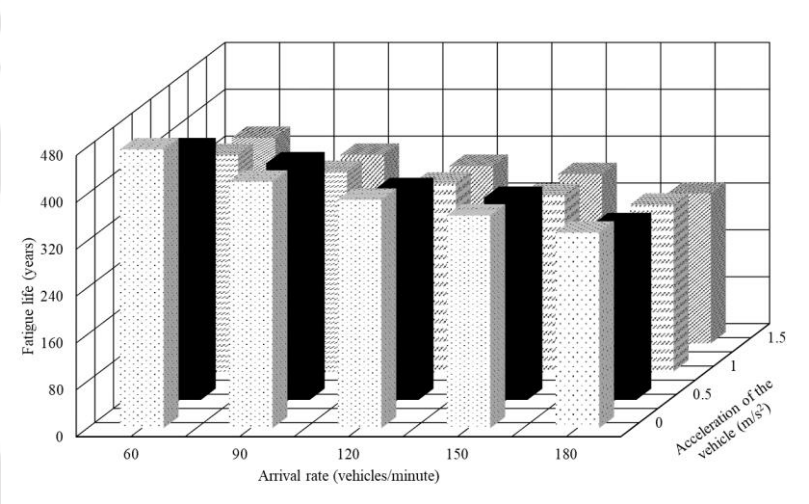

Fig. 6.46 Fatigue life for varying arrival rate and acceleration of the vehicle for entry velocity 40 km/hr for very poor road

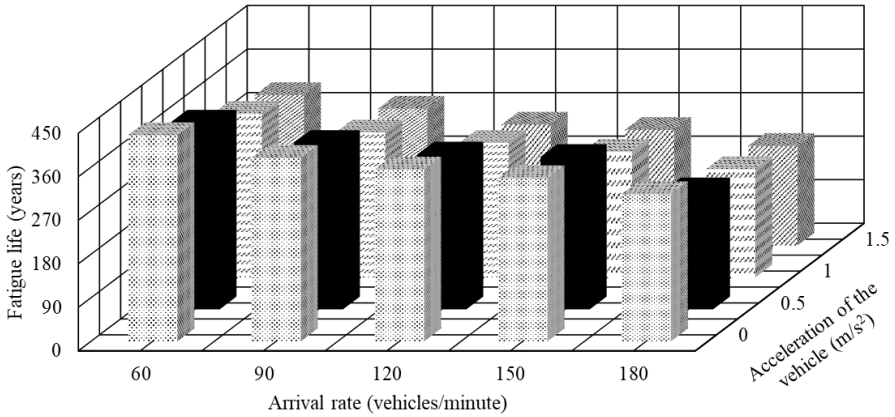

Fig. 6.47 Fatigue life for varying arrival rate and acceleration of the vehicle for entry velocity 60 km/hr for very poor road

The actual traffic flow can be divided into a dense state and sparse state. The randomness of traffic flow has been characterised by the parameter, arrival rate. The dense state of the traffic flow corresponds to higher arrival rate and sparse state of the traffic flow corresponds to lower arrival rate. Higher arrival rate of the vehicles indicates that maximum vehicles are present on the bridge and lower arrival rate indicates that less vehicles are present on the bridge. Since the arrival rate increases, more vehicles traverse the bridge leading to increase in dynamic force on the bridge. The number of stress cycles and the magnitude of stress range depends on the intensity and composition of traffic loads. It is also observed that the traffic load on the bridge will change over the lifetime of the bridge. Thus, multiple vehicles present on the bridge amplifies the stress range and increases the number of stress cycles. This leads to grater fatigue damage than that caused by a single vehicle (Fu et al., 2013). The bridge is subjected to higher stress cycles at lower and higher stress range with increase in arrival rate as observed from Figs. 6.41 to 6.44. The fatigue life decreases as the arrival rate of the vehicles increases which is observed from Figs. 6.45 to 6.47. It is also observed from Figs. 6.45 to 6.47 that the fatigue life decreases with the increase in vehicle velocity and acceleration of the vehicle. Thus, it is observed that since, fatigue is a time relevant issue, the time variant factors should be considered which includes the traffic growth on the bridge. The traffic growth on the bridge is represented by the factor arrival rate of the vehicles.

6.5.4.4 Effect of eccentricity of load

In the previous parametric study, the vehicle movement is on the centre lane of the bridge due to which the middle girder is subjected to higher flexural stresses as compared to the outer girder. The vehicle movement is shifted on the extreme lane to observe the effect on DAF and fatigue life. The velocity of the vehicle is considered to be uniform and is taken as 20 km/hr and arrival rate is considered as 120 vehicles per minute. The movement of multiple vehicles is considered. The pre-camber of the road is also considered along with the road roughness. The road roughness is taken as very poor and the magnitude of road roughness coefficient, $S_{GG}(\Omega_0)$ is 1024×10^{-6} m^2/cycle/m. The mean and standard deviation of flexural stresses for vehicles moving on the exterior lane is shown in Fig. 6.48.

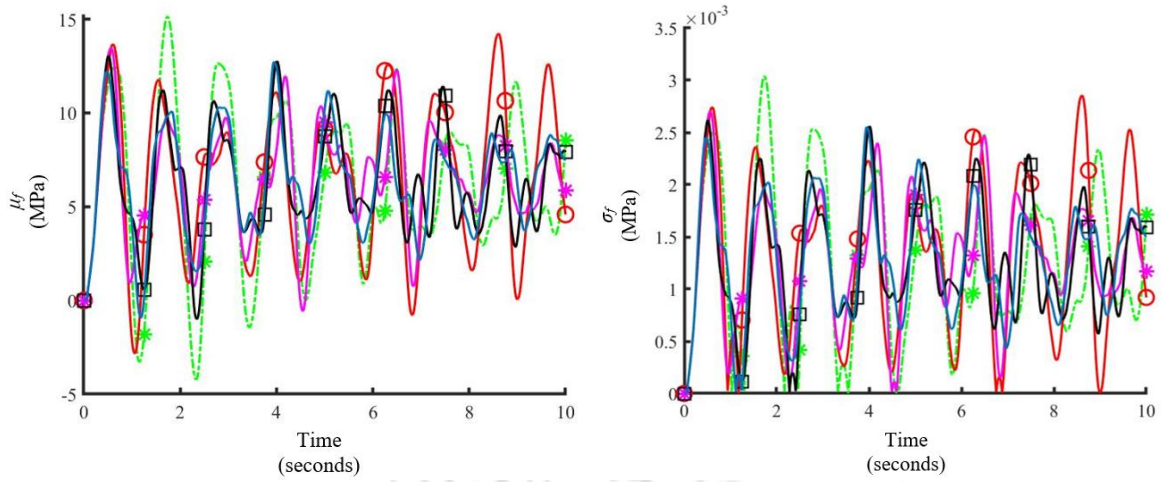

Fig. 6.48 (a): Mean and (b): standard deviation of flexural stress when the vehicle is moving on the extreme lane with uniform vehicle velocity 20 km/hr and arrival rate 120 vehicles per minute for very poor road

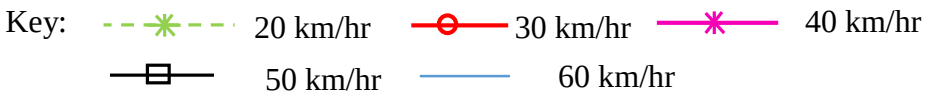

As observed from Fig. 6.48, the mean and standard deviation of the flexural stresses are higher on the extreme girder as compared to that of central girder (see Fig. 6.14). Since, the vehicles are moving on the extreme lane, the eccentric movement of the vehicle is causing higher flexural stresses on the extreme girder, which is observed from the Fig. 6.48. The flexural stress decreases with the increase in vehicle velocity. The average number of loads moving on the bridge decreases with the increase in vehicle velocity leading to lower flexural stress, as observed from Fig. 6.48.

Dynamic Amplification Factor (DAF)

The DAF for varying arrival rate and acceleration of the vehicle for entry velocities 20 km/hr, 40 km/hr and 60 km/hr are shown in Figs. 6.49 to 6.51. The acceleration of the vehicle is varied as 0.5 m/s^2, 1m/s^2 and 1.5 m/s^2. The road roughness considered is very poor ($S_{GG}(\Omega_0)$ = 1024 $\times$ 10^{-6} m^2/cycle/m). The pre-camber of the road is also considered. The arrival rate of vehicle is varied as 60 vehicles per minute, 90 vehicles per minute, 120 vehicles per minute, 150 vehicles per minute and 180 vehicles per minute.

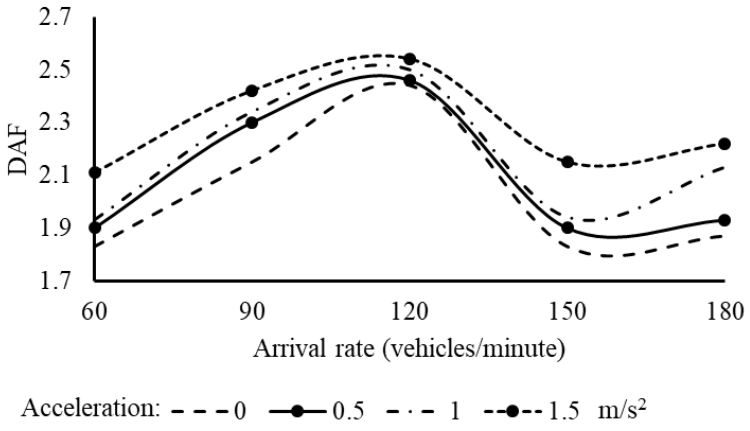

Fig. 6.49 DAF for varying arrival rate and acceleration of the vehicle for entry velocity 20 km/hr for very poor road

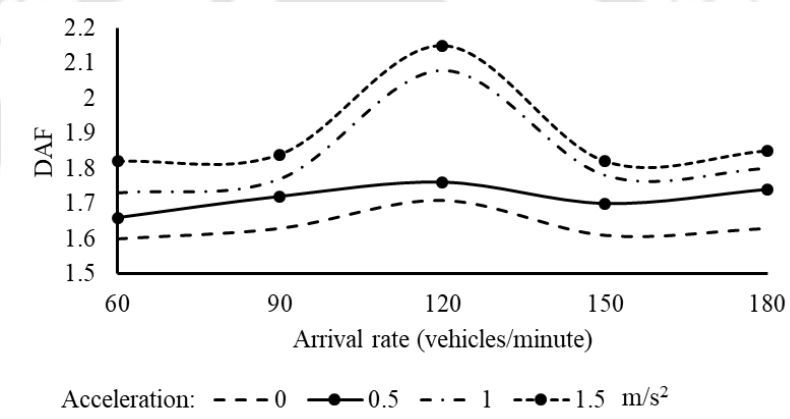

Fig. 6.50 DAF for varying arrival rate and acceleration of the vehicle for entry velocity 40 km/hr for very poor road

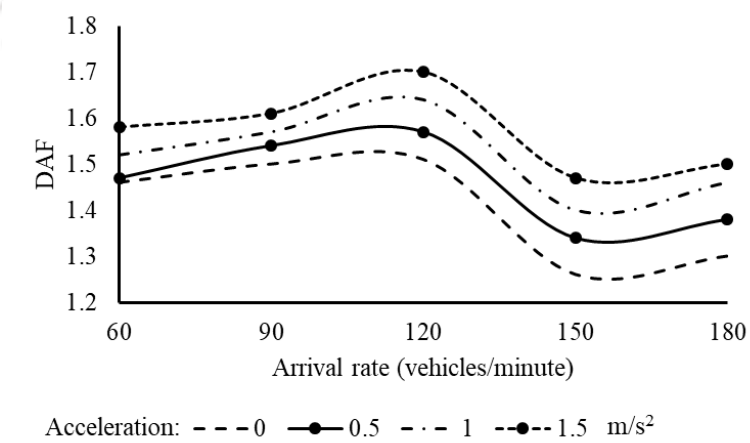

Fig. 6.51 DAF for varying arrival rate and acceleration of the vehicle for entry velocity 60 km/hr for very poor road

It is observed from Figs. 6.49 to 6.51, that the DAF decreases with increasing vehicle velocity. The DAF increases for arrival rate upto 120 vehicles per minute and then gradually decreases as the arrival rate increases. The variation is similar to that observed in the case of the middle girder. The static stresses play a significant role for higher arrival rates leading to lower DAF as observed from Figs. 6.49 to 6.51. The increase in the dynamic stresses with the increase in the acceleration of the vehicle causes the DAF to increase, which is observed from Figs. 6.49 to 6.51.

Fatigue Life

The comparison of fatigue life with arrival rate and acceleration of the vehicle for entry velocities 20 km/hr, 40 km/hr and 60 km/hr are shown in Figs. 6.52 to 6.54. The road roughness considered is very poor ($S_{GG}(\Omega_0)$ = 1024 × 10^{-6} m^2/cycle/m). The arrival rates are varied from 60 vehicles per minute to 180 vehicles per minute with an interval of 30 vehicles per minute. The mean profile of the road is also considered with the road roughness.

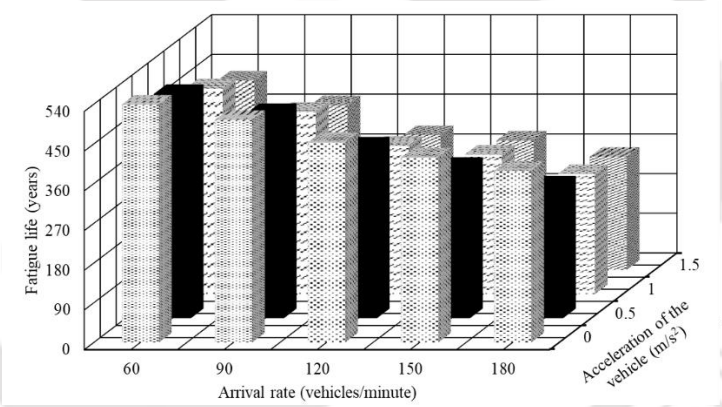

Fig. 6.52 Fatigue life for varying arrival rate and acceleration of the vehicle for entry velocity 20 km/hr for very poor road

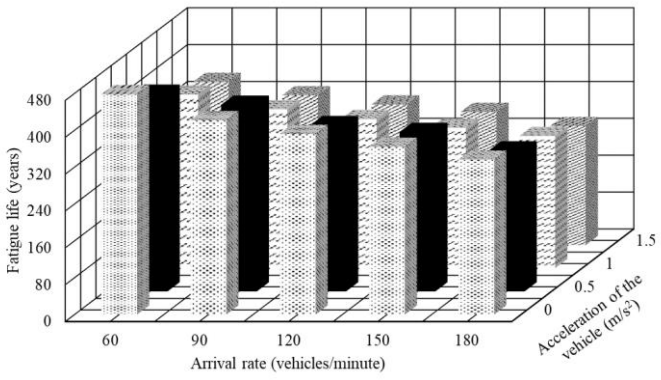

Fig. 6.53 Fatigue life for varying arrival rate and acceleration of the vehicle for entry velocity 40 km/hr for very poor road

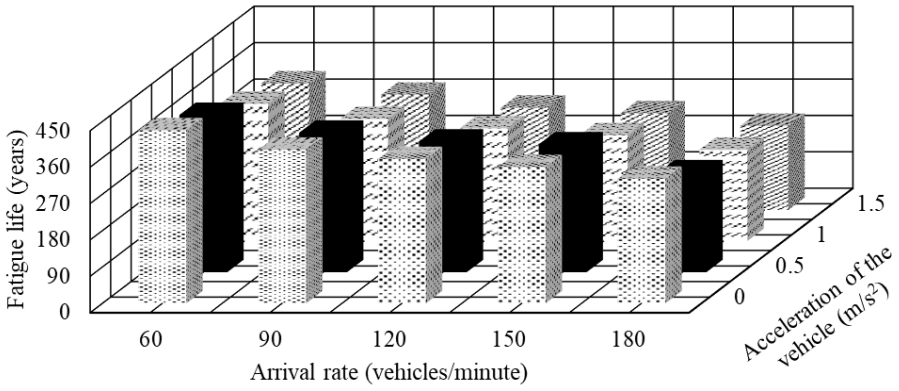

Fig. 6.54 Fatigue life for varying arrival rate and acceleration of the vehicle for entry velocity 60 km/hr for very poor road

The position of the vehicle on the bridge will affect the load distribution factors on the girders. The vehicle position can lead to stress in one girder more than the others. This is observed by the mean and standard deviation of flexural stresses shown in Fig. 6.48 when the vehicle traverses on the extreme lane. It is also observed that when a particular girder has exhibited more visual fatigue damage than other girders, allowing vehicles to traverse on the other extreme lane will help reduce the fatigue damage in the severely damaged girder for a short period of time. Since, the vehicle traverses on the extreme lane, the extreme girder is subjected to higher stress ranges than the central girder. This leads to more accumulation of fatigue damage in the extreme girder and reduced fatigue life which is observed from Figs. 6.52 to 6.54. Due to the increased crack propagation rate with increase in vehicle velocity and increasing traffic flow with increasing arrival rate of the vehicles, the fatigue life of the bridge decreases with increasing vehicle velocity and arrival rate of the vehicles as observed from Figs. 6.52 to 6.54. Since, the dynamic vibration of the bridge due to vehicular movement increases with increase in acceleration of the vehicles and deteriorated road conditions, the fatigue life of the plate girder bridge decreases with two parameters mentioned, which is observed from Figs. 6.52 to 6.54. The similar effect is observed in the middle girder when the vehicle is traversing through the centre lane which is presented in sub sections 6.5.4.1 to 6.5.4.3.

6.5.4.5 Effect of spacing of cross bracing

The effect of spacing of cross bracing on DAF and fatigue life of the plate girder bridge has been studied in this section. The spacing of the cross bracing is varied as 6 m, 12 m and 24 m. The vehicles are moving with constant velocity at 20 km/hr. The arrival rate of the vehicles is

considered as 120 vehicles per minute. The mean profile of the road is also considered with road surface roughness. The road roughness considered is very poor ($S_{GG}(\Omega_0)$ = 1024 × 10^{-6} m^2/cycle/m). The mean and standard deviation of flexural stresses obtained at mid span of the middle girder for uniform vehicle velocity 20 km/hr with arrival rate 120 vehicles per minute and very poor road condition are shown in Fig. 6.55.

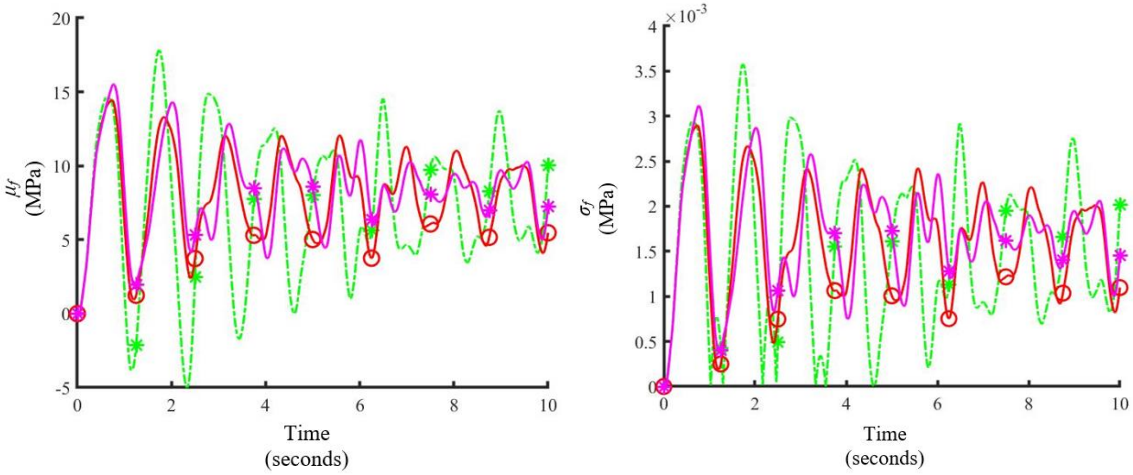

(a) (b)

Fig. 6.55 (a): Mean and (b): standard deviation of flexural stress at mid span of middle girder for different spacing of cross bracing for very poor road condition ($S_{GG}(\Omega_0)$ = 1024 × 10^{-6} m^2/cycle/m)

Key: 6 m 12 m 24 m

It is observed from Fig. 6.55 that, as the spacing of the cross bracing increases, the mean and standard deviation of flexural stresses also increases. The increase in the spacing of the cross bracing reduces the stiffness of the bridge leading to higher flexural stresses, which is observed from Fig. 6.55.

Dynamic Amplification Factor (DAF)

The DAF for the above mentioned vehicle and road parameters are obtained in this section. In case of variable velocity, the acceleration of the vehicles is varied as 0.5 m/s^2, 1 m/s^2 and 1.5 m/s^2 and the entry velocity is taken as 20 km/hr. The DAF for 12 m spacing and 24 m spacing of cross bracing for various arrival rates and acceleration of the vehicle for entry velocity 20 km/hr is shown in Figs. 6.56 and 6.57. The DAF for 6 m spacing of the cross bracing has already been presented in Fig. 6.38 under sub section 6.5.4.3.

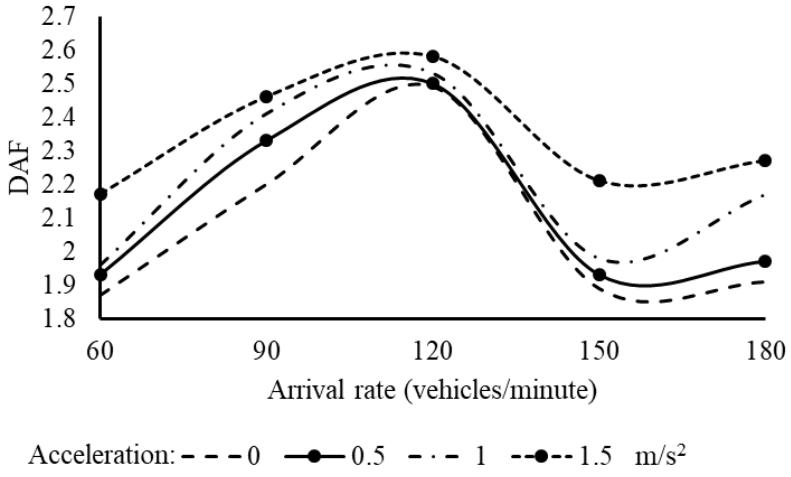

Fig. 6.56 DAF for varying arrival rate and acceleration of the vehicle for entry velocity 20 km/hr for very poor road for 12 m spacing of cross bracing

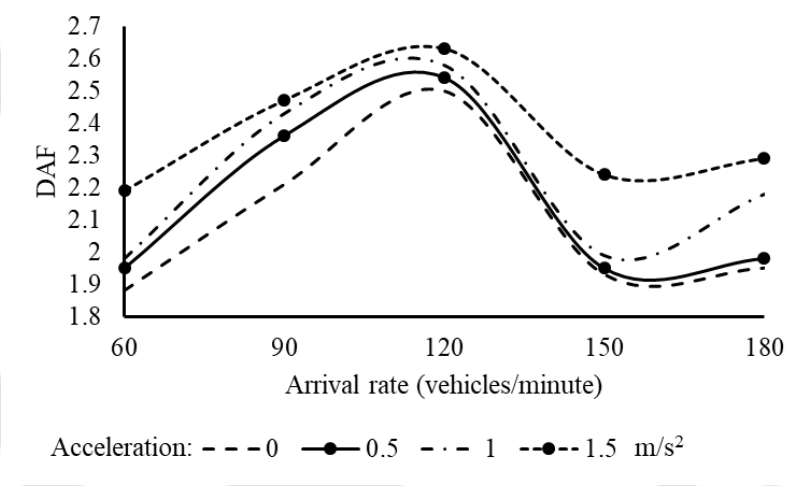

Fig. 6.57 DAF for varying arrival rate and acceleration of the vehicle for entry velocity 20 km/hr for very poor road for 24 m spacing of cross bracing

It is observed from Figs. 6.56 to 6.57 and 6.38 that the DAF increases as the spacing of the cross bracings increases. Since, the bridge stiffness reduces, the bridge deflection is higher leading to higher dynamic stresses. The static stresses also increase; however, the governing factor is the increase in dynamic stresses leading to higher DAF.

Fatigue Life

The stress range histogram for 12 m and 24 m spacing of cross bracing is shown in Fig. 6.58. The uniform vehicle velocity considered is 20 km/hr, arrival rate is 120 vehicles per minute and road roughness considered is very poor. The stress range histogram for 6 m spacing of

cross bracing has already been shown in Fig. 6.19 (a) in sub section 6.5.4.1. The comparison of fatigue life with arrival rate and acceleration of the vehicle for entry velocity 20 km/hr, very poor road roughness and spacing of cross bracing as 12 m and 24 m is shown in Figs. 6.59 to 6.60 respectively. The variation of fatigue life with arrival rate and acceleration of the vehicle for entry velocity 20 km/hr, very poor road roughness and spacing of cross bracing as 6 m has already been shown in Fig. 6.45 in sub section 6.5.4.3.

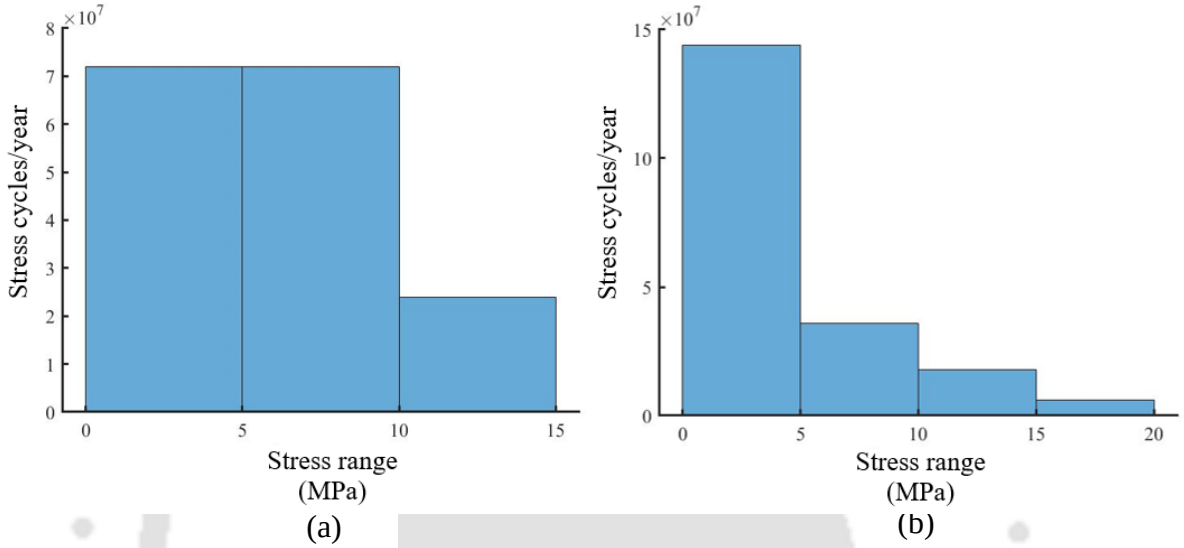

Fig. 6.58 Stress range histogram (a): 12 m spacing; (b): 24 m spacing for uniform vehicle velocity 20 km/hr, arrival rate 120 vehicles per minute and very poor road condition

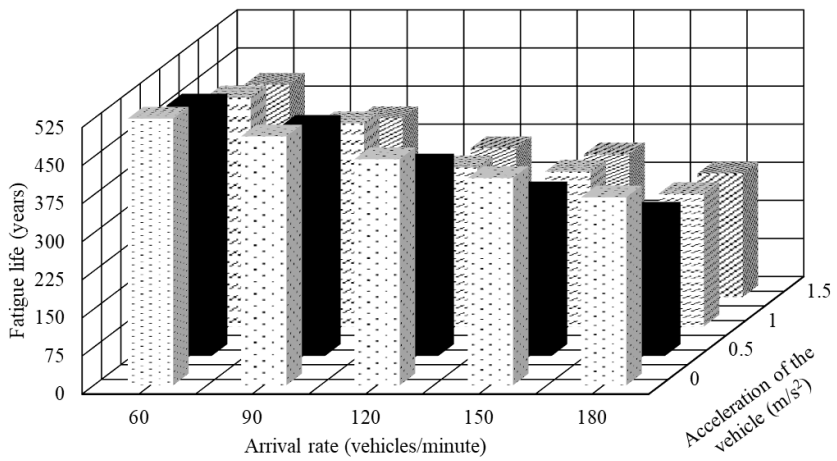

Fig. 6.59 Fatigue life for varying arrival rate and acceleration of the vehicle for entry velocity 20 km/hr for very poor road and 12 m spacing of cross bracing

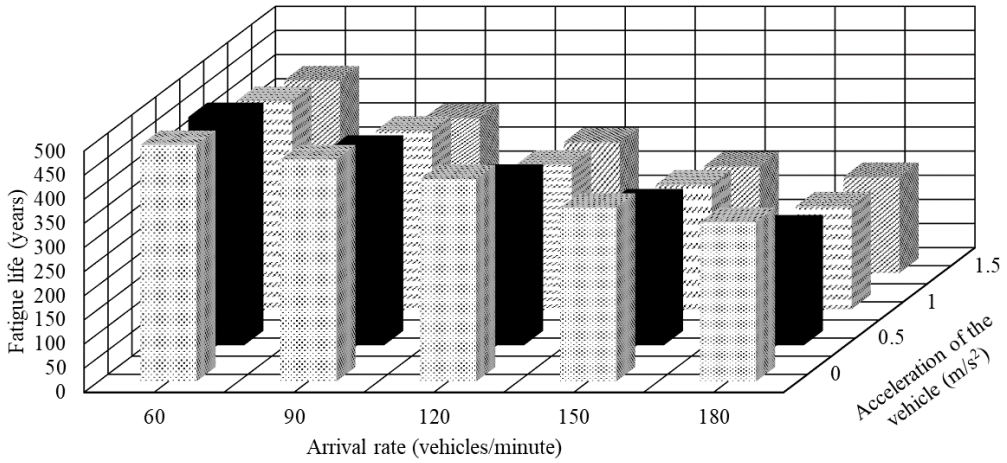

Fig. 6.60 Fatigue life for varying arrival rate and acceleration of the vehicle for entry velocity 20 km/hr for very poor road and 24 m spacing of cross bracing

The fatigue life of the bridge depends on the inherent variability of the fatigue response of the structural members, connection details and rate of accumulation of fatigue cycles which depends on the traffic flow in the past, present and future. Poorer structural design of the bridge can lead to higher dynamic flexural stresses and greater accumulation of fatigue damage on the bridge. It is observed that the spacing of the cross bracing affects the bridge dynamic response which is observed from the mean and standard deviation of flexural stresses, shown in Fig. 6.55. The stiffness of the bridge reduces as the spacing of cross bracing increases and this affects the dynamic behaviour of the bridge. The central girder is subjected to higher stress ranges and higher stress cycles as the dynamic stresses increases with the increase in the spacing of the cross bracing, which is observed from Figs. 6.58 and 6.19 (a). Due to this, the fatigue damage accumulation in the central girder is more leading to reduced fatigue life which is observed from Figs. 6.59 to 6.60 and 6.45. As observed in the previous parametric variations, the fatigue life decreases with increase in arrival rate, acceleration of the vehicle and vehicle velocity.

6.5.4.6 Effect of ratio of flange thickness to web thickness of girder

In this section, the effect of ratio of flange thickness to web thickness of girder on dynamic amplification factor (DAF) and fatigue life of the plate girder bridge has been studied. The web thickness of the girder is varied as 8 mm, 10 mm and 12 mm. The flange thickness is 25 mm. The ratio of flange thickness t_f to web thickness t_w is 2.08, 2.5 and 3.125. The vehicle velocity is kept constant and is considered as 20 km/hr, arrival rate is 120 vehicles per minute and road

roughness considered is very poor ($S_{GG}(\Omega_0)$ = 1024 × 10^{-6} m^2/cycle/m). The mean and standard deviation of flexural stresses obtained by varying t_f/t_w ratios are shown in Fig. 6.61.

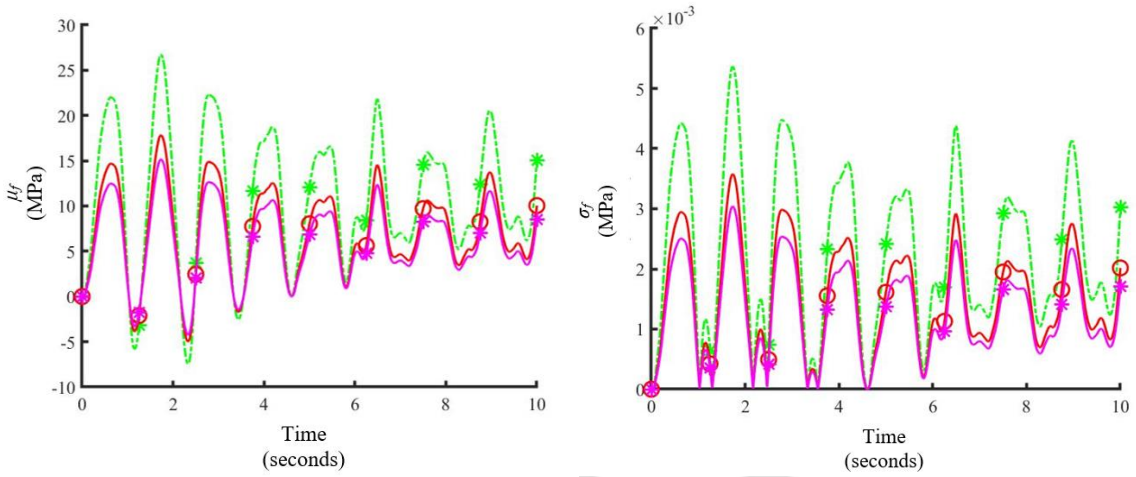

(a) (b)

Fig. 6.61 (a): Mean and (b): standard deviation of flexural stress at mid span of the middle girder for different t_f/t_w ratios for very poor road condition and uniform vehicle velocity 20 km/hr ($S_{GG}(\Omega_0)$ = 1024 × 10^{-6} m^2/cycle/m)

Key: t_f/t_w =3.125 t_f/t_w = 2.5 t_f/t_w = 2.08

It is observed from Fig. 6.61 that the plate girders with thin webs and heavy flanges are subjected to more dynamic flexural stresses than thick webs and heavy flanges. The section modulus of the plate girder decreases with the reduction in web thickness. This is the reason for increase in dynamic stresses in plate girders in case of thin webs and heavy flanges.

Dynamic Amplification Factor (DAF)

The DAF for various arrival rate and acceleration of the vehicle for t_f/t_w ratio as 2.08 and 3.125 is shown in Figs. 6.62 and 6.63 respectively. The entry velocity considered is 20 km/hr and road roughness considered is very poor ($S_{GG}(\Omega_0)$ = 1024 × 10^{-6} m^2/cycle/m). The acceleration of the vehicle is varied as 0.5m/s^2, 1m/s^2 and 1.5 m/s^2. It may be noted that DAF for t_f/t_w ratio as 2.5 has already been presented in Fig. 6.38 under sub section 6.5.4.3.

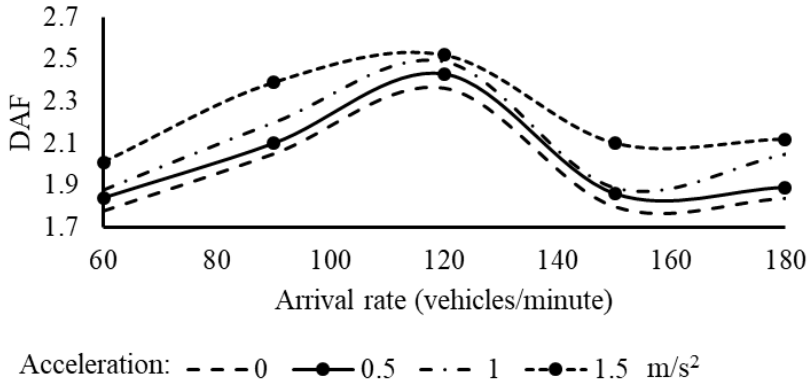

Fig. 6.62 DAF for various arrival rate and acceleration of the vehicle for entry velocity 20 km/hr and very poor road for t_f/t_w ratio as 2.08

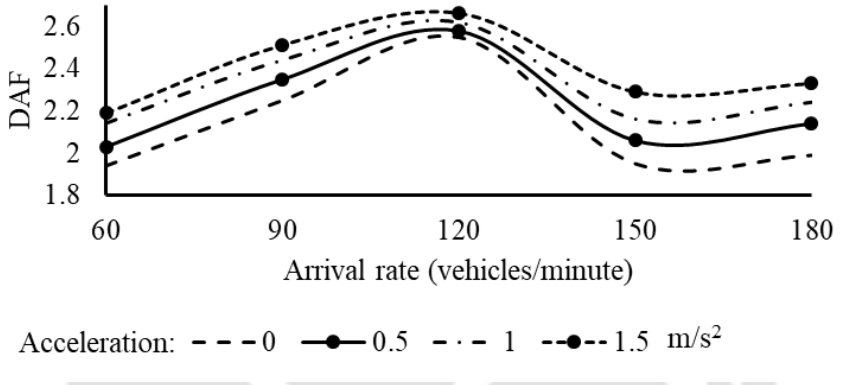

Fig. 6.63 DAF for various arrival rate and acceleration of the vehicle for entry velocity 20 km/hr and very poor road for t_f/t_w ratio as 3.125

As the dynamic stresses increase with the increasing t_f/t_w ratios, the DAF increases which is observed from Fig. 6.38 and Figs. 6.62 to 6.63. As acceleration of the vehicle increases, the DAF also increases. The DAF reaches maximum for arrival rate 120 vehicles per minute.

Fatigue Life

The stress range histogram for t_f/t_w ratio as 2.08 and 3.125 for constant vehicle velocity 20 km/hr, very poor road ($S_{GG}(\Omega_0)$ = 1024 × 10^{-6} m^2/cycle/m) and arrival rate 120 vehicles per minute is shown in Fig. 6.64. The stress range histogram for t_f/t_w ratio as 2.5 has been shown in Fig 6.19 (a) under sub section 6.5.4.1. The variation of fatigue life with arrival rate and acceleration of the vehicle for entry velocity 20 km/hr, very poor road and t_f/t_w ratios as 2.08 and 3.125 is shown in Figs. 6.65 to 6.66 while the fatigue life for t_f/t_w ratio as 2.5 has already been presented in Fig. 6.45 under sub section 6.5.4.3.

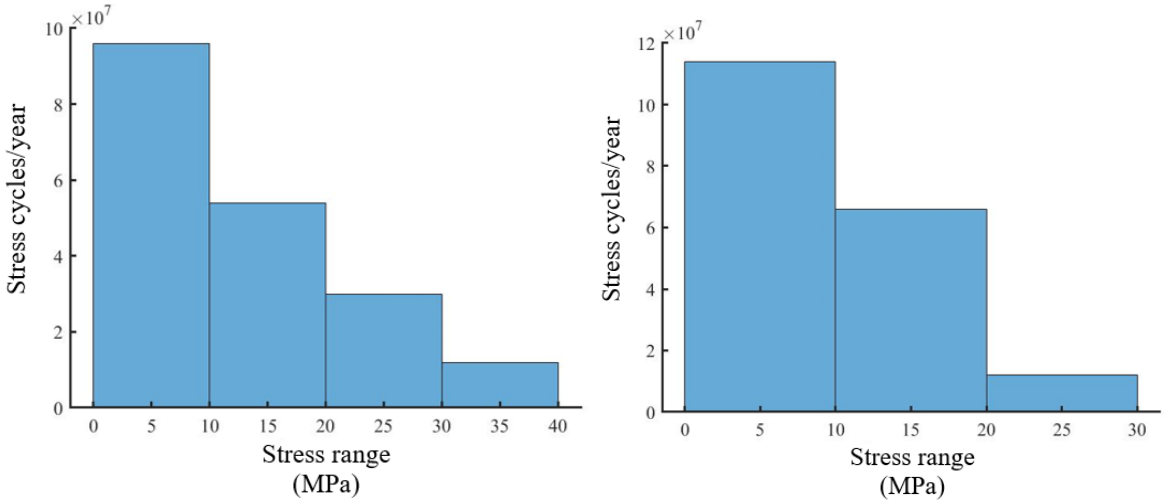

Fig. 6.64 Stress range histogram (a): t_f /t_w ratio 2.08 (b): t_f /t_w ratio 3.125 for entry velocity 20 km/hr, very poor road case and arrival rate 120 vehicles per minute

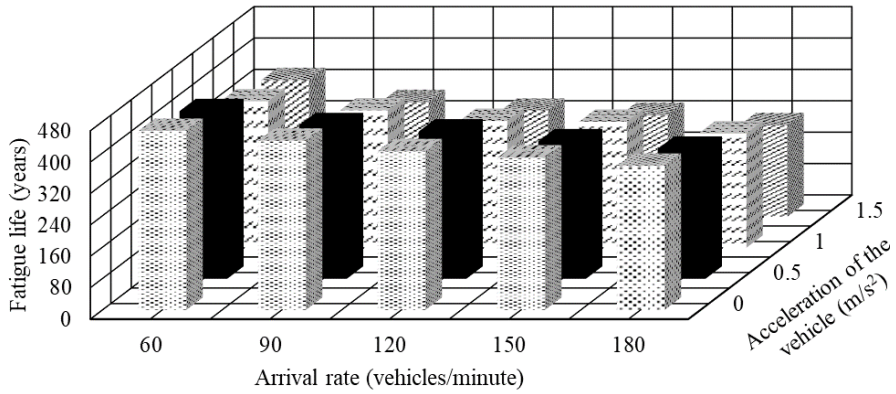

Fig. 6.65 Fatigue life for varying arrival rate and acceleration of the vehicle for entry velocity 20 km/hr for very poor road and t_f /t_w ratio 2.08

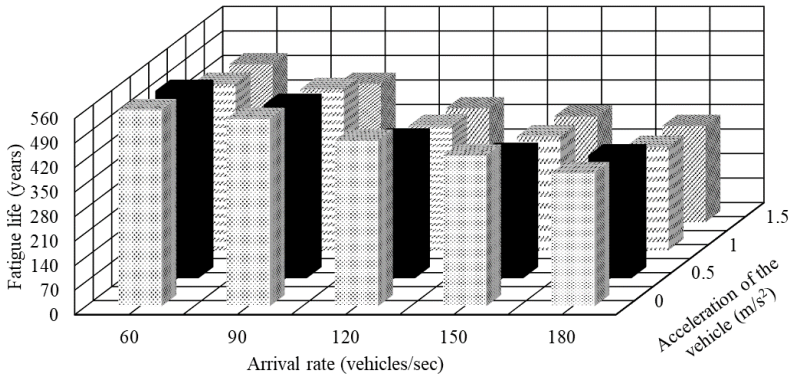

Fig. 6.66 Fatigue life for varying arrival rate and acceleration of the vehicle for entry velocity 20 km/hr for very poor road and t_f /t_w ratio 3.125

It is observed from Figs. 6.65 to 6.66 and Fig. 6.45 that the fatigue life of the bridge increases as the ratio of flange thickness to web thickness increases. Since the flanges contribute mainly to resist the bending of the girder, sectional capacity increase by increasing the flange thickness in relation to web thickness results in less fatigue damage. This is also evident that the bridge is subjected to higher stress cycles with the increase in the ratio of flange to web thickness as observed from Figs. 6.64 and 6.19 (a). The fatigue strength increases for plate girders with thin webs and heavy flanges. The point of crack initiation is at web-flange junction. In the crack propagation stage, the direction of initial crack propagation will be into the web. There is a reduction in the rate of crack propagation as the crack is propagated towards the neutral axis (Munse and Stallmeyer, 1962). The reduced crack growth rate in the crack propagation stage can be considered for the increase in fatigue strength for girders having thin webs and heavy flanges.

6.6 Comparison of DAF with Different Bridge Design Codes

In this section, a comparative study of impact factor obtained from the present dynamic analysis of plate girder bridge with the impact factors used in bridge design codes of different countries has been made. The codes referred for the study are:

(i). AASHTO LRFD Bridge Design Specification (AASHTO 2012)
(ii). IRC 6 (2017) Standard Specifications and Code of Practice for Road Bridges
(iii). BS 5400-2 Steel, Concrete and Composite Bridges. Part 2: Specifications for Loads (BSI 2006)
(iv). AS 5100 Bridge Design Standard Part 2: Design Load (Austroads 2004)
(v). Eurocode I: Actions on Structures-Part 2: Traffic Loads on Bridges (CEN 2003)
(vi). Specification for Highway Bridges by the Japan Road Association (JRA 1996)

It may be noted that the impact factors are used in design to magnify the static live load response in order to consider dynamic effect of vehicles over the bridge. However, it is not mentioned in the design codes that impact factors are dependent on various parameters such as velocity of vehicle, roughness of the deck, multiple vehicle effect. The impact factor I ($I < 1$) specified in the design codes are used to multiply the static live load effect by a factor (1+I). In this study the mean and standard deviation of dynamic flexural stress are used to obtain impact factor. The static and dynamic flexural stress at mid span of the central girder are shown

in Fig. 6.67. The vehicle velocity considered is 20 km/hr and road surface roughness considered is for good roads.

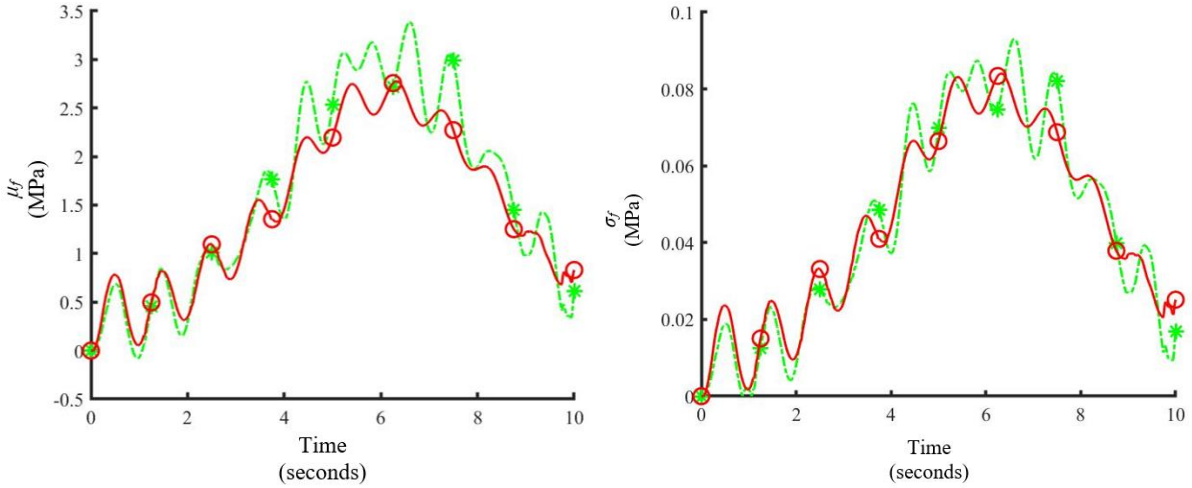

Fig. 6.67 (a): Mean and (b): standard deviation of flexural stress at mid span of the middle girder for single vehicle traversing on the bridge for good road condition and uniform vehicle velocity 20 km/hr ($S_{GG}(\Omega_0) = 32 \times 10^{-6}$ m^2/cycle/m)

Key: dynamic static

The dynamic amplification factor (DAF) is a non-dimensional parameter (DAF = impact factor + 1), which are then compared with those available in design codes of different countries mentioned earlier. The comparison is shown in Fig. 6.68.

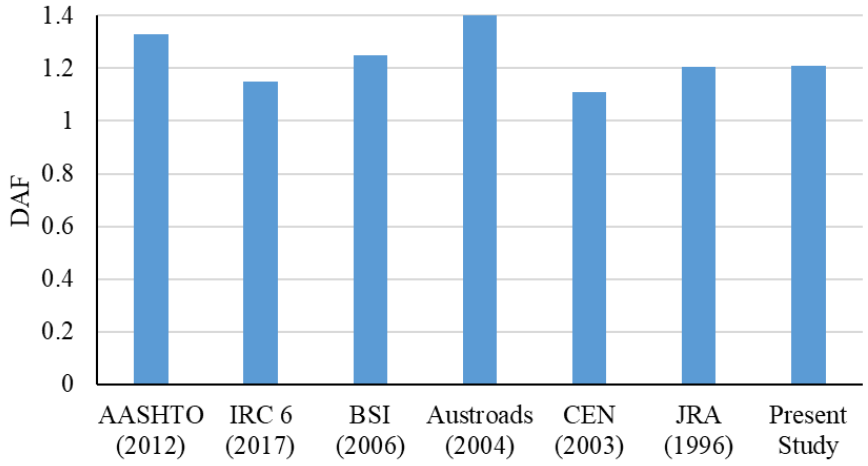

Fig. 6.68 Comparison of DAF obtained from bridge codes and present study

The result shows that the AASHTO (2012), BSI (2006) and Austroads (2004) overestimated the values of DAF, which is observed from Fig. 6.68. However, IRC 6 (2017) and CEN (2003)

underestimates the DAF. The value obtained from the present study and JRA (1996) is approximately the same. The effect of span length is only considered while evaluating DAF as per IRC 6 (2017) and CEN (2003) leading to lower DAF. However, DAF assumed in design may not remain same in service life since the traffic load increases with time and pavement deterioration occurs over time. These two aspects may be controlled by proper regulatory measures and maintenance of pavement surface. It is also worth mentioning that pavement repairing causes disruption of traffic and may also increase dead load due to increased thickness of wearing coat.

6.7 Closure

In this chapter, the FE model of a composite plate girder bridge for movement of multiple vehicles on the bridge is analysed for dynamic vehicular load. The arrival rate of the vehicles is assumed to follow Poisson process. The road surface roughness is considered in the FE model for dynamic analysis using an uncoupled iterative scheme. The DAF and fatigue life of a composite plate girder bridge for multiple vehicles traversing on the bridge is evaluated for various parameters such as vehicle velocity, arrival rate, road roughness, eccentricity of load, spacing of cross bracing and ratio of flange thickness to web thickness. The vehicle velocity is considered to be constant and also variable. It is observed from the study conducted that the DAF decreases with the increase in vehicle velocity. However, it increases with the increase in arrival rate upto 120 vehicles per minute and then gradually decreases for higher arrival rate. With increase in the acceleration of the vehicle, road roughness, spacing of cross bracing and ratio of flange thickness to web thickness, the DAF also increases. The fatigue life decreases with the increase in vehicle velocity, acceleration of the vehicle, road roughness, arrival rate and spacing of cross bracing. But, with the increase in the ratio of flange to web thickness, the fatigue life increases. The exterior girder is subjected to maximum flexural stresses when vehicle movement is on the exterior lane. Thus, the variation in DAF and fatigue life of the exterior girder for parameters discussed is similar to that of the middle girder when the vehicle is moving on the centreline of the bridge. The DAF for single vehicle obtained from the present study is compared with different bridge design codes. It is found that the value obtained from the present study is almost similar to that obtained from JRA (1996). However, impact factor in Austroads (2004) is overestimated as compared to present value. This is also observed in AASHTO (2012). The impact factor in IRC 6 (2017) and CEN (2003) are underestimated when compared with the values obtained in the present analysis.

7

CONCLUSIONS AND FUTURE SCOPE OF WORK

7.1 General

In the present work, fatigue life of bridges subjected to series of moving loads have been studied considering segregation of load cycles into crack initiation and crack propagation stage. The fatigue damage model in bilinear damage hypothesis has been improved considering crack opening stress in crack propagation phase. The models have been first tested for its sensitivity to stress range, loading frequency and damping of the system by considering a generic structural model of axially vibrating bar. Thereafter, models are further validated for prediction of failure cycles by conducting fatigue test of standard ASTM specimen in the laboratory with mixed stress range. In order to use the above models for prediction of fatigue failure in bridges, the stress time history of bridges have been obtained by a semi-analytical method which includes random arrival time and random road roughness. Once this approach is used in continuum representative models to find out the influencing parameters on fatigue life of the bridges, further investigation was carried out in a 3D finite element model of a plate girder bridge using an uncoupled iterative scheme to incorporate randomness in pavement roughness.

7.2 Conclusions

The major conclusions from experimental and theoretical study have been presented in the subsections given below.

7.2.1 Fatigue Damage Models and Experimental Works

The proposed fatigue damage methodologies i.e., Bilinear Damage Rule (BLDR) and Modified Bilinear Damage Rule (MBLDR) have been applied to a structural model of axially vibrating bar. The results are validated using experimental fatigue test results of specimen pertaining to ASTM standards. The effect of various influencing parameters on fatigue damage are also studied. The major conclusions from the study are:

(i). The number of stress cycles experienced by the damaged specimen is more for lower frequency of excitation. In addition to that, the slip systems causing crack propagation tend to be less active in higher frequency of loading. This results in higher activation

energy causing dislocation of grains. Thus, the fatigue damage increases with the increase in frequency of excitation.

(ii). With the increase in damping, the dynamic stresses in steady state part decrease slightly. However, increase in damping does not significantly affect the damage index because transient part of the stress does not contribute to the accumulation of damage leading to no change in damage index.

(iii). Increase in summation of modes beyond 3 lead to minor increase in stress due to which predicted life shows no significant change.

(iv). The fractured surface of the failed specimen was examined under FESEM and showed fracture initiation sites such as surface induced cracks, fish-eye formation, formation of slip-bands, grain boundaries and striations. These sites indicate that the specimen has undergone failure due to fatigue.

(v). The experimental fatigue test is conducted on small scale specimens based on constant amplitude loading. This loading does not consider the effect of random loading, which is usually observed in bridges. LDR has been formulated taking the constant loading condition. The improvement from LDR to MBLDR is not much observed since the loading condition is of constant amplitude and does not take into account the complexities of random loads. Thus, it can be observed that LDR works well for small scale specimens in laboratory tests whereas MBDLR works well for real structures like bridges, where the loading condition is random due to random arrival rate of vehicles and pavement roughness. In addition to that, the load sequence effects and complexities of fatigue damage process along with opening stress in crack propagation stage has been considered in MBLDR which were ignored in LDR.

(vi). The comparison of the failure cycles obtained from the proposed methods and that of the experimental results are in good agreement with each other. The average error is approximately 8%.

(vii). From the study conducted, MBDLR gives more accurate damage predictions as compared to BLDR since opening stresses are considered in the former case in Phase-2. It is also observed from the study that the propagation of crack can take place below the intrinsic fatigue limit and that considering a zero slope below the fatigue limit will tend to give over conservative damage values. Thus, it is observed that zero slope consideration can lead to inaccurate results. Both BLDR and MBLDR give less damage predictions as compared to LDR. This is because in LDR, the load sequence effects are neglected.

7.2.2 Fatigue Life Predictions using Semi Analytical Models

The dynamic flexural stresses of single span and multi span continuous bridge for multiple movement of vehicles have been obtained using the semi analytical method proposed in the study. MBLDR has been used in the study to obtain the fatigue life at critical location of single span and multi span continuous bridge. The dynamic amplification factor and fatigue damage of single span and multi span continuous bridge has been obtained for different bridge vehicle parameters. The major conclusions from the study are:

(i). The mean flexural stresses at centre of the single span, two and three span continuous bridge decrease with increase in vehicle entry velocity. Although a uniform time window is considered for all vehicle velocities, the action of each load is limited to time intervals of length L/v where L is the span of the bridge and v is the vehicle velocity. This implies that the average number of moving loads acting on the span decreases with increasing vehicle velocity. Thus, the mean flexural stresses are more for lower vehicle entry velocity. However, in case of single span bridge, the standard deviation of flexural stresses at mid span increases with the increase in vehicle velocity. A similar trend of standard deviation of flexural stresses at centre of the second span of two and three span continuous bridge is not observed.

(ii). The dynamic amplification factor (DAF) of single span, two and three span continuous bridge decreases with the increase in vehicle velocity. Due to the longer time span in lower vehicle velocity, the vehicle may experience low frequency excitation close to its own natural frequency, thus producing larger excitation force and large dynamic responses in the bridge deck.

(iii). The fatigue life of the single span, two and three span continuous bridge decreases with the increase in vehicle entry velocity. The number of stress cycles in low amplitude stress ranges increases with the increase in vehicle entry velocity. These stress cycles caused by vehicle bridge interaction contribute to fatigue damage accumulation.

(iv). The acceleration of the vehicle influences the mean and standard deviation of flexural stresses at centre of single span, two and three span continuous bridge. Since the vibration of the vehicle with acceleration is more, the transverse vibration of the bridge also increases as compared to that of the vehicle moving with uniform velocity. Thus, the mean and standard deviation of flexural stresses at centre of single span, two and three span continuous bridge increases with the increase in acceleration of vehicle.

(v). The dynamic amplification factor (DAF) of single span, two and three span continuous bridge increases with the increase in acceleration of the vehicle and fatigue life of the single span, two and three span continuous bridge decreases with the increase in acceleration of vehicle.

(vi). The vehicle traversing on a deteriorated road surface generate large excitation force on the bridge leading to large dynamic response. This causes the mean and standard deviation of flexural stresses at centre of single span, two and three span continuous bridge to increase with the increase in road surface irregularity.

(vii). The dynamic amplification factor (DAF) of single span, two and three span continuous bridge increases with the increase in road surface conditions. The fatigue life decreases with the increase in road surface irregularity. This fact indicates that during design phase, one should bear in mind some cases of poorly maintained pavement.

(viii). In the present study, traffic volume per unit time is represented by the arrival rate of the vehicles. Increase in arrival rate signifies higher traffic volume which implies increased vehicular movement on the bridge leading to higher mean and standard deviation of flexural stresses at centre of single span, two and three span continuous bridge.

(ix). A higher arrival rate indicates a higher traffic flow on the bridge. However, as the arrival rate increases, the static stresses caused by vehicular movement also increases in addition to the dynamic stresses, which become dominant for arrival rates greater than 120 vehicles per minute. This results in increase in DAF of single span, two and three span continuous bridge for arrival rates up to 120 vehicles per minute and reduction in DAF for arrival rates greater than 120 vehicles per minute.

(x). The presence of multiple vehicles on the bridge amplifies the stress range and increases the number of stress cycles. This causes more fatigue damage than a single vehicle. The fatigue life of single span, two and three span continuous bridge decreases as the vehicle arrival rate increases.

(xi). Crack propagation rate increases with the increase in vehicle entry velocity, road roughness and arrival rate leading to lower fatigue life in case of single span and multi span continuous bridge.

(xii). An overloaded truck can cause large dynamic vibrations on the bridge due to vehicular movement when the road roughness is very poor, as compared to that of a light weight vehicle. Due to this, the mean and standard deviation of flexural stresses at centre of single span as well as continuous span bridge increases with the increase in axle weight of the vehicle.

(xiii). The DAF decreases as the total vehicle weight increases from 200 kN to 400 kN and further increase in total vehicle weight does not show a significant change in DAF. The reason for reduced DAF may be attributed mainly due to increase of static stresses that appears superseding the corresponding dynamic part. The fatigue life of the bridge decreases as the total vehicle weight increases.

(xiv). The mean and standard deviation of flexural stresses at centre of single span, two and three span continuous bridge increases with the increase in the amplitude of mean profile. DAF of single span, two and three span continuous bridge increases with the increase in amplitude of mean profile. The fatigue life of single span, two and three span continuous bridge decreases as the amplitude of mean profile increases.

(xv). The mean flexural stresses at the centre of the single span bridge increases with the increase in span of the bridge. The number of vehicles crossing the bridge increases with the increase in span of the bridge, which increases the mean flexural stresses. The standard deviation of flexural stresses at mid span of the bridge does not follow a similar pattern.

(xvi). DAF of single span bridge decreases with the increase in the span of the bridge. The same trend is observed in codes of practice for bridge design. However, fatigue life of single span bridge increases with the increase in the span of the bridge. This is due to decrease in natural frequencies of the bridge in all modes which results in larger amplitude stress cycles.

(xvii). A structurally redundant system such as continuous bridge shows lower DAF and fatigue life as compared to single span bridge which becomes possible due to redistribution of bending moments.

7.2.3 Fatigue Life Prediction in Plate Girder Bridge

An uncoupled iterative scheme has been used in finite element model of steel concrete composite plate girder bridge in order to obtain dynamic stresses for assessment of fatigue damage. The major conclusions obtained from the studies are,

(i). The pattern of variation of the mean and standard deviation of flexural stresses at centre of the middle girder when vehicle moves on the centre line of the lane with different vehicle entry velocities, road surface roughness and arrival rate is similar to that obtained in single span bridge and multi span continuous bridge in semi-analytical models. The variation of dynamic amplification factor (DAF) and fatigue life with

different vehicle entry velocities is also similar to that of single span bridge and multi span continuous bridge.

(ii). When the vehicle traverses on the outer lane, the extreme girder is subjected to higher flexural stresses and the DAF and fatigue life varies in a similar way as that of central girder with parameters like vehicle entry velocity, road surface roughness and arrival rate of vehicles.

(iii). The increase in the spacing of the cross bracing reduces the stiffness of the bridge leading to higher flexural stresses at mid span of the central girder. DAF increases as the spacing of the cross bracings increases. This is also observed in case of fatigue damage analysis of the plate girder. Therefore, it is recommended to provide cross girder at suitable spacing to make the longitudinal girder more fatigue resistant.

(iv). The plate girders with thin webs and heavy flanges show better performance against fatigue. Since moment of resistance of the girder is mainly provided by the flanges, contribution of web mainly goes to shear buckling resistance. Fatigue life of plate girder bridge increases with the increase in ratio of flange thickness to web thickness. However, keeping in view of the shear criterion, one needs to provide adequate number of stiffeners.

(v). The DAF obtained from the present study is compared with the DAF used in bridge design codes of different countries. It is observed that AASHTO (2012), BSI (2006) and Austroads (2004) overestimate DAF, while IRC 6 (2017) and CEN (2005) underestimate the same. The effect of span length is only considered in IRC 6 (2017) and CEN (2005) leading to lower DAF. The value obtained from the present study and JRA (1996) are approximately same.

7.3 Future Scope

The future scope of the work is:

- To consider the bridge-vehicle interaction model taking pitching and rolling modes of vehicle and to observe their effects on fatigue life of bridge.
- To consider the non-linear suspension characteristics of vehicle on fatigue life of bridge.
- To take into account the non-linearity in crack opening stress using fracture mechanics approach to estimate the remaining life of the bridge when the structure is put to service.

- To consider the effect of environmental factors like corrosion to predict the fatigue life of the bridge.

7.4 Closure

The investigation carried out in the thesis has been summarized and conclusions are listed in different sub sections. The conclusions have been drawn from the results and discussions presented in the preceding chapters. Firstly, inferences from the numerical models of fatigue and experimental works have been discussed. Thereafter, the concluding remarks have been given on fatigue life and DAF of single span and multi span continuous bridge for various bridge vehicle parameters. The major findings from the analysis of 3D finite element model of plate girder bridge are then listed point wise. The possible extension of the present research work has also been discussed.

A.1.1 Natural Frequencies and Mode Shapes for Single-Span Beam

The equation of motion of the bridge in bending is given by

$$EI\frac{\partial^4 y(x,t)}{\partial x^4}+c\frac{\partial y(x,t)}{\partial t}+m_b\frac{\partial^2 y(x,t)}{\partial t^2}=f(x,t) \tag{A-1}$$

The undamped mode in free bending vibration is considered. The response is given by

$$y(x,t)=\phi(x)\sin(\omega t) \tag{A-2}$$

in which $\phi(x)$ is the mode shape function and ω is the circular natural frequency. Substituting Eq. (A-2) in Eq. (A-1)

$$\frac{d^4\phi}{dx^4}-\beta^4\phi=0;\beta^4=\frac{m_b\omega^2}{EI} \tag{A-3}$$

The general solution of Eq. (A-3) is

$$\phi(x)=A\sin\beta x+B\cos\beta x+C\sinh\beta x+D\cosh\beta x \tag{A-4}$$

where A, B, C and D are integration constants to be evaluated from the boundary conditions. The boundary conditions at the ends imply the following conditions on mode shape functions.

$$\begin{aligned} &y(0,t)=y(L,t)=0\\ &\Rightarrow \phi(0)=\phi(L)=0 \end{aligned} \tag{A-5}$$

$$\begin{aligned} &\frac{\partial^2 y(0,t)}{\partial x^2}=\frac{\partial^2 y(L,t)}{\partial x^2}=0\\ &\Rightarrow \phi''(0)=\phi''(L)=0 \end{aligned} \tag{A-6}$$

Substitution of boundary conditions in Eq. (A-4) results in following transcendental equation.

$$A\sin\beta L=0 \tag{A-7}$$

Excluding the trivial solution (A=0), the frequency equation is obtained as

$$\sin\beta L=0 \tag{A-8}$$

which will be satisfied for

$$\beta_n L = n\pi, n = 1,2,,... \tag{A-9}$$

The natural frequency in n^{th} mode is

$$\omega_n = (n\pi)^2 \sqrt{\frac{EI}{m_b L^4}} \tag{A-10}$$

The mode shape function n^{th} mode is

$$\phi_n(x) = \sqrt{\frac{2}{m_b L}} \sin\frac{n\pi}{L} x \tag{A-11}$$

A.1.2 System Matrices

The bridge-vehicle coupled equations given in Eqs. (3.31), (3.34) and (3.41) can be expressed in matrix form as

$$\mathbf{M}\ddot{\mathbf{X}} + \mathbf{C}\dot{\mathbf{X}} + \mathbf{K}\mathbf{X} = \mathbf{F}(t) \tag{A-12}$$

in which **M**, **C**, **K**, **F**(t) and **X** are the system mass matrix, damping matrix, stiffness matrix, force vector and response vector respectively and is given below

$$\mathbf{M} = \begin{bmatrix} m_s & 0 & 0 & 0 & \dots \\ 0 & m_w & 0 & 0 & \dots \\ 0 & 0 & 1 & 0 & \dots \\ 0 & 0 & 0 & 1 & \dots \\ . & . & . & . & \dots \\ . & . & . & . & \dots \\ . & . & . & . & \dots \end{bmatrix}, \mathbf{C} = \begin{bmatrix} c_s & -c_s & 0 & 0 & \dots \\ -c_s & c_w + c_s & -c_w\phi_1(x) & -c_w\phi_2(x) & \dots \\ 0 & A_1 & 2\xi\omega_1 + B_{11} & B_{12} & \dots \\ 0 & A_2 & B_{21} & 2\xi\omega_2 + B_{22} & \dots \\ . & . & . & . & \dots \\ . & . & . & . & \dots \\ . & . & . & . & \dots \end{bmatrix} \tag{A-13}$$

$$\mathbf{K}=\begin{bmatrix} k_s & -k_s & 0 & 0 & \ldots \\ -k_s & k_w+k_s & -k_w\phi_1(x) & -k_w\phi_2(x) & \ldots \\ 0 & C_1 & \omega_1^2+D_{11} & D_{12} & \ldots \\ 0 & C_2 & D_{21} & \omega_2^2+D_{22} & \ldots \\ & & & & \\ . & . & . & . & \ldots \\ . & . & . & . & \ldots \\ . & . & . & . & \ldots \end{bmatrix} \tag{A-14}$$

$$\mathbf{F}(t)=\begin{Bmatrix} 0 & c_w\dot{h}+k_w h & F_1 & F_2 & . & . & . \end{Bmatrix}^T,$$
$$\mathbf{X}=\begin{Bmatrix} z_1 & z_2 & \eta_1 & \eta_2 & . & . & . \end{Bmatrix}^T \tag{A-15}$$

The terms A_1, A_2, B_{11}, B_{12}, B_{21}, B_{22}, C_1, C_2, D_{11}, D_{12}, D_{21}, D_{22}, F_1, and F_2 in Eqs. (A-13), (A-14) and (A-15) are written in generalized form as

$$A_n=\frac{-c_w}{M_n}\sum_{j=1}^{N(t)}\phi_n\left\{v\left(t-t_j\right)\right\}, n=1,2,...,n_b \tag{A-16}$$

$$B_{in}=\frac{c_w}{M_n}\sum_{j=1}^{N(t)}\left[\phi_i(x)\phi_n\left\{v\left(t-t_j\right)\right\}\right], i,n=1,2,...,n_b \tag{A-17}$$

$$C_n=\frac{-k_w}{M_n}\sum_{j=1}^{N(t)}\phi_n\left\{v\left(t-t_j\right)\right\}, n=1,2,...,n_b \tag{A-18}$$

$$D_{in}=\frac{k_w}{M_n}\sum_{j=1}^{N(t)}\left[\phi_i(x)\phi_n\left\{v\left(t-t_j\right)\right\}\right], i,n=1,2,...,n_b \tag{A-19}$$

$$F_n=-\frac{c_w}{M_n}\sum_{j=1}^{N(t)}\phi_n\left\{v\left(t-t_j\right)\right\}\dot{h}-\frac{k_w}{M_n}\sum_{j=1}^{N(t)}\phi_n\left\{v\left(t-t_j\right)\right\}h- (m_s+m_w)g\sum_{j=1}^{N(t)}\phi_n\left\{v\left(t-t_j\right)\right\}, n=1,2,..,n_b \tag{A-20}$$

A.2.1 Natural Frequencies and Mode Shapes for Multi-Span Continuous Beam

The equation of transverse vibration for each span is given by

$$EI\frac{\partial^4 y_r}{\partial x_r^{\,4}} + c\frac{\partial y_r}{\partial t} + m_b\frac{\partial^2 y_r}{\partial t^2} = f_r(x_r,t),\ 0 \le x_r \le l_r,\ r = 1,2,3,.....N. \qquad \text{(A-21)}$$

Considering undamped free vibration, Eq. (A-21) can be written as

$$\frac{d^4\phi_r}{dx^4} - \beta_r^4\phi_r = 0; \beta_r^4 = \frac{m_b\omega_r^2}{EI} \qquad \text{(A-22)}$$

The homogeneous solution of the Eq. (A-21) is given by

$$\phi_r(x) = A_r \sin\beta_r x_r + B_r \cos\beta_r x_r + C_r \sinh\beta_r x_r + D_r \cosh\beta_r x_r \qquad \text{(A-23)}$$

The following boundary conditions of continuous beam need to be applied for calculation of frequency parameters and mode shape.

$$\begin{aligned}
&y_r(x_r = l_r, t) = 0\\
&y_{(r+1)}(x_{r+1} = l_r, t) = 0\\
&\frac{\partial y_r}{\partial x_r}(x_r = l_r, t) = \frac{\partial y_{(r+1)}}{\partial x_{(r+1)}}(x_{r+1} = 0, t) \qquad \text{(A-24)}\\
&\frac{\partial^2 y_r}{\partial x^2{}_r}(x_r = l_r, t) = \frac{\partial^2 y_{(r+1)}}{\partial x^2{}_{(r+1)}}(x_{r+1} = 0, t) \qquad r = 1,2,3...N
\end{aligned}$$

Using the boundary conditions given in Eq. (A-24), a set of homogeneous equations can be found in the matrix form as

$$[V(\beta_r)]\{W\} = \{0\} \qquad \text{(A-25)}$$

The non-trivial solution of the Eq. (A-25) necessitates that the determinant of the matrix $[V(\beta_r)]$ should be equal to zero. After expanding the determinant, the characteristic polynomial can be solved to find the frequency roots which when substituted in Eq. (A-25) yields the vector *{W}* and hence the mode shapes.

After solving the determinant, the lowest five frequency parameters of multi-span continuous beams can be determined (Fryba, 1996). The results are shown in Table A.1.

Table A.1 First five frequency parameters for continuous beams

Number of Spans (r)	Frequency parameters ($\beta_{nr}l_r$)				
	Mode 1	Mode 2	Mode 3	Mode 4	Mode 5
1	π	2π	3π	4π	5π
2	3.1416	3.9272	6.2832	7.0686	9.4248
3	3.1416	3.5500	4.3040	6.2832	6.6920

The natural frequency in nth mode of rth span ω_{nr} is given as

$$\omega_{nr} = (\beta_{nr}l_r)^2\sqrt{\frac{EI}{m_b l_r^4}} \tag{A-26}$$

The mode shape function for multi-span continuous beam is given by

$$\phi_{nr}(x) = \begin{cases} \sin(\beta_{nr}x_r) - \dfrac{\sin(\beta_{nr}l_r)}{\sinh(\beta_{nr}l_r)}\sinh(\beta_{nr}x_r) & r = 1 \\ P_r M_r(x_r) + Q_r N_r(x_r) & r = 2,3,...,N \end{cases} \tag{A-27}$$

in which

$$P_r = \frac{[\cosh(\beta_{nr}l_r) - \cos(\beta_{nr}l_r)][\sin(\beta_{nr}l_r)\sinh(\beta_{nr}l_r)]}{\sinh(\beta_{nr}l_r)[\{\cos(\beta_{nr}l_r) - \cosh(\beta_{nr}l_r)\}][\{\sinh(\beta_{nr}l_r) - \sin(\beta_{nr}l_r)\}]} - \frac{\sin(\beta_{nr}l_r)[\sinh(\beta_{nr}l_r)\cos(\beta_{nr}l_r) - \sin(\beta_{nr}l_r)\cosh(\beta_{nr}l_r)]}{\sinh(\beta_{nr}l_r)[\{\cos(\beta_{nr}l_r) - \cosh(\beta_{nr}l_r)\}][\{\sinh(\beta_{nr}l_r) - \sin(\beta_{nr}l_r)\}]} \tag{A-28}$$

$$Q_r = \frac{[\cos(\beta_{nr}l_r) - \cosh(\beta_{nr}l_r)][\sin(\beta_{nr}l_r)\sinh(\beta_{nr}l_r)]}{\sinh(\beta_{nr}l_r)[\{\cos(\beta_{nr}l_r) - \cosh(\beta_{nr}l_r)\}][\{\sinh(\beta_{nr}l_r) - \sin(\beta_{nr}l_r)\}]} + \frac{\sinh(\beta_{nr}l_r)[\sinh(\beta_{nr}l_r)\cos(\beta_{nr}l_r) - \sin(\beta_{nr}l_r)\cosh(\beta_{nr}l_r)]}{\sinh(\beta_{nr}l_r)[\{\cos(\beta_{nr}l_r) - \cosh(\beta_{nr}l_r)\}][\{\sinh(\beta_{nr}l_r) - \sin(\beta_{nr}l_r)\}]} \tag{A-29}$$

$$M_r(x_r) = [\cos(\beta_{nr}l_r) - \cosh(\beta_{nr}l_r)]\sinh(\beta_{nr}x_r) + \sinh(\beta_{nr}l_r)[\cosh(\beta_{nr}x_r) - \cos(\beta_{nr}x_r)] \tag{A-30}$$

$$N_r(x_r) = [\cos(\beta_{nr} l_r) - \cosh(\beta_{nr} l_r)]\sin(\beta_{nr} x_r) + \sin(\beta_{nr} l_r)[\cosh(\beta_{nr} x_r) - \cos(\beta_{nr} x_r)] \quad \text{(A-31)}$$

A.2.2 Second Derivative of Mode Shape Function

The second derivative of mode shape function which is needed to calculate the bending moment and flexural stress is given as

$$\phi''_{nr}(x) = \begin{cases} -(\beta_{nr} l_r)^2 \left(\sin(\beta_{nr} x_r) + \dfrac{\sin(\beta_{nr} l_r)}{\sinh(\beta_{nr} l_r)} \sinh(\beta_{nr} x_r) \right) & r = 1 \\ (\beta_{nr} l_r)^2 [P_r M''_r(x_r) + Q_r N''_r(x_r)] & r = 2, 3, \ldots, N \end{cases} \quad \text{(A-32)}$$

in which P_r and Q_r are given in Eq. (A-28) and Eq. (A-29). $M''_r(x_r)$ and $N''_r(x_r)$ are given below.

$$M''_r(x_r) = (\beta_{nr} l_r)^2 [\cos(\beta_{nr} l_r) - \cosh(\beta_{nr} l_r)]\sinh(\beta_{nr} x_r) + (\beta_{nr} l_r)^2 \sinh(\beta_{nr} l_r)[\cosh(\beta_{nr} x_r) + \cos(\beta_{nr} x_r)] \quad \text{(A-33)}$$

$$N''_r(x_r) = (\beta_{nr} l_r)^2 [\cosh(\beta_{nr} l_r) - \cos(\beta_{nr} l_r)]\sin(\beta_{nr} x_r) + (\beta_{nr} l_r)^2 \sin(\beta_{nr} l_r)[\cosh(\beta_{nr} x_r) + \cos(\beta_{nr} x_r)] \quad \text{(A-34)}$$

A.2.3 System Matrices

The vehicle dynamic equations given in Eqs. (3.42) and (3.45) and bridge equation given in Eq. (3.51) can be expressed in matrix form as

$$\mathbf{M}\ddot{\mathbf{X}} + \mathbf{C}\dot{\mathbf{X}} + \mathbf{K}\mathbf{X} = \mathbf{F}(t) \quad \text{(A-35)}$$

in which **M**, **C**, **K**, **F**(t) and **X** are the system mass matrix, damping matrix, stiffness matrix, force vector and response vector respectively and is given below.

$$\mathbf{M}=\begin{bmatrix} m_s & 0 & 0 & 0 & \dots \\ 0 & m_w & 0 & 0 & \dots \\ 0 & 0 & 1 & 0 & \dots \\ 0 & 0 & 0 & 1 & \dots \\ . & . & . & . & \dots \\ . & . & . & . & \dots \\ . & . & . & . & \dots \end{bmatrix},\quad \mathbf{C}=\begin{bmatrix} c_s & -c_s & 0 & 0 & \dots \\ -c_s & c_w+c_s & -c_w\phi_{1r}(x) & -c_w\phi_{2r}(x) & \dots \\ 0 & A_{1r} & 2\xi_1\omega_{1r}+B_{11r} & B_{12r} & \dots \\ 0 & A_{2r} & B_{21r} & 2\xi_2\omega_{2r}+B_{22r} & \dots \\ . & . & . & . & \dots \\ . & . & . & . & \dots \\ . & . & . & . & \dots \end{bmatrix} \tag{A-36}$$

$$\mathbf{K}=\begin{bmatrix} k_s & -k_s & 0 & 0 & \dots \\ -k_s & k_w+k_s & -k_w\phi_{1r}(x) & -k_w\phi_{2r}(x) & \dots \\ 0 & C_{1r} & \omega_{1r}^2+D_{11r} & D_{12r} & \dots \\ 0 & C_{2r} & D_{21r} & \omega_{2r}^2+D_{22r} & \dots \\ . & . & . & . & \dots \\ . & . & . & . & \dots \\ . & . & . & . & \dots \end{bmatrix} \tag{A-37}$$

$$\mathbf{F}(t)=\begin{Bmatrix} 0 & c_w\dot{h}+k_w h & F_{1r} & F_{2r} & . & . & . \end{Bmatrix}^T,\ \mathbf{X}=\begin{Bmatrix} z_1 & z_2 & \eta_1 & \eta_2 & . & . & . \end{Bmatrix}^T \tag{A-38}$$

The terms A_{1r}, A_{2r}, B_{11r}, B_{12r}, B_{21r}, B_{22r}, C_{1r}, C_{2r}, D_{11r}, D_{12r}, D_{21r}, D_{22r}, F_{1r}, and F_{2r} in Eqs. (A-36) to (A-38) are given as

$$A_{nr}=\frac{-c_w}{M_n}\sum_{j=1}^{N(t)}\phi_{nr}\left\{v\left(t-t_j\right)\right\}, n=1,2,\dots,n_b \tag{A-39}$$

$$B_{inr}=\frac{c_w}{M_n}\sum_{j=1}^{N(t)}\left[\phi_{ir}(x)\phi_{nr}\left\{v\left(t-t_j\right)\right\}\right], i,n=1,2,\dots,n_b \tag{A-40}$$

$$C_{nr}=\frac{-k_w}{M_n}\sum_{j=1}^{N(t)}\phi_{nr}\left\{v\left(t-t_j\right)\right\}, n=1,2,\dots,n_b \tag{A-41}$$

$$D_{inr}=\frac{k_w}{M_n}\sum_{j=1}^{N(t)}\left[\phi_{ir}(x)\phi_{nr}\left\{v\left(t-t_j\right)\right\}\right], i,n=1,2,\dots,n_b \tag{A-42}$$

$$F_{nr} = -\frac{c_w}{M_n}\sum_{j=1}^{N(t)}\phi_{nr}\left\{v\left(t-t_j\right)\right\}\dot{h} - \frac{k_w}{M_n}\sum_{j=1}^{N(t)}\phi_{nr}\left\{v\left(t-t_j\right)\right\}h - \left(m_s+m_w\right)g\sum_{j=1}^{N(t)}\phi_{nr}\left\{v\left(t-t_j\right)\right\}, n=1,2,...,n_b \quad \text{(A-43)}$$

REFERENCES

AASHTO. (2012). LRFD bridge design specifications, *American Association of State Highway and Transportation Officials*, 6th edition. Washington, DC.

AASHTO (2017). AASHTO LRFD Bridge Design Specifications, *American Association of State Highway Transport Officials*, 8th edition. Washington, DC.

Agerskov, H., and Nielsen, J. A. (1999). Fatigue in Steel Highway bridges under random loading. *Journal of Structural Engineering*, *125*(2), 152–162. https://doi.org/10.1061/(ASCE)0733-9445(1999)125:2(152)

Aïd, A., Amrouche, A., Bouiadjra, B. B., Benguediab, M., and Mesmacque, G. (2011). Fatigue life prediction under variable loading based on a new damage model. *Materials and Design*, *32*(1), 183-191. https://doi.org/10.1016/j.matdes.2010.06.010

Akin, J. E. and Mofid, M. (1989). Numerical solution for response of beams with moving mass. *Journal of Structural Engineering*, *115*(1), 120–131. https://doi.org/10.1061/(ASCE)0733-9445(1989)115:1(120)

Alampalli, S., and Lund, R. (2006). Estimating fatigue life of bridge components using measured strains. *Journal of Bridge Engineering*, *11*(6), 725–736. https://doi.org/10.1061/(ASCE)1084-0702(2006)11:6(725)

American Welding Society (AWS). (1995). Bridge welding code. ANSI/AAHSTO/AWS D1.5, Miami.

American Railway Engineering and Maintenance of Way Association (AREMA). (2000). Manual for railway engineering. Chapter 15, *Steel structures*, Landover, Md.

Austroads. (2004). *AS 5100 bridge design standard—Part 2: Design load*, Sydney, Australia.

Aygül, M., Bokesjö, M., Heshmati, M., and Al-Emrani, M. (2013). A comparative study of different fatigue failure assessments of welded bridge details. *International Journal of Fatigue*, *49*, 62-72. https://doi.org/10.1016/j.ijfatigue.2012.12.010

Ayre, R. S. and Jacobsen, L. S. (1950). Transverse vibration of a two-span beam under action of a moving alternate force. *Journal of Applied Mechanics*, *17*(3), 283-290. https://doi.org/10.1115/1.4010129

Ayre, R. S., Ford, G., and Jacobsen, L. S. (1950). Transverse vibration of a two-span beam under action of a moving constant force. *Journal of Applied Mechanics*, *17*(1), 1-12. https://doi.org/10.1115/1.4010050

Azimi, H., Galal, K., and Pekau, O. A. (2013). A numerical element for vehicle–bridge interaction analysis of vehicles experiencing sudden deceleration. *Engineering Structures*, *49*, 792-805. https://doi.org/10.1016/j.engstruct.2012.12.031

Bannantine, J. A., Corner, J.J., and Handrock, J. L. (1990). Fundamentals of metal fatigue analyses, *Prentice Hall*, N.J, USA.

Baptista, C., Reis, A., and Nussbaumer, A. (2017). Probabilistic S-N curves for constant and variable amplitude. *International Journal of Fatigue*, *101*(2), 312–327. https://doi.org/10.1016/j.ijfatigue.2017.01.022

Basquin, O. H. (1910). The Exponential Law of Endurance Tests. *Proceedings of the American Society for Testing and Materials*, *10*, 625-630.

Barsom, J. M. (1974). The development of the AASHTO fracture toughness requirements for bridge steels. *Proc., U.S.-Japan Cooperative Science Seminar*, American Iron and Steel Institute, Washington, D.C.

Barsom, J.M., and S.T. Rolfe. 1999. Fracture and Fatigue Control in Structures: Applications of Fracture Mechanics, *American Society for Testing and Materials*, 3rd Edition. West Conshohocken.

Batchelor, B. D., Hewitt, B. E., and Csagoly, P. (1978). An investigation of the fatigue strength of deck slabs of composite steel/concrete bridges. *Transportation Research Record*, *1*(664), 153-161. https://onlinepubs.trb.org/Onlinepubs/trr/1978/664/664v1-020.pdf

Batsoulas, N. D. (2016). Cumulative fatigue damage: CDM-based engineering rule and life prediction aspect. S*teel Research International*, *87*(12), 1670-1677. https://doi.org/10.1002/srin.201600048

Benasciutti, D., and Tovo, R. (2006). Comparison of spectral methods for fatigue analysis of broad-band Gaussian random processes. *Probabilistic Engineering Mechanics*, *21*(4), 287-299. https://doi.org/10.1016/j.probengmech.2005.10.003

Benkabouche, S., Guechichi, H., Amrouche, A., and Benkhettab, M. (2015). A modified nonlinear fatigue damage accumulation model under multiaxial variable amplitude loading. *International Journal of Mechanical Sciences*, *100*, 180-194. https://doi.org/10.1016/j.ijmecsci.2015.06.016

Bhowmik, S., and Ray, S. (2018). An improved crack propagation model for plain concrete under fatigue loading. *Engineering Fracture Mechanics*, *191*, 365-382. https://doi.org/10.1016/j.engfracmech.2018.01.003

Biezma, M. V, and Schanack, F. (2007). Collapse of steel bridges. *Journal of Performance of Constructed Facilities*, *21*(5), 398 – 405. https://doi.org/10.1061/(ASCE)0887-3828(2007)21:5(398)

Biggs, J. M. (1964). *Introduction to Structural Dynamics*, McGraw-Hill, New York, N.Y.

Blason, S., Correia, J. A. F. O., De Jesus, A. M. P., Calcada, R. A. B., and Fernandez-Canteli, A. (2016). A probabilistic analysis of Miner's law for different loading conditions. *Structural Engineering and Mechanics*, *60*(1), 71–90. https://doi.org/10.12989/sem.2016.60.1.071

Blejwas, T. E., Feng, C. C., and Ayre, R. S. (1979). Dynamic interaction of moving vehicles and structures. Journal of Sound and Vibration, 67(4), 513–521. https://doi.org/10.1016/0022-460X(79)90442-5

Bogsjö, K., Podgórski, K., and Rychlik, I. (2012). Models for road surface roughness. *Vehicle System Dynamics*, *50*(5), 725-747. https://doi.org/10.1080/00423114.2011.637566

Boyer, H. E. (Ed.). (1985). *Atlas of fatigue curves*. ASM International.

Brady, S. P., O'Brien, E. J., and Žnidarič, A. (2006). Effect of vehicle velocity on the dynamic amplification of a vehicle crossing a simply supported bridge. *Journal of Bridge Engineering*, *11*(2), 241-249. https://doi.org/10.1061/(ASCE)1084-0702(2006)11:2(241)

British Standards Institution (BSI). (2006). *Steel, concrete and composite bridges. Part 2: Specification for loads. BS 5400-2*, London.

Bui Quoc, T., Dubuc, J., Bazergui, A., and Biron, A. (1971). Cumulative fatigue damage under strain-controlled conditions. *Journal of Basic Engineering*, *93*(4), 691-698. https://doi.org/10.1115/1.3425328

Bui-Quoc, T., Choquet, J. A., and Biron, A. (1976). Cumulative fatigue damage on large steel specimens under axial programmed loading with nonzero mean stress. *Journal of Engineering Materials and Technology*, *98*(3), 249-255. https://doi.org/10.1115/1.3443375

Cai, C. S., and Chen, S. R. (2004). Framework of vehicle–bridge–wind dynamic analysis. *Journal of Wind Engineering and Industrial Aerodynamics*, *92*(7-8), 579-607. https://doi.org/10.1016/j.jweia.2004.03.007

Cai, C. S., Shi, X. M., Araujo, M., and Chen, S. R. (2007). Effect of approach span condition on vehicle-induced dynamic response of slab-on-girder road bridges. *Engineering Structures*, *29*(12), 3210-3226. https://doi.org/10.1016/j.engstruct.2007.10.004

Cai, Y., Chen, S. S., Rote, D. M., and Coffey, H. T. (1994). Vehicle/guideway interaction for high speed vehicles on a flexible guideway. *Journal of Sound and Vibration*, *175*(5), 625-646. https://doi.org/10.1006/jsvi.1994.1350

Cebon, D. (1999). *Handbook of vehicle-road interaction*. Taylor and Francis. London.

Chaboche, J. L., and Lesne, P. M. (1988). A non-linear continuous fatigue damage model. *Fatigue and Fracture of Engineering Materials and Structures*, *11*(1), 1-17. https://doi.org/10.1111/j.1460-2695.1988.tb01216.x

Chan, T. H., Guo, L., and Li, Z. X. (2003). Finite element modelling for fatigue stress analysis of large suspension bridges. *Journal of Sound and Vibration*, *261*(3), 443-464. https://doi.org/10.1016/S0022-460X(02)01086-6

Chan, T. H., Law, S. S., and Yung, T. H. (2000). Moving force identification using an existing prestressed concrete bridge. *Engineering Structures*, *22*(10), 1261-1270. https://doi.org/10.1016/S0141-0296(99)00084-X

Chan, T. H. T, and O'Connor, C. (1990). Vehicle model for highway bridge impact. *Journal of structural Engineering*, *116*(7), 1772-1793. https://doi.org/10.1061/(ASCE)0733-9445(1990)116:7(1772)

Chan, T. H. T., Zhou, T. Q., Li, Z. X., and Guo, L. (2005). Hot spot stress approach for Tsing Ma Bridge fatigue evaluation under traffic using finite element method. *Structural Engineering and Mechanics*, *19*(3), 261-279. https://doi.org/10.12989/sem.2005.19.3.261

Chang, D., and Lee, H. (1994). Impact factors for simple-span highway girder bridges. *Journal of Structural Engineering*, *120*(3), 704-715. https://doi.org/10.1061/(ASCE)0733-9445(1994)120:3(704)

Chatterjee, P. K., Datta, T. K., and Surana, C. S. (1993). Dynamic response of trussed bridges for moving loads. *Computers and structures*, *46*(6), 1085-1093. https://doi.org/10.1016/0045-7949(93)90094-T

Chatterjee, P. K., Datta, T. K., and Surana, C. S. (1994). Vibration of continuous bridges under moving vehicles. *Journal of Sound and Vibration*, *169*(5), 619-632. https://doi.org/10.1006/jsvi.1994.1037

Chatterjee, P. K., Datta, T. K., and Surana, C. S. (1994). Vibration of suspension bridges under vehicular movement. *Journal of Structural Engineering*, *120*(3), 681–703. https://doi.org/10.1061/(ASCE)0733-9445(1994)120:3(681)

Chatterjee, P. K. and Datta, T. K. (1995). Dynamic analysis of arch bridges under travelling loads. *International Journal of Solids and Structures*, *32*(11), 1585–1594. https://doi.org/10.1016/0020-7683(94)00193-Z

Chen, Y., Feng, M. Q., and Tan, C. A. (2009). Bridge structural condition assessment based on vibration and traffic monitoring. *Journal of Engineering Mechanics*, 135(8), 747-758. https://doi.org/10.1061/(ASCE)0733-9399(2009)135:8(747)

Chen, Y. H. (1978). Dynamic analysis of continuous beams subjected to moving loads. *Journal of the Chinese Institute of Civil and Hydraulic Engineering*,*5*(2), 1-7.

Chen, Y. H. and Li, C. Y. (2000). Dynamic response of elevated high-speed railway. *Journal of Bridge Engineering*, *5*(2), 124–130. https://doi.org/10.1061/(ASCE)1084-0702(2000)5:2(124)

Chen, Z. W., Xu, Y. L., Xia, Y., Li, Q., and Wong, K. Y. (2011). Fatigue analysis of long-span suspension bridges under multiple loading: Case study. *Engineering Structures*, *33*(12), 3246–3256. https://doi.org/10.1016/j.engstruct.2011.08.027

Cheung, Y. K., Au, F. T. K., Zheng, D. Y., and Cheng, Y. S. (1999). Vibration of multi-span non-uniform bridges under moving vehicles and trains by using modified beam vibration functions. *Journal of Sound and Vibration*, *228*(3), 611–628. https://doi.org/10.1006/jsvi.1999.2423

Chiewanichakorn, M., Aref, A. J., and Alampalli, S. (2007). Dynamic and fatigue response of a truss bridge with fiber reinforced polymer deck. *International Journal of Fatigue*, *29*(8), 1475–1489. https://doi.org/10.1016/j.ijfatigue.2006.10.031

Chopra, A. K. (2011). *Dynamic of Structures Theory and Applications to Earthquake Engineering*. (W. J. Hall, Ed.) (Fourth). Prentice Hall.

Chryssanthopoulos, M. K., and Righiniotis, T. D. (2006). Fatigue reliability of welded steel structures. *Journal of Constructional Steel Research*, *62*(11), 1199–1209. https://doi.org/10.1016/j.jcsr.2006.06.007

Chu, K. H., Garg, V. K., and Dhar, C. L. (1979). Railway–bridge impact: Simplified train and bridge model. *Journal of the Structural Division*, *105*(9), 1823–1844. https://doi.org/10.1061/JSDEAG.0005232

Chu, K. H., Garg, V. K., and Wang, T. L. (1986). Impact in railway prestressed concrete bridges. *Journal of Structural Engineering*, *112*(5), 1036–1051. https://doi.org/10.1061/(ASCE)0733-9445(1986)112:5(1036)

Corley, W. G., Hanson, J. M., and Helgason, T. (1978). Design of reinforced concrete for fatigue. *Journal of the Structural Division*, *104*(6), 921-932. https://doi.org/10.1061/JSDEAG.0004944

Corten, H. T, and Dolan, T. J. (1956). Cumulative fatigue damage. In *Proceedings of the International Conference on Fatigue of Metals*. Institution of Mechanical Engineering and American Society of Mechanical Engineers, *1*, 235-242

Costa, J. D., Ferreira, J. A. M., Borrego, L. P., and Abreu, L. P. (2012). Fatigue behaviour of AA6082 friction stir welds under variable loadings. *International Journal of Fatigue*, *37*, 8-16. https://doi.org/10.1016/j.ijfatigue.2011.10.001

Coussy, O., Said, M., and van Hoove, J. P. (1989). The influence of random surface irregularities on the dynamic response of bridges under suspended moving loads. *Journal of Sound and Vibration*, *130*(2), 313–320. https://doi.org/10.1016/0022-460X(89)90556-7

Cui, C., Chen, A., Ma, R., Wang, B., amd Xu, S. (2019). Fatigue life estimation for suspenders of a three-pylon suspension bridge based on vehicle–bridge-interaction analysis. *Materials*, *12*(16), 2617. https://doi.org/10.3390/ma12162617

D'Angelo, L., and Nussbaumer, A. (2017). Estimation of fatigue S-N curves of welded joints using advanced probabilistic approach. *International Journal of Fatigue*, *97*, 98–113. https://doi.org/10.1016/j.ijfatigue.2016.12.032

Daniel C. R., Diaz-Alvarez, H., McKenna, M. H., and Jordan, A. M. (2015). Vibration and acoustic analysis of trussed railroad bridge under moving loads. *Journal of Vibration and Acoustics*, *137*(3), 1-10. https://doi.org/10.1115/1.4029213

Dang-Van, K. (1993). Macro-micro approach in high-cycle multiaxial fatigue. In *Advances in Multiaxial Fatigue*. ASTM International, 120-130, https://doi.org/ 10.1520/STP24799S

Dattoma, V., Giancane, S., Nobile, R., and Panella, F. W. (2006). Fatigue life prediction under variable loading based on a new non-linear continuum damage mechanics model. *International Journal of Fatigue*, *28*(2), 89-95. https://doi.org/10.1016/j.ijfatigue.2005.05.001

DeCoursey, W. (2003). Statistics and probability for engineering applications. Elsevier.

Deng, L., and Cai, C. S. (2009). Identification of parameters of vehicles moving on bridges. *Engineering Structures*, *31*(10), 2474-2485. https://doi.org/10.1016/j.engstruct.2009.06.005

Deng, L, Wang, W, and Yu, Y. (2016). State-of-the-art review on the causes and mechanisms of bridge collapse. *Journal of Performance of Constructed Facilities*, *30*(2), https://doi.org/10.1061/(ASCE)CF.1943-5509.0000731

Deodatis, G. (1996). Simulation of ergodic multivariate stochastic processes. *Journal of Engineering Mechanics*, *122*(8), 778-787. https://doi.org/10.1061/(ASCE)0733-9399(1996)122:8(778)

Deodatis, G. (1996). Non-stationary stochastic vector processes: seismic ground motion applications. *Probabilistic Engineering Mechanics*, *11*(3), 149-167. https://doi.org/10.1016/0266-8920(96)00007-0

Dexter, R. J., and Fisher, J. W. (2000). Fatigue and fracture. *Bridge Engineering Handbook*, CRC Press, Boca Raton–Washington.

Dexter, R. J., Wright, W. J., and Fisher, J. W. (2004). Fatigue and Fracture of Steel Bridges. *Journal of Bridge Engineering*, *9*(3), 278–286. https://doi.org/10.1061/(ASCE)1084-0702(2004)9:3(278)

Dicleli, M., and Bruneau, M. (1995). Fatigue-Based Methodology for Managing Impact of Heavy-Permit Trucks on Steel Highway Bridges. *Journal of Structural Engineering*, *121*(11), 1651-1659. https://doi.org/10.1061/(ASCE)0733-9445(1995)121:11(1651)

Ding, L., Hao, H., and Zhu, X. (2009). Evaluation of dynamic vehicle axle loads on bridges with different surface conditions. *Journal of Sound and Vibration*, *323*(3-5), 826-848. https://doi.org/10.1016/j.jsv.2009.01.051

Ding, Y. L., Song, Y. S., Cao, B. Y., Wang, G. X., and Li, A. Q. (2016). Full-range SN fatigue-life evaluation method for welded bridge structures considering hot-spot and welding residual stress. *Journal of Bridge Engineering*, *21*(12), 04016096. https://doi.org/10.1061/(ASCE)BE.1943-5592.0000969

Dodds, C. J., and Robson, J. D. (1973). The description of road surface roughness. *Journal of Sound and Vibration*, *31*(2), 175-183. https://doi.org/10.1016/S0022-460X(73)80373-6

Dowling, N. E. (1972). *Fatigue life and inelastic strain response under complex histories for analloy steel*. University of Illinois at Urbana-Champaign.

Downing, S. D., and Socie, D. F. (1982). Simple rainflow counting algorithms. *International Journal of Fatigue*, *4*(1), 31-40. https://doi.org/10.1016/0142-1123(82)90018-4

Duan, Y. F., Wang, S. M., Wang, R. Z., Wang, C. Y., Shih, J. Y., and Yun, C. B. (2018). Vector form intrinsic finite-element analysis for train and bridge dynamic interaction. *Journal of Bridge Engineering*, *23*(1), 04017126. https://doi.org/10.1061/(ASCE)BE.1943-5592.0001171

Dubuc, J., Thang, B. Q., Bazergui, A., and Biron, A. (1971). Unified theory of cumulative damage in metal fatigue. *WRC Bulletin*, 162, 1-20.

Dugush, Y. A. and Eisenberger, M. (2002). Vibrations of non-uniform continuous beams under moving loads. *Journal of Sound and Vibration*, *254*(5), 911–926. https://doi.org/10.1006/jsvi.2001.4135

El Aghoury, I., and Galal, K. (2013). A fatigue stress-life damage accumulation model for variable amplitude fatigue loading based on virtual target life. *Engineering Structures*, *52*, 621-628. https://doi.org/10.1016/j.engstruct.2013.03.001

Ellobody, E. (2014). *Finite element analysis and design of steel and steel–concrete composite bridges*. Butterworth-Heinemann.

Erzurumlu, H., and Toprac, A. A. (1972). Fatigue of orthotropic steel decks. *Journal of the Structural Division*, *98*(4), 813-830. https://doi.org/10.1061/JSDEAG.0003201

European Committee for Standardization (CEN). (2003). *Eurocode 1: Actions on structures—Part 2: Traffic loads on bridges*, Brussels, Belgium.

Ewing, J. A. and Humphrey, J. C. W. (1903). The Fracture of Metals under Repeated Alternations of Stress. *Philosophical Transactions of the Royal Society of London. Series A, Containing Papers of a Mathematical or Physical Character*, 200, 241-250, http://doi.org/10.1098/rsta.1903.0006

Fairbairn, W. (1864). VIII. Experiments to determine the effect of impact, vibratory action, and long-continued changes of load on wrought-iron girders. *Philosophical Transactions of the Royal Society of London*, (154), 311-325.

Fertis, D. G. (1973). *Dynamics and vibration of structures*. Wiley-Interscience, New York.

Fisher, J. W. (1977). *Bridge Fatigue Guide Design and Details*. American Institute of Steel Construction, Chicago, USA.

Fisher, J. W. (1984). *Fatigue and fracture in steel bridges*, Wiley, New York.

Fisher, J. W., and Yuceoglu, U. (1981). *A survey of localized cracking in steel bridges: 1981 to 1988. Interim Report (DOT-FT-11-9506)*. Washington: Federal Highway Administration.

Fisher, J. W., Fisher, T. A., and Kostem, C. N. (1979). Displacement induced fatigue cracks. *Engineering Structures*, *1*(5), 252-257. https://doi.org/10.1016/0141-0296(79)90006-3

Fisher, J. W., Jian, J., Wagner, D. C., and Yen, B. T. (1990). Distortion induced fatigue cracking in steel bridges. *NCHRP Rep. 336*, Transportation Research Board, Washington, D.C.

Frank, K. H., and Galambos, C. F. (1972). Application of fracture mechanics to analysis of bridge failures. In Proceedings *Safety and Reliability of Metal Structures* ASCE, 279-306.

Frýba, L. (1968). Impacts of two-axle system traversing a beam. *International Journal of Solids and Structures*, *4*(11), 1107-1123. https://doi.org/10.1016/0020-7683(68)90026-7

Frýba, L. (1972). *Vibration of Solids and Structure*. Prague: Academia.

Frýba, L. (1996). *Dynamics of Railway Bridges*. Academia Praha.

Fu, T. T., and Cebon, D. (2000). Predicting fatigue lives for bi-modal stress spectral densities. *International Journal of Fatigue*, *22*(1), 11–21. https://doi.org/10.1016/S0142-1123(99)00113-9

Fu, G., Liu, L., and Bowman, M. D. (2013). Multiple presence factor for truck load on highway bridges. *Journal of Bridge Engineering*, *18*(3), 240-249. https://doi.org/10.1061/(ASCE)BE.1943-5592.0000330

Galdos, N. H., Schelling, D. R., and Sahin, M. A. (1993). Methodology for impact factor of horizontally curved box bridges, *Journal of Structural Engineering*, *119*(6), 1917–1934. https://doi.org/10.1061/(ASCE)0733-9445(1993)119:6(1917)

Gao, H., Huang, H. Z., Zhu, S. P., Li, Y. F., and Yuan, R. (2014). A modified nonlinear damage accumulation model for fatigue life prediction considering load interaction effects. *The Scientific World Journal*, https://doi.org/10.1155/2014/164378

Gao, J., Yuan, Y., and Xu, R. (2021). A framework for fatigue life prediction of materials under the multi-level cyclic loading. *Engineering Failure Analysis*, *127*, 1-14. https://doi.org/10.1016/j.engfailanal.2021.105496

Gao, K., Liu, G., and Tang, W. (2021). An improved Manson-Halford Model for Multi-level nonlinear fatigue life prediction. *International Journal of Fatigue*, *151*, 1-12. https://doi.org/10.1016/j.ijfatigue.2021.106393

Gao, Q., Wang, Z., Jia, H., Liu, C., Li, J., Guo, B., and Zhong, J. (2015). Dynamic responses of continuous girder bridges with uniform cross-section under moving vehicular loads. *Mathematical Problems in Engineering*, https://doi.org/10.1155/2015/951502

Gatts, R. R. (1961). Closure to Discussions of Application of a Cumulative Damage Concept to Fatigue. *Journal of Basic Engineering*, *83*, 539-540.

Gbadeyan, J. A. and Oni, S. T. (1995). Dynamic behaviour of beams and rectangular plates under moving loads. *Journal of Sound and Vibration*, *182*(5), 677–695. https://doi.org/10.1006/jsvi.1995.0226

Genin, J. and Chung, Y. I. (1979). Response of a continuous guideway on equally spaced supports traversed by a moving vehicle. *Journal of Sound and Vibration*, *67*(2), 245–251. https://doi.org/10.1016/0022-460X(79)90487-5

Genin, J., Ginsberg, J. H., and Ting, E. C. (1975). A complete formulation of inertial effects in the guideway–vehicle interaction problem. *Journal of Sound and Vibration*, *38*(1), 15–26. https://doi.org/10.1016/S0022-460X(75)80017-4

González, A. (2010). *Vehicle-bridge dynamic interaction using finite element modelling*. InTech, London, UK.

González, A., Cantero, D., and OBrien, E. J. (2011). Dynamic increment for shear force due to heavy vehicles crossing a highway bridge. *Computers and Structures*, *89*(23-24), 2261-2272. https://doi.org/10.1016/j.compstruc.2011.08.009

Green, M. F., and Cebon, D. (1994). Dynamic response of highway bridges to heavy vehicle loads: theory and experimental validation. *Journal of Sound and Vibration*, *170*(1), 51-78. https://doi.org/10.1006/jsvi.1994.1046

Green, M. F., and Cebon, D. (1997). Dynamic Interaction Between Heavy Vehicles and Highway Bridges. *Computers and Structures*, *62*(2), 253–264. https://doi.org/10.1016/S0045-7949(96)00198-8

Grover, H. J. (1960). An observation concerning the cycle ratio in cumulative damage. In *Symposium on fatigue of aircraft structures*. ASTM International.

Guowen, Y, Shicong, Y, Jinquan, Z, and Yanling, L. (2021). Analysis of Corrosion-Fatigue Damage and Fracture Mechanism of In-Service Bridge Cables/Hangers. *Advances in Civil Engineering*, 1-10. https://doi.org/10.1155/2021/6633706

Gupta, R. K., and Traill-Nash, R. W. (1980). Bridge dynamic loading due to road surface irregularities and braking of vehicle. *Earthquake Engineering and Structural Dynamics*, *8*(2), 83-96. https://doi.org/10.1002/eqe.4290080202

Gurney, T. R. (1979). *Fatigue of welded structures*. Cambridge University Press, London, UK.

Gu, M., Xu, Y. L., Chen, L. Z., and Xiang, H. F. (1999). Fatigue life estimation of steel girder

of Yangpu cable-stayed bridge due to buffeting. *Journal of Wind Engineering and Industrial Aerodynamics*, *80*(3), 383–400. https://doi.org/10.1016/S0167-6105(98)00209-8

Hahin, C., South, J. M., Mohammadi, J., and Polepeddp, R. K. (1993). Accurate and Rapid Determination of Fatigue Damage in Steel Bridges. *Journal of Structural Engineering*, *119*(1), 150–168. https://doi.org/10.1061/(ASCE)0733-9445(1993)119:1(150)

Han, S., and Shin, B. (2000). The use of hot spot stress for estimating the fatigue strength of welded components. *Steel research*, *71*(11), 466-473. https://doi.org/10.1002/srin.200005716

Hashin, Z., and Rotem, A. (1978). A cumulative damage theory of fatigue failure. *Materials Science and Engineering*, *34*(2), 147-160. https://doi.org/10.1016/0025-5416(78)90045-9

Hayashikawa, T., and Watanabe, N. (1981). Dynamic behavior of continuous beams with moving loads. *Journal of the Engineering Mechanics Division*, *107*(1), 229-246. https://doi.org/10.1061/JMCEA3.0002694

He, L., Akebono, H., Sugeta, A., and Hayashi, Y. (2020). Cumulative fatigue damage of stress below the fatigue limit in weldment steel under block loading. *Fatigue and Fracture of Engineering Materials and Structures*, *43*(7), 1419-1432. https://doi.org/10.1111/ffe.13204

Henchi, K., Fafard, M., Talbot, M., and Dhatt, G. (1998). An efficient algorithm for dynamic analysis of bridges under moving vehicles using a coupled modal and physical components approach. *Journal of Sound and Vibration*, *212*(4), 663-683. https://doi.org/10.1006/jsvi.1997.1459

Henry, D. L. (1955). A theory of fatigue damage accumulation in steel. *ASME Transactions*, 77, 913-918

Ho, H., and Nishio, M. (2020). Evaluation of dynamic responses of bridges considering traffic flow and surface roughness. *Engineering structures*, *225*, 1-10. https://doi.org/10.1016/j.engstruct.2020.111256

Hobbacher, A. (1996). *Fatigue design of welded joints and components: Recommendations of IIW Joint Working Group XIII-XV*. Woodhead Publishing, Sawston, UK.

Holmes, J. D. (2002). Fatigue life under along-wind loading - Closed-form solutions. *Engineering Structures*, *24*(1), 109–114. https://doi.org/10.1016/S0141-0296(01)00073-6

Honda, H., Kajikawa, Y., and Kobori, T. (1982). Spectra of road surface roughness on bridges. *Journal of the Structural Division*, *108*(9), 1956-1966. https://doi.org/10.1061/JSDEAG.0006035.

Huang, D. (2012). Vehicle-induced vibration of steel deck arch bridges and analytical methodology. *Journal of Bridge Engineering*, *17*(2), 241-248. https://doi.org/10.1061/(ASCE)BE.1943-5592.0000243

Huang, D., and Wang, T. L. (1992). Impact analysis of cable-stayed bridges. *Computers and Structures*, *43*(5), 897-908. https://doi.org/10.1016/0045-7949(92)90304-I

Huang, D., Wang, T. L., and Shahawy, M. (1992). Impact analysis of continuous multigirder bridges due to moving vehicles. *Journal of Structural Engineering*, *118*(12), 3427-3443. https://doi.org/10.1061/(ASCE)0733-9445(1992)118:12(3427)

Humar, J. L., and Kashif, A. M. (1993). Dynamic response of bridges under travelling loads. *Canadian Journal of Civil Engineering*, *20*(2), 287–298. https://doi.org/10.1139/l93-033

Hwang, E.-S., and Nowak, A. S. (1991). Simulation of Dynamic Load for Bridges. *Journal of Structural Engineering*, *117*(5), 1413–1434. https://doi.org/10.1061/(ASCE)0733-9445(1991)117:5(1413)

Hwang, J. H., and Kim, J. S. (2000). On the approximate solution of aircraft landing gear under nonstationary random excitations. *KSME international journal*, *14*(9), 968-977.

Iatsko, O., Babu, A. R., Stallings, J. M., and Nowak, A. S. (2020). Weigh-in-Motion-Based Fatigue Damage Assessment. *Transportation Research Record*, *2674*(8), 710-719. https://doi.org/10.1177/0361198120919758

Ichikawa, M., Miyakawa, Y., and Matsuda, A. (2000). Vibration analysis of the continuous beam subjected to a moving mass. *Journal of Sound and Vibration*, *230*(3), 492–506. https://doi.org/10.1006/jsvi.1999.2625.

Imine, H., M'Sirdi, N. K., and Delanne, Y. (2005). Sliding-mode observers for systems with unknown inputs: application to estimating the road profile. *Proceedings of the Institution of Mechanical Engineers, Part D: Journal of Automobile Engineering*, *219*(8), 989-997. https://doi.org/10.1243/095440705X34658

Inbanathan, M. J., and Wieland, M. (1987). Bridge vibrations due to vehicle moving over rough surface. *Journal of Structural Engineering*, *113*(9), 1994-2008. https://doi.org/10.1061/(ASCE)0733-9445(1987)113:9(1994)

Inglis, C. E. (1934). *A Mathematical Treatise on Vibration in Railway Bridges*, The University Press, Cambridge, England.

IRC 6 (2017). Standard specifications and code of practice for road bridges, section-II Loads and stresses. Indian Road Congress, New Delhi.

IRC 22 (2015). Standard specifications and code of practice for road bridges, Section VI Composite Construction. Indian Road Congress, New Delhi.

IRC 24 (2011). Standard specifications and code of practice for road bridges, section-v Steel Road Bridges. Indian Road Congress, New Delhi.

ISO 8608:1995. Mechanical Vibration-Road surface profiles reporting measured data.

Japan Road Association (JRA). (1996). *Specifications for highway bridges. Part 1: Common specifications*, Tokyo.

Jeffcott, H. H. (1929). On the vibrations of beams under the action of moving loads. *Phil. Magazine*, Ser. 7, *8*(48), 66–97. https://doi.org/10.1080/14786440708564857

Jin, Z., Pei, S., Li, X., and Qiang, S. (2015). Probabilistic evaluation approach for nonlinear vehicle–bridge dynamic performances. *Journal of Sound and Vibration*, *339*, 143-156. https://doi.org/10.1016/j.jsv.2014.11.008

Johansson, C., Pacoste, C., and Karoumi, R. (2013). Closed-form solution for the mode superposition analysis of the vibration in multi-span beam bridges caused by concentrated moving loads. *Computers and Structures*, *119*, 85-94. https://doi.org/10.1016/j.compstruc.2013.01.003

Ju, S. H. and Lin, H. T. (2003). Numerical investigation of a steel arch bridge and interaction with high speed trains. *Engineering Structures*, *25*(2), 241–250. https://doi.org/10.1016/S0141-0296(02)00148-7

Juvinall RC. (1967). *Stress, Strain and Strength*. McGraw-Hill Book Co., New York, 194-195.

Kang, D. H., Jang, C., Park, Y. S., Han, S. Y., and Kim, J. H. (2012). Fatigue reliability assessment of steel member using probabilistic stress-life method. *Advances in Mechanical Engineering*, *4*, 1-10. https://doi.org/10.1155/2012/649215

Keating, P. B., and Fisher, J. W. (1986). Evaluation of fatigue tests and design criteria on welded details. *NCHRP Rep. 286*, Transportation Research Board, Washington, D.C.

Kou, J. W. and DeWolf, J. T. (1997). Vibrational behavior of continuous span highway bridge- Influencing variables. *Journal of Structural Engineering*, *123*(3), 333–344. https://doi.org/10.1061/(ASCE)0733-9445(1997)123:3(333)

Kujawski, D., and Ellyin, F. (1984). A fatigue crack propagation model. *Engineering Fracture Mechanics*, *20*(5-6), 695-704. https://doi.org/10.1016/0013-7944(84)90079-1

Kun, F., Carmona, H. A., Andrade Jr, J. S., and Herrmann, H. J. (2008). Universality behind Basquin's law of fatigue. *Physical Review Letters*, *100*(9), 094301. https://doi.org/10.1103/PhysRevLett.100.094301

Kwofie, S., and Rahbar, N. (2013). A fatigue driving stress approach to damage and life prediction under variable amplitude loading. *International Journal of Damage Mechanics*, *22*(3), 393-404. https://doi.org/10.1177/1056789512449638

Kwon, K., and Frangopol, D. M. (2010). Bridge fatigue reliability assessment using probability density functions of equivalent stress range based on field monitoring data. *International Journal of Fatigue*, *32*(8), 1221–1232. https://doi.org/10.1016/j.ijfatigue.2010.01.002

Łagoda, T., Macha, E., and Będkowski, W. (1999). A critical plane approach based on energy concepts: application to biaxial random tension-compression high-cycle fatigue regime. *International Journal of Fatigue*, *21*(5), 431-443. https://doi.org/10.1016/S0142-1123(99)00003-1

Łagoda, T., Macha, E., and Niesłony, A. (2005). Fatigue life calculation by means of the cycle counting and spectral methods under multiaxial random loading. *Fatigue and Fracture of Engineering Materials and Structures*, *28*(4), 409-420. https://doi.org/10.1111/j.1460-2695.2005.00877.x

Langer, B. F. (1937). Fatigue Failure from Stress Cycle of Varying Magnitude. *Journal of Applied Mechanics*, *4*(4), A160- A162, https://doi.org/10.1115/1.4008807

Law, S. S., and Zhu, X. Q. (2005). Bridge dynamic responses due to road surface roughness and braking of vehicle. *Journal of Sound and Vibration*, *282*(3-5), 805-830. https://doi.org/10.1016/j.jsv.2004.03.032

Lee, S. B. (1996). Fatigue failure of welded vertical members of a steel truss bridge. *Engineering Failure Analysis*, *3*(2), 103-108, https://doi.org/10.1016/1350-6307(96)00003-9

Lefebvre, D., and Ellyin, F. (1984). Cyclic response and inelastic strain energy in low cycle fatigue. *International Journal of Fatigue*, *6*(1), 9-15. https://doi.org/10.1016/0142-1123(84)90003-3

Leipholz, H. H. E., Topper, T., and El Menoufy, M. (1983). Lifetime prediction for metallic components subjected to stochastic loading. *Computers and Structures*, *16*(1-4), 499-507. https://doi.org/10.1016/0045-7949(83)90190-6

Leipholz, H. H. E. (1985). Lifetime prediction for metallic specimens subjected to loading with varying intensity. *Computers and Structures*, *20*(1-3), 239-246. https://doi.org/10.1016/0045-7949(85)90073-2

Leipholz, H. H. E. (1986). On the modified SN curve for metal fatigue prediction and its experimental verification. *Engineering Fracture Mechanics*, *23*(3), 495-505. https://doi.org/10.1016/0013-7944(86)90158-X

Leitao, F. N., Silva, J. G. S., and Andrade, S. A. L. (2013). Fatigue analysis and life prediction of composite high- way bridge decks under traffic loading. *Latin American Journal of Solids and Structures*, *10*(3), 505–522. https://doi.org/10.1590/S1679-78252013000300004

Li, J., and Chen, J. (2009). *Stochastic dynamics of structures*. John Wiley & Sons (Asia) Pte Ltd.

Li, Z. X., Chan, T. H. T., and Ko, J. M. (2001). Fatigue analysis and life prediction of bridges with structural health monitoring data — Part I: methodology and strategy. *International Journal of Fatigue*, *23*(1), 45–53. https://doi.org/10.1016/S0142-1123(00)00068-2

Lin, Y. K. (1976). *Probabilistic theory of structural dynamics*. Krieger Publishing Company.

Liu, C., Huang, D., and Wang, T. L. (2002). Analytical dynamic impact study based on correlated road roughness. *Computers and structures*, *80*(20-21), 1639-1650. https://doi.org/10.1016/S0045-7949(02)00113-X

Liu, M. D., Xiong, J. J., and Wang, C. Q. (2019). A modified accumulation damage algorithm for predicting corrosion fatigue life by considering load interaction for aluminium alloys. *International Journal of Damage Mechanics*, *28*(2), 270-290. https://doi.org/10.1177/1056789518763707

Liu, Q., Gao, Y., Li, Y., and Xue, Q. (2020). Fatigue life prediction based on a novel improved version of the Corten-Dolan model considering load interaction effect. *Engineering Structures*, *221*, 111036. https://doi.org/10.1016/j.engstruct.2020.111036

Lou, P. (2005). A vehicle-track-bridge interaction element considering vehicle's pitching effect. *Finite Elements in Analysis and Design*, *41*(4), 397-427. https://doi.org/10.1016/j.finel.2004.07.004

Lu, F., Lin, J. H., Kennedy, D., and Williams, F. W. (2009). An algorithm to study non-stationary random vibrations of vehicle–bridge systems. *Computers and Structures*, *87*(3-4), 177-185. https://doi.org/10.1016/j.compstruc.2008.10.004

Lu, X., Kim, C. W., and Chang, K. C. (2020). Finite element analysis framework for dynamic vehicle-bridge interaction system based on ABAQUS. *International Journal of Structural Stability and Dynamics*, *20*(03), 2050034. https://doi.org/10.1142/S0219455420500340

Lutes, L. D., Corazao, M., Hu, S. J., and Zimmerman, J. (1984). Stochastic Fatigue Damage Accumulation. *Journal of Structural Engineering*, *110*(11), 2585–2601. https://doi.org/10.1061/(ASCE)0733-9445(1984)110:11(2585)

Lutes, L. D., and Larsen, C. E. (1990). Improved spectral method for variable amplitude fatigue prediction. *Journal of Structural Engineering*, *116*(4), 1149–1164. https://doi.org/10.1061/(ASCE)0733-9445(1990)116:4(1149)

Ma, R., Xu, S., Wang, D., and Chen, A. (2018). Vehicle models for fatigue loading on steel box-girder bridges based on weigh-in-motion data. *Structure and Infrastructure Engineering*, *14*(6), 701-713. https://doi.org/10.1080/15732479.2017.1359308

Maddox, S. J. (1991). *Fatigue strength of welded structures*. Woodhead publishing, Sawston, UK.

Manson, S. S, Freche, J. C, and Ensign, C. R. (1967). *Application of a double linear damage rule to cumulative fatigue*. National Aeronautics and Space Administration, Vol No. 3839.

Manson, S. S., and Halford, G. R. (1981). Practical implementation of the double linear damage rule and damage curve approach for treating cumulative fatigue damage. *International Journal of Fracture*, *17*(2), 169-192. https://doi.org/10.1007/BF00053519

Manson S.S. and Halford G. R. (2006). *Fatigue and Durability of Structural Materils.* ASM International, USA

Manual, Introduction to CSiBridge 2017. *Computers and Structures, Inc., Berkeley, California, USA*.

Manual, S. T. SAP2000 Integrated Finite Elements Analysis and Design of Structures Tutorial Manual. *Computers and Structures, Inc., Berkeley, California, USA*.

Marchesiello, S., Fasana, A., Garibaldi, L., and Piombo, B. A. D. (1999). Dynamics of multi-span continuous straight bridges subject to multi-degrees of freedom moving vehicle excitation. *Journal of Sound and Vibration*, *224*(3), 541–561. https://doi.org/10.1006/jsvi.1999.2197

Marco, S. M., and Starkey, W. L. (1954). A concept of fatigue damage. *Transactions ASME*, *76*(4), 627-632,

Marcondes, J., Burgess, G. J., Harichandran, R., and Snyder, M. B. (1991). Spectral analysis of highway pavement roughness. *Journal of Transportation engineering*, *117*(5), 540-549. https://doi.org/10.1061/(ASCE)0733-947X(1991)117:5(540)

Meirovitch L. (1986). *Elements of vibration analysis*, McGraw Hill.

Michaltsos, G., Sophianopoulos, D., and Kounadis, A. N. (1996). The effect of a moving mass and other parameters on the dynamic response of a simply supported beam. *Journal of sound and Vibration*, *191*(3), 357-362. https://doi.org/10.1006/jsvi.1996.0127

Miki, C., and Tateishi, K. (1997). Fatigue strength of cope hole details in steel bridges. *International Journal of Fatigue*, *19*(6), 445-455. https://doi.org/10.1016/S0142-1123(97)85727-1

Miller, K. J., and Zachariah, K. P. (1977). Cumulative damage laws for fatigue crack initiation and stage I propagation. *The Journal of Strain Analysis for Engineering Design*, *12*(4), 262-270. https://doi.org/10.1243/03093247V124262

Miner, M. A. (1945). Cumulative Damage in Fatigue. *Journal of Applied Mechanics, 12*(3), A159-A164, https://doi.org/10.1115/1.4009458

Mohammadi, J., Guralnick, A., and Polepeddi, R. (1998). Bridge Fatigue Life Estimation from Field Data. *Practice Periodical on Structural Design and Construction*, *3*(3), 128–133. https://doi.org/10.1061/(ASCE)1084-0680(1998)3:3(128)

Mori, T., Lee, H. H., and Kyung, K. S. (2007). Fatigue life estimation parameter for short and medium span steel highway girder bridges. *Engineering Structures*, *29*(10), 2762–2774. https://doi.org/10.1016/j.engstruct.2007.01.019

Munse, W. H., and Stallmeyer, J. E. (1962). Fatigue in welded beams and girders. *Highway Research Board Bulletin*.

Nallasivam, K., Talukdar, S., and Dutta, A. (2008). Fatigue life prediction of horizontally curved thin walled box girder steel bridges. *Structural Engineering and Mechanics: An International Journal*, *28*(4), 387-410. https://doi.org/10.12989/sem.2008.28.4.387

Nam, D. W., Choi, H. K., Kim, K. N., and Jung, K. S. (2008). Resonance Characteristics of a Arch Bridge for High-Speed Railways. *Journal of Korean Society of Steel Construction*, *20*(4), 455-467.

Newland, D.E. (1993). *An Introduction to Random Vibrations, Spectral and Wavelet Analysis.* 3Ed., Longman Scientific and Technical, Longman House, England.

Nigam, N. C. (1983). *Introduction to Random Vibrations*. The MIT Press Cambridge, Masachusetts, London, England.

Nigam, N. C., and Yadav, D. (1974). Dynamic response of accelerating vehicles to ground roughness. In *Proc., Noise Shock and Vibration Conf., Monash Univ.-Clayton, Victoria, Australia*. 280-285.

Oh, B. H. (1986). Fatigue analysis of plain concrete in flexure. *Journal of Structural Engineering*, *112*(2), 273-288. https://doi.org/10.1061/(ASCE)0733-9445(1986)112:2(273)

Oh, B. H. (1991). Fatigue life distributions of concrete for various stress levels. *Materials Journal*, *88*(2), 122-128.

Oliva, J., Goicolea, J. M., Antolín, P., and Astiz, M. Á. (2013). Relevance of a complete road surface description in vehicle-bridge interaction dynamics. Engineering Structures, 56, 466–476. https://doi.org/10.1016/j.engstruct.2013.05.029

Oller, S., Salomón, O., and Oñate, E. (2005). A continuum mechanics model for mechanical fatigue analysis. *Computational Materials Science*, *32*(2), 175-195. https://doi.org/10.1016/j.commatsci.2004.08.001

Ouyang, H. (2011). Moving-load dynamic problems: A tutorial (with a brief overview). *Mechanical Systems and Signal Processing*, *25*(6), 2039-2060. https://doi.org/10.1016/j.ymssp.2010.12.010

Papakyriacou M., Mayer H., Pypen C., Plenk H., Stanzl-Tschegg S. (2001). Influence of Loading frequency on high cycle fatigue properties of b.c.c. and h.c.p. metals. *Materials Science and Engineering: A*, *308*(1-2),143–152. https://doi.org/10.1016/S0921-5093(00)01978-X

Parida, S., and Talukdar, S. (2020). An Insight to the Dynamic Amplification Factor for Steel Truss Girder Bridge. *International Journal of Steel Structures*, *20*(4), 1341-1354. https://doi.org/10.1007/s13296-020-00364-y

Paris, P., and Erdogan, F. (1963). A critical analysis of crack propagation laws. *Journal of Basic Engineering*, *85*(4), 528-533. https://doi.org/10.1115/1.3656900

Pedikaris, P. C., Beim, S. R., and Bousias, S. N. (1989). Slab continuity effect on ultimate and fatigue strength of reinforced concrete bridge deck models. *Structural Journal*, *86*(4), 483-491.

Peng, Z., Huang, H. Z., Zhou, J., and Li, Y. F. (2018). A new cumulative fatigue damage rule based on dynamic residual SN curve and material memory concept. *Metals*, *8*(6), 456. https://doi.org/10.3390/met8060456

Pesterev, A. V., Yang, B., Bergman, L. A., and Tan, C. A. (2001). Response of elastic continuum carrying multiple moving oscillators. *Journal of Engineering Mechanics*, *127*(3), 260–265. https://doi.org/10.1061/(ASCE)0733-9399(2001)127:3(260)

Pesterev, A. V., Bergman, L. A., Tan, C. A., Tsao, T. C., and Yang, B. (2003). On Asymptotics of the Solution of the Moving Oscillator Problem. *Journal of Sound and Vibration*, *260*(3), 519–536. https://doi.org/10.1016/S0022-460X(02)00953-7

Piriera, H.S.F.G., DuQuesnay, D.L., DeJesus, A.M.P., and Silva, A.L.L. (2009). Analysis of Variable Amplitude Fatigue Data of the P355NL1 Steel using the Effective Strain Range Damage Model. *Journal of Pressure Vessel Technology*, *131*(5), 1-10. https://doi.org/10.1115/1.3147986

Pipinato, A., Molinari, M., Pellegrino, C., Bursi, O. S., and Modena, C. (2011). Fatigue tests on riveted steel elements taken from a railway bridge. *Structure and Infrastructure Engineering*, *7*(12), 907–920. https://doi.org/10.1080/15732470903099776

Poutiainen, I., Tanskanen, P., and Marquis, G. (2004). Finite element methods for structural hot spot stress determination—a comparison of procedures. *International Journal of Fatigue*, *26*(11), 1147-1157. https://doi.org/10.1016/j.ijfatigue.2004.04.003

Rabotnov, Y. N., Leckie, F. A., and Prager, W. (1970). Creep problems in structural members, John Wiley and Sons, New York, NY, USA.

Radaj, D. (1990). *Design and analysis of fatigue resistant welded structures*. Woodhead Publishing, Sawston, UK.

Radaj, D., Sonsino, C. M., and Fricke, W. (2006). *Fatigue assessment of welded joints by local approaches*. Woodhead publishing, Sawston, UK.

Rao, G. V. (2000). Linear dynamics of an elastic beam under moving loads, *Journal of Vibration and Acoustics*, *122*(3), 281–289. https://doi.org/10.1115/1.1303822

Rao, V. G., and Talukdar, S. (2003). Prediction of fatigue life of a continuous bridge girder based on vehicle induced stress history. *Shock and Vibration*, *10*(5–6), 325–338. https://doi.org/10.1155/2003/309413

Rao, J. S., Pathak, A., and Chawla, A. (2001). Blade life: a comparison by cumulative damage theories. *Journal of Engineering for Gas Turbines and Power*, *123*(4), 886-892. https://doi.org/10.1115/1.1384879

Ray, S., and Kishen, J. C. (2010). Fatigue crack propagation model for plain concrete–An analogy with population growth. *Engineering Fracture Mechanics*, *77*(17), 3418-3433. https://doi.org/10.1016/j.engfracmech.2010.09.008

Ray, S., and Kishen, J. C. (2011). Fatigue crack propagation model and size effect in concrete using dimensional analysis. *Mechanics of Materials*, *43*(2), 75-86. https://doi.org/10.1016/j.mechmat.2010.12.002

Ray, S., and Kishen, J. C. (2014). Analysis of fatigue crack growth in reinforced concrete beams. *Materials and structures*, *47*, 183-198. https://doi.org/10.1617/s11527-013-0054-0

Reed R.P., Smith J. H. and Christ B.W. (1983). *The economic effects of fracture in the United States*. Special Publications 647-1, National Bureau of Standards, U.S. Department of Commerce, Gaithersburg, MD.

Repetto, M. P. (2005). Cycle counting methods for bi-modal stationary Gaussian processes. *Probabilistic Engineering Mechanics*, *20*(3), 229–238. https://doi.org/10.1016/j.probengmech.2005.05.004

Ribeiro, D., Costa, B., Cruz, L., Oliveira, M., Alves, V., Montenegro, P., and Calçada, R. (2021). Simulation of the Dynamic Behavior of a Centenary Metallic Bridge under Metro Traffic Actions Based on Advanced Interaction Models. *International Journal of Structural Stability and Dynamics*, *21*(04), 2150057. https://doi.org/10.1142/S0219455421500577

Rice, J. R. (1968). A path independent integral and the approximate analysis of strain concentration by notches and cracks. *Journal of Applied Mechanics*, *35*(2), 379-386. https://doi.org/10.1115/1.3601206

Richart, F. E, and Newmark, N. M. (1948). An hypothesis for the determination of cumulative damage in fatigue. In *Selected Papers By Nathan M. Newmark: Civil Engineering Classics, ASCE,* 279-312

Rychlik, I., and Gupta, S. (2007). Rain-flow fatigue damage for transformed Gaussian loads. *International Journal of Fatigue*, *29*(3), 406–420. https://doi.org/10.1016/j.ijfatigue.2006.05.006

Sadiku, S. and Leipholz, H. H. E. (1987). On the dynamics of elastic systems with moving concentrated masses. *Ingenieur-Archiv*, *57*, 223–242. https://doi.org/10.1007/BF02570609

Salomon, O., Oller, S., and Oñate, E. (2002). Fatigue analysis of materials and structures using a continuum damage model. *International Journal of Forming Processes*, *5*(2-3-4), 493-503. doi:10.3166/ijfp.5.493-503

Sasidhar, M. N. V., and Talukdar, S. (2003). Nonstationary Response of Bridge Due to Eccentrically Moving Vehicles at Variable Velocity. *Advances in Structural Engineering*, *6*(4), 309-324. https://doi.org/10.1260/136943303322771691

Savin, E. (2001). Dynamic amplification factor and response spectrum for the evaluation of vibrations of beams under successive moving loads. *Journal of Sound and Vibration*, *248*(2), 267-288. https://doi.org/10.1006/jsvi.2001.3787

Schenk, C. A., and Bergman, L. A. (2003). Response of continuous system with stochastically varying surface roughness to moving load. *Journal of Engineering Mechanics*, *129*(July), 759–768. https://doi.org/10.1061/(ASCE)0733-9399(2003)129:7(759)

Schijve J. (2001). *Fatigue of structures and materials*. Kluwer Academic Publishers, Dordrecht, The Netherlands.

Schilling, C. G., and Klippstein, K. H. (1978). New method for fatigue design of bridges. *Journal of the Structural Division*, *104*(3), 425-438.

Schoutens, W. (2000). Lecture notes in statistics. In P. Bickel, P. Diggle, S. Fienberg, K. Krickeberg, I. Olkin, N. Wermuth, and S. Zeger (Eds.), *Stochastic Processes and Orthogonal Polynomials*. Springer. https://doi.org/10.1007/978-1-4612-1470-0

Shank, M.E. (1954). A Critical Survey of Brittle Failure in Carbon Plate Steel Structures Other than Ships. *National Research Council, Committee on Ship Structural Design*, Washington, DC, USA.

Shanley, F. R. (1952). *A theory of fatigue based on unbonding during reversed slip*. Rand Corp Santa Monica CA.

Shen, H., Lin, J., and Mu, E. (2000). Probabilistic model on stochastic fatigue damage. *International Journal of Fatigue*, *22*(7), 569–572. https://doi.org/10.1016/S0142-1123(00)00030-X

Shi, X., Cai, C. S., and Chen, S. (2008). Vehicle induced dynamic behavior of short-span slab bridges considering effect of approach slab condition. *Journal of Bridge Engineering*, *13*(1), 83-92. https://doi.org/10.1061/(ASCE)1084-0702(2008)13:1(83)

Shimokawa, T., and Tanaka, S. (1980). A statistical consideration of Miner's rule. *International Journal of Fatigue*, *2*(4), 165-170. https://doi.org/10.1016/0142-1123(80)90044-4

Shinozuka, M. (1971). Simulation of multivariate and multidimensional random processes. *The Journal of the Acoustical Society of America*, *49*(1B), 357-368. https://doi.org/10.1121/1.1912338

Shinozuka, M., and Deodatis, G. (1991). Simulation of Stochastic Processes by Spectral Representation. *Applied Mechanics Reviews*, *44*(4). 191–204. https://doi.org/10.1115/1.3119501

Sieniawska, R., and Śniady, P. (1990). Life expectancy of highway bridges due to traffic load. *Journal of Sound and Vibration*, *140*(1), 31-38. https://doi.org/10.1016/0022-460X(90)90904-E

Si-Jian, L., Wei, L., Da-Qing, T., and Jun-Bi, L. (2018). A new fatigue damage accumulation model considering loading history and loading sequence based on damage equivalence. *International Journal of Damage Mechanics*, *27*(5), 707-728. https://doi.org/10.1177/1056789517701531

Śniady, P. (1984). Vibration of a beam due to a random stream of moving forces with random velocity. *Journal of Sound and Vibration*, *97*(1), 23-33. https://doi.org/10.1016/0022-460X(84)90464-4

Śniady, P., Biernat, S., Sieniawska, R., and Zukowski, S. (2001). Vibrations of the beam due to a load moving with stochastic velocity. *Probabilistic Engineering Mechanics*, *16*(1), 53–59. https://doi.org/10.1016/S0266-8920(00)00007-2

Solnes J. (1997). *Stochastic processes and random vibrations: Theory and practice*. John Wiley and Sons, Chichester.

Sridharan, N., and Mallik, A. M. (1979). Numerical analysis of vibration of beams subjected to moving loads. *Journal of Sound and Vibration*. *65*(1), 147-150. https://doi.org/10.1016/0022-460X(79)90536-4

Subramanyan, S. (1976). A cumulative damage rule based on the knee point of the SN curve. *Journal of Engineering Materials and Technology*, *98*(4), 316-321. https://doi.org/10.1115/1.3443383

Stanisic, M. M. (1985). On a new theory of the dynamic behavior of the structures carrying moving masses. *Ingenieur-Archiv*, *55*, 176–185. https://doi.org/10.1007/BF00536412

Stanisic, M. M. and Hardin, J. C. (1969). On the response of beams to an arbitrary number of concentrated moving masses. *Journal of the Franklin Institute*, *287*(2), 115–123.

Stokes, S. G. G. (1849). Discussion of a differential equation relating to the breaking of railway bridges. *Transactions of the Cambridge Philosophical Society*, *8*(5), 707-735.

Subramanian, N. (2008). *Design of steel structures*. Oxford University Press.

Sun, L. (2013). An overview of a unified theory of dynamics of vehicle–pavement interaction under moving and stochastic load. *Journal of Modern Transportation*, *21*(3), 135-162. https://doi.org/10.1007/s40534-013-0017-8

Sun, L., and Kennedy, T. W. (2002). Spectral analysis and parametric study of stochastic pavement loads. *Journal of Engineering Mechanics*, *128*(3), 318–327. https://doi.org/10.1061/(ASCE)0733-9399(2002)128:3(318)

Sun, L., Zhang, Z., and Ruth, J. (2001). Modelling indirect statistics of surface roughness. *Journal of Transportation Engineering*, *127*(2), 105-111. https://doi.org/10.1061/(ASCE)0733-947X(2001)127:2(105)

Sun, Q., Dui, H. N., and Fan, X. L. (2014). A statistically consistent fatigue damage model based on Miner's rule. *International Journal of Fatigue*, *69*, 16–21. https://doi.org/10.1016/j.ijfatigue.2013.04.006

Tan, C. P. and Shore, S. (1968). Response of horizontally curved bridge to moving load. *Journal of the Structural Division*, *94*(9), 2135-2154. https://doi.org/10.1061/JSDEAG.0002068

Tan, G. H., Brameld, G. H., and Thambiratnam, D. P. (1998). Development of analytical model for treating bridge–vehicle interaction. *Engineering Structures*, *20*(1-2), 54–61. https://doi.org/10.1016/S0141-0296(97)00051-5

Tanaka, K., and Mura, T. (1981). A dislocation model for fatigue crack initiation. *Journal of Applied Mechanics*, 48(1): 97–103. https://doi.org/10.1115/1.3157599

Tanaka, K., and Mura, T. (1982). A theory of fatigue crack initiation at inclusions. *Metallurgical Transactions A*,*13*, 117-123. https://doi.org/10.1007/BF02642422

Theil, N. (2016). Fatigue life prediction method for the practical engineering use taking in account the effect of the overload blocks. *International Journal of Fatigue*, *90*, 23-35. https://doi.org/10.1016/j.ijfatigue.2016.04.006

Timoshenko, S. P. (1922). CV. On the forced vibrations of bridges. *The London, Edinburgh, and Dublin Philosophical Magazine and Journal of Science*, *43*(257), 1018-1019.

Ting, E. C., Genin, J., and Ginsberg, J. H. (1974). A general algorithm for the moving mass problem. *Journal of Sound and Vibration*, *33*(1), 49–58. https://doi.org/10.1016/S0022-460X(74)80072-6

Unsworth, J. F. (2003). Heavy axle load effects on fatigue life of steel bridges. *Transportation research record*, *1825*(1), 38-47. https://doi.org/10.3141/1825-06

Valluri, S. R. (1961). *A unified engineering theory of high stress level fatigue* (No. ARL-181). California. Inst. of Tech., Pasadena. Guggenheim Aeronautical Lab.

Van Delft, D. R. V. (1981). A two dimensional analyses of stress at the vicinity of weld toes of tubular structures. In *Stevin Report 6-81-8*. Delft University of Technology Delft, The Netherlands.

Veletsos, A. S. and Huang, T. (1970). Analysis of dynamic response of highway bridges. *J. Eng. Mech. Div.*, ASCE, *96*(5), 593–620. https://doi.org/10.1061/JMCEA3.0001277

Vellozzi, J. (1967). Vibration of suspension bridges under moving loads. *Journal of the Structural Division*, *93*(4), 123-138. https://doi.org/10.1061/JSDEAG.0001724

Virchis, V. J., and Robson, J. D. (1971). Response of an accelerating vehicle to random road undulation. *Journal of Sound and Vibration*, *18*(3), 423-427. https://doi.org/10.1016/0022-460X(71)90713-9

Wang, G. S. (1995). An EPFM analysis of crack initiation, stable growth and instability. *Engineering Fracture Mechanics*, *50*(2), 261-282. https://doi.org/10.1016/0013-7944(94)00189-O

Wang, R. T. (1997). Vibration of multi-span Timoshenko beams to a moving force, *Journal of Sound and Vibration*, *207*(5), 731–742. https://doi.org/10.1006/jsvi.1997.1188

Wang, T. L., Huang, D., and Shahawy, M. (1992). Dynamic response of multigirder bridges. *Journal of Structural Engineering*, *118*(8), 2222–2238. https://doi.org/10.1061/(ASCE)0733-9445(1992)118:8(2222)

Wang, T.-L., Liu, C., Huang, D., and Shahawy, M. (2005). Truck Loading and Fatigue Damage Analysis for Girder Bridges Based on Weigh-in-Motion Data. *Journal of Bridge Engineering*, *10*(1), 12–20. https://doi.org/10.1061/(ASCE)1084-0702(2005)10:1(12)

Wang, T. L., Shahawy, M., and Huang, D. Z. (1993). Dynamic response of highway trucks due to road surface roughness. *Computers and structures*, *49*(6), 1055-1067. https://doi.org/10.1016/0045-7949(93)90017-8

Wang, T. L., Shahawy, M., and Huang, D. Z. (1993). Probabilistic fatigue life analysis of highway steel bridges. *Computers and structures*, *48*(2), 241-248. https://doi.org/10.1016/0045-7949(93)90416-B

Wang, W., and Deng, L. (2016). Impact Factors for Fatigue Design of Steel I-girder Bridges Considering the Deterioration of Road Surface Condition. *Journal of Bridge Engineering*, *21*(5), 1-10. https://doi.org/10.1061/(ASCE)BE.1943-5592.0000885

Wang, W., Deng, L., and Shao, X. (2016). Number of stress cycles for fatigue design of simply-supported steel I-girder bridges considering the dynamic effect of vehicle loading. *Engineering Structures*, *110*, 70–78. https://doi.org/10.1016/j.engstruct.2015.11.054

Weaver Jr, W., Timoshenko, S. P., and Young, D. H. (1991). *Vibration problems in engineering*. John Wiley and Sons, New York, NY.

Wei, X., Xiao, L., and Pei, S. (2017). Fatigue assessment and stress analysis of cope-hole details in welded joints of steel truss bridge. *International Journal of Fatigue*, *100*, 136–147. https://doi.org/10.1016/j.ijfatigue.2017.03.032

Wen, R. K. (1960). Dynamic response of beams traversed by two-axle loads, *Journal of the Engineering Mechanics Division*, *86*(5), 91–111. https://doi.org/10.1061/JMCEA3.0000180

Willis, R. (1849). Preliminary essay to the Appendix B: Experiments for determining the effects produced by causing weights to travel over bars with different velocities. *Report of the commissions appointed to inquire into the application of iron to railway structures, London*.

Wirsching, P.H., Albrecht, P., Artley-Dean, M., Ellingwood, B., Schilling, C.G., and Zetrtlemoyer, N. (1982). Fatigue reliability: Variable amplitude loading. *Journal of Structural Engineering Division*,*108*, 47-69.

Wiriyachai, A., Chu, K. H., and Garg, V. K. (1982). Bridge impact due to wheel and track irregularities. *Journal of the Engineering Mechanics Division*, *108*(4), 648–666. https://doi.org/10.1061/JMCEA3.0002851

Wu, J. S. and Dai, C. W. (1987). Dynamic responses of multispan nonuniform beam due to moving loads, *Journal of Structural Engineering*, *113*(3), 458–474. https://doi.org/10.1061/(ASCE)0733-9445(1987)113:3(458)

Xia, F. L., Zhu, S. P., Liao, D., Dantas, R., Correia, J. A., and De Jesus, A. M. (2020). Isodamage curve-based fatigue damage accumulation model considering the exhaustion of static toughness. *Engineering Failure Analysis*, *115*, 104575. https://doi.org/10.1016/j.engfailanal.2020.104575

Xiao, X., Yan, Y., and Chen, B. (2019). Stochastic dynamic analysis for vehicle-track-bridge system based on probability density evolution method. *Engineering Structures*, *188*, 745-761. https://doi.org/10.1016/j.engstruct.2019.02.042

Xiao, Z. G., and Yamada, K. (2004). A method of determining geometric stress for fatigue strength evaluation of steel welded joints. *International Journal of Fatigue*, *26*(12), 1277-1293. https://doi.org/10.1016/j.ijfatigue.2004.05.001

Xu, Y. L., Li, Q., Wu, D. J., and Chen, Z. W. (2010). Stress and acceleration analysis of coupled vehicle and long-span bridge systems using the mode superposition method. *Engineering Structures*, *32*(5), 1356-1368. https://doi.org/10.1016/j.engstruct.2010.01.013

Xu, L., and Zhai, W. (2019). A three-dimensional model for train-track-bridge dynamic interactions with hypothesis of wheel-rail rigid contact. *Mechanical Systems and Signal Processing*, *132*, 471-489. https://doi.org/10.1016/j.ymssp.2019.04.025

Xu, X., Xue, Q., and He, Y. (2021). A Corten-Dolan model considering material strength degradation. *Mechanics of Solids*, 1-14. https://doi.org/10.3103/S002565442201006X

Yadav, D., and Nigam, N. C. (1978). Ground induced non-stationary response of vehicles. *Journal of Sound and Vibration*, *61*(1), 117-126. https://doi.org/10.1016/0022-460X(78)90046-9

Yadav, D., and Upadhyay, H. C. (1991). Non-stationary dynamics of train and flexible track over inertial foundation during variable velocity runs. *Journal of Sound and Vibration*, *147*(1), 57-71. https://doi.org/10.1016/0022-460X(91)90683-B

Yadav, D., and Upadhyay, H. C. (1993). Heave-pitch-roll dynamics of a vehicle with a variable velocity over a non-homogeneously profiled flexible track. *Journal of Sound and Vibration*, *164*(2), 337-348. https://doi.org/10.1006/jsvi.1993.1218

Yamada, K., and Albrecht, P. (1977). Fatigue behaviour of two flange details. *Journal of the Structural Division*, *103*(4), 781-791. https://doi.org/10.1061/JSDEAG.0004606

Yang, Y. B. and Lin, B. H. (1995). Vehicle–bridge interaction analysis by dynamic condensation method. *Journal of Structural Engineering*, *121*(11), 1636–1643. https://doi.org/10.1061/(ASCE)0733-9445(1995)121:11(1636)

Yang, Y. B., and Lin, C. W. (2004). Vehicle-bridge interaction dynamics and potential applications. World Scientific Publishing Co. Pte. Ltd. https://doi.org/10.1016/j.jsv.2004.06.032

Yang, Y. B., Chang, C. H., and Yau, J. D. (1999). An element for analysing vehicle–bridge systems considering vehicle's pitching effect. *International Journal* for *Numerical Methods in Engineering*, *46*, 1031–1047. https://doi.org/10.1002/(SICI)1097-0207(19991110)46:7<1031::AID-NME738>3.0.CO;2-V

Yang, Y. B., Lin, C. L., Yau, J. D., and Chang, D. W. (2004). Mechanism of resonance and cancellation for train-induced vibrations on bridges with elastic bearings. *Journal of Sound and Vibration*, *269*(1–2), 345–360. https://doi.org/10.1016/S0022-460X(03)00123-8

Yang, Y. B., Liao, S. S., and Lin, B. H. (1995). Impact formulas for vehicles moving over simple and continuous beams. *Journal of Structural Engineering*, *121*(11), 1644-1650. https://doi.org/10.1061/(ASCE)0733-9445(1995)121:11(1644)

Yang, Y. B. and Yau, J. D. (1997). Vehicle–bridge interaction element for dynamic analysis. *Journal of Structural Engineering*, *123*(11), 1512–1518. https://doi.org/10.1061/(ASCE)0733-9445(1997)123:11(1512)

Yang, X. H., Yao, W. X., and Duan, C. M. (2003). The review of ascertainable fatigue cumulative damage rule. *Engineering Science*, *5*(4), 82-87

Yen, T.B., Hodgson, I.C., Zhou, Y.E., Crudele, B. B. (2013). Bilinear S-N Curves and Equivalent Ranges for Fatigue Life Estimation. *Journal of Bridge Engineering*, *18*(1), 26–30. https://doi.org/10.1061/(ASCE)BE.1943-5592.0000325

Yin, X., Fang, Z., Cai, C. S., and Deng, L. (2010). Non-stationary random vibration of bridges under vehicles with variable speed. *Engineering Structures*, *32*(8), 2166–2174. https://doi.org/10.1016/j.engstruct.2010.03.019

Yuan, R., Li, H., Huang, H. Z., Zhu, S. P., and Gao, H. (2015). A nonlinear fatigue damage accumulation model considering strength degradation and its applications to fatigue reliability analysis. *International Journal of Damage Mechanics*, *24*(5), 646-662. https://doi.org/10.1177/1056789514544228

Zhang, B., and Shepard, W. S. (2014). Study of Moving Sinusoidal Wave Load Across Simple Supported Beam for Sensor Structural Configuration. *Journal of Vibration and Acoustics*, *136*(4), 1-11. https://doi.org/10.1115/1.4027481

Zhang, G., and Richter, B. (2000). A new approach to the numerical fatigue-life prediction of spot-welded structures. *Fatigue and Fracture of Engineering Materials and Structures*, *23*(6), 499-508. https://doi.org/10.1046/j.1460-2695.2000.00316.x

Zhang, L. J., Lee, C. M., and Wang, Y. S. (2002). A study on nonstationary random vibration of a vehicle in time and frequency domains. *International Journal of Automotive Technology*, *3*(3), 101-109.

Zhang, W., and Cai, C. S. (2012). Fatigue Reliability Assessment for Existing Bridges Considering Vehicle Speed and Road Surface Conditions. *Journal of Bridge Engineering*, *17*(3), 443–453. https://doi.org/10.1061/(ASCE)BE.1943-5592.0000272

Zhang, W., Cai, C. S., Pan, F., and Zhang, Y. (2014). Fatigue life estimation of existing bridges under vehicle and non-stationary hurricane wind. *Journal of Wind Engineering and Industrial Aerodynamics*, *133*, 135-145. https://doi.org/10.1016/j.jweia.2014.06.008

Zhang, Y., Zhao, H., and Lie, S. T. (2018). A nonlinear multi-spring tire model for dynamic analysis of vehicle-bridge interaction system considering separation and road roughness. *Journal of Sound and Vibration*, *436*, 112-137. https://doi.org/10.1016/j.jsv.2018.08.039

Zhao, Z., and Haldar, A. (1996). Bridge fatigue damage evaluation and updating using non-destructive inspections. *Engineering Fracture Mechanics*, *53*(5), 775–788. https://doi.org/10.1016/0013-7944(95)00136-0

Zhao, Z., Haldar, A., and Breen Jr., F. L. (1994). Fatigue-Reliability Evaluation of Steel Bridges. *Journal of Structural Engineering*, *120*(5), 1608–1623. https://doi.org/10.1061/(ASCE)0733-9445(1994)120:5(1608)

Zheng, D. Y., Cheung, Y. K., Au, F. T. K., and Cheng, Y. S. (1998). Vibration of multi-span non-uniform bridges under moving loads by using modified beam vibration functions. *Journal of Sound and Vibration*, *212*(3), 455–467. https://doi.org/10.1006/jsvi.1997.1435

Zheng, Y., Cao, Z., Guo, P., Gao, P., and Zhang, P. (2021). Fatigue Performance of Steel-Concrete Composite Continuous Box Girder Bridge Deck. *Complexity*, 1-15. https://doi.org/10.1155/2021/6610830

Zhong, H., Yang, M., and Gao, Z. J. (2015). Dynamic responses of prestressed bridge and vehicle through bridge–vehicle interaction analysis. *Engineering Structures*, *87*, 116-125. https://doi.org/10.1016/j.engstruct.2015.01.019

Zhou, H., Liu, K., Shi, G., Wang, Y. Q., Shi, Y. J., and De Roeck, G. (2013). Fatigue assessment of a composite railway bridge for high speed trains. Part I: Modeling and fatigue critical details. *Journal of Constructional Steel Research*, *82*, 234-245. https://doi.org/10.1016/j.jcsr.2012.12.006

Zhu, X. Q., and Law, S. S. (2003). Dynamic behaviour of orthotropic plates under moving loads. *Journal of Engineering Mechanics*, *129*(1), 79-87. https://doi.org/10.1061/(ASCE)0733-9399(2003)129:1(79)

Zuo, F. J., Huang, H. Z., Zhu, S. P., Lv, Z., and Gao, H. (2015). Fatigue life prediction under variable amplitude loading using a non-linear damage accumulation model. *International Journal of Damage Mechanics*, *24*(5), 767-784. https://doi.org/10.1177/1056789514553042

LIST OF PUBLICATIONS

Journal

1. Pillai A. J. and Talukdar S. (2021). Fatigue life estimation of continuous girder bridges based on the sequence of loading. *Structure and Infrastructure Engineering*, Taylor and Francis, *17* (7), 990-1006, DOI: 10.1080/15732479.2020.1784962
2. Pillai A. J., Talukdar, S. (2021). Stochastic model of bridge with moving load for aiding structural health monitoring. *Structural Engineering Digest, Quarterly Journal of Indian Association of Structural Engineers, 11* (3).
3. Pillai A. J. and Talukdar S. (2022). Fatigue life assessment of plate girder bridge using an uncoupled iterative scheme for bridge vehicle interaction (Manuscript no. BEENG-5703, Under Review in Journal of Bridge Engineering, ASCE)
4. Pillai A. J., Ahmed M. H and Talukdar S. (2022). Fatigue damage assessment of tensile specimen considering opening stress in crack propagation stage (Manuscript no. JSA-22-022, Under Review in Journal of Strain Analysis for Engineering Design, Sage Publications)

Conference

1. A. J. Pillai, S. Talukdar (2021), “Non-stationary response of bridge due to moving vehicle with random arrival rate”, Proceedings of 16th International Conference on Vibration Engineering and Technology of Machinery (VETOMAC), Paper ID: 015, p-63, December 16-18, BMS College of Engineering, Bangalore, India.
2. Anjaly J Pillai, S. Talukdar (2021), "Fatigue Damage Assessment of Axially Vibrating Steel Bar considering Opening Stress in Crack Propagation Stage", Proceedings of the International Conference in Futuristic Technologies, Paper ID: FT21012, p-G131, January 22-24, IIT Delhi, India. (Received Outstanding Research Paper Award)
3. Anjaly J Pillai, S. Talukdar (2020), "Dynamic Stresses in Bridge Girder caused by Randomly Moving Loads", Proceedings of First International Conference on Recent Advances in Computational and Experimental Mechanics (ICRACEM), Editors: D. K. Maiti, D. Maity, P. K. Patra, P. Jana, C. S. Mistry, R. Ghoshal and M. S. Afzal, Paper ID: VC-20-021, pp-502-503, September 04-06, 2020, IIT Kharagpur, India.

4. Pillai A.J, Parida S, and Talukdar S. (2020) Fatigue Life Estimation of a Box Girder Bridge Using Coupled and Uncoupled Bridge–Vehicle Dynamics. In: Maity D., Siddheshwar P., Saha S. (eds) Advances in Fluid Mechanics and Solid Mechanics. Lecture Notes in Mechanical Engineering. Springer, Singapore. http://doi-org-443.webvpn.fjmu.edu.cn/10.1007/978-981-15-0772-4_15
5. Kezhiyur A.J, Talukdar S, and Pillai A.J. (2020) Probability of Failure of a Beam Subjected to Randomly Moving Loads. In: Maity D., Siddheshwar P., Saha S. (eds) Advances in Fluid Mechanics and Solid Mechanics. Lecture Notes in Mechanical Engineering. Springer, Singapore. https://doi.org/10.1007/978-981-15-0772-4_29
6. A. J. Pillai, S. Talukdar (2022), "Fatigue Assessment of Bridge with Bifurcation of Load Cycles", 8th International Conference on Structural Engineering, Mechanics and Computation (SEMC), Paper ID: 586, September 5-7, University of Cape Town, South Africa (Paper ID: 586, Submitted)